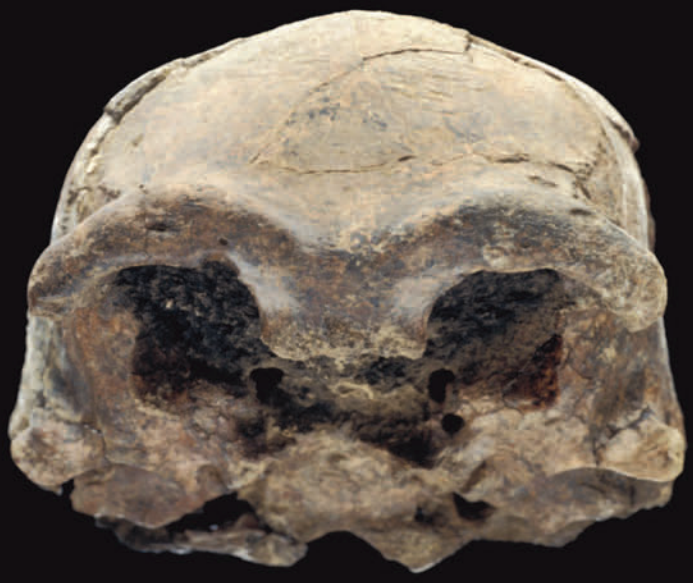

HOMO ERECTUS

Pleistocene Evidence from the Middle Awash, Ethiopia

EDITED BY

W. HENRY GILBERT AND

BERHANE ASFAW

Copyright 2008. University of California Press. All rights reserved. May not be reproduced in any form without permission from the publisher, except fair uses permitted under U.S. or applicable copyright law.

EBSCO Publishing : eBook Collection (EBSCOhost) - printed on 10/28/2022 4:53 AM via
AN: 305970 ; W. Henry Gilbert, Berhane Asfaw.; Homo Erectus : Pleistocene Evidence From the Middle Awash, Ethiopia
Account: s5302073

Homo erectus

Pleistocene Evidence from the Middle Awash, Ethiopia

EBSCOhost - printed on 10/28/2022 4:53 AM via . All use subject to https://www.ebsco.com/terms-of-use

The Middle Awash Series

Tim White, Editor

EBSCOhost - printed on 10/28/2022 4:53 AM via . All use subject to https://www.ebsco.com/terms-of-use

Homo erectus

Pleistocene Evidence from the Middle Awash, Ethiopia

EDITED BY **W. HENRY GILBERT** AND **BERHANE ASFAW**

UNIVERSITY OF CALIFORNIA PRESS *Berkeley Los Angeles London*

EBSCOhost - printed on 10/28/2022 4:53 AM via . All use subject to https://www.ebsco.com/terms-of-use

University of California Press, one of the most distinguished university presses in the United States, enriches lives around the world by advancing scholarship in the humanities, social sciences, and natural sciences. Its activities are supported by the UC Press Foundation and by philanthropic contributions from individuals and institutions. For more information, visit www.ucpress.edu.

University of California Press
Berkeley and Los Angeles, California

University of California Press, Ltd.
London, England

© 2008 by the Regents of the University of California

Library of Congress Cataloging-in-Publication Data

Homo erectus : Pleistocene Evidence from the Middle
Awash, Ethiopia / W. Henry Gilbert and Berhane Asfaw, editors.
p. cm. — (The Middle Awash series; 1)
Includes bibliographical references and index.
ISBN 978-0-520-25120-5 (cloth : alk. paper)
1. *Homo erectus*—Ethiopia—Middle Awash. 2. Geology, Stratigraphic—Pleistocene. 3. Paleontology—Pleistocene. 4. Excavations (Archaeology)—Ethiopia—Middle Awash. 5. Human remains (Archaeology)—Ethiopia—Middle Awash. 6. Middle Awash (Ethiopia)—Antiquities. I. Gilbert, W. Henry, 1970– II. Asfaw, Berhane.

GN284.H65 2007
569.9'70963—dc22
2007015647

Manufactured in the United States of America
10 09 08
10 9 8 7 6 5 4 3 2 1

The paper used in this publication meets the minimum requirements of ANSI/NISO Z39.48-1992 (R 1997) *(Permanence of Paper)*.

Cover illustration: Frontal view of *Homo erectus* calvaria BOU-VP-2/66 from the Daka Member. Photograph by David Brill.

EBSCOhost - printed on 10/28/2022 4:53 AM via . All use subject to https://www.ebsco.com/terms-of-use

Contents

Contributors *vii*
Foreword *ix*
Garniss Curtis
Series Preface *xi*
Tim White
Preface *xvii*
Berhane Asfaw and W. Henry Gilbert
Acknowledgments *xix*

1 Introduction 1
W. Henry Gilbert

2 Geology and Geochronology 13
Giday WoldeGabriel, W. Henry Gilbert, William K. Hart, Paul R. Renne, and Stanley H. Ambrose

3 Bovidae 45
W. Henry Gilbert

4 Carnivora 95
W. Henry Gilbert, Nuria García, and F. Clark Howell

5 Cercopithecidae 115
W. Henry Gilbert and Steve Frost

6 Equidae 133
W. Henry Gilbert and Raymond L. Bernor

7 Giraffidae 167
W. Henry Gilbert

EBSCOhost - printed on 10/28/2022 4:53 AM via . All use subject to https://www.ebsco.com/terms-of-use

8 Hippopotamidae 179
Jean-Renaud Boisserie and W. Henry Gilbert

9 Elephantidae 193
Haruo Saegusa and W. Henry Gilbert

10 Rhinocerotidae 227
W. Henry Gilbert

11 Suidae 231
W. Henry Gilbert

12 Rare Taxa 261
W. Henry Gilbert and Thomas Stidham

13 *Homo erectus* Cranial Anatomy 265
Berhane Asfaw, W. Henry Gilbert, and Gary D. Richards

14 Tomographic Analysis of the Daka Calvaria 329
W. Henry Gilbert, Ralph L. Holloway, Daisuke Kubo, Reiko T. Kono, and Gen Suwa

15 Hominid Systematics 349
W. Henry Gilbert

16 Daka Member Hominid Postcranial Remains 373
W. Henry Gilbert

17 Ecological and Biogeographic Context of the Daka Member 397
W. Henry Gilbert

18 Conclusions: Evolutionary Insights from the Daka Member 413
W. Henry Gilbert

Bibliography 427

Index 449

EBSCOhost - printed on 10/28/2022 4:53 AM via . All use subject to https://www.ebsco.com/terms-of-use

Contributors

W. Henry Gilbert
Department of Anthropology
California State University, East Bay; and
Human Evolution Research Center
University of California, Berkeley

Berhane Asfaw
Rift Valley Research Service
Addis Ababa, Ethiopia

Stanley H. Ambrose
Department of Anthropology
Center for African Studies
Nutritional Sciences Interdisciplinary Graduate Program
Program in Ecology and Evolutionary Biology
University of Illinois, Urbana

Raymond L. Bernor
Department of Anatomy
Laboratory of Evolutionary Biology
Howard University
Washington, DC; and
National Science Foundation
GEO/EAR Sedimentary Geology and Paleobiology Program
Arlington, Virginia

Jean-Renaud Boisserie
Unité Paléobiodiversité et Paléoenvironnements and Département Histoire de la Terre
Muséum National d'Histoire Naturelle
Paris, France; and
Human Evolution Research Center
University of California, Berkeley; and
Laboratoire de Géobiologie, Biochronologie et Paléontologie Humaine
Université de Poitiers, France

Steve Frost
Department of Anthropology
University of Oregon, Eugene

Nuria García
Departamento de Paleontología
Universidad Complutense de Madrid F. C. Geológicas
Madrid, Spain
Centro (UCM-ISCIII) de Evolución y Comportamiento Humanos
Madrid, Spain; and
Human Evolution Research Center
University of California, Berkeley

William K. Hart
Department of Geology
Miami University Geology Field Station
Miami University
Oxford, Ohio

EBSCOhost - printed on 10/28/2022 4:53 AM via . All use subject to https://www.ebsco.com/terms-of-use

Ralph L. Holloway
Department of Anthropology
Columbia University, New York

F. Clark Howell (deceased)
Human Evolution Research Center
University of California, Berkeley

Reiko Kono
Department of Anthropology
National Museum of Nature and Science, Tokyo

Daisuke Kubo
Department of Biological Sciences
Graduate School of Science
The University of Tokyo, Japan

Paul R. Renne
Berkeley Geochronology Center; and
Earth and Planetary Sciences Department
University of California, Berkeley

Gary D. Richards
Department of Anatomy
University of the Pacific
Arthur A. Dugoni School of Dentistry
San Francisco, California; and
Human Evolution Research Center
University of California, Berkeley

Haruo Saegusa
Museum of Nature and Human Activities
Sanda, Hyogo, Japan

Thomas Stidham
Faculty of Ecology and Evolutionary Biology
Texas Cooperative Wildlife Collection
Department of Biology
Texas A&M University, College Station

Gen Suwa
The University Museum
The University of Tokyo, Japan

Giday WoldeGabriel
Environmental Geology and Spatial Analysis Group
Earth and Environmental Sciences Division
Los Alamos National Laboratory
Los Alamos, New Mexico

EBSCOhost - printed on 10/28/2022 4:53 AM via . All use subject to https://www.ebsco.com/terms-of-use

Foreword

The great rifts of Africa are huge pull-apart or tensional zones whose numerous normal faults often drop their central parts thousands of meters below their margins. The Eastern Rift forms a natural hydraulic catchment almost everywhere it is exposed terrestrially. This dynamic system of horsts, grabens, accommodation faults, and uneven land surfaces complexly overlays the rift's axis. Shallow and ephemeral lakes form in the broken terrain, and rivers fill the lakes with sediment. Continued tectonic activity exposes these sediments and their contents to erosion—and to paleoanthropological research.

With nutrient-rich lakes, stream margins, gallery forests, and grassy sumplands, these geological systems provided ecological circumstances attractive to early hominids. Here the forerunners of humans lived and died. Some were entombed in sediments that possessed the right chemical array to fossilize their bones. The Middle Awash study area in the Afar Depression of eastern Ethiopia is a place where conditions were especially conducive to these processes.

Over the last 25 years the Middle Awash study area has proven to be one of the richest fossil areas in eastern Africa. It comprises the longest single record of human evolution on earth, with hominid fossils ranging in age from nearly six million years to around fifty thousand years. Middle Awash sediments regularly interred mammalian remains and archaeological traces, and subsequent erosion has exposed scores of vantages into the deep past. Through these portals we see our ancestors across geological time, from small-brained, ape-like *Ardipithecus*, through the development of tool use, to the first of our species, *Homo sapiens*.

I have had the good fortune of working in the Middle Awash on several occasions. In the months I have spent there, I joined and observed a large group of staff, students, and researchers working under extreme conditions. I never once heard a complaint. Local Afar pastoralists and world-renowned scientists worked side-by-side, digging wells, gathering firewood, cutting roads, surveying, excavating, sieving, and performing the countless other tasks that are required to bring fossils from where they occur naturally to a state that allows their presentation in volumes like this one.

One of my fondest memories is of the late Desmond Clark. By the early 1990s, I had known and admired him for over 30 years. Work was intensifying at Bouri, and

EBSCOhost - printed on 10/28/2022 4:53 AM via . All use subject to https://www.ebsco.com/terms-of-use

Desmond—then in his late seventies—with dimming eyesight but a brightly shimmering passion for paleoanthropology—loaded his gear into the vehicle early in the morning. He and his crew unloaded at a Daka archaeology site, sent the car on its way, put up a large canvas tarpaulin over the excavation, and commenced working. I was dropped nearby, and began surveying Bouri sediments, making interpretations, and looking for good volcanic samples. In so doing, I came across a site with numerous hippo fossils and five basalt hand axes.

The nearest basalt flow was over two kilometers away, and the hominids that made them, Daka Member hominids, had transported the raw tool material over this distance to the site. When I went to tell Desmond of this, I suggested that we have a look when the landcruiser returned. He objected—he couldn't wait to see the site. So we walked the sun-baked kilometer from his excavation to the handaxes I had found, excitedly discussing the potential vindication for his hypothesis that Acheulean tools were occasionally made at the site of butchery.

"This is proof," he said upon arrival. I asked, "Do you think they killed the hippo or were they exploiting an already-dead carcass?" He responded quickly, "Oh, I think they killed it." Clearly he had thought about it before and did not perceive *Homo erectus* as a stupid brute. Later, an excellent Ar/Ar date was derived from a tuff overlying the site. It was close to one million years old. Within 500 meters of this fossilized carcass were several other such localities variously preserving associations of fossils, Acheulean tools, and debitage, all within chronologically-controlled contexts.

Exploration of the human past at Bouri and other Middle Awash locales will continue for centuries to come. The initial archaeological background of the Daka Member discoveries has already been presented by Jean de Heinzelin, Desmond Clark, and others (de Heinzelin et al. 2000a). The pages that follow in the current volume represent the second major published component of Daka-related research. They document the paleontology, revise the stratigraphy, characterize the paleoenvironment, and present Daka *Homo erectus* fossils in the comprehensive manner that Desmond anticipated.

Garniss Curtis
Professor Emeritus of Geology,
Department of Earth and Planetary Science,
University of California, Berkeley
Founder, Berkeley Geochronology Center
September 2007

EBSCOhost - printed on 10/28/2022 4:53 AM via . All use subject to https://www.ebsco.com/terms-of-use

Series Preface

The Middle Awash valley of Ethiopia is a unique natural laboratory for the study of human origins and evolution. Sediments measuring more than a kilometer in thickness lie exposed here on the floor and margins of the Afar Rift. They provide an unparalleled composite geological, paleontological, and archaeological record of the human past. This is Earth's longest and deepest record of early hominid occupation, environment, technological development, and evolution.

The Middle Awash study area is a paleoanthropological resource very different from the nearby richly fossiliferous, stratigraphically simple, and temporally limited deposits at Hadar, where *Australopithecus afarensis* was found in the 1970s. The Middle Awash also differs from the more continuous depositional sequence of the Omo Shungura Formation of southern Ethiopia and from the time-compressed and spatially constrained strata of Olduvai Gorge in Tanzania. In contrast, the Middle Awash affords a series of radioisotopically calibrated "windows" opening on different time slices of the deep past, rather than a continuous accumulation of Miocene through Holocene deposits. Here, in a single valley in the Horn of Africa, it is now possible to sample dozens of biological lineages, including our own, through geological time.

The study area occupies the southwestern corner of the Afar Depression where it sits atop an active segment of the African rift system. Here, crustal extension through the last six million years created shifting centers of fluviatile and lacustrine sedimentary deposition. Today, the modern landscape of the Middle Awash is a tectonically and geomorphologically created patchwork of eroding sediments. These deposits yield the remains of ancient organisms and their environments.

The paleoanthropological importance of the Middle Awash was first revealed in the late 1960s and early 1970s by the pioneering work of geologist Maurice Taieb. Taieb and colleagues focused their efforts on the Hadar fossil field 75 kilometers to the north. Meanwhile, Jon Kalb and his Rift Valley Research Mission in Ethiopia extended Taieb's preliminary Middle Awash surveys. Their field investigations ended in 1978. In 1981 the late Berkeley professor J. Desmond Clark invited me to join him in initiating multidisciplinary work on the geological, archaeological, and paleontological resources of this unique part of the Afar. The Middle Awash project was born.

EBSCOhost - printed on 10/28/2022 4:53 AM via . All use subject to https://www.ebsco.com/terms-of-use

This project is an ongoing multidisciplinary effort to elucidate human origins and evolution. A carefully planned program of exploration, focused research, and resource management has maximized results. Middle Awash field investigations can be loosely divided into three stages for each of the many fossiliferous packages in the study area. Exploration identifies and constrains the package. Focused research then establishes its contents and chronostratigraphic relationships, generating most primary data. Long-term management then allows additional data recovery as erosion and excavation continue. Meanwhile, ground-truth information is synthesized with space- and aerial-based imagery to guide further fieldwork, while other field-based data are subjected to laboratory analyses.

This integrated research strategy matches ongoing problems of human evolutionary studies with the unique resources of the rich and complex Middle Awash repository. Hundreds of team members from nearly 20 different nations play key roles in this process. Paleoanthropology, by definition, is multidisciplinary. In this historical science most objects of investigation are often unique, fragile, and irreplaceable, derived from contexts that are erased during their extraction. This is a science best done deliberately, carefully, and thoroughly. At 25 years, the Middle Awash research effort is both complex and protracted compared to many laboratory-based efforts in modern science. Project success is owed to this long-term perspective and to sustained funding for simultaneous research on multiple fronts.

In its efforts to illuminate African prehistory and paleontology, including the origin and evolution of hominids and their technologies, the Middle Awash project encompasses three basic areas of research: geology, archaeology, and paleontology. A fourth dimension, crucial to the project, is capacity building. During the last century, paleoanthropological research in Ethiopia was traditionally conducted by foreign-based expeditions, with little or no scientific collaboration by Ethiopian institutions or individuals. From its nascence, the Middle Awash project has dedicated itself to developing local scientific personnel and infrastructure that today characterize internationally prominent Ethiopian field and laboratory paleoanthropology.

The Middle Awash project gives priority to constructing an accurate time-stratigraphic framework for its fossil discoveries and to nesting these discoveries into paleoenvironmental contexts. As of the time of this writing, the Middle Awash research project has recovered >260 hominids from 15 separate temporal horizons. Many of these fossils are pivotal to an understanding of the evolution of our family, genus, and species. The recovered hominid remains are but a tiny fraction of the paleobiological evidence amassed by the Middle Awash project to date. Totals as of this writing (2007) are more than 17,000 cataloged vertebrate specimens; more than 1,200 geological samples; and thousands of lithic artifacts. All recovered fossils and artifacts are permanently housed in the collections of the National Museum of Ethiopia. These data, all painstakingly extracted from radioisotopically calibrated and stratigraphically controlled sedimentary contexts, constitute an exceptional record of Africa's past.

This progress has been realized by a global scientific consortium of involved laboratories and facilities. The research has been conducted by team members working under challenging field and laboratory conditions in roles as diverse as translator, archaeologist, Ethiopian government representative, mechanic, geochronologist, cook, paleobotanist, guide, fossil

EBSCOhost - printed on 10/28/2022 4:53 AM via . All use subject to https://www.ebsco.com/terms-of-use

preparator, and dozens more. A full listing of fieldwork participants and primary laboratory researchers resides at the web site of the Middle Awash Project (http://middleawash.berkeley.edu). Middle Awash research results are realized through the support of institutions within Ethiopia and beyond. The continuous financial support of the National Science Foundation and the Institute of Geophysics and Planetary Physics at Los Alamos National Laboratory in New Mexico, with additional assistance from many other organizations and individuals, is gratefully acknowledged (see acknowledgments to each volume).

The Middle Awash project, like most scientific endeavors, uses peer-reviewed publications as the primary means by which its data are shared. Publication of the primary data generated by any such large multidisciplinary project is a formidable and essential undertaking. In paleoanthropology, the most important discoveries are traditionally first announced in high-impact journals and then, after more detailed analysis, published in specialty journals and monographs. In envisioning how to present the most significant discoveries of the Middle Awash study area in book form, we had the advantage of more than a century of scholarly publication in this field.

The Middle Awash Series concept launches with the publication of this volume on the geological background and paleontological content of the Daka Member of the Bouri Formation. The series will proceed as each subsequent, edited, stand-alone volume features the original research results of collaborating teams of project scientists who work together to illuminate a particular temporal period of paleoanthropological significance. Forthcoming volumes detail the project's discoveries of *Ardipithecus kadabba*, *A. ramidus*, and the early anatomically near-modern *Homo sapiens idaltu* from Herto Bouri. Additional volumes will be added to document the project's active ongoing field research.

The research team envisions a set of volumes that shares similar production values, organization, and methods of coverage. Within each volume, richly illustrated chapters contributed by project scientists will be organized by topic. The accounts of the fossils, particularly the hominid fossils, will go beyond mere anatomical description and will be explicitly comparative. This series will place on permanent record the definitive accounts of the most major discoveries of the Middle Awash research project.

To take advantage of the opportunities opened by the rise of information technology, we have taken steps to integrate the series with online digital resources. We have established a Middle Awash web site (http://middleawash.berkeley.edu) that features an accessible, user-friendly portal to project activities and accomplishments, including a full bibliographic listing of all paleoanthropologically relevant work published on the area since the earliest Italian geological explorations in the 1930s.

Another feature of the electronic interface to the Middle Awash discoveries is its specimen-level presentation. Modern digital informatics has allowed a proliferation of web-based faunal lists and other compendia that are increasingly used in meta-analyses ostensibly designed to explore global relationships between data sets as diverse as proxies of global climatic change and fossil evidence for biological evolution. Vertebrate paleontology and paleoanthropology have both witnessed an explosion of uncritical uses of secondary- and tertiary-level faunal lists and other accounts to explore these relationships. These analyses, and the conclusions based upon them, are only as good as the primary data upon which they are constructed.

EBSCOhost - printed on 10/28/2022 4:53 AM via . All use subject to https://www.ebsco.com/terms-of-use

Specimen-level catalog detail must form the empirical foundation of any such synthetic investigations. However, the necessary comprehensive detail on individual specimens and their provenience is traditionally lacking from project-level syntheses in paleoanthropology. Therefore, we have endeavored to accompany each of the volumes in the Middle Awash Series with full and free electronic access to specimen-based catalog detail for each and every collected vertebrate fossil. Furthermore, our accompanying web site archive will release, with the publication of each respective volume in the Middle Awash Series, digital photographic coverage of all cataloged fossils and special micro-CT-generated animations for selected hominid specimens. We hope these efforts to integrate and archive scholarly printed and digital resources will move paleoanthropology forward into a new century of data sharing.

This series is dedicated to the late F. Clark Howell (see tributes at http://herc.berkeley.edu/fc_howell_memorial), whose global vision, detailed knowledge, and passion for paleoanthropology inspires all the participants of the Middle Awash research project.

Tim White
Human Evolution Research Center
Berkeley, California
July 2007

EBSCOhost - printed on 10/28/2022 4:53 AM via . All use subject to https://www.ebsco.com/terms-of-use

I am afraid a good many scientists have the same feelings about Rhodesian Man. Even his fossilized skull has been the source of continual anthropological headaches. He is unique, isolated, and problematical. It is difficult to know where to place him or why he existed at all. He cannot be dismissed as an unmitigated nuisance, for there stand his bones, indisputable evidence that this extraordinary human once lived in Africa. His problem is almost as baffling as that of Piltdown Man, although the dilemma is not the same.

—Roy Chapman Andrews, *Meet Your Ancestors: A Biography of Primitive Man* (1945)

It seems to me more likely that the Far Eastern *Pithecanthropus* and our East African skull have a common ancestor much further back, and that it was these African hominids (with some Pithecanthropine resemblances in a few characters) that gave rise eventually to *Homo*.

—Louis S. B. Leakey, "Very Early East African Hominidae and Their Ecological Setting" (1963)

Lastly, the discovery in upper levels of the Olduvai gorge of a skull of primitive appearance associated with stone implements assigned to the Chellean phase of palaeolithic culture has raised the possibility that *H. erectus*—or a type closely related to it—extended its geographical distribution to East Africa.

—W. E. Le Gros Clark, *The Antecedents of Man* (1971)

Human evolutionary studies are equally historical and processual. The historical documentation afforded by fossil and archaeological records affords the basic stuff from which hypotheses are generated, tested through analysis and controlled comparisons, and ultimately eventuates in development of sustainable and productive theoretical frameworks.

—F. Clark Howell, "Evolutionary Implications of Altered Perspectives on Hominine Demes and Populations in the Later Pleistocene of Western Eurasia" (1998)

EBSCOhost - printed on 10/28/2022 4:53 AM via . All use subject to https://www.ebsco.com/terms-of-use

This Page Left Intentionally Blank

EBSCOhost - printed on 10/28/2022 4:53 AM via . All use subject to https://www.ebsco.com/terms-of-use

Preface

Our ever-expanding synthetic knowledge of human evolution comes from the integration of data sets from contemporary, actualistic, paleontological, archaeological, and geological contexts. The evidence of the prehistoric record represents a major concrete basis for testing hypotheses, predictions, speculations, and conjectures about the human past. This prehistoric evidence is always partial, but often profoundly important. It is evidence that accumulates through time, and is continuously subjected to critical inquiry. The presentation of such evidence in detail sufficient to underpin that inquiry is fundamentally important in modern paleoanthropology.

The Daka Member of Ethiopia's Bouri Formation dates to the early Pleistocene, about one million years ago. Several *Homo erectus* fossils, hundreds of vertebrate remains from diverse taxa, and abundant archaeology have all been recovered from spatiotemporally controlled contexts within sediments exposed by tectonics and erosion along the Bouri Peninsula.

This volume presents the geological and paleontological evidence from the Daka Member. This evidence has been amassed by the research of the Middle Awash project since 1981. The archaeological context of these deposits is presented in the 2000 Belgian monograph entitled *The Acheulean and the Plio-Pleistocene Deposits of the Middle Awash Valley, Ethiopia,* edited by J. Desmond Clark, Jean de Heinzelin, Kathy Schick, and Henry Gilbert.

Of particular focus in the present volume is a very well-preserved *Homo erectus* calvaria, BOU-VP-2/66. This is one of only a few hominid remains of this antiquity from Africa. It is described and compared here in detail; analyzed metrically, morphologically, and tomographically; and interpreted in an evolutionary context. Hominid postcranial elements from the Daka Member, including three femora, are also described and compared here.

The relatively few hominid fossils from the Daka Member are spatially and stratigraphically associated with a fossil vertebrate fauna that is unique in its quality and abundance. This rich and diverse assemblage provides data on paleoecology, evolutionary patterns,

EBSCOhost - printed on 10/28/2022 4:53 AM via . All use subject to https://www.ebsco.com/terms-of-use

and paleoclimate in early Pleistocene Africa. The acquisition and presentation of all this evidence from the Daka Member allows the emergence of an unparalleled composite diorama of the natural history of *Homo erectus* in Pleistocene Africa.

Berhane Asfaw
W. Henry Gilbert
Addis Ababa and Berkeley
February 2007

EBSCOhost - printed on 10/28/2022 4:53 AM via . All use subject to https://www.ebsco.com/terms-of-use

Acknowledgments

The Middle Awash research project, active in Ethiopia since 1981, incorporates the work of dozens of Ph.D.-level scientists conducting field and laboratory research. Not all are co-authors of the chapters to follow, but all have contributed, in some logistical or intellectual manner, to the results presented here. Permission to conduct the research reported here was granted by the Authority for Research and Conservation of Cultural Heritage, Ministry of Culture and Tourism, Ethiopia. We also thank the National Museum of Ethiopia for its logistical and scientific support, and we acknowledge the many Antiquities Officers who have served with the project since 1981.

The Middle Awash research project was initiated in 1981 by the late Professor J. Desmond Clark. Both editors of this volume had the great privilege of being his graduate students, and later, two of his many colleagues (see http://herc.berkeley.edu/jdesmond_clark_memorial for tributes). During the 1990s, Desmond Clark and Tim White enlisted Dr. Jean de Heinzelin to lead the geological work on Acheulean-bearing deposits at Bodo and Bouri. His work was instrumental in establishing the stratigraphic context of the discoveries reported here. It is to these passed friends and giants of African paleoanthropology that we dedicate this volume.

We owe our families undying gratitude for their support during the production of this volume. Thanks to Olivia, John, and Sandra Gilbert for their patience and encouragement. Thanks to Frehiwot and the family for their support and tolerance of long absences from the house to do field work. Without her encouragement none of this research would be possible.

We thank the following individuals for their scientific contributions to understanding the Acheulean-bearing deposits of the Middle Awash: Don Adamson, Alemu Ademassu, Alan Almquist, Alemayehu Asfaw, Mesfin Asnake, Tadewos Assebework, Zelalem Assefa, Yonas Beyene, Raymonde Bonnefille, David Brill, Alison Brooks, Jose Miguel Carretero, Tadewos Chernet, Sylvia Cornero, Garniss Curtis, Brianne Daniels, Alban Defleur, David DeGusta, Eric Delson, Ann Getty, Erksin Guleç, Yohannes Haile-Selassie, Jack Harris, Grant Heiken, David Helgren, Leslea Hlusko, Girma Hundie, Ferhat Kaya, Leonard Krishtalka, Hiro Kurashina, Tonja Larson, Bruce Latimer, Ken Ludwig, Agazi Negash, Jim Parham, Çesur Pehlevan, Scott Simpson, Denise Su, Carole Susman, Solomon

EBSCOhost - printed on 10/28/2022 4:53 AM via . All use subject to https://www.ebsco.com/terms-of-use

Teshome, Nick Toth, Elisabeth Vrba, Robert Walter, Martin Williams, John Yellen, and Yohannes Zeleke.

Research by these scientists in the remote corners of the Afar depression is made possible and tolerable by the support of a variety of individuals who have repeatedly assumed the logistical responsibilities of organizing and maintaining field camps under difficult conditions. No science would be possible without the support of the collectors, cooks, camp managers, and drivers for the project. A full listing of the approximately 600 people engaged in the project's field activities during the last quarter-century can be found at web site http://middleawash.berkeley.edu.

We thank the Afar Regional Government of Ethiopia for its support, and, in particular, we thank the late Neina Tahiro and his brother Mohammed Tahiro for their encouragement and friendship. The Afar people of Gewane, Bouri, Aramis, Uma D'ah, Enito, and many other smaller villages have provided invaluable assistance, sharing their skills and knowledge of navigation, excavation, security, and natural history with the project at its various field camps. In particular, we thank Hamed Elema and his family for their untiring work in support of the project's activities at Bouri.

Most of the work described here was supported by grants from the National Science Foundation (NSF) of the United States (grants BNS 80-19868, BNS 82-10897, SBR-9318698, SBR-9512534, SBR-9521875, SBR-9632389, and BCS-9910344). The Institute for Geophysics and Planetary Physics (IGPP) at the Los Alamos National Laboratory in New Mexico provided critical support for the field geology and laboratory geochemical work associated with the project during the last 15 years. The National Geographic Society provided a vehicle for fieldwork in 1982. Gilbert's dissertation research on the Daka Member was funded by the L. S. B. Leakey Foundation.

We would like to thank the anonymous reviewers for their comments on individual chapters and the overall presentation. We are very grateful to Phillip Rightmire for his comments on the hominid-based chapters.

For the cover presentation and the plates embedded in the various individual chapters, we extend our deepest appreciation to David Brill for his photographs, and so much more, over the years of the research at Bouri and elsewhere in the Middle Awash. We also thank Lorenzo Rook for the Buia photographs, and David Lordkipanidze for the Dmanisi photograph.

We appreciate the support of all those at the University of California Press who contributed to the production of the volume. In particular, Chuck Crumly provided constant, patient guidance throughout the process of completing this volume, and Francisco Reinking and Scott Norton had the difficult task of handling the submission package. Tim White and Kyle Brudvik provided thorough proofreads.

In addition to those acknowledged above, the following individuals and institutions made specific contributions to the individual chapters:

Chapter 2. Access to electron microprobe and other support from the Earth Environmental Sciences Division at LANL facilitated the characterization of volcanic samples. Stable isotope analysis was performed at the Environmental Isotope Paleobiogeochemistry Laboratory at the University of Illinois, Urbana. The National Science Foundation (SBR 98-71480) and the University of Illinois provided additional support for mass

EBSCOhost - printed on 10/28/2022 4:53 AM via . All use subject to https://www.ebsco.com/terms-of-use

spectrometry instrumentation. Janet Atkinson assisted in fieldwork and analysis. Any opinions, findings, and conclusions or recommendations expressed in this publication are those of the author(s) and do not necessarily reflect the views of the NSF, LANL, and the University of Illinois.

Chapter 3. Elizabeth Vrba gave consultation on bovid identifications and evolutionary patterns, as well as advice on format. Faysal Bibi provided a thorough review.

Chapter 4. The Spanish Ministry of Education, Culture, and Sports supported N. Garcia's postdoctoral research at the Human Evolution Research Center, UC Berkeley.

Chapter 5. Nelson Ting provided some of the comparative femoral data; Eric Delson and three anonymous reviewers provided valuable comments. The L. S. B. Leakey Foundation, the Wenner-Gren Foundation, the University of Oregon, and the New York College of Osteopathic Medicine provided support to S. Frost.

Chapter 6. Miranda Armour-Chelu provided unpublished measurements. Some work was funded by NSF (grant EAR 0125009).

Chapter 8. J.-R. B. thanks J. Surault, A. Foray, E. Lavertu in Addis Ababa and G. Florent in Poitiers for their kind help, as well as M. Brunet, F. C. Howell, P. Vignaud for their advice and support. His research was funded by the Ministère Français de l'Education Nationale et de la Recherche (Université de Poitiers), the Mission Paléoanthropologique Franco-Tchadienne, the Fondation Fyssen (postdoctoral research grant), the Ministère des Affaires Etrangères (program Lavoisier and SCAC, French Embassy in Ethiopia), the Fondation Singer-Polignac (postdoctoral research grant), and the NSF-HOMINID program RHOI at the Human Evolution Research Center, UC Berkeley.

Chapter 9. The following individuals provided invaluable assistance: J. Hooker and A. Currant (Natural History Museum, London), R. Ziegler (Staatliches Museum für Naturkunde Stuttgart), L. Ginsburg (Muséum National d'Histoire Naturelle, Paris), W.-D. Heinrich (Institut für Paläontologie, Museum für Naturkunde, Berlin), Y. Tominda (National Science Museum, Tokyo) and M. G. Leakey (National Museum of Kenya, Nairobi). P. Vingnaud provided literature, and financial support was provided to H. Saegusa by the Japanese Ministry of Education, Culture, Sports, Science and Technology.

Chapter 10. Çesur Pehlevan provided guidance on systematics and identifications.

Chapter 11. Tim White provided guidance and discussion. Gen Suwa provided access to Konso fossils and contributed substantial helpful advice regarding *Metridiochoerus* evolution. Scott Simpson provided helpful information and conversation about *Metridiochoerus* and *Phacochoerus*.

Chapter 12. Hank Wesselman provided assistance in identifying the *Arvicanthis* cranium.

Chapter 13. The description protocol used was developed in the Human Evolution Research Center, UC Berkeley, by (in alphabetical order) Berhane Asfaw, David DeGusta, Henry Gilbert, Gary Richards, and Tim White.

Chapter 14. Tim White provided helpful discussions and comments.

Chapter 15. The character list is in large part derived from a literature review of characters used in Pleistocene hominid systematics conducted by Tim White and developed with Berhane Asfaw, David DeGusta, Henry Gilbert, and Gary Richards. Clark Howell provided helpful discussions and comments.

EBSCOhost - printed on 10/28/2022 4:53 AM via . All use subject to https://www.ebsco.com/terms-of-use

Chapter 16. The Phoebe Apperson Hearst Museum of Anthropology provided access to the comparative modern human femoral collection. Brianne Daniels provided assistance in scoring the modern human femoral collection.

Chapter 17. Elizabeth Vrba provided valuable discussions on bovid natural history.

Chapter 18. Tim White and Clark Howell provided helpful discussions and comments.

EBSCOhost - printed on 10/28/2022 4:53 AM via . All use subject to https://www.ebsco.com/terms-of-use

1

Introduction

W. HENRY GILBERT

The rich Dakanihylo (Daka) Member of the Bouri Formation in the Afar Rift of Ethiopia is today exposed by active erosion along the northeast slope of the Bouri Peninsula (Figures 1.1 and 1.2). Geochronological results on interbedded volcanic strata indicate an age for these fossiliferous sediments of one million years (Ma). The Daka Member has preserved a very rich array of fossil mammals (>750 collected specimens), including several *Homo erectus* specimens (Vrba 1997; Asfaw et al. 2002; Gilbert 2003b). Numerous Acheulean archaeological localities are documented. This volume presents the fossil content of the Daka Member, provides geological background, and explores the assemblage's significance for studies of African Pleistocene paleobiology.

Importance of the Daka Member to African Pleistocene Studies

The richness, stratigraphic integrity, and temporal placement of Ethiopia's Daka Member make it key to exploring the development of the Afar Rift, African Pleistocene fauna, and our own evolution. The Daka Member comprises a single, well-constrained stratigraphic interval. Much of the detail possible in this volume is the result of employing a coherent methodology that began with detection of the fossils on the eroding landscape.

Plio/Pleistocene global cooling and its effects on African biology have been a topic of considerable debate, and numerous links between paleoclimate and biology have been explored for the late Pliocene and earliest Pleistocene (Vrba et al. 1995; Bromage and Shrenk 1999; deMenocal 2004; Behrensmeyer 2006). The rise of intense, cyclical glaciation, involving change from a 0.04 Ma to a 0.1 Ma glacial/interglacial cycle with more intense ice ages, began between 1.2 and 0.8 Ma (deMenocal and Bloemendal 1995; deMenocal 2004). This Pleistocene transition has received less attention than earlier transitions, and sampling of fossils from this time period in Africa has, before now, been extremely poor. With two volcanic horizons dated to approximately 0.96 and 1.04 Ma (see Chapter 2), the Daka Member constitutes one of the richest paleoanthropological sites in Africa dated to this period.

EBSCOhost - printed on 10/28/2022 4:53 AM via . All use subject to https://www.ebsco.com/terms-of-use

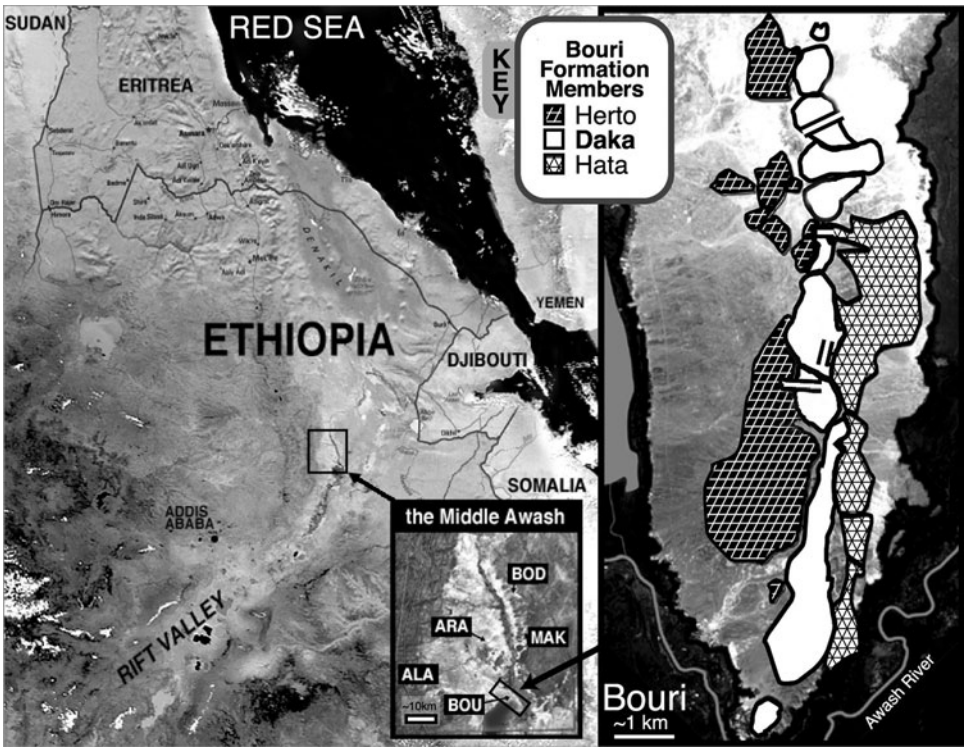

FIGURE 1.1
The Middle Awash, Bouri (BOU in Middle Awash inset), and the Daka Member.

TABLE 1.1 Significant African Fossiliferous Sites Dating to Near 1.0 Ma

Site	*Date*	*Date Reference*
Olduvai Bed IV	Dated to between 0.78 and 1.2 Ma	Tamrat et al. 1995
Tighenif	Biochronologically placed in the middle Pleistocene	Geraads et al. 1986
Aïn Maarouf	Biochronologically placed in the early middle Pleistocene	Geraads et al. 1992
Buia	Dated to approximately 1.0 Ma using biochronology and paleomagnetism	Abbate et al. 1998
Olorgesailie Member 1	Dated to between 0.974 and 0.992 Ma	Potts et al. 1999
Olorgesailie Member 10	Dated to between 0.662 and 0.746 Ma	Potts et al. 1999
Kanjera North	Biochronologically and paleomagnetically placed in the late early Pleistocene or early middle Pleistocene	Ditchfield et al. 1999
Thomas Quarries	Biochronologically placed at the early to middle Pleistocene transition	Raynal et al. 2001
West Turkana Nariokotome Member	Dated to between approximately 0.78 and 1.4 Ma	Harris et al. 1988a
East Turkana Chari Member	Dated to between approximately 0.78 and 1.4 Ma	McDougall 1985; McDougall et al. 1985
Omo Member L	Dated to between approximately 1.0 and 1.4 Ma	Feibel et al. 1989

EBSCOhost - printed on 10/28/2022 4:53 AM via . All use subject to https://www.ebsco.com/terms-of-use

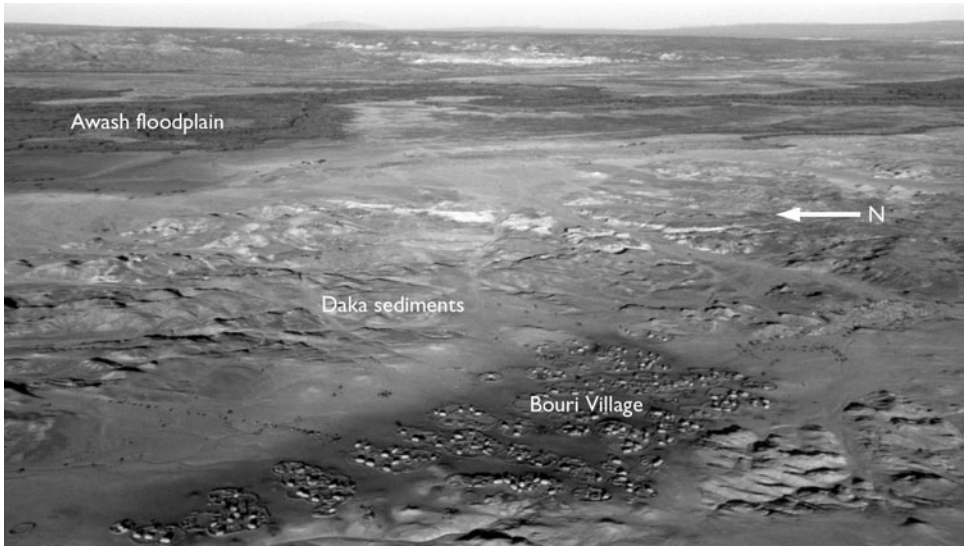

FIGURE 1.2

Low-altitude aerial view of the Afar Bouri Village, January 11, 2003. View is to the east, across the Awash River. The dark background of the village reflects the large number of domestic livestock, which are penned at night within the rings of thorn tree branches that surround the lighter-colored, loaf-shaped dwellings. These houses are made by the local pastoralists by placing grass mats atop curved branches. Pliocene sediments at Asa Barrie are center top, beyond the river. Erosional outcrops of the Daka and Hata Member sediments are between the village and the swampy river floodplain. Herto Member sediments are eroding at the bottom of the image, west and southeast of the village. Video frame capture by Rod Paul, January 11, 2003.

Table 1.1 enumerates other significant fossiliferous sites in Africa dating to near 1.0 Ma. Of these, the richest radiometrically dated unit is Olduvai Bed IV, which has fewer than half as many identified large mammal specimens as the Daka Member (in general, the fossil remains from there are far less complete; Leakey 2000). Tighenif, Aïn Maarouf, and Thomas Quarries are large localities in northern Africa that rely on geomagnetic and biochronological dating, as does Kanjera North in eastern Africa. Faunal samples from the West Turkana Nariokotome Member, Olorgesailie, and Buia are small compared to the Daka Member assemblage (Koch 1986; Harris and Leakey 1993; Abbate et al. 1998; Martínez-Navarro et al. 2004).

History of Fieldwork at Bouri

Although fossils from the southern portion of the Ethiopian Rift have been known since the early twentieth century, the paleoanthropological potential of the Awash River basin, which traces the Afar Rift, was not realized until the 1965 discovery of Melka Kunture by United Nations Development Programme water project personnel and its excavation by Chavaillon (Chavaillon et al. 1979). Chavaillon influenced geology student Maurice Taieb, who explored farther north in the Afar basin in the late 1960s. Taieb discovered many fossiliferous areas, including what would later become the Middle Awash and Hadar paleoanthropological study areas. After his reconnaissance work, Taieb was joined by Jon Kalb, Yves Coppens, and Donald Johanson. They formed the International Afar Research Expedition (IARE) and began work at Hadar. Kalb seceded from the group and initiated the Rift Valley Research Mission in Ethiopia (RVRME). This group engaged in reconnaissance survey of the Awash basin in 1975 and 1976. Most of the survey was on the east side of the Awash River, but the Bouri area was also visited. In December 1975, Seleshi Tebedge and Jon Kalb visited the Bouri Peninsula and found Acheulean artifacts and fossils at a location called Dakanihylo. In November 1976, after Alemayehu Asfaw's discovery

EBSCOhost - printed on 10/28/2022 4:53 AM via . All use subject to https://www.ebsco.com/terms-of-use

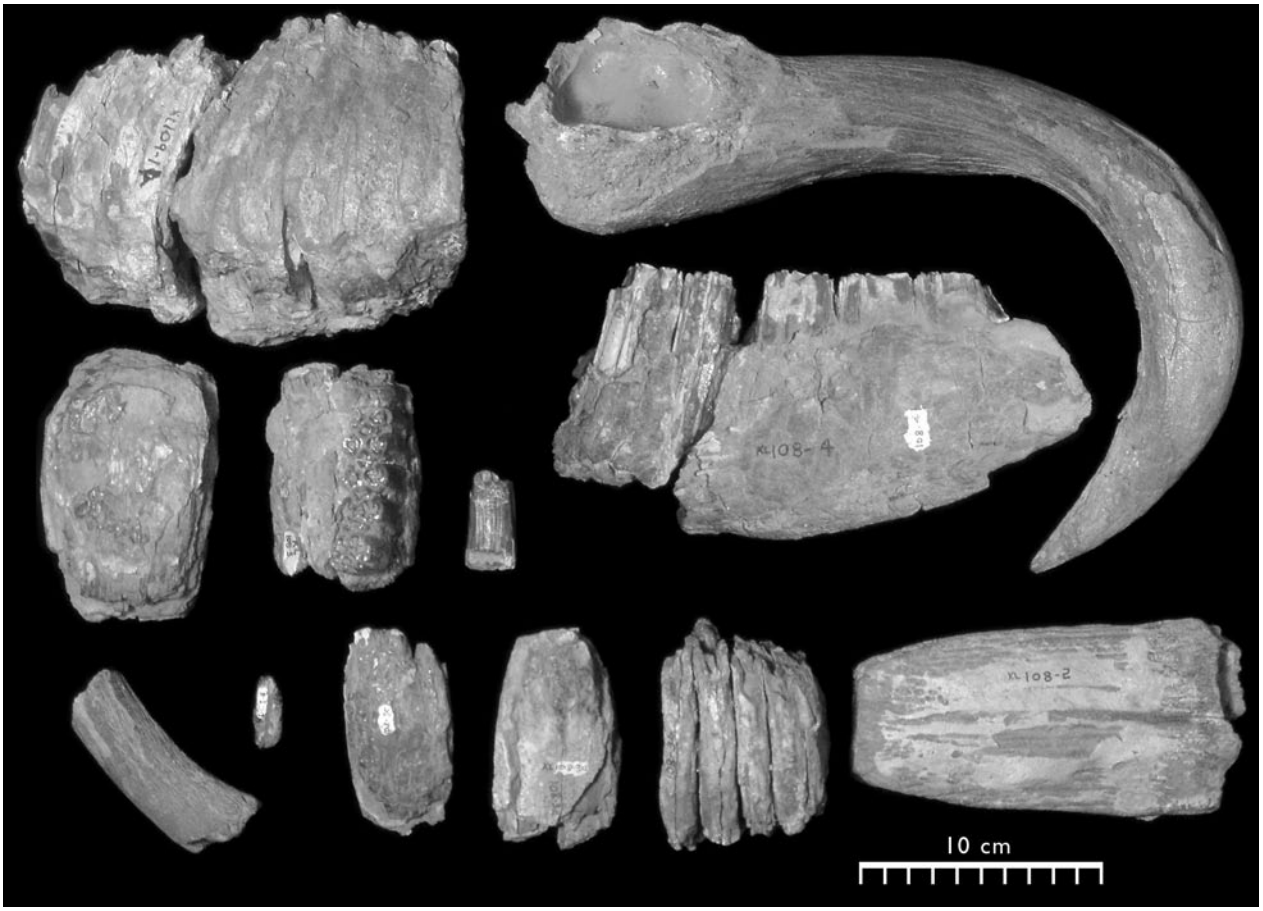

FIGURE 1.3
Eleven possible Daka Member specimens collected by the RVRME.

of the Bodo cranium east of the Awash River, Jon Kalb returned to the Bouri Peninsula briefly with Charles Smart. During this venture they collected a sample of the artifacts and fossils that Kalb had seen the year before, and they performed a cursory survey of the peninsula.

Kalb et al. (1982c) described the Wehaietu Formation based mainly on the RVRME's fieldwork east of the Awash. "Dakanihylo" sediments, however, were included in this formation based on transects made west of the Awash, and four small collection localities were noted. The name "Dakanihylo" is misplaced on maps published by Kalb (1982a, b) several kilometers from Bouri (both locations are included in Kalb's maps), but the Dakanihylo rock formation, well known to local Afar-speaking residents, occurs *on* the Bouri Peninsula. The eleven mammalian fossils (Figure 1.3) collected by Kalb et al. (1982c) from Kalb's "Dakanihylo" localities 108, 109, 178, and 179 are thus of questionable stratigraphic provenience based on current geological understanding of the three stratigraphic members exposed on the Bouri Peninsula (Kalb did not recognize the older Hata or younger Herto units; see figure 6 in Kalb et al. 1982b). Furthermore, we have examined the 11 RVRME Daka specimens housed in the National Museum of Ethiopia and have found that they do not significantly

EBSCOhost - printed on 10/28/2022 4:53 AM via . All use subject to https://www.ebsco.com/terms-of-use

FIGURE 1.4
Crossing the Awash River from south to north on the initial trip to Bouri in 1981. The lack of bridges and roads in the study area is a constant hindrance to paleoanthropological research in the Middle Awash study area. Photograph by Tim White, November 17, 1981.

depart from the faunal assemblage reported in the chapters that follow. Because of the positional and stratigraphic uncertainty associated with the RVRME collections from Bouri, we have excluded them from the analysis that follows.

Data collected by the RVRME have been published in several places. Kalb et al. (1982b, c) present the most coherent data syntheses in a largely repetitive series of papers published soon after our work began at Bouri in 1981. In these RVRME publications the "Dakanihylo Member" was described as follows: "Consists of 15–20 m or more of strata. . . . A stratigraphic position for this unit above the Meadura Member is inferred from its basinward and generally lower altitudinal position and from its more derived fauna" (Kalb et al. 1982c, 113). The 1981 work demonstrated that this chronostratigraphic placement of the Daka Member was erroneous: "The fauna associated with the Dakanihylo Member of the Wehaietu Formation may antedate, rather than postdate, the Bodo and Meadura Members" (Clark et al. 1984, 426). This conclusion has been substantiated by all subsequent geochronological, stratigraphic, and biochronological work at Bouri.

The Middle Awash research project began work on the Bouri Peninsula in 1981 (Figure 1.4), but this was interrupted between 1982 and 1990 as new Ethiopian antiquities legislation was developed. Archaeological, paleontological, and geological work commenced at Bouri in 1992 under the direction of J. Desmond Clark, Tim White, Berhane Asfaw, and Jean de Heinzelin. No work occurred at Bouri during the 1994 season. Research during 1995 and 1996 focused on stratigraphy and archaeology (Figure 1.5), and was reported in de Heinzelin et al. (2000a). The 1997, 1998, and 1999 field seasons were characterized by intensive fossil collection and further stratigraphic revision of Bouri sediments. Fossils described in this volume were mostly collected between 1992 and 2002. Stratigraphic data were collected in 1997, 1998, 1999, and 2000 by Henry Gilbert, Giday WoldeGabriel, William Hart, and Paul Renne.

EBSCOhost - printed on 10/28/2022 4:53 AM via . All use subject to https://www.ebsco.com/terms-of-use

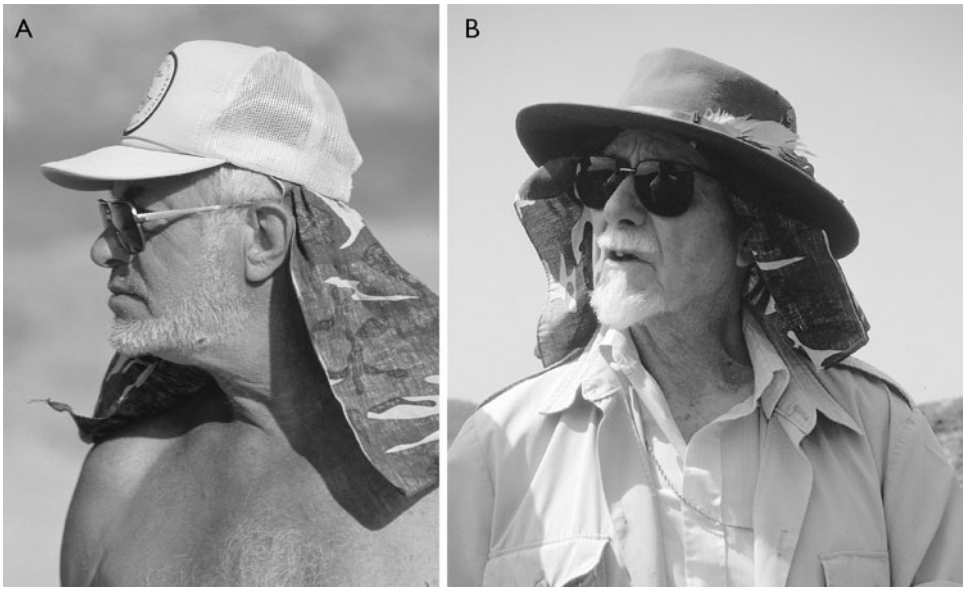

FIGURE 1.5
Daka Member archaeological work team leaders. A. Jean de Heinzelin, chief geologist for the Pleistocene archaeology effort on the Bouri Peninsula between 1993 and 1996. Photograph by Tim White, November 12, 1990. B. Middle Awash project founder J. Desmond Clark. Photograph by Tim White, November 21, 1995.

Archaeological Evidence in the Daka Member

Numerous artifacts were recovered from 17 designated archaeological localities in the Daka Member during active work in the 1990s (de Heinzelin et al. 2000a; Schick and Clark 2000). Daka Member technology (Figure 1.6) was classified by Schick and Clark (2000) as early Acheulean and is composed of unrefined handaxes, cleavers, picks, flakes, flake cores, bifaces, retouched flakes, and hammerstones. Artifacts were formed using a hard-hammer technique. Some of the archaeological sites are associated with hippopotamus and elephant remains. Several fossils found outside designated archaeological localities, including an equid femur (BOU-VP-1/165) and other mammal bone fragments, bear cut marks. The Acheulean of the Daka Member was treated extensively by de Heinzelin et al. (2000a). In that monograph, Middle Awash project mapping, nomenclature and locality/specimen designation protocols, and collection protocols are outlined.

Fieldwork, Curation, and Analytical Methods

The present volume rests on a foundation of data assimilated and analyzed according to a sequence of methodologies and protocols. Understanding these methods is a necessary first step to interpreting the results presented here. Operational procedures are grouped into discrete subsets that are applied at various stages of analysis. This section follows fossils from recovery in the field to their analysis in the National Museum of Ethiopia, where they are permanently stored.

Survey, Collection, and Transportation

The Middle Awash research project fossil recovery protocols vary according to research focus. The project has protocols governing the establishment of new localities to ensure

EBSCOhost - printed on 10/28/2022 4:53 AM via . All use subject to https://www.ebsco.com/terms-of-use

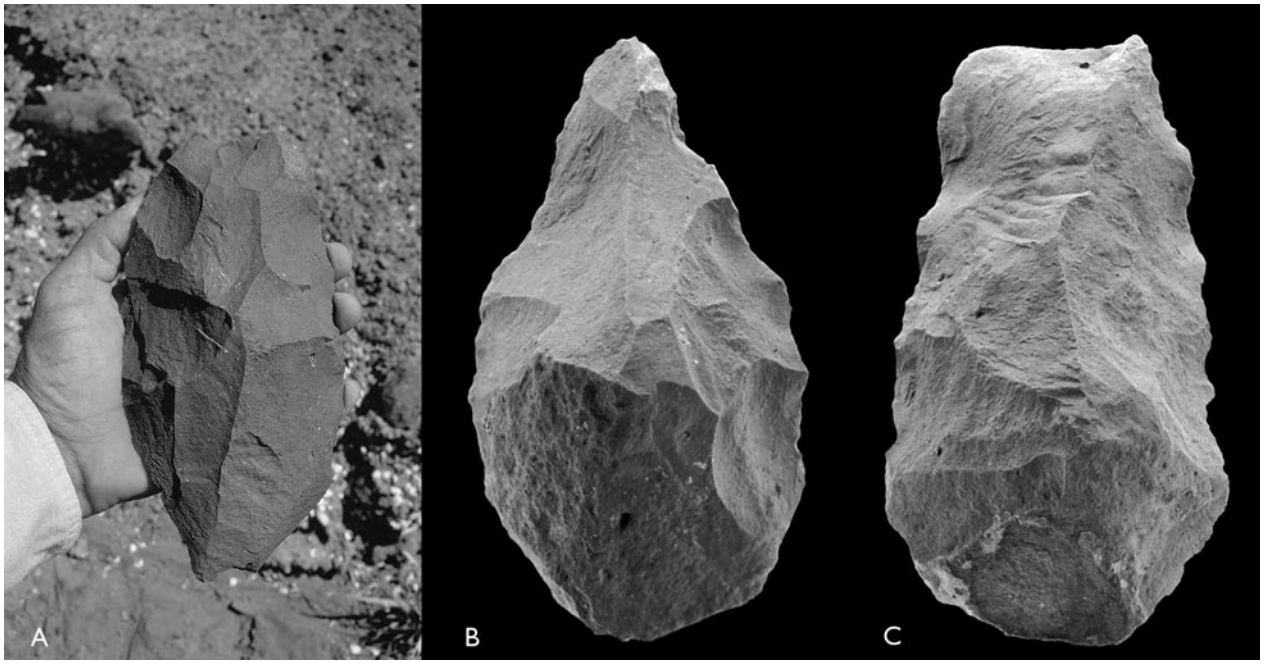

FIGURE 1.6

A. Early Acheulean artifacts in the field in the Daka Member. Photograph by Tim White, January 3, 1998. B. Representative early Acheulean handaxe. C. Representative cleaver from the Daka Member. Photographs courtesy David Brill.

that these are based on consistent geological and geographic boundaries, are accurately circumscribed, and follow a logical numbering scheme. The survey and collection methods used in the Daka Member follow these guidelines. In contrast to procedures employed at many other African Plio-Pleistocene study areas, the precise stratigraphic and spatial placement of each cataloged Middle Awash specimen is individually recorded. This renders "site" and "locality" definition relatively less important and more flexible than is the case for many other research areas.

The first stage in the development of a paleontological area is broad-scale survey of a region within the study area. Our project's initial efforts on the Bouri Peninsula took place in 1981 and continued in 1992 and 1993. During the 1981 survey, extensive fossil fields were identified and archaeological sites were visited and photographed. No fossils were collected because there was not yet a properly established stratigraphic framework.

The first collection from the Daka Member, at BOU-VP-1, was made in 1992 (Figure 1.7). This first locality was established based on a laterally continuous, homogeneous outcrop above the Hata Member/Daka Member unconformity. It is the largest Daka Member locality. Like BOU-VP-1, the remaining Bouri vertebrate paleontology localities were established using two criteria: geology and geography. Localities were established only where the geological context was apparent and the risk of contamination from other adjacently exposed strata was low. This meant that some rich surface assemblages were left in the field because they were mixed. The geological basis for each locality is presented in Chapter 2.

The second criterion for the establishment of a vertebrate paleontology locality is geography. In many cases it was practical to subdivide geologically equivalent units

EBSCOhost - printed on 10/28/2022 4:53 AM via . All use subject to https://www.ebsco.com/terms-of-use

FIGURE 1.7

In the 1992 field camp on the Hatayae floodplain, Gen Suwa (left), Bruce Latimer, and antiquities officer Tadewos Assebework prepare Daka Member fossils for transport to the National Museum of Ethiopia. Photograph by Tim White, December 10, 1992.

to facilitate collection and organization. Geologically equivalent localities established at different locations can sometimes meet at the borders as they grow, as was the case for BOU-VP-2 and BOU-VP-3. When coeval fossiliferous deposits were thus subdivided, a discrete modern geographic landmark, such as a streambed, was used as a boundary. Each locality has been carefully plotted and its perimeter traced on the ground to ensure correspondence with geological boundaries. This strict definition of locality borders has been necessary when working the Bouri Peninsula because of the proximity of the adjacent Herto and Hata Members, often in unconformity and/or fault contact.

Accurate placement of individual fossils is crucial for documenting spatial and stratigraphic provenience. During the 1980s and 1990s, before differential GPS (DGPS) became available, each specimen collected was pinpointed and plotted on high-resolution 1:30,000 aerial photos. In field tests using a differentially corrected GPS unit with submeter accuracy, these air photo plots were shown to be accurate to within 5–10 meters. We transferred the air photo plots to the Middle Awash Digital Map Archive (MADMA) in the 1990s and have now generated latitude and longitude coordinates by aligning the aerial photo scans with georeferenced satellite imagery.

During systematic paleontological collection, recovery crews pin-flagged all potentially collectable fossils on a locality's surface. It was not possible to collect every piece of fossilized bone from this large area because of logistical constraints involved in transportation and museum space. For this reason a specific collection protocol was employed. All bovid craniodental material was collected, with the exception of horn core midshafts that did not preserve the base. All material identifiable as avian,

EBSCOhost - printed on 10/28/2022 4:53 AM via . All use subject to https://www.ebsco.com/terms-of-use

carnivore, cecopithecid, rodent, or hominid was collected. All material identifiable as equid and giraffid was collected, with the exception of broken teeth. Hippopotamid third molars, mandibles with dentition, and crania were collected. Suid complete third molars, mandibles, and cranial material were collected. Elephant molars, crania, and complete mandibles were collected. Fish fossils were generally not collected, but one complete cranium was recovered because of its excellent preservation. Crocodile fossils were not collected.

After pin flags had been placed, a team of two people with an understanding of the stratigraphy and collection protocols then recovered and plotted each collectable flagged specimen, closely following imagery to make sure the recovery team covered all areas. Each Daka locality was systematically collected in this way numerous times over several field seasons. Despite intensive search, no micromammal quarries were established in Daka Member sediments, presumably because these largely sandy units were deposited by high-energy flow. This meant that most collected fossils were found by foot survey rather than excavation, although many partially exposed and in situ fossils were identified during surface transects and released by excavation.

Upon collection, each fossil was wrapped in an individual bag and given a specimen number, which was written on a weatherproof paper tag. This number accompanied the fossil through the process of water-washing and drying, staying with the specimen until it was permanently labeled and cataloged at night in the field camp.

Field catalog entries were made in camp as the fossils were labeled and bagged. Provisional field identifications of the specimens were made at that time, and this record became the official inventory of fossils for each field season. Fossils were wrapped in several layers of tissue paper, then wrapped in newspaper, then labeled and placed in padded plastic containers for vehicle transport to the National Museum of Ethiopia.

Restoration and Curation

Upon arrival in the museum, nonfragmentary, matrix-free specimens were unpacked, removed from their protective wrapping, placed in permanent, numbered clear plastic bags, and shelved or organized within labeled wooden trays (Figure 1.8). Specimens collected as fragments or embedded in matrix were separated into one of three categories: those that needed only cleaning, those that needed only gluing, or those that needed both.

The Middle Awash research project employs a fossil restoration methodology that uses several different compounds and procedures for various types of specimens and conditions of preservation. For small, non-porous fossils such as teeth, where the joins recognized are certain to be correct, cyanoacrylate is sometimes used. Larger fossils are bonded with epoxies of various viscosities, and fossils that might later be taken apart are joined with an acetone-soluble adhesive such as polyvinyl acetate. Matrix removal, particularly for the Daka Member fossils, often required extended time periods. It was common for a bovid horn core, for example, to require two or three days to harden, clean with an air scribe, and restore. Fossils requiring restoration or cleaning joined the others on shelves or in trays as they were finished. Fossils from the Daka Member

EBSCOhost - printed on 10/28/2022 4:53 AM via . All use subject to https://www.ebsco.com/terms-of-use

FIGURE 1.8
Washing prior to cleaning and reassembly of fossils collected from the Daka Member. From left to right, Scott Simpson, Doug Pennington, Ann Getty, and W. Henry Gilbert do the work, which involves careful cleaning and control over the many fragments that will be reassembled into the more complete specimens illustrated in this volume. Photograph by Tim White, October 1994.

all currently reside in the National Museum of Ethiopia. They are sorted by taxon and element and deposited on open-air shelves and in trays. Smaller specimens are in labeled bags.

Documentation and Analysis

The bulk of laboratory research on the Daka vertebrate fossils was done in the fall of 2001 and in the spring and summer of 2002. Fossils were measured and photographed, and the most complete and important specimens were described. Description was done at various levels of detail according to several factors, including the rarity of the taxon, its systematic significance, and the degree to which the taxon had been previously described elsewhere.

Digital photography has overtaken film photography as the most practical means of visually documenting a large collection of fossils. All Daka Member specimens have been imaged in several views all accessible in digital format at http://middleawash.berkeley.edu.

This volume constitutes the official presentation of the overall Daka Member faunal assemblage and significantly revises and supplants the assessments presented in Gilbert (2003b). As discussed, the archaeology and general stratigraphy of the Daka Member were published previously (de Heinzelin et al. 2000a). Major updates to the stratigraphy presented there are made in Chapter 2.

EBSCOhost - printed on 10/28/2022 4:53 AM via . All use subject to https://www.ebsco.com/terms-of-use

TABLE 1.2 Daka Member Faunal List

- MAMMALIA
  - Primates
    - Cercopithecidae
      - Colobini
        - *Cercopithecoides alemayehuii* sp. nov.
      - Papionini
        - *Theropithecus oswaldi leakeyi*
    - Hominidae
      - Hominini
        - *Homo erectus*
  - Rodentia
    - Muridae
      - *Arvicanthis*
  - Carnivora
    - Hyaenidae
      - *Crocuta crocuta yangula* ssp. nov
    - Felidae
      - *Panthera* cf. *leo*
      - *Panthera* cf. *pardus*
  - Proboscidea
    - Elephantidae
      - *Elephas recki recki*
  - Perissodactyla
    - Equidae
      - Equini
        - *Equus* sp.
      - Hipparionini
        - *Eurygnathohippus* cf. *cornelianus*
    - Rhinocerotidae
      - Dicerotini
        - *Ceratotherium simum*
        - *Diceros* sp.
  - Artiodactyla
    - Suidae
      - Potamochoerini
        - *Kolpochoerus majus*
        - *Kolpochoerus olduvaiensis*
      - Phacochoerini
        - *Metridiochoerus compactus*
        - *Metridiochoerus* cf. *hopwoodi*
        - *Metridiochoerus modestus*
        - *Phacochoerus* sp.
    - Hippopotamidae
      - *Hippopotamus* cf. *gorgops*
    - Giraffidae
      - Giraffini
        - *Giraffa* sp.
      - Sivatherini
        - *Sivatherium* sp.
    - Bovidae
      - Aepycerotini
        - *Aepyceros* cf. *melampus*
      - Alcelaphini
        - *Connochaetes taurinus*
        - *Damaliscus* sp.
        - *Megalotragus kattwinkeli*
        - *Nitidarcus asfawi*
        - *Numidocapra crassicornis*
        - *Parmularius angusticornis*
      - Antilopini
        - *Gazella* sp.
        - cf. *Antidorcas* sp.
      - Bovini
        - *Pelorovis antiquus*
        - *Pelorovis oldowayensis*
        - *Syncerus* sp.
      - Caprini
        - *Bouria anngettyae*
      - Hippotragini
        - *Hippotragus* cf. *gigas*
        - *Oryx gazella*
      - Reduncini
        - *Kobus* aff. *ancestrocera*
        - *Kobus ellipsiprymnus*
        - *Kobus kob*
      - Tragelaphini
        - *Tragelaphus* cf. *imberbis*
        - *Tragelaphus* cf. *scriptus*
        - *Tragelaphus strepsiceros*
- OSTEICHTHYES
- AVES

EBSCOhost - printed on 10/28/2022 4:53 AM via . All use subject to https://www.ebsco.com/terms-of-use

Overall Format

The chapters that follow present detailed descriptions and interpretations of the hominids and the nonhominid fauna collected in the Daka Member (listed in Table 1.2), provide background information on stratigraphy and methodology necessary to understand these interpretations, and summarize the overall importance of this material in the context of African Pleistocene paleontology. Faunal chapters vary in approach and depth according to several factors. First, some taxa are more common than others and thus present more salient morphology. For example, murids are represented by a single, partially exposed molar row, whereas *Kolpochoerus majus* is represented by several crania. The latter is thus afforded far more descriptive text. Second, the bibliographic history of each taxon varies according to paleogeographic and temporal distribution, abundance, and subsequent differential academic treatment. For example, the broadly distributed genus *Elephas* has a vast, complex literature that must be addressed, whereas the bovid genus *Bouria* is known only from a single species from a single site and is treated in a single publication (Vrba 1997). Third, fossils of some taxa are more informative of previously undocumented morphology. For this reason the *Homo erectus* calvaria and the *Crocuta* cranium are described in detail, while the several *Kobus kob* crania, much more common in the fossil record, are not. Finally, bovids were much more diverse than other families represented in the Daka Member and could easily have filled another volume of this size by themselves. It was decided, for this reason, to abridge the chapter on bovids in the interest of a more timely presentation of the rest of the taxa, including hominids. Unless otherwise noted, all tabular data are in millimeters.

The overarching goal of paleoanthropological work in the Middle Awash study area is the portrayal of a rich, tangible picture of the prehistoric worlds in this unique corner of Africa. The Daka Member is a major window on one of those worlds, and through it we can access elements of an ancient landscape that includes several hominid individuals, a well-documented Acheulean cultural tradition, and a diverse, well-preserved fauna that occupied a tectonically active rift valley. The Daka Member is the most important African site dated to the 1.0 Ma horizon, a time slice on the eve of the Pleistocene ice age cycles that would mold the modern geography of the planet.

EBSCOhost - printed on 10/28/2022 4:53 AM via . All use subject to https://www.ebsco.com/terms-of-use

2

Geology and Geochronology

GIDAY WOLDEGABRIEL, W. HENRY GILBERT, WILLIAM K. HART, PAUL R. RENNE, AND STANLEY H. AMBROSE

The Daka Member of the Plio-Pleistocene Bouri Formation, located within the south-central part of the Middle Awash region of the Afar Rift, encompasses diverse lithologic units dominated by sedimentary deposits with minor interbedded distal tephra markers that crop out along the strike of the NNW-SSE trending and westward-tilted Bouri Fault Block (Figure 2.1). The Bouri Fault Block occurs on the west side of the tectonically controlled Awash River, which flows northward parallel to the Quaternary axial rift zone (de Heinzelin et al. 2000b). The fault block is bounded by Yardi Lake to the southwest and the Awash River floodplain to the south. On the east side, the Awash and the Hatayae Rivers and the floodplain at their confluence bound it. To the north, the fault block extends into structurally complex and densely faulted terrain that consists of altered Pliocene basalt lava flows and tephra overlain by successive deposits of sedimentary units with multiple distal silicic tephra beds. The fault block is expressed as the Bouri Peninsula because it is surrounded on three sides by bodies of water: Yardi Lake to the southwest and the Awash River drainage system to the south, east, and northeast (Figure 2.2).

The Bouri Formation is exposed in the southern two-thirds of the fault block over a distance of approximately 10 km from north to south and about 4 km from east to west. There are no volcanic centers in the immediate vicinity of the Bouri Peninsula. The closest volcanic flow and center is the NE-SW trending Dulu Ali Basaltic Ridge, which represents the southeastern part of the domed early Pliocene Central Awash Complex, located about 10 km to the north of the Bouri Peninsula. Moreover, the Quaternary Ayelu silicic center, which forms the highest topographic feature in the area, is 20 to 30 km to the southeast of the Bouri Peninsula. Except for the floodplain, the area between the dormant Ayelu Volcano and the Awash River directly south of the Bouri Peninsula is covered by partially to strongly welded tuff deposits with minor interbedded fallout tephra. Although the Bouri Peninsula and the surrounding areas were explored in the middle 1970s with additional reconnaissance survey in 1981, detailed geological, paleontological, and archaeological investigations were not initiated until the early 1990s (see Chapter 1).

EBSCOhost - printed on 10/28/2022 4:53 AM via . All use subject to https://www.ebsco.com/terms-of-use

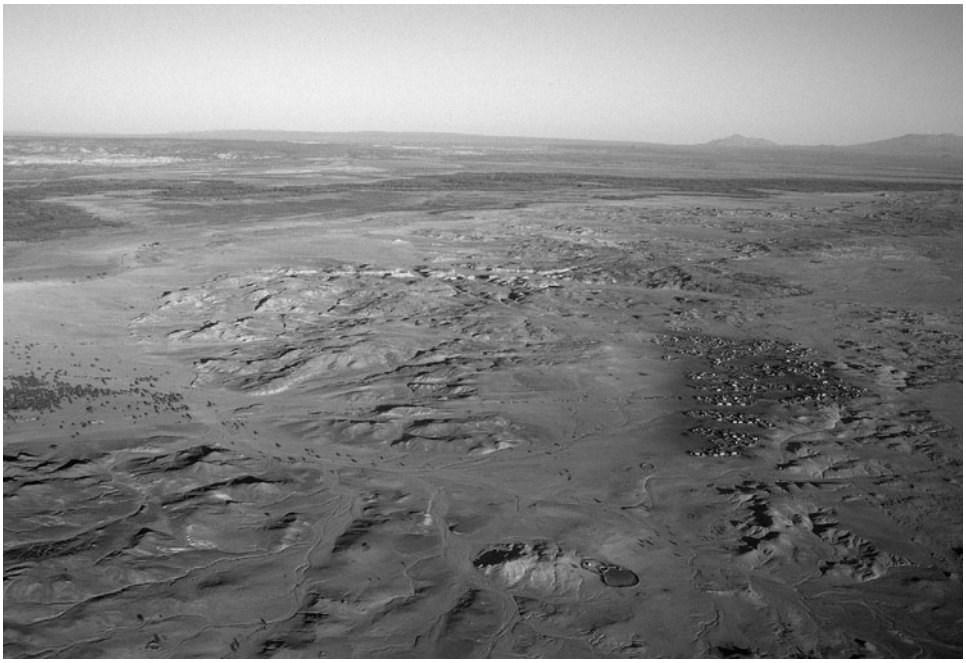

FIGURE 2.1
Low-altitude aerial view to the southeast over Bouri Village (dark area with Afar corrals and houses at right center frame) and the eastern side of the Bouri Peninsula. The light-colored rocks seen between the Awash floodplain to the top of the photo and the village are tuffs of the Hatayae and Dakanihylo Members of the Bouri Formation. Herto Member sediments are exposed west and south of the village. Light-colored sediments east of the Awash river are Pliocene deposits at Asa Barrie. Photograph by Tim White, January 11, 2003.

Landscape Evolution of the Bouri Peninsula

Late Pleistocene tectonic and sedimentological forces, consisting of cross-cutting faults coupled with fluvial, lacustrine, and aeolian processes, primarily shaped the current geomorphic features of the Bouri Peninsula. A major NW-SE trending transverse fault that runs along the northeast margin of the peninsula triggered its uplift and subsequent westward tilting, and resulted in a long, narrow horst (Clark et al. 2003). The transverse fault zone continues southward across the Awash River and runs into the Ayelu-Abidu volcanic complex. This structure is located in close proximity to an inferred intersegment accommodation zone that runs from the west side of the Bouri Fault Block to the Ayelu-Abidu volcanic complex (Hayward and Ebinger 1996). The peninsula is also cut by multiple generations of NE-SW trending, densely spaced normal faults that are closely associated with the Quaternary axial rift zone. Most of these faults are inconspicuous within the Bouri Formation because they cut through poorly to moderately indurated sedimentary deposits that do not preserve the fault scarps. Swarms of rift-oriented faults along the basalt-covered western edge of the axial rift zone directly east of the Bouri Peninsula are truncated by the transverse fault, indicating multiple generations and reactivations of cross-cutting fault episodes that are dominated by the main NE-SW trending Quaternary axial fault zone.

The uplifted Bouri Peninsula blocked the ancestral Awash River to create a large, shallow lake that subsequently breached this fault-generated dam, diminishing the lake to the current, smaller remnant reservoir (Clark et al. 2003). The area currently occupied by the villages of Herto and Bouri was flooded by the ancestral lake, as indicated by the lateral distributions of coarse and rounded beach gravels, well-sorted sandstone, and platy limestone deposits. Once the tectonic dam was breached, the ancestral Awash River reestablished

EBSCOhost - printed on 10/28/2022 4:53 AM via . All use subject to https://www.ebsco.com/terms-of-use

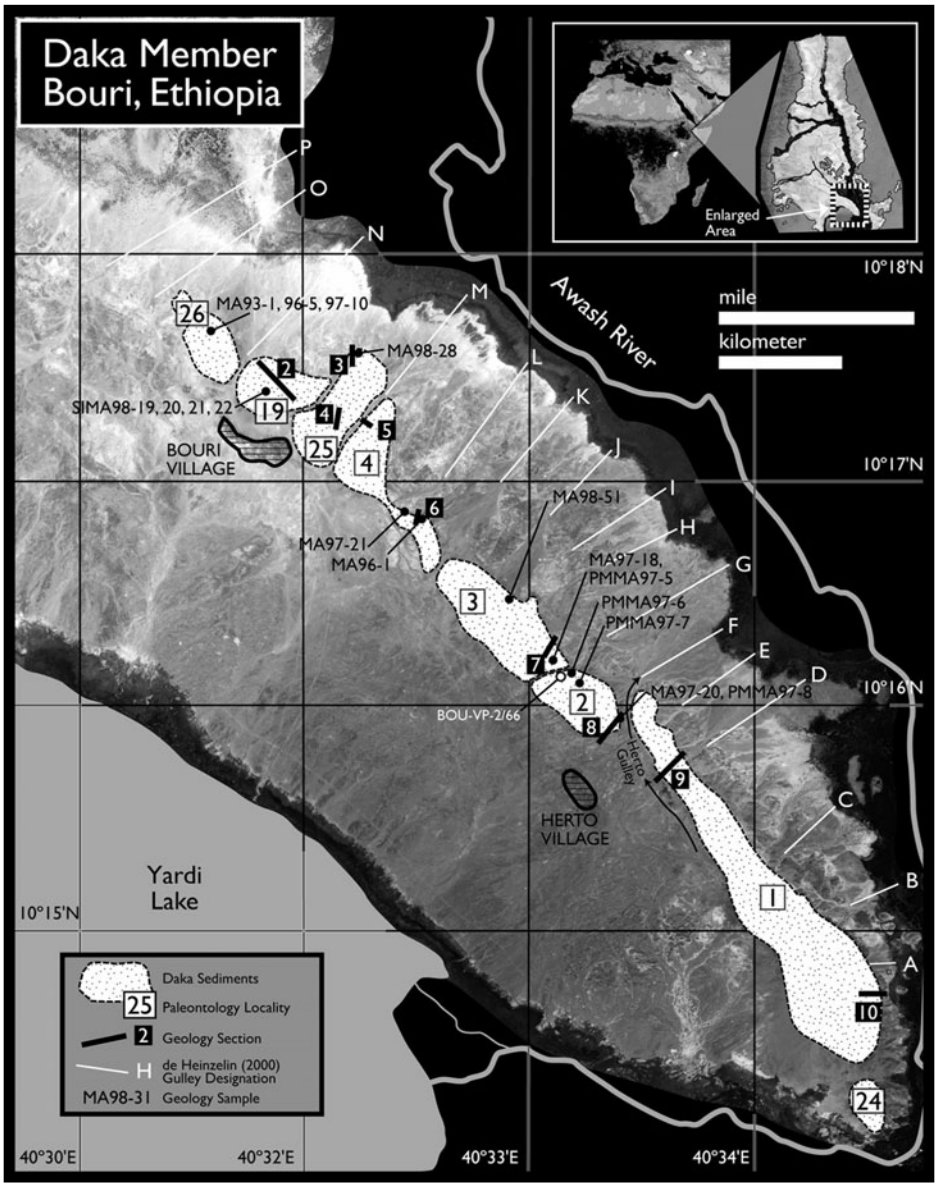

FIGURE 2.2

Map of the Daka Member. Sections are detailed in Figure 2.4.

itself by flowing southward around the southern tip of the Bouri Horst into its old channel. A broad flood plain has developed on the hanging wall of the transverse fault between the modern Awash River and the eastern part of the Bouri Fault Block.

The westward-tilted Bouri Horst gently increases its elevation to the northwest, forming an arched drainage divide between Yardi Lake and the flood plain of the Awash and the Hatayae Rivers (Figure 2.2). The peninsula is extensively dissected by east-trending, densely spaced narrow and broad drainage gullies, resulting in a badlands topography. Most of these gullies are developed on the eastern half of the Bouri Fault Block except for some of the deeper and broader channels that have cut across to the western part of the horst. Differential weathering

EBSCOhost - printed on 10/28/2022 4:53 AM via . All use subject to https://www.ebsco.com/terms-of-use

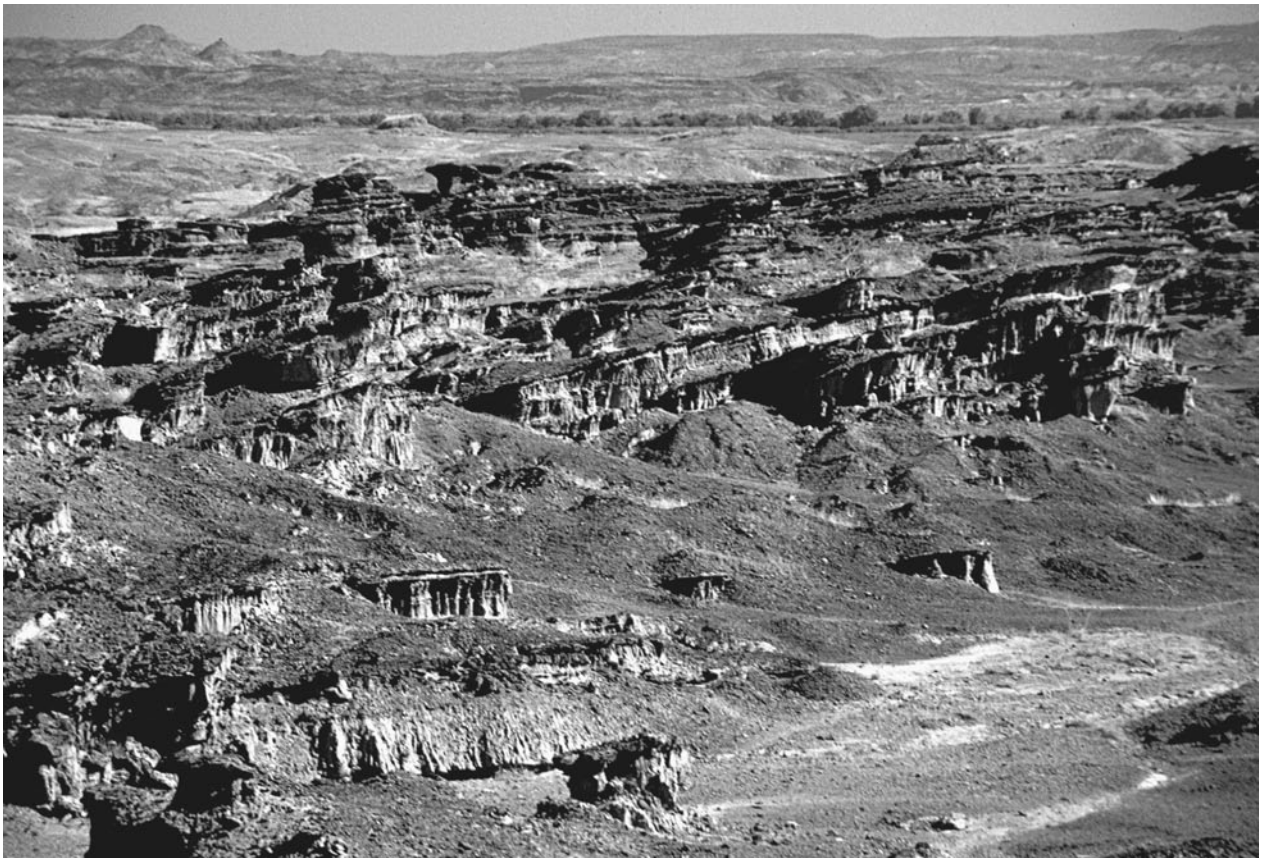

FIGURE 2.3
The "hyaena condominium," part of the "castellated" sandstone facies described by de Heinzelin (2000). Photograph taken December 1997.

and erosion accelerated by faulting with eastward and westward offsets are responsible for the rugged topography commonly observed in the eastern half of the peninsula. Resistant units such as the Wokari Tuff and the "castellated facies" (Figure 2.3), the basal sandstone beds of the Daka Member, and the underlying carbonate and sandstone layers in the upper and middle sections of the Hata Member are responsible for the formation of the rugged terrain. The western half of the Bouri Fault Block gently slopes toward Yardi Lake and exhibits minimal erosional scars. However, erosional landscapes related to fluctuating lake levels represented by multiple ancestral strandlines are apparent along the eastern margin of the shallow lake.

Aeolian processes have also contributed to the landscape evolution at Bouri. This is mostly developed in the western half of the fault block between Bouri Village and the Awash River. The aeolian deposits are unconsolidated and well-sorted, forming poorly defined sand dunes. In some areas between Bouri and Herto Villages, the sand dunes were removed by fluvial and aeolian erosions, creating undulating badlands. The Arari sandstone, which is considered here as being in the upper Herto Member, directly underlies the sand dunes and forms isolated patches of 5–7 m residual mesas above the rolling badlands between the Bouri and Herto Villages. The cross-bedded Arari sandstone contains altered pumice clasts that are about 4 cm in diameter. Unlike the west-dipping units of the Daka and Hata Members, the Arari sandstone is tilted to the east.

EBSCOhost - printed on 10/28/2022 4:53 AM via . All use subject to https://www.ebsco.com/terms-of-use

Another notable but localized geomorphic feature defined by east-west trending ridges of the 1.65 m thick Waidedo Vitric Tuff (WAVT) occurs in the western half of the Bouri Peninsula. Dated to 154 ka (Clark et al. 2003), the WAVT forms the youngest volcanic unit within the Bouri Fault Block. The ridge segments of the WAVT are made up of indurated vitric tuff that probably accumulated along older gullies. These were protected from subsequent erosion as the adjacent land surface eroded away, giving rise to the "inverted channel," or raised ridges of the Bouri Peninsula (de Heinzelin 2000). Unlike the mesa-like Arari Sandstone, the "inverted channel" tuff forms narrow ridge segments (50–100 m long) across the gently west-dipping terrain between Bouri and Herto Villages. Although no stratigraphic contact was observed in the field, the Arari Sandstone probably predates the tuff. Both the localized mesa of the Arari Sandstone and the ridges of the Waidedo Vitric Tuff (WAVT) are erosional remnants of fluvial and volcanic deposits, respectively, that blanketed the Bouri Peninsula before most of these units were removed by erosion since the late Pleistocene (154 ka). Considering the thicknesses of the ridge-forming WAVT (1.65 m) and the thick (≥5 m) Arari Sandstone residual mesa, it appears that intense fluvial and aeolian erosions removed most of the deposits except for those layers that accumulated in low-lying areas and along old stream channels. Despite low topographic elevation, the current Bouri Peninsula landscape is continuing to evolve as a result of erosional forces driven by faulting, coupled with fluvial and wind processes. While fluvial and aeolian erosion appear to be equally important on the west side, the occurrence of numerous gullies on the eastern side suggests fluvial erosion as the dominant process there.

Chronostratigraphy of the Bouri Peninsula

Despite the initial assignment of the Bouri Peninsula lithostratigraphic units to the late Pleistocene Wehaitu Formation (Kalb 1993), detailed stratigraphic and lithologic investigations of the Bouri Fault Block, coupled with geochemical and geochronological analyses of several tuff markers interbedded within the fluvial and lacustrine sediments, revealed that the units were deposited during the Plio-Pleistocene (de Heinzelin et al. 1999, 2000b; Asfaw et al. 2002; Clark et al. 2003). The sedimentary sequences deposited along floodplains, distributary and deltaic channels, and lake margin primarily constitute the uplifted NW-SE trending fault block. The oldest strata are exposed on the eastern half of the block and form a band of well-defined stratigraphic zones that decrease in age from east to west. Most of the sedimentary deposits are fossiliferous and contain abundant aquatic and terrestrial fauna, including three hominid species that were recovered from different stratigraphic levels of the Bouri Formation (Asfaw et al. 1999, 2002; White et al. 2003). Moreover, numerous archaeological sites with artifacts and modified bones (including the oldest known butchered bones) were discovered in the sedimentary succession (de Heinzelin et al. 1999; Clark and Schick 2000).

The stratigraphic sequence of the Bouri Peninsula is assigned to the ~80 m thick Bouri Formation and is subdivided from oldest to youngest into the Hatayae Member (Hata Member), Dakanihylo Member (Daka Member), and Herto Member. Tuff beds, unconformities, and fault boundaries bracket the individual members of the Bouri Formation. On the east and south sides of the peninsula the Bouri Formation disappears under the Awash River floodplain.

EBSCOhost - printed on 10/28/2022 4:53 AM via . All use subject to https://www.ebsco.com/terms-of-use

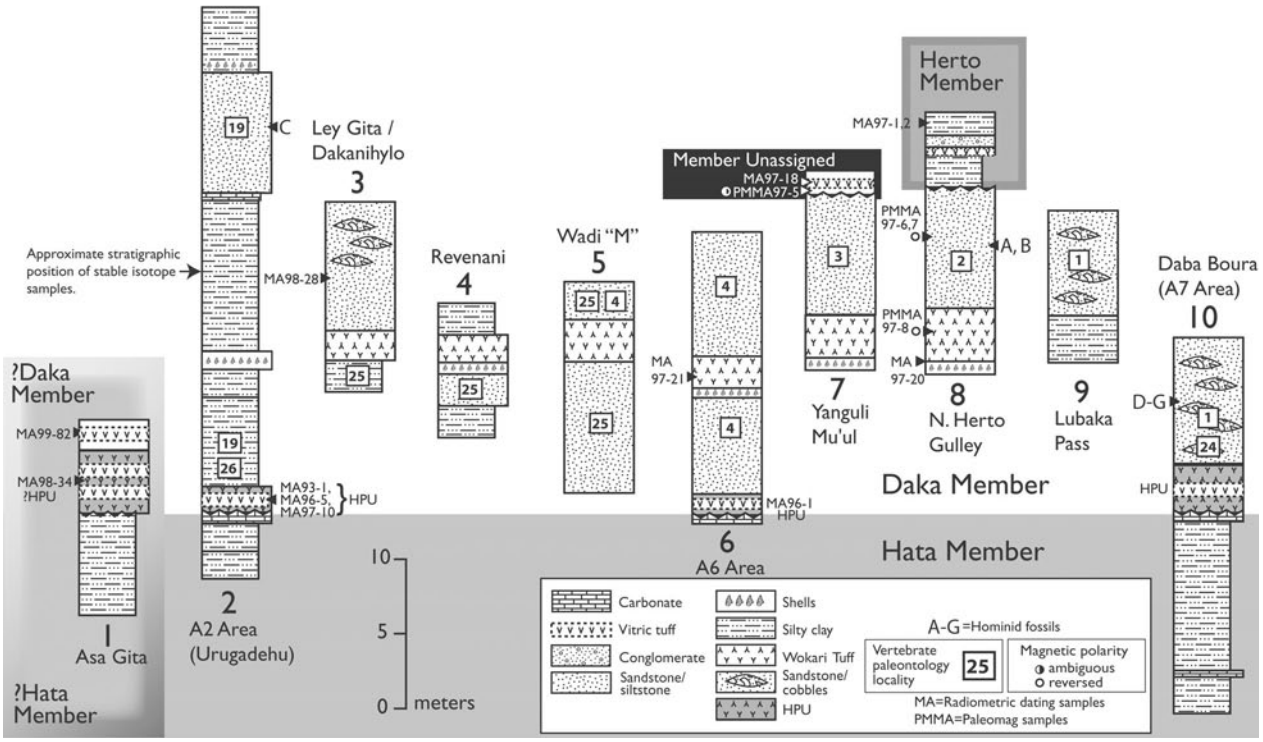

FIGURE 2.4

Daka Member sections. Locations of sections are indicated in Figure 2.2. Hominid specimens: A. BOU-VP-2/66 (calvaria). B. BOU-VP-2/15 (femur). C. BOU-VP-19/63 (femur). D. BOU-VP-1/75 (femur). E. BOU-VP-1/108 (vault fragments). F. BOU-VP-1/109 (tibia). G. BOU-VP-1/114 (vault fragment).

On the west side, the tilted fault block is covered by upper Herto Member sediments and by Yardi Lake (Figure 2.2). The Bouri Formation is poorly defined on the northwest side of the peninsula because of faulting and excessive erosion. Although the focus of this chapter is on the Daka Member volcanic and sedimentary stratigraphic units, a summary of the chronostratigraphic and lithostratigraphic characteristics, geographic distributions, geomorphic features, and the paleontological and archaeological records of the underlying Hata and overlying Herto Members is presented in the subsequent sections.

Hata Member

Most of the Bouri Formation stratigraphic sequence belongs to the 40 m thick Hata Member (de Heinzelin et al. 1999). In ascending stratigraphic order, the Hata Member consists of variegated light yellowish to dark gray silty clays capped by the yellow-green, partially zeolitized, 2.5 Ma Maoleem Vitric Tuff (MOVT). This is followed by several beds of silty clays and paleosols that grade to thin carbonate, calcareous silty clays, and coarse sandstone in the middle part of the section (de Heinzelin et al. 1999; de Heinzelin 2000). The middle section also contains more silty clays with interbedded mudstone and two thin, altered tephra layers separated by about 5 m of silty clays, coarse and poorly sorted sandstone, and limestone. The lower altered tephra is white, 6 cm thick, diatomaceous, and localized, whereas the upper altered ash layer is pinkish with abundant accretionary lapilli. The upper part of the member contains light to dark brown silty clay beds that grade to yellowish and light

EBSCOhost - printed on 10/28/2022 4:53 AM via . All use subject to https://www.ebsco.com/terms-of-use

FIGURE 2.5

Survey team on Daka Member sediments at BOU-VP-2. View is to the south, with Ayelu Volcano dominating the horizon above the horizontal line of trees indicating the course of the modern Awash River. Herto Village is at the top secondary horizon line, and Yardi Lake is to the right of the image. In this area, Daka sediments are not in proximity with either overlying or underlying deposits. Photograph by Tim White, January 4, 2005.

brown coarse sand, platy sandstone, and dark gray mudstone with bivalves. A distinctive, highly resistant cream-colored carbonate layer characterizes the uppermost unit of the Hata Member. The transition to the overlying Daka Member is unconformable and is represented by coarse sandstone with a conglomeratic lens, clasts of limestone, and a gastropod-rich horizon (Figure 2.4).

The cyclothemic Hata Member deposits likely originated along a deltaic margin of a fluctuating paleo-lake (de Heinzelin et al. 1999; de Heinzelin 2000). The Hata Member contains abundant fossils, including hominids assigned to *Australopithecus garhi* (Asfaw et al. 1999). The transition from the Hata Member to the overlying Daka Member is easily distinguishable at several locations along the strike of the Bouri Peninsula. The resistant Hata Member carbonate (~20–30 cm thick) is unconformably capped by the distinctive cross-bedded Hereya Pumice Unit (HPU) of the Daka Member. There is, however, substantial erosional infilling of Daka Member units into paleo-channels cut into Hata sediments during Daka Member deposition, and the distinctive transition described above is not always visible in outcrops (de Heinzelin 2000; Figure 2.5). For this reason, areas containing fossils of questionable stratigraphic provenience were avoided during collection.

EBSCOhost - printed on 10/28/2022 4:53 AM via . All use subject to https://www.ebsco.com/terms-of-use

Herto Member

Herto Member units cover most of the western half of the Bouri Peninsula. The 15–20 m thick Herto Member is generally divided into lower lacustrine and upper fluvial units and represents the youngest stratigraphic sequence of the Bouri Formation. The basal lacustrine units and bentonites mostly crop out close to the drainage divide of the peninsula in close proximity to the underlying Daka Member, whereas the upper mixed fluvial and lacustrine units occur mostly to the west of the Bouri and Herto Villages. The lower Herto Member is older than 240 ka, whereas the base of the upper Herto Member has been dated to ca. 160 ka (Clark et al. 2003). The Herto Member consists of silty clays, lacustrine limestone, beach sand and gravels with bentonite beds and clasts, paleosols, lignite, and cross-bedded pumiceous sandstone (de Heinzelin 2000; Clark et al. 2003). In most sections, the division between the Herto and Daka Members is defined by fault contacts. For example, in the vicinity of BOU-VP-4, buff silt layers of the lower Herto Member make sharp fault contact with the dark gray, carbonate-cemented silts and sandstone of the Daka Member. Lithologic contacts are also noted at other outcrops. In the south, Herto Member gray silts and silty clays from beneath the MA97-1 bentonite (Clark et al. 2003) unconformably crop out on Daka Member sandstone. Along the trail between Herto and Bouri Villages, the basal section of the Herto Member, which consists of fossiliferous mudstone with fish fossils, a thin (~1 cm) pinkish bentonitic layer, and silty clay beds, is exposed above Daka Member sandstone. Except for a platy limestone that is widespread to the south and west of Bouri Village, the upper units of the Herto Member are dominated by yellowish, cross-bedded tuffaceous sandstone with interbedded shelly layers, which underlie the Arari Sandstone. The 154 ka Waidedo Vitric Tuff represents the uppermost unit of the Herto Member and crops out as east-west trending ridge segments in the southern and northern parts of the Bouri Fault Block (Clark et al. 2003). In most places, Herto Member units are blanketed by poorly consolidated sand dunes.

The Herto Member contains both late Acheulean and middle Stone Age artifacts and abundant terrestrial fauna, including hominid remains that have greatly contributed to understanding the origin of *Homo sapiens* (de Heinzelin et al. 2000b; Clark et al. 2003). Aquatic fossil remains from hippos, crocodiles, fish, bivalves, and gastropods are common within the Herto Member units. The Upper Herto Member archaeological assemblages were recovered from erosional surfaces within the hominid-bearing, partially consolidated yellowish sand unit. These are characterized by spatially variable lithological and typological contents (Clark and Schick 2000; Clark et al. 2003). Archaeological evidence from the upper Herto Member suggests hominid activity along a fluctuating lake margin where records of butchery sites of large mammals such as hippos were preserved. Similar occurrences are noted within the lower Herto Member (Clark and Schick 2000; Clark et al. 2003).

Daka Member

The Pleistocene Daka Member is unconformably sandwiched between the underlying Hata Member and the overlying Herto Member of the Bouri Formation and crops out mostly along the strike of the ridgeline that forms the drainage divide of the Bouri Horst (de Heinzelin 2000; Asfaw et al. 2002). It is mostly composed of multiple silt and sandstone layers, unlike the Herto and Hata Member stratigraphic units. Except along fault

EBSCOhost - printed on 10/28/2022 4:53 AM via . All use subject to https://www.ebsco.com/terms-of-use

FIGURE 2.6

View to the southeast over Daka Member sediments in BOU-VP-19. Photograph by Tim White, December 28, 1997.

contacts, the base of the Daka Member is well defined by the cross-bedded Hereya Pumice Unit (HPU), a volcaniclastic deposit that unconformably overlies a carbonate layer at the top of the Hata Member. The HPU is exposed at several sections along the strike of the Bouri Horst from Daba Boura in the south to Urugadehu in the north. The Wokari Tuff, an altered yellowish-gray diatomaceous tuff in the middle part of the Daka Member section, is another diagnostic stratigraphic marker. It is commonly exposed in the central part of the Bouri Fault Block. The top of the Daka Member is mostly represented by pebbly sandstone with pumice cobbles. Lithologic variations are noted along the strike of the Daka Member sedimentary deposits. For example, more alternating silty clay beds occur in the northern part, compared with those sandstone-dominated sections exposed in the central and southern parts of the Daka Member.

Daka Member Sections

Sections along the strike of the Bouri Peninsula were measured and described to document the stratigraphic, paleontological, archaeological, and paleoenvironmental records of the Daka Member (Figures 2.2 and 2.4). The stratigraphic descriptions for each of the Daka Member sections measured along the strike of the Bouri Horst (and numbered

EBSCOhost - printed on 10/28/2022 4:53 AM via . All use subject to https://www.ebsco.com/terms-of-use

sequentially from northwest to southeast) are highlighted in the following paragraphs. The first section, Asa Gita, is not directly correlated with the rest of the unit, and it is presented here only as a possible Daka Member section.

Asa Gita (Section 1)

While not traceable to the Daka Member directly, a cross-bedded pumiceous deposit similar to the HPU deposit was encountered in the Asa Gita area, located at the north of the Bouri Peninsula. The Bouri Peninsula north of this area transitions to the Adlalita Plain. The same transverse fault zone that runs along the eastern part of the Bouri Peninsula bounds the eastern edge of this plain. A fault scarp, which has been modified by erosion, exposes an important section that consists of different sedimentary lithologic units. The section was measured and the various units described. At the top of the section, a poorly consolidated aeolian sand deposit caps a 1.5 m thick vitric tuff (MA99-82). About 30 m of alternating sandstone and silty clay deposits underlie the tuff. Hominid fossil remains were recovered from the basal sandstone. About a kilometer to the north of this section, two mesas rise above the surrounding Hatayae River floodplain.

Both mesas are capped by vitric tuff. However, the eastern mesa contains more than 5 m thick cross-bedded pumiceous sandstone beneath the bedded vitric tuff (MA98-34). The pumiceous deposit is very similar to the HPU, which defines the base of the Daka Member along the middle section of the Bouri Peninsula. Although no fossiliferous silty clays occur above this cross-bedded pumiceous sandstone, most of the section below it consists of pebbly sandstone and dark brown silty clay, in descending stratigraphic order. The cream-colored carbonate layer commonly noted at the top of the Hata Member and beneath the HPU along the strike of the Bouri Peninsula was not observed in the Asa Gita section. If the pumiceous deposit is indeed correlative to the HPU, then the section at Asa Gita represents the northernmost outcrop of the basal section of the Daka Member.

A2 Area (Urugadehu) (Section 2)

The Urugadehu section at the northern end of the Bouri Peninsula represents the thickest (~35 m) stratigraphic sequence of the Daka Member (Figures 2.2 and 2.4). It is located near the HPU-type section and transects the BOU-VP-19 fossiliferous site. At this outcrop, orange silts and light gray silty clays of the Hata Member capped by the diagnostic 20–30 cm thick cream-colored carbonate are clearly visible below the HPU. The interface between the Hata Member carbonate and the HPU at the base of the Daka Member is a characteristic feature at a number of sections exposed along the strike of the Bouri Formation on the peninsula, spanning a distance of approximately 9 km. The thickness of the HPU is variable along the strike and ranges from 0 to 2 m. The matrix-free HPU consists of a partially altered, medium- to coarse-grained, cross-bedded pumice deposit. Different lithologic units, consisting of alternating silty clays, shelly layers, and sandstone, crop out above the HPU. In the Urugadehu area more than 7 m of gray to dark gray silty clay with calcium carbonate concretions, about 4 m of dark brown silty clay, and a meter of abundant bivalves and gastropods crop out above the HPU in ascending stratigraphic order. In the upper half of the section above the shelly horizon there are about 10 m of gray to brown silty clays, which are the lateral equivalent of the unit from which stable

EBSCOhost - printed on 10/28/2022 4:53 AM via . All use subject to https://www.ebsco.com/terms-of-use

carbon isotope samples were taken. Above this there is a thin (20 cm) calcium carbonate horizon and a thick (6–10 m) sandstone with abundant root casts. This sandstone constitutes the upper fossiliferous horizon of the BOU-VP-19 vertebrate paleontology locality. At this section the uppermost unit of the Daka Member is about 5 m thick and consists of gray silty clay with a basal shelly horizon.

In the Urugadehu area, the middle section of the Daka Member is highly fossiliferous. Based on lithological and paleontological records, alternating fluvial and lacustrine deposits accumulated along a fluctuating shallow lake margin. The cross-bedded and matrix-free pumiceous deposit of the HPU was deposited by a fluvial system where the fine matrix was depleted by sedimentation. However, the occurrence of thick silty clays capped by mixed bivalve- and gastropod-rich layers suggests that the dynamics of the depositional environment changed from fluvial to lacustrine, resulting in the accumulation of fine silt and clay materials. The lacustrine deposits are associated with abundant invertebrate fossils. The deposition of thick sandstone with abundant root casts above these suggests that the lake margin had retreated and was replaced by a fluvial depositional landscape.

Ley Gita/Dakanihylo (Section 3)

Daka Member units largely dominate the rugged landscape northeast of Bouri Village. The Ley Gita section occurs within this area and largely consists of at least three major lithologic units: a basal silty clay, the diatomaceous Wokari Tuff, and a thick (~8 m) partially cemented sandstone with pumice cobbles, in ascending stratigraphic order. The crystal-poor Wokari Tuff is totally altered, diatomaceous, and fine grained with abundant bioturbation features. The outcrops in this area have less vertical exposure than those in the Urugadehu section. On the north side of the Ley Gita area, a poorly preserved HPU layer at the base of the section is less pumice-laden compared with the outcrop at the northern end of the Daka Member. Pumice wisps are fainter, and there are no sizable clasts. This HPU can, however, be traced laterally southward from the Urugadehu to the Ley Gita area. Above the HPU is approximately 2 m of silt with basal gastropod and bivalve fossils. The Wokari Tuff is dominant and widespread in the surrounding sections. The majority of the BOU-VP-25 paleontological and archaeological loci occur below and above the diatomaceous Wokari Tuff horizon. The occurrences of silty clays with invertebrate fossil remains, the diatomaceous Wokari Tuff, and the thick sandstone with pumice cobbles suggest that the depositional environment was characterized by alternating fluvial and shallow lacustrine settings, similar to the Urugadehu area to the north.

Revenani (Section 4)

This section is located east of the main Bouri Village cemetery. Unlike the Ley Gita section to the north, the diatomaceous Wokari Tuff occurs at or near the top of the section, with silty clays locally cropping out on top of the altered diatomaceous tuff. Moreover, to the northeast of the Revenani section the Wokari Tuff is capped by alternating sandstone with conglomerate lenses and sand deposits. The basal section of the Wokari Tuff is undulating, typical of predepositional erosional channels. In the Revenani area, multiple faults transect the ridgeline of the Bouri Peninsula. As a result, the

EBSCOhost - printed on 10/28/2022 4:53 AM via . All use subject to https://www.ebsco.com/terms-of-use

faulted blocks are tilted in opposite directions to the west and east. In most cases, the diatomaceous Wokari Tuff dips to the east. The lower half of the section beneath the Wokari Tuff consists of sandstone, a thin gravel layer with mixed bivalve and gastropod fossils, and a basal olive gray silty clay, in descending stratigraphic order. Although the lithologic units and depositional environments are similar to those of the previous sections, fewer paleontological or archaeological localities were established in this area.

Wadi "M" (Section 5)

A broad channel defines Wadi "M," and its floor is covered by recent alluvium. Daka sediments exposed along the sides of the channel were deposited in a lower-energy environment compared with those described from sections in the northern part of the Daka Member. The main section contains 10–15 m of gray-buff sandstone, and the majority of the BOU-VP-25 vertebrate paleontology locality occurs within this unit. The locality is less fossiliferous in its southern part, where the section was measured. In some places a cemented silty sandstone horizon that is approximately 5 m thick represents the uppermost part of the fossiliferous unit. Above this silty sandstone is the diatomaceous Wokari Tuff. Bivalve and gastropod fossils occur at the base of this 3–4 m thick altered tuff unit. Above the tuff, another 2–3 m of sandstone caps the section. A small number of BOU-VP-25 fossils were collected from this unit, and these are in the same stratigraphic position as those at the northern part of the BOU-VP-4 fossil locality.

A6 Area (Section 6)

The section, informally called "A6" for its proximity to the archaeological locality BOU-A6 occurs south of Wadi "M." It is an area where both the HPU and the Wokari Tuff occur in a single section. Jean de Heinzelin, J. Desmond Clark, W. Henry Gilbert, and their team excavated a step trench at the BOU-A6 locality, and the stratigraphic, paleontological, and archaeological records were documented (Clark and Schick 2000; de Heinzelin 2000). The section includes an erosional contact with the underlying Hata Member, which is defined by a diagnostic orange silt and carbonate-cemented claystone. The HPU, which overlies the carbonate at the top of the Hata Member, contains small, concentrated lenses of pure pumice here, as it does in the Ley Gita area. The diatomaceous Wokari Tuff occurs in the same section, but not within the step trench (de Heinzelin 2000: figures 3.17 and 3.18). The small outcrop of stratified yellow Wokari Tuff with bivalve shells at its base occurs about 50 m north of the step trench and clearly overlies the HPU. This outcrop is not described in de Heinzelin (2000), although he was aware of another outcrop of the Wokari Tuff approximately 400 m south of the BOU-A6 locality that could not be directly related to the HPU section (de Heinzelin, personal communication). In the vicinity of this section, abundant BOU-VP-4 fossils occur above and below the Wokari Tuff.

Yanguli Mu'ul (Section 7)

This section is centered within the BOU-VP-3 fossil site and represents the northernmost Daka Member vertebrate paleontology locality that occurs entirely above the Wokari Tuff.

EBSCOhost - printed on 10/28/2022 4:53 AM via . All use subject to https://www.ebsco.com/terms-of-use

The section contains partially exposed shelly sandstone, the Wokari Tuff, a thick (~10 m) sequence of moderately cemented sandstone, and a 2 m thick moderately altered vitric tuff, in ascending stratigraphic order. The thick sandstone contains several variably cemented silt and clay lenses and partially cemented silty sands that have been scoured by erosion to create a unique landscape consisting of pedestals and caverns (Figure 2.3). The locality is part of what de Heinzelin (2000) called the "castellated facies." The area around the BOU-VP-3 vertebrate paleontology locality is informally called the "hyaena condominium," and it is very rich in fossils. The section was measured at the eastern edge of BOU-VP-3 and does not include the transition to Herto Member sediments located to the west of the locality. North of the "hyaena condominium" and the Yanguli Mu'ul section the sequence is capped by an isolated patch of a partially altered yellowish gray vitric tuff (sample MA98-51; see Figure 2.2) that may be correlative to the Waidedo Vitric Tuff. Capping the section is an isolated outcrop of silts and altered tuff that is paraconformable with the underlying Daka sequence. Samples (MA97-18; Figure 2.4) from the tuff were not datable, and paleomagnetic data (PMMA97-5; Figure 2.4) from the silts were ambiguous. The BOU-VP-3 fossils come from the lower, magnetically reversed silts and siltstones of the "castellated facies." Apart from the diatomaceous Wokari Tuff, the remaining Daka Member lithologies in this area were deposited along distributary channels close to a fluctuating lake margin, consistent with the occurrence of mixed bivalve and gastropod layers within the basal sandstone.

Homo erectus calvaria BOU-VP-2/66 was recovered to the south of the Yanguli Mu'ul section (Figure 2.2). The stratigraphic sequence at the hominid site is similar to the Yanguli Mu'ul section and consists of a bivalve-rich basal shelly sandstone, the stratified diatomaceous Wokari Tuff, and a well-sorted coarse- to fine-grained sandstone. West of the hominid site, the thick "castellated" sandstone of the "hyaena condominium" forms the uppermost unit of the Daka Member, and it is unconformably overlain by silty clays of the lower Herto Member (Figure 2.4). The *H. erectus* calvaria was recovered from the middle part of the "castellated" sandstone horizon (Asfaw et al. 2002). Paleomagnetic samples from this stratigraphic horizon yield reversed geomagnetic polarity.

North Herto Gully (Section 8)

This section occurs to the east of the *Homo erectus* site. Identical lithologic units occur at both sections, but the Wokari Tuff is thicker (~2 m) at the North Herto Gully outcrop than in the vicinity of the hominid site. Samples of pumice (MA97-20) were taken from small lenticular occurrences just below the base of the Wokari Tuff in this area. Two NW-SE trending normal faults with about 1.5 m northeast offsets occur along the south-facing section of the Wokari Tuff. Sandstone beds of the "castellated facies" make up most of the section above the Wokari Tuff. This fossil-bearing unit can be traced laterally to the correlative section at the hominid site. To the west of the hominid site, the lithologic units of the Herto Member that consist of dark brown silty clay, bentonite, calcrete, and yellowish pumiceous sandstone, in ascending stratigraphic order, unconformably crop out above the "castellated" sandstone facies of the uppermost unit of the Daka Member (Clark et al. 2003).

EBSCOhost - printed on 10/28/2022 4:53 AM via . All use subject to https://www.ebsco.com/terms-of-use

Lubaka Pass (Section 9)

A narrow ridgeline defines the southwestern edge of the Bouri Horst where it transitions to the Herto Plain. The measured section is located east of Herto Village in the northern part of the BOU-VP-1 locality (Figures 2.2 and 2.4). The Daka Member crops out in a narrow zone at this area, and it is bounded to the east by Hata Member sediments and to the southwest by a shallow, potentially fault-generated gully that is covered by Herto Member sediments. The ridgeline is defined by partially weathered coarse sandstone with isolated remnants of resistant ledges that cap the section. Despite its resemblance to the "castellated facies" sandstone unit of the previous sections to the north, the coarse and sometimes pebbly sandstone at this location represents the basal stratigraphic unit of the Daka Member. The Wokari Tuff is absent from the section. While no HPU outcrop exists at the base of this section, the stratigraphic sequence is otherwise similar to the Daba Boura section located to the south of the Lubaka Pass area (Figures 2.2 and 2.4).

Daba Boura (Section 10)

The Daba Boura section represents the southernmost outcrop of the Daka Member and is located in close proximity to the BOU-G4 Daba Boura promontory of de Heinzelin (2000: figure 3.32). A major part of the Hata Member stratigraphic sequence is exposed here unconformably beneath the lower half of the Daka Member units. A thin (20 cm) cream-colored limestone defines the top part of the Hata Member, and it occurs directly beneath a thick (>3 m) layer of the cross-bedded Hereya Pumice Unit (HPU). About 1.5 m of cross-bedded olive silt and sand beds capped by nodular carbonate occur above the HPU. The BOU-VP-1 and BOU-VP-24 fossil localities occur within partially cemented sandstone above the HPU layer. Thick (~1.5 m) buff-colored sandy layers occur between the carbonate and thick, pebbly sandstone that represents the ridgeline of the uplifted Bouri Horst. The pebbly sandstone at the Daba Boura section is at the same stratigraphic level and along the strike of the ledge-forming pebbly sandstone that crops out along the drainage divide in the vicinity of the Lubaka Pass section (Figures 2.2 and 2.4).

Daka Member Paleontological Localities

All individual fossils collected from the Daka Member have been temporally and spatially placed within the well-defined localities plotted in Figure 2.2. Faunal lists from the different localities are relatively homogeneous, with diversity scaling as a function of the number of specimens collected. Locality BOU-VP-3, which seems to evade this trend somewhat, has a very low diversity of bovid taxa and has only few alcelaphines. *Kobus kob,* however, is disproportionately abundant at the BOU-VP-3 locality, suggesting that this locality's representation might be biased by localized taphonomic phenomena, especially considering that the adjacent BOU-VP-3 is the lateral continuation of the BOU-VP-2 locality (which has typical Daka Member bovid diversity). Faunal

EBSCOhost - printed on 10/28/2022 4:53 AM via . All use subject to https://www.ebsco.com/terms-of-use

representation and correlation of the Daka Member localities are consistent with the stratigraphic evidence.

BOU-VP-1

In 1992, locality BOU-VP-1 was designated upon the discovery of a set of *Elephas recki* molars. The BOU-VP-1 locality was initially surveyed and collected by a team led by Tim White and Berhane Asfaw in December 1992. A total of 92 specimens were collected that year. The following year, Berhane Asfaw led a team that surveyed and collected additional fossils at the site. A total of 21 fossils were collected in 1993. The BOU-VP-1 locality was not surveyed again until 1997. Only 6 specimens were collected in 1997. More intensive collection took place in 1998. During that season, 83 specimens were collected. The latest collection made in 1999 was smaller, and seven specimens were recovered. Locality BOU-VP-1 is rich and will continue to erode and expose new surfaces and fossils with time.

Locality BOU-VP-1, which measures roughly 3 km north to south, is the largest of the Bouri localities. It is stratigraphically well defined, and it occurs directly above the unconformity atop the Hata Member. The upper boundary, a long southern extension of Gully F northeast of the Herto Village, occurs along the locality's western border, and it is most likely defined by a fault. This north-south trending unnamed gully separates BOU-VP-1 from the Herto Member's BOU-VP-16 and BOU-VP-9 localities. All of the fossils from BOU-VP-1 were recovered from a widespread unit of bedded silts with partial carbonate cementation that occurs just above the Hata and Daka Member contact in the north and just above the HPU in the south. The Lubaka Pass and the Daba Boura sections in Figure 2.4 present the BOU-VP-1 locality stratigraphy. The fossil-bearing facies of the BOU-VP-1 locality is very similar in field aspect to those of the BOU-VP-2 and BOU-VP-3 localities. Although Gully F prevents their physical linkage, the localities are probably laterally correlative. There is direct contact between fossil-bearing Hata Member deposits and the Daka Member BOU-VP-1 locality. As the geology was refined, some fossils collected in 1992 and 1993 were redesignated as Hata fossils based on their plotted location. As collection intensified, the 20–50 meter contact zone was avoided to prevent incorrect provenience attribution. One fossil hominid was discovered at BOU-VP-1: a right femur (BOU-VP-1/75) found in 1992 by Tim White. Archaeological localities BOU-A7 and -A18 occur within the boundaries of the BOU-VP-1 locality.

BOU-VP-2

Locality BOU-VP-2 was designated in 1992 and was initially collected by a survey team led by Tim White and Berhane Asfaw. The first fossil collected was a *Theropithecus oswaldi* cranium, found by Berhane Asfaw. A total of 22 specimens were collected at this locality in the first season. In 1993 a small team led by Berhane Asfaw collected briefly at the locality, recovering six more specimens. The site was resurveyed in 1997 and subsequent years (Figure 2.5), and 59 additional specimens have been collected.

Locality BOU-VP-2 fossils were recovered from the "castellated" sandstone. Sections 8 and 9 in Figure 2.4 indicate the BOU-VP-2 stratigraphy. The locality is

EBSCOhost - printed on 10/28/2022 4:53 AM via . All use subject to https://www.ebsco.com/terms-of-use

bounded to the east and northeast by Gully F (de Heinzelin 2000), which separates it from Hata Member localities BOU-VP-8 and BOU-VP-12. Gully F, located northeast of Herto Village, is a faulted basin that is clearly defined along its northern fork, adjacent to the eastern boundary of the BOU-VP-3 locality. At this section, the Hata Member's Maoleem Vitric Tuff outcrops to the east of the fault contact. The Wokari Tuff that is exposed along the southeastern locality boundary forms the basal unit of BOU-VP-2. This unit is traceable for approximately 500 m along the eastern border of the BOU-VP-2 locality. However, the southern boundary of BOU-VP-2 is not well defined. The distinctive "castellated" sandstone unit is poorly exposed in the central southern part, and the contact with the overlying Herto Member is not apparent. This contact is, however, visible along the southern portion of the western border. The "castellated" sandstone deposit is unconformably capped by the distinct Herto Member sequence of gray silt, bentonite, calcrete, and yellow pumiceous sandstone. The northern part of the western boundary of the BOU-VP-2 locality does not make direct contact with the Herto Member. Instead, there is an intervening unit of uncertain provenience between the Herto and Daka Members, designated BOU-VP-21. The BOU-VP-3 locality borders the BOU-VP-2 fossil site on the north side. The drainage divide separating the "hyaena condominium" in the west and the drainage into Gully G to the east define this boundary. Two hominid fossils were recovered at this locality; a shaft of a right femur (BOU-VP-2/15) and calvaria (BOU-VP-2/66) were collected by Gen Suwa and by Henry Gilbert in 1992 and 1997, respectively. Archaeological locality BOU A5 occurs within the boundaries of BOU-VP-2.

BOU-VP-3

Locality BOU-VP-3 was designated in December 1992. The first fossil collected was a bovid cranium found by Alemayehu Asfaw. A group led by Tim White collected a total of 26 specimens in 1992, all from the "hyaena condominium." The area was not surveyed again until 1997.

Locality BOU-VP-3 samples a distinctive outcrop of the "castellated" sandstone (Figure 2.3), the appropriately named "hyaena condominium," as well as a series of fossil-rich low hills to the north. The "hyaena condominium" is a dramatic topographic feature produced by differential weathering and erosion of somewhat cyclic deposits of carbonate-cemented sandstone and unconsolidated silt horizons. These layers have eroded differentially into a bowl-like feature that is dotted with numerous small mesas isolated by winding, deep channels. Many spotted hyaenas *(Crocuta crocuta)* make their dens in the small erosional caves that are common in the area. The stratigraphic sequence is the same as that of the BOU-VP-2 locality. Tracing the fossiliferous outcrop northward appears to indicate a transition up the stratigraphic section, but the unit is represented by a similar facies until it disappears beneath recent alluvium. This area defines the northern boundary of the BOU-VP-3 locality. The eastern locality boundary is defined by NNE-SSW trending fault contact with the Hata Member. On the south, BOU-VP-3 is bounded by the BOU-VP-2 locality that was described above. The western boundary of the locality is effectively the drainage divide of the Bouri

EBSCOhost - printed on 10/28/2022 4:53 AM via . All use subject to https://www.ebsco.com/terms-of-use

Peninsula. Herto Member sediments that are exposed by erosion at some places overlie the Daka Member along the western locality boundary. The archaeological locality BOU-A4 occurs within the BOU-VP-3 locality.

BOU-VP-4

Locality BOU-VP-4 was designated in 1992. The first fossil collected was a *Kolpochoerus majus* RM_3 found by Tadewos Assebework. During the first season, a survey team led by Tim White and Berhane Asfaw collected only five fossils at the BOU-VP-4 site. Single specimens were collected there in 1996 and 1997. In 1998 a team led by Henry Gilbert collected 49 specimens at the locality, and a follow-up survey in 1999 yielded additional fossils.

Locality BOU-VP-4 has one of the most complete geological sections in the Daka Member, although not all of the fossils derive from areas where the sections were measured. The BOU-VP-4 locality is shaped like an hourglass. The Wokari Tuff underlies the northwestern portion of the locality, and the fossils there are in a stratigraphically correlative position to those from the western part of BOU-VP-25. Gully M separates both localities along its northern border (Figure 2.2). Some of the fossils in the eastern part of the northern sector of BOU-VP-4 come from isolated outcrops of Daka Member sediments that are not connected to the rest of the locality. A major fault defines the eastern border of the northern sector of BOU-VP-4. Gully L incises the bottleneck of BOU-VP-4 locality, and fossils to the south of this drainage were recovered from both above and below the Wokari Tuff. The best exposure of the Wokari Tuff and the Hereya Pumice Unit in a single section occurs in this area. Some of the fossils in the southern sector of the BOU-VP-4 locality were collected between these two marker horizons, but most are from above the Wokari Tuff. The southern sector of BOU-VP-4 is bounded to the east by the underlying Hata Member and to the west by fault contact with the Herto Member. On the south side, a minor alluvium-covered gully at the north end of BOU-VP-3 locality bounds the BOU-VP-4 locality. No hominid fossils have been found at the BOU-VP-4 locality. Archaeological locality BOU-A6 occurs within the BOU-VP-4 locality.

BOU-VP-19

Locality BOU-VP-19 was designated in 1997 (Figure 2.6). The first fossil collected was a bovid cranial fragment, found by Henry Gilbert. In 1997, 30 specimens were collected at BOU-VP-19, whereas in 1998 a total of 33 specimens were recovered from this locality. The VP-19 locality predominantly yielded fossils from two horizons in a relatively deep section of diverse lithology above the HPU. The first zone is a shell-rich horizon just about 1 m above the HPU. The second is a sandy-silt with iron-stained calcrete about 7–10 m above the HPU. The locality is bounded to the west by debris middens and aeolian deposits around Bouri Village, to the south by Ley Gita (water trail), and to the east by the distinctive HPU/Hata contact. A hominid left femur (BOU-VP-19/63) was found by Tim White at this locality. Archaeological localities BOU-A2 and -A3 occur within BOU-VP-19.

EBSCOhost - printed on 10/28/2022 4:53 AM via . All use subject to https://www.ebsco.com/terms-of-use

BOU-VP-24

Locality BOU-VP-24 was designated in 1998. The first fossil collected was a *Kobus kob* cranium, found by Ounda Heis. Two specimens were recovered from this locality. The BOU-VP-24 locality is bounded to the south by the Awash floodplain gallery forest, to the west by Holocene alluvium, and to the north by an unnamed large gully. Although the BOU-VP-24 locality represents a portion of the Daka Member, de Heinzelin (2000) incorrectly assigned it to the Hata Member. No hominid fossils were recovered at this locality, nor were any archaeological localities established.

BOU-VP-25

Locality BOU-VP-25 was designated in 1998. Hola Kadir collected the first fossil here. In 1998, the survey team collected 46 specimens. A total of 42 additional specimens were collected at this locality in 1999. The fossils from locality BOU-VP-25 were recovered from two stratigraphic intervals (see Figure 2.4). The lower unit occurs between pumiceous sand, a lateral variant of the HPU, and the overlying Wokari Vitric Tuff. It is likely the stratigraphic equivalent of the lower fossiliferous unit of BOU-VP-19. The second fossil-bearing horizon is above the Wokari Tuff in similar stratigraphic position to the fossil-bearing strata in the northern sector of BOU-VP-4. BOU-VP-25 is bounded to the north by the Ley Gita area, to the east by the Awash floodplain, to the south by Gully M, and to the west by the debris midden pile around Bouri Village. No hominid fossils have been found in this locality. Archaeological localities BOU-A1, -A14, -A15, and -A17 are located within the borders of the BOU-VP-25 locality.

BOU-VP-26

Locality BOU-VP-26 was designated in 1998. The first fossil collected was a *Kolpochoerus* molar. In 1998, 26 specimens were collected at the BOU-VP-26 locality. The BOU-VP-26 locality encompasses a stratigraphic horizon of the Daka Member just above the HPU type section. It is bounded to the north by a prominent normal fault with a north-south strike, to the east by the HPU and underlying Hata Member contact, and to the south by Gully N. Its western boundary is a possibly conformable contact with the Herto Member. Unfortunately, the landscape is nearly flat, and it is largely masked by recent aeolian deposits and disturbed by bioturbation. No archaeological localities have been established within the BOU-VP-26 locality.

$^{40}Ar/^{39}Ar$ and Paleomagnetic Results

An array of $^{40}Ar/^{39}Ar$ dates on single feldspar crystals separated from HPU pumices yielded an average age of 1.042 ± 0.009 Ma (Renne 2000). The sample location for the dated HPU in BOU-VP-26 (MA93-1) is presented in Figure 2.2**.** The crystal-poor diatomaceous Wokari Tuff was not dated. However, 10 pumice clasts 5–10 cm in diameter taken from a tuffaceous sand above the Wokari Tuff (sample MA98-28) in the area close to the Ley Gita section were dated to 0.966 ± 0.006 Ma (see Table 2.1).

Sanidine crystals separated from the pumice clasts were irradiated with the 28.02 Ma Fish Canyon sanidine standard (Renne et al. 1998) and analyzed by laser fusion of 6–11

EBSCOhost - printed on 10/28/2022 4:53 AM via . All use subject to https://www.ebsco.com/terms-of-use

individual crystals using methods and facilities described previously (Renne et al. 1999). Analytical data are shown in Table 2.1. The weighted mean ages for individual pumice clasts range from 0.949 ± 0.007 to 1.002 ± 0.020 Ma (1 σ uncertainties) and are mutually indistinguishable at 95 percent confidence. The weighted mean age of all 10 pumice clasts is 0.966 ± 0.006 Ma, which we infer to date a single eruption, essentially synchronous with deposition of the tuffaceous, pumice-bearing sand.

This new result effectively brackets the Wokari Tuff to between 1.043 ± 0.009 and 0.966 ± 0.006 Ma, providing broad chronological control for the Daka Member. Paleomagnetic samples have been analyzed from throughout the unit (see Figure 2.4). All Daka Member samples (PMMA97-6, 7, and 8) have reverse polarity, consistent with their deposition prior to the Bruhnes-Matuyama geomagnetic polarity reversal at ca. 0.790 Ma. Because the deposits are all younger than 1.043 ± 0.009 Ma and all reversed, it can be deduced that they postdate the Jaramillo subchron.

Paleosol Stable Isotope Analysis

Paleosol (fossil soil) geomorphology and stable isotope analysis can provide useful, often mutually reinforcing, lines of evidence for environmental reconstruction. A step trench excavated in 1998 at Urugadehu BOU-VP-19 exposed a 3.5 m sequence of silty clays with a prominent paleosol. Figure 2.7 shows the stratigraphic section and plots of the carbon isotopic composition of disseminated organic carbon and nodular carbonate carbon and oxygen. Results of isotopic analyses are listed in Table 2.2. Three stratigraphic units, numbered from the top, were recognized in the field. Unit 1 (>108 cm thick) is a very dark brown/gray clay loam with vertical cracks creating well-defined small/medium columnar peds. The top of this unit is the modern eroded land surface. Carbonate nodules up to 25 cm in diameter are concentrated at the undulating base of this vertic horizon. The sedimentary and nodule matrix includes a small amount of poorly sorted coarse sand–sized mineral grains (0.2–2.0 mm), including subrounded basaltic lava, subangular black and gray glassy fragments and clear crystals, and rounded yellow and gray tuffaceous grains, possibly derived from the HPU tuff or the Wokari Tuff. The carbonate nodule matrix is micritic (fine-grained, noncrystalline) under 15 × magnification. Unit 2 (213 cm thick) is a brown subangular medium block silty clay with disseminated carbonate and small (1–10 cm) irregular/rounded micritic carbonate nodules. This is interpreted as the paleosol B horizon with illuvial (translocated) carbonate (Btk). Unit 3 (>30 cm thick, base not exposed) is a brown subangular to angular medium blocky clay with less disseminated carbonate, and micritic carbonate nodules up to 10 cm in diameter. This is interpreted as the Bk/C horizon of the paleosol. Sand grains were not observed during low magnification microscopic examination of the sedimentary matrix and carbonate nodules of units 2 and 3. The carbonate content of sedimentary matrix of unit 1 was not quantitatively determined, but it reacts weakly with 10 percent HCl. The acid-insoluble matrix content of unit 2 is lower than that of unit 3 (Table 2.2), which indicates more disseminated carbonate in unit 2 than in unit 3. The apparently higher silt content of unit 2 is likely a function of its higher carbonate content. The sedimentary matrix microfabric of these units comprises small (1–4 mm) dark brown rounded clay pellets surrounded by lighter brown

EBSCOhost - printed on 10/28/2022 4:53 AM via . All use subject to https://www.ebsco.com/terms-of-use

TABLE 2.1 Argon Isotopic Data for MA98-28

	^{40}Ar (nA)	$\pm s$ (nA)	^{39}Ar (nA)	$\pm s$ (nA)	^{38}Ar (nA)	$\pm s$ (nA)	^{37}Ar (nA)
MA98-28A							
32410-01	0.1537	0.0003	0.0241	0.0001	0.00030	0.00001	0.0016
32410-02	0.2024	0.0005	0.0448	0.0001	0.00055	0.00001	0.0020
32410-03	0.2422	0.0005	0.0564	0.0001	0.00069	0.00001	0.0018
32410-04	0.1165	0.0003	0.0239	0.0001	0.00030	0.00001	0.0006
32410-05	0.3391	0.0005	0.0569	0.0001	0.00076	0.00001	0.0041
32410-06	0.2800	0.0006	0.0586	0.0001	0.00075	0.00001	0.0025
Wtd. Mean $\pm$ 1 s							
MA98-28B							
32411-01	0.5302	0.0008	0.0683	0.0001	0.00094	0.00002	0.0030
32411-02	0.2090	0.0005	0.0431	0.0001	0.00054	0.00001	0.0019
32411-03	0.2755	0.0005	0.0293	0.0001	0.00046	0.00001	0.0008
32411-04	0.3105	0.0005	0.0663	0.0001	0.00085	0.00001	0.0030
32411-05	0.1485	0.0003	0.0239	0.0001	0.00031	0.00001	0.0009
32411-06	0.1772	0.0004	0.0397	0.0001	0.00049	0.00001	0.0014
Wtd. Mean $\pm$ 1 s							
MA98-28C							
32412-01	0.1201	0.0002	0.0275	0.0000	0.00032	0.00001	0.0005
32412-02	0.5992	0.0007	0.0375	0.0000	0.00075	0.00001	0.0014
32412-03	0.1451	0.0003	0.0307	0.0001	0.00039	0.00001	0.0016
32412-04	0.1483	0.0003	0.0339	0.0001	0.00040	0.00001	0.0014
32412-05	0.1777	0.0004	0.0413	0.0001	0.00053	0.00001	0.0020
32412-06	0.1915	0.0006	0.0462	0.0001	0.00057	0.00001	0.0017
32412-07	0.1338	0.0002	0.0289	0.0001	0.00037	0.00001	0.0012
32412-08	0.4749	0.0005	0.0482	0.0001	0.00079	0.00001	0.0024
32412-09	0.2573	0.0005	0.0599	0.0001	0.00075	0.00001	0.0026
32412-10	0.2117	0.0006	0.0470	0.0001	0.00059	0.00001	0.0020
32412-11	0.2993	0.0004	0.0492	0.0001	0.00068	0.00001	0.0015
Wtd. Mean $\pm$ 1 s							
MA98-28D							
32414-01	0.3732	0.0031	0.0867	0.0002	0.00105	0.00002	0.0030
32414-02	0.1989	0.0031	0.0296	0.0001	0.00042	0.00001	0.0008
32414-03	0.3579	0.0031	0.0808	0.0002	0.00099	0.00001	0.0036
32414-04	0.4850	0.0031	0.0552	0.0002	0.00080	0.00002	0.0038
32414-05	0.1882	0.0031	0.0411	0.0002	0.00051	0.00001	0.0017
32414-06	0.2228	0.0031	0.0506	0.0001	0.00063	0.00001	0.0020
Wtd. Mean $\pm$ 1 s							

EBSCOhost - printed on 10/28/2022 4:53 AM via . All use subject to https://www.ebsco.com/terms-of-use

± s (nA)	^{36}Ar (nA)	± s (nA)	$^{40}Ar^*/^{39}ArK$	± s	$\%^{40}Ar^*$	Age (Ma)	± s (Ma)
0.0001	0.00019	0.00001	4.00551	0.15237	62.8	0.972	0.037
0.0001	0.00007	0.00001	4.06100	0.07839	89.9	0.986	0.019
0.0001	0.00007	0.00001	3.91606	0.06586	91.1	0.951	0.016
0.0001	0.00007	0.00001	4.04506	0.14249	83.1	0.982	0.035
0.0001	0.00040	0.00002	3.87335	0.08369	65.0	0.940	0.020
0.0001	0.00017	0.00001	3.93376	0.06700	82.4	0.955	0.016
						0.960	0.008
0.0001	0.00086	0.00002	4.04360	0.08259	52.1	0.982	0.020
0.0001	0.00012	0.00001	3.99807	0.09131	82.5	0.971	0.022
0.0001	0.00055	0.00001	3.82648	0.15710	40.7	0.929	0.038
0.0001	0.00017	0.00001	3.91726	0.05697	83.7	0.951	0.014
0.0001	0.00017	0.00001	4.05693	0.16257	65.3	0.985	0.039
0.0001	0.00005	0.00001	4.06104	0.09802	91.1	0.986	0.024
						0.965	0.009
0.0001	0.00002	0.00002	4.16939	0.16814	95.5	1.012	0.041
0.0001	0.00153	0.00001	3.90840	0.12012	24.4	0.949	0.029
0.0001	0.00007	0.00001	4.03993	0.11507	85.6	0.981	0.028
0.0001	0.00007	0.00001	3.78457	0.11044	86.6	0.919	0.027
0.0001	0.00006	0.00001	3.88628	0.08120	90.3	0.943	0.020
0.0001	0.00002	0.00001	4.00634	0.07684	96.6	0.973	0.019
0.0001	0.00007	0.00001	3.88573	0.11282	83.9	0.943	0.027
0.0001	0.00098	0.00002	3.83853	0.11171	38.9	0.932	0.027
0.0001	0.00008	0.00001	3.92110	0.05621	91.3	0.952	0.014
0.0001	0.00010	0.00001	3.87265	0.07722	86.0	0.940	0.019
0.0001	0.00038	0.00001	3.83042	0.08025	62.9	0.930	0.019
						0.949	0.007
0.0003	0.00010	0.00002	3.97780	0.08653	92.4	0.966	0.021
0.0003	0.00026	0.00002	4.11148	0.25246	61.1	0.998	0.061
0.0003	0.00013	0.00002	3.97437	0.09284	89.7	0.965	0.023
0.0003	0.00087	0.00002	4.11228	0.14774	46.8	0.998	0.036
0.0004	0.00007	0.00002	4.07881	0.17466	89.1	0.990	0.042
0.0003	0.00009	0.00002	3.86818	0.14197	87.9	0.939	0.034
						0.969	0.012

EBSCOhost - printed on 10/28/2022 4:53 AM via . All use subject to https://www.ebsco.com/terms-of-use

TABLE 2.1 *(continued)*

	^{40}Ar (nA)	$\pm s$ (nA)	^{39}Ar (nA)	$\pm s$ (nA)	^{38}Ar (nA)	$\pm s$ (nA)	^{37}Ar (nA)
MA98-28E							
32415-01	0.1301	0.0031	0.0239	0.0001	0.00029	0.00001	0.0005
32415-02	0.1144	0.0031	0.0255	0.0001	0.00032	0.00001	0.0005
32415-03	0.1549	0.0031	0.0282	0.0001	0.00036	0.00001	0.0015
32415-04	0.2057	0.0031	0.0437	0.0002	0.00056	0.00001	0.0019
32415-05	0.1176	0.0031	0.0285	0.0001	0.00035	0.00001	0.0011
32415-06	1.0079	0.0032	0.0493	0.0001	0.00111	0.00002	0.0019
Wtd. Mean $\pm$ 1 s							
MA98-28F							
32416-01	0.2607	0.0031	0.0536	0.0002	0.00067	0.00001	0.0026
32416-02	0.0728	0.0031	0.0156	0.0001	0.00019	0.00001	0.0002
32416-03	0.1264	0.0031	0.0282	0.0001	0.00036	0.00001	0.0006
32416-04	0.1244	0.0031	0.0275	0.0001	0.00033	0.00001	0.0011
32416-05	0.1229	0.0031	0.0274	0.0001	0.00035	0.00001	0.0008
32416-06	0.5298	0.0032	0.0536	0.0002	0.00085	0.00002	0.0022
Wtd. Mean $\pm$ 1 s							
MA98-28G							
32418-01	0.2347	0.0031	0.0526	0.0001	0.00068	0.00001	0.0014
32418-02	0.2954	0.0031	0.0498	0.0002	0.00069	0.00002	0.0015
32418-03	0.1571	0.0031	0.0365	0.0001	0.00044	0.00001	0.0009
32418-04	0.1483	0.0031	0.0332	0.0001	0.00042	0.00001	0.0019
32418-05	0.2789	0.0031	0.0643	0.0002	0.00079	0.00001	0.0027
32418-06	0.1606	0.0031	0.0374	0.0002	0.00045	0.00001	0.0011
Wtd. Mean $\pm$ 1 s							
MA98-28H							
32419-01	0.2728	0.0031	0.0618	0.0002	0.00079	0.00001	0.0026
32419-02	0.2978	0.0031	0.0648	0.0002	0.00082	0.00002	0.0018
32419-03	0.1963	0.0031	0.0450	0.0002	0.00057	0.00001	0.0022
32419-04	0.2034	0.0031	0.0346	0.0001	0.00046	0.00001	0.0012
32419-05	0.2181	0.0031	0.0394	0.0001	0.00053	0.00001	0.0017
32419-06	0.3041	0.0031	0.0726	0.0002	0.00088	0.00002	0.0031
Wtd. Mean $\pm$ 1 s							
MA98-28I							
32420-01	0.2432	0.0031	0.0421	0.0001	0.00056	0.00001	0.0014
32420-02	0.4392	0.0032	0.0823	0.0002	0.00103	0.00002	0.0031
32420-03	0.1070	0.0031	0.0238	0.0001	0.00028	0.00001	0.0002
32420-04	0.3770	0.0031	0.0335	0.0001	0.00057	0.00001	0.0021

EBSCOhost - printed on 10/28/2022 4:53 AM via . All use subject to https://www.ebsco.com/terms-of-use

± s (nA)	^{36}Ar (nA)	± s (nA)	$^{40}Ar^*/^{39}ArK$	± s	$\%^{40}Ar^*$	Age (Ma)	± s (Ma)
0.0003	0.00012	0.00002	3.97824	0.29263	73.1	0.966	0.071
0.0003	0.00004	0.00002	4.03447	0.28010	90.0	0.979	0.068
0.0003	0.00014	0.00002	4.04305	0.25424	73.5	0.982	0.062
0.0003	0.00010	0.00002	4.02721	0.15921	85.7	0.978	0.039
0.0003	0.00001	0.00002	4.05321	0.24469	98.3	0.984	0.059
0.0003	0.00280	0.00003	3.65441	0.21029	17.9	0.887	0.051
						0.961	0.022
0.0003	0.00015	0.00002	4.06787	0.13183	83.6	0.988	0.032
0.0003	0.00004	0.00002	3.92784	0.44527	84.4	0.954	0.108
0.0003	0.00002	0.00002	4.22740	0.24970	94.2	1.026	0.061
0.0003	0.00006	0.00002	3.89014	0.25109	85.9	0.944	0.061
0.0003	0.00002	0.00002	4.30245	0.25380	95.8	1.044	0.062
0.0003	0.00103	0.00002	4.22235	0.15353	42.7	1.025	0.037
						1.002	0.020
0.0003	0.00007	0.00002	4.08049	0.13353	91.5	0.991	0.032
0.0003	0.00036	0.00002	3.81401	0.14800	64.3	0.926	0.036
0.0003	0.00003	0.00002	4.08862	0.19277	95.1	0.993	0.047
0.0003	0.00003	0.00002	4.23176	0.21046	94.8	1.027	0.051
0.0003	0.00006	0.00002	4.04426	0.11006	93.3	0.982	0.027
0.0003	0.00002	0.00002	4.11213	0.18776	95.6	0.998	0.046
						0.981	0.015
0.0003	0.00005	0.00002	4.18843	0.11367	95.0	1.017	0.028
0.0004	0.00010	0.00002	4.15971	0.11344	90.5	1.010	0.028
0.0004	0.00005	0.00002	4.05198	0.15696	93.0	0.984	0.038
0.0003	0.00021	0.00002	4.05396	0.20775	69.0	0.984	0.050
0.0003	0.00017	0.00002	4.22614	0.17957	76.4	1.026	0.044
0.0004	0.00005	0.00002	3.99783	0.09927	95.5	0.971	0.024
						0.997	0.013
0.0003	0.00021	0.00002	4.29058	0.17138	74.3	1.042	0.042
0.0004	0.00036	0.00002	4.05091	0.09210	75.9	0.983	0.022
0.0003	0.00004	0.00002	4.01693	0.29524	89.2	0.975	0.072
0.0003	0.00080	0.00002	4.22974	0.23251	37.5	1.027	0.056

EBSCOhost - printed on 10/28/2022 4:53 AM via . All use subject to https://www.ebsco.com/terms-of-use

TABLE 2.1 *(continued)*

	^{40}Ar (nA)	± s (nA)	^{39}Ar (nA)	± s (nA)	^{38}Ar (nA)	± s (nA)	^{37}Ar (nA)
32420-05	0.1606	0.0031	0.0345	0.0001	0.00043	0.00001	0.0020
32420-06	0.1351	0.0031	0.0295	0.0001	0.00036	0.00001	0.0009
Wtd. Mean ± 1 s							
MA98-28J							
32421-01	0.1918	0.0031	0.0431	0.0001	0.00053	0.00001	0.0019
32421-02	0.2009	0.0031	0.0395	0.0002	0.00050	0.00001	0.0013
32421-03	0.0865	0.0031	0.0205	0.0001	0.00025	0.00001	0.0004
32421-04	0.0979	0.0031	0.0225	0.0001	0.00028	0.00001	0.0006
32421-05	0.2210	0.0031	0.0400	0.0001	0.00053	0.00001	0.0016
32421-06	0.1757	0.0031	0.0260	0.0001	0.00037	0.00001	0.0006
Wtd. Mean ± 1 s							

NOTE: Relative abundances of argon isotopes are given in nanoAmperes (nA) of amplified ion beam current, corrected for background, mass discrimination, and radioactive decay. Mass spectrometer sensitivity is approximately 4×10^{-16} moles/nA. Mass discrimination, based on automated analysis of air pipettes and applied as a power law correction, is 1.0041 ± 0.0016 per atomic mass unit for samples MA98-28A–C, and 1.0048 ± 0.0014 for samples MA98-28D–J. Neutron fluence was monitored by Fish Canyon sanidine (28.02 Ma) with a J-value of $(1.346 \pm 0.001) \times 10^{-4}$ applicable to all samples. Age calculations employ nuclear interference corrections reported by Renne et al. (1999).

void and crack-filling clayey silt matrix enriched with disseminated carbonate. The original parent material of units 2 and 3 was probably very fine silty clay lacking detrital or disseminated carbonate. Primary sedimentary bedding structures and root marks have been obliterated by expansion and contraction of the clays with seasonal wetting and drying, so it is impossible to determine whether the parent material was fine-grained shallow water lacustrine, paludal, or distal floodplain overbank sediments. The thick, well-developed A horizon (unit 1) of this soil reflects a depositional hiatus or sharp drop in sedimentation rate, permitting in-situ subaerial weathering and soil formation.

The closest modern analog for this type of soil profile is a vertisol, which is a soil type characteristic of semiarid to mesic grasslands of volcanic regions. Vertisols are typically dark gray brown to black, with a deep A horizon with strong columnar structure, and they often contain substantial amounts of disseminated carbonate and carbonate nodules (Driese et al. 2000; Retallack 2001).

Disseminated organic carbon was prepared for isotopic analysis by treating the ground, sieved fine fraction (<0.25 mm mesh) of the sedimentary matrix of units 2 and 3, and a carbonate nodule from unit 1 with 1 *M* HCl, in order to remove carbonates. Acid-insoluble residue samples weighing ~900 mg were loaded in Vycor glass tubes with 1 g granular CuO, 1 g granular Cu, and 50 mg Ag foil, and pumped under high vacuum at 55°C for 20 hours to remove adsorbed water. Sealed tubes were combusted for 3 hours at 900°C. CO_2 was purified by cryogenic distillation, collected in sealed Pyrex tubes, and analyzed on

EBSCOhost - printed on 10/28/2022 4:53 AM via . All use subject to https://www.ebsco.com/terms-of-use

± s (nA)	^{36}Ar (nA)	± s (nA)	$^{40}Ar^*/^{39}ArK$	± s	$\%^{40}Ar^*$	Age (Ma)	± s (Ma)
0.0003	0.00008	0.00002	3.98625	0.19921	85.7	0.968	0.048
0.0004	0.00005	0.00002	4.07553	0.23648	89.0	0.989	0.057
						0.994	0.016
0.0004	0.00005	0.00002	4.11593	0.16199	92.6	0.999	0.039
0.0004	0.00015	0.00002	3.99189	0.17918	78.5	0.969	0.043
0.0003	0.00000	0.00002	4.23525	0.33632	100.3	1.028	0.082
0.0003	0.00004	0.00002	3.75669	0.30599	86.5	0.912	0.074
0.0004	0.00021	0.00002	4.01349	0.18052	72.6	0.974	0.044
0.0003	0.00022	0.00002	4.28356	0.27692	63.4	1.040	0.067
						0.985	0.021

a Finnegan MAT 252 isotope ratio mass spectrometer. Carbonate was prepared from the cores of freshly fractured nodules with a diamond burr minidrill. Samples were heated to 380–400°C under vacuum for 3 hours to reduce organic matter and remove adsorbed water and weakly bound clay hydroxyls. CO_2 for carbon and oxygen isotope analysis was generated by reaction with 100 percent phosphoric acid at 70°C in a Kiel III automated carbonate reaction–cryogenic distillation device interfaced with the MAT 252. Isotope ratios are expressed using the δ notation as permil (‰, or parts per thousand) difference from the PDB standard. Replicate pairs of 18 different pedogenic carbonate samples collected during the 1998 field season produce a mean difference of 0.1 ± 0.09‰ in $\delta^{13}C$ and 0.16 ± 0.14‰ in $\delta^{18}O$ values.

Cerling et al. (2003) and Quade et al. (2004) provide detailed explanations of the foundations of environmental reconstruction with pedogenic carbonate carbon and oxygen isotope ratios in eastern Africa. Plants with the C_3 photosynthetic pathway comprise trees, shrubs and most leafy (dicotyledous) plants, as well as grasses from cool and/or shaded habitats. They have a mean $\delta^{13}C$ value of −26.5‰. C_4 plants are mainly tropical grasses in open habitats and have a mean $\delta^{13}C$ value of −12.5‰. The difference between C_3 and C_4 end-members is thus 14‰. Soil organic matter $\delta^{13}C$ values are enriched during decomposition by 1–2‰ over standing plant biomass (Nadelhoffer and Fry 1988); pedogenic carbonate $\delta^{13}C$ values are enriched by 13.5–17‰ (Cerling 1984; Quade and Levin, in review). In this study we assume an average enrichment of 1.5‰ for soil organic

EBSCOhost - printed on 10/28/2022 4:53 AM via . All use subject to https://www.ebsco.com/terms-of-use

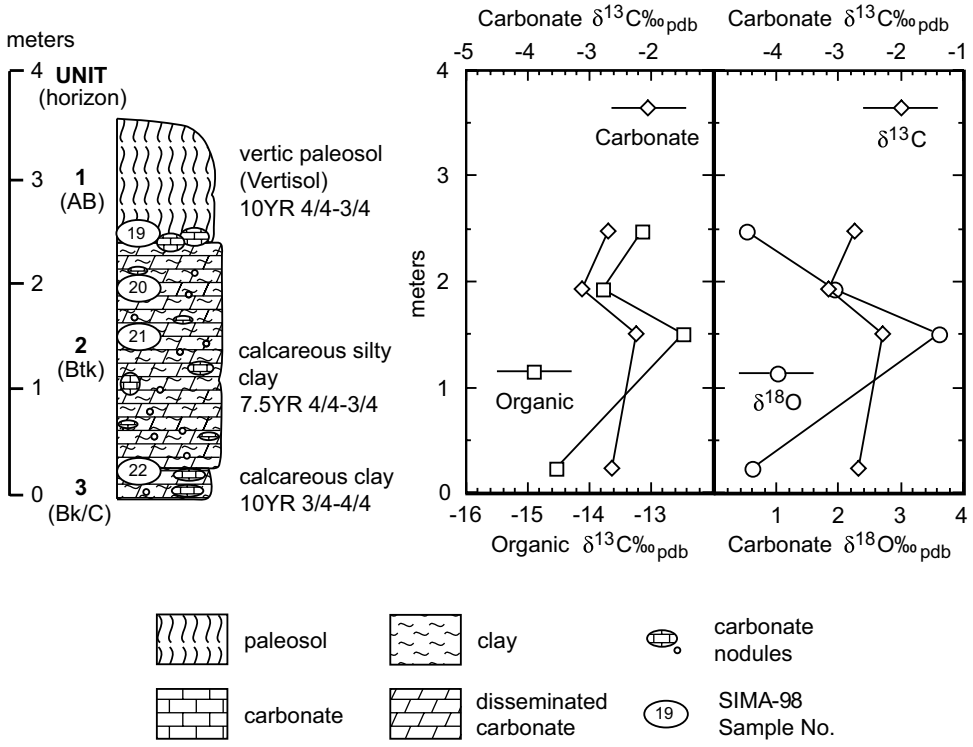

FIGURE 2.7

Stratigraphic section of soil sampling trench dug in 1998 showing locations of carbonate nodule and sedimentary matrix samples, stable isotope ratios of included and disseminated organic carbon, and carbonate nodule carbon and oxygen. The trench was dug near the A2 Area section in BOU-VP-19 (see Figure 2.4).

matter and 15.4‰ for pedogenic carbonates. Because $\delta^{13}C$ enrichment can vary by ± 1.5 to 2.0‰ around these average values (Cerling 1984; Krull and Skjemstad 2003; Quade et al. 2004), the accuracy of estimates of percent C_4 biomass from both carbonates and organic matter are approximately ± 15 percent. When soil organic matter and associated carbonates are formed in equilibrium with a plant community, the difference between carbonate and organic $\delta^{13}C$ values ($\Delta^{13}C_{carb\text{-}org}$) is expected to be 13.5–17‰ (Cerling 1984; Quade and Levin, in review). Deviations from equilibrium may reflect diagenesis or contamination of one or both fractions or formation at different times under floras with different isotopic compositions.

Oxygen isotope ratios of pedogenic carbonates reflect those of soil water. The isotopic composition of meteoric waters is controlled by polar ice volume, altitude, temperature, humidity, and evapotranspiration (Gat 1980). Precipitation $\delta^{18}O$ values are highest in hot, arid habitats and at low latitudes and altitudes (Craig 1961). Although interpretation of oxygen isotope ratios of pedogenic carbonate nodules is complex because of the number of sources of variation, they can provide relative evidence for humidity, temperature, and micro- and macroclimate (Cerling 1984; Cerling et al. 2003).

Soil organic $\delta^{13}C$ values range from -12.5 to -14.5‰, reflecting 75–90 percent C_4 plant biomass. Carbonate $\delta^{13}C$ values range from -2.2 to -3.1‰, reflecting 55–65 percent C_4 plant biomass. This difference in estimates of percent C_4 biomass is reflected by $\Delta^{13}C_{carb\text{-}org}$ values that are smaller than expected for soils in which carbonate

EBSCOhost - printed on 10/28/2022 4:53 AM via . All use subject to https://www.ebsco.com/terms-of-use

TABLE 2.2 Results of Isotopic Analysis of Paleosol Samples from Urugadehu BOU-VP-19, Daka Member, Bouri Formation, Bouri Peninsula, Middle Awash Valley

Strat. unit (depth cm)	*SIMA field #*	*Organic material*	*MAW lab #*	*Wt.% HCl-insoluble*	*Wt.% org carbon*	*Organic $\delta^{13}C‰_{pdb}$*	*MAW lab #*
1 (103)	98-19	Nodule	132	34.26	0.107	−13.15	207
2 (50)	98-20	Matrix	133	73.53	0.125	−13.79	208
2 (92)	98-21	Matrix	134	69.08	0.121	−12.49	209
3 (7)	98-22	Matrix	135	83.3	0.097	−14.53	210

Strat. unit (depth cm)	*SIMA field #*	*Carbonate material*	*Wt.% $CaCO_3$*	*Carbonate $\delta^{13}C‰_{pdb}$*	*Carbonate $\delta^{13}O‰_{pdb}$*	*$\Delta^{13}C‰$ carb-org*	*$\%C_4$ carb*	*$\%C_4$ org*
1 (103)	98-19	Nodule	53.8	−2.64	0.8	10.52	59.8	84.6
2 (50)	98-20	Nodule	99.6	−3.12	1.99	10.67	56.3	80.1
2 (92)	98-21	Nodule	93.5	−2.22	3.67	10.27	62.7	89.4
3 (7)	98-22	Nodule	83.2	−2.63	0.65	11.9	59.8	74.8

NOTE: Depths are midpoints of sample points measured from the top of each stratigraphic unit. Organic carbon concentration and stable carbon isotopic composition of acid-insoluble residue included in carbonate nodule 98-19, and disseminated in sedimentary matrix associated with carbonate nodules 98-20, 21 22, carbonate concentration and stable carbon and oxygen isotopic composition of paleosol nodule carbonate, and estimates of percent C_4 plant biomass from carbon isotope ratios. $\Delta^{13}C_{carb\text{-}org}$ is the difference between carbonate and organic $\delta^{13}C$ values. The precision of estimates of percent C_4 biomass is approximately ± 15 percent.

and organic matter formed in equilibrium, so it is uncertain which fraction retains a more accurate record of the floral composition. Organic samples prepared by heating to 55°C under vacuum have somewhat lower weight percent carbon and higher $\delta^{13}C$ values than unheated samples (S. Ambrose, unpublished data). If the isotopically light fraction is more volatile at higher temperatures, then the organic fraction may overestimate percent C_4 in this study. Figure 2.7 shows that carbonate and organic $\delta^{13}C$ values covary within the soil profile, which suggests that both reflect variation in proportions of C_3 and C_4 plant biomass through time. Carbonate $\delta^{18}O$ values range from 0.7 to 3.7‰ and do not systematically covary with $\delta^{13}C$ values. Comparatively high $\delta^{18}O$ values suggest relatively high soil temperatures and evaporation rates. This suggestion is consistent with the carbon isotope evidence for predominantly unshaded grassy habitats. Combined with paleosol geomorphology, these data suggest open, warm, seasonally dry, wooded grassland to open grassland environments in this section of the Daka Member. This environmental reconstruction is explained in more detail in the following section.

Paleolandscape and Paleoenvironmental Features of the Daka Member

The occurrences of similar lithologic units such as mudstone, silty clays, sandstone, limestone, sands, and intercalated bivalve and gastropod beds within the Bouri Formation suggest recurrent patterns of sedimentation and erosional processes that are

EBSCOhost - printed on 10/28/2022 4:53 AM via . All use subject to https://www.ebsco.com/terms-of-use

defined by paraunconformities and diastems during the Plio-Pleistocene. Tectonic features coupled with lithologic and faunal evidence provide fundamental information about the paleolandscape and paleoenvironmental features of the Bouri Peninsula during the Plio-Pleistocene. The sedimentary rocks were deposited by fluvial processes in a depositional setting characterized by floodplains, distributary deltaic channels, and margins of fluctuating shallow lakes. For example, silty clays and sandstone units generally dominate the lower and upper parts of the older Hata Member stratigraphic sequence, respectively. The cream-colored limestone layer at the top of the Hata Member was probably deposited in a lacustrine environment like the widespread platy limestone unit of the late Pleistocene upper Herto Member, currently exposed between Yardi Lake and Bouri Village (Clark et al. 2003). Although the lithologic units of the Hata and Daka Members are generally similar, the Daka Member stratigraphic sequence is dominated by fine- to coarse-grained, moderately sorted sandstone with minor silty clays mostly confined to the northern part of the Bouri Peninsula. Again, fluvial processes were primarily responsible for the accumulation of the Daka Member except for those units in the upper part of the sequence that contain bivalve and gastropod fossil–bearing silty clays and sandstone layers and the interbedded diatomaceous Wokari Tuff. The Wokari Tuff was deposited in a shallow lake, as indicated by the abundant bivalve and gastropod shells in the underlying silty sandstone. The Herto Member at the top of the Bouri Formation also contains similar sedimentary units that were mostly deposited by fluvial processes. Sediments were deposited on flood plains, along distributary deltaic channels and within the large shallow lake margin of the ancestral Yardi Lake. Outcrops of lignite, silty clays with aquatic invertebrate fossils, widespread platy limestone, sands and a mixture of bentonite clasts, rounded beach gravels, and well-sorted and partially cemented sandstone define the lateral extent of the ancestral Yardi Lake.

Comparison of the Bouri Formation's lithologic units with their depositional settings and formative tectonic processes implies that the paleolandscape and paleoenvironment of the Bouri Peninsula did not drastically fluctuate during the Plio-Pleistocene. However, multiple episodes of faulting, uplift, and subsidence and the close proximity of the Bouri Formation to the Quaternary axial rift zone did influence the paleolandscape history of the area. For example, the current Yardi Lake provides a modern natural analog, highlighting the impact of faulting on landscape evolution and subsequent sedimentological processes. Yardi Lake formed when a major transverse fault uplifted the Bouri area and blocked the ancestral Awash River during the late Pleistocene (Clark et al. 2003). As a result, the Herto area became a major sedimentary trap, accumulating both fluvial and lacustrine sediments. Today, both erosional and depositional processes are taking place side by side in the vicinity of the Bouri Peninsula. For example, abundant sediments are being removed by fluvial and wind erosion from the uplifted Bouri Fault Block into the adjacent Awash River and Yardi Lake. In contrast, major ephemeral streams from the adjacent western rift escarpment and highlands seasonally deposit extensive amounts of sediments within Yardi Lake and the surrounding floodplain. In light of the similarity of the lithologic units of the Herto and Daka Members, it is possible to assess the depositional settings and the paleolandscape of the Daka Member.

EBSCOhost - printed on 10/28/2022 4:53 AM via . All use subject to https://www.ebsco.com/terms-of-use

High-energy fluvial processes were probably responsible for the accumulation of the cross-bedded, coarse, and matrix-free Hereya Pumice Unit (HPU) at the base of the Daka Member. In contrast, the cream-colored limestone at the top of the Hata Member, which preceded a nondepositional environment prior to the onset of the Daka Member deposition, probably formed in a lacustrine environment. The stratigraphic interval between the Hata and Daka Members suggests that the Bouri area probably experienced an erosional diastem and/or tectonic and sedimentological quiescence. However, by the time of HPU deposition, the Bouri area was transformed again into a shallow lacustrine depositional environment, most likely as a result of faulting and subsidence or as a result of blockage of an ancestral drainage system. This likely resulted in a shallow-lake environment like Yardi Lake. As deposition continued, silty clays started to accumulate above the coarse sandstone beds at the base of the Daka Member. The increased thickness of the diatomaceous Wokari Tuff in the vicinity of Wadi "M" implies that the deposystem was deeper in that area. The sandstone units above and below the Wokari Tuff are also thicker in that area. Between Wadi "M" and Ley Gita the pebbly sandstone above the Wokari Tuff contains abundant cobbles. In the southern half, the uppermost unit of the Daka Member is dominated by well-sorted and bedded "castellated facies" sandstone of the Yanguli Mu'ul section, which was probably deposited by fluvial processes. West of this section, Daka Member sandstone underlies Herto Member lacustrine sediments, consisting of silty clay beds with fossil fish remains. This implies that the paleolandscape was undergoing another cycle of subsidence at the beginning of Herto Member sedimentation. The recurrent transitions from fluvial to lacustrine sediments and vice versa probably reflect episodes of tectonic-driven subsidence and uplift that controlled the rift-bound sedimentation processes. The thick Plio-Pleistocene sedimentary deposits and minor interbedded volcanic rocks of the Bouri Formation represent records of the complex tectonic-driven sedimentation processes that are currently preserved within the rift floor.

The paleosol profile at Urugadehu BOU-VP-19 can be classified as a vertisol ("black cotton soil"). Vertisols typically form in tropical savanna grassland environments on sediments weathered from basaltic parent materials, under subhumid to semiarid climates with mean annual rainfall of 180–1,520 mm (Retallack 2001). By considering the distribution of carbonates within the profile, the range of environments and climates represented in this paleosol can be narrowed. Pedogenic carbonate nodules form at greater depths in soil profiles with higher mean annual rainfall, and nodules rarely form when precipitation exceeds 1,000 mm (Cerling 1984; Retallack 1994). Pedogenic carbonate nodules formed at least 1 m below the top of the vertic A horizon, and substantial amounts of disseminated carbonate were leached from the A horizon and accumulated in the Btk and Bk/C horizons. Assuming that the depth of carbonate nodule formation in the A horizon was around 100 cm, then mean annual precipitation was likely to have been 600–800 mm (Retallack 1994).

Carbonate nodule and organic $\delta^{13}C$ values reflect ~55–90 percent C_4 plant biomass, indicating wooded grasslands to open grasslands in this area of the Daka Member. These results can be compared to those from other time periods in the Middle Awash Valley (Figure 2.8), and to those in surrounding regions in eastern Africa (Quade et al. 2004). Aduma A5, a late Pleistocene MSA site located ~10 km north of Bouri has a similar geomorphic setting to BOU-VP-19. Aduma A5 has a vertisol with a well-developed carbonate horizon, as well as

EBSCOhost - printed on 10/28/2022 4:53 AM via . All use subject to https://www.ebsco.com/terms-of-use

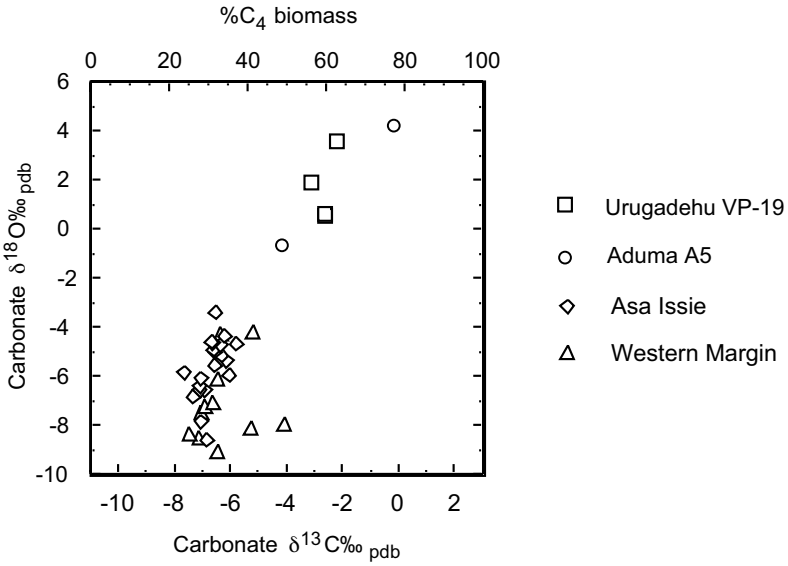

FIGURE 2.8

Stable carbon and oxygen isotope ratios of pedogenic carbonate nodules from BOU-VP-19 (see Figure 2.4, Az Area section) compared to those of other time periods in the Middle Awash Valley: Aduma A5: late Pleistocene,~0.1 Ma (Yellen et al. 2005). Asa Issie: early Pliocene, 4.1–4.2 Ma (White et al. 2006). Western Margin: terminal Miocene, 5.2–5.6 Ma (WoldeGabriel et al. 2001; Haile-Selassie et al. 2004).

high carbonate and organic $\delta^{13}C$ values and high $\delta^{18}O$ values (Yellen et al. 2005). Terminal Miocene and early Pliocene sites in the Western Margin and Asa Issie of the Middle Awash Valley have substantially lower carbonate carbon and oxygen isotope ratios (WoldeGabriel et al. 2001; Haile-Selassie et al. 2004; White et al. 2006). Penecontemporary sites in the Tugen Hills, Lothagam, Gona, and Kanapoi (Kingston 1999; Wynn 2000; Cerling et al. 2003; Levin et al. 2004) also have low values. These data reflect predominantly higher rainfall, and woodland to wooded grassland environments throughout eastern Africa before 2.9 Ma. Late Pliocene and early Pleistocene sites at Olduvai Gorge, Kanjera, Baringo, Koobi Fora, Gona, and Olorgesailie have relatively high carbonate $\delta^{13}C$ and values (Cerling and Hay 1986; Cerling et al. 1988; Plummer et al. 1999; Sikes et al. 1999; Quade et al. 2004; Liutkus et al. 2005), reflecting predominantly warmer, drier, more open, grassy woodlands and grasslands after 2.6 Ma. These data show that open and drier environments predominated after 1.6 Ma (Cerling et al. 1988; Quade et al. 2004). As in other parts of eastern Africa, the environment of *Homo erectus* in the Daka Member around 1.0 Ma was a relatively warm, mesic to semiarid wooded to open savanna mosaic that probably resembled those of the present highlands of eastern Africa, including parts of the main Ethiopian Rift near Lake Besaka, and the Lake Nakuru basin of the central Rift Valley of Kenya. Because the Middle Awash region is 10° north of the equator, it lies near the northern edge of the intertropical convergence zone, so there was probably one long wet season rather than the two shorter seasons that characterize equatorial savannas. Seasonal variation in water, temperature, and food availability may thus have been greater in the Middle Awash Valley than near the equator.

Summary and Conclusion

The sedimentary and volcanic units of the Bouri Formation, which are divided into the Hata, Daka, and Herto Members, in ascending stratigraphic order, crop out along the strike of the NW-SE trending Bouri horst. The uplifted structural block, which is obliquely

EBSCOhost - printed on 10/28/2022 4:53 AM via . All use subject to https://www.ebsco.com/terms-of-use

oriented to the NE-SW trending Quaternary axial fracture zone of the rift floor, was subsequently tilted to the southwest during the late Pleistocene. The early Pleistocene Daka Member, which is dominated by fluvial sedimentary rocks, crops out between the Pliocene Hata Member and the late Pleistocene Herto Member of the Bouri Formation. Two major tephra stratigraphic markers, represented by the 1.04 Ma HPU and the diatomaceous Wokari Tuff, are intercalated within the basal and middle parts of the Daka Member stratigraphic section, respectively. Pumice cobbles within conglomerate lenses above the Wokari Tuff yield a mean age of 0.966 ± 0.006 Ma, thus providing a minimum age for the underlying Wokari Tuff. The Daka Member lithological units were primarily deposited along distributary channels, along lake margins, and in fluctuating shallow lakes. Finally, paleosol geomorphology stable carbon isotope data suggest open, warm, seasonally dry, wooded grassland to open grassland environments for a section centrally located in the Daka Member.

EBSCOhost - printed on 10/28/2022 4:53 AM via . All use subject to https://www.ebsco.com/terms-of-use

This Page Left Intentionally Blank

EBSCOhost - printed on 10/28/2022 4:53 AM via . All use subject to https://www.ebsco.com/terms-of-use

3

Bovidae

W. HENRY GILBERT

Bovidae comprise the most diverse array of genera for any family represented in the Daka Member. Fossil bovid specimens include more than 25 well-preserved crania and hundreds of dental and horn core specimens. The 17 different genera include extinct and living representatives. The assemblage is especially rich in bovines (Figures 3.1 and 3.2), alcelaphines, and reduncines, but also includes hippotragines, tragelaphines, antilopines, caprines, aepycerotines, neotragines, and possibly ovibovines. The diversity of taxa and the large number of specimens from the Daka Member prevent treatment of Bovidae with as much detail as is given to taxa in other chapters. Some Daka Member bovids, including the holotypes of *Nitidarcus asfawi* and *Bouria anngettyae,* have already been described and published (Vrba 1997). The aim of this chapter is to present the entire Daka bovid assemblage as a unit and to provide brief descriptions and evolutionary backgrounds for the bovid taxa present. More research is warranted on Daka bovids, some of which is identified here. Bovids contribute substantial paleoecological information as a result of the tendency for niche specificity among bovid tribes, genera, and species. These paleoecological indications are discussed in Chapter 17.

Daka bovid specimens have been identified conservatively, and many cannot be identified to the level of genus or species. In this chapter, a more fragmentary specimen is described in the text only if it represents the sole Daka representative of the most refined taxonomic rank that can be effectively determined. For example, although its generic status is uncertain, the single representative of Neotragini, BOU-VP-25/11, is described in the text because there are no other neotragines in the assemblage. Most isolated dental specimens and many horn cores are assigned only to tribe and listed in Appendices 3.1 and 3.2.

The monophyly of Bovidae is supported by molecular and morphological phylogenetic analyses (Gatesy et al. 1997; Hassanin and Douzery 1999a, b; Hernández-Fernández and Vrba 2005a). The tribal groupings of Bovidae made by Simpson (1945) have changed little in over a half-century, but hypotheses regarding their evolutionary relationships remain controversial. Many phylogenetic analyses have been undertaken: molecular (Allard et al. 1992; Gatesy 1992; Essop et al. 1997; Hassanin and Douzery 1999a, b; Matthee and Robinson 1999; Kostia et al. 2000; Matthee and Davis 2001; Kuznetsova and Kholodova 2003) and morphological (Gentry 1992; Vrba and Gatesy 1994; Vrba 1997; Vrba and Schaller 2000). In addition, synthetic approaches to bovid phylogeny have yielded robust

EBSCOhost - printed on 10/28/2022 4:53 AM via . All use subject to https://www.ebsco.com/terms-of-use

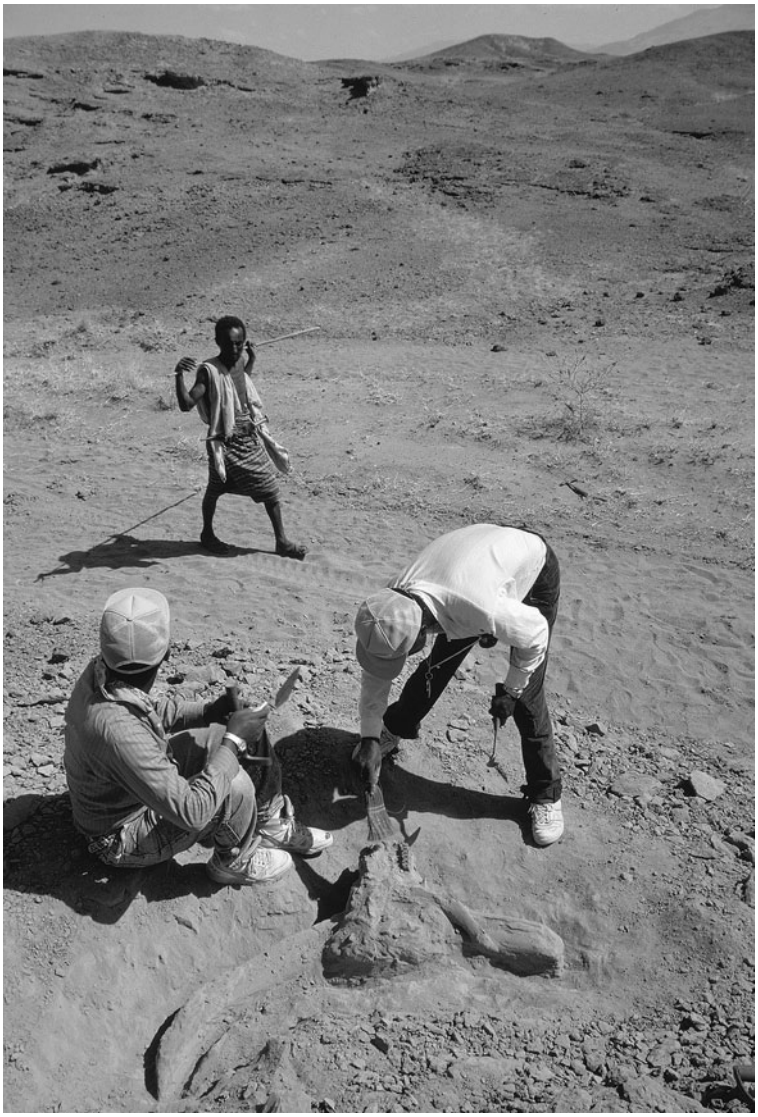

FIGURE 3.1
Alemayehu Asfaw (right) and antiquities officer Tadewos Assebework excavating *Pelorovis* cranium BOU-VP-3/8. Photograph by Tim White, December 29, 1992.

results (Gatesy et al. 1997; Hernández-Fernández and Vrba 2005a). Figure 3.3 presents the conservative view of African bovid phylogeny used in this chapter. This figure is based on Gatesy et al. (1997), Vrba and Schaller (2000), and Hernández-Fernández and Vrba (2005a). This chapter employs the taxonomy used by Grubb (2001) because it corresponds well to these recent phylogenetic studies.

Bovid fossils identified by horn cores first appear in the early Miocene of Eurasia and Africa, but the family probably originated in the Oligocene (Harris 1991a; Vrba 1995b; Gentry 2000b; Hernández-Fernández and Vrba 2005a). Authors with both molecular and morphological perspectives suggest a series of bovid migrations between Eurasia and Africa during the Miocene (Vrba 1995b; Matthee and Davis 2001). Early Miocene first appearances of Bovidae in Africa are based on dental specimens (Gentry 1990), which,

EBSCOhost - printed on 10/28/2022 4:53 AM via . All use subject to https://www.ebsco.com/terms-of-use

FIGURE 3.2
W. Henry Gilbert and Hamed Elema examine specimen BOU-VP-3/8 (see Figure 3.1) from the Daka Member at the National Museum of Ethiopia. Other Daka faunal remains are on the tabletop. Photograph by David Brill.

unfortunately, are not as diagnostic of bovid status as are horn cores. An early Miocene first appearance of Bovidae in Africa does, however, fit well with estimates of divergence times for African bovid groups (Hernández-Fernández and Vrba 2005a). The middle Miocene record of Bovidae in Africa includes representatives of Boselaphini, Caprinae, and Antilopinae (Gentry 1990), but fossils and localities are extremely sparse until the late Miocene. The late Miocene Adu-Asa Formation of the Middle Awash has representatives of Bovini, Boselaphini, Tragelaphini, Reduncini, Hippotragini, Antilopini, and Neotragini (Haile-Selassie 2001).

Alcelaphinae

Alcelaphinae includes a single tribe, Alcelaphini. Hernández-Fernández and Vrba (2005a) suggest that the alcelaphine radiation began in the later middle Miocene. Further diversification appears to have followed, with an exceptional diversity of lineages appearing between 2.0 and 3.0 Ma (Vrba 1995b). The five extant alcelaphine genera appear in the Pliocene. Another major alcelaphine clade, the extinct genus *Parmularius,* also likely originated in the Pliocene and went extinct in the middle Pleistocene (Vrba 1997). Vrba (1997) names two cladistic subtribes: Alcelaphina and Damaliscina. Subtribe Damaliscina includes the existing genus *Damaliscus* (topi) and the extinct

EBSCOhost - printed on 10/28/2022 4:53 AM via . All use subject to https://www.ebsco.com/terms-of-use

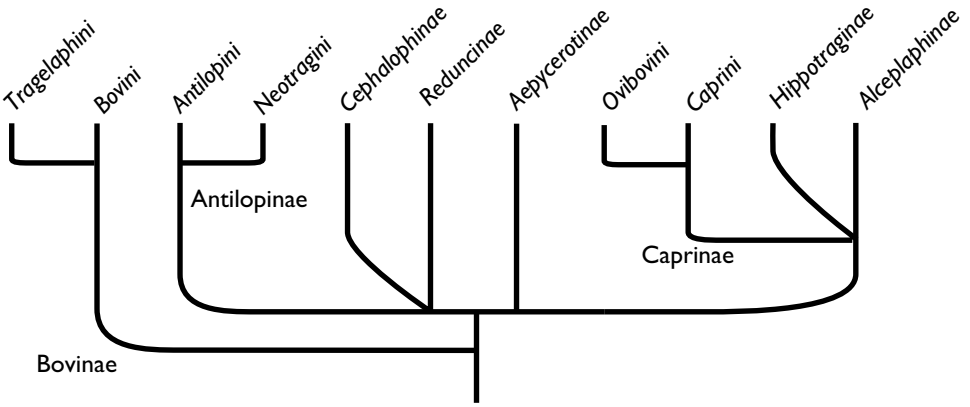

FIGURE 3.3
Phylogeny of Bovidae based on conservative synthesis of data presented in Gatesy et al. (1997), Vrba and Schaller (2000), and Hernández-Fernández and Vrba (2005a).

genera *Awashia* and *Parmularius*. Alcelaphina comprises all other alcelaphines, including the extinct genus *Megalotragus*.

Different alcelaphine species are recognized by unique horn morphologies. From the diversity of shapes seen among modern and fossil forms, alcelaphine horns appear to have changed shape rapidly during their evolutionary history. Annulation (latitudinal horn corrugation), a primitive feature of nonbovinae bovids, may allow selection to alter horn shape relatively quickly. Alcelaphine genera possess an additional feature potentially adding to the evolutionary malleability of their horn core shape: a pneumatized frontal bone. Variation in this morphology can significantly affect the shape of the base, and thus the growing horn.

Alcelaphina

Vrba (1997) divides Alcelaphini into two subtribes: Alcelaphina and Damaliscina. Alcelaphina includes the modern genera *Alcelaphus* (hartebeest), *Connochaetes* (wildebeest), and *Beatragus* (hirola) and the extinct genera *Megalotragus, Damalops, Damalacra, Rabaticeras, Numidocapra,* and *Oreonager*.

Connochaetes Lichtenstein, 1812

GENERIC DIAGNOSIS "Fairly large alcelaphines with skulls tending to be low and wide; horn cores inserted widely apart and behind the orbits, strongly divergent in earlier species. Where torsion exists in the horn cores it is clockwise from the base upwards on the right side. Suture of the parietofrontals centrally indented behind horn core insertions; preorbital fossae shallow or absent and without an upper rim; posterior tuberosities of basioccipital more localized than in *Alcelaphus* or *Damaliscus;* auditory bullae large and inflated; occipital surface faces backwards rather than laterally; premolar rows very short with P_2s tending to disappear" (Gentry and Gentry 1978, 364).

Connochaetes taurinus (Burchell, 1823)

DIAGNOSIS "A larger wildebeest with a more convexly domed forehead than *C. gnou;* horn cores inserted at the back of the skull above the occipital surface, emerging transversely,

EBSCOhost - printed on 10/28/2022 4:53 AM via . All use subject to https://www.ebsco.com/terms-of-use

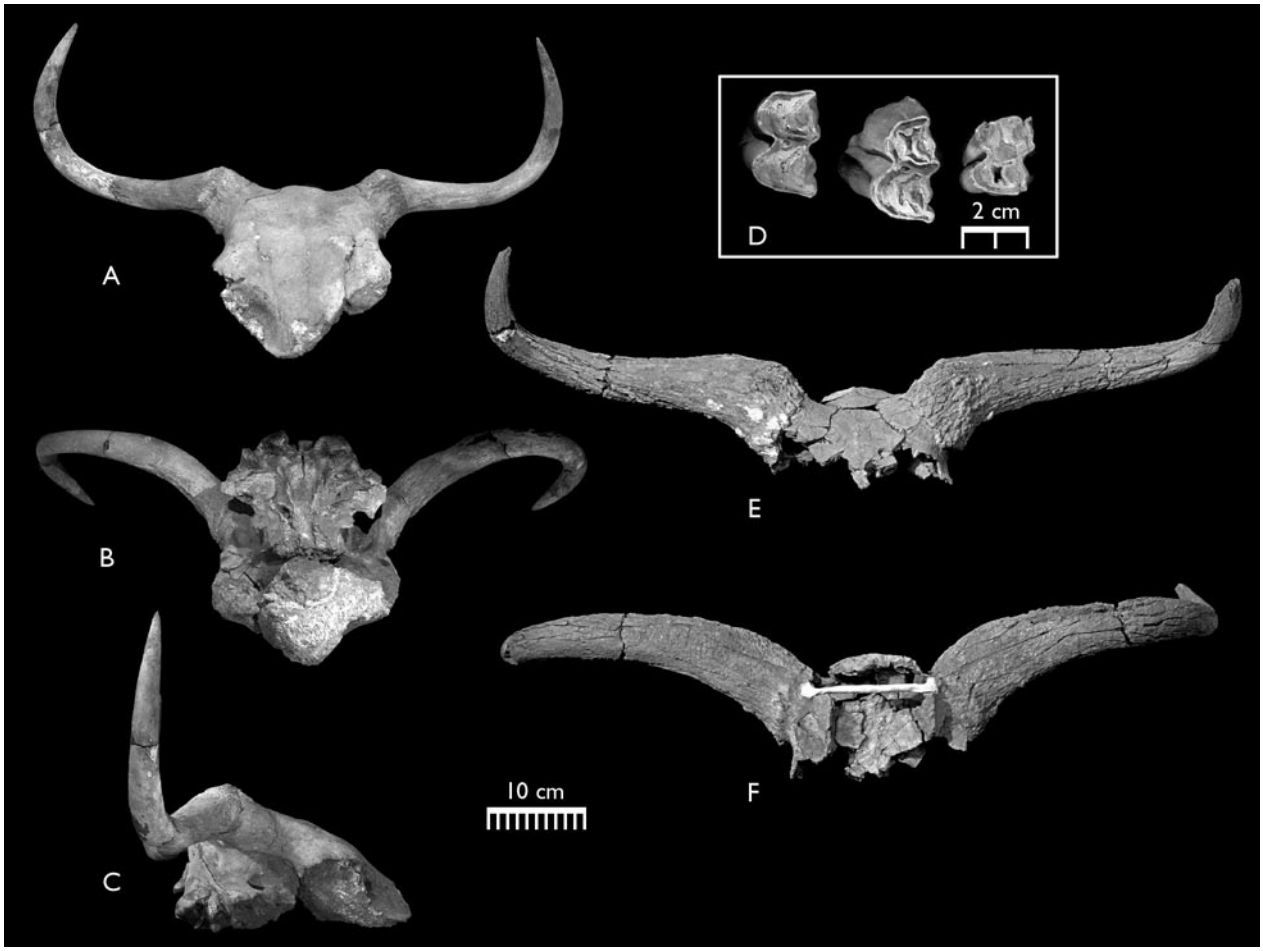

FIGURE 3.4

Connochaetes taurinus. A. BOU-VP-1/123 Cranial view. B. BOU-VP-1/123 Basal view. C. BOU-VP-1/123 Lateral view. D. BOU-VP-25/72 Occlusal view. E. BOU-VP-2/49 Cranial view. F. BOU-VP-2/49 Basal view.

having tips turned upwards and inwards; a long face and nasals; zygomatic arch deep anteriorly below the orbits; large shallow preorbital fossa; jugal with two broad anterior lobes; wide premaxillae ascending to a long contact on the nasals; no median vertical ridge on the occipital" (Vrba 1997, 157).

DESCRIPTION BOU-VP-2/49 (Figure 3.4E and F) is a partial cranium consisting of nearly complete right and left horn cores as well as a substantial portion of the right and left frontal. The coronal suture is present, and some endocranial surface remains intact. The nasal portion of the frontal is missing. The large frontal sinuses at the bases of each horn core are preserved.

BOU-VP-1/5 is a right horn core and a portion of the right frontal. A small fragment of left frontal just lateral to the metopic suture is the only remnant of that bone. Most of the right horn core base is present, preserving much of the sinus. Some of the ectocranial cortex of the right frontal remains intact.

Cranium BOU-VP-1/123 (Figure 3.4A, B, and C) is the most complete of the Daka *Connochaetes* crania. It comprises the complete right and left horn cores, frontals,

EBSCOhost - printed on 10/28/2022 4:53 AM via . All use subject to https://www.ebsco.com/terms-of-use

parietal(s), and occipital. Large portions of the right and left temporals are present, but the zygomatic processes are broken away. The basisphenoid is present, as is the sphenoid. Most of the right lacrimal is preserved. The zygomatics, maxillae, premaxillae, palatines, and left lacrimal are all missing.

DISCUSSION The genus *Connochaetes (C. gentryi)* first appears in the upper Lomekwi Member of the Nachukui Formation, dating to 2.6 Ma (Vrba 1997). *Connochaetes gentryi* persists until the earliest Pleistocene, around the time when possible daughter species *C. africanus* and *C. taurinus* diverge (Vrba 1997). Modern species of *Connochaetes* include *C. taurinus* and *C. gnou*. Many synapomorphies besides those listed in the diagnosis unite *Connochaetes* (Gentry and Gentry 1978; see Vrba 1997).

Some Daka *Connochaetes* specimens are similar to *C. t. olduvaiensis* (Gentry and Gentry 1978) in horn core morphology, but other specimens are less gracile. The distance from basal horn core to orbit would have been significantly shorter than in modern *C. taurinus* (Vrba 1997). Because *Connochaetes* and *Megalotragus* dentitions are so similar, no attempt was made to identify individual teeth potentially from these taxa to genus. One upper dentition, BOU-VP-25/72 (Figure 3.4D), is assigned here to *Connochaetes* by an associated horn core. Other teeth are identified as "Alcelaphini" in Appendix 3.1. Some horn cores that did not preserve enough of the frontal to determine their orientation were also impossible to differentiate between *Connochaetes* and *Megalotragus* and are also identified to the tribal level (Appendix 3.2).

Megalotragus Schwarz, 1932

GENERIC DIAGNOSIS "Very large extinct alcelaphines, including the largest known, with narrow skulls and horn cores inserted obliquely in side view, behind the level of the orbits and close together, and with torsion that is clockwise from the base upwards on the right side; molar teeth tending to have a simple occlusal pattern; very short premolar rows; long legs" (Gentry and Gentry 1978, 356).

Megalotragus kattwinkeli Schwarz, 1932

DIAGNOSIS "An alcelaphine that varies in size from large-medium to very large. Horn cores short to moderately long, with transverse ridges that are better developed above the base. Insertions that vary from far behind the orbits to very far such that their bases overhang the occipital surface, with associated variation in the distance from horn core bases to occiput; horn core bases strongly angled to the midfrontal suture, with compression that is mostly low at the base and increases towards the mid-horn core. Divergence above the horn core bases varies from low to moderate, with tips that have a greater tendency to reapproach and to curve inwards distally in the smaller individuals, whereas in larger individuals they curve less inwards and rather more upwards. In smaller individuals most of the basal part of the horn core is anteriorly concave. Towards larger skull sizes there is an increasing tendency to strong backwards curvature of the horn core above a more upright basal stem. The horn cores have anterior basal swellings that are especially marked in larger horn cores with well-developed basal backward curvatures. There is a variable tendency,

EBSCOhost - printed on 10/28/2022 4:53 AM via . All use subject to https://www.ebsco.com/terms-of-use

increasing in larger specimens, for the frontals between the horn cores to be raised such that the pedicels appear fused into an incipient joint boss. The orbits project prominently relative to the narrow distance across the horn pedicels. A prominent nasal rest, formed by upwards-doming of the posterior nasals and adjacent bones, is present. The cranium has an occipital surface that faces mainly backwards and only a little laterally and has a median vertical ridge, a wide basioccipital with large anterior tuberosities, and small, little inflated auditory bullae" (Vrba 1997, 147–148).

DESCRIPTION Cranium BOU-VP-2/21 (Figure 3.5) preserves most of the left horn core and about half of the right. The frontals are nearly complete, with the exception of a fragment missing from the posterior right frontal and cortical bone adjacent to the fragment. The posterior part of the occipital is missing, and the basicranium, while partially preserved, lacks surface detail. The right temporal is missing, as is most of the inferior portion of the left. Only the central portion of the sphenoid is preserved. Large portions of the left and right nasals are preserved. Bones of the maxilla and the lacrimals are missing, as are all other facial elements.

Cranium BOU-VP-1/99 preserves most of the left horn core and both frontals. It preserves most of the braincase, with the exception of the posterior occipital, the basisphenoid, the zygomatic processes, and the inferior portions of the temporals. The facial skeleton is missing.

Partial cranium BOU-VP-2/20 preserves the right horn core, frontal, and a small part of the anterior parietal. A small fragment of the endocranial surface of the left parietal adjacent to the metopic suture is preserved. The right frontal is broken through the frontal sinuses and is missing all portions anterior to them, including the orbits.

Cranium BOU-VP-1/97 preserves most of the horn cores and braincase with the exception of the right occipital condyle and the zygomatic processes and inferior portions of both temporals. The basicranium is reasonably well preserved, and it includes some of the sphenoid. The orbits and facial skeleton are missing. Note that this specimen has provenience issues and might not be from the Daka Member (see above). It is listed here, but referred to cf. *Megalotragus*.

DISCUSSION *Megalotragus kattwinkeli* first appears at approximately 3.5 Ma in the Sidi Hakoma Member of the Hadar Formation, at the site of Matabaeitu in the Middle Awash, and in Sterkfontein Member 4. Its last appearance is in Olduvai Bed IV (Vrba 1997). Vrba (1997) discusses the attribution of Daka material to *M. kattwinkeli* at great length, breaking down seven salient features of cranial morphology useful in comparing *Megalotragus* species. She compares specimens from the Daka Member to counterparts from Omo, Koobi Fora, and Olduvai, and asserts that they are all part of a single polymorphic species. Specimen BOU-VP-1/97, reported by Vrba (1997), should be regarded with caution, however, as it comes from close to the Pliocene Hata Member contact and was collected prior to the establishment of precise locality boundaries. It is possibly Pliocene. This would reduce the amount of variation noted by Vrba (1997) for the taxon in the Daka Member. Specimen BOU-VP-1/97, while

EBSCOhost - printed on 10/28/2022 4:53 AM via . All use subject to https://www.ebsco.com/terms-of-use

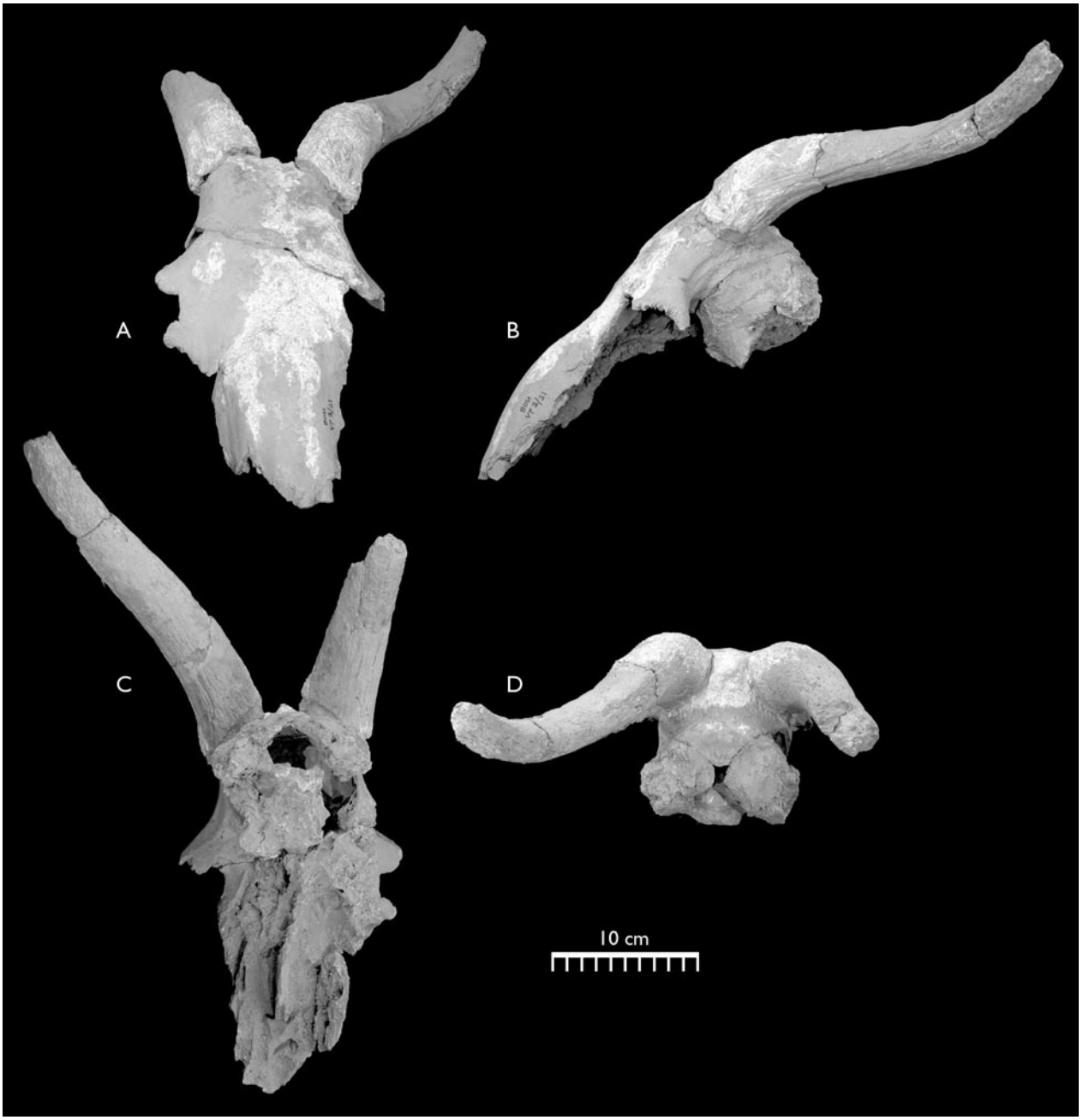

FIGURE 3.5
Megalotragus kattwinkeli, BOU-VP-2/21. A. Cranial view. B. Lateral view. C. Basal view. D. Caudal view.

presented here to ensure bibliographic traceability of the specimen, is referred to cf. *Megalotragus*.

Numidocapra Arambourg, 1949

GENERIC DIAGNOSIS This genus has a single species and the diagnosis is presented below.

EBSCOhost - printed on 10/28/2022 4:53 AM via . All use subject to https://www.ebsco.com/terms-of-use

Numidocapra crassicornis Arambourg, 1949

DIAGNOSIS "Medium to large alcelaphines with skulls nearer to high and narrow than to low and wide; frontals between horn core bases strongly raised; horn cores have an oval cross-section and are more massive, longer, and often basally more strongly compressed and less basally and distally divergent, with weaker clockwise torsion from the base up on the right side, than in *Rabaticeras*. The horn cores pass forwards and upwards from the base such that their basal to middle part appears gently concave-forward in lateral view; basal horn cores with low divergence and inserted closely, with small posterior angles of their maximum diameters to the midfrontal suture, and very uprightly with a large angle to the dorsal braincase; the frontal surface anterior to the horn cores is not convex, but slightly concave with a shallow valley towards the midfrontal suture; supraorbital foramina widely separated; keels and basal swellings are absent on horn cores and transverse ridges absent to weak; parietofrontal suture straight to gently indented anteriorly; dorsal orbital rims project less strongly than in *Rabaticeras;* postcornual fossa small to absent; braincase strongly angled relative to the face with sides parallel to slightly narrower towards the rear; no parietal boss; moderately large, somewhat shallow preorbital fossa that lacks definite rims; the nasal bones are narrow; occipital surface facing mainly backwards, narrowing a bit dorsally, with a slight vertical ridge. The teeth are large relative to skull size among the alcelaphines. The occlusal morphology is quite advanced, with large, fairly complex central cavities and pinched buccal and lingual lobes. The premolar row is reduced" (Vrba 1997, 141).

DESCRIPTION Two specimens represent *N. crassicornis* in the assemblage. Specimen BOU-VP-1/21 (Figure 3.6) is the more complete specimen. Its anterior frontals are missing, as are the lateral portions of the temporals, including the zygomatic processes. The remainder of the braincase and basicranium are present. A portion of the sphenoid is present, but most of the right half is missing. The lacrimals are entirely absent, while much of the snout is preserved. The maxillary palate and left and right tooth rows are preserved, with the exception of the left P_2 and the palatal area anterior to the premolars. The anterior nasals are preserved, as is the right maxilla between the tooth row and the preserved nasal. The maxillary portion of the fossil does not articulate with the neurocranium.

Cranium BOU-VP-1/31 preserves the left and right horn cores and nearly complete frontals. The entire parietal is present as is a small portion of the most superior occipital. The squama and zygomatic root of the left temporal are present. The right temporal, the basicranium, and all cranial elements anterior to the frontal are missing.

Daka *N. crassicornis* is separated from *Rabaticeras arambourgi,* its closest sister taxon, by the following cranial features: horn cores that are more weakly compressed, more transversely separated and divergent, with intensified clockwise torsion proximo-distally on the right side, a very subtle cornual fossa, shorter parietal relative to braincase width, and more projecting dorsal orbital rims (Vrba 1997). Contra Gentry and Gentry's (1978) contemplation that *Numidocapra* might have some caprine affinities, Daka *N. crassicornis* dental morphology and metrics are less caprine than alcelaphine, affirming its inclusion in the latter (Vrba 1997).

EBSCOhost - printed on 10/28/2022 4:53 AM via . All use subject to https://www.ebsco.com/terms-of-use

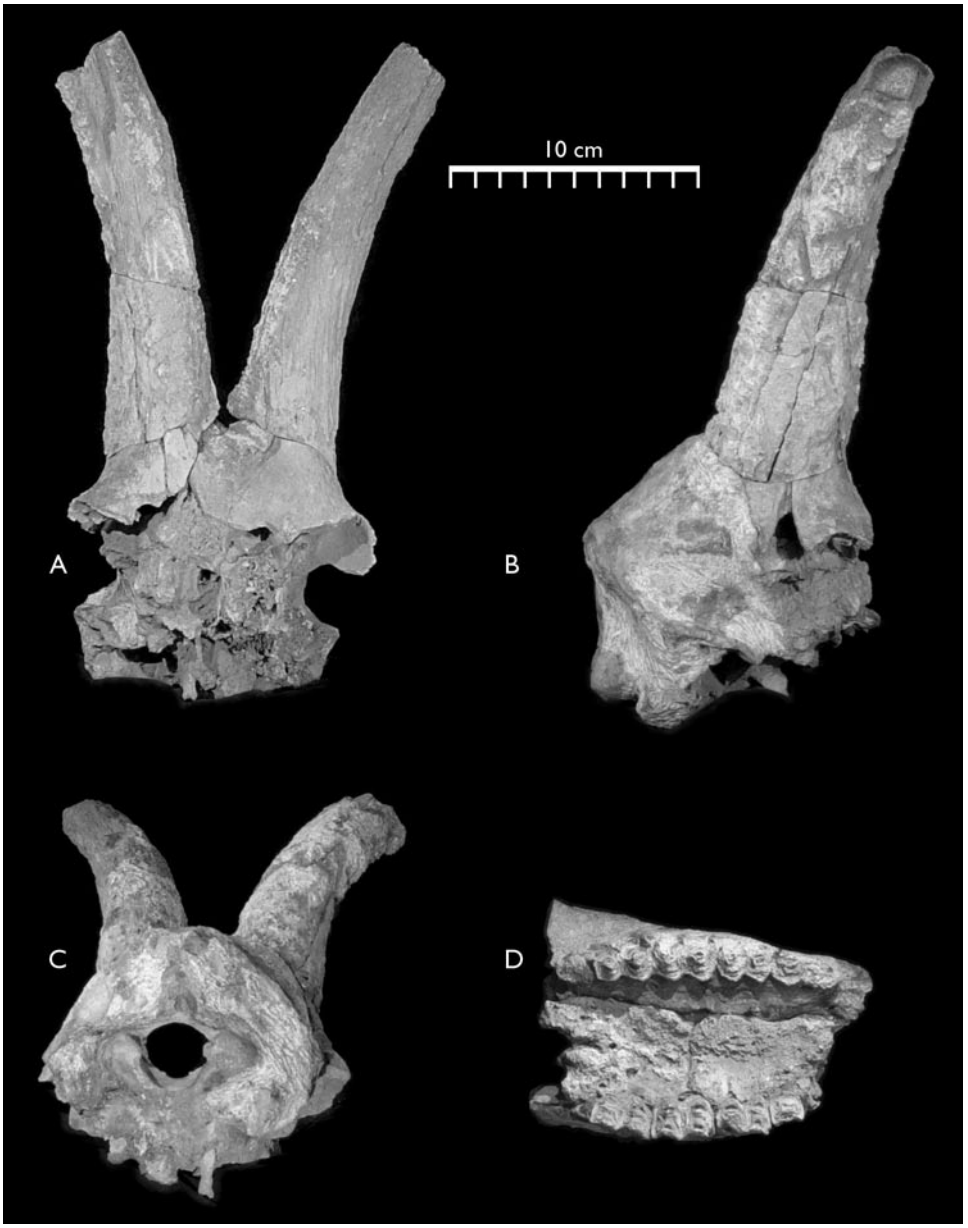

FIGURE 3.6
Numidocapra crassicornis, BOU-VP-1/21. A. Cranial view. B. Lateral view. C. Caudal view. D. Occlusal view.

DISCUSSION *Numidocapra crassicornis,* the single known species of the genus, first appears in earliest Pleistocene deposits at Aïn Hanech, Algeria. Its last appearance is in the Daka Member. There is some disagreement over the tribal status of *Numidocapra*. While most consider it a member of Alcelaphini, some have placed the taxon in Caprini (Gentry and Gentry 1978; Gentry 1990). Daka Member fossils support its inclusion in the former tribe (Vrba 1997). Vrba (1997) suggests that *Numidocapra* is likely sister to *Rabaticeras* and that as such it should subsume it, but she postpones doing so formally because it is also possible that further systematic work will see both genera subsumed into a larger *Alcelaphus*.

EBSCOhost - printed on 10/28/2022 4:53 AM via . All use subject to https://www.ebsco.com/terms-of-use

Damaliscina

Damaliscina is the second subtribe of Alcelaphini named by Vrba (1997). It includes the extant genus *Damaliscus* (topi) and the extinct genera *Parmularius* and *Awashia*. *Damaliscus* first appears in the Pliocene. *Damaliscus* "*hadari*," the earliest representative of the genus, first appears in the Pliocene in the Sidi Hakoma Member of Hadar Formation (Vrba 1997). *Damaliscus ademassuai* has been recovered from the 2.5 Ma Gamedah locality of the Middle Awash. *Damaliscus agelaius* occurs in Beds II and III of Olduvai Gorge, and *D. niro* occurs in several localities in Africa spanning the Pleistocene, including Olduvai Bed II. Both *D. lunatus* and *D. dorcas* are living species. *Damaliscus dorcas* first appears in the later early Pleistocene, and *D. lunatus* in the middle Pleistocene (Vrba 1997). *Parmularius* first appears ca. 3.6 Ma at Laetoli as *P. pandatus*. Later taxa *P. braini, P. eppsi,* and *P. altidens* are known from later in the Pliocene into the early Pleistocene. Numerous species are known from the early and middle Pleistocene. *Parmularius* disappears from the record in the middle Pleistocene. There are no known modern *Parmularius* species.

Damaliscus Sclater and Thomas, 1894

GENERIC DIAGNOSIS "Small to medium sized antelopes. The skulls are high and narrow. The distance across the supraorbital margins is low except for departure from this basal condition in *D. lunatus lunatus*. The basal horn core slopes smoothly upwards and backwards from the base without sudden alteration in course close above the base. The basal horn core is flattened laterally but not posteriorly, although this condition may have reversed in *D. agelaius*. The basal horn cores are relatively strongly compressed with secondary loss of this feature in two taxa. The supraorbital foramina tend to not be so widely separated and not as far from the horn cores as in most other alcelaphines. There is a slightly developed parietal boss. The braincase roof is slightly to markedly convex. The braincase is moderately long to long. The occipital height is low. Weak anticlockwise torsion in the right horn core is present in most species. The premolar rows tend to be relatively long for alcelaphines" (Vrba 1997, 168).

Damaliscus sp.

Three horn cores can be assigned to *Damaliscus*. The best preserved, BOU-VP-1/149, is shown in Figure 3.7. All specimens display pronounced hollowing of the base that extends into the proximal horn core, annulation, smooth upward and backward sloping from the base, and moderate basal lateral flattening. All three specimens appear to be from the same species.

Parmularius Hopwood, 1934

GENERIC DIAGNOSIS "Extinct alcelaphines about the size of *Alcelaphus buselaphus*. Horn cores moderate to long, slightly compressed mediolaterally, without keels or torsion, occasionally with transverse ridges in their distal parts, inserted obliquely over the back of or behind the orbits and close together, usually not very divergent but more so distally, and tending to have posteromedial, posterior or posterolateral swellings at the base. Horn core

EBSCOhost - printed on 10/28/2022 4:53 AM via . All use subject to https://www.ebsco.com/terms-of-use

FIGURE 3.7
Damaliscus sp., BOU-VP-1/149. A. Cranial view. B. Basal/medial view.

pedicles long (partly connected with the oblique insertions); horns in females; postcornual fossae present; braincase short and strongly angled on the facial axis; a parietal boss placed centrally on the braincase roof; orbital rims moderately projecting; supraorbital pits not set notably wide apart; preorbital fossae small; auditory bullae rather small and not very inflated; premolar rows short; lower molar row sometimes appearing rather small relative to the mandible size" (Gentry and Gentry 1978, 371).

Parmularius angusticornis Schwarz, 1937

DIAGNOSIS "A species of *Parmularius* about the size of *Alcelaphus buselaphus* or slightly larger; horn cores more massive with thicker bases and often more divergent in their distal parts than in *P. altidens;* parietal boss less marked than in *P. altidens;* suture or parietofrontals without a central indentation; large occipital surface retaining its median vertical ridge but facing backwards more clearly than in *P. altidens* or *P. rugosis;* auditory bullae small and little inflated; basisphenoid strongly bent upwards on plane of basioccipital" (Gentry and Gentry 1978, 382).

REMARKS Daka *Bouria anngettyae* and *P. angusticornis* are very similar, differing primarily in the larger amount of lateral basal swelling on horn cores, the less pronounced horn

EBSCOhost - printed on 10/28/2022 4:53 AM via . All use subject to https://www.ebsco.com/terms-of-use

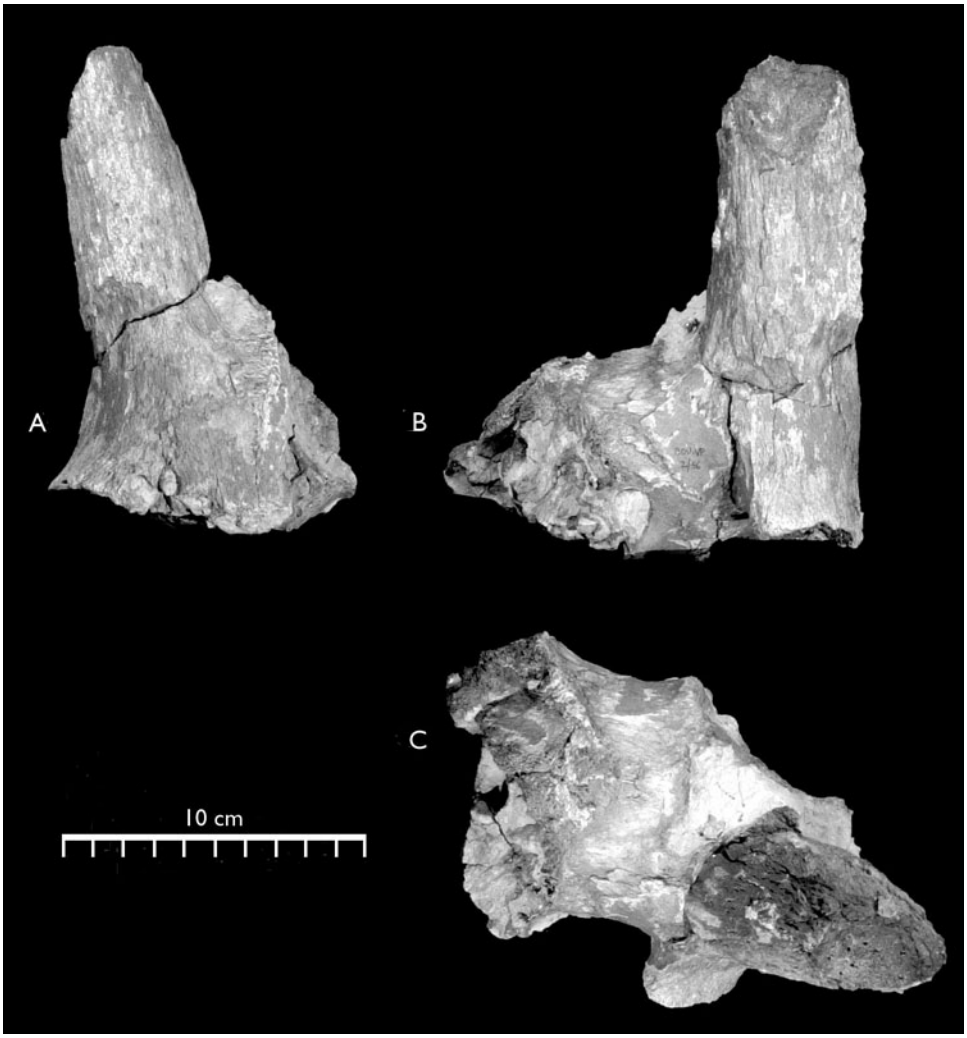

FIGURE 3.8
Parmularius angusticornis, BOU-VP-2/56. A. Cranial view. B. Lateral view. C. Dorsal view.

core basal mediolateral compression, and the shorter overall horns found in *P. angusticornis*. Distinguishing the two taxa was difficult for some recovered Daka specimens. Specimens BOU-VP-2/61, BOU-VP-2/42, and BOU-VP-2/58 are identified as cf. *Bouria* cf. *anngettyae* for this reason.

DESCRIPTION Cranium BOU-VP-2/56 (Figure 3.8) is the most complete of the *Parmularius* cranial specimens. It preserves the right horn core base, right frontal including the orbital rim, the portion of the left frontal deep to the sinus, the parietal, and much of the occipital. The basisphenoid is present, but surface morphology is missing. The sphenoid is also present, but poorly preserved. None of the cranium anterior to the frontals is present.

Partial cranium BOU-VP-2/78 preserves the right and left horn core bases and portions of their associated frontals. The anterior portion of the parietal is also present. The metopic suture is intact between and just anterior to the horn core bases, but the orbital rims and

EBSCOhost - printed on 10/28/2022 4:53 AM via . All use subject to https://www.ebsco.com/terms-of-use

most of the anterior frontals have been lost. The posterior portion of the frontal endocranial surface is well preserved, as is the anterior portion of the parietal endocranial surface.

Aepycerotini

Some workers have considered Aepycerotini a sister tribe to Alcelaphini (Simpson 1945; Vrba 1984; Gentry 1985, 1992), but molecular phylogenetic analyses of *Aepyceros* do not suggest a firm phylogenetic nesting within any established bovid tribes or subfamilies (Gatesy et al. 1992; Gatesy et al. 1997; Matthee and Davis 2001; Kuznetsova and Kholodova 2003; Hernández-Fernández and Vrba 2005a). Thus, Aepycerotini is presented here as a tribe and is not presented within Antilopinae or Alcelaphinae. Aepycerotini first appears in the late Miocene as *Aepyceros,* and even early forms are readily placed in the modern genus (Vrba 1984). There is no conclusive evidence of more than one species of *Aepyceros* at any one time, and it is the single genus of the tribe (Vrba 1984). Aepycerotini has changed little over its evolutionary history since its first record in the late Miocene. Modern *Aepyceros* (impala) is notable for variation in size between subspecies. This diminishes the systematic significance of size differences in *Aepyceros* fossils from various sites, which might otherwise seem to imply an anagenetic increase in size (discussed in Vrba 1984).

Aepyceros Sundevall, 1845

GENERIC DIAGNOSIS "Small or medium sized antelopes. Horn cores are found in males, and are long, not very compressed, with flattened lateral surfaces and a posterolateral keel, with transverse ridges, inserted fairly uprightly, close together and above the back of the orbits, curving backwards in side view, strongly divergent in their lower parts but with a change of course in their centre and with distal parts parallel or re-approaching. Postcornual fossae deep, frontals hollowed internally and slightly higher between the horn core bases than the dorsal rim of the orbits, complicated mid frontals and parieto-frontal sutures on the skull top, braincase roof bent downwards posteriorly, side walls of braincase more or less parallel, temporal lines approaching fairly closely posteriorly, small supraorbital pits situated widely apart on a flat or slightly convex surface of the frontals, preorbital fossa very reduced or absent, ethmoidal fissure narrow or absent, a long narrow foramen between premaxilla and maxilla only known otherwise in *Neotragus moschatus* and *N. batesi* among Bovidae; premaxilla with a long contact with the nasal; mastoid large, occipital surface facing partly laterally on each side as well as backwards, and auditory bullae well inflated. Basioccipital with quite small anterior tuberosities with slight to moderate longitudinal ridges behind them, and with a wide shallow central longitudinal groove."

"Hypsodont teeth without basal pillars on the molars, strong styles and poor ribs on the lateral walls of the upper molars, a tendency to complicated central cavities on the upper molars, lower molars without transverse flanges (goat folds), M_3 with a large rear (third) lobe, P_4 with paraconid-metaconid fusion."

"The tuber scapulae is far from the lateral edge of the glenoid facet in ventral view. On the proximal end of the radius the lateral tubercle is small and situated at a lower level than the articular surface. The lateral articular facet is anteroposteriorly long and noticeably concave, and there is a medial rim on the medial facet" (Gentry 1985, 170–171).

EBSCOhost - printed on 10/28/2022 4:53 AM via . All use subject to https://www.ebsco.com/terms-of-use

FIGURE 3.9
Aepyceros cf. *melampus,* BOU-VP-2/50. A. Cranial view. B. Lateral view.

Aepyceros cf. *melampus* (Lichtenstein, 1812)

The Daka Member has two *Aepyceros* horn cores, both right sides. Specimen BOU-VP-2/50 (Figure 3.9) is attached to a large portion of frontal bone, and BOU-VP-4/18 retains most of the horn core to the tip. With maximum diameters of 34.7 mm and 40.6 mm, the two Daka Member *Aepyceros* horn cores are larger than any from the Shungura Formation and within the size range of modern *A. melampus* (Gentry 1985).

Antilopinae

Antilopinae is composed of the tribes Neotragini (dik-diks, pygmy antelopes, and allies) and Antilopini (gazelles and allies). The first fossil antilopines appear in the middle Miocene (Gentry 1990), and molecular work points to an early Miocene origin of the subfamily. Antilopini speciated during the middle and upper Miocene, predominantly in Eurasia (Vrba 1995b). Neotragini, which is likely paraphyletic or polyphyletic (Gentry 1992; Hernández-Fernández and Vrba 2005a), appears to have arisen in Africa toward the end of the Miocene, although fossil recovery biases likely influence such first appearances (Gentry 1990; Vrba 1995b).

EBSCOhost - printed on 10/28/2022 4:53 AM via . All use subject to https://www.ebsco.com/terms-of-use

Antilopini

Antilopini appears in Eurasia and Africa in the middle Miocene (Vrba 1995b). Hernández-Fernández and Vrba (2005a) suggest an early Miocene origin of the tribe. Kingdon (1982) posits that the modern distribution of the tribe is a relict of Miocene radiations. The proboscis is generally reduced in Antilopini, extremely so in some specialized taxa. Sight and hearing are well developed, and orbits and auditory bullae are large (Kingdon 1982). The internal systematics of Antilopini are not well resolved (Matthee and Robinson 1999; Hassanin and Douzery 1999a, b; Matthee and Davis 2001). Modern antilopines include the African genera *Gazella* (gazelles), *Antidorcas* (springboks), *Litocranius* (gerenuks), *Ammodorcas* (dibitags), and the Asian genera *Panthalops* and *Saiga*.

There are two different groups of antilopine horn cores in the Daka Member: a larger, annulated form and a smaller form without significant annulation. These groups are presented here as cf. *Antidorcas* and *Gazella*. The decision to place these in different genera follows Gentry's (1985) and Gentry and Gentry's (1978) work on Omo and Olduvai antilopines.

cf. *Antidorcas* Sundevall, 1845

Daka cf. *Antidorcas* consists of two horn cores, the most complete of which, BOU-VP-1/106 (Figure 3.10A and B), has an attached frontlet. Several features are consistent with *Antidorcas:* horn cores are not exceedingly compressed, horn cores have some annulation, and there is some hollowing of the frontal and horn core bases.

Gazella de Blainville, 1816

GENERIC DIAGNOSIS "Horn cores subcircular or elliptical in cross-section, with some mediolateral compression, the lateral surface often flatter than the medial, fairly uprightly inserted with backward curvature in side view, generally more obliquely set in females than in males of the same species, slightly divergent in anterior view, without keels or torsion; frontals without or almost without internal sinuses and the area between the horn core bases hardly raised above the level of the top of the orbital rims; moderately large triangular supraorbital pits at the base of the horn core pedicels slightly medial to the anteriormost edge of the pedicels; ethmoidal fissure present; moderate to large preorbital fossa; premaxilla generally contacting the sides of the nasals which have shortened during evolution; occipital low with each half often facing partly laterally as well as backwards; moderate to large auditory bullae; living species with hypsodont teeth but less hypsodont than in earlier fossil species; upper molars with moderately prominent styles and little development of ribs between them; lower molars without goat folds; M_3s often with the rearmost (third) lobe greatly enlarged; except in the east Asian subgenus *Procapra,* P_4s are without metacoid-paraconid fusion to form a complete medial wall at the front of the tooth" (Gentry and Gentry 1978, 436).

DESCRIPTION Right mandible BOU-VP-1/93 (Figure 3.10E) retains M_1 and M_2. Most of the mandibular body is present, with the exception of a few fragments of cortical bone. The sutural surface of the symphysis is intact, and the alveoli of all of the teeth, including that of the P_2, are visible. The molars present are worn, but otherwise intact. The mandibular ramus, condyle, and coronoid process are well preserved. The presence of a P_2 is not an *Antidorcas* feature, and this specimen is thus referred to *Gazella*.

EBSCOhost - printed on 10/28/2022 4:53 AM via . All use subject to https://www.ebsco.com/terms-of-use

FIGURE 3.10

Antilopini. cf. *Antidorcas.* A. BOU-VP-1/106 cranial view. B. BOU-VP-1/106 lateral view. *Gazella.* C. BOU-VP-2/35 lateral view. D. BOU-VP-2/35 cranial view. E. BOU-VP-1/93 occlusal view.

Specimen BOU-VP-2/35 (Figure 3.10C and D) is a good representative of Daka *Gazella* horn cores. It preserves the right horn core and frontlet. The superior border of the orbit is present, although the orbital rim is eroded. The specimen is relatively mediolaterally compressed, without annulation, and without internal hollowing of the frontal.

DISCUSSION *Gazella* has the broadest geographic range of any modern African bovid genus, with representatives in temperate Eurasia. *Gazella* is present in Africa beginning in the middle Miocene (Gentry and Gentry 1978; Harris 1991a). It is highly speciose. Gentry and Gentry (1978) separate the genus into four groups: the Asian subgenus *Procapra* with the Persian *G. subgutturosa;* a west Asian and African group comprising *G. bennetti* of the Levant and *G. dorcas* of northern and eastern Africa (possibly also including *G. cuvieri* of North Africa, *G. leptoceros* of the Sahara, and *G. spekei* of Somalia); *G. rufifrons* of western Africa with *G. thomsoni;* and finally the western African *G. dama* with the northeastern

EBSCOhost - printed on 10/28/2022 4:53 AM via . All use subject to https://www.ebsco.com/terms-of-use

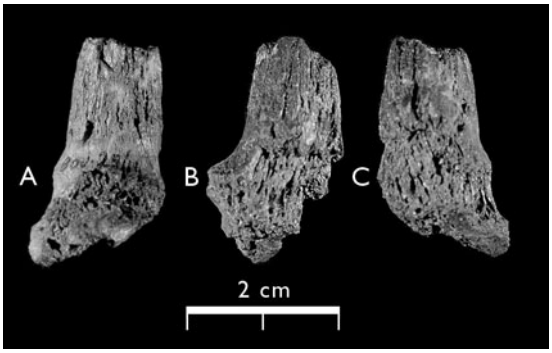

FIGURE 3.11
Neotragini, BOU-VP-25/11. A. Medial view. B. Cranial view. C. Lateral view.

African *G. soemmerringi* and the eastern African *G. granti* (Gentry and Gentry 1978). The eastern African group, *G. nanger* (subgenus), has been given subgeneric status by some and has been suggested by others to be a separate species. Morphological differences between species are subtle (Gentry 1978), and Daka *Gazella* is not assigned to species.

Gazella fossils from the Daka Member are relatively rare. They comprise four horn cores and one mandible. Horn core specimens have been identified as *Gazella* based on compression with minimal annulation and no internal hollowing.

Neotragini

Neotragines are widespread in Africa by the Pliocene (Gentry 1990). Molecular evidence suggests that traditionally defined Neotragini is not monophyletic (Kuznetsova and Kholodova 2003; Hernández-Fernández and Vrba 2005a). Modern neotragines, all small, are assigned to six genera: *Neotragus, Raphiceras, Ourebia, Oreotragus, Dorcotragus,* and *Madoqua*.

Daka Member Neotragini comprises a single specimen, BOU-VP-25/11 (Figure 3.11). This specimen preserves the base of the left horn core and a small amount of frontal. It is assigned to Neotragini based on its very small size and upright horn core projection.

Bovinae

Bovinae is composed of the tribes Tragelaphini, Boselaphini, and Bovini, and its monophyly is well resolved (Hernández-Fernández and Vrba 2005a). *Eotragus*, the first known fossil representative of Bovinae to appear, is placed in Boselaphini, and there is general acceptance of its Bovinae status, if not its boselaphine one (Gentry 2000b). Hernández-Fernández and Vrba (2005a) suggest a late Oligocene divergence of Bovinae from the rest of Bovidae. The two living Indian boselaphines, *Boselaphus* and *Tetracerus* (Nigali and Chousinga), are relicts of a once broader distribution of the tribe, and it is thought that Bovinae's earliest radiations were boselaphines (Gentry 2000b).

Bovini

Gentry (1990) suggests that Bovini is a descendant of Boselaphini. Bovini and Tragelaphini do not appear in the fossil record until the late Miocene, well after Boselaphini's wide

EBSCOhost - printed on 10/28/2022 4:53 AM via . All use subject to https://www.ebsco.com/terms-of-use

dispersal (Vrba 1995b). Hernández-Fernández and Vrba (2005a) suggest that Bovini and Tragelaphini diverged in the early Miocene. Modern bovines include the genera *Bison* (buffalos), *Bos* (cows and allies), *Bubalus* (Asian water buffalo), and *Syncerus* (cape buffalo). Molecular phylogenetic analyses split the group, suggesting that African and Asian buffaloes *(Syncerus/Bubalus)* form one clade and that yaks, bison, oxen, cows, zebus, and gaurs form another (Buntjer et al. 2002). Bovini is diagnosed by low, broad crania with short muzzles and smooth, laterally oriented horns with frontal sinuses (Kingdon 1982). Gentry (1992) suggests that the Plio-Pleistocene genus *Pelorovis* is more similar to the African buffalo *Syncerus* than to the Asian buffalo *Bubalus* and that *Simatherium* and *Ugandax* are its probable ancestors. Geraads (1995) performed a cladistic analysis on African Bovini, resulting in *Ugandax* and *Simatherium* being sister taxa to a clade containing *Pelorovis* and *Syncerus*.

Bovine teeth were not separated by species. Isolated dental specimens from the Daka Member were identified as Bovini, and their dimensions are presented in Appendix 3.1. The average mesiodistal length of the lower second molars in Daka specimens is approximately equal to a combined average of Olduvai Bed II *Syncerus* and *Pelorovis* measurements (Gentry and Gentry 1978).

Massive, broad, and arching horn cores characterize *Pelorovis* (Gentry 1967). The genus is present as early as Members D and F of the Shungura Formation, and these early representatives are smaller than later forms (Gentry 1985, 1990). *Pelorovis* is present from the late Pliocene to the Holocene. The earliest form, *P. turkanensis,* is known from the KBS member at Koobi Fora (Harris 1991a). *Pelorovis antiquus* likely survived late, as paintings of it are reported from Holocene prehistoric sites (Gautier and Muzzolini 1991; Klein 1994). There is some disagreement regarding the generic status of late *Pelorovis*. Gentry and Gentry (1978) and Klein (1994) include *antiquus* in *Pelorovis,* while others suggest that *antiquus* might belong in *Syncerus* (Geraads 1992; Peters et al. 1994). Gautier and Muzzolini (1991) go further, suggesting that *P. antiquus,* a long horned, late member of the genus, and others of the genus are *Syncerus caffer* subspecies. Klein (1994) disagrees, suggesting that *P. antiquus* is a distinct species. Daka *Pelorovis* specimens present two distinct horn core morphologies. One form is similar to *P. turkanensis* and *P. oldowayensis,* with horns that emerge from the frontal caudally, then curve tightly ventrally (see Figures 3.12 and 3.13). The other morphotype is similar to *P. antiquus,* with horn cores that emerge from the frontal with a slight ventral orientation, extend laterally with little curvature, then curve cranially at the tips. The co-occurrence of *P. antiquus* and *Syncerus* in the Daka Member supports generic separation of *Syncerus* and *P. antiquus* (contra Gautier and Muzzolini 1991).

Pelorovis Reck, 1928

GENERIC DIAGNOSIS "Extinct large African bovines with massive, long, curved horn cores, slightly compressed dorsoventrally and without keels; both sexes with horns; frontals hollowed internally; no ethmoidal fissures; nor preorbital fossae; premaxillae either not reaching the nasals or having only a short contact; nasals fairly short; vomer not fused to the back of the palate; occipital low and wide; P_4s with paraconid and metaconid growing close together and usually fusing in late wear" (Gentry and Gentry 1978, 310).

EBSCOhost - printed on 10/28/2022 4:53 AM via . All use subject to https://www.ebsco.com/terms-of-use

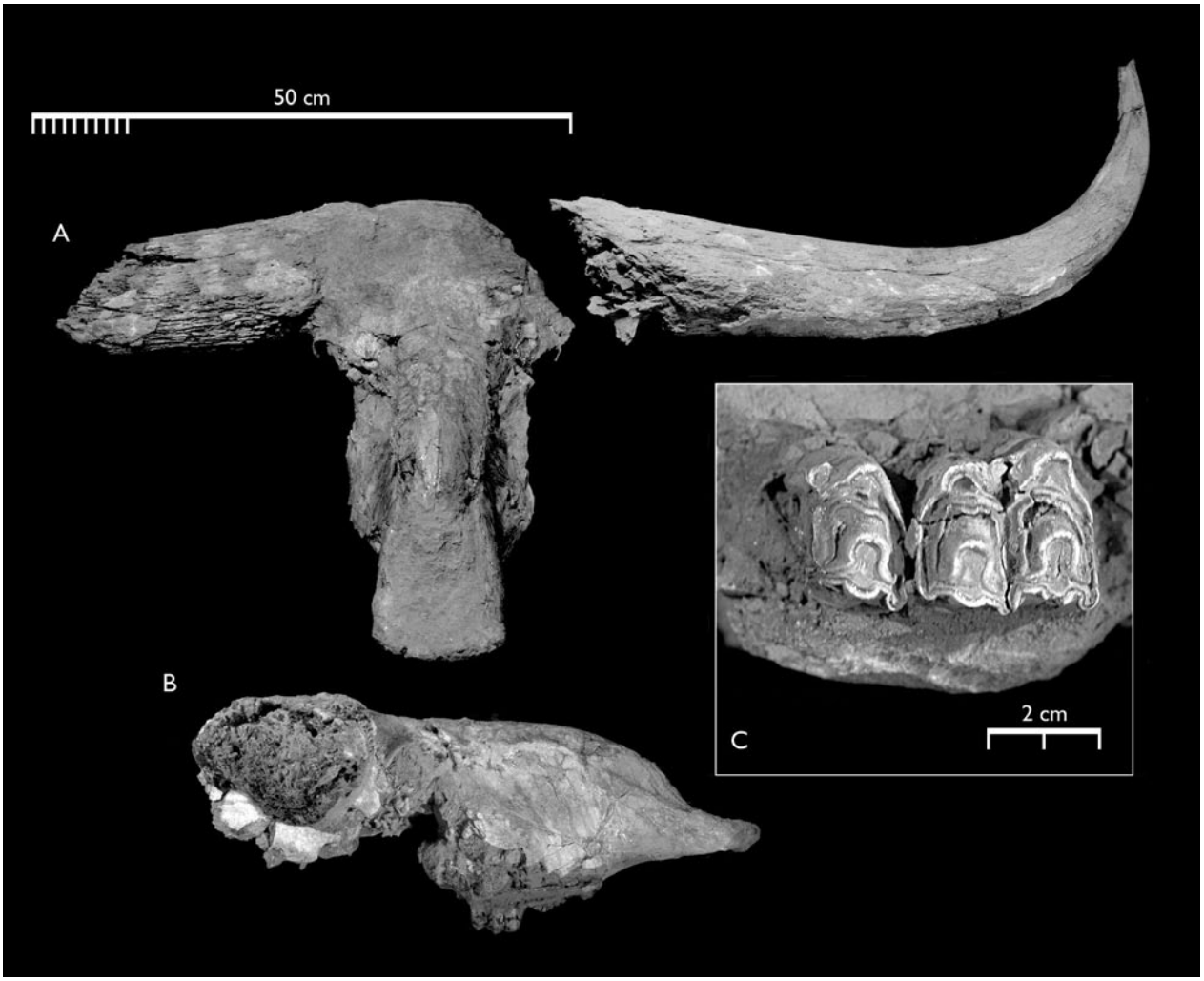

FIGURE 3.12

Pelorovis antiquus, BOU-VP-3/1. A. Cranial view. B. Lateral view. C. Occlusal view.

Pelorovis sp.

One specimen, BOU-VP-3/109 (Figure 3.14), represents *Pelorovis* sp. While this specimen cannot be attributed to species, its juvenile status renders it important enough to note. Specimen BOU-VP-3/109 preserves right and left horn cores, parietal, partial right and left maxillae, and several other cranial fragments. The maxillae bear a complete RM^2, LM^1, LM^2, an unerupted RM^3, and an unerupted LM^3. The cranium is fragmentary and presents portions of the frontal, parietal, and maxillae. The frontoparietal (coronoid) suture is not ossified. The horn cores are in an early stage of growth and project laterally from the frontals. This specimen is placed in *Pelorovis* based on the moderate basal and nasal projection of its horns from the frontals and their length. Both of these features differ from *Syncerus*.

Pelorovis oldowayensis Reck, 1928

DIAGNOSIS "Horn cores not hollowed internally, inserted close together and so far posteriorly as frequently to overhang the occipital surface, curved backwards from the base,

EBSCOhost - printed on 10/28/2022 4:53 AM via . All use subject to https://www.ebsco.com/terms-of-use

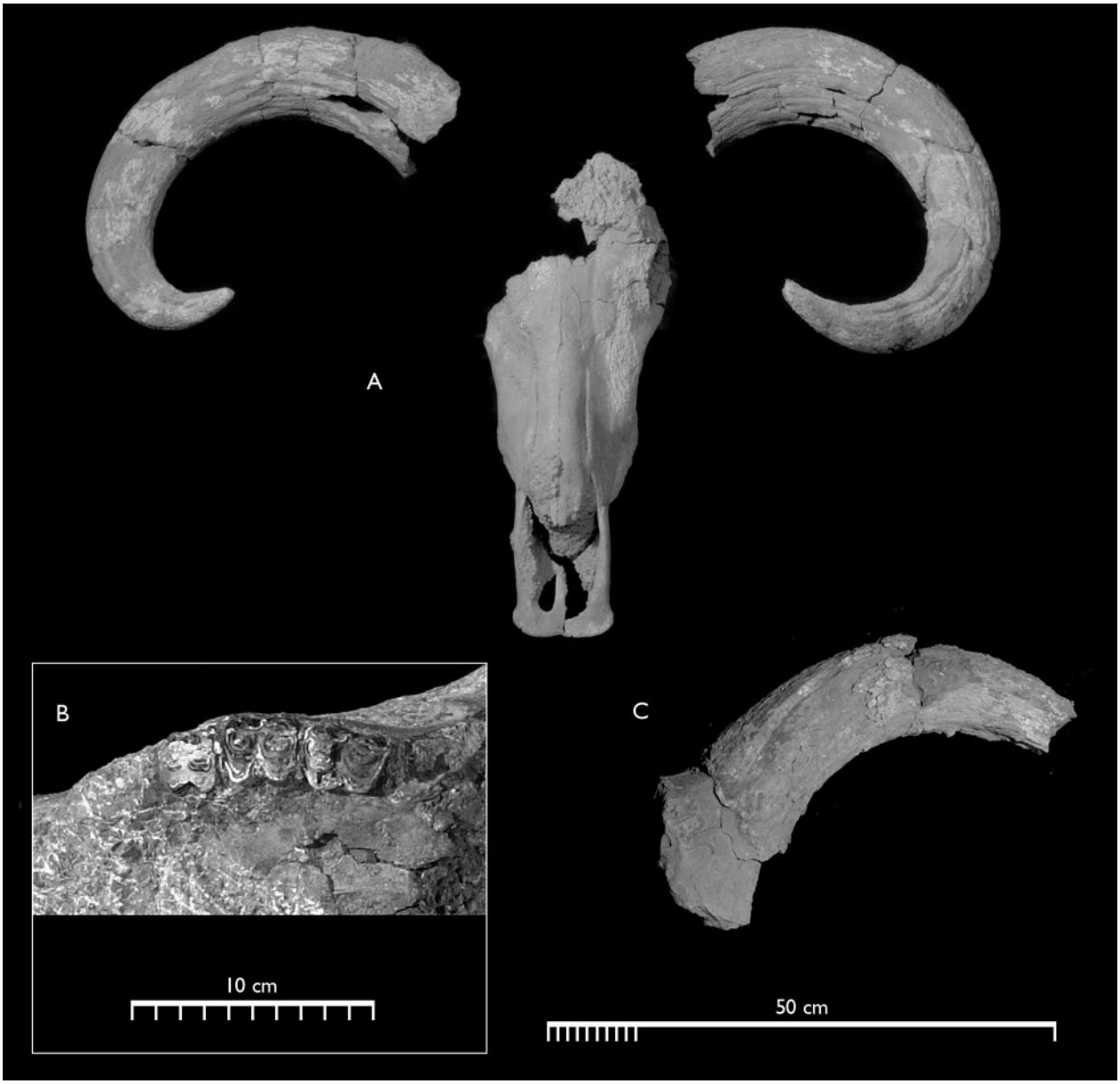

FIGURE 3.13

Pelorovis oldowayensis. A. BOU-VP-1/78 cranial view. B. BOU-VP-1/78 occlusal view. C. BOU-VP-1/77 cranial view.

then outwards and finally forwards and a little bit upwards; nasals domed transversely; anterior part of the zygomatic arch thickened below the orbits; anterior tuberosities of the basioccipital rather wide apart for a bovine; molars with small basal pillars and central cavities simple in outline; upper molars with poorly localized and outbowed ribs between the lateral styles; mandibles with deep horizontal rami" (Gentry and Gentry 1978, 310).

DESCRIPTION Partial cranium BOU-VP-1/78 preserves the snout and horn cores. The premaxilla is present, as are nasals, maxillae, left lacrimal, left anterior zygomatic, and some of the proximal frontal. Some vault fragments are present, but they are not articulated. None

EBSCOhost - printed on 10/28/2022 4:53 AM via . All use subject to https://www.ebsco.com/terms-of-use

FIGURE 3.14

BOU-VP-3/109. Juvenile *Pelorovis* sp. A. Cranial (maxillae a view from lateral) view. B. Occlusal view. Note that many more fragments of this fossil exist than are figured here.

of the basicranium is preserved. Neither right nor left horn core preserves a base, but their orientations can be determined by means of their completeness via comparison to BOU-VP-1/77, which preserves the connection of the horn core to the frontal (see Figure 3.13). The horn cores project from the frontal caudally and laterally, and they curve tightly for their whole length nasally and cranially. While preservation of the specimen prevented taking any of the metrics reported in Appendix 3.3, it is clear that BOU-VP-1/78 is more gracile than the *P. antiquus* specimens from the Daka Member.

EBSCOhost - printed on 10/28/2022 4:53 AM via . All use subject to https://www.ebsco.com/terms-of-use

Specimen BOU-VP-1/77 preserves the base of the horn core, allowing assessment of the projection of the horn from the base. It emerges with a caudal orientation and has an even curvature similar to that seen in BOU-VP-1/78. The horn core emerges from the most posterior part of the cranium, overhangs the occipital, and does not present a thick bony ridge that would have extended between the horn core bases.

DISCUSSION Specimens BOU-VP-1/78 (Figure 3.13A and B) and BOU-VP-1/77 (Figure 3.13C) have tightly curved, inferiorly oriented horn cores. In the latter specimen, where more-or-less complete morphology is preserved, the spiral curvature exceeds 270°, and the spiral is also tight in the former. The morphology of these specimens is consistent with *Pelorovis oldowayensis*.

Pelorovis antiquus (Duvernoy, 1851)

DIAGNOSIS "A species of *Pelorovis* with horn cores normally curved forwards and downwards from the base, inserted widely apart and behind the orbits but less posteriorly than in *P. oldowayensis;* anterior part of the zygomatic arch not thickened below the orbits; face shorter and tooth row set less anteriorly than in *P. oldowayensis;* occipital surface low and wide; molars with larger basal pillars and central cavities more complicated in outline, and upper molars with more localized and outbowed ribs between the styles than in *P. oldowayensis*" (Gentry and Gentry 1978, 312).

DESCRIPTION Cranium BOU-VP-3/1 is a very complete *Pelorovis* cranium. It preserves both horn cores, the frontals including the superior orbital rims, the parietal, and the superior portions of the temporals. The occipital, basisphenoid, zygomatic processes, sphenoid, and palatine are absent. The lacrimals, maxillae, and premaxillae are present and the maxilla preserves the left M^2 and the mesial half of the M^3. Other teeth are not present. The alveolar row of the right maxilla is damaged and eroded. The horns of BOU-VP-3/1 project from the bases with a slight basal orientation and curve upwards laterally, with tighter curvature toward the tip.

Cranium BOU-VP-3/8 is the most complete Daka Member *Pelorovis*. It lacks the anterior premaxillae, the distal end of the left horn core, and some of the right side of the cranial vault, which has been cleanly broken away lateral to the sagittal plane defined by the buccal margin of the molars and the mastoid process. On the left side, the M^3 through M^1 remain intact, and premolars are fractured just above the roots, which remain in the alveoli. On the right side the M^2 and M^3 are visible, but mesial to these teeth the alveolar bone and additional teeth are missing. The preserved right horn core does not emerge from the frontal with any basal orientation as it does in BOU-VP-3/1. Rather, it emerges with a caudal orientation. Specimen BOU-VP-3/8 also has shorter, more evenly curved horn cores and is a smaller individual.

DISCUSSION The two specimens referred to *P. antiquus,* BOU-VP-3/1 (Figure 3.12) and BOU-VP-3/8, are considerably larger than those specimens referred to *P. oldowayensis*. Both Daka *P. antiquus* specimens present upturned horns that differ strikingly in their morphology from those referred to *P. oldowayensis*. Daka *P. antiquus,* while larger overall,

EBSCOhost - printed on 10/28/2022 4:53 AM via . All use subject to https://www.ebsco.com/terms-of-use

has a relatively shorter face and horns that insert less posteriorly than those of Daka *P. oldowayensis*.

Syncerus Hodgson, 1847

GENERIC DIAGNOSIS "Moderate-sized to large African bovines with wide skulls and short faces; horn cores short to moderately long, dorsoventrally compressed, often with keels, and emerging transversely from just behind the orbits; females with horns; supraorbital pits fairly close together; occipital surface low and wide; molars with moderate-sized basal pillars and central cavities without such an extremely complicated outline as in *Bos*; upper molars without such pronounced ribs between the styles as in *Bos*; the occlusal complexity of the teeth increasing with increased body size; P_4 with paraconid and metaconid growing towards one another or fused."

"The following characters, known only from living species, are also quite likely to be valid for the genus; nasals fairly short, without lateral flanges anteriorly, and in a plane nearly parallel to the tooth row giving the face quite a high profile; no ethmoidal fissures; no preorbital fossae; premaxillae with only a short or no contact on the nasals; vomer not fused to the back of the palate" (Gentry and Gentry 1978, 313).

DESCRIPTION Cranium BOU-VP-1/36 (Figure 3.15) preserves the right and left horn cores, frontals, parietal, and occipital. Anterior portions of the frontals are broken away to expose frontal sinuses. Cranium BOU-VP-1/36 preserves most of the right temporal, including the petrous portion, glenoid fossa, mastoid region, and some of the left temporal. The zygomatic processes have been broken from both sides. The basisphenoid is present, as is most of the sphenoid. The lower face is missing.

Specimen BOU-VP-1/36 differs from robust modern *S. caffer* in lacking basal bossing on the horn cores and in its more triangular basal cross section. The horn cores are only internally hollowed toward the base and are markedly keeled posteriorly. Both of these features and the lack of basal bossing are similar to *S. acoelotus* from Olduvai (Gentry and Gentry 1978). Gentry and Gentry (1978) contrast the keeled horn cores of *Syncerus* with the unkeeled horns of *Pelorovis*.

DISCUSSION *Syncerus* first appears conclusively at Omo in lower Member G. The genus includes the modern Cape buffalo, *S. caffer,* and the late Pliocene and Pleistocene *S. acoelotus*. The co-occurrence of *Syncerus* with *Pelorovis antiquus* in the Daka Member diminishes the likelihood that the latter is a *Syncerus caffer* subspecies (contra Gautier and Muzzolini 1991). The presence of *Syncerus* in the Daka Member is consistent with genetic work indicating a Pleistocene origination and range expansion of the genus (Hooft et al. 2002).

Tragelaphini

Hernández-Fernández and Vrba (2005a) suggest that Bovini and Tragelaphini diverged in the early Miocene. Tragelaphini fossils first appear in Africa in the late Miocene (Gentry 1985; Vrba 1995b), and multiple forms are present in the late Miocene Adu-Asa Formation of the Middle Awash (Haile-Selassie 2001). There are several Pliocene

EBSCOhost - printed on 10/28/2022 4:53 AM via . All use subject to https://www.ebsco.com/terms-of-use

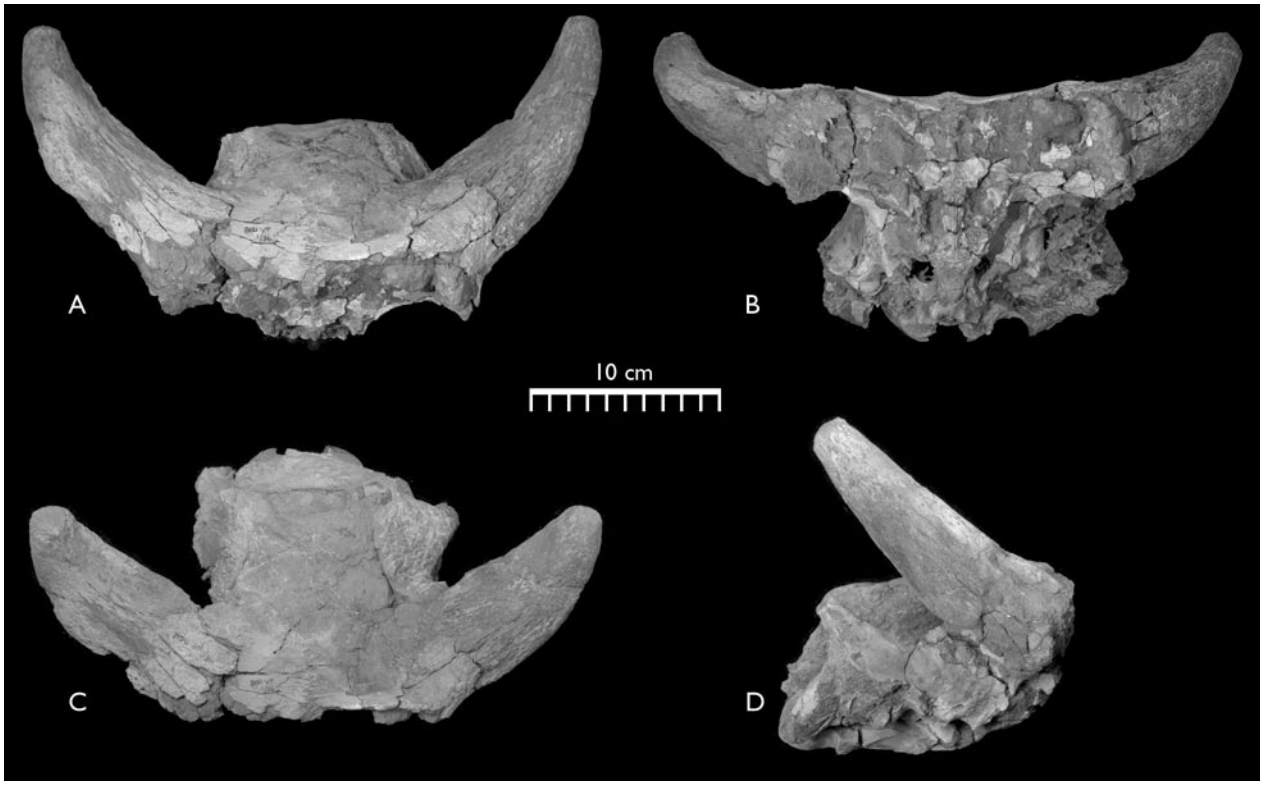

FIGURE 3.15

Syncerus, BOU-VP-1/36. A. Cranial view. B. Basal view. C. Dorsal view. D. Lateral view.

tragelaphine species from eastern Africa. Modern tragelaphines include elands, bongos, kudus, nyalas, bushbucks, and sitatungas. All are exclusively African. Tragelaphini horn cores are spiraled and keeled. Cheek teeth are brachydont, lack basal pillars, and lack ribs between the styles of upper molars (Gentry 1990). There are two commonly recognized modern genera: *Taurotragus*, the eland, and *Tragelaphus,* the kudu. A separate *Taurotragus* clade, however, has not withstood molecular phylogenetic analysis (Gatesy et al. 1997), and the eland is now thought of as a derived group within *Tragelaphus*. Tragelaphine teeth are primitive, yet highly distinctive, possessing the following characters to the exclusion of other bovids: roots, molars with pronounced crests on the lophs when viewed from a lateral perspective, crested premolars, deep fissures separating lophs on lingual upper and buccal lower molars, and a central island of enamel on molars that is crescent shaped.

Except for the eland, *Tragelaphus* is easily defined. It includes all spiral-horned bovids. The earliest representatives are from the late Miocene (Gentry 1985; Haile-Selassie 2001). Modern taxa include the nyala, sitatunga, bushbuck, bongo, greater and lesser kudus, and the eland. Greater and lesser kudus, *T. strepsiceros* and *T.* cf. *imberbis,* both have relatively long horns with respect to other *Tragelaphus*. The helices of kudu horns are high in both spiral amplitude and frequency relative to those of non-kudu species.

The Daka member has two groups of kudu-clade *Tragelaphus* that are differentiated based on horn core size. Non-kudu *Tragelaphus* in the Daka Member is represented by *T.* cf.

EBSCOhost - printed on 10/28/2022 4:53 AM via . All use subject to https://www.ebsco.com/terms-of-use

scriptus, which has less tightly spiraled horns. There is only one *Tragelaphus* dental specimen in the assemblage, BOU-VP-3/130, a left mandible. It is larger than *T.* cf. *imberbis* but is not assigned to a species.

Tragelaphus Blainville, 1816

GENERIC DIAGNOSIS "Medium to large tragelaphines with spiraled horn cores inserted closely together and having an anterior keel and sometimes a strong posterolateral one; small to medium sized supraorbital pits, which are frequently long and narrow; occipital surface tending to have a flat top edge and straight sides" (Gentry and Gentry 1978, 297).

Tragelaphus cf. *imberbis* Blyth, 1869

Tragelaphus cf. *imberbis* in the Daka Member comprises 11 horn cores with bases. Identification of these specimens as kudus is based on horn core morphology, specifically the amplitude and wavelength of the helical spiral. The most complete *T.* cf. *imberbis* horn core is BOU-VP-26/15 (Figure 3.16B). This specimen presents a right horn core with some of the base. Approximately 20 cm of the proximal horn core remains intact. Specimen BOU-VP-26/15 presents a tight spiral and pronounced keels. Most of the *T.* cf. *imberbis* specimens in the Daka Member preserve only the horn core bases. Their provisional assignment to species is based on keeling and small size.

Tragelaphus cf. *scriptus* (Pallas, 1766)

Tragelaphus cf. *scriptus* in the Daka Member is based on a single specimen, BOU-VP-25/8 (Figure 3.16A). This specimen preserves the left horn core, the frontlet, and the base of the right horn core. It is intermediate in size between *T.* cf. *imberbis* and *T. strepsiceros* in the assemblage and does not present the tight helices of the kudus in the sample.

Tragelaphus strepsiceros (Pallas, 1766)

DIAGNOSIS "A large species of *Tragelaphus* with strongly and openly spiraled horn cores, anterior keel present but posterolateral keel reduced and tending to be present only distally; compared with other *Tragelaphus* species the horn cores are more uprightly inserted and are not anterior-posteriorly compressed; braincase short; a low occipital" (Gentry and Gentry 1978).

DESCRIPTION The most complete *T. strepsiceros* horn core is BOU-VP-1/32 (Figure 3.16C). This specimen comprises right and left horn cores and much of the frontal. The left supraorbital margin is partially intact. Some of the endocranial surface of the frontal is preserved. The horns show a pronounced keel, starting at the anteromedial aspect of the proximal horn core base and twisting clockwise on the right horn. Approximately 20 cm of each proximal horn core remains intact.

DISCUSSION *Tragelaphus strepsiceros* and *T.* cf. *strepsiceros* in the Daka Member consist of two horn cores and a partial cranium with horn core bases. Identification of these specimens as kudus is based on horn core morphology, specifically the amplitude

EBSCOhost - printed on 10/28/2022 4:53 AM via . All use subject to https://www.ebsco.com/terms-of-use

FIGURE 3.16
Tragelaphini. Cranial views. A. BOU-VP-25/8 (*Tragelaphus* cf. *scriptus*). B. BOU-VP-26/15 (*Tragelaphus imberbis*). C. BOU-VP-1/32 (*Tragelaphus strepsiceros*).

and wavelength of the helical spiral. Their attribution to *T. strepsiceros* is based on their large size.

Caprinae

Grubb (2001) includes the tribes Caprini, Ovibovini, Naemorhedini, and Rupicaprini in Caprinae. Hernández-Fernández and Vrba (2005a) present Caprinae as monophyletic, but point out that with the exception of Caprini's relatively robust signal of monophyly, the positions of other tribes in the subfamily, including Ovibovini (which is possibly represented in the Daka Member), remain ambiguous. Caprinae tribes appear to have diverged in the early middle Miocene (Hernández-Fernández and Vrba 2005a).

EBSCOhost - printed on 10/28/2022 4:53 AM via . All use subject to https://www.ebsco.com/terms-of-use

Caprini

The roots of Caprini potentially extend into the middle Miocene (Gentry 2000a, b; Hernández-Fernández and Vrba 2005a). After initial Miocene radiations, caprines were probably replaced in richer areas of Eurasia by cervids and bovines, and their modern relict distribution in marginal, high-elevation habitats is likely the result of this evolutionary event (Kingdon 1982). Modern caprines are distributed mostly in temperate zones, with only one undomesticated species in Africa, the ibex *(Capra ibex)*.

Bouria Vrba, 1997

GENERIC DIAGNOSIS This genus has a single species, and the diagnosis is presented below.

Bouria anngettyae Vrba, 1997

DIAGNOSIS "Extinct medium-sized caprines with a new combination of plesiomorphic and advanced features: horn cores that are long and large for the skull as in living *Capra,* resembling the living *C. ibex* in being basally very close, medially flattened, compressed, but little angled to the midfrontal suture, very upright to the braincase, and strongly backbent with hardly any tendency to torsion; strong raising of frontals between horn core bases and elongation of the frontal between the horn core and orbit as in *Hemitragus* and more advanced than in *C. ibex;* braincase roof shorter than living *Capra* and with a higher angle to the occipital surface; and a longer, narrower basioccipital, less flat and with less widened anterior tuberosities, and larger auditory bullae than in advanced living caprines but resembling the extinct *Tossunnoria* and *Sivacapra*. Horn core bases have a greatest mediolateral diameter situated posteriorly, an anteromedial keel that sharpens progressively higher up, and a posterior cross-section that is more rounded basally but also develops a progressively sharper keel towards the horn core tip" (Vrba 1997, 182 and 186).

DESCRIPTION Cranium BOU-VP-1/44 (Figure 3.17) is the holotype and most complete of the *B. anngettyae* crania in the Daka Member. It preserves nearly the entire left horn core and the base of the right. The anterior frontal is broken away, but portions of the orbital rims of the left and right orbits remain. Most of the braincase and basicranium are well preserved, but the occipital condyles and inferior temporals are missing. The lower face is not present. This specimen is described in detail in Vrba (1997).

Cranium BOU-VP-2/18, also discussed by Vrba (1997), preserves a right horn core, complete with the exception of its distal tip. It preserves much of the right frontal, with the metopic sutural surface and a portion of the right orbit. Frontal sinus and the basal horn core sinus are exposed. A large portion of the right parietal with some endocranial surface is preserved. The anterior portion of the right temporal is also present, including some petrous bone.

Cranium BOU-VP-1/17, also discussed by Vrba (1997), preserves a nearly complete calvaria that is missing the left horncore and most of the exterior cortex of the left frontal. Some fragments of the right orbital rim are missing, as is some of the cortex surrounding the right frontal sinus. Both zygomatic processes are missing, as are the inferior portions of both orbital rims. Surface detail is generally well preserved. The lower face is missing.

EBSCOhost - printed on 10/28/2022 4:53 AM via . All use subject to https://www.ebsco.com/terms-of-use

FIGURE 3.17

Bouria anngettyae, BOU-VP-1/44. A. Cranial view. B. Lateral view. C. Dorsal view. D. Basal view.

EBSCOhost - printed on 10/28/2022 4:53 AM via . All use subject to https://www.ebsco.com/terms-of-use

Cranium BOU-VP-2/60 preserves the right horn core and much of the cranium. The left horn core base is present. The right and left orbital rims are missing, and the anterior frontal is broken away. The occipital, inferior temporals, and basisphenoid are missing. Matrix encases the left half of the cranium, but the surface of the right half is well preserved. The basicranium is eroded, but present. The lower face is absent.

DISCUSSION *Bouria*'s first and last appearance dates are currently in the Daka Member. Although it is similar in many ways, *Bouria* has many features that distinguish it from ibexes, indicating that it is not a member of this lineage (Vrba 1997). Vrba suggests that it is possibly a sister to *Hemitragus* (tahrs), a Eurasian caprine genus with species in the Himalayas, India, and Oman. *Bouria* also shares some features with early caprines such as *Sivacapra* and *Tossunnoria,* also possible ancestors to tahrs.

Bouria anngettyae is relatively common in the Daka Member. There are four crania from which measurements could be taken (Appendix 3.3), and ten specimens from which horn core measurements could be taken (Appendix 3.2).

Daka *B. anngettyae* and *Parmularius angusticornis* are very similar. The taxa differ primarily in the larger amount of lateral basal swelling on horn cores, the less pronounced horn core basal mediolateral compression, and the shorter overall horns found in *P. angusticornis*. *Bouria* horn cores are more compressed mediolaterally, with cross sections that become tight ellipses at their base. In profile, *Bouria* horn cores are longer and more crescent-shaped, and the horn core pedicles do not have large lateral bulges. Three specimens (BOU-VP-2/51, BOU-VP-2/42, and BOU-VP-2/58) are referred to cf. *Bouria* cf. *anngettyae* because of the difficulty in distinguishing them from *P. angusticornis*.

aff. *Ovibovini*

Fossil ovibovines appear in Africa in the late Miocene (Gentry 1992). Ovibovini's modern distribution is Eurasian, and the taxon includes modern musk oxen and takins, two very different creatures. Gentry (1992) considers these large differences evidence for an early dispersal. Gentry also notes that late Miocene ovibovines were morphologically diverse in horn core and occipital morphology but share with each other and modern taxa a number of discrete morphological characters. Many workers note that Ovibovini, as traditionally defined, might not be monophyletic (Gentry 1996; Vrba 1997; Hernández-Fernández and Vrba 2005a). The single Daka representative associated with this group is only provisionally placed in the tribe (see Vrba 1997).

Nitidarcus Vrba, 1997

GENERIC DIAGNOSIS This genus has a single species, and the diagnosis is presented below.

Nitidarcus asfawi Vrba, 1997

DIAGNOSIS "A medium to large sized bovid with moderately long horn cores that pass forward at the base at a very high angle to the braincase and recurve backward strongly towards the tip; a large, smooth walled sinus in frontals and pedicles extending into the horn core base; horn cores basally compressed, inserted moderately closely together and

EBSCOhost - printed on 10/28/2022 4:53 AM via . All use subject to https://www.ebsco.com/terms-of-use

above the back and behind the orbit, moderately divergent, without transverse ridges, and with fairly strong clockwise torsion on the right; supraorbital foramina in small pits and wide apart on a broad, slightly convex forehead; dorsal orbital margins projecting strongly and closely beneath the horn core bases; midfrontal suture simple; temporal lines poorly marked and very far apart; braincase without a parietal boss, and with sides nearly parallel, moderately to strongly bent relative to the face and fairly short; occipital surface facing mostly backwards, with a rounded dorsal outline, and with the mastoid situated entirely on it; basioccipital with an approach to shape that is triangular rather than rectangular because the laterally splayed posterior tuberosities are distinctly wider apart than the anterior ones; anterior tuberosities posteriorly further apart than anteriorly with a shallow space rather than a deep groove between them, a slight spine extending backwards behind the anterior tuberosities, followed by a valley that widens posteriorly towards a broad hollow between posterior tuberosities; in the central part of the basioccipital there is some lateral constriction and marked longitudinal ridges are absent; auditory bulla moderately sized; paroccipital process quite wide, with mediolaterally broadened proximal parts and distal parts pointing downwards rather than recurving in a medial direction" (Vrba 1997, 177).

REMARKS Vrba (1997) described BOU-VP-1/9 (Figure 3.18) in detail. Since Vrba's work, two additional horn cores have been identified, BOU-VP-19/23 and BOU-VP-1/15g *Nitidarcus asfawi* is not abundant in the Daka fauna.

DESCRIPTION Cranium BOU-VP-1/9 (Figure 3.18) is the complete calvaria and the holotype of *N. asfawi*. It preserves the right and left horn cores in their entirety and is very well preserved. The most anterior part of the frontal is broken away, but most of the orbital rims remain intact. The zygomatic processes are missing, and the inferior temporals are abraded, but the basicranium is otherwise intact. None of the facial skeleton anterior to the frontals remains.

Hippotraginae

Simpson (1945), Gentry (1992), and Hernández-Fernández and Vrba (2005a) suggest a sister relationship between subfamilies Hippotraginae and Alcelaphinae. Hernández-Fernández and Vrba (2005a) suggest that these two groups diverged from one another in the later early Miocene. The earliest known hippotragine fossils date to the late Miocene and derive from Lothagam, Kenya, and the Adu-Asa Formation of the Middle Awash (Leakey and Harris 2003; Haile-Selassie 2001). It is likely that these late first appearance dates are artifacts of an incomplete fossil record. Numerous genera and species are known from the Pliocene and Pleistocene of Africa and Asia (Vrba and Gatesy 1994). Modern forms include three genera: *Hippotragus, Oryx,* and *Addax*. *Hippotragus* includes *H. equinus* and *H. niger*, the roan antelope and sable antelope. *Oryx* includes three species: *O. gazella* (oryx), *O. leucoryx* (Arabian oryx), *O. dammah* (scimitar-horned oryx). *Addax nasomaculatus*, the Saharan addax, is the lone species of its genus.

Hippotraginae is united by an array of morphological characters, including long horn cores that have a large basal area, no keeling, little divergence in projection, and

EBSCOhost - printed on 10/28/2022 4:53 AM via . All use subject to https://www.ebsco.com/terms-of-use

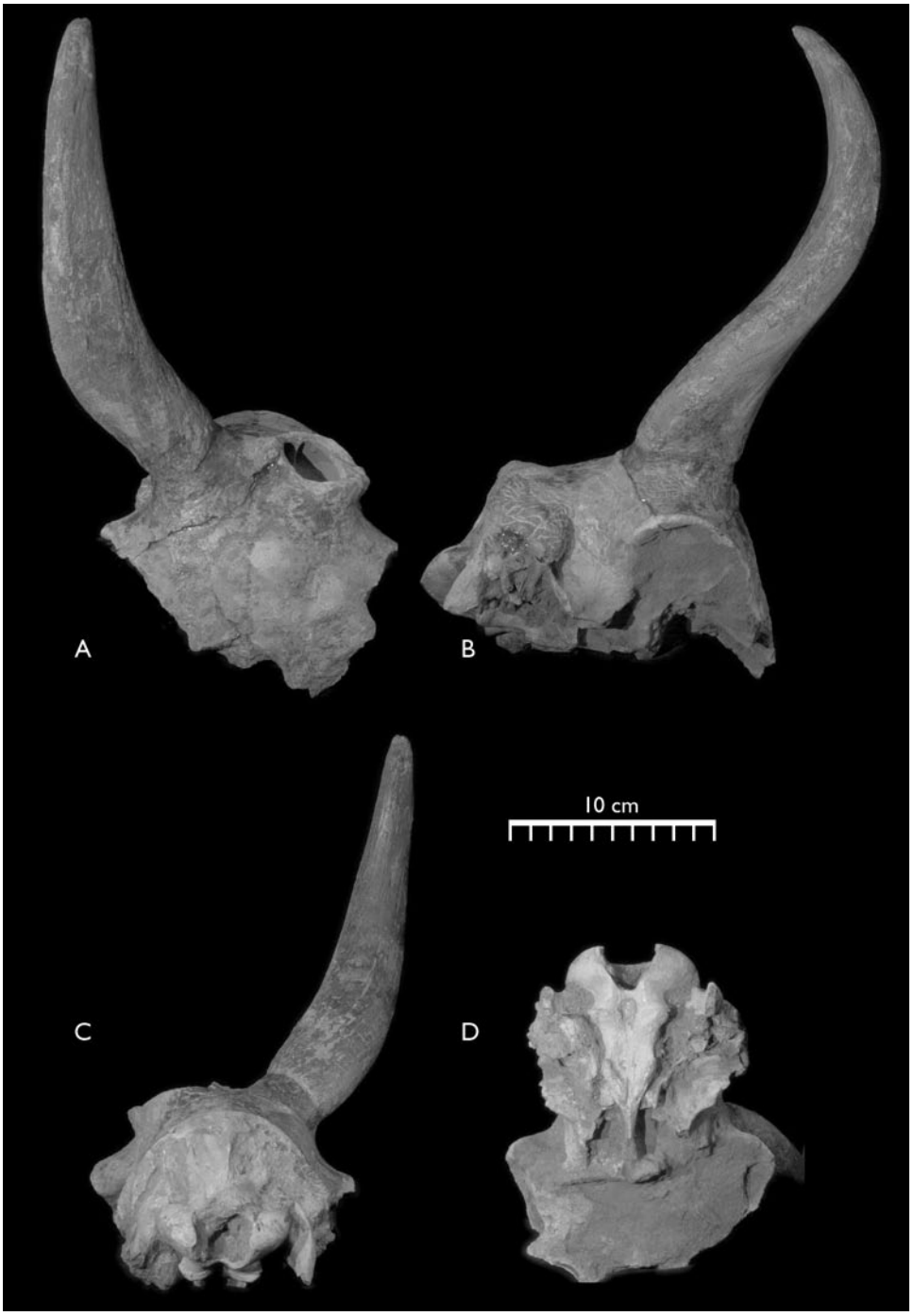

FIGURE 3.18

Nitidarcus asfawi, BOU-VP-1/9. A. Cranial view. B. Lateral view. C. Caudal view. D. Basal view.

EBSCOhost - printed on 10/28/2022 4:53 AM via . All use subject to https://www.ebsco.com/terms-of-use

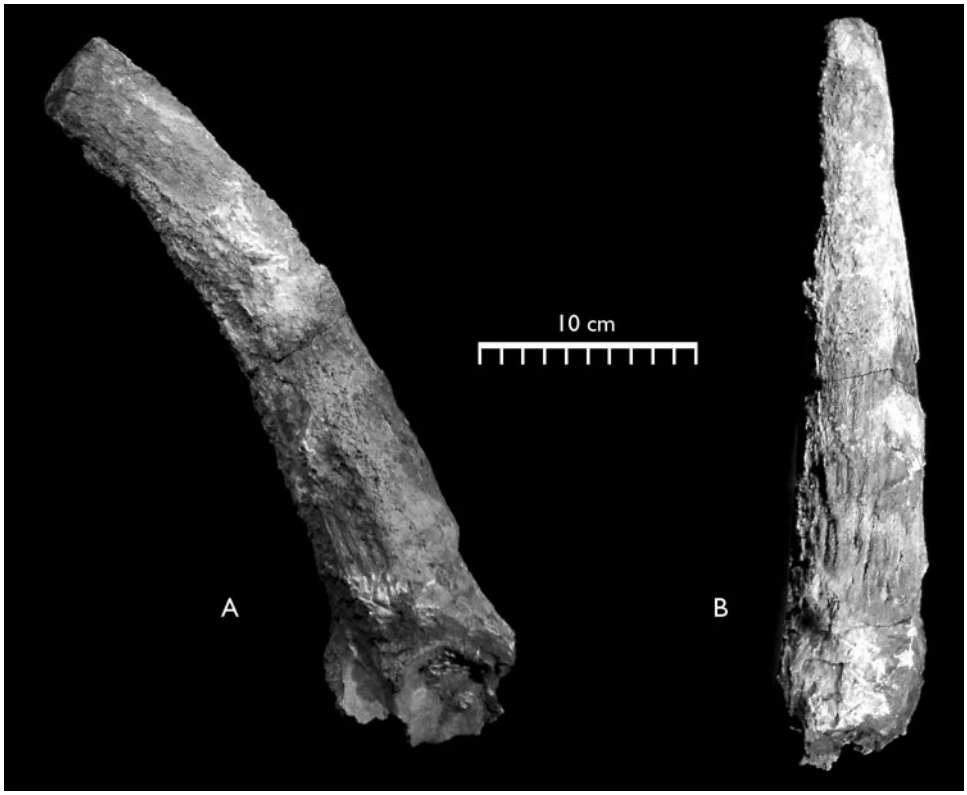

FIGURE 3.19
Hippotragus cf. *gigas,* BOU-VP-19/47. A. Lateral view. B. Cranial view.

shallow post-cornual fossae (Gentry 1978; Vrba and Gatesy 1994). Additionally, sinuses in horn core pedicles extend superiorly into the base of the horn core. Lingually bulbous metaconids occur on P_4s (Gentry 1978; Vrba and Gatesy 1994). Hippotragine crania are also characterized by moderately complicated midfrontal and parietofrontal sutures, widely divided temporal lines, an infraorbital foramen situated some distance superior to the P^2-P^3 junction, premaxillae that make a short articulation medially, and moderate to large mastoids (Gentry and Gentry 1978).

Hippotragus Sundevall, 1846

GENERIC DIAGNOSIS "Horn cores mediolaterally compressed, strongly curved backwards, inserted uprightly above the orbits and closer together than in *Oryx;* ethmoidal fissures blocked by bone internally; nasals more domed than in *Oryx;* mastoid facing partly laterally as well as backwards; longitudinal ridges behind the anterior tuberosities of the basioccipital are stronger than in *Oryx;* lower molars with stronger goat folds than in *Oryx*" (Gentry and Gentry 1978, 342).

Hippotragus cf. *gigas* Leakey, 1965

Specimen BOU-VP-19/47 (Figure 3.19) has very large horn cores with little mediolateral compression. Mediolateral compression of the horn core (see Appendix 3.2) is similar to compression reported by Gentry and Gentry (1978) for *H. gigas* from Olduvai and

EBSCOhost - printed on 10/28/2022 4:53 AM via . All use subject to https://www.ebsco.com/terms-of-use

Elandsfontein. Horn cores from the Daka specimen are less compressed than those of *H. niger* and larger than those of *H. equinus* (measurements from Gentry and Gentry 1978).

DESCRIPTION Specimen BOU-VP-19/47 preserves the proximal portion of a right horn core and its base. Some of the frontal, including the superior margin of the orbit, is present. The proximal horn core projects vertically above the orbit and begins curving strongly backwards at about 15 cm above the base. The horn core displays moderate transverse ridges.

Oryx Blainville, 1816

GENERIC DIAGNOSIS "A large hippotragine, a little smaller than living *Hippotragus* species; skull lower and wider than in *Hippotragus*; horn cores straighter and less compressed, inserted very obliquely, farther behind the orbits and wider apart" (from Harris 1991a, 159).

Oryx gazella (Linnaeus, 1758)

DIAGNOSIS *Oryx* species with longer, straighter, more anteroposteriorly compressed, and more obliquely inserted horn cores compared to others in the genus.

DESCRIPTION Specimen BOU-VP-3/149 (Figure 3.20) consists of a partial cranium with complete horn cores. The frontals are broken in front of and behind the horn core insertion, but the two frontals are joined. The anterior portion of the parietal is also present, allowing assessment of the insertion angle of the horn cores and the angular difference in the sagittal profiles of the face and cranial vault. Specimen BOU-VP-3/149 possesses morphology exemplary of *O. gazella,* including straight, anteroposteriorly compressed horn cores with oblique insertions. The horn cores are nearly parallel and are approximately 0.75 m long.

Specimen BOU-VP-19/31 is a proximal horn core and its base. It is referred to *O. gazella* for its obliquely inserted horn cores and low basal compression. Its overall morphology is very similar to BOU-VP-3/149.

DISCUSSION *Oryx* first appears at approximately 2.5 Ma, occurring in Member C of the Omo Shungura Formation and at Matabaeitu in the Middle Awash (Vrba and Gatesy 1994). Representatives are known from the Plio-Pleistocene of eastern Africa, northern Africa, and Asia. Asian specimens from this time have been referred to *O. sivalensis,* advanced African specimens are referred to *O. gazella,* and a few early specimens remain unassigned (Vrba and Gatesy 1994). *Oryx* species are characterized by long, linear horn cores that have a reduced angle between the facial profile and the postpedicle braincase, particularly in more advanced *O. gazella*. There is little sexual dimorphism (Kingdon 1982). The neurocranium is reduced in anteroposterior dimension, and horn cores are less curved than those of other hippotragine genera.

Reduncinae

The first African fossil reduncines appear between 6.0 and 7.0 Ma (Vrba 1995b). While Reduncini is monophyletic, its position relative to other tribes is controversial (Gentry 1992; Vrba et al. 1994; Matthee and Davis 2001). Hernández-Fernández and

EBSCOhost - printed on 10/28/2022 4:53 AM via . All use subject to https://www.ebsco.com/terms-of-use

FIGURE 3.20
Oryx gazella, BOU-VP-3/149. A. Cranial view. B. Lateral view.

EBSCOhost - printed on 10/28/2022 4:53 AM via . All use subject to https://www.ebsco.com/terms-of-use

Vrba (2005a) resolve a Cephalophinae/Peleinae/Reduncinae clade and suggest that this clade originated in the early Miocene. They suggest that Reduncinae and Peleinae diverged in the middle Miocene. Reduncines have specialized in the exploitation of seasonal grasses and in tolerating the flooding associated with marshlands, floodplains, and vegetation galleries surrounding waterways (Kingdon 1982). Molars with accessory enamel folds are characteristic of Reduncini, and many, but not all, members of the tribe have long, robust horns. Reduncini synapomorphies include relatively small cheek teeth, a large maxillary tuberosity in basal view, pronounced transverse ridges on horns, temporal lines that approach the cranial roof, and a host of other dental characters (Gentry 1992).

Within Reduncini, *Kobus* is firmly established as a monophyletic sister clade to *Redunca* both on molecular (Gatesy et al. 1997; Matthee and Davis 2001) and morphological (Vrba et al. 1994) grounds. A number of soft tissue and cranial osteological characters separate the two taxa, but the most useful with regard to the Daka material relate to horn core morphology. *Kobus* horn cores tend to have a portion of the midsection that is cylindrical and elongate, curving neither toward the base nor toward the tip. Additionally, *Kobus* species have "upright horn core stems," horn cores that extend perpendicularly from the base before curving posteriorly (Vrba et al. 1994). *Redunca* horns are less sigmoid and are oriented posteriorly from the base (see figure 1 of Vrba et al. 1994).

Kobus Smith, 1840

GENERIC DIAGNOSIS "Larger sized reduncines; horn cores usually long, their bases sometimes curving backwards instead of being concave anteriorly, usually with a flattened lateral surface but with no tendency towards a flattened posteromedial surface; frontals sometimes with a small system of internal sinuses" (Gentry 1985, 145).

Kobus kob (Erxleben, 1777)

DIAGNOSIS "A species of *Kobus* smaller than waterbuck or lechwe; horn cores with some mediolateral compression, curving backwards at the base, inserted close together and fairly uprightly; large supraorbital pits; skull not wide; braincase angled quite strongly on the facial axis; occipital surface with an evenly rounded top edge; narrow mastoids often having a strong ventral rim in males" (Gentry and Gentry 1978, 332).

REMARKS *Kobus kob* is a common element in the Daka Member fauna and comprises numerous horn cores, crania, and dental specimens (Figure 3.22; Appendices 3.1, 3.2, and 3.3). It is the most abundant bovid species in the Daka assemblage. Several of the complete crania come from a single locality, BOU-VP-3. Cranial metrics are similar to those of modern *K. kob* and earlier crania reported from Olduvai Bed II and Omo Member G (Gentry and Gentry 1978; Gentry 1985). The several crania and partial crania of *K. kob* are presented in Appendix 3.3 and in the following paragraphs.

DESCRIPTION The most complete cranial specimens are briefly outlined here. Besides these specimens, there are several horn core specimens assigned to *K. kob*, listed in Appendix 3.2.

Cranium BOU-VP-3/2 preserves the complete right horn core, most of the left horn core, and the complete neurocranium, including the frontals, parietal, occipital, temporals,

EBSCOhost - printed on 10/28/2022 4:53 AM via . All use subject to https://www.ebsco.com/terms-of-use

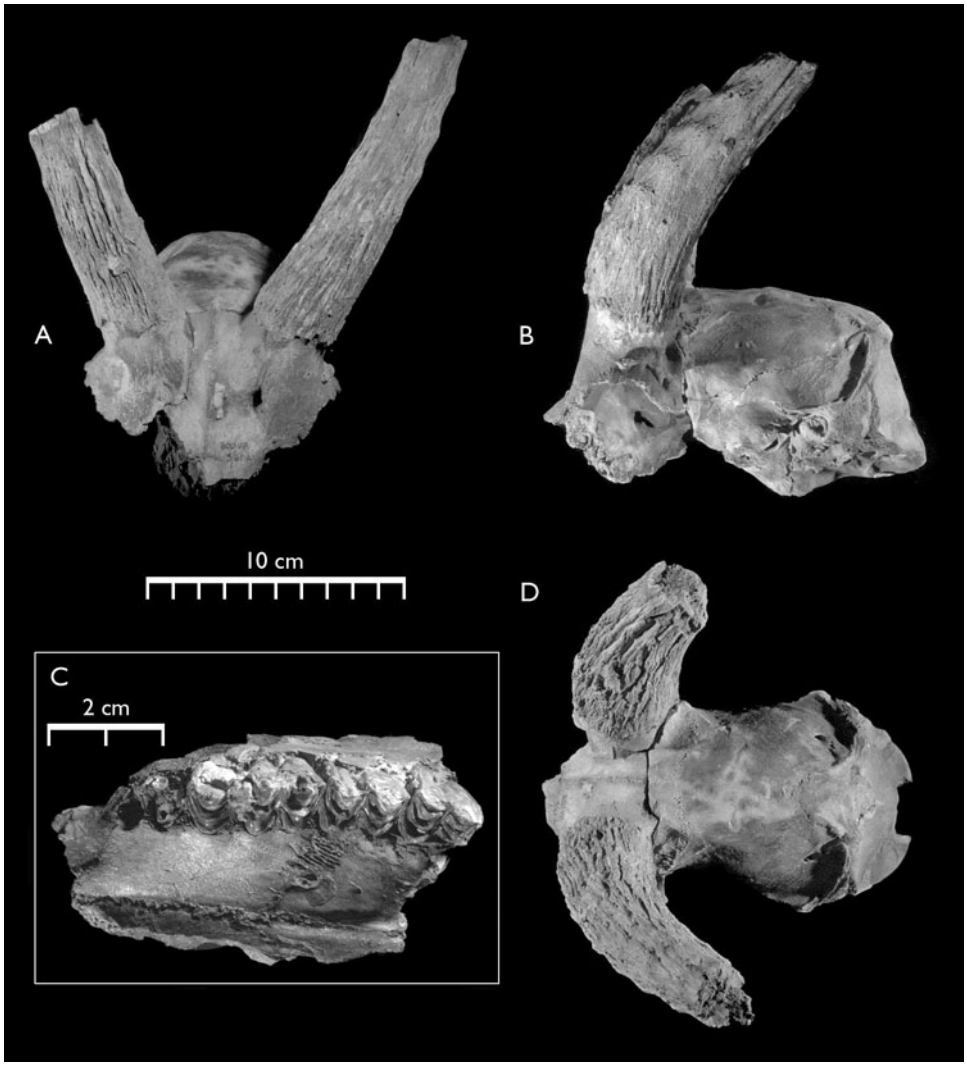

FIGURE 3.21
Kobus kob, BOU-VP-3/61. A. Cranial view. B. Lateral view. C. Occlusal view. D. Dorsal view.

and basicranium. The facial skeleton, including the maxillae, premaxillae, and nasals, is not preserved. Surface detail is good.

Cranium BOU-VP-3/9 preserves the complete right horn core, and the complete neurocranium, including the frontals, parietal, occipital, temporals, and basicranium. The maxillae, premaxillae, and nasals are not preserved. Surface detail is good.

Cranium BOU-VP-3/37 has two parts. One preserves the complete right and left horn cores and the frontals, with superior orbits and supraorbital foramina present. The second part preserves the posterior parietal, the occipital, and the posterior temporals. Surface detail is good.

Cranium BOU-VP-3/61 (Figure 3.21) is one of the best preserved *K. kob* crania in the assemblage. Although the tips of the left and right horn cores are missing, the

EBSCOhost - printed on 10/28/2022 4:53 AM via . All use subject to https://www.ebsco.com/terms-of-use

complete neurocranium, including the frontals, parietal, occipital, temporals, and basicranium, is immaculately preserved. Surface detail is excellent. In addition to the neurocranium, portions of the maxillae and premaxillae are present. The left maxilla and premaxilla preserve P^4–M^3 and the roots of P^2 and P^3. The right maxilla and premaxilla are represented only by a small strip of bone adjacent to the intermaxillary and interpremaxillary suture.

Cranium BOU-VP-3/87 preserves the complete right and left horn cores and the complete neurocranium, including the frontals, parietal, occipital, temporals, and basicranium. The facial skeleton, including the maxillae, premaxillae, and nasals, is not preserved. Surface detail is good on the basicranium, but parts of the horn cores, frontals, and parietal are encased in matrix.

Cranium BOU-VP-4/2 is easily the largest of the Daka *K. kob* sample. It is identified as *K.* cf. *kob* for this reason. It preserves the complete right and left horn cores and the superior part of the neurocranium, including the frontals, parietal, occipital, and parts of the temporals. The facial skeleton, including the maxillae, premaxillae, and nasals, is not preserved. Surface detail is obscured by resistant matrix.

Cranium BOU-VP-24/1 preserves the complete right and left horn cores and the frontals, with superior orbits and supraorbital foramina present. These anterior portions articulate with preserved portions of the sphenoid and basisphenoid. The rest of the neurocranium and facial skeleton is missing.

Kobus ellipsiprymnus Ogilby, 1833

DIAGNOSIS "A large reduncine species; horn cores moderately long with some mediolateral compression, little or moderate divergence, transverse ridges generally well marked, without any backwards curvature at the base but rising with their concave edge anteriorly; temporal ridges of the cranial roof may approach closely or remain more widely apart; top edge of occipital not evenly rounded, median ridge on the occipital flanked by small depressions near its top; mastoid not narrow, without a strong ventral rim but with a marked depression around the mastoid foramen, and tending to face laterally in males. In late wear P_4s may show fusion of paraconid and metaconid" (Gentry and Gentry 1978, 330).

DESCRIPTION Cranium BOU-VP-2/62 (Figure 3.22) preserves the proximal portion of the right horn core and most of the neurocranium, including the frontals, parietal, occipital, temporals, and basicranium. Surface detail is good. Differences between BOU-VP-2/62 and Omo *Kobus sigmoidalis* include the Daka specimen's possession of less mediolaterally compressed horn cores emerging from the frontal with slightly less divergence. Both of these features become even less pronounced in later *K. ellipsiprymnus*.

DISCUSSION *Kobus ellipsiprymnus* is represented in the Daka Member by a cranium, several horn cores, and dental material. Cranial metrics are similar to those reported

EBSCOhost - printed on 10/28/2022 4:53 AM via . All use subject to https://www.ebsco.com/terms-of-use

FIGURE 3.22

Kobus ellipsiprymnus, BOU-VP-2/62. A. Cranial view. B. Lateral view. C. Dorsal view.

from the taxon by Gentry (1985). Gentry (1985) suggests that *K. sigmoidalis* is a chronospecies ancestral to *K. ellipsiprymnus*, and the intermediate morphology of the Daka *K. ellipsiprymnus* is consistent with this hypothesis.

Kobus aff. *ancystrocera* Arambourg, 1947

Specimen BOU-VP-2/19 (Figure 3.23) is referred to *Kobus* aff. *ancystrocera* for its quick recurve, which is forwardly concave from the base. Other features aligning it with this taxon include pronounced longitudinal grooving, upright pedicles, and a slightly flattened lateral surface of the horn core. All of these features readily distinguish it from other reduncines in the Daka Member.

EBSCOhost - printed on 10/28/2022 4:53 AM via . All use subject to https://www.ebsco.com/terms-of-use

FIGURE 3.23

Kobus aff. *ancystrocera,* BOU-VP-2/19. A. Cranial view. B. Lateral view.

Conclusions

The Daka Member bovid assemblage presents a wealth of information from the poorly sampled African 1.0 Ma time period. Two new genera and species, *Bouria anngettyae* and *Nitidarcus asfawi,* have been named from Daka material (Vrba 1997). *Nitidarcus asfawi* is of particular interest, because it potentially indicates biogeographic interchange with Asia (see Vrba 1997). Daka Member bovid fossils document the last appearances of several taxa, including *Numidocapra crassicornis.* Daka *Syncerus* coexists with two *Pelorovis* species, including *P. antiquus*. This diminishes the possibility that *P. antiquus* is a *S. caffer* subspecies (contra Gautier and Muzzolini 1991). Also, the Daka Member presents a relatively complete juvenile *Pelorovis* cranium. The diversity of Bovini in the Daka Member calls for a review of the tribe in Plio-Pleistocene Africa. Daka *Kobus ellipsiprymnus* is transitional between *K. sigmoidalis* and later *K. ellipsiprymnus,* supporting Gentry's (1985) hypothesis that the two are chronospecies. Finally, the Daka bovid assemblage conveys several paleoecological and paleoclimatic implications presented in Chapter 17.

EBSCOhost - printed on 10/28/2022 4:53 AM via . All use subject to https://www.ebsco.com/terms-of-use

APPENDIX 3.1 Daka Bovid Dental Metrics

Specimen	*Element*	*Tribe*	*Genus*	*Species*	*MD*	*BL*
BOU-VP-25/72	L.$P^{3 \text{ or } 4}$	Alcelaphini	*Connochaetes*	*taurinus*	15.7	15.6
BOU-VP-25/72	R.M^1	Alcelaphini	*Connochaetes*	*taurinus*	e 24.6	18.5
BOU-VP-25/72	R.M^2	Alcelaphini	*Connochaetes*	*taurinus*	30.6	19.4
BOU-VP-25/72	R.M^3	Alcelaphini	*Connochaetes*	*taurinus*	30.7	1.9
BOU-VP-25/72	R.$P^{3 \text{ or } 4}$	Alcelaphini	*Connochaetes*	*taurinus*	15.8	15.7
BOU-VP-2/21	R.M^1	Alcelaphini	*Megalotragus*	*kattwinkeli*	26.3	19.3
BOU-VP-1/21	L.$M^{1 \text{ or } 2}$	Alcelaphini	*Numidocapra*	*crassicornis*	22.3	14.5
BOU-VP-1/21	L.M^2	Alcelaphini	*Numidocapra*	*crassicornis*	25.8	15.4
BOU-VP-1/21	L.M^3	Alcelaphini	*Numidocapra*	*crassicornis*	26.3	13.4
BOU-VP-1/21	L.P^4	Alcelaphini	*Numidocapra*	*crassicornis*	14	14.2
BOU-VP-1/21	R.M^1	Alcelaphini	*Numidocapra*	*crassicornis*	23.3	14.9
BOU-VP-1/21	R.M^2	Alcelaphini	*Numidocapra*	*crassicornis*	25.5	15.3
BOU-VP-1/21	R.M^3	Alcelaphini	*Numidocapra*	*crassicornis*	25.4	13.6
BOU-VP-1/21	R.P^3	Alcelaphini	*Numidocapra*	*crassicornis*	e 14.7	e 13.9
BOU-VP-1/21	R.P^4	Alcelaphini	*Numidocapra*	*crassicornis*	14.5	14.4
BOU-VP-1/26	R.M^3	Alcelaphini			24.3	14.8
BOU-VP-1/34	L.$M^{1 \text{ or } 2}$	Alcelaphini			30.8	20.1
BOU-VP-1/41	L.M^3	Alcelaphini			28.7	14.1
BOU-VP-1/63	R.M_3	Alcelaphini			30.7	9.9
BOU-VP-1/64	L.$M^{1 \text{ or } 2}$	Alcelaphini			31.1	18.4
BOU-VP-1/67	R.P_4	Alcelaphini			e 15.1	11.7
BOU-VP-1/68	L.$M^{1 \text{ or } 2}$	Alcelaphini			29.1	18.3
BOU-VP-1/69	R.$M^{1 \text{ or } 2}$	Alcelaphini			30.6	18.4
BOU-VP-1/70	R.M^3	Alcelaphini			31.7	e 18.6
BOU-VP-1/82	R.$M^{1 \text{ or } 2}$	Alcelaphini			31.8	22.2
BOU-VP-1/88	R./M1	Alcelaphini			23.8	13.2
BOU-VP-1/88	R.M_2	Alcelaphini			30.5	e 15.2
BOU-VP-1/88	R.M_3	Alcelaphini			41.7	14.2
BOU-VP-1/88	R.P_3	Alcelaphini			17.5	e 12.7
BOU-VP-1/88	R.P_4	Alcelaphini			20.2	13.2
BOU-VP-1/91	R.M^3	Alcelaphini			21.5	12.7
BOU-VP-1/101	R.M_3	Alcelaphini			40.8	13.7
BOU-VP-1/102	L.M^3	Alcelaphini			31.2	15.6
BOU-VP-1/129	R.M_3	Alcelaphini				8.9
BOU-VP-1/131	R.M_3	Alcelaphini			26.8	9.2
BOU-VP-1/138	L.$M^{1 \text{ or } 2}$	Alcelaphini			25.3	e 18.8
BOU-VP-1/139	L.$M^{1 \text{ or } 2}$	Alcelaphini			35.9	13.8
BOU-VP-1/142	L.M_3	Alcelaphini				
BOU-VP-1/146	R.M_2	Alcelaphini			29.7	12.7
BOU-VP-1/148	R.M^3	Alcelaphini			29.1	
BOU-VP-1/153	R.M_1	Alcelaphini			23.9	13.5
BOU-VP-1/153	R.M_2	Alcelaphini			27.3	13.3
BOU-VP-1/153	R.M_3	Alcelaphini			38.3	12.7
BOU-VP-1/153	R.P_4	Alcelaphini			16.2	10.8
BOU-VP-1/157	R.$M^{1 \text{ or } 2}$	Alcelaphini			19.9	13.9
BOU-VP-1/158	R.M^3	Alcelaphini			22	13.3
BOU-VP-1/160	R.M^3	Alcelaphini			28.6	16.9
BOU-VP-1/166	R.M_1	Alcelaphini			21.8	11.55
BOU-VP-1/171	R.M^3	Alcelaphini			27.6	
BOU-VP-1/189	R.M_3	Alcelaphini			37.3	13.5
BOU-VP-1/195	L.M_3	Alcelaphini				8.2

EBSCOhost - printed on 10/28/2022 4:53 AM via . All use subject to https://www.ebsco.com/terms-of-use

APPENDIX 3.1 *(continued)*

Specimen	*Element*	*Tribe*	*Genus*	*Species*	*MD*	*BL*
BOU-VP-1/202	L.M_1	Alcelaphini			20.9	13.2
BOU-VP-1/206	R.$M^{1 \text{ or } 2}$	Alcelaphini			21.8	12
BOU-VP-1/214	L.M_2	Alcelaphini			23.4	10.9
BOU-VP-1/214	L.M_3	Alcelaphini			32.5	11.9
BOU-VP-1/220	L.$M_{1 \text{ or } 2}$	Alcelaphini			25.5	13.5
BOU-VP-1/222	L.$M^{1 \text{ or } 2}$	Alcelaphini			24.7	16.3
BOU-VP-1/225	L.M_1	Alcelaphini			17.1	8.6
BOU-VP-1/225	L.M_2	Alcelaphini			22.07	9.1
BOU-VP-1/225	L.M_3	Alcelaphini			e 30.9	7.5
BOU-VP-1/230	R.M^3	Alcelaphini			31.7	19.6
BOU-VP-1/234	L.M^3	Alcelaphini			25.5	15.1
BOU-VP-1/235	L.^{M}	Alcelaphini			28.8	17.7
BOU-VP-1/238	R.$M^{1 \text{ or } 2}$	Alcelaphini			22	13.9
BOU-VP-1/240	L.M_2	Alcelaphini			26.5	13.2
BOU-VP-1/240	L.M_3	Alcelaphini			34.8	12.8
BOU-VP-1/240	L.P_4	Alcelaphini			14.9	9.4
BOU-VP-2/5	R.M^2	Alcelaphini			23.7	15.8
BOU-VP-2/12	L.M^3	Alcelaphini			28.7	11.8
BOU-VP-2/33	L.M^3	Alcelaphini			24.4	13.9
BOU-VP-2/52	R.M_3	Alcelaphini			38.3	13.8
BOU-VP-2/63	L.M_3	Alcelaphini			29	9.7
BOU-VP-2/71	L.$M^{1 \text{ or } 2}$	Alcelaphini			26.8	
BOU-VP-2/83	R.dp_4	Alcelaphini			e 31.6	10.7
BOU-VP-2/90	R.M_3	Alcelaphini				10.2
BOU-VP-3/3	R.M_1	Alcelaphini			24.8	12.6
BOU-VP-3/3	R.M_2	Alcelaphini			29.9	12.9
BOU-VP-3/3	R.M_3	Alcelaphini			e 36.7	e 11.8
BOU-VP-3/4	L.M_1	Alcelaphini			e 14.1	9.7
BOU-VP-3/4	L.M_2	Alcelaphini			19.5	11.2
BOU-VP-3/4	L.M_3	Alcelaphini			29.7	10.5
BOU-VP-3/29	L.M^3	Alcelaphini			34.1	18.1
BOU-VP-3/44	L.M^1	Alcelaphini			18.9	13.5
BOU-VP-3/48	R.M_2	Alcelaphini			e 27.3	11.6
BOU-VP-3/93	R.$M^{1 \text{ or } 2}$	Alcelaphini			19.6	12.8
BOU-VP-3/97	R.$M^{1 \text{ or } 2}$	Alcelaphini			28.6	18.1
BOU-VP-4/8	L.M_3	Alcelaphini			e 27.5	9.4
BOU-VP-4/9	L.M_3	Alcelaphini				e 11.3
BOU-VP-4/19	R.M^3	Alcelaphini			24.5	11.8
BOU-VP-4/20	R.M^3	Alcelaphini			e 20.3	13.5
BOU-VP-4/21	R.M_2	Alcelaphini			34.3	12.1
BOU-VP-4/22	L.M_2	Alcelaphini			30.8	13
BOU-VP-4/26	R.M^3	Alcelaphini			24.5	11.5
BOU-VP-4/28	R.M^3	Alcelaphini			23.9	12.7
BOU-VP-4/34	R.M^2	Alcelaphini			28	13.7
BOU-VP-4/34	L.M^3	Alcelaphini				14
BOU-VP-4/52	L.$M^{1 \text{ or } 2}$	Alcelaphini			20.9	12.3
BOU-VP-4/54	L.M^3	Alcelaphini			25.6	15.8
BOU-VP-4/56	L.M_1	Alcelaphini			24.1	13.2
BOU-VP-4/56	L.M_2	Alcelaphini			31.5	13.1
BOU-VP-4/56	L.M_3	Alcelaphini			e 34.8	12.4
BOU-VP-19/7	R.M^3	Alcelaphini			23	12.2

EBSCOhost - printed on 10/28/2022 4:53 AM via . All use subject to https://www.ebsco.com/terms-of-use

APPENDIX 3.1 *(continued)*

Specimen	*Element*	*Tribe*	*Genus*	*Species*	*MD*	*BL*
BOU-VP-19/18	L.M_3	Alcelaphini			29.7	10.4
BOU-VP-19/24	L.M_3	Alcelaphini			34.9	10.9
BOU-VP-19/25	L.M_2	Alcelaphini			30	e 11.6
BOU-VP-19/27	L.\M	Alcelaphini			26.9	
BOU-VP-19/28	L.M_3	Alcelaphini			35.9	13
BOU-VP-19/30	L.M_1	Alcelaphini			26.5	14.4
BOU-VP-19/33	L.$M^{1\text{ or }2}$	Alcelaphini			27.3	19.3
BOU-VP-19/37	R.$M_{1\text{ or }2}$	Alcelaphini			26.7	11.5
BOU-VP-19/38	L.M^2	Alcelaphini			29.2	17.5
BOU-VP-19/41	L.M^3	Alcelaphini			28.4	18.3
BOU-VP-19/52	L.$M^{1\text{ or }2}$	Alcelaphini			18.5	29.6
BOU-VP-19/54	L.M_2	Alcelaphini			22	10.1
BOU-VP-19/57	L.M^3	Alcelaphini			24.1	13
BOU-VP-19/59	R.$M^{1\text{ or }2}$	Alcelaphini			19.4	12.5
BOU-VP-25/1	L.M^1	Alcelaphini			e 28.6	14.2
BOU-VP-25/5	L.$M_{1\text{ or }2}$	Alcelaphini			29.6	12.2
BOU-VP-25/7	L.$M^{1\text{ or }2}$	Alcelaphini			20.5	14.2
BOU-VP-25/13	L.M_3	Alcelaphini			e 36.8	e 11.5
BOU-VP-25/17	L.M_2	Alcelaphini			32.4	12.9
BOU-VP-25/20	L.M_1	Alcelaphini			29.5	14.1
BOU-VP-25/25	L.$M^{1\text{ or }2}$	Alcelaphini			26.4	16.2
BOU-VP-25/44	L.M_2	Alcelaphini			29.7	12.2
BOU-VP-25/60	L.M^3	Alcelaphini			23.5	9.8
BOU-VP-25/66	R.M^3	Alcelaphini			25.5	12.8
BOU-VP-25/73	L.$M^{1\text{ or }2}$	Alcelaphini			29.6	18.5
BOU-VP-25/91	L.$M_{1\text{ or }2}$	Alcelaphini			31.5	14.1
BOU-VP-25/92	R.M^3	Alcelaphini			28.2	12.3
BOU-VP-25/93	L.M_2	Alcelaphini			21.8	8.8
BOU-VP-25/96	L.M_2	Alcelaphini			11.4	10.8
BOU-VP-25/96	L.M_3	Alcelaphini			29.5	20.7
BOU-VP-26/4	R.M_3	Alcelaphini			34.2	10.5
BOU-VP-26/14	R.M^1	Alcelaphini			18.7	13.5
BOU-VP-26/14	R.P^2	Alcelaphini			12.8	10.2
BOU-VP-26/14	R.P^3	Alcelaphini			10.9	9.9
BOU-VP-26/17	L.$M^{1\text{ or }2}$	Alcelaphini			17.2	12.2
BOU-VP-26/20	L.$M^{1\text{ or }2}$	Alcelaphini			21.5	12.3
BOU-VP-1/93	R.M_1	Antilopini	*Gazella*		8.8	5.9
BOU-VP-1/93	R.M_2	Antilopini	*Gazella*		10.3	6.6
BOU-VP-1/161	L.M_3	Antilopini			e 17.1	e 6.3
BOU-VP-3/1	R.M^2	Bovini	*Pelorovis*	aff. *antiquus*	e 31	e 28
BOU-VP-3/8	L.M_1	Bovini	*Pelorovis*	aff. *antiquus*	29.2	18.9
BOU-VP-3/8	L.M_2	Bovini	*Pelorovis*	aff. *antiquus*	33.4	19.2
BOU-VP-3/8	L.M_3	Bovini	*Pelorovis*	aff. *antiquus*	46	18.1
BOU-VP-3/8	L.P_3	Bovini	*Pelorovis*	aff. *antiquus*	21.9	15.3
BOU-VP-3/8	L.P_4	Bovini	*Pelorovis*	aff. *antiquus*	25.2	16.2
BOU-VP-3/8	R.M_1	Bovini	*Pelorovis*	aff. *antiquus*		
BOU-VP-3/8	R.M_2	Bovini	*Pelorovis*	aff. *antiquus*	35.9	18.1
BOU-VP-3/8	R.M_3	Bovini	*Pelorovis*	aff. *antiquus*	45.8	17.7
BOU-VP-3/8	R.M_3	Bovini	*Pelorovis*	aff. *antiquus*	45.8	17.7
BOU-VP-3/8	R.P_3	Bovini	*Pelorovis*	aff. *antiquus*	24.2	15.8
BOU-VP-3/109	L.dp_3	Bovini	*Pelorovis*	sp.	28.1	15

EBSCOhost - printed on 10/28/2022 4:53 AM via . All use subject to https://www.ebsco.com/terms-of-use

APPENDIX 3.1 *(continued)*

Specimen	*Element*	*Tribe*	*Genus*	*Species*	*MD*	*BL*
BOU-VP-3/109	L.dp_4	Bovini	*Pelorovis*	sp.	32	16.7
BOU-VP-3/109	R.dp_4	Bovini	*Pelorovis*	sp.	e 32.8	17.5
BOU-VP-1/2	L.dm^1	Bovini				e 16.3
BOU-VP-1/2	L.dm^2	Bovini			20.4	17.9
BOU-VP-1/2	L.M^1	Bovini			26.8	16.6
BOU-VP-1/2	L.M^2	Bovini			30.1	19.2
BOU-VP-1/2	L.M^3	Bovini				
BOU-VP-1/55	L.M_1	Bovini			31.5	14.6
BOU-VP-1/55	L.M_2	Bovini			e 32.4	13.3
BOU-VP-1/55	L.M_3	Bovini			e 40.5	12.3
BOU-VP-1/100	R.^{M}	Bovini			35.3	24
BOU-VP-1/111	R.M_1	Bovini			29.6	20.6
BOU-VP-1/111	R.M_2	Bovini			35.6	21.1
BOU-VP-1/111	R.M_3	Bovini			50.1	17.7
BOU-VP-1/111	R.M_3	Bovini			50.1	17.7
BOU-VP-1/111	R.P_2	Bovini			15.3	12.4
BOU-VP-1/111	R.P_3	Bovini			20.4	14.1
BOU-VP-1/111	R.P_4	Bovini			26.1	14.4
BOU-VP-1/126	R.$M^{1 \text{ or } 2}$	Bovini			33.2	23.5
BOU-VP-1/127	R.$M_{1 \text{ or } 2}$	Bovini			33.7	18
BOU-VP-1/128	R.M^2	Bovini			33.6	e 22.3
BOU-VP-1/173	R.M_1	Bovini			27.5	21.2
BOU-VP-1/173	R.M_2	Bovini			e 31.6	16.7
BOU-VP-1/173	R.P_4	Bovini			23	20.3
BOU-VP-1/177	R.$M_{1 \text{ or } 2}$	Bovini			38.3	15.5
BOU-VP-1/197	R.P_4	Bovini			21.2	15.1
BOU-VP-1/200	R.M_2	Bovini			16.9	10.6
BOU-VP-1/200	R.M_3	Bovini			23.5	9.5
BOU-VP-2/4	L.$M^{1 \text{ or } 2}$	Bovini			37.1	20.5
BOU-VP-2/10	L.M_3	Bovini			48	16.3
BOU-VP-2/13	L.M_2	Bovini			33.9	17.9
BOU-VP-2/13	L.M_3	Bovini			47.3	18
BOU-VP-2/24	L.M^3	Bovini			32.2	20.7
BOU-VP-2/32	L.M_2	Bovini			31	14.1
BOU-VP-2/38	R.M^1	Bovini			30.4	21.4
BOU-VP-2/38	R.M^2	Bovini			29.4	25
BOU-VP-2/38	R.M^3	Bovini			26.1	
BOU-VP-2/38	R.P^3	Bovini			e 16.6	18.8
BOU-VP-2/38	R.P^4	Bovini			17.3	18.6
BOU-VP-2/43	L.$M_{1 \text{ or } 2}$	Bovini			29.8	17.8
BOU-VP-2/46	L.M_3	Bovini				14.8
BOU-VP-3/15	R.$M^{1 \text{ or } 2}$	Bovini			35.7	24.7
BOU-VP-3/28	R.$M_{1 \text{ or } 2}$	Bovini			35.8	18.5
BOU-VP-3/45	R.P_3	Bovini			20.6	13.2
BOU-VP-3/45	R.P_4	Bovini			24.5	15.3
BOU-VP-3/52	L.M_1	Bovini			26.2	17.8
BOU-VP-3/52	L.M_2	Bovini			31.8	17.6
BOU-VP-3/52	L.P_3	Bovini			22.2	13
BOU-VP-3/52	L.P_4	Bovini			24.6	15
BOU-VP-3/53	L.M^3	Bovini			40	24.9

EBSCOhost - printed on 10/28/2022 4:53 AM via . All use subject to https://www.ebsco.com/terms-of-use

APPENDIX 3.1 *(continued)*

Specimen	*Element*	*Tribe*	*Genus*	*Species*	*MD*	*BL*
BOU-VP-3/73	L.$M_{1\text{ or }2}$	Bovini			32.8	16.3
BOU-VP-3/75	R.$M_{1\text{ or }2}$	Bovini			40.6	23.9
BOU-VP-3/84	L.M_3	Bovini			41.9	17.8
BOU-VP-3/85	L.$M_{1\text{ or }2}$	Bovini			38.1	14.8
BOU-VP-3/92	R.M_1	Bovini			24.5	18.9
BOU-VP-3/92	R.M_2	Bovini			31.8	19
BOU-VP-3/92	R.P_4	Bovini			23.7	17.7
BOU-VP-3/99	R.M_2	Bovini			32.2	16.8
BOU-VP-3/102	R.M_1	Bovini			29.4	20.9
BOU-VP-3/102	R.M_2	Bovini			30.6	20.7
BOU-VP-3/102	R.M_3	Bovini			45.8	20.5
BOU-VP-3/126	L.M^1	Bovini			e 23.6	25.6
BOU-VP-3/126	L.M^2	Bovini			30.2	24.6
BOU-VP-4/29	R.$M^{1\text{ or }2}$	Bovini			27.3	22.1
BOU-VP-19/4	L.M_1	Bovini			e 26.1	20
BOU-VP-19/4	L.M_2	Bovini			32.2	19.8
BOU-VP-19/4	L.M_3	Bovini			47.7	19.5
BOU-VP-19/4	L.P_3	Bovini			23.6	16.8
BOU-VP-19/4	L.P_4	Bovini			22.8	16.1
BOU-VP-19/11	L.$M^{1\text{ or }2}$	Bovini			35	17.3
BOU-VP-19/20	L.M^2	Bovini			38.3	21.4
BOU-VP-19/43	R.$M_{1\text{ or }2}$	Bovini			32.2	14.9
BOU-VP-24/2	R.$M^{1\text{ or }2}$	Bovini				e 17.2
BOU-VP-25/18	L.$M_{1\text{ or }2}$	Bovini			33.2	14.4
BOU-VP-25/19	L.M_1	Bovini			31.4	15.2
BOU-VP-25/19	L.M_2	Bovini			36.4	15.7
BOU-VP-25/19	L.P_4	Bovini			25.6	15.3
BOU-VP-25/99	R.M_1	Bovini			29.6	18.6
BOU-VP-25/99	R.M_2	Bovini			34.6	18.4
BOU-VP-25/99	R.M_3	Bovini				18.8
BOU-VP-25/99	R.M_3	Bovini				18.8
BOU-VP-25/99	R.P_3	Bovini			22.2	13.2
BOU-VP-25/99	R.P_4	Bovini			21.2	15.6
BOU-VP-25/23	R.$M_{1\text{ or }2}$	Bovini			31.8	15.1
BOU-VP-25/34	L.$M_{1\text{ or }2}$	Bovini			34.1	e 14.7
BOU-VP-25/83	L.$M_{1\text{ or }2}$	Bovini			39.7	14.7
BOU-VP-26/24	R.$M_{1\text{ or }2}$	Bovini			e 31.1	16.6
BOU-VP-25/35	L.$M^{1\text{ or }2}$	indet			31.6	19.8
BOU-VP-25/86	L.M_3	indet			37.1	16.5
BOU-VP-1/85	R.$M^{1\text{ or }2}$	Reduncini	*Kobus*	*ellipsiprymnus*	24.4	15.1
BOU-VP-1/98	R.M_1	Reduncini	*Kobus*	*ellipsiprymnus*	23.1	16.5
BOU-VP-1/98	R.M_2	Reduncini	*Kobus*	*ellipsiprymnus*	27.8	16.8
BOU-VP-1/98	R.M_3	Reduncini	*Kobus*	*ellipsiprymnus*	40.9	15.4
BOU-VP-1/98	R.P_3	Reduncini	*Kobus*	*ellipsiprymnus*	11.5	9.5
BOU-VP-1/98	R.P_4	Reduncini	*Kobus*	*ellipsiprymnus*	15.5	13.8
BOU-VP-1/150	L.M^3	Reduncini	*Kobus*	*ellipsiprymnus*	22.8	15.2
BOU-VP-1/233	R.P_3	Reduncini	*Kobus*	*ellipsiprymnus*	18	10.4
BOU-VP-1/233	R.P_4	Reduncini	*Kobus*	*ellipsiprymnus*	21.4	12.5
BOU-VP-1/239	L.P_2	Reduncini	*Kobus*	*ellipsiprymnus*	18.4	13.3
BOU-VP-2/65	R.M_3	Reduncini	*Kobus*	*ellipsiprymnus*	31	14.8

EBSCOhost - printed on 10/28/2022 4:53 AM via . All use subject to https://www.ebsco.com/terms-of-use

APPENDIX 3.1 *(continued)*

Specimen	*Element*	*Tribe*	*Genus*	*Species*	*MD*	*BL*
BOU-VP-1/47	R.M^3	Reduncini	*Kobus*	*kob*	16.2	11.4
BOU-VP-1/50	R.$M_{1\text{ or }2}$	Reduncini	*Kobus*	*kob*	15.2	7.2
BOU-VP-1/52	L.M_2	Reduncini	*Kobus*	*kob*	14.6	7.8
BOU-VP-1/56	L.M^3	Reduncini	*Kobus*	*kob*	16	9.8
BOU-VP-1/122	L.M^3	Reduncini	*Kobus*	*kob*	14.9	10.1
BOU-VP-1/125	L.M_2	Reduncini	*Kobus*	*kob*	13.66	8.1
BOU-VP-1/141	R.M^3	Reduncini	*Kobus*	*kob*	13.8	9.5
BOU-VP-1/152	L.M^2	Reduncini	*Kobus*	*kob*	17.7	9.6
BOU-VP-1/167	R.M^3	Reduncini	*Kobus*	*kob*	20	11
BOU-VP-1/179	R.$M_{1\text{ or }2}$	Reduncini	*Kobus*	*kob*	16	7.7
BOU-VP-1/217	R.M_3	Reduncini	*Kobus*	*kob*	17.1	8.3
BOU-VP-2/73	L.M_2	Reduncini	*Kobus*	*kob*	15.3	7.6
BOU-VP-3/6	R.M^3	Reduncini	*Kobus*	*kob*	18.5	11.7
BOU-VP-3/46	R.M_2	Reduncini	*Kobus*	*kob*	15.2	8.2
BOU-VP-3/46	R.M_3	Reduncini	*Kobus*	*kob*	20.6	7.5
BOU-VP-3/63	L.M_1	Reduncini	*Kobus*	*kob*	e 13.4	e 7.5
BOU-VP-3/63	L.P_4	Reduncini	*Kobus*	*kob*	10.2	6.1
BOU-VP-3/82	R.M_3	Reduncini	*Kobus*	*kob*	20	7.4
BOU-VP-3/96	R.$M^{1\text{ or }2}$	Reduncini	*Kobus*	*kob*	14.3	9.8
BOU-VP-4/24	R.M_1	Reduncini	*Kobus*	*kob*	12	8
BOU-VP-4/24	R.M_2	Reduncini	*Kobus*	*kob*	14.1	8.1
BOU-VP-4/24	R.P_2	Reduncini	*Kobus*	*kob*	6.6	4.5
BOU-VP-4/24	R.P_3	Reduncini	*Kobus*	*kob*	8.6	6.2
BOU-VP-4/24	R.P_4	Reduncini	*Kobus*	*kob*	9.9	6.9
BOU-VP-4/40	L.M_1	Reduncini	*Kobus*	*kob*	e 12.2	e 9.4
BOU-VP-4/40	L.M_2	Reduncini	*Kobus*	*kob*	e 15.6	10.4
BOU-VP-4/40	L.M_3	Reduncini	*Kobus*	*kob*	e 23.4	9.6
BOU-VP-4/47	L.M^1	Reduncini	*Kobus*	*kob*	14.4	9.5
BOU-VP-4/47	L.M^2	Reduncini	*Kobus*	*kob*	1.4	8.1
BOU-VP-25/22	L.$M_{1\text{ or }2}$	Reduncini	*Kobus*	*kob*	15.9	7.4
BOU-VP-1/119	L.M^2	Reduncini	*Kobus*	*sp.*	18.8	10.5
BOU-VP-19/29	R.M^3	Reduncini	*Kobus*	*sp.*	21.3	13.1
BOU-VP-1/94	L.M_3	Reduncini	*Kobus*		26.4	10.6
BOU-VP-1/184	L.$M_{1\text{ or }2}$	Reduncini	*Kobus*		24.6	12.7
BOU-VP-1/218	L.M_3	Reduncini	*Kobus*		25.8	8.4
BOU-VP-1/236	L.$P_{3\text{ or }4}$	Reduncini	*Kobus*		15.1	10.4
BOU-VP-2/72	R.$M_{1\text{ or }2}$	Reduncini	*Kobus*		e 18.1	10.3
BOU-VP-3/104	L.dp_4	Reduncini	*Kobus*		e 17.7	6
BOU-VP-3/117	L.M^3	Reduncini	*Kobus*		22	12.4
BOU-VP-19/32	R.M_1	Reduncini	*Kobus*		17.1	8.8
BOU-VP-19/32	R.M_3	Reduncini	*Kobus*		25.2	9
BOU-VP-19/32	R.P_2	Reduncini	*Kobus*		7.2	5.2
BOU-VP-19/32	R.P_3	Reduncini	*Kobus*		10.2	7.5
BOU-VP-19/32	R.P_4	Reduncini	*Kobus*		13.9	7.7
BOU-VP-19/34	R.M_3	Reduncini	*Kobus*		22.7	7.5
BOU-VP-25/2	L.M_2	Reduncini	*Kobus*		21.9	9.4
BOU-VP-25/24	L.$M^{1\text{ or }2}$	Reduncini	*Kobus*		18.2	12.4
BOU-VP-1/80	L.M_2	Tragelaphini	*Tragelaphus*		47	29.1
BOU-VP-1/80	L.M_3	Tragelaphini	*Tragelaphus*		e 64.2	29.5
BOU-VP-3/130	L.M_2	Tragelaphini	*Tragelaphus*		29.9	12.6

NOTE: MD: mesiodistal, BL: buccolingual, e: estimate.

EBSCOhost - printed on 10/28/2022 4:53 AM via . All use subject to https://www.ebsco.com/terms-of-use

APPENDIX 3.2 Daka Bovid Horn Core Metrics

Specimen	*Tribe*	*Genus*	*Species*	*Side*	*Max*	*Min*
BOU-VP-2/50	Aepycerotini	*Aepyceros*	cf. *melampus*	r	38.7	
BOU-VP-4/18	Aepycerotini	*Aepyceros*	cf. *melampus*	r	40.6	
BOU-VP-1/57	Alcelaphini	*Connochaetes*	*taurinus*	r	59.6	e 46.9
BOU-VP-1/144	Alcelaphini	*Connochaetes*		l	68.7	57.8
BOU-VP-1/155	Alcelaphini	*Connochaetes*		r	e 56	e 56
BOU-VP-1/163	Alcelaphini	*Connochaetes*		l	e 65.1	e
BOU-VP-1/193	Alcelaphini	*Connochaetes*		l	e 95.5	65
BOU-VP-2/59	Alcelaphini	*Connochaetes*		l	89.1	63.2
BOU-VP-19/62	Alcelaphini	*Connochaetes*		r	74.5	62.6
BOU-VP-1/149	Alcelaphini	*Damaliscus*	sp.	r	53.6	
BOU-VP-3/98	Alcelaphini	*Damaliscus*	sp.		47.9	e 35.8
BOU-VP-25/9	Alcelaphini	*Damaliscus*	sp.	r	e 59.2	e
BOU-VP-1/6	Alcelaphini	*Megalotragus*	*kattwinkeli*		89.6	71.9
BOU-VP-4/14	Alcelaphini	cf. *Megalotragus*			e 54.1	e
BOU-VP-1/21	Alcelaphini	*Numidocapra*	*crassicornis*	r	64.9	52.7
BOU-VP-1/31	Alcelaphini	*Numidocapra*	*crassicornis*	r	59.9	46.9
BOU-VP-1/11	Alcelaphini	*Parmularius*	*angusticornis*	l	e 64.5	e 53.2
BOU-VP-2/36	Alcelaphini	*Parmularius*	*angusticornis*		57	42.9
BOU-VP-2/40	Alcelaphini	*Parmularius*	*angusticornis*		e 67.5	67.5
BOU-VP-2/56	Alcelaphini	*Parmularius*	*angusticornis*	r	59.3	50.8
BOU-VP-3/83	Alcelaphini	*Parmularius*	*angusticornis*	l	61.5	48.7
BOU-VP-4/10	Alcelaphini	*Parmularius*	*angusticornis*	r	62.4	48.5
BOU-VP-4/31	Alcelaphini	*Parmularius*	*angusticornis*		60	45.8
BOU-VP-4/35	Alcelaphini	*Parmularius*	*angusticornis*	r	66.9	53.1
BOU-VP-4/46	Alcelaphini	*Parmularius*	*angusticornis*	r	64.2	54.1
BOU-VP-19/10	Alcelaphini	*Parmularius*	*angusticornis*	r	70.5	47.3
BOU-VP-1/13	Alcelaphini				73	
BOU-VP-4/41	Alcelaphini			r	74.5	60.5
BOU-VP-26/11	Alcelaphini				80.9	
BOU-VP-1/106	Antilopini	cf. *Antidorcas*		r	34.7	33.2
BOU-VP-2/47	Antilopini	cf. *Antidorcas*			41.9	26.6
BOU-VP-1/74	Antilopini	*Gazella*		l	30	20.4
BOU-VP-1/115	Antilopini	*Gazella*			25.7	17.7
BOU-VP-1/227	Antilopini	*Gazella*			31.9	20.6
BOU-VP-2/35	Antilopini	*Gazella*		l	28.7	21.2
BOU-VP-1/17	Caprini	*Bouria*	*anngettyae*	l	76.6	
BOU-VP-1/17	Caprini	*Bouria*	*anngettyae*	r	74.4	46.4
BOU-VP-1/44	Caprini	*Bouria*	*anngettyae*	l	69.1	43.5
BOU-VP-1/140	Caprini	*Bouria*	*anngettyae*	r	84.1	
BOU-VP-2/18	Caprini	*Bouria*	*anngettyae*	l	89	55.8
BOU-VP-2/34	Caprini	*Bouria*	*anngettyae*	l	71.7	
BOU-VP-2/41	Caprini	*Bouria*	*anngettyae*	l	e 77.3	e
BOU-VP-2/42 cf.	Caprini	cf. *Bouria*	cf. *anngettyae*	l	66.8	47.3
BOU-VP-2/42 cf.	Caprini	cf. *Bouria*	cf. *anngettyae*	r	71.1	e 49.4
BOU-VP-2/58 cf.	Caprini	cf. *Bouria*	cf. *anngettyae*	l	70.6	46.9
BOU-VP-2/60	Caprini	*Bouria*	*anngettyae*	r	70.3	48.7
BOU-VP-2/61 cf.	Caprini	cf. *Bouria*	cf. *anngettyae*		87.4	48
BOU-VP-2/75	Caprini	*Bouria*	*anngettyae*	l	e 75.5	49.4
BOU-VP-2/79	Caprini	*Bouria*	*anngettyae*	r	e 65.5	e
BOU-VP-3/103	Caprini	*Bouria*	*anngettyae*	r	79.6	46.9
BOU-VP-3/103	Caprini	*Bouria*	*anngettyae*	r	40.2	35.8

EBSCOhost - printed on 10/28/2022 4:53 AM via . All use subject to https://www.ebsco.com/terms-of-use

APPENDIX 3.2 *(continued)*

Specimen	*Tribe*	*Genus*	*Species*	*Side*	*Max*	*Min*
BOU-VP-19/47	Hippotragini	*Hippotragus*	cf. *gigas*	r	e 69	e 60.6
BOU-VP-3/149	Hippotragini	*Oryx*	*gazella*		52.5	51.7
BOU-VP-19/31	Hippotragini	*Oryx*	*gazella*	l	51.7	47.3
BOU-VP-1/12	indet				37.1	27.1
BOU-VP-1/159	aff. Ovibovini	*Nitidarcus*	*asfawi*		48.1	
BOU-VP-19/23	aff. Ovibovini	*Nitidarcus*	*asfawi*	r	e 50	e 40
BOU-VP-2/19	Reduncini	*Kobus*	aff. *ancystrocera*	l	47.8	44.4
BOU-VP-1/38	Reduncini	*Kobus*	*ellipsiprymnus*	r	63	54.3
BOU-VP-1/60	Reduncini	*Kobus*	*ellipsiprymnus*	r	59.5	46.3
BOU-VP-1/164	Reduncini	*Kobus*	*ellipsiprymnus*	r	56.9	44.3
BOU-VP-1/231	Reduncini	*Kobus*	*ellipsiprymnus*	l	63.8	49.2
BOU-VP-2/62	Reduncini	*Kobus*	*ellipsiprymnus*	r	55	46.7
BOU-VP-2/64	Reduncini	*Kobus*	*ellipsiprymnus*	l	53	44.1
BOU-VP-4/45	Reduncini	*Kobus*	*ellipsiprymnus*	l	53.9	49
BOU-VP-1/10	Reduncini	*Kobus*	*kob*	r	41.6	36.8
BOU-VP-1/14	Reduncini	*Kobus*	*kob*	r	46.1	41
BOU-VP-1/15	Reduncini	*Kobus*	*kob*	l	37.2	28.9
BOU-VP-1/45	Reduncini	*Kobus*	*kob*	r	39.1	36.2
BOU-VP-1/49	Reduncini	*Kobus*	*kob*	l	38.6	33.1
BOU-VP-1/51	Reduncini	*Kobus*	*kob*	l	45	38.4
BOU-VP-1/168	Reduncini	*Kobus*	*kob*	l	51.4	40
BOU-VP-1/169	Reduncini	*Kobus*	*kob*	r	46.3	38.5
BOU-VP-1/196	Reduncini	*Kobus*	*kob*	l	50.3	44.6
BOU-VP-2/54	Reduncini	*Kobus*	*kob*	r	40.5	34.1
BOU-VP-2/92	Reduncini	*Kobus*	*kob*	l	43.4	39.2
BOU-VP-2/93	Reduncini	*Kobus*	*kob*	r	42.6	e 33
BOU-VP-2/94	Reduncini	*Kobus*	*kob*	r	35.4	31.2
BOU-VP-3/2	Reduncini	*Kobus*	*kob*	r	37.3	31
BOU-VP-3/9	Reduncini	*Kobus*	*kob*	r	37.6	30.5
BOU-VP-3/27	Reduncini	*Kobus*	*kob*	r	38.3	32.5
BOU-VP-3/34	Reduncini	*Kobus*	*kob*	r	39.5	34.3
BOU-VP-3/35	Reduncini	*Kobus*	*kob*		44.3	e 34
BOU-VP-3/36	Reduncini	*Kobus*	*kob*	l	43.3	36.9
BOU-VP-3/37	Reduncini	*Kobus*	*kob*	r	40.5	33.7
BOU-VP-3/43	Reduncini	*Kobus*	*kob*	l	e 39.5	e 35.3
BOU-VP-3/49	Reduncini	*Kobus*	*kob*	r	37.5	33
BOU-VP-3/56	Reduncini	*Kobus*	*kob*	l	43.2	40
BOU-VP-3/57	Reduncini	*Kobus*	*kob*	r	38.6	e 33.6
BOU-VP-3/61	Reduncini	*Kobus*	*kob*	r	40.6	32
BOU-VP-3/66	Reduncini	*Kobus*	*kob*	l	37.6	35
BOU-VP-3/70	Reduncini	*Kobus*	*kob*	r	39.5	35.8
BOU-VP-3/79	Reduncini	*Kobus*	*kob*	l	38.6	34.1
BOU-VP-3/81	Reduncini	*Kobus*	*kob*	r	43.3	36.1
BOU-VP-3/95	Reduncini	*Kobus*	*kob*	l	37.6	31
BOU-VP-3/107	Reduncini	*Kobus*	*kob*	l	38.6	32.6
BOU-VP-3/128	Reduncini	*Kobus*	*kob*	r	44.5	39.2
BOU-VP-3/144	Reduncini	*Kobus*	*kob*	r	41.4	39
BOU-VP-4/2	Reduncini	*Kobus*	cf. *kob*	r	49.2	42.9
BOU-VP-4/13	Reduncini	*Kobus*	*kob*	l	e 44.3	e 35.6

EBSCOhost - printed on 10/28/2022 4:53 AM via . All use subject to https://www.ebsco.com/terms-of-use

APPENDIX 3.2 *(continued)*

Specimen	*Tribe*	*Genus*	*Species*	*Side*	*Max*	*Min*
BOU-VP-4/39	Reduncini	*Kobus*	*kob*	r	52.8	43.3
BOU-VP-19/9	Reduncini	*Kobus*	*kob*	r	40	e 36
BOU-VP-19/48	Reduncini	*Kobus*	*kob*	l	39.2	35.4
BOU-VP-19/60	Reduncini	*Kobus*	*kob*	l	42.7	36.8
BOU-VP-24/1	Reduncini	*Kobus*	*kob*	r	41	38
BOU-VP-25/6	Reduncini	*Kobus*	*kob*	r	44.1	37.3
BOU-VP-25/27	Reduncini	*Kobus*	*kob*	l	43.4	35
BOU-VP-25/32	Reduncini	*Kobus*	*kob*	r	44.6	39.7
BOU-VP-25/33	Reduncini	*Kobus*	*kob*	l	40	36
BOU-VP-25/38	Reduncini	*Kobus*	*kob*	l	33.2	27.9
BOU-VP-25/47	Reduncini	*Kobus*	*kob*	l	43.6	40.8
BOU-VP-25/52	Reduncini	*Kobus*	*kob*	r	49.4	42.9
BOU-VP-25/67	Reduncini	*Kobus*	*kob*	l	39.5	29.6
BOU-VP-25/80	Reduncini	*Kobus*	*kob*		36.5	31.2
BOU-VP-25/87	Reduncini	*Kobus*	*kob*	l	37.6	30.7
BOU-VP-25/88	Reduncini	*Kobus*	*kob*	r	42.4	36.8
BOU-VP-25/100	Reduncini	*Kobus*	*kob*	l	50.6	44.8
BOU-VP-26/22	Reduncini	*Kobus*	*kob*	l	36.4	30.8
BOU-VP-1/201	Reduncini	*Kobus*		l	52.6	43.2
BOU-VP-25/76	Reduncini	*Kobus*		r	50.9	43.3
BOU-VP-1/8	Tragelaphini	*Tragelaphus*	cf. *imberbis*	l	35	25.8
BOU-VP-1/107	Tragelaphini	*Tragelaphus*	cf. *imberbis*	l	43.6	34.2
BOU-VP-1/198	Tragelaphini	*Tragelaphus*	cf. *imberbis*	r	44.4	31.7
BOU-VP-1/216	Tragelaphini	*Tragelaphus*	cf. *imberbis*	r	31.9	26.2
BOU-VP-2/53	Tragelaphini	*Tragelaphus*	cf. *imberbis*	l	38.7	35
BOU-VP-19/8	Tragelaphini	*Tragelaphus*	cf. *imberbis*	r	36.6	33.4
BOU-VP-19/15	Tragelaphini	*Tragelaphus*	cf. *imberbis*	r	33.8	24.5
BOU-VP-19/16	Tragelaphini	*Tragelaphus*	cf. *imberbis*	r	36.9	30.5
BOU-VP-25/39	Tragelaphini	*Tragelaphus*	cf. *imberbis*	r	41.2	32.9
BOU-VP-25/102	Tragelaphini	*Tragelaphus*	cf. *imberbis*	l	37.4	29.7
BOU-VP-26/15	Tragelaphini	*Tragelaphus*	cf. *imberbis*	r	37.7	29.2
BOU-VP-25/8	Tragelaphini	*Tragelaphus*	cf. *scriptus*	l	e 51.6	42.8
BOU-VP-1/32	Tragelaphini	*Tragelaphus*	*strepsiceros*	l + r	73.3	60.5
BOU-VP-2/28	Tragelaphini	*Tragelaphus*	*strepsiceros*	r	64.3	50.7

NOTE: Max: maximum diameter, Min: maximum diameter, e: estimate. See also Appendix 3.3.

EBSCOhost - printed on 10/28/2022 4:53 AM via . All use subject to https://www.ebsco.com/terms-of-use

EBSCOhost - printed on 10/28/2022 4:53 AM via . All use subject to https://www.ebsco.com/terms-of-use

APPENDIX 3.3 Daka Member Bovid Cranial Metrics

Specimen	*Tribe*	*Genus*	*Species*	*A*	*B*	*C*	*D*	*E*	*F*	*G*	*H*	*I*	*J*	*K*	*L*
BOU-VP-1/123	Alcelaphini	*Connochaetes*	*taurinus*	77.2	57.7	184.1	102.6	40.1		100.8	125.9	38.4	51.1	197.8	158.3
BOU-VP-2/49	Alcelaphini	*Connochaetes*	*taurinus*	84.4	54.2	194.9									
BOU-VP-1/99	Alcelaphini	*Megalotragus*	*kattwinkeli*	72.9	60	154.3				100.9					134.4
BOU-VP-2/20	Alcelaphini	*Megalotragus*	*kattwinkeli*	83.3	69.2										
BOU-VP-2/21	Alcelaphini	*Megalotragus*	*kattwinkeli*	68.2	53	115.5	110								
BOU-VP-2/57	Alcelaphini	*Megalotragus*	*kattwinkeli*	52.7	48.4	135									
BOU-VP-1/97	Alcelaphini cf.	*Megalotragus*		67.5	57.8	133.1				94.1	106	36.6	40.1		
BOU-VP-2/56	Alcelaphini	*Parmularius*	*angusticornis*	65.7	52	128.6	75.4			91.7				146.8	
BOU-VP-2/78	Alcelaphini	*Parmularius*	*angusticornis*	72.1		103									
BOU-VP-1/21	Alcelaphini	*Numidocapra*	*crassicornis*	64.5	53.3	109.3				97.3	105.5		35.3	147.5	
BOU-VP-2/61 cf.	Caprini cf.	*Bouria* cf.	*anngettyae*	87		108.4									99.7
BOU-VP-3/1	Bovini	*Pelorovis* aff.	*antiquus*	150.5	94.1		122.4							235.6	
BOU-VP-3/8	Bovini	*Pelorovis* aff.	*antiquus*	145.1	81.8		153.2		221.2	150			59.6	175.4	276.4
BOU-VP-1/36	Bovini	*Syncerus*		70.5	66.4	230.5					147.5	37.7	37.5		224.2
BOU-VP-1/17	Caprini	*Bouria*	*anngettyae*	74.6	48	104		33.9		85	87.5	25.8	33.8		90.7
BOU-VP-1/44	Caprini	*Bouria*	*anngettyae*	62	43.6	81.7		36.3		78.1	91.6			124.5	95.8
BOU-VP-2/18	Caprini	*Bouria*	*anngettyae*	88	55	120									
BOU-VP-2/60	Caprini	*Bouria*	*anngettyae*	67.1	46.3	95.8									e97.7
BOU-VP-1/31	Alcelaphini	*Numidocapra*	*crassicornis*	57.9	48.3	103.9	66	48.1		100.5				75.8	
BOU-VP-3/149	Hippotragini	*Oryx*	*gazella*	39	44	44									
BOU-VP-1/9 aff.	Ovibovini	*Nitidarcus*	*asfawi*												125.9
BOU-VP-2/93	Reduncini	*Kobus*	*kob*	39.1	35.8	92.5	40								
BOU-VP-3/2	Reduncini	*Kobus*	*kob*	36.4	33.2	94.4	48	44.7	119.4	66.1	80.3		34		87.7
BOU-VP-3/9	Reduncini	*Kobus*	*kob*	39	33.7	93.6	45.2	46.8	119.5	63.8	79.7	23.3	32.4		
BOU-VP-3/37	Reduncini	*Kobus*	*kob*	40.2	36.1	97	46.6							102	
BOU-VP-3/61	Reduncini	*Kobus*	*kob*	38.2	33.4	86	41.2	48.6	106.7	63.6			29.4	100.2	80.1
BOU-VP-3/81	Reduncini	*Kobus*	*kob*	38.6	39.1	96.5	42.2								
BOU-VP-3/87	Reduncini	*Kobus*	*kob*	38.2	35.2	99.2	45.5			69.3		23.8		110.2	87.4
BOU-VP-3/139	Reduncini	*Kobus*	*kob*	40.2	35.8	107.8	38.2								
BOU-VP-3/128	Reduncini	*Kobus*	*kob*	42.6	40.8	112.4	52.7								
BOU-VP-4/2	Reduncini	*Kobus* cf.	*kob*	47	44	113	54			79.8	95.3				104.8
BOU-VP-24/1	Reduncini	*Kobus*	*kob*	45	39.3	98.8	47.7			67.7		17.1	36.3	108.8	
BOU-VP-25/6	Reduncini	*Kobus*	*kob*	47	33.2	111.1	52.2								
BOU-VP-2/62	Reduncini	*Kobus*	*ellipsiprymnus*	51.7	46.1	145		63.6	150	93.4	111.7	35.6	31.3		127.3

NOTE: A = anteroposterior length of horn core base, B = mediolateral breadth of horn core base, C = breadth between lateral horn core bases, D = distance between lateral margins of supraorbital foramina, E = lambda-bregma length, F = length from midfrontal suture at level of supraorbital foramina to top of occiput, G = minimum cranial breadth, H = breadth between tips of mastoid processes, I = breadth across anterior tuberosities of basioccipital, J = breadth across posterior tubercles of the basioccipital, K = cranial breadth at orbits, L = maximum breadth at mastoid process (lateral margins, not tips), e = estimate.

4

Carnivora

W. HENRY GILBERT,
NURIA GARCÍA,
AND
F. CLARK HOWELL

Carnivores are less common than most other ordinal taxa in both present communities and those preserved by the fossil record. This trend is realized in the small number (10 specimens) of carnivore fossils in the Daka Member. What is lacked in quantity in the assemblage is made up for in quality: the unit has produced one of the best-preserved Pleistocene hyaenid crania known (Figure 4.1). This new specimen, a large *Crocuta,* along with remains of both *Panthera* cf. *leo* and *P.* cf. *pardus*, indicate the presence of numerous large carnivores in the community represented by the Daka Member.

All of the large carnivores from the Daka assemblage, which includes leopards, lions, and crocutoid hyaenas, have modern analogs with broad geographic ranges. Modern *Crocuta crocuta, Panthera leo,* and *P. pardus* are not ecologically specific. For this reason, carnivores from the Daka Member are not given detailed treatment as environmental indicators.

Felidae

Turner and Antón's (1997) review of Felidae suggests that the first felids, genus *Proailurus*, come from the middle Oligocene of France, but they are not seen in significant numbers until the late Miocene. The saber-tooth clade, Machairodontinae, first appears in the late middle Miocene and is the dominant felid group until the Pliocene (Turner and Antón 1997). Modern cats, Felinae, make their first appearance in the later Miocene, and the big cats, *Panthera*, are known first from Laetoli (Turner 1990a, b; Turner and Antón 1997) and have since dispersed across the globe. Recent phylogenetic studies, both molecular and morphological, have focused on small cats, Felinae. The monophyly of the big cats (with the exception of the puma, *Puma concolor*, and the cheetah, *Acinonyx jubatus*) is well established (Salles 1992; Johnson and O'Brien 1997; Mattern and McLennan 2000), although relationships within *Panthera* are less well established.

Panthera pardus

Panthera pardus is first known from Laetoli (Turner 1990a, b; Turner and Antón 1997), although this attribution, based on size, is controversial because of lack of discrete osteological

EBSCOhost - printed on 10/28/2022 4:53 AM via . All use subject to https://www.ebsco.com/terms-of-use

FIGURE 4.1
Crocuta crocuta yangula calvaria BOU-VP-1/204 immediately after excavation of the fossil. The specimen was cleaned and removed from the protective matrix block in the museum. Photograph by Tim White, November 9, 1998.

characters that separate the members of *Panthera* (Uphyrkina et al. 2001; O'Regan 2002). Numerous subspecies have been named based on coat color, on subtle morphological characteristics, and more recently on molecules (Miththapala et al. 1996; Uphyrkina et al. 2001), but these are not apparent on isolated postcranial skeletal elements. Leopards range throughout the tropical and subtropical Old World. The coalescence date for modern leopards in Africa has been estimated at 0.47–0.825 Ma and the more recent divergence of Asian populations at 0.17–0.3 Ma (Uphyrkina et al. 2001).

Panthera Oken, 1816
Panthera cf. *pardus* (Linnaeus, 1758)

REMARKS BOU-VP-1/73 is the well-preserved proximal and distal ends of a single left femur. None of the shaft remains. BOU-VP-25/55 is a carbonate-encrusted distal right humerus. Most of the shaft is present, but expanding matrix distortion has severely affected the specimen.

DISCUSSION *Panthera pardus* in the Daka Member is distinguished from *Acinonyx* or *P. leo* on the basis of size, and identification should therefore be considered provisional. Table 4.1 provides weight estimates for Daka Member *P.* cf. *pardus*.

Weight estimations of *P.* cf. *pardus* were calculated using 19 species, represented by 81 individuals of both sexes, and regression equations used in the estimations included only

EBSCOhost - printed on 10/28/2022 4:53 AM via . All use subject to https://www.ebsco.com/terms-of-use

TABLE 4.1 Weight Estimates for Daka Member *Panthera pardus* Based on Femur (BOU-VP-1/73) Measurements

Variable	*Value (mm)*	*r*	*Estimated Weight (kg)*	*RE*
APD-PX-FE	27.9	0.98	55.3	0.7
TD-PX-FE	25.3	0.98	56.8	0.9
APD-DT-FE	50.9	0.97	59.6	0.7

NOTE: Abbreviations: *r:* correlation; RE: ratio estimator; PX: proximal epiphysis; DT: distal epiphysis; APD: anteroposterior diameter; TD: transverse diameter; FE: femur.

the family Felidae. Least-squares regressions of $\log_{10}$-transformed data were used to model the association between body weight and skeletal elements. The equations used for estimating body weight are of the form $\log Y = b \log X + \log a$, where X is a metric variable taken on the fossil specimen and Y is the unknown body weight. During this estimation procedure, variables were measured on a linear scale and transformed to logarithms, and estimated values were subsequently transformed back to a linear scale. Because this procedure biases the estimate of Y, several methods of transformation have been suggested. Among them, the Ratio Estimator (RE) seems to underestimate Y the least and has been recommended when logarithmic transformation procedures are applied (Smith 1993). The weights of the different carnivore species were obtained from published sources (Grzimek 1988; Eisenberg 1989; Estes 1991; Beltrán and Delibes 1993; Blanco 1998; Eisenberg and Redford 1999; García and Arsuaga 1999; Nowak 1999).

The Daka leopard falls within the average size range of its modern relatives. Estes (1991) gives weight values for females between 28 and 58 kg and for males between 35 and 65 kg. Kingdon (1997) gives females means of 50 kg and male means of 60 kg. The Daka specimen is placed between these two means, so the sex of the Daka leopard cannot be predicted on basis of its weight.

Panthera leo

Panthera leo is also first known from Laetoli (Turner 1990a, b; Turner and Antón 1997), although its identification is, like that of *P. pardus*, controversial for its basis on size alone (Uphyrkina et al. 2001; O'Regan 2002). Lions once had a broad Old World distribution but are currently restricted to Africa except for a precarious relict population of 300 Asiatic lions in the Gir Forest of northwest India (Vijayan and Pati 2002; Singh et al. 2002). Lions are noted outside Africa from the early middle Pleistocene (García and Arsuaga 1999).

Panthera cf. *leo* (Linnaeus, 1758)

BOU-VP-3/86 is a curved felid fourth metacarpal. It is assigned to *P. leo* and distinguished from *Acinonyx* or *P. pardus* in the Daka Member on the basis of size. Being the largest candidate feline by a substantial margin, *P. leo* is a more certain identification than *P. pardus*, although one must be aware that species of *Dinofelis*, a jaguar-sized machairodontine, might still have been present in Africa at this time.

EBSCOhost - printed on 10/28/2022 4:53 AM via . All use subject to https://www.ebsco.com/terms-of-use

Hyaenidae

There are four living species of Hyaenidae: *Crocuta crocuta* (the spotted hyaena), *Hyaena hyaena* (the striped hyaena), *Parahyaena brunnea* (the brown hyaena), and *Proteles cristatus* (the aardwolf). The largest and most common is *C. crocuta*, although *H. hyaena* is the only living taxon to range outside Africa. No hyaenid species is an exclusive scavenger, and the aardwolf feeds almost exclusively on termites. Aside from the estimated divergence dates of *Hyaena* from *Crocuta* (Wayne et al. 1989), the relationships among living taxa have not yet been approached molecularly.

The first appearance of Hyaenidae is from Europe in the early Miocene (Werdelin and Solounias 1991; Werdelin and Turner 1996). Hyaenids are united morphologically by auditory bulla features: a posteriorly expanded ectotympanic and a reduced caudal entotympanic (Werdelin and Solounias 1991). Several genera are present throughout the Old World in the early Miocene. The Miocene *Plioviverrops* clade was small and had dental adaptations suggestive of omnivory and insectivory (Werdelin and Solounias 1991). Another Miocene clade, represented by *Ictitherium*, is united by a reduced M_1 protoconid. Due to a paucity of preserved morphology, other large groups from the early and middle Miocene ("*Thalassictis*," "*Hyaenictitherium*") are referred to grades (Werdelin and Solounias 1991; Werdelin and Turner 1996). The aardwolf, *Proteles*, diverges from the clade containing the modern species by approximately 17.0 Ma (Wayne et al. 1991; Binninda-Edmonds et al. 1999). A clade distinguished by the loss of the upper and lower M2s shows up in the late Miocene. This group is composed of two subsidiary clades: a clade (*Hyaenictis*/*Chasmaporthetes*) that exapts back toward shearing in the molars and persists into the Pleistocene, and a bone-crushing clade containing the extinct genera *Pachycrocuta*, *Adcrocuta,* and all extant hyaenids except *Proteles* (Werdelin and Solounias 1991). The following features unite this latter clade: reduced M^1, a sagittally oriented upper carnassial (associated with bone crushing), and an anteriorly placed foramen magnum (except *Parahyaena brunnea*) (Werdelin and Solounias 1990, 1991). This group, of which *Crocuta crocuta* is a member, is found throughout the Old World as early as the late Miocene and is especially prevalent during the Quaternary (Petter and Howell 1989; Werdelin and Solounias 1991; Werdelin and Turner 1996; Werdelin and Kurtén 1999).

The evolutionary relationships of *Hyaena*, *Parahyaena*, *Pachycrocuta*, *Adcrocuta*, and *Crocuta* are not solidly established. Detailed molecular analyses of the modern taxa, as previously mentioned, have not yet been undertaken, and morphological systematic assessments are controversial at this phylogenetic level (Howell and Petter 1980; Werdelin and Solounias 1991; Mutter et al. 2001). Much of the systematic work on fossil specimens that would fall within or near the crown group of modern non-*Proteles* hyaenids is based exclusively on dental features, which are not always free of homoplastic or epigenetic biases.

Crocuta

The first appearance of a *Crocuta*-lineage distinct from what would become *Parahyaena* and *Hyaena* is at approximately 10 Ma with *Adcrocuta eximia* (Howell and Petter 1980, 1985;

EBSCOhost - printed on 10/28/2022 4:53 AM via . All use subject to https://www.ebsco.com/terms-of-use

Wayne et al. 1991; Werdelin and Solounias 1991; Bininda-Edmonds et al. 1999). This clade is distinguished by the presence of sutural contact between the premaxilla and frontal (Werdelin and Solounias 1991).

Kurtén (1968) strongly promoted the Asian origin of *Crocuta crocuta*, focussing his argument on the Plio-Pleistocene taxon *C. sivalensis* from the Siwaliks. According to Kurtén, these hyaenas would have migrated into Europe, establishing a population ranging from southern Russia to the Levant. Arambourg (1958, 1979) also defends an Asiatic origin of *C. crocuta* but allows the possibility of an Indo-Ethiopian emergence.

Ficarelli and Torre (1970) disagree with Kurtén's idea, referring to evidence of *Crocuta crocuta* from early Pleistocene deposits from Africa: Swartkrans, Kromdraai, and Olduvai Bed I. This is contrasted with the presence of another *Crocuta* species of similar age in Asia, *C. sivalensis* from the Siwalik Hills. Additionally, the description of *C. dietrichi* (Barry 1987; Petter and Howell 1989) recovered from the Laetoli Beds in Tanzania, sets the first appearance of *Crocuta sensu stricto* at about 3.5 to 3.8 Ma.

Four named species compose *Crocuta*: *C. crocuta*, *C. sivalensis*, *C. ultra*, and *C. dietrichi*. Ficarelli and Torre (1970) group *C. sivalensis* in the genus based on the relative lengths of the lobes on the upper carnassials, which are similar to those in *C. crocuta* in that the parastyles are short. *Crocuta ultra ultra* and *C. u. latidens* are named by Ewer (1954) from Kromdraai and Clyde Trading Co. deposits, respectively. However, Ewer (1967) later suggests including these forms, together with *C. spelaea capensis* and *C. crocuta angella*, into a single species and suggests a possible lineage-wide size increase over time. These are synonymized with *C. crocuta* Erxleben, 1777 by Werdelin and Solounias (1991). *Crocuta dietrichi* is based on maxillary and mandibular dental specimens, and Petter and Howell (1989) align it with *Crocuta* based on an elongated P^4 metacone, the absence of P_1 and M_2, reduction of the M_1 metaconid, and M_1 trigonid shape. *Crocuta dietrichi* has been argued as a *C. crocuta* synonym (Turner 1990a), and some authors suggest that it is possible that *C. sivalensis* is as well (Werdelin and Solounias 1991; Werdelin and Turner 1996). Others (Barry 1987) have synonymized *C. dietrichi* with *C. sivalensis* to the exclusion of *C. crocuta*. The first entry of *C. crocuta* into Europe was historically thought to date to the middle Pleistocene in Süssenborn and Gombasek and slightly later during the Cromerian interglacial at Forest Bed or Mosbach (Kurtén 1968). Since then, *C. crocuta* fossils were recovered from earlier deposits of Trinchera-Dolina, Atapuerca. García and Arsuaga (1999) suggest an entry of *C. crocuta* into Europe by at least 900 Ka based on this evidence.

Crocuta crocuta is very derived in morphology related to crushing of large mammal bones. Ewer (1954) notes that the teeth involved in *C. crocuta* primary bone crushing are the upper and lower P3s. These teeth become very worn in older individuals. The carnassial and other teeth are also somewhat involved, but not as heavily (Werdelin 1989). The unworn *C. crocuta* P^3 is higher crowned than that of *Parahyaena* or *Hyaena*. The buccal alveolar margin bounding the P^3 and the P^4 parastyle is buttressed by thick maxillary bone, and the plane of occlusion on these teeth is more perpendicular to the force vector generated by the temporalis muscle than in other modern taxa. Werdelin (1989) outlines the *C. crocuta* masticatory apparatus. This morphological array is adapted for powerful masticatory force generation and a heavy-use-resistant bone-crushing apparatus. This morphology is easily observed in the maxillary dentition when

EBSCOhost - printed on 10/28/2022 4:53 AM via . All use subject to https://www.ebsco.com/terms-of-use

viewing it from a lateral perspective. Apices of the *C. crocuta* P^2 and P^3 tend to converge more than in other living taxa, and the P^3 is distinctly cone shaped with a reduced distal cusplet. This condition differs from the P^3 of *Parahyaena* and *Hyaena*, which have a less hypsodont apex and a proportionally larger distal cusplet. Neither *C. dietrichi* nor the type of *C. sivalensis*, specimen Dublin 42, retain as derived a morphology in these features as living *C. crocuta* or the Daka *Crocuta* cranium. Some specimens referred to the *C. sivalensis* holotype more recently are closer to the condition seen in *C. crocuta* than the holotype of *C. sivalensis* (Matthew 1929; Werdelin and Solounias 1991).

Comparisons of the Daka material were made with modern *Crocuta* as well as *Crocuta* from various Plio-Pleistocene sites from Africa and Eurasia (Table 4.2). It has been suggested that there is significant regional variation in modern *Crocuta* (Kurtén 1956; Turner 1990a), but detailed morphometric studies are lacking. This morphological issue is somewhat tempered, however, by the group's lack of sexual dimorphism (Hamilton et al. 1986), which promotes clean, Gaussian distributions of size within *Crocuta* populations.

Crocuta Erxleben, 1777
Crocuta crocuta Erxleben, 1777
Crocuta crocuta yangula subsp. nov.

ETYMOLOGY The subspecies name *yangula* is from the Afar language, in which it means hyaena.

HOLOTYPE BOU-VP-1/204 (Figures 4.2–4.5) consists of an adult cranium with dentition. The holotype resides in the paleontology collections of the National Museum of Ethiopia, Addis Ababa.

LOCALITY AND HORIZON BOU-VP-1/204 was collected in November 1998 by Yohannes Haile-Selassie from Bouri Vertebrate Paleontology Locality 1 of the Daka Member.

DIAGNOSIS *Crocuta crocuta yangula* is placed in *Crocuta* by the following features: M^1 is absent. The P^4 protocone slopes forward; its parastyle is small, and its metacone is long. P^3 is hypsodont and conelike, with a reduced posterior cusplet. Sagittal crest does not project substantially posterior to lambda. Frontal process of the jugal is less prominent than that of *Hyaena*. Nuchal crest is reduced along its central portion and more prominent bilaterally. Nuchal crest bends when viewed laterally, extending steeply from the porion region, then decreasing slope abruptly as it extends toward the sagittal crest. *Crocuta crocuta yangula* can be distinguished from other *C. crocuta* subspecies by its significantly larger size, which is close to *Pachycrocuta brevirostris* based on a comparative sample that included modern eastern African and Pleistocene *P. brevirostris* from Eurasia and eastern and southern African sites (Table 4.2), and also by a diastema between I^3 and the upper canine and between the upper canine and P^1.

REMARKS BOU-VP-1/204 is a nearly complete hyaena cranium. BOU-VP-1/112 is a distal femur, with both condyles intact and reasonable surface integrity. Very little remains

EBSCOhost - printed on 10/28/2022 4:53 AM via . All use subject to https://www.ebsco.com/terms-of-use

EBSCOhost - printed on 10/28/2022 4:53 AM via . All use subject to https://www.ebsco.com/terms-of-use

TABLE 4.2 Measurements from Fossil and Modern *Crocuta* used in Principal Components Analysis

	Modern C. crocuta, eastern Africa					*BOU-VP-1/204*	*Laetoli*						*Siwaliks*	*Elands-fontein*		*Ata-puerca*	P. brevirostris, *Eurasia and Africa*				
	N	MEAN	MIN	MAX	SD		158	4132	4092	5278	4008	494	DUBLIN 42	15833	EC5	TD4-5	N	MEAN	MIN	MAX	SD
Prosthion-acrocranium	35	259.2	237.5	283.0	9.4	304.2										261.7					
Prosthion-synsphenion	35	150.5	139.8	162.0	5.0	168.0										146.2					
Frontal-acrocranium	33	145.3	129.8	169.9	7.5	181.4										158.2					
Prosthion-nasion	34	95.4	78.5	107.1	6.5	109.7										92.8					
Prostion-frontal	35	132.9	103.5	143.4	7.1	150.4										130.1					
Palatal length	35	119.1	110.8	126.8	4.4	135.2										119.7					
Premolar length	35	77.8	67.3	84.0	3.2	85.4										77.3					
Length C-P^4	35	97.1	91.4	103.5	2.9	109.6										96.9					
P^2 length	34	14.7	12.9	17.9	1.0	16.1	13.7				12.5		18.3	15.6		15.2	23	20.6	17.5	23.2	1.5
P^2 breadth	34	11.1	9.6	15.8	1.2	12.3	9.5				8.1			11.5		11.3	22	14.2	11.4	19.0	1.7
P^3 length	35	21.2	12.2	23.2	2.1	23.1	18.6	18.8	20.2	19.5		19	21.8	23.4	24.2	23.6	28	26.5	24.4	29.0	1.1
P^3 breadth	35	15.7	10.2	17.2	1.2	17.8	12.7	12.5	14.1	13.1		11.4		17.5	17.4	17.2	25	18.9	17.0	21.2	1.2
P^4 length	35	34.9	28.8	38.3	1.9	38.7	31.3				29.9		38.1	36.4	41	34.8	27	42.4	36.5	45.1	2.3
P^4 breadth at parastyle	35	19.6	13.7	21.6	1.4	20.3	15.5				16.3			20	22	21.8	28	24.0	21.4	27.1	1.4
Anteroposterior diameter I^3	35	12.2	10.3	13.8	0.8	15.4										13.5					
Transversal diameter I^3	35	9.3	8.2	10.5	0.6	11.1										9.0					
Anteroposterior diameter C	35	15.7	13.4	17.6	0.9	17.7								17.2		15.7	11	21.6	18.0	24.0	1.6
Transversal diameter C	35	11.7	10.7	13.0	0.6	13.8								12.4		12.6	10	15.5	11.5	17.2	1.6
Otion-otion	35	95.3	90.0	99.8	2.3	102.4										97.8					
Ectorbital-ectorbital	35	78.2	63.1	95.3	6.9	75.0										73.3					
Palatal breadth	33	101.0	93.5	111.5	4.7	107.2										110.2					

NOTE: See Figure 4.3 and Tables 4.4 and 4.5. Sources: Pei 1934; Kurtén 1972; Schutt 1972; Hendey 1974; Pons-Moyá 1987; Harris et al. 1988a; Martínez-Navarro 1992; Turner and Antón 1997.

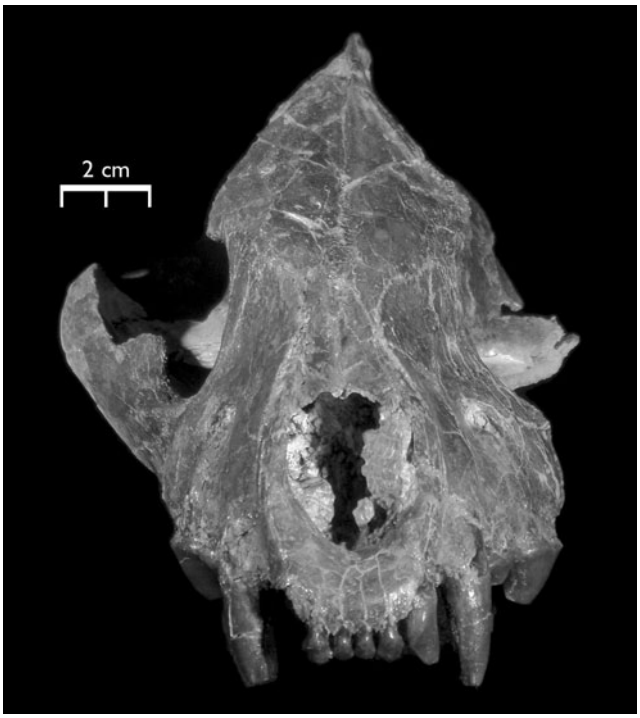

FIGURE 4.2
BOU-VP-1/204.
Anterior view.

of the shaft. BOU-VP-2/16 is a complete, well-preserved right calcaneus. BOU-VP-1/143 is a well-preserved right distal tibia, with little shaft but complete distal epiphysis. The noncranial material is not presented here as a paratype but is provisionally identified as *C. c. yangula*.

DESCRIPTION BOU-VP-1/204 was discovered by Yohannes Haile-Selassie in 1998. One zygomatic process was exposed at the surface, and upon removal of some of the surrounding matrix it was revealed that the specimen was largely intact. The specimen was jacketed and collected without the removal of any more matrix. Cleaning took place in the National Museum of Ethiopia over the next several years. The specimen is largely intact, preserving the entire premaxilla and maxilla with at least one tooth of each pair preserved. The cranial vault, including frontal, parietals, and much of the temporals, is present, but the occipital portion of the basicranium and nuchal planum are missing. There is some distortion to the overall shape, rendering many cranial metrics untenable, but surface anatomy is very well preserved. The following description compares BOU-VP-1/204 to two *C. crocuta* and two *Hyaena hyaena* crania in the comparative collection in the paleoanthropology laboratory of the National Museum of Ethiopia. It should be noted that there is considerable variation in both of the modern forms. For this reason, the recent taxa described here should not be taken to represent species norms, but are used as a device to better describe the Daka specimen.

EBSCOhost - printed on 10/28/2022 4:53 AM via . All use subject to https://www.ebsco.com/terms-of-use

FIGURE 4.3
BOU-VP-1/204. Superior view. One-half natural size.

Cranium The sagittal crest of BOU-VP-1/204 begins more posterior on the cranium than that of either *Hyaena hyaena* or *C. crocuta,* and the frontal trigon is a more acute triangle than that of either, although it is much closer to the *C. crocuta* condition. In contrast to either taxon, there is a deep midline valley between the two halves of the frontal that emanates anterior from the bifurcation of the sagittal crest. The relative anteroposterior length of the sagittal crest is substantially longer than that of either *C. crocuta* or *H. hyaena.* The intersection of the sagittal and lambdoidal keels is different than in *C. crocuta* or *H. hyaena.* In the latter the two meet without complexity, and both the adjacent occipital bone and the keels are smoothly curved. In *C. crocuta,* the area around lambda projects posteriorly, so there is an overhanging portion of the midline keel posterior to lambda, and the occipital portion of the crest undulates. Also in *C. crocuta,* the superior portion of the occipital similarly lacks smoothness. This, together with lipping of the nuchal crest superiorly, forms two distinct hooded fossae just inferolateral to lambda and tends to circumscribe the area, distinguishing it visually as a morphological unit. BOU-VP-1/204 more closely resembles the *C. crocuta* condition. Although the area is broken, the hooding of the nuchal crest and the overhanging posterior sagittal keel are observable. Unlike that of *H. hyaena,* but similar to what is seen in *C. crocuta,* the sagittal crest is convex along its entire course in BOU-VP-1/204. Most of the occipital is missing on BOU-VP-1/204.

There is a marked fossa on the posterior temporal at the root of the zygomatic, but because of the destruction of the occipital, this region cannot be directly compared to that

EBSCOhost - printed on 10/28/2022 4:53 AM via . All use subject to https://www.ebsco.com/terms-of-use

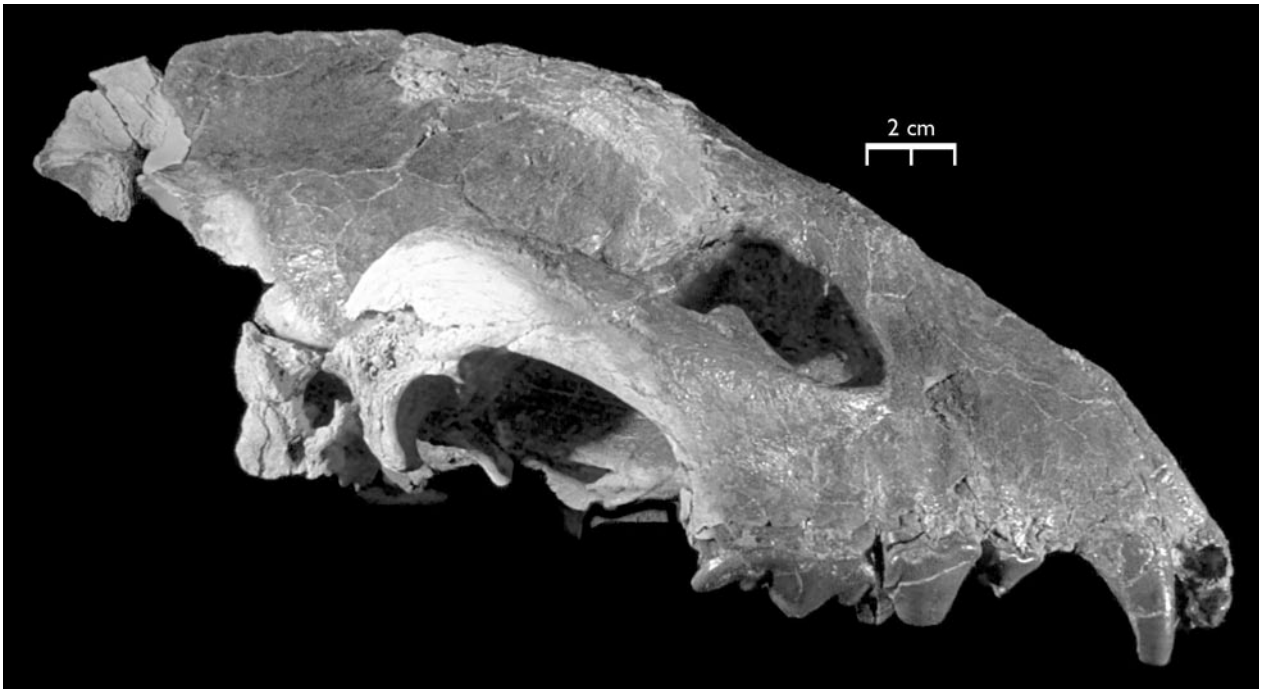

FIGURE 4.4
BOU-VP-1/204. Lateral view.

of either *C. crocuta* or *Hyaena hyaena*. There is a slight spicule of bone centrally located in the zygomatic root, where it forms a buttress into the squamosal portion of the temporal. This condition is likely subject to intraspecific variation, as it appears to be variably expressed in both existing genera. The distance between the medial wall of the temporal and the inside of the zygomatic arch is wider in BOU-VP-1/204 than in either modern taxon, and the posterior border of the zygomatic root extends at a right angle from the cranial base. The roots seen in *C. crocuta* and *H. hyaena* are oriented anteriorly. There is a portion of the zygomatic root that forms a horizontal plane prior to twisting laterally into the arch. Viewed from a superior perspective the temporal fossa appears to have a flat posterior border, and the whole fossa/arch complex has a more triangular appearance in BOU-VP-1/204 than that of either *C. crocuta* or *H. hyaena*. Viewed laterally, the superior border of the crest rises more steeply from the root in BOU-VP-1/204 than in either *C. crocuta* or *H. hyaena*.

As with *C. crocuta*, the mastoid crest of BOU-VP-1/204 is pronounced and bifurcates inferiorly, one portion leading to the posteroinferior tympanic bone around the meatus, the other following the paramastoid process. Also resembling the condition in *C. crocuta*, the entire region projects laterally, so there is a pronounced shelf of bone above the supramastoid crest. The inferior portion of the paramastoid process is missing, but its superior morphology suggests a downward orientation as seen in *C. crocuta*. Although damaged, the recess superior and anterior to the tympanic plate, between the plate itself and the postglenoid process, resembles the *C. crocuta* condition in that it would have been long and crescent shaped. In *Hyaena hyaena* specimens there is a concavity at the medial root of

EBSCOhost - printed on 10/28/2022 4:53 AM via . All use subject to https://www.ebsco.com/terms-of-use

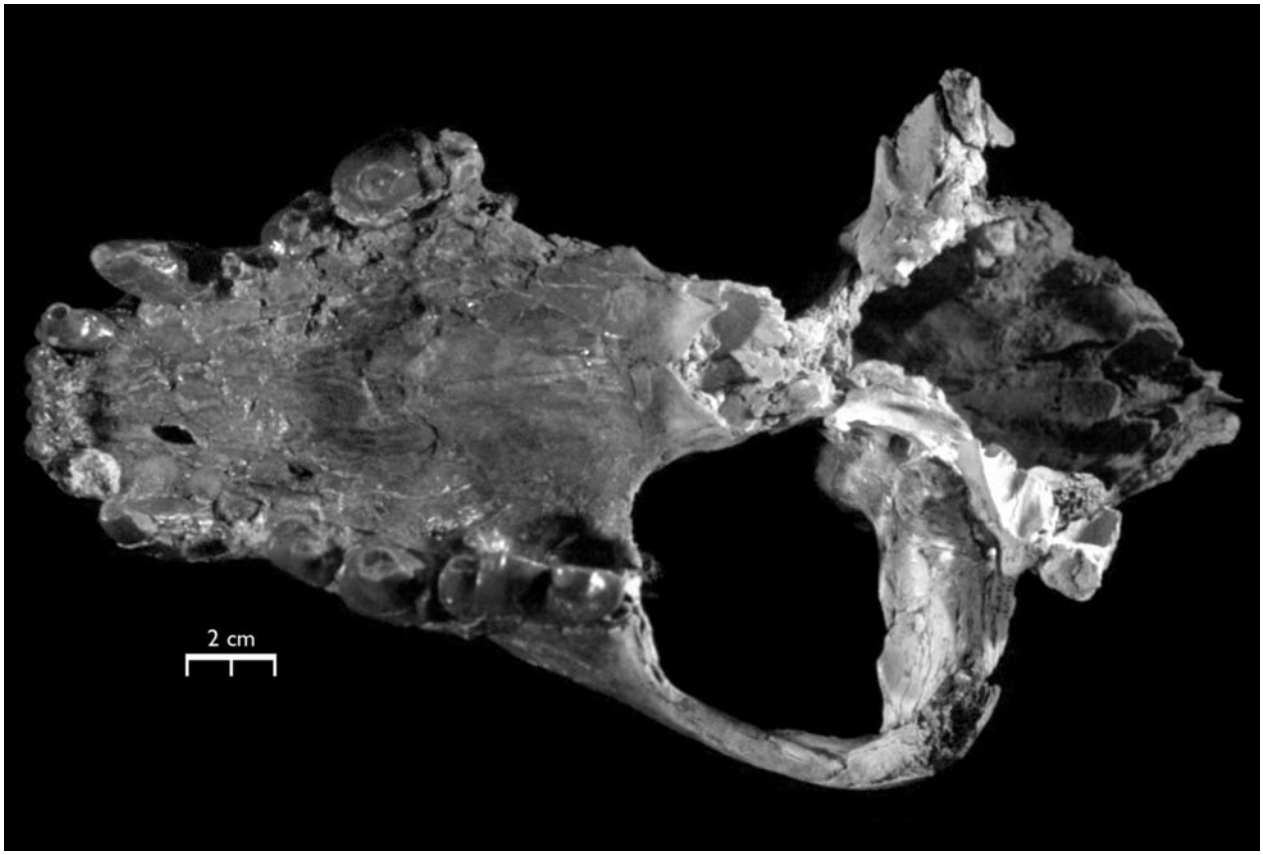

FIGURE 4.5
BOU-VP-1/204. Inferior view.

the tympanic bone, giving it the appearance of projecting farther laterally. BOU-VP-1/204 resembles the *C. crocuta* condition in this feature. The tympanic plate is oriented more mediolaterally and less anteroposteriorly than in *H. hyaena*, similar to the condition in *C. crocuta*. Also as in *C. crocuta*, the shelf of bone between the tympanic plate and the anterolateral bulla encasing the cochlea is cornucopia-shaped, with the lateral portion of the shelf much wider than the medial portion. The shelf in BOU-VP-1/204 is divided by bony septa into several haustra, adding to its resemblance to a cornucopia and to *C. crocuta*.

The basicranium is absent in BOU-VP-1/204, save some of the right sphenoid around the foramen ovale. Separating the Daka specimen from *C. crocuta crocuta* (reference to modern forms below are all to this living subspecies) is a small ridge dividing the foramen ovale from the foramen rotundum, which produces a fossa just anterior to the former. Additionally, this foramen is situated so that the anterior margin of its opening is tangent to the anterior border of the glenoid fossa. In *C. crocuta* it is positioned farther back. There is more anterolateral lipping of the glenoid fossa than in *C. crocuta*, and the small, subtly demarcated anteromedial contact facet within the glenoid is absent in BOU-VP-1/204. In this way the glenoid fossa superficially resembles *H. hyaena*. Sutures in this area, and on the cranium in general, are fused as with *C. crocuta*. The postglenoid

EBSCOhost - printed on 10/28/2022 4:53 AM via . All use subject to https://www.ebsco.com/terms-of-use

process is relatively wider mediolaterally than what is seen in either *C. crocuta* or *Hyaena hyaena*. The crest separating the foramen rotundum from the superior orbital fissure is more pronounced in BOU-VP-1/204 than it is in *C. crocuta*, and the fissure itself is divided by a bony crest on its medial wall. This differs from both modern taxa, which have no bony separation. The crest is collinear with a crest that extends from the inferior border of the optic canal. The superior border of the orbital fissure extends as a crest anteriorly beyond the optic canal.

In both modern taxa and in BOU-VP-1/204 there is a torus along the superior border of the sphenoid, straddling its suture with the frontal. In the Daka specimen and in *C. crocuta* it is somewhat horizontally elongated, and this tendency is exaggerated in the former. Anterior to it in BOU-VP-1/204 is a distinct, triangular fossa, with its base composed of the crest extending anterior from the superior orbital fissure.

Most of the pterygoid plate is absent, but some of the palatine portion of the bone is present. The crest that would continue posterior into the medial pterygoid lamina is situated more medially than in modern taxa, and there is an incipient groove between it and the most lateral part of the posterior palatine. The posterior opening of the nasal aperture is relatively wide compared with *Hyaena hyaena* morphology, resembling that seen in *C. crocuta*. A large, unjoined portion of the pterygoid plate indicates that it was significantly larger than in the *C. crocuta* condition.

As previously mentioned, the temporal fossa/zygomatic arch complex is swept back in BOU-VP-1/204, giving the slight impression of a barbed arrowhead when viewed from a superior perspective. This makes the posterior border of the zygomatic arch look superficially like the *Hyaena hyaena* condition when viewed from a lateral perspective, as described previously. Its distinctly *C. crocuta*–like zygomatic-temporal suture and the superior border of the zygomatic process of the temporal, however, which is flat all the way to the frontal process of the zygomatic bone, betrays this illusion. It is markedly different from the concave *H. hyaena* condition. Also as in *C. crocuta*, the superior border of the temporal process of the zygomatic posterior to the frontal process is short. The jugal-maxillary suture is long in BOU-VP-1/204, similar to that seen in *C. crocuta* and contra *H. hyaena* morphology. The frontal process of the zygomatic is not as pronounced as in *H. hyaena*, and is similar to the *C. crocuta* condition.

The inferior border of the orbit resembles the *C. crocuta* condition: The horizontal portion of it, formed by the union of the zygomatic and temporal bones, is separated from the lacrimal canal by a crest, rather than running smoothly into it as in *Hyaena hyaena*. Further differentiating BOU-VP-1/204 from *H. hyaena*, but aligning it with *C. crocuta*, is a triangular depression between the medial border of the orbit, the infraorbital foramen, and the frontal-maxillary suture. It is divided by a linear torus into inferior and superior components. While vestiges of the overall depression exist in *H. hyaena*, there is no torus, and it is not as deep. The inferior, triangular portion of the depression is deeper than the superior in both *C. crocuta* and BOU-VP-1/204. The superior extent of the zygomatic-frontal suture is superior to the superior border of the orbit, differing substantially from the *C. crocuta* condition. The lacrimal foramen is bounded by both the maxilla and the lacrimal bone, differentiating it from *H. hyaena* and aligning it with *C. crocuta*.

EBSCOhost - printed on 10/28/2022 4:53 AM via . All use subject to https://www.ebsco.com/terms-of-use

The fossa for the inferior oblique muscles is variable in living hyaenids. Illustrations of modern taxa and descriptions given in Werdelin and Solounias (1991) do not match the comparative specimens employed in this description in this feature. In BOU-VP-1/204, the fossa is situated at the junction of the frontal, maxilla, lacrimal, and palatine, and is shaped as a horizontally inclined oval. A crest more pronounced than the one in *C. crocuta* extends posterior from the inferior border of this fossa, invoking a groove along the superior border of the palatine. Further differentiating it from *C. crocuta*, a slightly raised portion of bone continues linearly posterior from this crest, joining eventually the crest defining the inferior border of the superior orbital fissure. *Hyaena hyaena* does not have such a pronounced crest anteriorly, but it has a better-defined crest along the greater wing of the sphenoid.

The internal opening of the infraorbital foramen is in a deep recess in BOU-VP-1/204, the maxillary portion of the inferior orbital margin overhanging the depression. This recess extends posterior from the infraorbital foramen to just below the frontal process of the zygomatic. The depth of this groove is situated on the maxillary side of the posterior palatine-maxilla suture. Much less of the medial wall of this impression is composed of the maxilla than in *C. crocuta*, where the maxilla continues posterior beyond the fossa for the internal oblique muscles. The sphenoidal and postpalatine foramina are quite different in *Hyaena hyaena* and *C. crocuta*. In *H. hyaena* they are situated close together in a slightly recessed area that opens posteriorly, with a more crested border anteriorly. In the Daka specimen and in *C. crocuta*, the posterior border of the recessed area is more crested.

The maxilla is substantially longer anteroposteriorly than in *C. crocuta* and is proportionally similar to that of *Hyaena hyaena*. In BOU-VP-1/204 the posterior border of the P^2 is slightly nasal to the most anterior part of the orbital margin. There is a bulge of bone above the mesial root of the P^4 and the distal root of the P^3, with a slight impression between the two. There is another columnar bulge extending distinctively from the mesial root of the P^3 and terminating in the infraorbital foramen. This is quite different from the condition of either modern taxon. There is a slight triangular bulge above the P^2 that gives way anteriorly to a pronounced fossa, which is subsequently bounded by a large canine jugum. This depression is oriented more anteroposteriorly than in *C. crocuta*, especially superiorly toward the entrance of the infraorbital foramen. The jugum itself is long, curved, and swept similarly posteriorly. A substantial portion of the posterior jugum is parallel with the superior border of the snout, resembling the *H. hyaena* condition.

Superior to the jugum is a linear fossa that starts just posterior to the I^3 and ends at the most superior point of the premaxilla. This portion of the premaxilla makes angular contact with the frontal, the two bones together looking something like an hourglass. This differs from the *Hyaena hyaena* condition, where a short length of single suture separates them. The nasal bones are crushed inwards, but much of the morphology is apparent. The portions surrounding the nasal aperture do not extend as far anterior as they do in *C. crocuta,* and the notch formed between the two is more acute. The overall shape of the nasal aperture in the Daka specimen is much more ovoid than that of *C. crocuta*, superficially resembling the *H. hyaena* condition. The lateral margins of the aperture, composed of the premaxilla,

EBSCOhost - printed on 10/28/2022 4:53 AM via . All use subject to https://www.ebsco.com/terms-of-use

are rounded and do not make a sharp crest superiorly, more closely resembling those of *C. crocuta*. The nasal wings of the premaxilla are flared laterally as in *C. crocuta*, contra the more vertical wing of *H. hyaena.* The U-shaped inferior and lateral borders of the nasal aperture are more robust than those of *C. crocuta*.

The maxillary portion of the palate of BOU-VP-1/204 has a deep impression and appears substantially deeper than in *C. crocuta*, although there is some distortion. The palatine-maxillary suture extends more linearly posteroinferiorly from the midline than it does in *C. crocuta* or, especially, *Hyaena hyaena*. The incisive foramen opens into a deep groove anteriorly, similar to the *C. crocuta* condition, and the foramen itself is more rounded than either of the modern taxa studied. The groove and palatal aspect of the premaxilla are longer in the Daka specimen than in *C. crocuta*, with proportions more similar to those seen in *H. hyaena*. The foramen on the maxillary palate is a relatively greater distance posterior of the incisive foramen. The anteroposterior length of the inferior palatine is relatively larger than in either *C. crocuta* or *H. hyaena*. The cervical margin of the P^4 protocone is reinforced by thicker alveolar bone than that of *C. crocuta*.

Dentition There is no M^1 on BOU-VP-1/204, although the socket for a *C. crocuta*–sized, vestigial M^1 is present. The P^4 of the specimen is longer mesiodistally than in most specimens of *C. crocuta*. Its paracone has a slight mesial orientation like that seen in *C. crocuta*. The P^3 of BOU-VP-1/204 is very similar to that of modern *C. crocuta*, both in size and morphology. The Daka specimen's P^2 is relatively large compared to modern *C. crocuta* but is encompassed within its range of variation.

DISCUSSION The dental dimensions of BOU-VP-1/204 are closer to the Siwaliks specimen (Dublin 42) *C. sivalensis* (Lydekker 1884) and fall well within the range of the giant hyaena (*Pachycrocuta brevirostris*). Nevertheless, both preserve a large M^1 and are more primitive in this feature than Daka, which retains a socket for a diminutive vestigial M^1, and all other specimens of *C. crocuta*, which have either vestigial or absent M^1s. This reduced M^1 indicates that the Daka specimen already presents the derived crocutoid condition. This is also observed in the Atapuerca (level TD4-5) specimen, but its smaller size differs considerably from that of BOU-VP-1/204 and falls with a modern eastern African range.

Some comparative upper tooth dimensions from a small ($n = 10$) southern African modern *C. crocuta* sample reveal some slightly larger values than their eastern African counterparts: (S. Africa, $n=10$: $LP^2 = 16.2$ mm; $LP^3 = 22.9$ mm; $LP^4 = 37.2$ mm). Furthermore, specimens 15833 and EC5 from the Pleistocene site of Elandsfontein (South Africa) seem to be considerably large and close to BOU-VP-1/204 in size (Table 4.2).

Harris et al. (1988a) assigned three mandibles from West Turkana, Lomekwi Member (LO4, LO5, and LO10), spanning the temporal interval from 3.36 to 2.52 Ma, to "*Crocuta* new species." The lower teeth dimensions from Lomekwi are very large and placed out of the modern eastern African *Crocuta* sample. Nevertheless, Werdelin (1999) reports parts of this material as having been mistakenly identified and suggests that the Lomekwi hyaenid material is distinct from *Crocuta* and should be referred to

EBSCOhost - printed on 10/28/2022 4:53 AM via . All use subject to https://www.ebsco.com/terms-of-use

Pachycrocuta based on overall dimensions and the morphology of the P_2 and other morphological traits.

One of the first to note a significant size difference between southern African and eastern African spotted hyaenas was Roberts (1954), who explained his observations as a relationship between temperature and mean adult size. Kurtén (1957) used modern spotted hyaena samples from South Africa, Tanzania, Uganda, and Somalia and Eurasian fossil samples to show that mean lower carnassial length (as representative of size) increased with distance from the equator. He also noted this was consistent with Bergmann's rule. The difference in size observed among the eastern African *C. crocuta* and their southern African counterparts, explained as a "cline" (size increase with distance from the equator), does not explain the large size of BOU-VP-1/204, which, following this criterion, should fall within the eastern African "smaller" range close to the equator. A subspecific attribution is justified on the basis of the large dimensions observed on BOU-VP-1/204 considering the eastern African location of the Daka Member. The Laetoli tooth dimensions (closer to the modern eastern African ones) are also smaller than Daka, as are values for European *Crocuta* arriving into Eurasia during the late early Pleistocene.

Several methods were employed to determine the systematic position of BOU-VP-1/204, including cladistic analysis of discrete characters and a principal components analysis of multivariate metrics. Cladistic analysis to place BOU-VP-1/204 phylogenetically was performed using the data matrix constructed by Werdelin and Solounias (1991). This analysis was undertaken using their data, which was exactly reproduced except for the inclusion of BOU-VP-1/204. Detailed information on the mechanics of the analysis can be found in Werdelin and Solounias (1991). Scores for the Daka specimen are listed in Table 4.3, and the strict consensus of the nine most parsimonious trees is shown in Figure 4.6. Some interesting patterns emerge from the analysis. The first is that BOU-VP-1/204 is positioned firmly in a clade that unites *Crocuta* and *Adcrocuta* by its distinct premaxilla-frontal articulation and in a second clade that unites the first with *Pachycrocuta* for lack of a derived *Parahyaena*/*Hyaena*-like medial orbit.

More precise placement of BOU-VP-1/204 was obtained by comparison of the cranium to modern and fossil *Crocuta*. BOU-VP-1/204 is aligned with *C. crocuta*, to the exclusion of the *C. dietrichi* and *C. sivalensis* (type specimen) by highly derived dental specializations related to bone crushing. The cranium and teeth of BOU-VP-1/204 are at the extremely large end of the modern *C. crocuta* range (see Table 4.2). The teeth are substantially larger that those of *C. dietrichi* and similar in size, except for the P^2, to the type specimen of *C. sivalensis*, and the cranium is larger than any compared modern *Crocuta*.

To address these issues and other issues outside of *Crocuta* systematics methodologically, we conducted multivariate analyses comparing modern spotted hyaenas with BOU-VP-1/204, and the cranial remains from the lowermost levels of Trinchera Dolina (TDW4-5) from Atapuerca, Spain. These units are of a slightly younger chronology than the Daka Member, dating to around 0.9 Ma (García 2003). We also included *C. sivalensis* from the Siwaliks (Lydekker 1884).

EBSCOhost - printed on 10/28/2022 4:53 AM via . All use subject to https://www.ebsco.com/terms-of-use

TABLE 4.3 Scores Assigned to BOU-VP-1/204 from Characters Used in Werdelin and Solounias (1991)

Character	*Score*	*Definition*	*Coding*
9	1	Position of P^4 protocone	Protocone extends anterior of parastyle = 0; anterior face of paracone level with face of parastyle = 1; anterior face of protocone does not extend anterior to face of parastyle = 2
10	1	Shape of tooth row	Straight = 0; curved = 1
11	1	Relative length of paracone and metastyle of P^4	Metastyle equal or shorter than paracone = 1; metastyle longer than paracone = 2
12	1	Placement of carnassials in tooth row	Carnassials in line with tooth row = 0; carnassial in sagittal plane = 1
21	0	Length of palate	Ends at level of last upper molar = 0; continues past last upper molar = 1
22	2	Position of infraorbital foramen	Placed above posterior end of P^3 or P^3, P^4 junction = 0; positioned above middle of P^3 = 1; positioned anterior to middle of P^3 = 2
23	1	Position of anterior margin of orbit	Above anterior end of P^4 = 0; above P^3 = 1
24	0	Suture between premaxilla and frontal on snout	Absent = 0; present = 1
25	0	Size of inferior oblique muscle fossa at maxillary-lacrimal suture posterodorsal to infraorbital foramen	Small = 0; large = 1
26	0	Inferior oblique muscle fossa II at juncture between maxillary, lacrimal, and frontal	Absent = 0; present = 1
27	1	Sphenoid foramen and postpalatine foramen position	Well-separated, distinct foramina = 0; formamina located close together in a single depression = 1
28	1	Contribution of the maxilla to the anterointernal rim of zygomatic arch	Small to none = 0; maxilla makes up substantial portion = 1
29	1	Lacrimal-palatine suture in orbital mosaic	Present = 0; absent = 1
30	0	Nasal wings of premaxilla	Divergent = 0; vertical = 1
33	1	Position of premaxillary-maxillary suture on palate	Near middle of the incisive fossa = 0; at posterolateral margin of incisive fossa = 1
34	0	Shape of incisive fossa	Broad = 0; narrow = 1
35	1	Position of major palatine foramen	At palatine-maxillary suture = 0; far forward on palate = 1
36	1	Shape of jugal-maxillary suture in external view	Angled downward posteriorly = 0; straight = 1
40	1	Placement of septum bullae	Vertical = 0; semihorizontal to horizontal = 1
41	0	Shape of caudal entotympanic	Uniform = 0; local to ventral expansion = 1
42	1	Size of tympanic	Small = 0; medium = 1; large = 2
43	1	Position of external auditory meatus	Far forward of nuchal crest = 0; level with nuchal crest = 1
44	1	Shape of nuchal crest	Antero-posteriorly inclined = 0; nearly vertical or vertical = 1

EBSCOhost - printed on 10/28/2022 4:53 AM via . All use subject to https://www.ebsco.com/terms-of-use

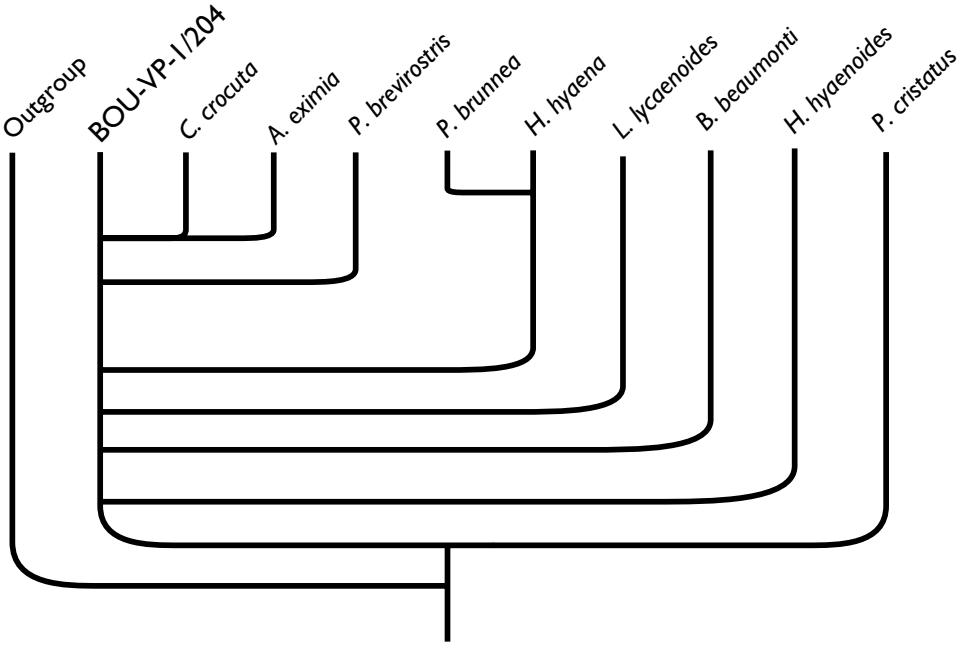

FIGURE 4.6

Phylogeny of crown group Hyaenidae that includes BOU-VP-1/204. See Table 4.3 for BOU-VP-1/204 character states. Scores for other specimens are found in Werdelin and Solounias (1991).

The modern sample of *C. crocuta* skulls was measured at the Museum of Vertebrate Zoology (University of California, Berkeley), where this collection is housed, and is mainly composed of Kenyan specimens from the Masai Mara region, but it also includes three skulls of Ethiopian origin. The modern sample size was originally larger ($n > 65$), but after conducting multiple multivariate analyses we realized that the resulting variability observed was somewhat confused by the presence of subadult individuals. These specimens mimic adult morphology in most of the features but differ in some cranial metrics. BOU-VP-1/204 is a fully mature adult, so the modern subadults were eliminated from the analyses, resulting in a sample of 35 modern *Crocuta* crania.

Metrics were addressed by a factor analysis of the principal components of an array of cranial and dental metrics. Principal components analysis reduces the number of variables to only those that are the most important (those that express most of the variability) and facilitates visualization and understanding. The method also detects structure in the relationships between variables, projecting combinations of the original variables linearly while keeping the maximum variance of the data. We have employed the widely used Kaiser criterion, dropping eigenvalues less than 1, which assumes that factors must retain at least as much variance as the average of the original variables. To obtain a clear pattern of loadings, we conducted orthogonal (varimax) rotations of the axes. This type of rotation maximizes the variance of the new axes, the factors, obtaining the most diverse pattern of loadings on each factor, resulting in an easier interpretation. See Tables 4.4 and 4.5 and Figure 4.7 for a presentation of the principal components data.

Although similar in size, both *Crocuta* species reported from the Siwaliks, *C. sivalensis* (Falconer and Cautley 1867) and *C. felina* (Bose 1880), differ significantly from the Daka

EBSCOhost - printed on 10/28/2022 4:53 AM via . All use subject to https://www.ebsco.com/terms-of-use

TABLE 4.4 Rotated Component Loadings for Recent and Fossil *Crocuta* (Varimax Normalized)

Measurement	*Factor 1*	*Factor 2*
Prosthion-acrocranium	**0.928659**	0.178528
Prosthion-synsphenion	**0.905553**	0.025098
Frontal-acrocranium	**0.790466**	0.201624
Prosthion-nasion	**0.801983**	−0.014531
Prosthion-frontal	0.340579	0.186991
Palatal length	**0.836338**	0.211677
Premolar length	0.322287	0.451287
Length C-P^4	**0.863617**	0.324498
P^2 length	0.186571	**0.686577**
P^2 breadth	−0.110178	**0.671542**
P^3 length	0.105199	0.512245
P^3 breadth	0.167054	**0.778416**
P^4 length	0.299272	0.632198
P^4 breadth (at parastyle)	−0.028365	**0.831237**
P^4 breadth	0.20222	**0.813119**
Anteroposterior diameter I^3	0.502718	0.618045
Transversal diameter I^3	0.434544	0.542844
Anteroposterior. diameter C	0.470805	0.53532
Transversal diameter C	0.344666	**0.799928**
Otion-otion	0.673364	0.342696
Ectorbital-ectorbital	0.553218	0.041614
Palatal breadth	0.666293	0.410415
Expl. Var	7.056920	6.105323
Proportion of Total	0.306823	0.265449

NOTE: Extraction: Principal components. Marked loadings (bold) are > 0.65. $n = 31$. See plot in Figure 4.7.

cranium. *Crocuta sivalensis*, using the holotype specimen Dublin 42 promoted by Matthew (1929), is reported by Pilgrim (1932) to retain a "moderately large" M^1. Very small vestigial M^1s are found in a small percentage of modern *Crocuta*, but developed M^1s are not found in any *Crocuta* other than *C. sivalensis*. *Crocuta felina*, as presented in BM 15902, lacks a P^1 and retains a very small diastema between the P^2 and the upper canine. This contrasts with BOU-VP-1/204's distinct P^1 and large diastema.

TABLE 4.5 Eigenvalues for Factors 1 and 2

	Eigenvalue	*% Total*	*Cumulative*	*Cumulative*
Factor 1	10.01049	43.52389	10.01049	43.52389
Factor 2	3.15175	13.70325	13.16224	57.22714

EBSCOhost - printed on 10/28/2022 4:53 AM via . All use subject to https://www.ebsco.com/terms-of-use

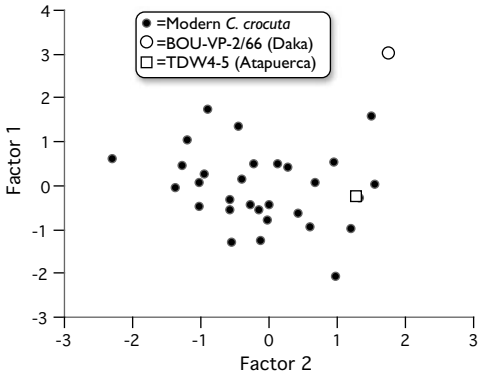

FIGURE 4.7

Principal components analysis of skull and upper dentition variables for fossil and recent *Crocuta* listed in Table 4.4. See Tables 4.4 and 4.5 for parameters.

Conclusion

Daka carnivores include *Crocuta crocuta yangula*, *Panthera* cf. *pardus*, and *Panthera* cf. *leo*. Carnivores potentially influenced the lives of Daka Member hominids, and preburial modifications on *Homo erectus* cranium BOU-VP-2/66 are likely the result of carnivore activity. The Daka Member carnivore assemblage presents one of the best preserved Pleistocene *Crocuta* crania known. This cranium, significantly larger than any recent or prehistoric eastern African *Crocuta*, has been placed in a new subspecies, *C. crocuta yangula*.

EBSCOhost - printed on 10/28/2022 4:53 AM via . All use subject to https://www.ebsco.com/terms-of-use

This Page Left Intentionally Blank

EBSCOhost - printed on 10/28/2022 4:53 AM via . All use subject to https://www.ebsco.com/terms-of-use

5

Cercopithecidae

W. HENRY GILBERT
AND
STEVE FROST

Cercopithecidae is the most speciose and geographically widespread extant nonhuman primate family. It includes two universally accepted extant clades, usually recognized as the subfamilies Cercopithecinae and Colobinae (e.g., Delson 1975; Szalay and Delson 1979; Strasser and Delson 1987; Fleagle 1999; Disotell 2000; Grubb et al. 2003; Brandon-Jones et al. 2004), and occasionally as families (e.g., Jablonski 2002). Many morphological features distinguish these two groups, including soft-tissue features (e.g., Delson 1975; Szalay and Delson 1979; Strasser and Delson 1987; Fleagle 1999; Jablonski 2002). Frost (2001a) provides a relatively complete list. All molecular analyses to date have corroborated this split (e.g., Disotell 2000).

Seventeen fossil Cercopithecidae have been collected from the Daka Member. Both subfamilies of Cercopithecidae are present in the Daka sample, with the Cercopithecinae predominating. Of this subfamily, all specimens identifiable to genus belong to the large extinct baboon *Theropithecus oswaldi leakeyi*. This taxon is represented by both cranial and postcranial material, including an adult calvaria, a juvenile partial cranium (Figure 5.1), three mandibular fragments, a premolar, three femora, and two tibiae. Only two specimens are diagnostically colobine. One is a partial cranium of a new species of the extinct genus *Cercopithecoides,* and the other is an isolated lower molar, which could potentially be from this new species or *Colobus*. There are also three femoral fragments and one scapular fragment that cannot be allocated to subfamily with certainty. This is a relatively low number compared with some middle Pleistocene localities within the Afar region, such as Asbole and Andalee (Kalb et al. 1982a; Alemseged and Geraads 2001; Geraads et al. 2004), and closer to that from Bodo (Kalb et al. 1980).

The extinct genera *Prohylobates* and *Victoriapithecus* are generally considered to be sister taxa to the Colobinae and Cercopithecinae (e.g., Szalay and Delson 1979; Strasser and Delson 1987; Fleagle 1999; Jablonski 2002), and they are recognized either as the subfamily Victoriapithecinae within the family Cercopithecidae (e.g., Szalay and Delson 1979; Leakey et al. 2003) or as a separate family, Victoriapithecidae (Benefit and McCrossin 2002). They are known from several middle and late Miocene sites in northern and eastern Africa, as well as Arabia (Szalay and Delson 1979; Benefit and

EBSCOhost - printed on 10/28/2022 4:53 AM via . All use subject to https://www.ebsco.com/terms-of-use

FIGURE 5.1
Berhane Asfaw with cranium of cercopithecid BOU-VP-2/1 in 1992. Initial visits to localities such as this often produce very well preserved specimens on the lag surfaces, but since these surfaces armor the underlying soft sediments, revisits are rarely rewarded with an abundance of intact specimens like this one. Photograph by Tim White, December 28, 1992.

McCrossin 2002). One of the main reasons for their taxonomic status is that their molar teeth are incompletely bilophodont, retain cristae obliquae, and variably lack distal loph(id)s (Benefit 1999).

Colobinae

There are only two specimens that are diagnostically colobine from the Daka Member. One is a well-preserved calvaria with an upper face and associated maxilla that represents a new species of *Cercopithecoides*. The other, an isolated lower molar, is clearly colobine and is of a size compatible with extant *Colobus* as well as with the new taxon.

The subfamily Colobinae is divided into two geographically distinct clades, typically recognized at the subtribe level: the African Colobina and the Asian Presbytina (e.g., Delson

EBSCOhost - printed on 10/28/2022 4:53 AM via . All use subject to https://www.ebsco.com/terms-of-use

1975; Szalay and Delson 1979; Strasser and Delson 1987; Disotell 2000). The extant members of the latter group are far more diverse than those of the former in both morphology and generic diversity. There are now six extinct genera of colobines known from the African fossil record (e.g., Delson 1994; Frost 2001b; Jablonski 2002), but the taxonomic position of most of these relative to the two subtribes is not clear.

Cercopithecoides Mollet, 1947

SYNONYMY (= or including *Parapapio* Jones 1937; Broom 1940; Broom & Robinson 1950; Freedman 1957, in part. *Brachygnathopithecus* Kitching 1952, in part. Colobinae cf. *Cercopithecoides* Leakey & Leakey 1973. cf. Colobinae gen. et sp. nov. A: Eck 1976; 1977; Colobinae gen. et sp. indet. smaller Szalay & Delson, 1979).

TYPE SPECIES *Cercopithecoides williamsi* Mollet, 1947.

OTHER SPECIES *C. kimeui* Leakey 1982; *C. meaveae* Frost and Delson 2002; *C. kerioensis* Leakey et al. 2003.

GENERIC DIAGNOSIS See Frost and Delson (2002).

Cercopithecoides alemayehui sp. nov.

ETYMOLOGY Named to honor the discoverer of this and many other Middle Awash fossils, Alemayehu Asfaw.

HOLOTYPE BOU-VP-1/95 (calvaria and right maxilla; Figures 5.2 and 5.3).

LOCALITIES AND HORIZONS Bouri Formation, Daka Member.

DIAGNOSIS Cranium is smaller than in *Cercopithecoides kimeui* and *C. williamsi,* and is comparable to *C. meaveae* and *C. kerioensis*. Supraorbital torus is more projecting than in either *C. meaveae* or *C. kerioensis*. Teeth are significantly smaller than those of *C. kimeui,* and generally smaller than those of *C. williamsi,* although there is some overlap with the lower end of the *C. williamsi* molar size range. Dental dimensions close in overall size to *C. kerioensis* and *C. meaveae*. The nasals bones are longer than those of any other *Cercopithecoides* species, and they extend inferior of the inferior orbital rims. The supraorbital tori are more projecting than those of *C. kerioensis* or *C. meaveae,* and are more similar to those of *C. williamsi*. In dental proportions, the molars are relatively larger in comparison to cranial size than those of *C. meaveae*. Additionally, the molars are relatively broader than those of *C. meaveae,* being similar in proportion to those of the other species of *Cercopithecoides*.

REMARKS This taxon is represented by a single specimen: BOU-VP-1/95, a partial cranium. The calvaria is preserved, as is the basicranium, but the latter was eroded prior to discovery and it has not been possible to completely reassemble it. The right maxilla, with the roots of the lateral incisor and canine as well as the crowns of P^3–M^3, is pres-

EBSCOhost - printed on 10/28/2022 4:53 AM via . All use subject to https://www.ebsco.com/terms-of-use

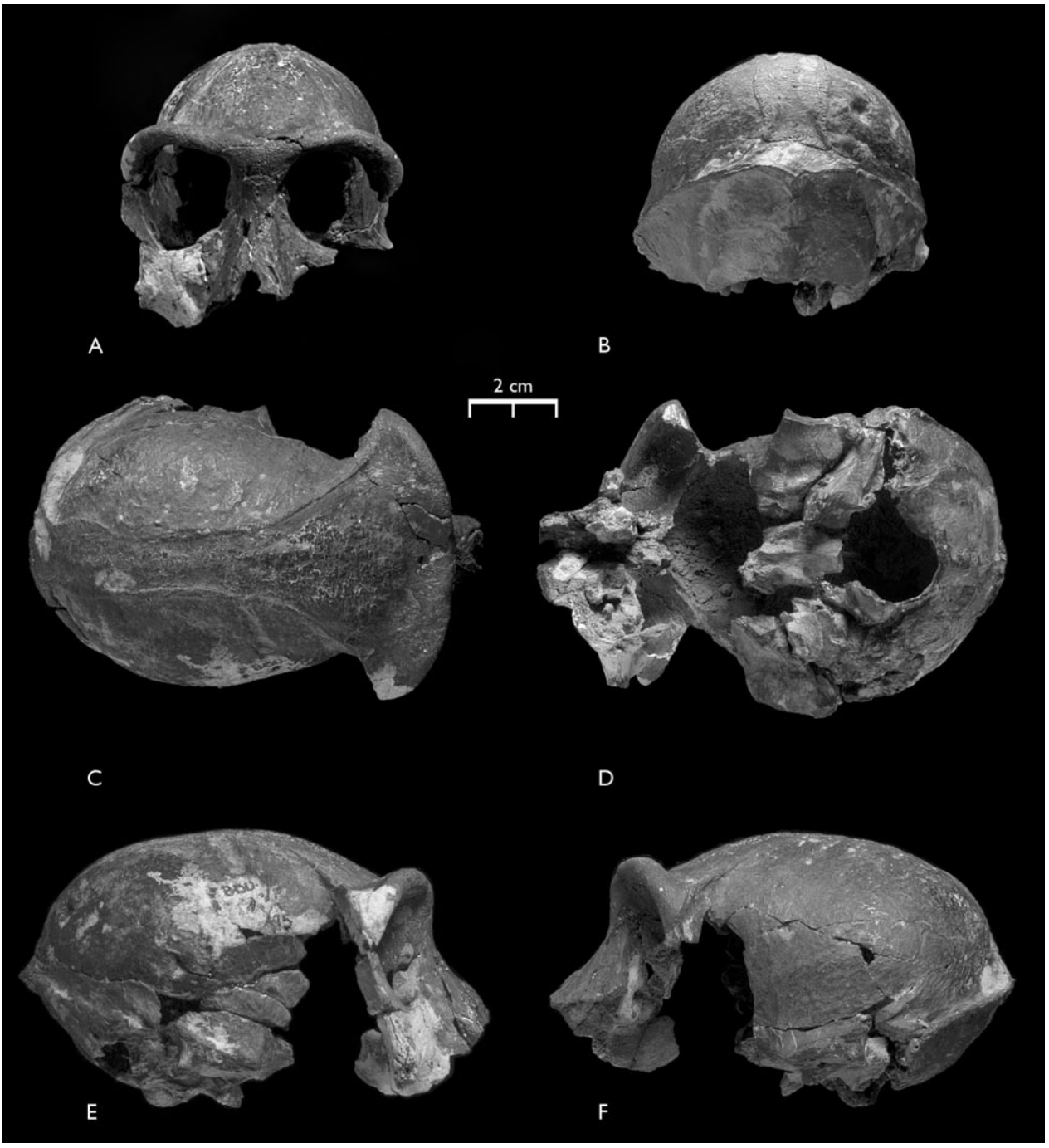

FIGURE 5.2

Cercopithecoides alemayehui sp. nov. cranium BOU-VP-1/95. A. Anterior view. B. Posterior view. C. Superior view. D. Inferior view. E. Right lateral view F. Left lateral view.

EBSCOhost - printed on 10/28/2022 4:53 AM via . All use subject to https://www.ebsco.com/terms-of-use

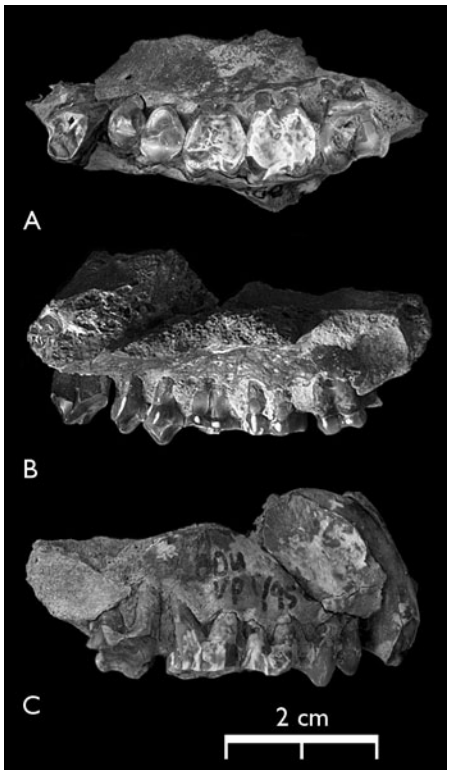

FIGURE 5.3

Cercopithecoides alemayehui sp. nov. maxilla: BOU-VP-1/95.
A. Occlusal view.
B. Lingual view.
C. Buccal view.

ent, but separate from the calvaria. Surface detail is well preserved. The cranium is not symmetrical, with distortion especially apparent in basal view and on the temporal lines. However, it does not appear that this asymmetry was the result of in situ plastic distortion or expanding matrix distortion. Rather, it seems that the individual sustained in vivo injuries. There are unusual occlusion facets on the lingual roots of the right maxillary tooth row. As the teeth of BOU-VP-1/95 also have substantial normal occlusal wear, presumably developed prior to the event initiating asymmetrical occlusion, it is possible that trauma led to the observed asymmetry in this individual. There are also two depressions on the posterior right parietal that appear to be healed injuries.

DESCRIPTION In cranial size, BOU-VP-1/95 is larger than extant colobines (other than larger subspecies of *Semnopithecus entellus*), although it overlaps the upper ranges of some extant taxa in some dimensions. It is smaller than known species of *Paracolobus, Rhinocolobus*, *C. kimeui,* and most *C. williamsi,* and slightly smaller than the holotype of *C. meaveae*. The molars are larger than those of extant *Colobus,* including the Pleistocene sample from Andalee (Kalb et al. 1982a; Frost 2001a), and *Procolobus,* and smaller than those of *Paracolobus, Rhinocolobus,* and *C. kimeui,* and overlapping the smaller end of the *C. williamsi* range. Cranial and dental dimensions are presented in Tables 5.1 and 5.3, respectively.

EBSCOhost - printed on 10/28/2022 4:53 AM via . All use subject to https://www.ebsco.com/terms-of-use

TABLE 5.1 Cranial Dimensions

Crania	*BOU-VP-1/95*	*BOU-VP-1/132*	*BOU-VP-2/1*
Nasospinale–Rhinion			(29)
Rhinion–Nasion	22		25
Nasion–Inion	100		122
Nasion–Basion	(64)		(80)
Glabella–Inion	101		124
Bregma–Inion	55	74	57
Biorbital Breadth	58		60
Interorbital Breadth	13		
Postorbital Breadth	45	56	
Biporionic Breadth	(72)	113	105
Orbit Height	25		
Orbit Breadth	24		
Alveolar process length from mesial C to distal M^3	44		

NOTE: Values in parentheses are estimated.

In general shape, the calvaria is long and narrow. Postorbital constriction is modest (Table 5.1). The brow ridge is projecting, and arches over each orbit separately. In lateral view glabella is prominent and positioned anterior to nasion. Superiorly, there is a marked ophryonic groove, with the frontal rising posteriorly, a feature common in *Cercopithecoides* and *Procolobus*. The temporal lines are strongly marked, and turn posteriorly so that they are parallel at bregma, and remain approximately 1.0 cm apart to lambda. The lines are slightly asymmetrical, the left being somewhat closer to the sagittal suture than the right. The left line is also slightly discontinuous, with a hiatus halfway along its parietal course. Posteriorly, the temporal lines meet the nuchal crests, which are relatively prominent.

On the basicranium, the postglenoid process is broken bilaterally, but its base can be seen to project posteroinferiorly at approximately 45 degrees. Although the lateral portions of the glenoid fossae are broken at the zygomatic bases on both sides, both anterior and posterior articular facets can be observed. The sphenoid, including the pterygoid plates, is missing, and it is therefore impossible to determine whether the pterygoid fossae were perforated. The tympanic plate is not separated anteriorly from the postglenoid process, although a deep crevasse divides it from the lateral aspect of the posterior lobe of the glenoid fossa and the groove medial to it.

TABLE 5.2 Mandibular Dimensions

Mandibles	*BOU-VP-1/3*	*BOU-VP-26/3*
Corpus Depth at P_4/M_1 Contact		38
Corpus Depth at M_2/M_3 Contact	44	
Corpus Breadth at M_2/M_3 Contact	26	

EBSCOhost - printed on 10/28/2022 4:53 AM via . All use subject to https://www.ebsco.com/terms-of-use

TABLE 5.3 Colobine Dental Dimensions

Specimen	*Sex*	*Tooth*	*WS*	*W*	*PW*	*L*
BOU-VP-1/95	M	C^1		6.8		8.9
BOU-VP-1/95	M	P^3	7	5.7		4.3
BOU-VP-1/95	M	P^4	6	6.9		5.1
BOU-VP-1/95	M	M^1	16	7.7		7.3
BOU-VP-1/95	M	M^2	16	8.9		8.9
BOU-VP-1/95	M	M^3	16	9.3	7.5	8.9
BOU-VP-2/26	?	M_X	9	5.5	6.0	7.0

NOTE: WS indicates wear stage of the tooth (see Frost 2001a for definitions); W indicates buccolingual crown width, or in the case of molars width across the mesial loph(id); PW indicates buccolingual width across the distal molar loph(id); L indicates mesiodistal crown length.

The interorbital pillar is broad (Table 5.1). The orbits are tall and narrow and ovoid. The most inferior portion of the orbital rim is approximately 2.0 mm lateral to the zygomaticomaxillary suture, but lies superior to rhinion. The nasals are long for a colobine, extending over 1.0 cm inferiorly beyond the inferior orbital rim. The lacrimal groove extends onto the maxilla. The superior extreme of the piriform aperture is preserved, and shows that rhinion was not prominent. The face is deep due in part to the tall orbital area and deep, vertical zygoma. The infraorbital foramina are moderate in size and multiple, being smaller than those of *Procolobus*. They are distributed only on the coronally oriented portion of the maxilla. The base of the zygomatic process of the maxilla is positioned superior to the M^2. A slight postcanine fossa is present, which is deepest superiorly. The superior portion of the zygoma is broken, revealing a smooth-walled space that may represent a maxillary sinus. The premaxilla was likely squared in superior view, with a small incisive area, but it is difficult to be certain of this. In any event, it is less projecting than the same area of most specimens of *Colobus*.

The crown of the upper canine is not preserved other than the area immediately occlusal to the cervix. It is typical of the family, and its size and morphology clearly mark this individual as male. It is also substantially smaller than male upper canines of *C. williamsi*. The P^3 protocone is greatly reduced, so that it is nearly absent. The P^4 is a typical bicuspid tooth. It is considerably broader than the P^3. The molars are all marked by heavy wear so that little occlusal enamel remains and the lophs and cusps are completely worn away, rendering details of the morphology absent. Interestingly, the M^3 shows the most advanced state of wear. This degree of wear is rare among extant colobines, but common among individuals of *Cercopithecoides*. What is preserved of the crowns appears to indicate a relatively low amount of basal flare and crowns that are relatively broad for their length. The M^3 appears to be the largest of the molars, and the M^1 the smallest. This is also unusual among colobines, where the M^2 is typically the largest tooth.

DISCUSSION Morphologically this specimen fits best within *Cercopithecoides,* although its inclusion extends the morphological and chronological range of the genus. It is

EBSCOhost - printed on 10/28/2022 4:53 AM via . All use subject to https://www.ebsco.com/terms-of-use

distinct from *Colobus,* including that reported from Andalee (Kalb et al. 1982a; Frost 2001a), as well as *Procolobus*. It shows none of the derived morphological facial features of *Rhinocolobus* or *Paracolobus*. The supraorbital torus is thicker and projects farther anteriorly than that of *Colobus,* which is similar to *Procolobus* and *Cercopithecoides*. Unlike *Procolobus (Piliocolobus)* the torus is not marked by supraorbital foramina. The interorbital region is broad, which is similar to most colobines, but unlike *Rhinocolobus, Dolichopithecus,* and *Nasalis*. The nasals are at the longest extreme for individuals of *Colobus, Procolobus, Paracolobus*, and *Cercopithecoides,* longer than those of *Rhinocolobus,* but shorter than those of *Nasalis* and cercopithecines. The infraorbital foramina are smaller than those of *Procolobus*. The calvaria lacks a sagittal crest, which is different from *Paracolobus* and *Libypithecus,* and most male individuals of *Procolobus*. The temporal lines are, however, more strongly marked than those of *Colobus*. In fact, they are most similar to the less common condition in male *Procolobus* where they are strongly marked, but do not quite converge. The zygomatic process of the maxilla is positioned superior to the middle of the M^2, which overlaps the range for males of most colobine genera, but it is generally posterior to the position found in males of *Pygathrix* and *Kuseracolobus,* and anterior to that of *Nasalis* and *Rhinocolobus*. If the space in the zygomatic portion of the maxilla is a true sinus, then this would be inconsistent with any extant genus of colobine (but not inconsistent with *Cercopithecoides*). The P^3 protocone is reduced, a similarity to *Colobus, Procolobus,* and some *Cercopithecoides*. The molars are at an extreme state of wear unusual for extant colobines, but common among *Cercopithecoides*. The M^3 appears to have been the largest of the maxillary molars, though it is close in size to the M^2. This pattern is also unusual among colobines. It is for these reasons that BOU-VP-1/95 is here included in *Cercopithecoides*.

Colobinae gen. et sp. indet. cf. *Colobus*

MATERIAL BOU-VP-2/26 (left M_1 or M_2).

DESCRIPTION This specimen preserves the entire crown with the roots intact. It is either a first or second lower molar, but the former is more probable. It is moderately worn with dentine exposed on the tips of the protoconid and hypoconid, and very small areas of eroded enamel on the metaconid and entoconid. It is typical of the subfamily in morphology, with tall, widely spaced cusps, a low lingual notch, and well-developed lophids. The hypolophid is bucco-lingually broader than the protolophid. In size it is compatible with extant *Colobus*, *Procolobus*, as well as Colobinae sp. nov. (above). Given the presence of *Colobus* at other, although more recent, Pleistocene sites in the Afar region (Kalb et al. 1982; Alemseged and Geraads 2001; Frost 2001b) it cannot be allocated further here on the basis of morphology.

Cercopithecinae

All 11 specimens that are diagnosable to this subfamily are of the large baboon *Theropithecus oswaldi leakeyi*. This taxon can often be easily identified on size alone, but many elements in the Daka assemblage show diagnostic morphology as well. The material includes cranial and postcranial specimens, including the first juvenile cranium of this subspecies.

EBSCOhost - printed on 10/28/2022 4:53 AM via . All use subject to https://www.ebsco.com/terms-of-use

The Cercopithecinae are divided into two clades, one being the highly speciose and often arboreal tribe Cercopithecini that includes the guenons and allies (see Tosi et al. 2004 for recent taxonomic discussion of genera). There are no cercopithecins represented in the Daka Member sample to date. The other major clade is the tribe Papionini, including the Asian and northern African genus *Macaca,* usually placed in its own subtribe Macacina, and the sub-Saharan African genera in the subtribe Papionina (e.g., Delson 1975; Szalay and Delson 1979; Strasser and Delson 1987). Molecular data have generally supported these divisions (e.g., Disotell 2000; Tosi et al. 2000, 2002). Furthermore, molecular phylogenies have shown that within the papioninans, there are two main clades, which have not been assigned formal taxonomic status. These are *Papio, Lophocebus,* and *Theropithecus* in one group, and *Mandrillus* and *Cercocebus* in the other (Disotell 1994; Harris and Disotell 1998). Fleagle and McGraw (1999, 2002) have found several morphological features that seem to support this taxonomic arrangement.

Theropithecus Geoffroy, 1843

Theropithecus oswaldi (Andrews, 1916)

REVISED DIAGNOSIS The concept of *T. oswaldi* used here follows that of Leakey (1993). Three chronologically sequential subspecies are recognized within Africa, each of which spans a large geographic area. This species is distinguished from the other undisputed members of the genus *Theropithecus, T. gelada* and *T. brumpti,* largely on the basis of characters in the cranium and anterior dentition.

There are several morphological trends displayed by the subspecies of *Theropithecus oswaldi*, which show their origins in *T. o. darti* and their most extreme expressions in *T. o. leakeyi*. These trends are also features that distinguish this species from *T. brumpti* and to a lesser extent *T. gelada*.

Through time there is a general increase in body size from early *T. o. darti* (similar in size to *T. gelada*) to the largest *T. o. leakeyi* (similar in size to gorilla females) (e.g., Jolly 1972; Eck 1987; Krentz 1993; Delson et al. 2000; Frost and Delson 2002). Thus, early members of this species can be separated from *T. brumpti* partly because they are smaller, and later members can be distinguished from *T. gelada* because they are larger. There are also a large number of shape differences through time. At the same time, there is a decrease in the size of the premaxilla relative to the maxilla and a decrease in the length of the rostrum relative to overall cranial size, a pattern that is opposite to that seen in most other papionines. There is also a trend toward increased facial depth and airorhynchy. Finally, there is an increase in the size of the sagittal and nuchal crests.

The symphysis has only weakly marked mental ridges, and in early *T. o. darti,* it is more sloping than that of *T. brumpti* or *T. gelada*. The mandible either entirely lacks corpus fossae, or they are only lightly developed (except for some *T. o. darti* that may have larger fossae). This is distinct from both *T. brumpti* and *T. gelada,* which typically have well-developed corpus fossae.

Related to the decrease in premaxillary size through time, there is a progressive decrease in incisor size, and a decrease in canine height, if not caliber (Leakey 1993). The reduction in canine size leads to a shortening of the P^3 mesiobuccal flange, particularly in males. Both of these features separate *T. oswaldi* from *T. brumpti* and *T. gelada* and may be atypical of

EBSCOhost - printed on 10/28/2022 4:53 AM via . All use subject to https://www.ebsco.com/terms-of-use

size trends in other papionines. Finally, there is a substantial increase in dental size, particularly of the distal molars, through time. Along with the increased size, there is an increase in crown complexity, which makes *T. o. leakeyi* molars distinct from those of *T. gelada*.

Theropithecus oswaldi leakeyi (Hopwood, 1934)

REVISED DIAGNOSIS This subspecies is distinguished from both *T. o. darti* and *T. o. oswaldi* by its larger cranial, molar, and postcranial size. The rostrum is shorter relative to cranial size and the zygomatic is positioned more anteriorly (typically near M^2). Cranial superstructures are larger than in any other known cercopithecid. The posterior maxilla is deeper. The mandibular symphysis lacks mental ridges, and often has a triangular fossa on the anterior surface between the roots of the canines. The area for the incisors is very small, and the canine roots converge inferiorly. The mandible completely lacks corpus fossae, and the ramus is tall and vertical. The molar teeth are larger than those of other subspecies. The M_3 is larger relative to the M_2, which is in turn larger relative to the M_1 than in other subspecies. This relationship is generally true for the upper molars as well. Molar enamel complexity is also greater in this subspecies than in the older subspecies. The incisors are relatively smaller. The canines are relatively shorter, though often still very broad. The P_3 mesiobuccal flange is likewise short.

REMARKS This taxon is represented by several elements. BOU-VP-1/132 (Figure 5.4) is a calvaria lacking the area anterior to ophryonic groove, the right temporal, as well as most of the basicranium. BOU-VP-2/1 (Figure 5.5) is a heavily worn and eroded juvenile partial cranium, missing the right zygomatic and temporal bones, most of the right side of the face, and the area around the foramen magnum. A small portion of the endocast is preserved on the right side. Most of the surface detail has been lost or is covered by a highly calcified, irremovable matrix. While none of the dentition is preserved, the $dp^{3–4}$ and M^1 would have been erupted and in wear, while the M^2 was still in the crypt. Two mandibular corpora are present. BOU-VP-1/3 preserves the roots of the distal M_2 and M_3 and the entire corpus underneath, as well as a small portion of the base of the ramus. BOU-VP-26/3 preserves the symphysis and corpus distally to the mesial root of M_3. The crowns of P_4-M_2 are preserved, but damaged, as are the alveoli for the canine and P_3. A single isolated P_3, BOU-VP-1/212, is present. There are two proximal femora, BOU-VP-1/81 and BOU-VP-1/86, the latter with one-third of the shaft. The surface detail of the former is well preserved, whereas that of the latter is somewhat cracked, distorted, and filled with matrix. The distal end of a femur with both condyles and 3.5 cm of shaft is represented by BOU-VP-1/113, but the cortical bone is missing over much of the surface, exposing the trabecular bone on both of the condyles. Two proximal tibiae are present, BOU-VP-1/28 and BOU-VP-2/88. The former preserves the proximal one-half to two-thirds of the shaft, while the latter only preserves about 2.0 cm of the shaft below the condyles. The cortical bone is well preserved on BOU-VP-2/88 except on the anterior surface of the tuberosity, but that of BOU-VP-1/28 is more extensively damaged, particularly on the medial and anterior surfaces.

EBSCOhost - printed on 10/28/2022 4:53 AM via . All use subject to https://www.ebsco.com/terms-of-use

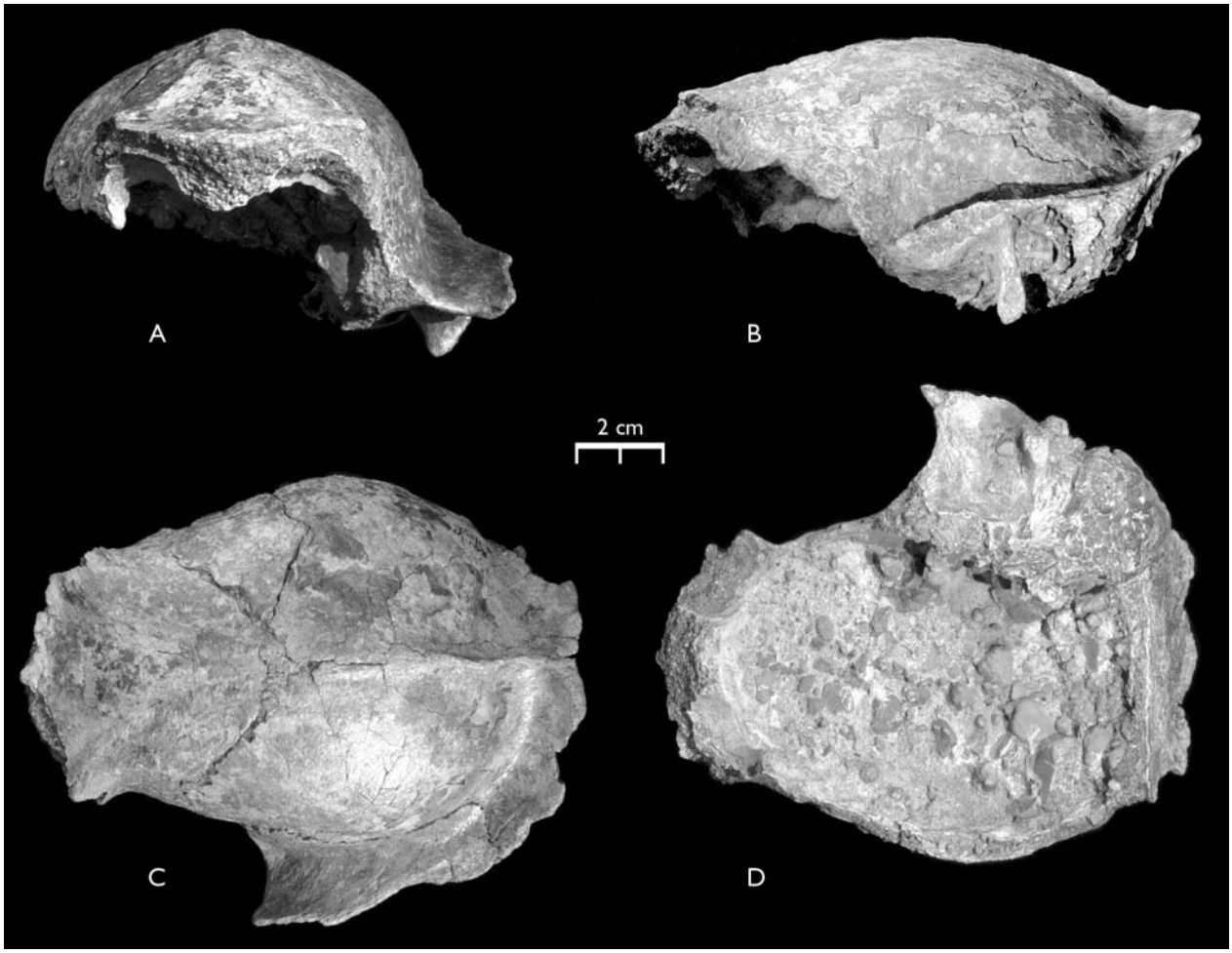

FIGURE 5.4
Theropithecus oswaldi leakeyi calvaria BOU-VP-1/132. A. Anterior view. B. Left lateral view. C. Superior view. D. Inferior view.

DESCRIPTION In size and morphology, BOU-VP-1/132 is similar to the female partial cranium DAW-VP-1/1 (Gilbert et al. 2000; figured in Frost 2001a). In overall calvaria size, it is smaller than the probable male calvaria KGA7-350 (Frost, in preparation) from Konso, and much smaller than the males KL337-1 and HAR-VP-1/1 (figured in Delson et al. 2000; Gilbert et al. 2000; Frost 2001a). In spite of its relatively young age, the calvaria of BOU-VP-2/1 overlaps the largest adults of extant *Papio hamadryas* and *Mandrillus sphinx*. The face, however, is relatively short, due to both the young age of this specimen and the generally short face of *T. o. leakeyi* (Figure 5.5; Table 5.1).

The brow ridge of BOU-VP-2/1 is strongly eroded and mostly absent so that little of the supraorbital morphology can be determined, but it was probably quite prominent. As is typical of *T. o. leakeyi* calvaria, postorbital constriction is strong in both Daka specimens, when the juvenile nature of BOU-VP-2/1 is taken into account (Figures 5.4 and 5.5; Table 5.1), and there is evidence for large temporal muscles. The temporal lines of BOU-VP-1/132 are marked, but not as prominent as those of the males. They meet immediately posterior to bregma and form a sagittal crest that

EBSCOhost - printed on 10/28/2022 4:53 AM via . All use subject to https://www.ebsco.com/terms-of-use

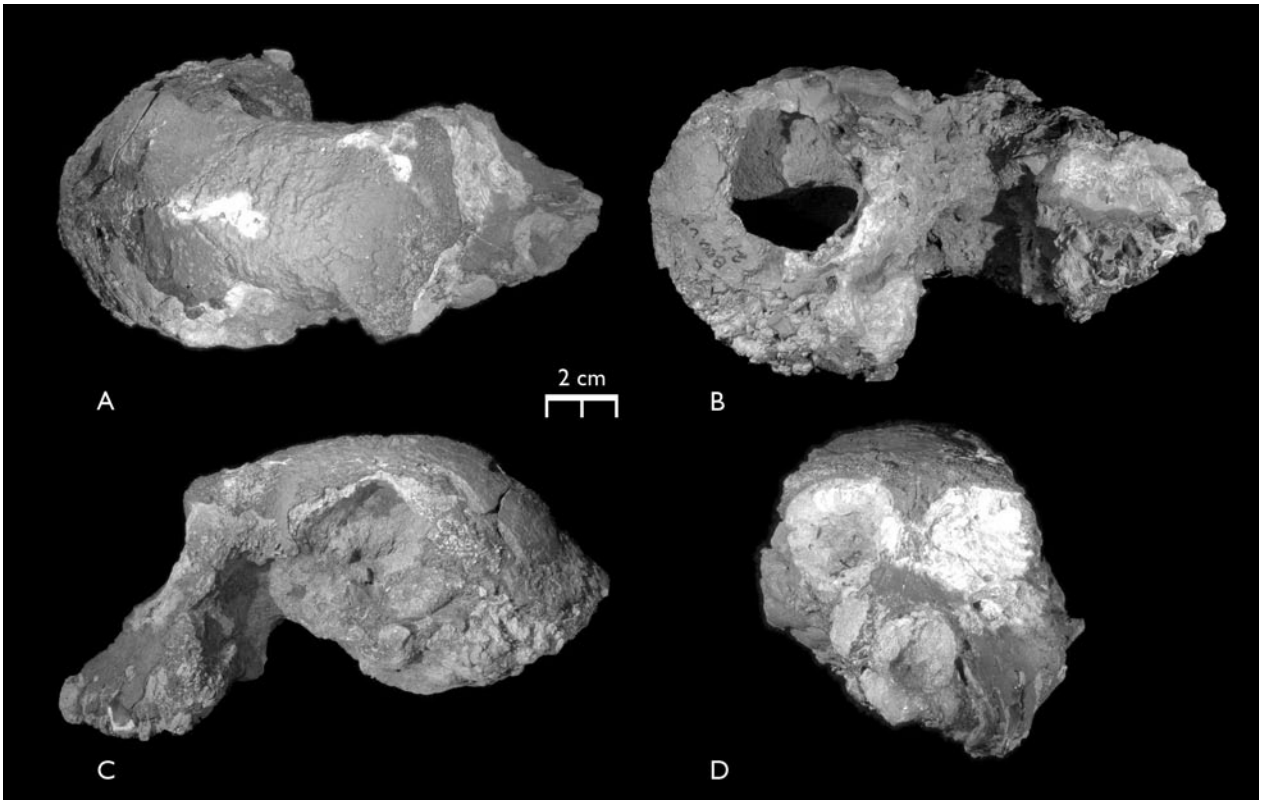

FIGURE 5.5
Theropithecus oswaldi leakeyi cranium BOU-VP-2/1.
A. Superior view.
B. Inferior view.
C. Left lateral view.
D. Anterior view.

reaches its greatest height, less than 5.0 mm, near inion. Here it meets a prominent nuchal crest that is over 1.0 cm high and roughly semicircular in superior view. In general, these crests are smaller than those of the males HAR-VP-1/1, KL337-1, and KGA3-750, and also slightly smaller than those of the female DAW-VP-1/1. Therefore, this specimen is probably an adult, or near adult, female. A bony ledge continuous with the superior surface of the zygomatic process of the temporal, the nuchal crest, forms a nearly continuous shelf, lateral and posterior to the neurocranium, that provides a large area for attachment of the temporalis muscle. The temporal lines of BOU-VP-2/1 do not form a sagittal crest, as would be expected of a juvenile, but the nuchal crest has already begun to form. Viewed posteriorly, the neurocranium is widest inferiorly, at the level of porion, and the temporal squamae are inclined more medially than they are in earlier subspecies of *T. oswaldi*.

The face is only preserved on BOU-VP-2/1. As the specimen is juvenile, the face is very short relative to the neurocranium, but the characteristic *T. o. leakeyi* morphology can already be observed. The interorbital region is present, though partly eroded and the dacryonic areas are partly obscured by matrix. As a result the interorbital breadth cannot be directly measured, but it appears broad. The lateral orbital margins are not well preserved, but matrix fills the orbits so that their general shape can be seen, and it is essentially ovoid. The nasals are quite short, extending approximately 2.0 cm rostral to the maxillary zygomatic process. As would be expected for an individual of this age there is no evidence of maxillary ridges or fossae. As a result, this individual does not possess the

EBSCOhost - printed on 10/28/2022 4:53 AM via . All use subject to https://www.ebsco.com/terms-of-use

TABLE 5.4 *Theropithecus* Dental Dimensions

Specimen	*Sex*	*Tooth*	*WS*	*W*	*FL*	*L*
BOU-VP-1/212	F	P_3		6.9	10.8	9.2
BOU-VP-26/3	F	P_4	7	(8.3)		9.1
BOU-VP-26/3	F	M_1	16	10		12.9
BOU-VP-26/3	F	M_2	16	(13.3)		17.1

NOTE: Dimensions as for Table 5.2. FL indicates length of the mesiobuccal honing flange from protoconid to mesiobuccal extreme.

concave-convex-concave muzzle dorsum shown by adult males of the subspecies from the Dawaitoli Formation (Frost 2001a). Whether or not this individual would have had it as an adult is not certain. The dorsal surface of the rostrum has the typical sellar morphology: it is U shaped in paracoronal section, and smoothly and deeply concave in profile. The midface is already quite deep, and the zygomatics are positioned far anteriorly, even for a juvenile.

Most of the basicranium of BOU-VP-2/1 is obscured by matrix. A few details of the basicranium of BOU-VP-1/132 can be observed. The postglenoid process is approximately 1.5 cm tall and resembles an equilateral triangle in shape. It is separated from the glenoid articulation by a wide sulcus, although this area is partially obscured by matrix. The articular facet for the mandibular condyle is sellar in morphology, being concave-down in the coronal plane and convex-down in the parasagittal plane. Viewed inferiorly, its outline is mediolaterally elongate and similar to an L in shape, with the foot at the medial end and the toe pointed anteriorly. The medial aspect of the facet (i.e., the foot of the L) faces more laterally, whereas the lateral portion is flatter and faces more inferiorly. In these aspects, BOU-VP-1/132 is similar to the material from Kanjera and Olorgesailie (Jolly 1972). In the anterior part of the medial half of the mandibular articulation there is a slightly flattened area that may have accommodated the condyle while the mandible was maximally depressed. The tympanic is angled slightly posterolaterally and marked by a prominent crest. The mastoid area is inflated, but erosion renders it impossible to determine if the mastoid process was prominent.

Mandible The symphysis is only represented by BOU-VP-26/3 (Figure 5.6). Anteriorly, the symphysis is marked by a median mental foramen and moderately sized mental ridges. In lateral view the profile is deep and steeply sloping. The transverse tori are large and robust, with the superior extending posteriorly to the mesial P_4 and the inferior to the distal P_4. All three mandibular specimens preserve some aspects of the corpus, which is thick and robust (Table 5.2). In lateral view, the surface lacks fossae, and appears to shallow posteriorly in BOU-VP-26/3 (the only specimen where this can be judged). The mental foramen is positioned under the P_4/M_1 contact. BOU-VP-1/3 preserves the anteroinferior extreme of the ramus. In superior view, the corpus is thick, exceeding 2.5 cm under the M_3, and the buccinator sulcus is deep and broad. In all of these features, the corpus is similar to other *T. o. leakeyi* mandibles from Olduvai, Olorgesailie, Hopefield, Thomas Quarries, and Tighenif (i.e., Ternifine) (Leakey and Whitworth 1958; Singer 1962; Jolly 1972; Dechow and Singer 1984; Delson 1993).

EBSCOhost - printed on 10/28/2022 4:53 AM via . All use subject to https://www.ebsco.com/terms-of-use

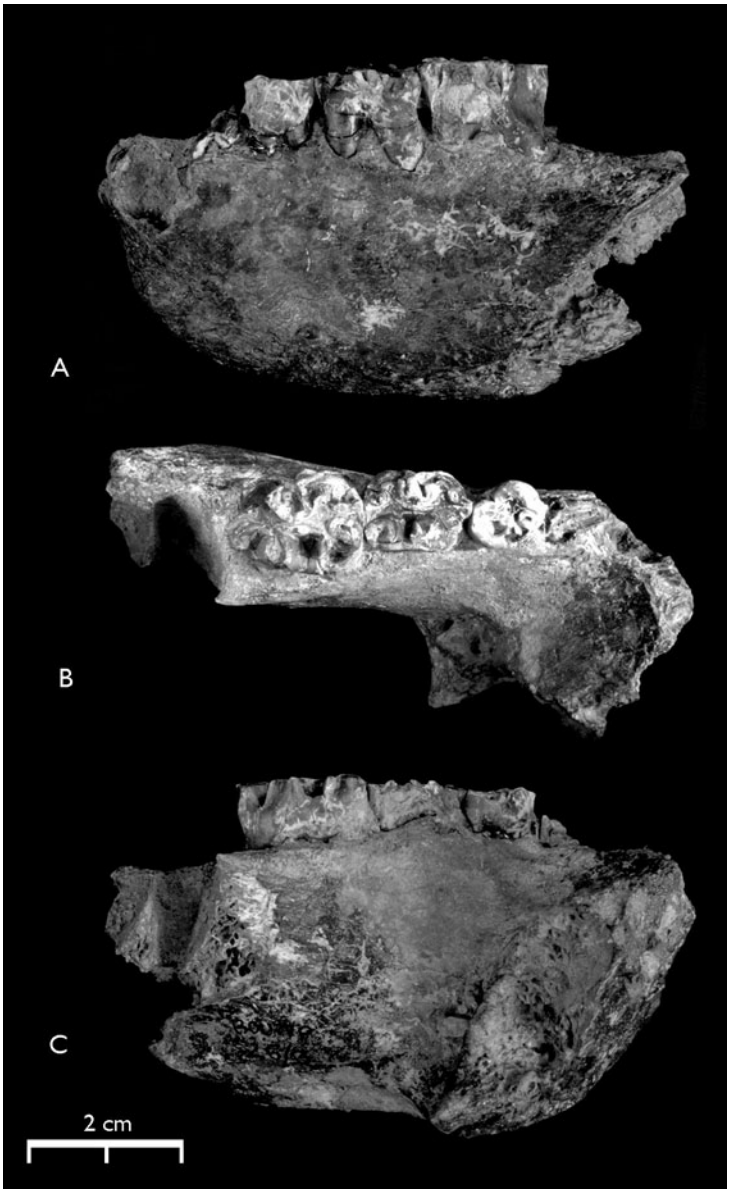

FIGURE 5.6
Theropithecus oswaldi leakeyi mandibles BOU-VP-26/3. A. Buccal view. B. Occlusal view. C. Lingual view.

Dentition Only the lower postcanine dentition is preserved. In general it is similar to other known samples of *T. o. leakeyi.* The only preserved P_3 is from a female individual. It is typical for the family in that it has a prominent protoconid with a relatively small talonid. The mesiobuccal flange is very short, being shorter relative to overall tooth size than those of females of other baboon species. This is consistent with other known populations of *T. o. leakeyi* and consistent with the reduction of the anterior dentition in this taxon. The P_4 is a large and molarized tooth. The protolophid has the same enamel folding seen on the molars. The talonid is relatively large, with its perimeter formed by a prominent cristid. The molars show all of the diagnostic features of the genus (Jolly 1972; Szalay and

EBSCOhost - printed on 10/28/2022 4:53 AM via . All use subject to https://www.ebsco.com/terms-of-use

TABLE 5.5 Postcranial Dimensions

Measurement	*BOU-VP-1/28*	*BOU-VP-1/29*	*BOU-VP-1/39*	*BOU-VP-1/62*	*BOU-VP-1/81*	*BOU-VP-1/86*	*BOU-VP-2/88*	*BOU-VP-1/113*
Femora								
Anterioposterior Head Diameter		(26)	20		31	(28)		
Maximum Mediolateral Breadth			41		61	(50)		
Greater Trochanter Projection				16	19	(16)		
Shaft Anterioposterior Diameter				17		(22)		
Shaft Mediolateral Diameter				16		(19)		
Bicondylar Breadth								53
Anterioposterior Condyle Length								(39)
Tibiae								
Proximal Anterioposterior Depth	41						45	
Proximal Mediolateral Breadth	49						49	

Delson 1979), but they are developed to an extreme as in other samples of *T. o. leakeyi* (Figure 5.6). The lower molars show a distinct increase in size from M_1 to M_3.

Femur The proximal end of the femur is typical of terrestrially adapted cercopithecines, but, in addition to its extreme size, it also shows some features unique to *T. o. leakeyi*. The larger of the two, BOU-VP-1/81, is close in size to the smaller of the two femora identified as possibly male from Olorgesailie and Bodo, and BOU-VP-1/86 is slightly smaller than the Olorgesailie females (Table 5.5; Jolly 1972; Frost 2001a). The head is spherical and marked by a large and oval fovea capitis. The posterior aspect of the articular surface has a prominent extension onto the neck, which is elevated above the surrounding nonarticular bone surface, with its posteromedial extreme arching superiorly and posteriorly. While the articular surface in several cercopithecid taxa does extend onto the posterior neck, it is never as prominent and well marked as that of *T. o. leakeyi*. This feature is unknown in any other cercopithecid taxa including *T. o. oswaldi*. It likely indicates a hip that is habitually abducted, and may show this extreme expression due to a gait or posture of *Theropithecus* in combination with the extreme size of *T. o. leakeyi* (Krentz 1993; Iwamoto 1993). The neck shaft angle is low (approximately 105° and 108° in BOU-VP-1/81 and BOU-VP-1/86, respectively; Figure 5.8), and the neck is short. The greater trochanter is straight and extends more than 1.0 cm proximal to the head, and projects nearly 2.0 cm above the neck (Figure 5.7, Table 5.5). In both specimens the gluteal fossa is extensive. The *quadratus femoris* muscle insertion is prominent (though damaged on BOU-VP-1/81). The lesser trochanter is long and posteriorly oriented. The shaft of BOU-VP-1/86 is strongly curved in the anteroposterior plane. The distal end of the femur is typical of the family, but also shows the reverse valgus angle typical of *T. oswaldi,* possibly associated with the "bottom-shuffling" gait known in *T. gelada* (Krentz 1993; Iwamoto 1993).

Tibia In general the proximal tibial morphology is typical of the family but also shows some features typical of *T. oswaldi* and is so large that it can represent only this

EBSCOhost - printed on 10/28/2022 4:53 AM via . All use subject to https://www.ebsco.com/terms-of-use

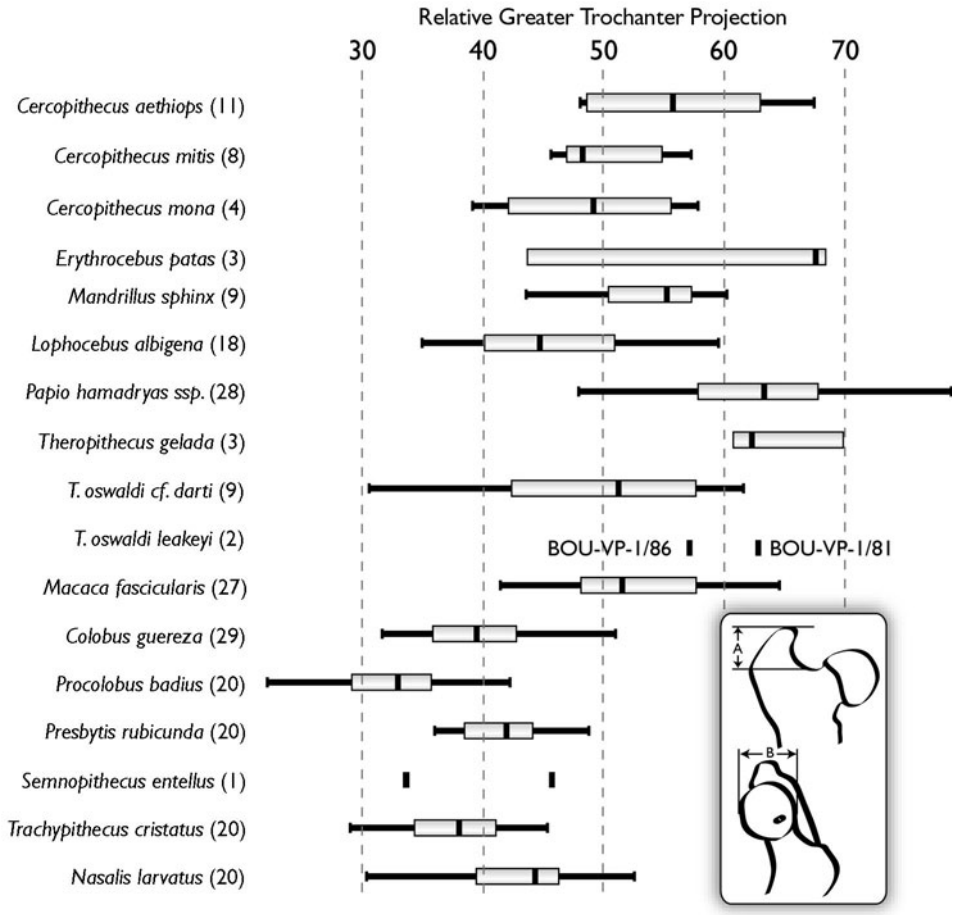

FIGURE 5.7

Box and whisker plot of greater trochanter projection. The central bar of each box represents the median or 50th percentile. The left and right of each box represent the value of the 25th and 75th percentiles, respectively. The whiskers extend to the farthest observation that is less than 1.5 times the length of the box. Any individuals outside of the whisker range are marked separately.

taxon. The proximal end is large and deep in the anteroposterior plane compared with its mediolateral breadth (Table 5.5). The medial and lateral condylar facets are more asymmetrical than in most other cercopithecid taxa, including earlier subspecies of *T. oswaldi,* with the medial facet being substantially larger than the lateral. The condylar facets are also relatively flat with the intercondylar area low. Although there is damage to the cortical bone of both specimens (especially BOU-VP-1/28), enough can be seen to determine that the tibial tuberosity is broad and flat, and does not project far anteriorly beyond the condylar facets, particularly in BOU-VP-2/88. In anterior view, the shaft of BOU-VP-1/28 shows a strong medial curvature, but too little of the shaft of BOU-VP-2/88 is preserved to determine if it was similarly formed. A partial *T. o. leakeyi* skeleton from Olduvai shows a similar medial curvature to its tibial shaft (illustrated in Szalay and Delson 1979), but this curvature is otherwise unknown among cercopithecids. Both specimens show a well-excavated fossa on the lateral surface of the tuberosity.

Cercopithecidae Subfamily Indet.

REMARKS There are four elements, BOU-VP-1/29, BOU-VP-1/39, BOU-VP-1/62, and BOU-VP-1/65, that cannot be diagnosed with confidence to specific taxa based on the

EBSCOhost - printed on 10/28/2022 4:53 AM via . All use subject to https://www.ebsco.com/terms-of-use

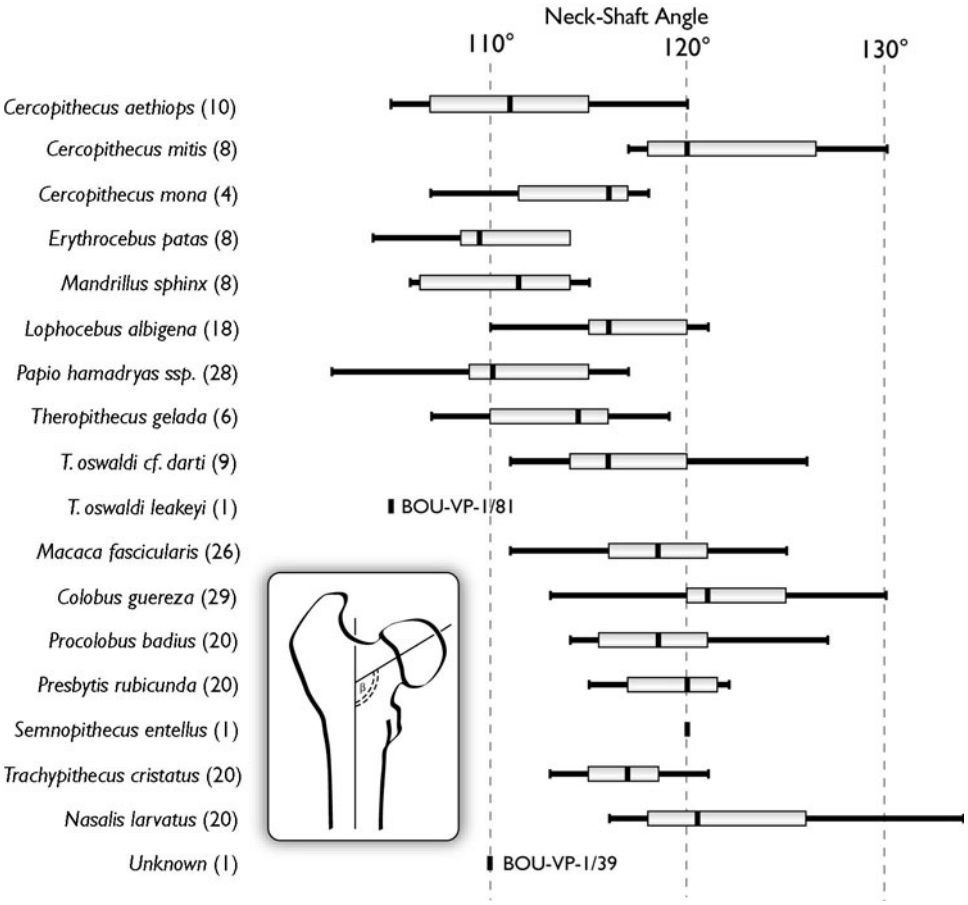

FIGURE 5.8
Box and whisker plot of neck-shaft angle.

available morphology. These specimens comprise three proximal femora and the distal portion of a scapula. Each is described individually here. Their dimensions are reported in Table 5.5.

BOU-VP-1/29 is the proximal end of a right femur. The proximal end is eroded so that trabecular bone is exposed on the head, gluteal tubercle, and greater trochanter, which is also missing the tip. It most likely would have been a slightly larger animal than BOU-VP-1/62. The head, eroded as it is, is at the top of the observed range for *Papio hamadryas,* so if one accounts for the eroded bone, it is higher. Without the approximated volume of the eroded bone taken into account, it is still at least 3.0 mm below the bottom of the Olorgesailie range (ca. 29.0 mm) and the Olduvai *leakeyi* range (28.0 mm). It is also about 2 mm below the distorted BOU-VP-1/86. Given that the *P. hamadryas* dental material from the Afar is generally in the small- to mid-range for extant *Papio* (excluding *P. h. kindae*), and that this specimen is larger than possibly male *Papio* femora from Talalak and Halibee, it seems most probable that this is a female *T. o. leakeyi*.

BOU-VP-1/39 is a left femur preserving the head, neck, and much of the proximal area other than the greater trochanter, as well as much of the shaft distal to the area just proximal to the patellar groove. The shaft distal to the lesser trochanter is preserved as fragments held together by the mineralized cast of the marrow cavity, rendering shaft

EBSCOhost - printed on 10/28/2022 4:53 AM via . All use subject to https://www.ebsco.com/terms-of-use

dimensions difficult to measure. Distally it is broken just proximal to the condyles. From the head, 17.4 cm of the shaft are preserved, so a total length of approximately 19.0–20.0 cm is likely. In size, the head is in the high end of modern *Colobus guereza* males and the low end of modern *Papio hamadryas* sp. females (other than *P. h. kindae*). The shaft is comparatively straight. The articular surface of the head does not extend medially onto the posterior surface of the neck. The fovea is large and oval in outline. The neck shaft angle is approximately 110º, below that of most colobines. The neck is also relatively long. The lesser trochanter projects medially.

BOU-VP-1/62 is the proximal one-third of a left femur. It is similar in size to modern *Papio*, too small to be *Theropithecus oswaldi leakeyi,* and probably too large to represent the same species as BOU-VP-1/95. The head is missing but the greater and lesser trochanters are preserved. The greater trochanter projects about 16 mm above the neck. The greater trochanter hooks medially at its apex. The intertrochanteric line is strongly marked, and the *quadratus femoris* muscle insertion is prominent. The gluteal fossa is deep. The lesser trochanter is oriented posteriorly. The preserved portion of the shaft is strongly curved in the anteroposterior plane.

BOU-VP-1/65 is a right scapula preserving the glenoid fossa, the base of the acromion and spine, and about 3.0 cm. of the posterior edge of the blade. Unfortunately, the medial and lateral borders of the distal (and widest) portion of the glenoid are missing. The glenoid is approximately 3.0 cm in anteroposterior diameter, which is within the upper limit of the extant *Papio hamadryas* and *Mandrillus sphinx* ranges. The fossa is not particularly deep or tightly curved. In spite of the damage, the glenoid fossa was probably relatively broad in its mediolateral diameter. It can be determined that the lateral margin of the fossa shows a prominent bulge at the distal end. This specimen could possibly represent a female *T. o. leakeyi*.

Conclusion

Cercopithecid fossils make up a relatively small component of the Daka fauna, yet they contribute substantial information about African monkey evolution. The partial colobine cranium is from a new species of colobine, *Cercopithecoides alemayehui*. Among the cercopithecines, the large extinct baboon *Theropithecus oswaldi leakeyi* is predominant, and other cercopithecine taxa known to occur at other Pleistocene Afar sites are absent. This may indicate that a different environment is being sampled at Daka. The preserved elements of *Theropithecus* substantiate the anagenetic trends observable throughout the record of this species, and represent a time period between Olduvai Bed IV and Olorgesailie Member 7, helping to close one of the larger temporal gaps in that record.

EBSCOhost - printed on 10/28/2022 4:53 AM via . All use subject to https://www.ebsco.com/terms-of-use

6

Equidae

W. HENRY GILBERT
AND
RAYMOND L.
BERNOR

The family Equidae has a rich and well-studied fossil record. The earliest known equids are of the genus *Hyracotherium* and derive from the early Eocene of North America (MacFadden 1992). Equidae dispersed from North America to the Old World in several events since the Eocene, and the *Equus* and hipparionine lineages separated in the early middle Miocene (MacFadden 1984; Hulbert and MacFadden 1991). Hipparionines of the genus *Cormohipparion* immigrated into the Old World during the early late Miocene (ca. 11.2–10.8 Ma) and rapidly dispersed across Eurasia and Africa (Bernor et al. 1996; Woodburne 1996; Bernor et al. 2004). The hipparionine genus *Eurygnathohippus* is known strictly from Africa between 7.5 and 0.6 Ma and is most closely related to the Indopakistan "*Sivalhippus*" clade (Bernor and Harris 2003). Monodactyl horses including the lineage leading to *Equus* had a protracted New World evolutionary history prior to their entry into the Old World during the late Pliocene (Lindsay et al. 1980, 1981; Bernor et al. 1996; Azzarolli 2003). The first occurrence of *Equus* in Africa is in the Omo Shungura F Member, 2.32–2.36 Ma (Feibel et al. 1989).

Both *Eurygnathohippus* and *Equus* are common faunal elements of the Daka Member, with *Equus* being roughly twice as common (based on the number of individual specimens present). At approximately 1.0 Ma, Daka *Eurygnathohippus* is a relatively late African occurrence of the genus. Remains of both genera include mandibular, dental, and postcranial specimens. In addition, two partial crania of *Equus* have been recovered (BOU-VP-3/54 and BOU-VP-25/94), but neither are well enough preserved to allow for a detailed metric analysis.

Terminology

The taxonomic nomen "hipparion" has been applied in a variety of ways by different authors. We define "hipparionine" or "hipparion" as referring to horses with an isolated protocone on maxillary premolar and molar teeth and, as far as known, tridactyl feet, including species of the following genera: *Cormohipparion*, *Neohipparion*, *Nannippus*, *Pseudhipparion*, *Hippotherium*, *Cremohipparion*, *Hipparion*, "*Sivalhippus*," *Eurygnathohippus* (= senior synonym of "*Stylohipparion*"), *Proboscidipparion*, and *Plesiohipparion*.

EBSCOhost - printed on 10/28/2022 4:53 AM via . All use subject to https://www.ebsco.com/terms-of-use

TABLE 6.1 Abbreviations and Codes Used in Text and Figures

Symbols used in tables

A	*Equus asinus*	a	MAK hipparions
B	*Equus burchelli boehemi*	b	MAT hipparions
C	*Equus burchelli chapmani*	c	BOU 2.5 Ma (Hata Member)
D	Bouri Daka (1.0 Ma) *Eurygnathohippus*	d	Bouri Daka (1.0 Ma) *Equus*
E	Eppelsheim *Hippotherium primigenium* s.s.	f	Olduvai General
G	*Equus grevyi*	v	Olduvai Bed IV
H	Höwenegg *Hippotherium primigenium*	w	Olduvai Bed III
I	*Equus burchelli* [subspecies not indicated]	x	Olduvai Bed II
L	*Equus burchelli selousi*		
M	*Equus hemionus*	y	Olduvai Bed I?/General
Q	*Equus quagga* [measurements from cast]	z	Hadar
S	*Equus asinus somaliensis*		
Z	*Equus zebra*		

Anatomical abbreviations

MC	Metacarpal
MCIII	Metacarpal of the third (central) digit
MTIII	Metatarsal of the third (central) digit
MPIII	Either metacarpal III or metatarsal III
1PH3	1st phalanx III (central digit) of either the anterior or posterior limb, which are difficult to distinguish in hipparion.
A1PH3	Anterior 1st phalanx III, certainly identifiable for extant zebras plotted herein
P1PH3	Posterior 1st phalanx III, certainly identifiable for extant zebras plotted herein

Characterizations of these taxa have been most recently reviewed by Bernor and Armour-Chelu (1999a, b) and Bernor et al. (1996, 2005).

The osteological nomenclature and the enumeration and/or lettering of the figures have been adapted from Nickel et al. (1986). Getty (1982) was also consulted for morphological identification and comparison. Anatomical abbreviations are used in the text and tables, and many figures present plots with codes for different taxa and fossil samples. These abbreviations and codes are listed in Table 6.1.

Metric Procedures

Measurements in Tables 6.2-6.5 are all given in millimeters and rounded to 0.1 mm. Measurement numbers (M1, M2, M3, etc.) refer to those published by Eisenmann et al. (1988) and Bernor et al. (1997) for the skulls and postcrania. Tooth measurement numbers refer to those published by Bernor et al. (1997) and Bernor and Harris (2003).

Bernor and Armour-Chelu (1999b), Bernor and Harris (2003), Bernor and Scott (2003), and Bernor et al. (2005) compared African hipparions to an extensive series of late Miocene-Pleistocene Eurasian and African assemblages. In various studies, Eisenmann (see Eisenmann 1995 for a comprehensive summary) has used log10 ratio diagrams to evaluate differences in hipparion metapodial proportions as a basis for

EBSCOhost - printed on 10/28/2022 4:53 AM via . All use subject to https://www.ebsco.com/terms-of-use

TABLE 6.2 *Equus* Maxillary Check Teeth

Specimen	*Element*	*M1*	*M2*	*M3*	*M5*	*M6*	*M7*	*M8*	*M9*	*M10*	*M11*
BOU-VP-1/24	L.P^3	30.6	27.5	28.1	64.9	1	4	1	1	8.6	5.2
BOU-VP-1/42	L.P^3	30.3	28.8	32.9	38.5	1		1	1	10.2	6.2
BOU-VP-1/87	R.M^1	22.3		27.5						11.5	6.6
BOU-VP-1/87	R.M^2	24.2		27.6						12.5	5.6
BOU-VP-1/87	R.M^3	29.4		26.1						12	4.9
BOU-VP-1/103	R.M^3	22.4		20.8						9.8	
BOU-VP-1/176	R.P^3	26								11.1	5
BOU-VP-1/187	L.P^4	26.4	24.5	26.7	52.8	0	1	0	0	12.2	6.6
BOU-VP-1/199	R.M^1	21.5		27.2						10	4.5
BOU-VP-2/3	L.M^1	21.7		24.8						11.4	5.1
BOU-VP-2/6	R.P^2	28.7	26.3	29.7	71.6	1	1	1	2	10.7	5.6
BOU-VP-2/11	L.P^3	31.5	28.3	29.2	55.2	1	2	1	1	11.7	5.3
BOU-VP-2/44	L.M^1	26.4		24.7						10.2	4.9
BOU-VP-2/45	R.M^2	22		26						11.1	5.3
BOU-VP-2/48	L.M^2	29.9		26.1						11.1	4
BOU-VP-2/51	L.M^1										
BOU-VP-2/55	L.M^1	24.5	23.3	27.9	76.7	1			0	10.3	4.9
BOU-VP-2/69	L.P^4	27.6	26.3	29.6	53.8	1			2	9.6	4.5
BOU-VP-2/70	L.M^3	28.8									
BOU-VP-2/76	L.P^4	24.3	21.6	25.4	37.3	0	1		0	9.6	4.6
BOU-VP-3/18	R.M^3	29.6		25.3						11.4	4.3
BOU-VP-3/20	L.P^3	28.1		28.5						12.5	6.3
BOU-VP-3/21	R.P^3	27.8	25.2	27.8						11.6	4.8
BOU-VP-3/23	L.P^4	26	25.9		48.8	1	3	1	1	8.3	5
BOU-VP-3/32	L.M^1	29.7	22.6	24	83.4	2	1	1	1	10.1	4.6
BOU-VP-3/32	L.P^4	30.9	25.3	29.1	76.4	0		0	1	11.5	6.1
BOU-VP-3/54	M^1	29.7	29.1	31.8	43.4	1			1	12.5	6.2
BOU-VP-3/54	M^2	27.7	51.2	29.7						12.2	5.9
BOU-VP-3/54	M^3	33.3		28	39.3	1			2	13.4	4.9
BOU-VP-3/54	R.P^2	39.2		29.3		1	1	5	2		
BOU-VP-3/54	L.P^2	40.5	38.2	29.7	39.1	1	2	4	1		
BOU-VP-3/54	L.P^4	30.9	28.7	31.9	45.7					12	4.5
BOU-VP-3/58	R.M^1	28		27.1						11.3	12.2
BOU-VP-3/58	R.M^2	27.8		26.1						12.3	11.9
BOU-VP-3/58	R.M^3	28									
BOU-VP-3/58	R.P^2	38.5		27.5	71.2	2				10.7	6.7
BOU-VP-3/58	R.P^3	31.8		29.1						12.8	6.4
BOU-VP-3/58	R.P^4	30.9		27.4	78.1						
BOU-VP-3/59	R.P^4	31.5		30.4	81.5	1				11.8	6.4
BOU-VP-3/90	R.P^3	29.8		27.8						11.2	
BOU-VP-3/90	L.P^4	27.5		25.9	71.3						
BOU-VP-3/94	R.P^4	26.9			53.9	0	1	1	1	8.7	4.5
BOU-VP-3/115	L.M^1	33.5		29	38.4	1	1	2		10.4	3.6
BOU-VP-3/135	L.P^4	24.7	23.3	26.7	42.5	0	1	1	1	10.8	4.9
BOU-VP-3/145	R.M^3	25.8		21.7						12.7	
BOU-VP-4/43	R.P^4					1	4	1	1		
BOU-VP-19/2	L.M^1	33.8		29.1						13.8	4.8
BOU-VP-19/61	R.M^3	31.2		28.4							
BOU-VP-25/10	R.M^1	29.2		26.5						11.2	2.7
BOU-VP-25/31	L.P^4	31.9		25.7						11.8	3.9

EBSCOhost - printed on 10/28/2022 4:53 AM via . All use subject to https://www.ebsco.com/terms-of-use

TABLE 6.2 *(continued)*

Specimen	*Element*	*M1*	*M2*	*M3*	*M5*	*M6*	*M7*	*M8*	*M9*	*M10*	*M11*
BOU-VP-25/36	L.P^4	27.9	24.7	32.2	40	1	0	0	1	14	6
BOU-VP-25/64	L.P^3										
BOU-VP-25/74	R.P^3	25.5	22.4		46.6	1	2	2	0	11.2	5.7
BOU-VP-25/84	L.P^4	20.8	24.1	28.4	50.2	0	1	1	1	10	4.8
BOU-VP-25/94	L.M^1	29.5		23.6						12.4	
BOU-VP-25/94	L.M^2			29.6	61.9		5	2	1		5.7
BOU-VP-25/94	L.M^3	30.1	35.9	25.7	65.1	0	4	2	1	12.6	4.9
BOU-VP-25/94	L.P^2	40.7	40	29.7	37.8	1	1	3	3	9.4	5.3
BOU-VP-25/94	L.P^4										
BOU-VP-26/6	R.P^2	39		25.3							

NOTE: Tooth measurement numbers refer to those published by Bernor et al. (1997) and Bernor and Harris (2003)

recognizing taxa and their evolutionary relationships. Bernor et al. (2003) and Bernor and Harris (2003) have used multiple statistical tests, sometimes including univariate, bivariate, and multivariate statistics as well as log10 ratio diagrams (re: Bernor et al. 2004) to evaluate and resolve the alpha systematics of hipparionine horses. Bernor et al. (2005) used log10 ratio diagrams together with multivariate statistics to evaluate metapodial and 1st phalangeal evidence for postcranial evolution in 6.0+ to 2.95 Ma Ethiopian hipparions.

We incorporate these previously used methodologies in this work. The Daka equid material is the first where we have analyzed both *Equus* and a hipparionine together in the same fauna. While the differences in the cheek teeth are obvious, the differences in the postcrania are not always so. Because of this we exercise caution, where needed, in their identification. Our statistical analysis uses two recognized population standards. For postcrania we use the skeletal population from Höwenegg (Hegau, southern Germany, 10.3 Ma; Bernor et al. 1997) for calculating 95 percent confidence ellipses used in bivariate plots, and log10 mean standard values for all log10 ratio diagrams (MPIIIs and 1PHIIIs). We use the Eppelsheim standard for calculating 95 percent confidence ellipses for cheek tooth variables (re: Bernor and Franzen 1997; Kaiser et al. 2000; Bernor and Harris 2003). In these comparisons we include Ethiopian hipparions between 3.4 and 1.0 Ma age, Olduvai Gorge material, and extant zebra material from the American Museum of Natural History (New York) and the Smithsonian Museum Support Center (Washington, DC).

Analysis

Statistical analysis of Daka Equidae, *Eurygnathohippus* and *Equus*, were undertaken simultaneously between both genera and extant zebras housed by the Smithsonian Institution's Support Center. For this reason, overall results of the multivariate analyses are presented prior to specific sections on each of the genera. Analyses are discussed broadly here and later applied more specifically to the two Daka taxa.

EBSCOhost - printed on 10/28/2022 4:53 AM via . All use subject to https://www.ebsco.com/terms-of-use

TABLE 6.3 *Equus* Mandibular Check Teeth

Specimen	*Element*	*M1*	*M2*	*M3*	*M4*	*M5*	*M6*	*M8*	*M9*	*M10*
BOU-VP-1/22	L.P_4	31.6	29.7	17.6	9.9	14.1	17.7	15.3	14.1	73.7
BOU-VP-1/23	R.M_1	32.5	28.8	20.4	9.3	16	16.1	15.2	14.8	59
BOU-VP-1/25	R.M_2	26		13.5						53
BOU-VP-1/40	L.P_4	26.7	25.1	13.7	7.5	8.9	15.3	13.6	12.1	62.1
BOU-VP-1/71	L.M_3	28.1		11.7						60.2
BOU-VP-1/83	R.M_2	25.9		13.7		10.7		13.0	12.5	
BOU-VP-1/83	R.P_2	28.1		12.5	7.3	16.7		11		
BOU-VP-1/83	R.P_3	30.7								
BOU-VP-1/83	R.P_4	28.7		16.3	8.7	13.2		5.1`	13.2	56.8
BOU-VP-1/130	L.M_3		24.6	13	8.3	8.5	12.7	11.7	9.8	60.9
BOU-VP-1/135	L.M_1	24.9		14.7						43.4
BOU-VP-1/135	L.M_2	26.3		14.6						
BOU-VP-1/135	L.M_3			13.5						
BOU-VP-1/174	R.M_1	24		13.7						
BOU-VP-1/174	R.M_2	24.7		13.8						
BOU-VP-1/174	R.M_3	33.2		13						
BOU-VP-1/174	R.P_3	28.4		17.6						46
BOU-VP-1/174	R.P_4	27.4		15.3	9.4	13.5	18.9	16.8	12.8	
BOU-VP-1/175	L.P_4	29.4	28	18.3	8.6	14.9	15.4	16.1	14.9	40.1
BOU-VP-1/190	L.M_1	29.3		16	9.3	14	15.1	14.6	14.4	57.7
BOU-VP-1/205	L.M_1	29.9		17.7	9.5	13.7	18	15	14	61.8
BOU-VP-1/207	L.M_3									
BOU-VP-1/211	R.M_2	26.1		13.8	8.1	8.9	13.7	14.4	12.1	
BOU-VP-1/232	L.M_2	29		16.1						52.2
BOU-VP-2/23	R.dp_2	36.6		13.9	10.9	14.1	9.5	8.4	10.6	
BOU-VP-2/23	R.dp_3	31.2		13.2	9	10.2	9.4	8.4	9.6	
BOU-VP-2/23	R.dp_4	32.1		12.5	9.8	10.1	7.7		7	
BOU-VP-2/29	L.P_4	28.5	26.1	16.1	8.9	14.5	15.2	14.5	13.5	58.3
BOU-VP-2/74	L.M_1	24.5	23.7	13.7	7.2	7.8	14.1	12.9	12.4	49.6
BOU-VP-2/77	L.M_3	32.6		13.9						
BOU-VP-2/80	R.P_4	27.2	24.5	15.3	9.2	12.5	16.9	14.4	13.9	58.5
BOU-VP-2/81	R.M_2	27.5		14.4						56
BOU-VP-2/82	R.M_1	32.5		19.2	9.9	13.8	19.9	16.9	16.6	43.4
BOU-VP-2/84	R.M_1	25.2	25	13.9	6.5	9.5	16.3	14.5	12.7	52
BOU-VP-2/85	L.M_1	27.3		15.1	8.1					
BOU-VP-2/85	L.M_2	27.8		14.2	8.3					
BOU-VP-2/85	L.M_3	31.5		12.9	8.2					
BOU-VP-2/85	L.P_2	36.9		15.3	9.7	12.1	13.7	12.1	13.6	
BOU-VP-2/85	L.P_3	30.4		18.1	10					
BOU-VP-2/85	L.P_4	31.7		17	9.11	13.7	17.6	16.4	13.3	
BOU-VP-3/5	R.P_2			15.5						
BOU-VP-3/5	R.P_3	28.8		17.7						
BOU-VP-3/11	L.M_1	25.6		14.5						
BOU-VP-3/11	L.M_2	27.6		13.1						
BOU-VP-3/11	L.M_3	28		11.1						
BOU-VP-3/11	L.P_2	33.6		14.5	9.3	15.4	13.5	10.8	10.6	
BOU-VP-3/11	L.P_3	27.8		16.4						
BOU-VP-3/11	L.P_4	27.5		14.8	10.1	11.8	14.3	10.2	10.2	
BOU-VP-3/12	R.M_1	32.4		18.1						
BOU-VP-3/12	R.M_2	31.9		14						

EBSCOhost - printed on 10/28/2022 4:53 AM via . All use subject to https://www.ebsco.com/terms-of-use

TABLE 6.3 *(continued)*

Specimen	*Element*	*M1*	*M2*	*M3*	*M4*	*M5*	*M6*	*M8*	*M9*	*M10*
BOU-VP-3/12	$R.M_3$									
BOU-VP-3/12	$R.P_4$	32.1		18.6	9.3	7.9	14	13.5	12.5	11.3
BOU-VP-3/13	$R.M_1$	28.1		15.5						
BOU-VP-3/13	$R.M_2$	26		14						
BOU-VP-3/13	$R.M_3$	27.4		12.2						
BOU-VP-3/13	$R.P_3$	30.9								
BOU-VP-3/13	$R.P_4$	29.6		16.5	7.7	7.4	14.3	13.1	12.8	
BOU-VP-3/14	$R.M_2$	18.9		12.8						35.8
BOU-VP-3/14	$R.M_3$	23.9		14.4						
BOU-VP-3/16	$L.M_2$	28		16.2	8.6	12.8	18.6	16.9	14.4	
BOU-VP-3/22	$R.P_4$	34.5		18.5			15.4			59.7
BOU-VP-3/24	$R.M_2$			12.7						54.2
BOU-VP-3/25	$R.P_4$									
BOU-VP-3/30	$L.M_3$	28		10.4						66.2
BOU-VP-3/55	$R.M_2$	27.7		13.9						39.7
BOU-VP-3/60	$L.P_2$	33.4		15.6	7.5	16.4		12.3	14.9	
BOU-VP-3/64	$L.M_2$	27.8		13						70.6
BOU-VP-3/68	$L.M_1$	25.6		13.1						51.3
BOU-VP-3/101	$L.P_2$	31.8		10.9	10.3		13.5	10.2	12.8	
BOU-VP-4/6	$L.M_3$	30.2		12.9						44
BOU-VP-4/16	$R.M_2$	27.3		13.4	10.9	10.2	11.7	12.4	11.4	48.4
BOU-VP-4/48	$L.M_2$	31.7		17.1						82.6
BOU-VP-4/49	$R.M_1$	28.3	25.2	15	8.7	9.8	17	14.6	12.7	73.9
BOU-VP-19/5	$R.M_1$	25.5		14.7						
BOU-VP-19/5	$R.M_2$	28.5		14.4						
BOU-VP-19/5	$R.M_3$	29.1		11.8						
BOU-VP-19/5	$R.P_2$	35.8		14.5	10.5	12.8	15	13.6	15.1	
BOU-VP-19/5	$R.P_3$	30.4		17.8						
BOU-VP-19/5	$R.P_4$	27.9		15.9	9.6	11.6	18.3	15.5	15.2	
BOU-VP-19/19	$L.M_1$	29		14.5						43.5
BOU-VP-19/21	$L.P_4$	32.2	28.1	19.9	9.5	17.2	17.7	15.7	15.7	63.5
BOU-VP-19/22	$L.M_2$	28.6		14.7						54.4
BOU-VP-19/22	$L.M_3$	34.3		13.3						51
BOU-VP-19/42	$L.M_1$	23.1		13.1						
BOU-VP-19/42	$L.M_2$	23.1		12.3						
BOU-VP-19/42	$L.M_3$	36.3		12						
BOU-VP-19/42	$L.P_3$	31.6		18.7						
BOU-VP-19/42	$L.P_4$	28		16.3	7.7	8.2	21.5	15.1	12.6	
BOU-VP-19/53	$L.M_1$	28.8		14.8						49.1
BOU-VP-25/29	$L.M_1$	26.4		13.9	7.5	8.8	14.3	13.1	11.1	55.2
BOU-VP-25/48	$R.P_4$	30.9		18.2	8.4	14.8		15.5	15	60.5
BOU-VP-25/49	$R.M_2$	28.1		14	8.7	9.8	13.6	14.3	12.6	48.6
BOU-VP-25/61	$L.M_3$	31.4		13.1						53.8
BOU-VP-25/68	$L.M_1$	26.8	23.4	14.9	7.5	8.5	14	15.6	13	68.2
BOU-VP-25/68	$L.M_2$	28.1	25.6	15.4	9	9.8	11.6	15.2	12.7	71.1
BOU-VP-25/77	$R.M_1$	29.4	27.9	16.1	8.1	14.2	17.9	15.8	13.7	68.8
BOU-VP-25/78	$R.M_1$	27.5		14.1						70.1
BOU-VP-25/82	$R.M_1$	29.9	27	16.6						40.3
BOU-VP-25/105	$L.M_3$	30.2		13.4						63.4

EBSCOhost - printed on 10/28/2022 4:53 AM via . All use subject to https://www.ebsco.com/terms-of-use

TABLE 6.3 *(continued)*

Specimen	*Element*	*M1*	*M2*	*M3*	*M4*	*M5*	*M6*	*M8*	*M9*	*M10*
BOU-VP-26/10	L.M_1	25.9		13.9						
BOU-VP-26/10	L.M_2	26.1		13						
BOU-VP-26/10	L.M_3	29.6		11.7						
BOU-VP-26/10	L.P_3	28.4		17.5						
BOU-VP-26/10	L.P_4	27.9		15.8	8.6	10.1	16.3	14.6	13.6	
BOU-VP-26/16	L.M_3	35.1		13.2						33
BOU-VP-26/21	R.P_2			14.6		17.3				
BOU-VP-26/25	R.M_2	27		14.5						45.8

NOTE: Tooth measurement numbers refer to those published by Bernor et al. (1997) and Bernor and Harris (2003).

Maxillary P^2

Bernor et al. (2003) argued that maxillary P^2 is the best tooth to statistically analyze for length and width measurements because it varies the least in these dimensions through ontogeny. In the fossil sample (Figure 6.1A), Daka has four *Equus* individuals ("d" for *Equus*, "D" for *Eurygnathohippus*), Hadar ("z") has two individuals and Maka ("a") has one individual with measurement M1 dimension falling outside (larger) than the Eppelsheim standard. The Hadar and Maka samples are clearly hipparion, and simply large compared to European hipparion. Daka, however, has one individual that plots in the center of the Eppelsheim ellipse, and this individual, BOU-VP-3/88, is the only Daka hipparion in the figure. The other four Daka specimens are *Equus*. From Figure 6.1B one can see that most zebra populations overlap in their measurement M3 versus measurement M1 dimensions with the Eppelsheim ellipse; however, Grevy's zebra ("G") has a large number of specimens that have a longer P^2 (measurement M1) than the Eppelsheim sample.

Figure 6.2 plots P^2 protocone width (measurement M11) versus protocone length (measurement M10). Figure 6.2A plots the fossil sample, and one can see that a single Maka and four Hadar specimens plot to the right, above, or on the edge of the ellipse. Three Daka *Eurygnathohippus* specimens plot within the ellipse, one Daka *Equus* specimen plots above and to the right of the ellipse, and another Daka *Equus* specimen plots inside but to the right of the ellipse. Figure 6.2B shows that most zebra measurements fall within the Eppelsheim ellipse, with some Grevy's zebra individuals and a single *E. burchelli* ("I") plotting above the ellipse; hence, these are wider protocones than the Eppelsheim sample.

Astragali

Figure 6.3 plots astragalus maximum length (measurement M1) versus distal articular width (measurement M5). Figure 6.3A plots Eppelsheim, Hadar, and Daka. Hadar's hipparion *Eurygnathohippus hasumense* is large, with all points plotting well outside and to the right of the Höwenegg ellipse. Hata member equid BOU-VP-11/5, ("c") in Figure 6.3, dated to 2.5 Ma, is undoubtedly a small hipparion. This is an important documentation that

EBSCOhost - printed on 10/28/2022 4:53 AM via . All use subject to https://www.ebsco.com/terms-of-use

TABLE 6.4 *Equus* Nondental Specimens

Specimen	*Taxon*	*Element*	*M1*	*M2*	*M3*	*M4*	*M5*	*M6*	*M7*	*M8*
BOU-VP-25/42	*Equus*	Astragalus	58.6	56.5	29.9	59.4	51.7	32.3	48.5	
BOU-VP-2/7	*Equus*	Astragalus	61.9	57.1	33	62.8	53.8	29.2	50.5	
BOU-VP-2/8	*Equus*	Astragalus	68.1	65.6	33.1			35.8	58.4	
BOU-VP-2/86	*Equus*	Astragalus	66.2	55.4	32.5			34		
BOU-VP-2/9	*Equus*	Astragalus		55.8	29.5	62.9	54.2	33.8		
BOU-VP-3/111	*Equus*	Astragalus	63.5	62.7	30.8	65.3	53	33.7	53.7	
BOU-VP-3/113	*Equus*	Astragalus	30	57.8	28.3					
BOU-VP-1/178	*Equus*	Mandible							61.3	
BOU-VP-1/213	*Equus*	Mandible		125.7	97.8	89.7	184.1		67.9	
BOU-VP-1/83	*Equus*	Mandible			95.1					
BOU-VP-19/42	*Equus*	Mandible				87.1				
BOU-VP-19/5	*Equus*	Mandible			95.5	88	185.1	142		
BOU-VP-2/23	*Equus*	Mandible								
BOU-VP-2/25	*Equus*	Mandible								
BOU-VP-26/10	*Equus*	Mandible				80.4				
BOU-VP-2/85	*Equus*	Mandible			98.7	88.4	189.9	139		
BOU-VP-3/11	*Equus*	Mandible			88.5	81.8	173.5	125.2		243
BOU-VP-3/13	*Equus*	Mandible				84.5				
BOU-VP-3/31	*Equus*	Mandible				87.7				
BOU-VP-25/94	*Equus*	Maxilla								
BOU-VP-3/54	*Equus*	Maxilla								
BOU-VP-3/58	*Equus*	Maxilla							102	86.9
BOU-VP-1/43	*Equus*	MCIII	216.4	206.5	32.9	28.4	48.3	36.1	41.7	12.7
BOU-VP-3/116	*Equus*	MCIII	218.1	207.6	37.4	29.5	54.4	36.8	43.5	15.6
BOU-VP-3/118	*Equus*	MTIII					45.7	35.7	42.7	
BOU-VP-1/43	*Equus*	PHLX 1	69.9	61.7	33.3	49.2	33.8	39.8	38.7	24.1
BOU-VP-3/108	*Equus*	PHLX 2	50.7	37.3	46.3	53.3	33.5	48.5		

NOTE: Measurement numbers (M1, M2, M3, etc.) refer to those published by Eisenmann et al. (1988) and Bernor et al. (1997).

at 2.5 Ma the Middle Awash sequence has a smaller species of *Eurygnathohippus* present than is known from the Sidi Hakoma–Kada Hadar sequence (3.4–2.9 Ma). There is also one Daka Member *Euryganthohippus* astragalus in the sample, ("D") in Figure 6.3A, that compares closely in size with the Hata specimen. Both of these specimens are similar in size to the Höwenegg hipparion. Most of our modern *Equus* sample (Figure 6.3B) plots outside the ellipse, the majority of which is to the right (greater width measurement) or below (smaller maximum length).

Figure 6.4 provides yet another pair of dimensions for the astragalus: distal articular depth (measurement M6) versus distal articular width (measurement M5). In Figure 6.4A, the entire Hadar hipparion sample plots at the right edge or to the right of the Höwenegg ellipse. The Daka sample includes one specimen within the Höwenegg ellipse, four to the right of the ellipse, and one above and to the right of the ellipse. As before, this leads us to suggest that the astragali with a measurement M5 dimension plotting to the right of the Höwenegg ellipse are those of *Equus*, while those in and below the ellipse are of

EBSCOhost - printed on 10/28/2022 4:53 AM via . All use subject to https://www.ebsco.com/terms-of-use

M9	*M10*	*M11*	*M12*	*M13*	*M14*	*M15*	*M16*	*M17*	*M18*	*M19*	*M20*	*M21*	*M22*
				74	39.5								
	129.2	86.2	66.9	86.1	39.2								
	138.2	102.9	75.6										
				63.5	32.8								
	185.4	86.9											
	140	98.4	67.7										
129	114.4	81.6	63.5										
		77.9											
												100	76.4
											82.4		
183.3													
	44.1	45.5	33.8	25.9	29.1	120	6.9						
4.3	52.4	52.7	38.3	29.7	32.8	110	15.2						
10.5													
35.9	51.4	50.6	17.9	18.1									

Eurygnathohippus. These are smaller specimens of the *Eu.* cf. *cornelianus* lineage (sensu Armour-Chelu et al. 2006). The Daka specimen has a narrower distal articular width and an overall smaller size (see Figure 6.5D). In Figure 6.4B, most of the zebra material plots outside the Höwenegg ellipse, either to the right (various zebras), below (*E. asinus* = *A*), or to the left (*E. hemionus* = *M*) of the ellipse.

Metacarpal III

Figure 6.6 plots MCIII maximum length (measurement M1) versus distal articular width (measurement M11). Figure 6.6A plots three Olduvai specimens within the Höwenegg ellipse and three outside and to the right of the ellipse. We believe that this likely discriminates the Olduvai hipparions (= f, within the ellipse) from *Equus* (outside the ellipse). All Hadar specimens plot above and to the right of the ellipse and reveal a large, elongate MCIII for specimens likely referable to either *Eurygnathohippus hasumense* or *Eu. afarense*

EBSCOhost - printed on 10/28/2022 4:53 AM via . All use subject to https://www.ebsco.com/terms-of-use

EBSCOhost - printed on 10/28/2022 4:53 AM via . All use subject to https://www.ebsco.com/terms-of-use

TABLE 6.5 *Eurygnathohippus* Specimens

Specimen	*Taxon*	*Element*	*M1*	*M2*	*M3*	*M4*	*M5*	*M6*	*M7*	*M8*	*M9*	*M10*	*M11*	*M12*	*M13*	*M14*
BOU-VP-25/26	*Eurygnathohippus* cf. *cornelianus*	M_1	21.7	20.7	12.6	6.0	9.1	14.0		12.3	10.5	42.5	6.3	4.0	28.9	
BOU -VP-25/81	*Eurygnathohippus* cf. *cornelianus*	P_3	24.7		15.0	7.8	12.6	14.9		13.6	11.8	24.7	7.3	2.7		
BOU-VP-25/81	*Eurygnathohippus* cf. *cornelianus*	P_4	22.9	0.0	14.0	7.6	12.4	14.7	0.0	13.2	12.3	30.5	6.7	2.9		
BOU-VP-25/77	*Eurygnathohippus* cf. *cornelianus*	dp_3 or 4	27.1	25.1	19.1	21.1	22.8	0	3	0	0	7.9	3.3			
BOU-VP-1/221	*Eurygnathohippus* cf. *cornelianus*	M_1	24.4	22.5	14.1	9.3	12.8	15.5	14.0	8.6	10.8	22.9	9.1	4.2	26.2	
BOU-VP-25/45	*Eurygnathohippus* cf. *cornelianus*	M_1	23.5	21.9	14.8	7.7	10.8	14.1	13.3	11.4	11.9	14.6	5.5	2.0	34.5	
BOU-VP-26/5	*Eurygnathohippus* cf. *cornelianus*	M_1	24.7	22.6	15.5	8.6	12.0	13.9	13.4	10.9	11.5	58.1	6.3	3.1	57.1	
BOU-VP-25/59	*Eurygnathohippus* cf. *cornelianus*	M_2	25.7	19.9	14.8	10.2	12.9	11.7	13.3	9.7	7.3	61.2	2.2	1.0	57.2	
BOU-VP-3/17	*Eurygnathohippus* cf. *cornelianus*	M_2	22.7	19.9	12.0	6.6	11.0	13.2	11.6	9.9	11.4	60.2	4.1	2.0	62.9	
BOU-VP-3/40	*Eurygnathohippus* cf. *cornelianus*	M_2	23.5	22.0	14.0	7.4	10.5	13.1	12.8	10.4	11.2	50.9	4.8	2.5	42.2	
BOU-VP-3/51	*Eurygnathohippus* cf. *cornelianus*	M_2	21.4	20.4	12.0	6.5	10.1	13.1	11.9	9.8	10.5	54.7	3.5	2.0	49.0	
BOU-VP-1/183	*Eurygnathohippus* cf. *cornelianus*	M_3			11.7	8.4	9.1	10.4	10.1	9.3	7.1	54.4	3.1	2.9	44.4	
BOU-VP-25/4	*Eurygnathohippus* cf. *cornelianus*	M_3	24.3	25.5	10.4	7.6	8.4	10.1	10.9	8.7	8.5	54.5	3.5	1.7	50.3	
BOU-VP-26/18	*Eurygnathohippus* cf. *cornelianus*	M_3	24.1	24.9	11.4	7.7	11.3	12.2	11.7	9.9	9.7	43.2	2.6	1.5	37.0	
BOU-VP-26/2	*Eurygnathohippus* cf. *cornelianus*	M_3	27.3	28.9	13.1	8.8	11.0	12.1	10.9	11.6	10.4	44.9	3.7	2.0	38.2	
BOU-VP-26/26	*Eurygnathohippus* cf. *cornelianus*	M_3	25.1		11.9							45.6	8.4	3.1		
BOU-VP-2/30	*Eurygnathohippus* cf. *cornelianus*	P_2	26.6	23.4	14.6	10.1		12.8	11.5	10.5	11.9	45.9				
BOU-VP-25/70	*Eurygnathohippus* cf. *cornelianus*	P_2	29.0	28.1	12.4	6.6	12.8	16.1	15.2	11.4	12.1	28.4	7.0	3.3	29.0	
BOU-VP-3/142	*Eurygnathohippus* cf. *cornelianus*	P_2	35.4		17.6		14.5	11.6		11.6	14.6	35.5	9.0			

EBSCOhost - printed on 10/28/2022 4:53 AM via . All use subject to https://www.ebsco.com/terms-of-use

BOU-VP-25/46	*Eurygnathohippus* cf. *cornelianus*	P_3	22.1	21.0	12.6	7.2	11.7	14.6	14.1	11.8	10.9	18.5	7.4	3.3	21.4
BOU-VP-1/19	*Eurygnathohippus* cf. *cornelianus*	P_4	25.5	24.6	13.7	9.3	12.8	17.3	15.9	13.2	11.8	40.8	7.1	3.6	38.0
BOU-VP-1/84	*Eurygnathohippus* cf. *cornelianus*	P_4	27.2	24.8	13.8	9.8	12.8	12.7	15.3	12.5	11.4	49.3	9.2	4.2	50.1
BOU-VP-19/8	*Eurygnathohippus* cf. *cornelianus*	P_4	23.0	22.2	13.4	8.7	12.3	14.5	14.4	12.2	11.6	25.4	6.9	3.0	31.8
BOU-VP-25/3	*Eurygnathohippus* cf. *cornelianus*	P_4	22.5	21.4	12.6	7.6	11.7	15.1	13.1	12.1	11.1	29.4	4.4	2.6	32.8
BOU-VP-25/40	*Eurygnathohippus* cf. *cornelianus*	P_4	27.4	24.8	8.6			13.5	13.4	8.8	9.7	53.3	6.5		50.8
BOU-VP-25/53	*Eurygnathohippus* cf. *cornelianus*	P_4	25.1	23.8	14.5	8.7	13.2	12.6	15.3	12.0	11.7	38.4	8.6	3.7	44.5
BOU-VP-3/38	*Eurygnathohippus* cf. *cornelianus*	P_4	25.7	24.3	13.9	10.3	14.5	17.2	15.7	13.1	12.5	33.8	9.7	4.2	
BOU-VP-3/41	*Eurygnathohippus* cf. *cornelianus*	P_4	23.6	22.4	12.4	8.1	12.2	15.1	14.6	11.9	11.7	44.4	6.7	2.5	36.2
BOU-VP-3/143	*Eurygnathohippus* cf. *cornelianus*	M^1	19.1	19.1	21.8		10.6	0	0	0	0	10	6.8		
BOU-VP-25/16	*Eurygnathohippus* cf. *cornelianus*	M^1	22.0	21.3	22.5	19.4	51.3	1	6	1	0	10.6	3.4		
BOU-VP-3/89	*Eurygnathohippus* cf. *cornelianus*	M^1	24.8	20.3	18.5	19.9	69.2	0	1	1	0	9.0	2.3		
BOU-VP-4/50	*Eurygnathohippus* cf. *cornelianus*	M^1	20.9	20.0	21.0	20.5	43.3	0	5	2	0	9.2	2.5		
BOU-VP-25/63	*Eurygnathohippus* cf. *cornelianus*	M^2	24.8	20.5	23.3	22.7	68.6	3	7	2	0	10.4	4.0		
BOU-VP-19/21	*Eurygnathohippus* cf. *cornelianus*	M^3	20.8	21.1	18.0	18.6	52.1	0	3	1	0	9.0	3.8		
BOU-VP-25/79	*Eurygnathohippus* cf. *cornelianus*	M^3	22.2	23.0	17.4	18.8	56.9	1	5	2	1	8.3	2.8		
BOU-VP-3/136	*Eurygnathohippus* cf. *cornelianus*	M^3	20.3		17		65.8	1	2	1	0	8.5	2.6		
BOU-VP-3/146	*Eurygnathohippus* cf. *cornelianus*	M^3	23.9		18.2							8.6	1.6		
BOU-VP-19/26	*Eurygnathohippus* cf. *cornelianus*	P^2			22.9	20.8	30.5	1	4	4	0	9.4	4.3		

EBSCOhost - printed on 10/28/2022 4:53 AM via . All use subject to https://www.ebsco.com/terms-of-use

TABLE 6.5 *(continued)*

Specimen	*Taxon*	*Element*	*M1*	*M2*	*M3*	*M4*	*M5*	*M6*	*M7*	*M8*	*M9*	*M10*	*M11*	*M12*	*M13*	*M14*
BOU-VP-25/85	*Eurygnathohippus* cf. *cornelianus*	P^2			22.3	21.6	48.9	1	4	4	0	9.2	3.7			
BOU-VP-3/88	*Eurygnathohippus* cf. *cornelianus*	P^2	33.1	31.5	24.3	22.1	42.3	1	2	3	0	7.7	3.9			
BOU-VP-19/39	*Eurygnathohippus* cf. *cornelianus*	P^3	22.2	17.0	21.7	22.0	32.7	1	5	3	0	9.1	3.5			
BOU-VP-19/40	*Eurygnathohippus* cf. *cornelianus*	P^3	24.0	19.7	22.8	20.8	53.6				0	11.6				
BOU-VP-25/97	*Eurygnathohippus* cf. *cornelianus*	P^3	26.6	24.9	20.6		23.7	1	4	2	1	8.2	2.2			
BOU-VP-3/39	*Eurygnathohippus* cf. *cornelianus*	P^3	27.3	22.9	24.8	23.6	46.6	1	3	4	0	9.6	3.7			
BOU-VP-1/192	*Eurygnathohippus* cf. *cornelianus*	P^4	24.2	20.9	19.5	20.8	29.9	3	3	3	0	9.5	3.0			
BOU-VP-25/12	*Eurygnathohippus* cf. *cornelianus*	P^4	24.9	24.0		23.9	23.5	2	5	2	0	9.1				
BOU-VP-25/30	*Eurygnathohippus* cf. *cornelianus*	P^4	21.7	19.3	19.6	19.6	40.6	1	4	0	0	9.3	3.2			
BOU-VP-3/19	*Eurygnathohippus* cf. *cornelianus*	P^4	22.4	21.4	24.2	23.4	25.1	3	5	3	0	9.2	4.0			
BOU-VP-19/36	*Eurygnathohippus* cf. *cornelianus*	Lateral MC			17.2	24.7										
BOU-VP-26/9	*Eurygnathohippus* cf. *cornelianus*	Astra-galus	56.6	57.6	28.9	55.1	45.4	32.4	49.7							
BOU-VP-1/104	*Eurygnathohippus* cf. *cornelianus*	MCIII										42.5	40	31.1	24.7	28.3
BOU-VP-26/13	*Eurygnathohippus* cf. *cornelianus*	MTIII	259.2	252.6	30.6	29.5	43.1	29.4	36.9			42.1	42.7	35.3	26.3	29.5

NOTE: Measurement numbers (M1, M2, M3, etc.) refer to those published by Eisenmann et al. (1988) and Bernor et al. (1997) for the skulls and postcrania. Tooth measurement numbers refer to those published by Bernor et al. (1997) and Bernor and Harris (2003).

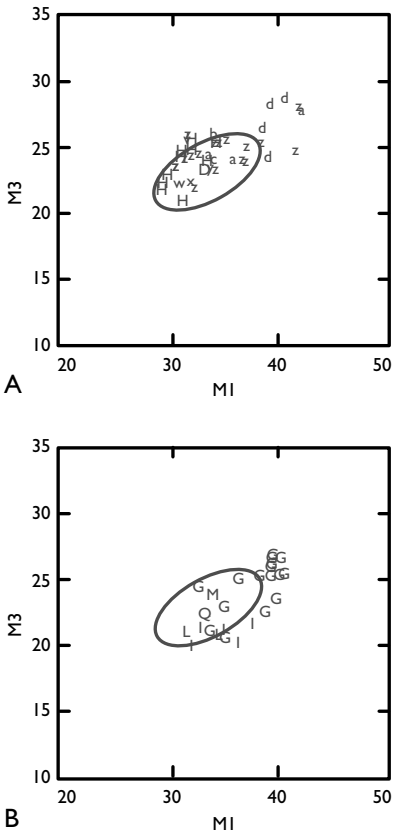

FIGURE 6.1

Bivariate plots of maxillary P^2 occlusal width (measurement M3) versus occlusal length (measurement M1). Plot A compares the fossil sample with a 95 percent confidence ellipse based on the Eppelsheim sample. Plot B provides a plot of modern zebras compared to the same Eppelsheim ellipse. Refer to the section on terminology for abbreviation codes.

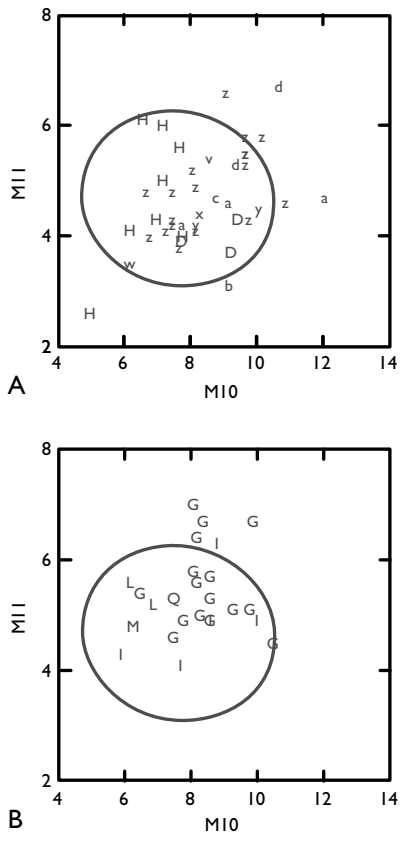

FIGURE 6.2

Plots of P^2 protocone width (measurement M11) versus length (measurement M10). Plot A compares the fossil sample with a 95 percent confidence ellipse based on the Eppelsheim sample. Plot B provides a plot of modern zebras compared to the same Eppelsheim ellipse. Refer to the section on terminology for abbreviation codes.

(or both; Bernor et al. 2005). The two Daka specimens are short and broad, one is especially broad, and both are likely referable to *Equus*.

Figure 6.6B shows that the entire *Equus* sample other than a single *E. burchelli* individual and a single *E. asinus* individual plots well to the right of the Höwenegg ellipse. We also plot here the Eppelsheim (E) *Hippotherium primigenium* for scale comparisons. Of this sample the largest *Equus* in both length and width dimensions is *E. grevyi. Equus zebra* (Z), *E. burchelli* (I), *E. b. boehemi* (B), and *E. quagga* (Q) are notable for their relatively short and broad MCIIIs.

EBSCOhost - printed on 10/28/2022 4:53 AM via . All use subject to https://www.ebsco.com/terms-of-use

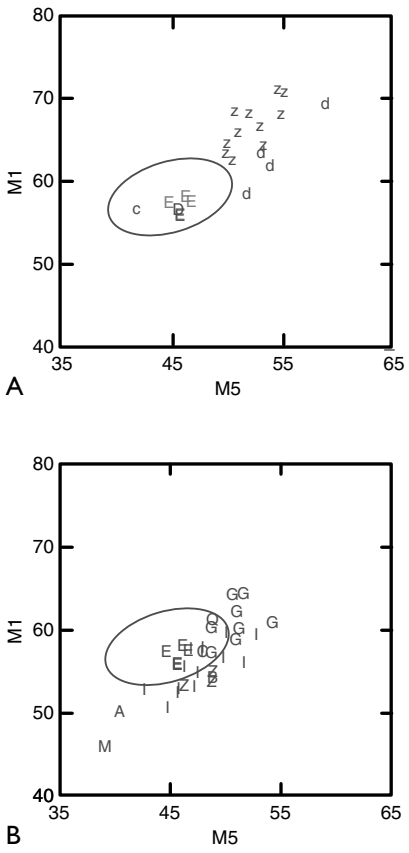

FIGURE 6.3

Plots of astragalus maximum length (measurement M1) versus distal articular width (measurement M5). Plot A compares the fossil sample with a 95 percent ellipse of the Höwenegg sample. Plot B provides a plot of modern zebras compared to the same Höwenegg ellipse. Refer to the section on terminology for abbreviation codes.

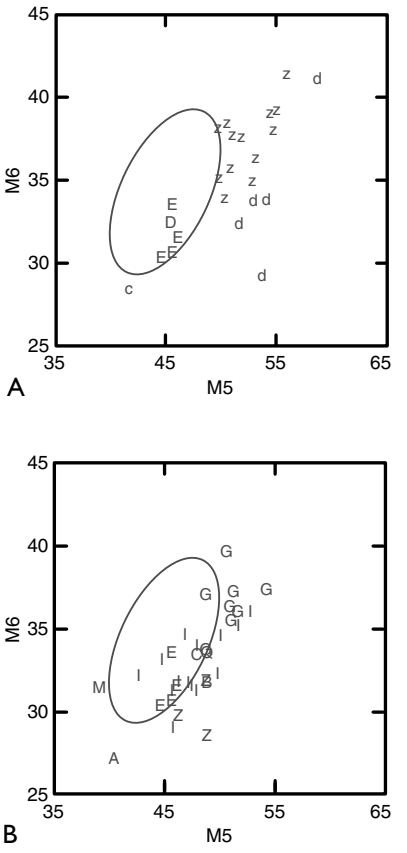

FIGURE 6.4

Plots of astragalus distal articular depth (measurement M6) versus distal articular width (measurement M5). Plot A compares the fossil sample with a 95 percent ellipse of the Höwenegg sample. Plot B provides a plot of modern zebras compared to the same Höwenegg ellipse. Refer to the section on terminology for abbreviation codes.

We generated a number of log10 ratio plots for our total sample of MCIIIs, of which we present an illustrative sample herein. Figure 6.7A plots two Daka MCIIIs, BOU-VP-1/43 and BOU-VP-3/116. The Daka MCIIIs differ substantially from the Höwenegg standard in their greater M3–M14 dimensions, particularly BOU-VP-3/116. The M3 and M4 dimensions differ markedly in their relative proportions, which have M3 and M4 progressively diverging away from the Höwenegg standard. The Daka specimens likewise differ from the Hadar sample of *Eurygnathohippus hasumense* in their shorter length and, again, M3 versus M4 proportions. Bernor et al. (2005: figure 2D) noted that the single Kada Hadar MCIII, AL361-1, also figured here (Figure 6.7B), was smaller than other Hadar hipparions, and this

EBSCOhost - printed on 10/28/2022 4:53 AM via . All use subject to https://www.ebsco.com/terms-of-use

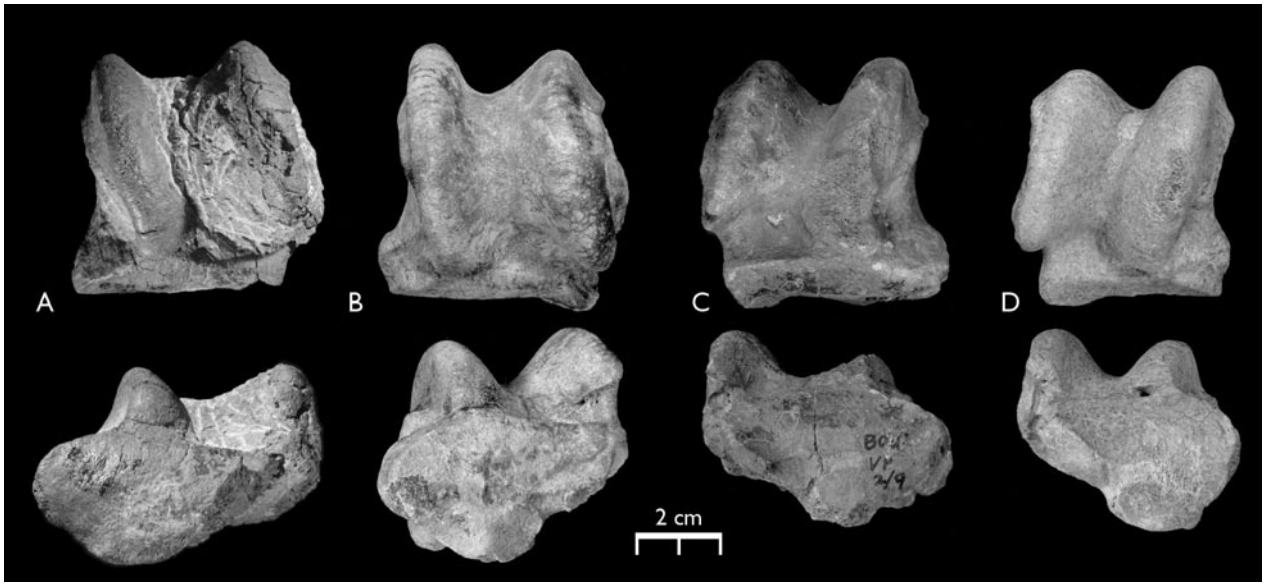

FIGURE 6.5

Daka Member equid astragali. Top row is cranial views; bottom row is distal views. A. BOU-VP-2/7, *Equus* sp. B. BOU-VP-3/111, *Equus* sp. C. BOU-VP-2/9, *Equus* sp. D. BOU-VP-26/9, *Eurygnathohippus* cf. *cornelianus*.

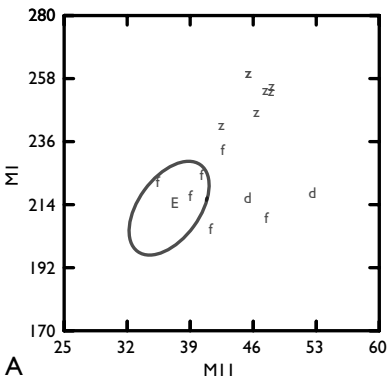

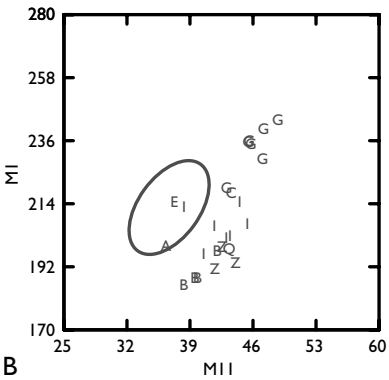

FIGURE 6.6

Plots of MCIII maximum length (measurement M1) versus distal articular width (measurement M11). Plot A compares the fossil sample with a 95 percent ellipse of the Höwenegg sample. Plot B provides a plot of modern zebras compared to the same Höwenegg ellipse. Refer to section on terminology for abbreviation codes.

EBSCOhost - printed on 10/28/2022 4:53 AM via . All use subject to https://www.ebsco.com/terms-of-use

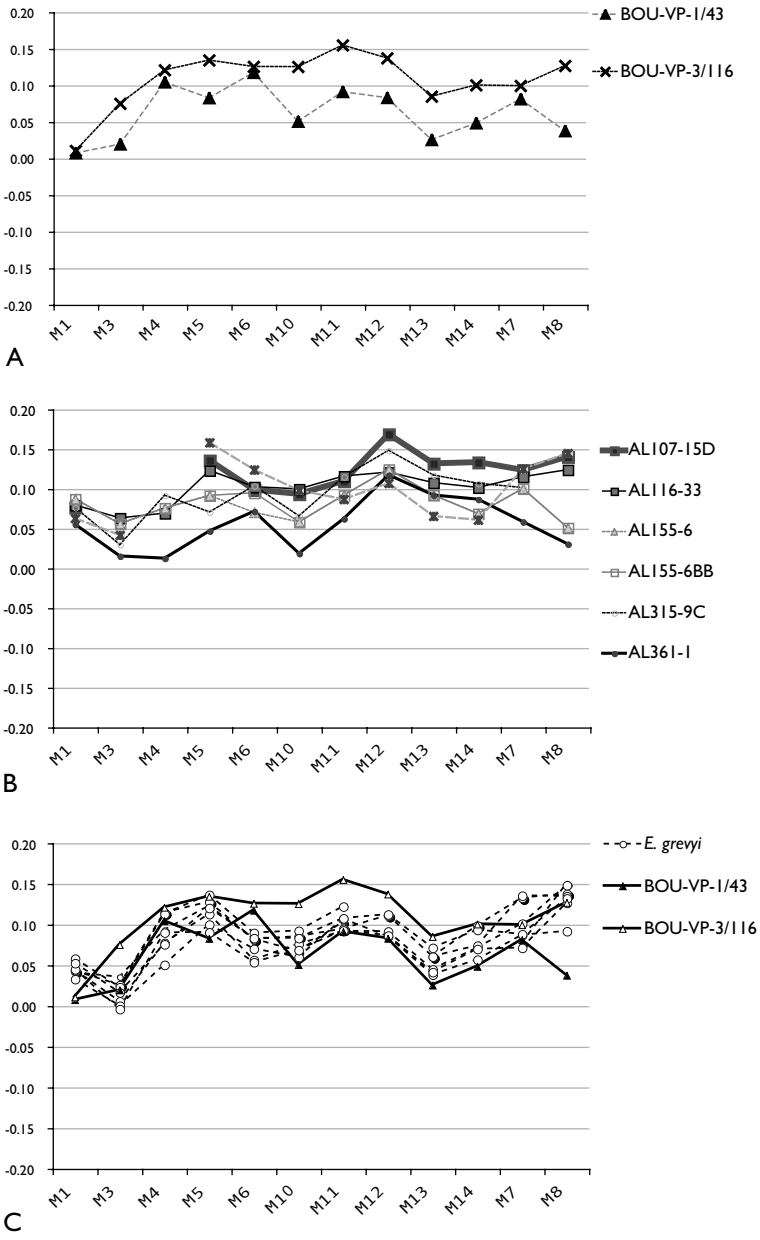

FIGURE 6.7

Log10 ratio plots of MCIIIs. Plot A compares two Daka MCIIIs, BOU-VP-1/43 and BOU-VP-3/116, to the Höwenegg sample average. Plot B compares Hadar *Eurygnathohippus* to the Höwenegg sample average. Plot C compares the two Daka MCIIIs and our *Equus grevyi* sample to the Höwenegg sample average.

could indicate the emergence of a new species of *Eurygnathohippus* at 2.9 Ma. For its relatively short length, BOU-VP-3/116 also has elevated proximal (measurements M5 and M6) and distal (measurements M10, M11, and M12) articular dimensions. Specimen BOU-VP-1/43 is more similar in these dimensions to some Hadar hipparions, in particular, AL155-6. Figure 6.7C plots the two Daka specimens against our *Equus grevyi* sample. The Daka specimens have a maximum relative length comparable to the Höwenegg sample and shorter than *E. grevyi*. However, the midshaft dimensions, as well as the proximal and distal articular dimensions, overlap and have similar trajectories to the *E. grevyi* sample. Figure 6.8A, the

EBSCOhost - printed on 10/28/2022 4:53 AM via . All use subject to https://www.ebsco.com/terms-of-use

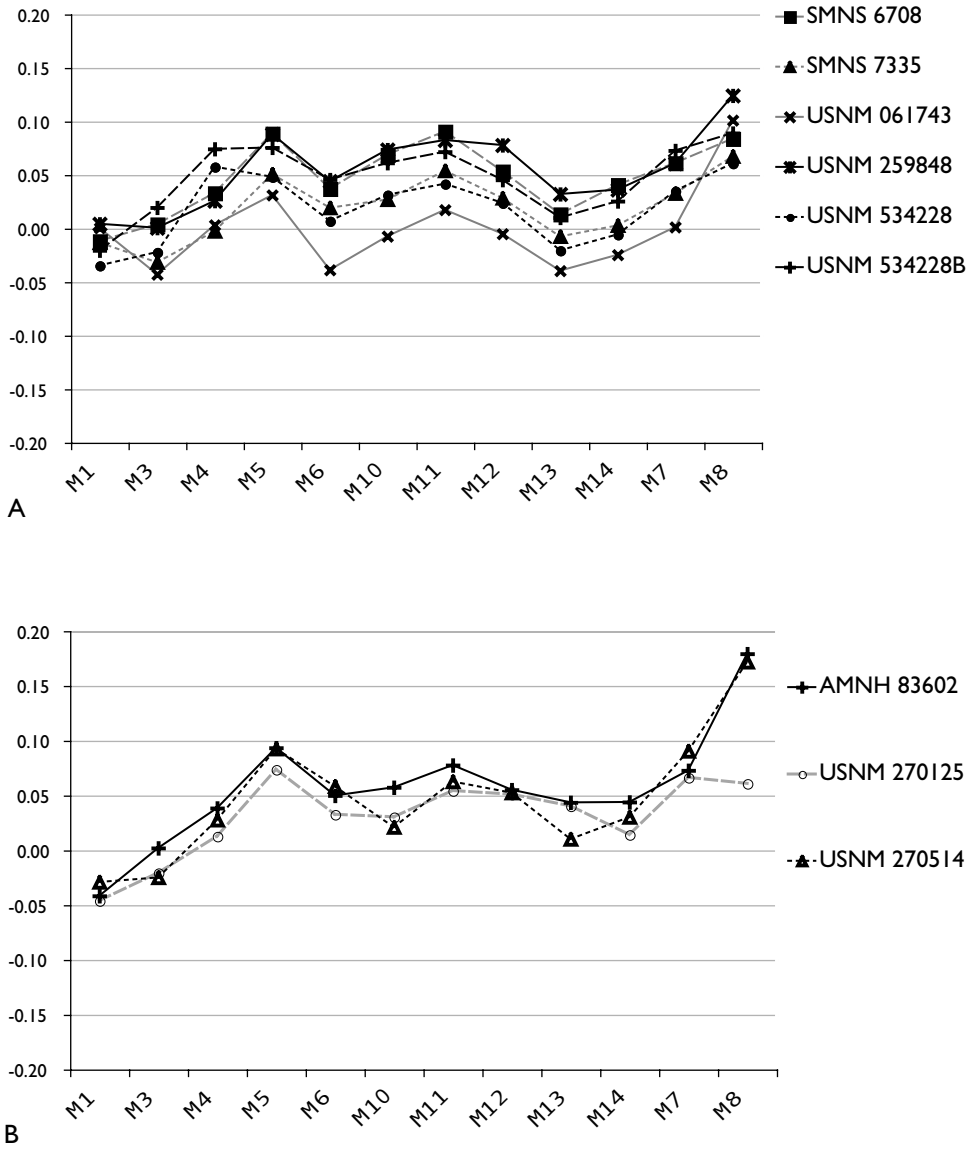

FIGURE 6.8

Log10 ratio plots of MCIIIs. Plot A compares *Equus burchelli* to the Höwenegg sample average. Plot B compares *Equus zebra* to the Höwenegg sample average.

E. burchelli sample, is more similar to BOU-VP-1/43 than to BOU-VP-3/116 and most of the *E. burchelli* sample plots as being similar to or smaller than the Daka sample. Important here are that the M3 versus M4 proportions again related the Daka specimens with extant African zebras, not hipparions. Figure 6.8B plots our *E. zebra* sample, which again is similar to the Daka sample, with the obvious differences being in *E. zebra*'s shorter length (measurement M1) and smaller midshaft width (measurement M3) and depth (measurement M4) dimensions. We conclude from this analysis and from overall morphology that the two Daka MCIIIs considered here are referable to a form of *Equus*. They have a length shorter than *E. grevyi*, a log10 ratio trajectory similar to *E. grevyi* and *E. burchelli*, are as long as *E. burchelli*, and are larger and longer than *E. zebra*.

EBSCOhost - printed on 10/28/2022 4:53 AM via . All use subject to https://www.ebsco.com/terms-of-use

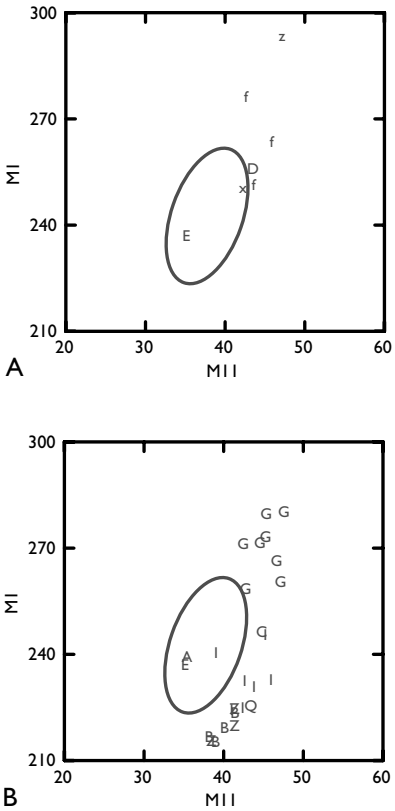

FIGURE 6.9

Plots of MTIII maximum length (measurement M1) versus distal articular width (measurement M11). Plot A compares the fossil sample with a 95 percent ellipse of the Höwenegg sample. Plot B provides a plot of modern zebras compared to the same Höwenegg ellipse. Refer to section on terminology for abbreviation codes.

Metatarsal III

Figure 6.9 is a bivariate plot of MTIII length (measurement M1) versus width (measurement M11). Figure 6.9A plots a single Daka specimen just outside the upper right quadrant of the Höwenegg ellipse. This single specimen plots closely to a specimen from Olduvai Bed II (x) and three Olduvai General (f) specimens. The (x) specimen and smallest (f) specimen (just outside the ellipse) are likely attributable to *Eurygnathohippus*, while the two larger Olduvai General (f) specimens are not presently identifiable to genus until we restudy the articular surfaces. Olduvai Bed II is known to have the very advanced species, *Eu. cornelianus*, and being similar in proportions to Daka, as well as similar in age to Daka (1.2 vs. 1.0 Ma), we find that this is evidence that the Daka hipparion is referable to *Eu.* cf. *cornelianus* (Armour-Chelu et al. 2006; see further discussion following in the *Eurygnathohippus* section). Figure 6.9B plots our modern *Equus* sample against our Höwenegg 95 percent confidence ellipse for measurements M1 and M11. There is only a single individual of *E. asinus* and a single individual of *E. burchelli* that plot within the ellipse; all the remainder of our sample plots outside the Höwenegg ellipse (along with the Eppelsheim *Hippotherium primigenium* MTIII for additional comparison). *Equus grevyi* is the single zebra species that plots outside, above, and/or to the right of the Höwenegg ellipse. Other zebras plot to the right and low within the bivariate frame: *E. burchelli*,

EBSCOhost - printed on 10/28/2022 4:53 AM via . All use subject to https://www.ebsco.com/terms-of-use

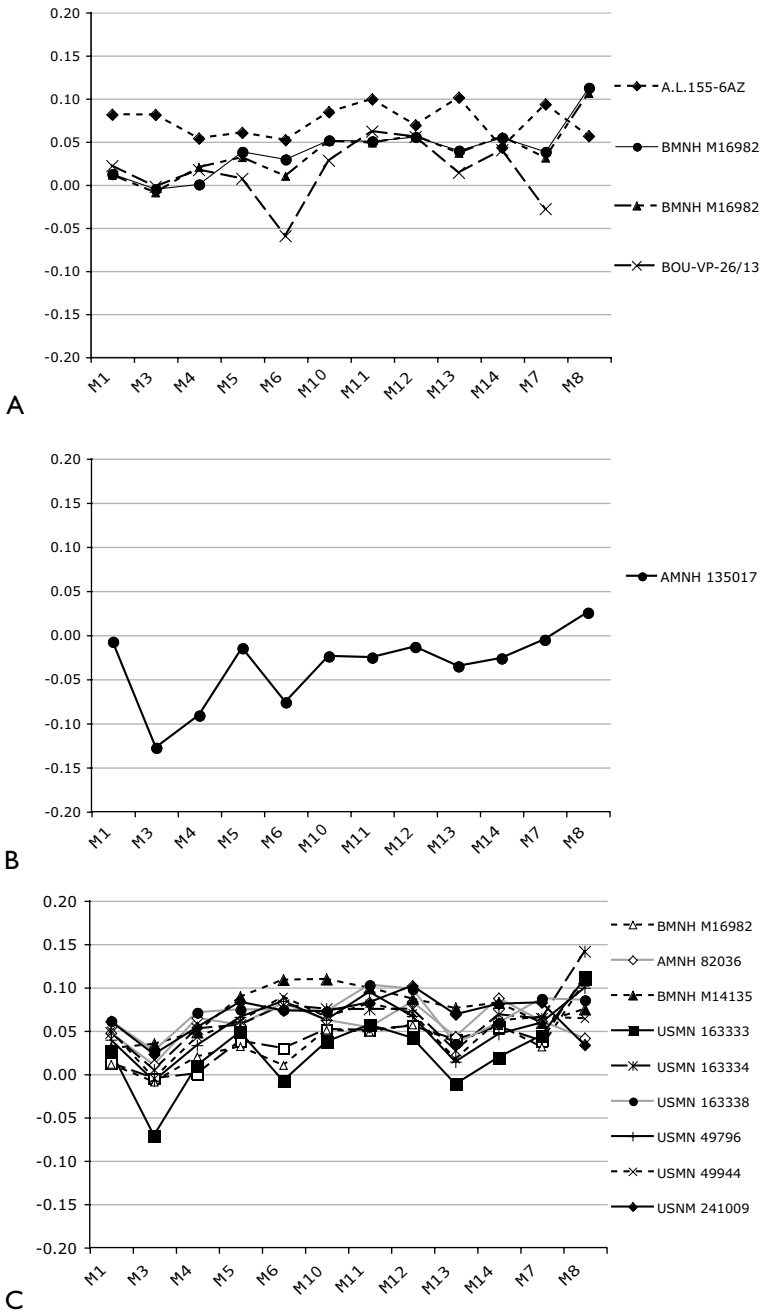

FIGURE 6.10

Log10 ratio plots of MTIIIs. Plot A compares Pleistocene eastern African *Eurygnathohippus* to the Höwenegg sample average. Plot B compares *Equus asinus* to the Höwenegg sample average. Plot C compares *Equus grevyi* to the Höwenegg sample average. Refer to section on terminology for abbreviation codes.

E. burchelli boehemi, *E. quagga*, and *E. zebra* are remarkable for their short, wide metapodials. As with the MCIIIs, we generated a series of MTIII log10 ratio plots, of which we present an illustrative sample herein (Figures 6.10 and 6.11). Figure 6.10A plots BOU-VP-26/13 along with what we believe are all species of eastern African hipparion. Hadar specimen AL155-6AZ is referable to *Eu. hasumense* (Bernor et al. 2005) and is characterized as having large, elongate, and rather robust MTIIIs. BOU-VP-26/13 plots very similarly to

EBSCOhost - printed on 10/28/2022 4:53 AM via . All use subject to https://www.ebsco.com/terms-of-use

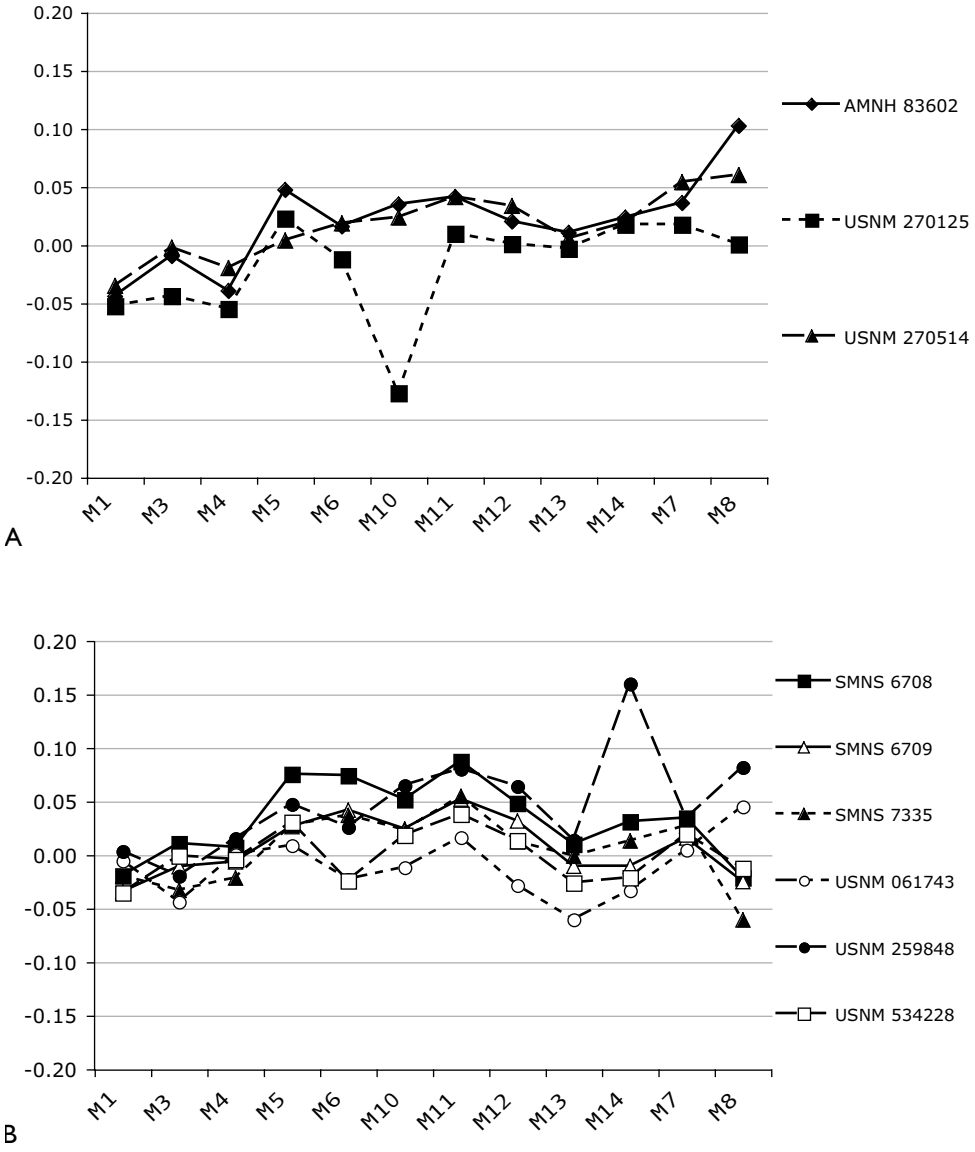

FIGURE 6.11

Log10 ratio plots of MTIIIs. Plot A compares *Equus zebra* to the Höwenegg sample average. Plot B compares *Equus burchelli* to the Höwenegg sample average. Refer to section on terminology for abbreviation codes.

BMNH M16982 from Bed II Olduvai Gorge, where diagnostic premaxillary and mandibular incisor dentitions are found (Leakey 1965), making them most likely referable to *Eu. cornelianus*. These smaller (than *Eu. hasumense*) hipparions are characterized by having a length slightly greater than the Höwenegg hipparion log10 mean, midshaft width and depth being very similar to the Höwenegg hipparion log10 mean, proximal, and distal articular dimensions being somewhat elevated compared to the Höwenegg hipparion log10 mean. *Equus asinus* (Figure 6.10B) contrasts with these hipparions by having strikingly smaller midshaft width (measurement M3) and depth (measurement M4) dimensions. Our *E. grevyi* sample (Figure 6.10C) overlaps, and at the same time has individuals with longer log10 lengths, with a sharper contrast in the midshaft width (measurement

EBSCOhost - printed on 10/28/2022 4:53 AM via . All use subject to https://www.ebsco.com/terms-of-use

M3) to midshaft depth (measurement M4) dimensions. Also, *E. grevyi* proximal articular width (measurement M5) and depth (measurement M6) vary more and have individuals with more elevated dimensions; distal articular dimensions (measurements M10, M11, and M12) range from being similar to strikingly more elevated.

Equus zebra (Figure 6.11A) is shorter (measurement M1) than the Höwenegg standard and has an inverted (and relatively greater) midshaft width (measurement M3) versus midshaft depth (measurement M4) dimensional relationship. Our *E. burchelli* sample (Figure 6.11B) is characterized as having its maximum length (measurement M1) the same or shorter than the Höwenegg standard; midshaft width (measurement M3) and depth (measurement M4) overlap and are smaller than the Höwenegg standard, and proximal (measurements M5, M6) and distal (measurements M10, M11, M12) articular dimensions vary and overlap with the Höwenegg standard.

Equus

There is a general consensus among equid systematists about the alpha taxonomy of modern *Equus* species (Oakenfull and Clegg 1998; Eisenmann and Baylac 2000). *Equus przewalskii* is usually recognized as a distinct species and is broadly agreed to be the ancestor of *E. caballus*, the domestic horse (Vilá 2001). African *Equus* species include the mountain zebra *(E. zebra)*, Grevy's zebra *(E. grevyi)*, the plains zebra *(E. burchelli)*, the African wild ass and its sister-taxon, the domestic donkey *(E. africanus/asinus)*. Asian species of *Equus* include asses (half-asses): *E. hemionus* and *E. kiang* (which some consider a subspecies of *E. hemionus*) (Klein and Cruz-Uribe 1999). Most workers also recognize *E. quagga*, a Southern African relative of *E. burchelli* that became extinct in the late 19th century, as a distinct species.

While the alpha taxonomy of *Equus* is relatively well understood, there remains substantial controversy concerning the evolutionary relationships of the Old World species of *Equus*. This has been most recently discussed by Eisenmann and Baylac (2000) and Azzaroli (2003). *Equus simplicidens* first occurred in the New World at approximately 3.7 Ma, and its first appearance in the Old World is calibrated as being 2.6 Ma (Lindsay et al. 1980, 1981; Bernor and Armour-Chelu 1999a, b). Many Eurasian late Pliocene and early Pleistocene equines are believed to have resembled modern-day zebras and have been referred to *E. stenonis*. However, recognition of samples as being referable to *E. stenonis* may be in error because they are recognized by plesiomorphic characters (Forsten 1999). *Equus*'s first appearance in Africa is apparently recorded in the late Pliocene/early Pleistocene deposits at Gladysvale, South Africa (Berger 1993), as well as in lower Omo Shungura Member G (Eisenmann 1985; Feibel et al. 1989). Molecular data suggest that modern zebras and donkeys are part of a second, more recent biogeographic extension into Africa by a Eurasian group in the middle to late lower Pleistocene (Oakenfull and Clegg 1998), but this view is not shared universally by paleontologists (Eisenmann and Baylac 2000).

Recent molecular studies have addressed relationships among living *Equus* taxa and the timing of speciation events. Oakenfull and Clegg (1998) have analyzed alpha and theta globin genes and suggest that zebras and asses diverged from the *E. caballus/przewalskii* group relatively early, approximately 2.4 million years ago. They go on to suggest that the

EBSCOhost - printed on 10/28/2022 4:53 AM via . All use subject to https://www.ebsco.com/terms-of-use

zebra/donkey clade has undergone a rapid recent radiation. Oakenfull and Clegg approximate the dispersal time of the zebra/donkey clade and Eurasian asses at approximately 0.9 Ma. They suggest the initial divergence of Asian half-asses and the African zebra/donkey clade would have been somewhat earlier than this. The earliest reported ass is from the middle of Bed II, Olduvai Gorge (Churcher 1982), and the earliest definitive zebra is the northern African species, *E. mauritanicus*, 0.7 Ma (Eisenmann and Baylac 2000).

Equus Linnaeus, 1758

Equus sp.

GENERIC DIAGNOSIS Monodactyl horses possessing upper cheek teeth with protocone connected to protoloph by a narrow isthmus and few to no enamel plis on the pre- and postfossettes. Preorbital facial region shallow with lacrimal fossae absent or rudimentary. Sagittal crest absent. Fossae on occiput for nuchal attachment small, and those directly above occipital condyles poorly developed. Bony auditory meatus variable in length and orientation. Basicranial region variable in length, with or without low longitudinal crest. Coronoid process of dentary lower than in hipparionine horses, and ascending ramus with oblique-posterior orientation. Grooves on lower incisors variably developed. Canines usually absent in females. Cheek teeth very hypsodont. Lower cheek teeth with well-developed metaconid-metastylid; metaconid often rounded while metastylid has a straight, mesial edge; protostylids usually lacking; mesial valley (metaflexid) with unequal arms, distal long and mesial short and transverse; ectoflexid variably developed; M_3 with bipartite talonid; ptychostylid lacking on lower milk molars. Metapodials more robustly built than contemporary African hipparion belonging to the genus *Eurygnathohippus*. Extremities always monodactyl, lateral digits lacking except as shortened splints that contact with the metapodial IIIs for no more than two-thirds of their length; A1PH3 usually longer than P1PH3; no rudiment of MPV apparent. Hoofed phalanges lack developed median slits on their anterior margin (adapted from Churcher and Richardson 1978).

DESCRIPTION In the descriptions that follow we will describe and figure the best representative specimens of the diagnostic skeletal material. For teeth, we will figure and describe a representative sample for each tooth position.

The best cranial fragment is an occipital region, likely attributable to *Equus* (Figure 6.12A–D). In this specimen the nuchal crest is prominent, rising above the plane of the middorsal cranium. The specimen is abraded and preserves very little other useful morphological information. We were able to take the following standard measurements for this specimen: measurement M21 = 100 mm and measurement M22 = 76.4 mm. A second, more fragmentary partial cranium, BOU-VP-3/54, provides the following measurement: measurement M20 = 82.4 mm.

Specimen BOU-VP-3/58 (Figure 6.13) is a subadult right maxillary fragment with dp^1 and P^2–M^3 (M^3 emerging). This specimen preserves the entire toothrow from dp^1 to M^3. The M^1 is the most worn tooth of the series and as such exhibits the clearest *Equus* features

EBSCOhost - printed on 10/28/2022 4:53 AM via . All use subject to https://www.ebsco.com/terms-of-use

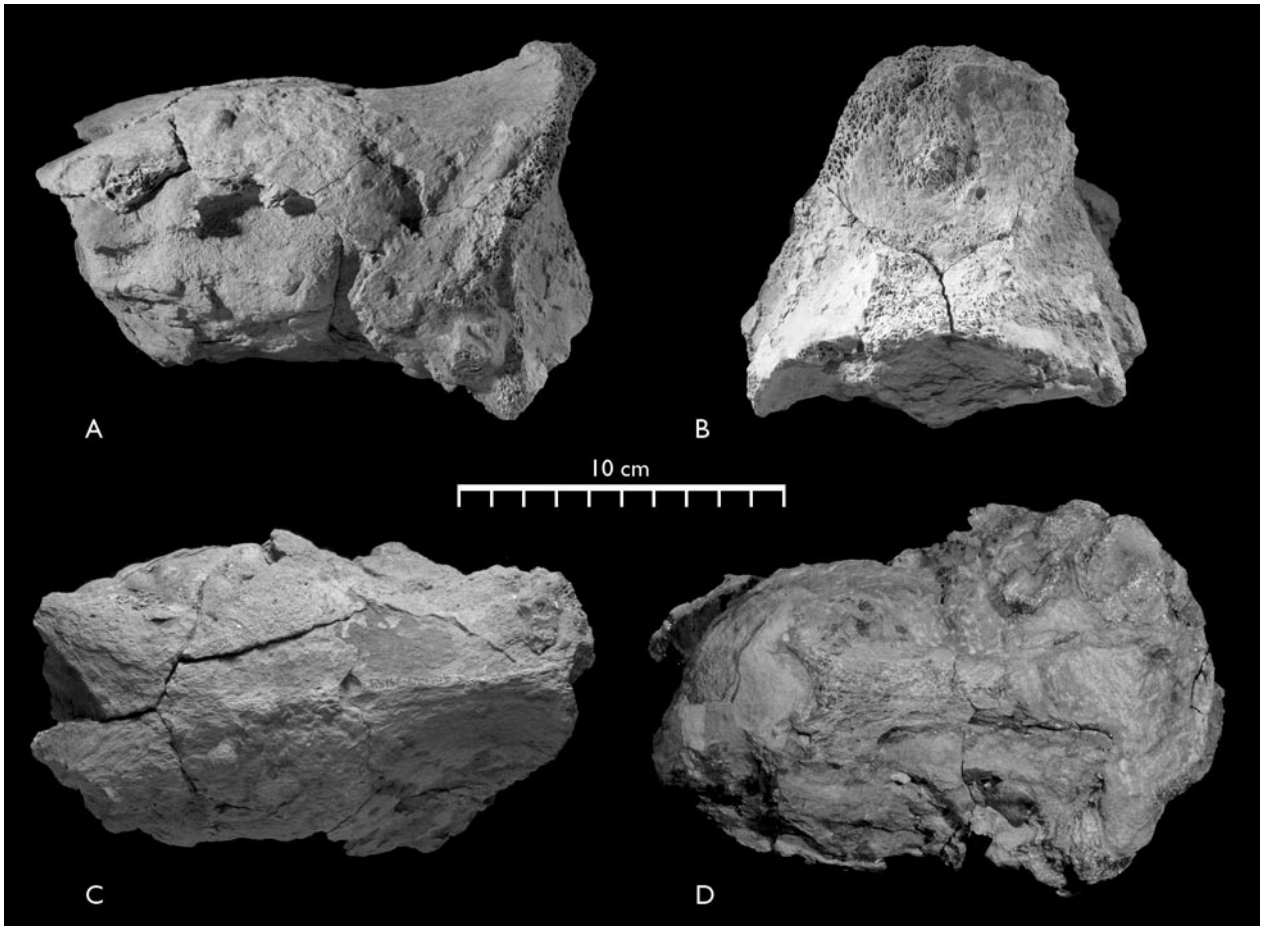

FIGURE 6.12
Equus sp. partial cranium BOU-VP-25/94. A. Lateral view. B. Caudal view. C. Dorsal view. D. Basal view.

(Figure 6.13B): the protocone shows distinct connection with the protoloph. On M^1, enamel plications are modestly developed on the posterior surface of the prefossette and opposing anterior surface of the postfossette, the hypoglyph is only moderately deeply incised, and the pli caballin is not at all apparent. The P^2 presents a short, "stubby" anterostyle. The protocone on P^2–M^2 is flat to concave on the lingual surface. Figure 6.13A shows that despite the early stage of wear the ectoloph is worn nearly flat on P^2–M^1, and the cusp relief is relatively low. This indicates high attrition and a grazing feeding adaptation.

There is a mandible including the corpus, ramus, and P_2–M_3, BOU-VP-3/11 (Figure 6.14). The mandibular P_2 is similar to the maxillary P^2 in its abbreviated anterostyle. All cheek teeth lack an ectostylid, the hallmark of the three-toed Daka equid, *Eurygnathohippus*. The premolars have mostly elongate metaconids and metastylids that are elongate on P_2 and P_3 and square shaped on P_4. The molars likewise have elongate metaconids on M_1 and M_2 and are squared medially on M_3. Molar metastylids are square and distolingually pointed on M_1 and are more elongate-rounded on M_2 and M_3. The mandibular P_2 preflexid is typical for *Equus*, with a strong, mesiolabially projecting pli. This same pli is present, but less strongly expressed, on P_4, M_1, and M_2. Preflexids and

EBSCOhost - printed on 10/28/2022 4:53 AM via . All use subject to https://www.ebsco.com/terms-of-use

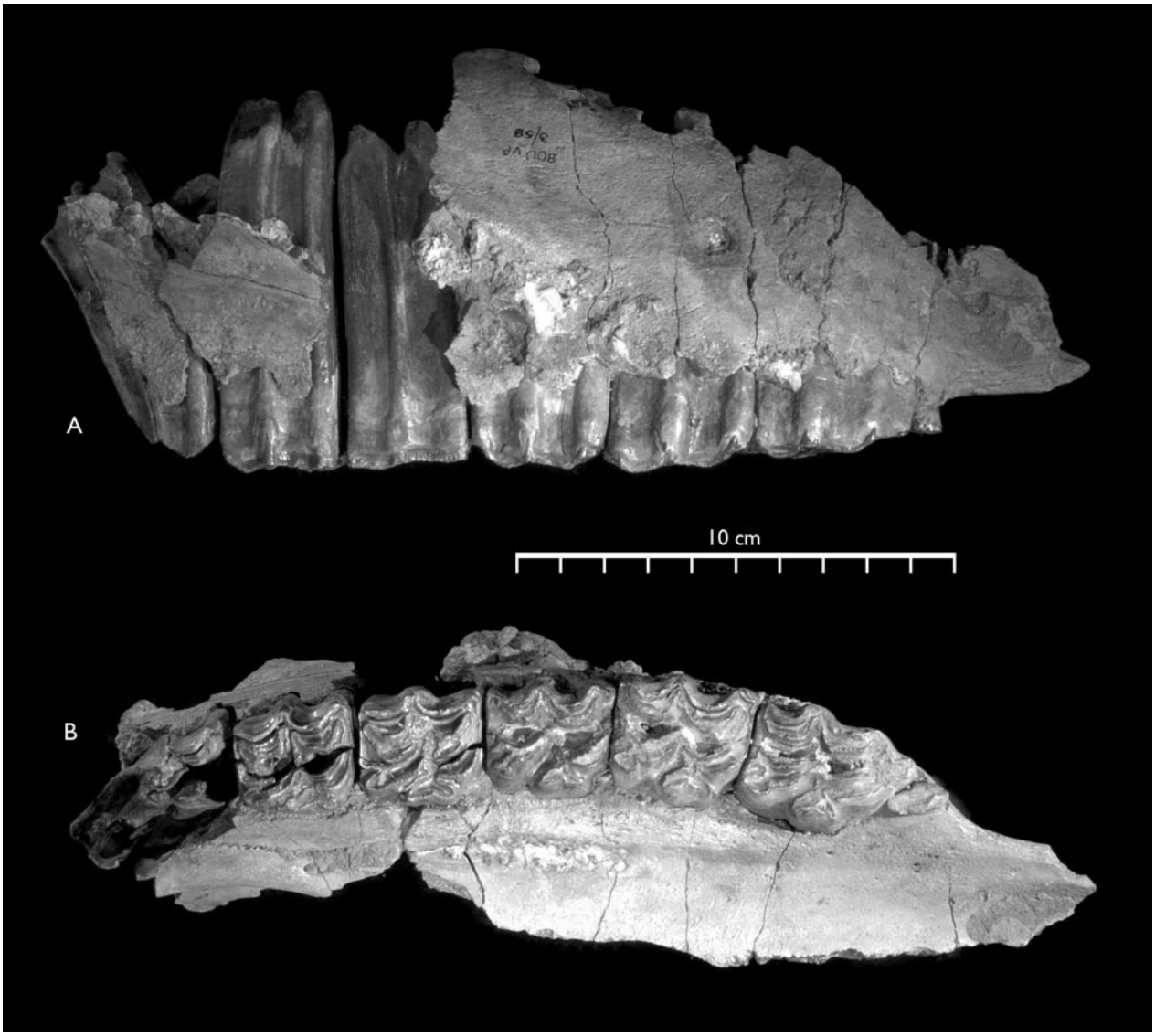

FIGURE 6.13
Equus sp. maxilla BOU-VP-3/58. A. Labial view. B. Occlusal view.

postflexids are labiolingually constricted and show minimum complexity, the P_3 postflexid having the only complex morphology. The mandibular M_3 is newly emergent and has a short talonid, particularly in comparison to hipparionine equids. Protostylids are not apparent on any of the cheek teeth.

Specimen BOU-VP-1/213 (Figure 6.15) is a mandibular symphysis with right and left I_1–I_3. The canine is lacking in this individual, which is typical for *Equus*. The incisor arcade is subarcuate in shape, with right and left I_1–I_2 being horizontally aligned, but I_3 being placed labiodistally. The I_1 is very worn, preserving a very small, circular infundibulum. The I_2 and I_3 are less worn, with correspondingly larger and more elongate infundibulae. The I_3 is only modestly elongate, tapering slightly distally. There are no vertical grooves apparent on the labial or lingual surfaces.

EBSCOhost - printed on 10/28/2022 4:53 AM via . All use subject to https://www.ebsco.com/terms-of-use

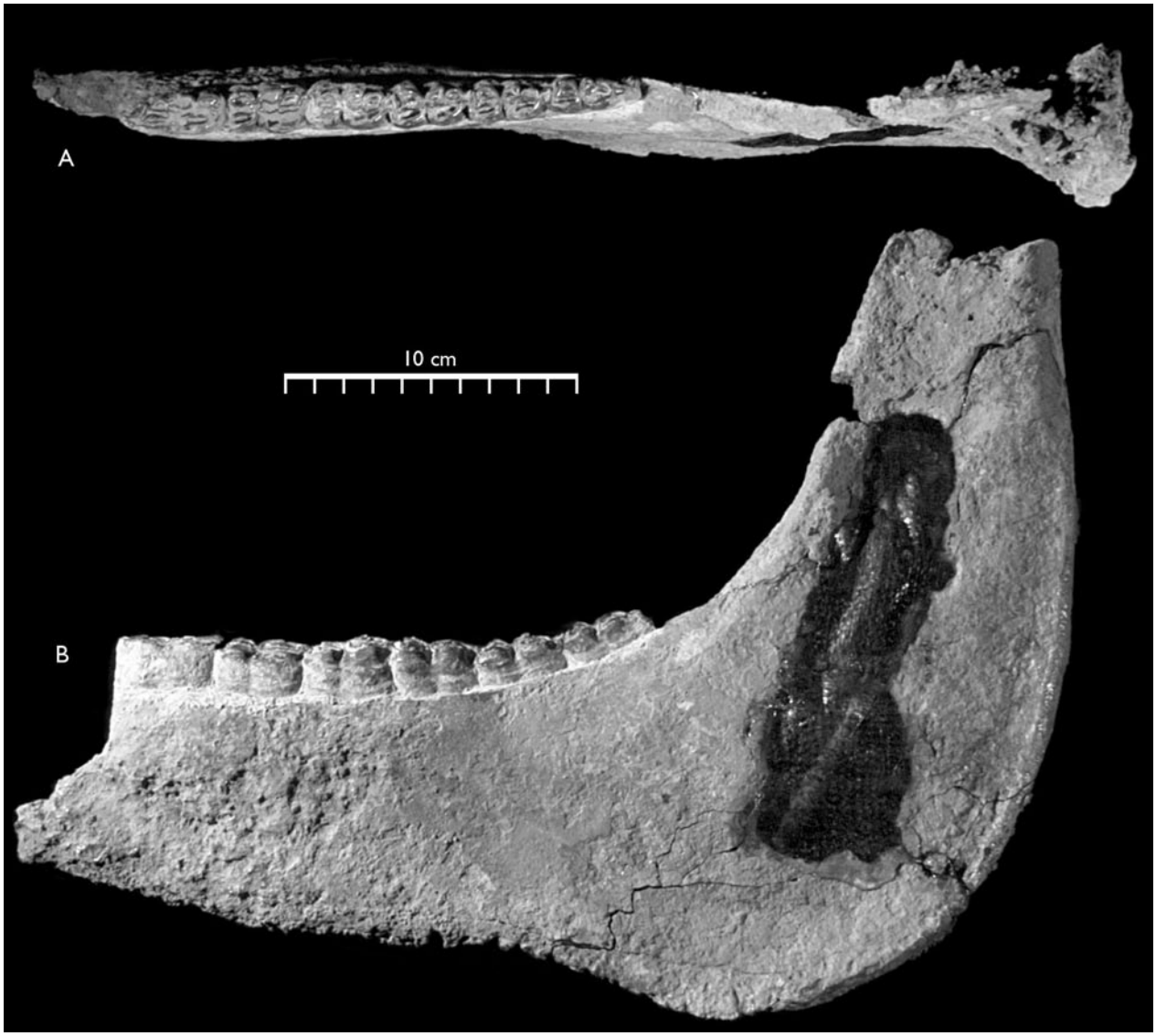

FIGURE 6.14
Equus sp. mandible BOU-VP-3/11.
A. Occlusal view. B. Buccal view.

The postcranial remains have been statistically analyzed in preceding sections. We summarize the salient morphologic features below for those elements that were statistically analyzed. Specimen BOU-VP-1/43 (Figure 6.16) is a complete right MCIII remarkable for its relatively short and stout appearance. The proximal surface (Figure 6.16B) is broad, with a prominent, laterally flaring uncinate facet, distomedially a distinct and deep fossa nudutae, and a distinct and large facet for the proximal MCIV splint. The log10 ratio diagram presented earlier (Figure 6.7A) exhibited proportions akin to our *E. grevyi* and *E. burchelli* samples, differing mostly from that species in its shorter length.

DISCUSSION Daka *Equus* provisionally appears more similar to *E. grevyi* and *E. burchelli* than to *E. zebra* or *E. quagga* based on astragalus and MCIII metrics

EBSCOhost - printed on 10/28/2022 4:53 AM via . All use subject to https://www.ebsco.com/terms-of-use

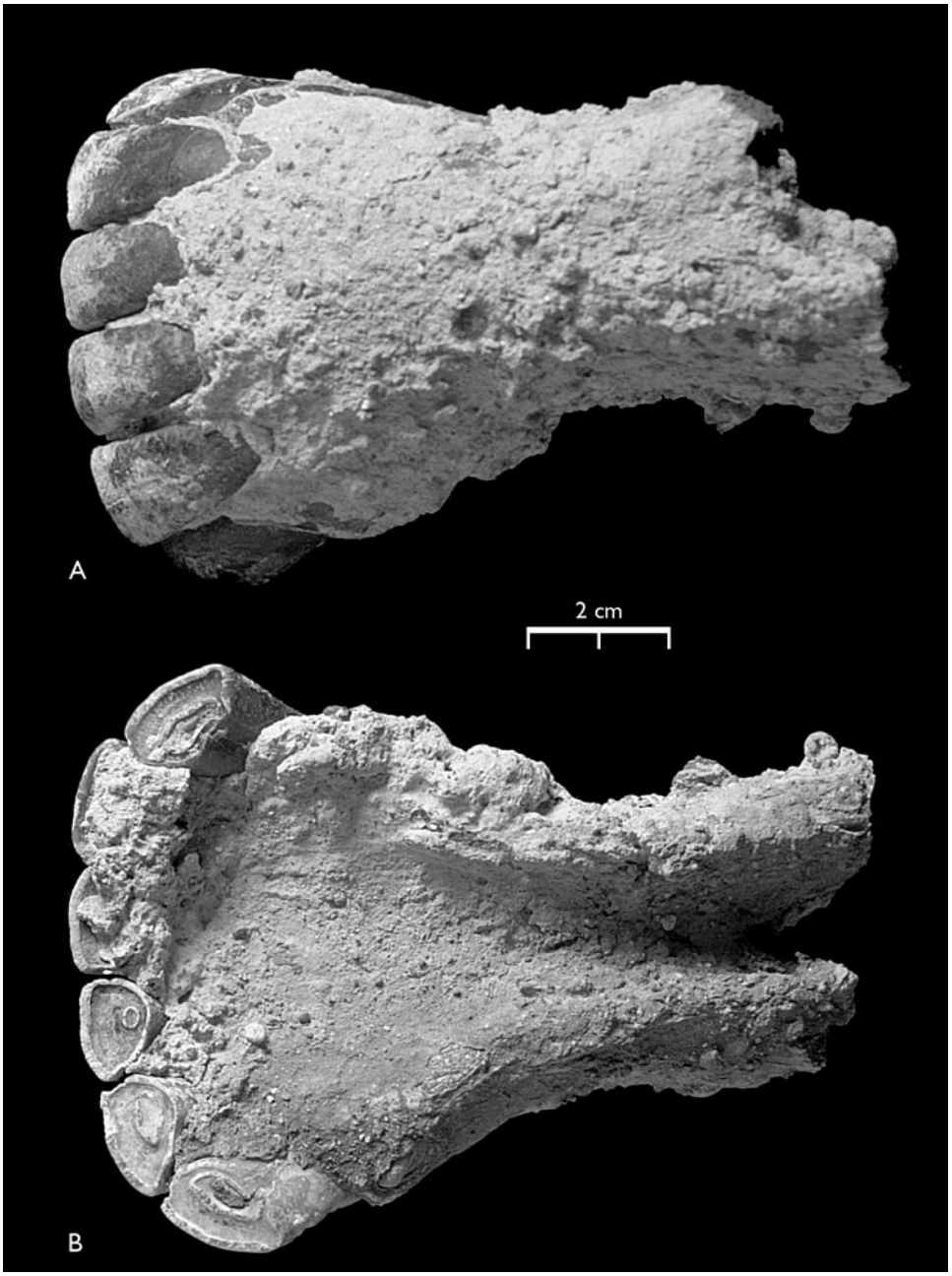

FIGURE 6.15
Anterior portion of *Equus* sp. mandible BOU-VP-1/213. A. Ventral view. B. Occlusal view.

(see Figures 6.3, 6.4, and 6.6). The Daka Member is roughly contemporaneous with the first appearance dates of the zebra/ass group in Africa. This potentially places Daka *Equus* near the base of the African zebra radiation predicted by molecular studies (Oakenfull and Clegg 1998). The Daka Member is younger than the earliest reported occurrence of the zebra/ass lineage at Olduvai Bed II (Churcher 1982) and older than the earliest reported zebra (Eisenmann and Baylac 2000).

EBSCOhost - printed on 10/28/2022 4:53 AM via . All use subject to https://www.ebsco.com/terms-of-use

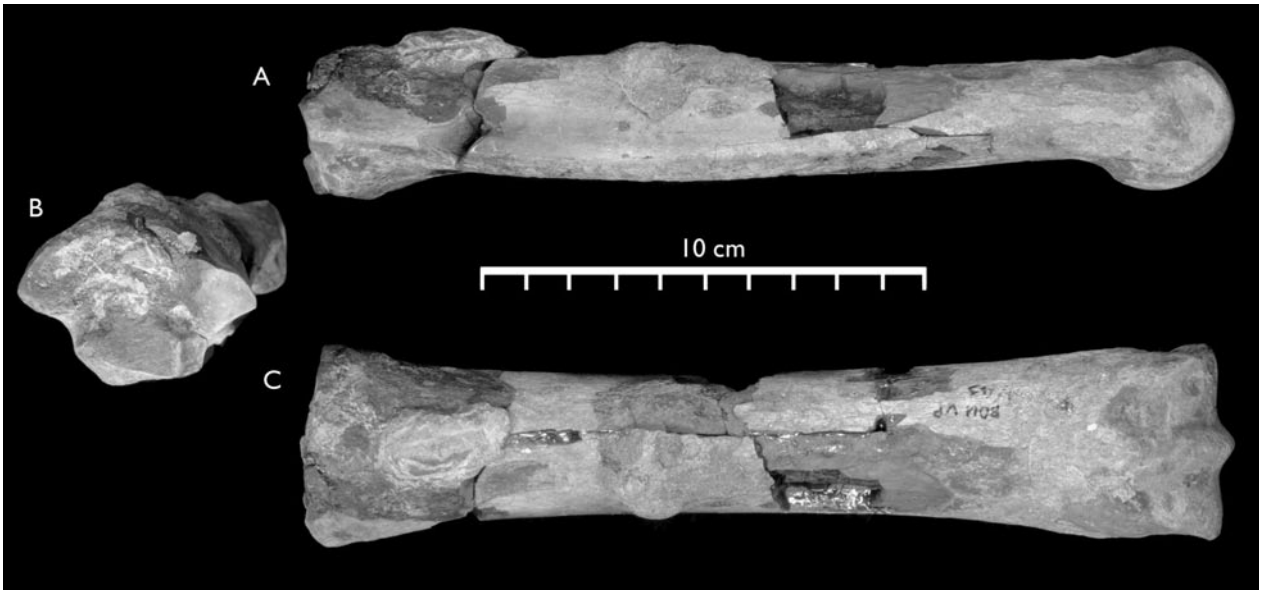

FIGURE 6.16
Equus sp. MCIII BOU-VP-1/43. A. Lateral view. B. Proximal view. C. Dorsal view.

Eurygnathohippus

Several workers have applied the nomen *Hipparion* for all Old World hipparions of late Miocene to Pleistocene age (Alberdi 1989; Eisenmann 1995). This taxonomic convention is most remarkable in the application of the nomen *Hipparion* for African hipparions that, over approximately 7 million years, evolved extremely high crowns and large ectostylids on the permanent cheek teeth (Hooijer 1975; Churcher and Richardson 1978; Eisenmann 1983) independent of Eurasian hipparions (Bernor and Armour-Chelu 1999a, b; Bernor and Harris 2003; Bernor et al. 2004, 2005).

Woodburne and Bernor (1980) early recognized a number of superspecific groups of Old World Neogene hipparions, and most recently Bernor and Armour-Chelu (1999a, b) and Bernor et al. (1996) have recognized several genera of hipparionines that include two major evolutionary radiations. The initial late Miocene radiation of species of *Cormohipparion*, *Hippotherium*, and *Cremohipparion* was species-diverse and largely restricted to Eurasia. Species of this predominantly Eurasian radiation mostly became extinct at the end of the late Miocene. A secondary radiation, likely rooted in a species of *Cormohipparion*, was apparently restricted to Indo-Pakistan, eastern and southern Africa for most of the late Miocene, and then exhibited distinct species-diverse clades in southern Asia ("*Sivalhippus*" spp.), China (*Plesiohipparion* spp. and *Proboscidipparion* spp.), and eastern and southern Africa (*Eurygnathohippus* spp.). Apparently, species of *Plesiohipparion* and *Proboscidipparion* extended their ranges into Europe and even Greenland in the early Pliocene.

The earliest known African hipparion, "*Cormohipparion*" sp., is from Chorora, Ethiopia, between 10.6 and 10.3 Ma (Geraads et al. 2002), or alternatively 10.7 and 10.1 Ma (Bernor et al. 2004) in age. The earliest recognized *Eurygnathohippus* is known from the lower Nawata Member of the Nawata Formation, Lothagam Hill, Kenya. *Eurygnathohippus* is initially recognized by tiny, diminutive ectostylids that rose only slightly on the labial

EBSCOhost - printed on 10/28/2022 4:53 AM via . All use subject to https://www.ebsco.com/terms-of-use

wall of the cheek teeth. The occurrence of the oldest recognized species of *Eurygnathohippus*, *Eu. turkanense*, evidently extended to fossiliferous levels as old as 7.4 Ma (McDougall and Feibel 2003). *Eurygnathohippus* exhibits low species diversity in the late Miocene and Plio-Pleistocene, but later in its chronologic range had dispersed across Africa. There is no evidence that Eurasian *Plesiohipparion*/*Proboscidipparion* overlapped geographically with *Eurygnathohippus*. Plio-Pleistocene *Eurygnathohippus* remains a poorly represented and understudied hipparion clade.

Middle Awash hipparions referable to the smaller sister taxon of *Eu. feibeli* are known to occur at the oldest levels, 6.0 Ma, and are very closely correlated with the upper Nawata Member type specimen of *Eu. feibeli* (KNM-LT 139; Bernor and Harris 2003; Bernor et al. 2005; Haile-Selassie and WoldeGabriel 2008). The *Eu. feibeli*/*hasumense* lineage dominates the Ethiopian succession between 6.0 and 2.9 Ma, and shows very conservative evolution in the postcranial skeleton (Bernor et al. 2005) and dentition (Bernor and Haile-Selassie in press).

Churcher and Richardson (1978) referred all Pleistocene African hipparions to the species "*Hipparion libycum,*" citing the commonality of cheek teeth in excess of 70 mm maximum crown height. This attribution, as well as the referral to the genus *Hipparion*, has been shown to be entirely inadequate. There is no compelling reason whatsoever to assume that all African Pleistocene hipparions belong to a single species, nor that any Pleistocene African hipparion species must be referred to a genus other than *Eurygnathohippus* (Bernor and Armour-Chelu 1999a, b). The highly derived species *Eu. cornelianus* is clearly recognized from the type locality of Cornelia, South Africa, and Olduvai Gorge Bed II (Tanzania; Leakey 1965) by its extreme hypsodonty and very wide mandibular symphysis, with hypertrophied I_1 and I_2, and atrophied I_3 placed posterior to I_2 in the lower dentition. *Eurygnathohippus* may include more than a single evolving lineage within Africa, but resolution of this scientific problem awaits further study. *Stylohipparion* and *Notohipparion* are junior synonyms of *Eurygnathohippus* by year priority (Bernor and Armour-Chelu 1999a, b).

Eurygnathohippus van Hoepen, 1930

GENERIC DIAGNOSIS All African hipparions of the genus *Eurygnathohippus* are united by the synapomorphy of ectostylids on the permanent cheek teeth. Eurasian and North American hipparions do not have this character except very rarely in extremely worn hipparion teeth from the Dinotheriensandes. Within *Eurygnathohippus* species, crown height, and ectostylid length, width, and maximum height increase from older to younger stratigraphic horizons.

Eurygnathohippus cf. *cornelianus* van Hoepen, 1930

REMARKS We have assembled a composite left cheek tooth series here composed of the following specimens, with their crown heights (Figure 6.17): P^2, BOU-VP-25/85 (mesostyle height [MH] = 48.9 mm); P^3, BOU-VP-19/39 (32.7 mm); P^4, BOU-VP-3/19 (MH = 25.1 mm); M^1, BOU-VP-4/50 (43.3 mm.); M^2, BOU-VP-25/16 (MH = unknown); LM^3, BOU-VP-19/21 (MH = 52.1 mm). The highest-crowned Daka *Eurygnathohippus* cheek tooth is 68.6 mm recorded in BOU-VP-3/89, a right M^1 (Figure 6.18).

We have also composed a composite lower cheek tooth series of the following individual *Eurygnathohippus* specimens (Figure 6.19): P_2, BOU-VP-2/30 (height = 45.9 mm); P_3, BOU-VP-25/81 (height = 24.7 mm); P_4, BOU-VP-25/81 (height = 30.5 mm); M_1,

EBSCOhost - printed on 10/28/2022 4:53 AM via . All use subject to https://www.ebsco.com/terms-of-use

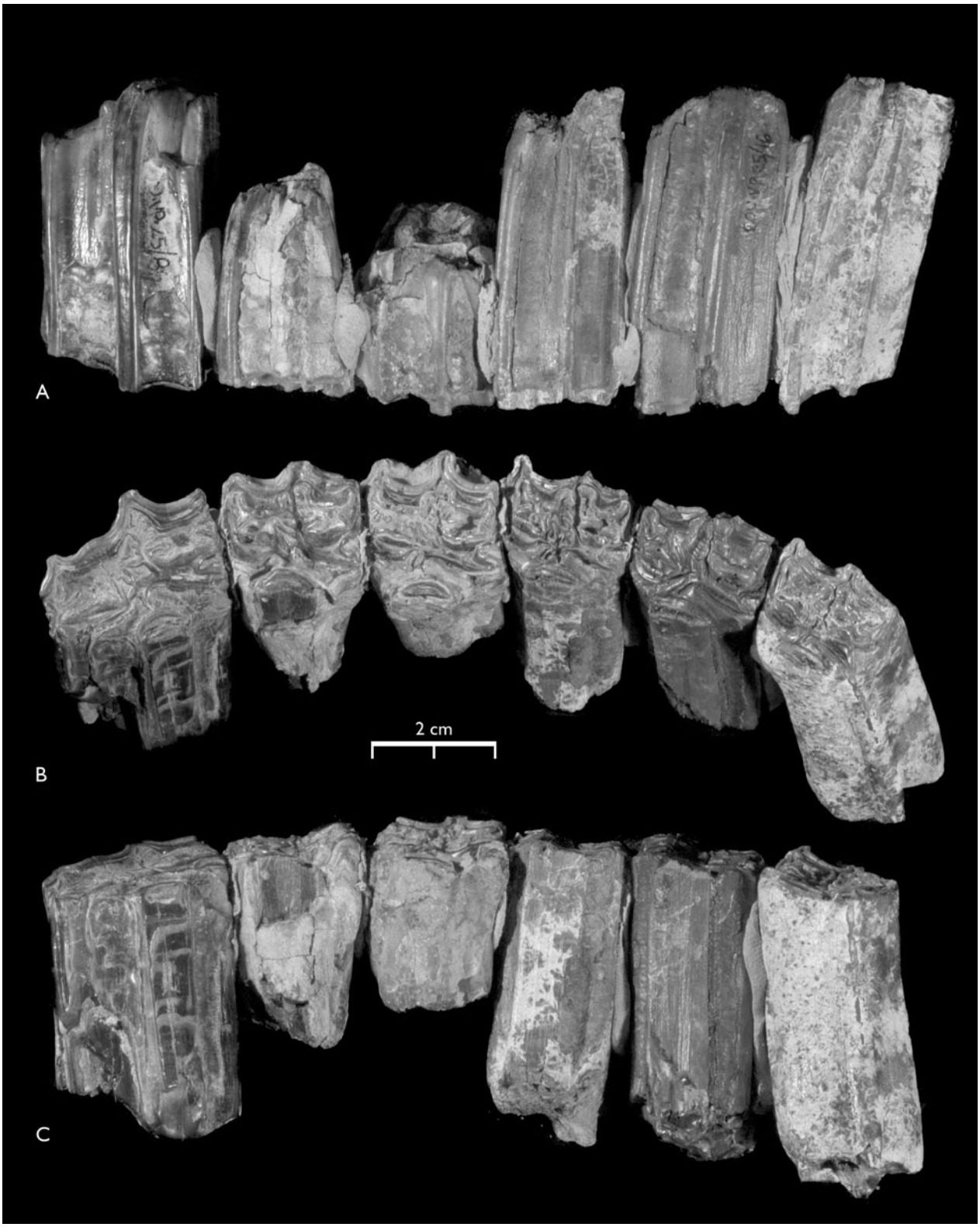

FIGURE 6.17

Eurygnathohippus cf. *cornelianus* composite maxillary dentition using multiple specimens. A. Buccal view. B. Occlusal view. C. Lingual view.

EBSCOhost - printed on 10/28/2022 4:53 AM via . All use subject to https://www.ebsco.com/terms-of-use

FIGURE 6.18

Eurygnathohippus cf. *cornelianus* M^1 BOU-VP-3/89. A. Labial view. B. Occlusal view. Maximum crown height is 68.6 mm.

BOU-VP-25/45 (height = 14.6 mm); M_2, BOU-VP-3/40 (height = 50.9 mm); M_3, BOU-VP-26/18 (height = 43.2 mm). The highest-crowned lower cheek tooth is BOU-VP-25/59, a right M_2 with a crown height of 61.2 mm.

DESCRIPTION

Maxilla (Composite) The P^2 has the following salient features: a broken anterostyle and mesiolingual margin; mesostyle with a somewhat squared appearance; prefossette has a slightly complex anterior margin and a more complex posterior margin; postfossette anterior margin is moderately complex and the posterior margin is less complex; there is a single pli caballin; hypoglyph is deeply incised; protocone is elongate with a strongly flattened lingual margin and rounded labial margin. The P^3 is substantially more worn than P^2, having an even more square mesostyle; prefossette has a very simple anterior margin and only moderately complex posterior margin; postfossette is simpler yet has a moderately complex anterior margin and very simple posterior margin; hypoglyph is still deeply incised; pli caballin is lacking; protocone is elongate as in P^2 and has the same strong flattening lingually and rounding labially. The P^4 is even more worn than the P^3 and has all the same characters as the P^3 except that there is a double pli caballin and the protocone is more labiolingually compressed. The M^1 is in middle wear and exhibits slightly different characters in some aspects: while the prefossettes and postfossettes have a similar degree of complexity as the P^2, the mesostyle has a more pointed, bladelike aspect; pli caballins are strongly double; hypoglyph is again deeply incised; protocone is elongate and very strongly compressed labiolingually. The M^2 lacks a mesostyle height measurement, but the occlusal surface appears to be in relatively early wear compared to the other teeth described herein, exhibiting the following salient characters: mesostyle has a squared appearance; fossette margins are simple (due to early wear) except for the posterior surface of the prefossette; pli caballin is single, but elongate and directed anteriorly; protocone is elongate and strongly compressed labiolingually; hypoglyph is deeply incised. The M^3 is also in relatively early wear and has the following features: mesostyle has a squared outline; all fossettes are relatively simple; pli caballin is small; protocone is an elongate oval; hypoglyph is deeply incised, but directed anterolabially. The most remarkable characteristics of all these cheek teeth are the labiolingually compressed protocones and the orientation of the hypoglyphs. Normally, deeply incised hypoglyphs virtually encircle the hypocone. In this species, the hypoglyph, though deeply incised, is directed mesiolabially, not mesiolingually. Pli caballin variability is not unusual through wear, especially when cheek tooth occlusal surfaces have been planed flat, as in these specimens. The flat, or blunt (*sensu* Fortelius and Solounias 2000; Kaiser et al. 2000), occlusal surfaces seen in Figure 6.17A are indicative of a dedicated grazing diet, characteristic of early Pleistocene eastern and southern African hipparions and especially *Eu. cornelianus* (Bernor and Armour-Chelu 1999a, b).

Beyond the composite maxillary cheek tooth series, there is a single M^1 that warrants description—BOU-VP-3/89, the highest crowned individual in the *Eurygnathohippus* sample, with a mesostyle height of 69.2 mm. This individual is in an early wear stage, and we estimate that the tooth would have had an unworn crown height of nearly 75 mm, but not likely much more than 75 mm. Given that it originated from the middle of the tooth row, we can use this as an effective and empirical estimate of the maximum crown height of

EBSCOhost - printed on 10/28/2022 4:53 AM via . All use subject to https://www.ebsco.com/terms-of-use

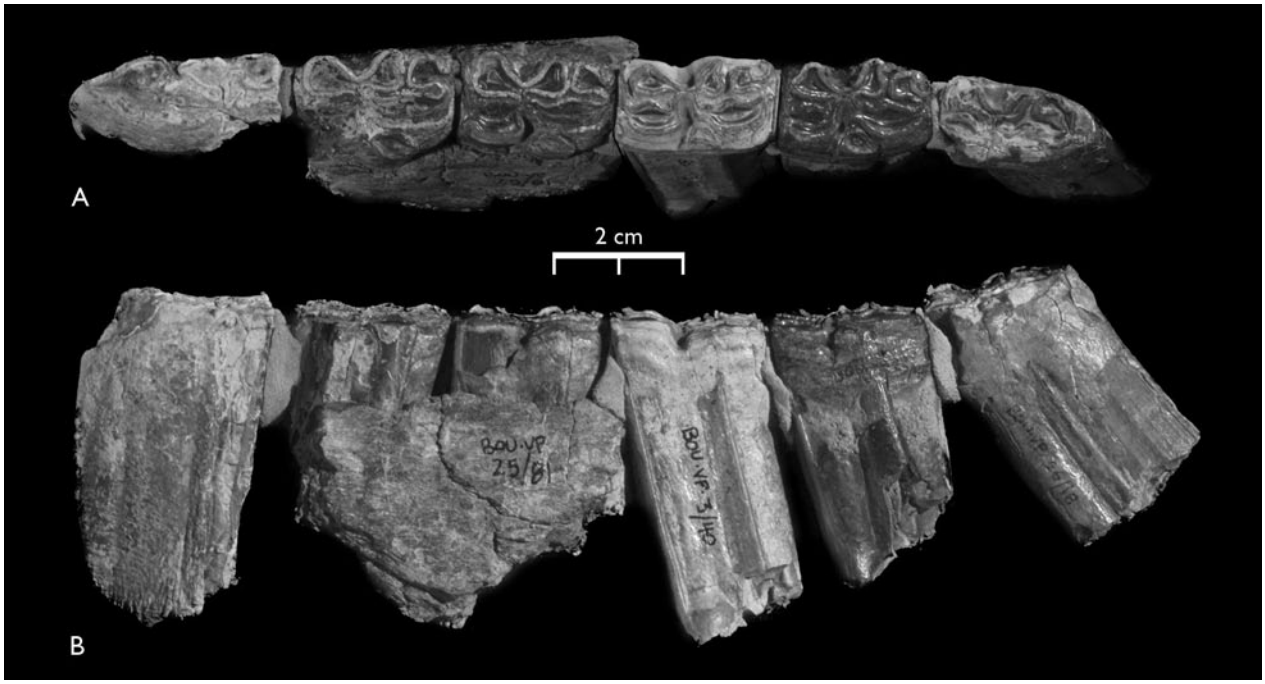

FIGURE 6.19
Eurygnathohippus cf. *cornelianus* composite mandibular dentition using multiple specimens.
A. Occlusal view.
B. Labial view.

the Daka *Eurygnathohippus*. The occlusal surface of this specimen (Figure 6.18) has a very pointed and blade-like parastyle and mesostyle; pre- and postfossettes are beginning to wear and show relatively simple plication amplitude. The hypoglyph is very deeply incised and fully encircles the hypocone, but the constriction is on the midlabial side, not more mesial as is typical for most hipparions. The protocone is extremely long and extremely compressed.

Mandible The P_2 would appear to be in a relatively early stage of wear and, in addition, has the mesial and the distolabial portions of the crown broken away and has the following salient morphological characters: metaconid has an unusual labiolingually compressed, mesially pointed, beak-like appearance; metastylid is round with a squared distal border; preflexid is strongly compressed labiolingually and has simple margins while postflexid is rectangular; ectoflexid continues mesially from the postflexid and is inverted, being directed labialward rather than lingualward, which is the usual condition. The P_3 and P_4 are of a single individual in an advanced stage of wear. Both teeth express the following salient characters: metaconid and metastylid are rounded, with slight pointing to the metastylid; linguaflexid has a very deep and wide V-shape; pre- and postflexids are very elongate, labiolingually compressed, and entirely lacking complexity to the enamel margins; pli caballinid is preserved only on the P_4 and is an open, labially directed loop; protoconid enamel band is likewise only preserved on the P_4 and exhibits only modest flattening; ectoflexid is shallow in both teeth, abutting against, but not separating the pre- and postflexids; ectostylids are large, ovate-shaped structures on both P_3 and P_4. The M_1 is in a medial stage of wear. It is similar to the P_3 and P_4 except for the following features: metastylid is very pointed; linguaflexid is as deep, but has a broader U shape; ectoflexid extends fully between pre- and postflexids, making contact with

EBSCOhost - printed on 10/28/2022 4:53 AM via . All use subject to https://www.ebsco.com/terms-of-use

the linguaflexid; ectostylid has a flat labial margin and a more rounded lingual surface; protostylid is not well developed on the occlusal surface because of early wear. The M_2 is more worn than the M_1, but fundamentally similar to M_1, differing in having a pointed M_1 metaconid and more oval, yet still large, ectostylid. The M_3 is unusual in a number of morphological features including: exceedingly deep and broad U-shaped linguaflexid that presents a rounded metaconid and a very mesiodistally constricted metastylid not seen in any other hipparion we have studied; unusually abbreviated distally, with an underdeveloped talonid occlusal morphology; ectostylid is a very large, labiolingually compressed ovate structure.

In summary, the most remarkable morphological features of this species' lower cheek teeth are the very large, mostly ovate ectostylids; the markedly pointed morphology of metastylids (particularly in the molars); the extremely compressed and often elongate pre- and postflexids; and the extremely derived M_3 where the linguaflexid is exceptionally deep and wide, the metastylid is compressed mesiodistally, and the talonid is sharply reduced.

Specimen BOU-VP-26/13 (Figure 6.20) is a left MTIII of a Daka *Eurygnathohippus*. The specimen is elongate and moderately heavily built. The proximal surface (Figure 6.20D) is obscured by a calcareous matrix, but the outline has the relatively deep cranial-caudal dimension typical of hipparions. The distal surface has medial trochlea metatarsi considerably larger than its lateral trochlea, also a hipparion-like feature. Referral to the previously described log10 ratio diagram (Figure 6.10A) shows that this specimen compares closely with BMNH 16982. Specimen BOU-VP-26/13 differs markedly from Hadar *Eu. hasumense* (Bernor et al. 2005) in its smaller size, its shorter maximum length dimension, and markedly narrower (measurement M3 [mediolateral]) and shallower (measurement M4 [craniocaudal]) midshaft dimensions. This specimen would appear most closely related to Olduvai Bed II *Eu. cornelianus*.

DISCUSSION Daka specimens are securely referred to *Eurygnathohippus* based on the presence of ectostylids and isolated protocones. There are few published metrics of Pleistocene hipparionines. Overall, dental metrics fall within the range of Omo representatives from all levels (Eisenmann 1985).

Despite the fact that the Daka hipparion sample does not include a mandibular symphysis or a premaxilla with hypertrophied incisors, we believe it is very similar to, or identical to, *Eu. cornelianus*. If this is proven to be true, the Daka occurrence is one of the later occurrences of *Eu. cornelianus* known. The Daka *Eu.* cf. *cornelianus* is characterized by its extremely derived cheek teeth with: elongated, labiolingually compressed ovate protocones; anterolabially directed hypoglyphs; pointed metastylids, broad linguaflexids, large, mostly ovate shaped ectostylids, mesiodistally compressed M_3 metastylid and abbreviated talonid. The maximum crown height of the Daka *Eurygnathohippus* would appear to have been about 75 mm. The metapodials were elongate and relatively slender (compared to *Equus*) and, together with the astragali, suggest a species of hipparion that approximated the Höwenegg hipparion (10.3 Ma, Hegau, southern Germany) in its stature and robustness of build. It was substantially smaller than the relatively well-known form from the early late Pliocene of Hadar, Ethiopia (ca. 3.2 Ma), *Eu. hasumense* (Bernor et al. 2005).

The last appearance of the genus *Eurygnathohippus* is potentially in Members 10 and 11 of Olorgesailie (although Eisenmann 1979 questions this; Koch 1986). Alternatively, the

EBSCOhost - printed on 10/28/2022 4:53 AM via . All use subject to https://www.ebsco.com/terms-of-use

FIGURE 6.20
Daka *Eurygnathohippus* cf. *cornelianus* MTIII BOU-VP-26/13. A. Cranial view. B. Distal view. C. Lateral view. D. Proximal view.

latest occurrence may be Cornelia, the type locality of *Eu. cornelianus*, which Vrba (personal communication) believes to be on the order of 0.6 Ma. The latest occurring species of *Eurygnathohippus* was clearly a dedicated grazer. Its high crowns, reportedly approximating 90 mm height, and its very broad symphyseal gape with procumbent and hypertrophied first and second incisors, are the hallmarks of a committed short-grass-grazing diet (Bernor and Armour-Chelu 1999a, b). It remains a mystery why *Eurygnathohippus* failed to survive the Pleistocene when other committed short-grass grazers such as the wildebeest and white rhinoceros did.

The evolutionary relationships of pan-African late Miocene-Pleistocene hipparions remain unstudied, but it is clear that there was at least some degree of biogeographic provinciality in *Eurygnathohippus* through the duration of its African evolutionary history.

Conclusions

The Daka Member provides a large sample of fossil equids, including both an *Equus* form similar to modern zebra species and an extinct hipparionine, *Eurygnathohippus* cf. *cornelianus*. *Equus* outnumbers *Eurygnathohippus* in the Daka Member by an approximate 2:1 ratio (Figure 6.21). The two taxa are very abundant, together representing approximately 20 percent of the total Daka Member faunal assemblage in terms of number of identifiable specimens present (NISP).

Daka equids are of only moderate use as paleoenvironmental indicators. Archaic Old World hipparions were high crowned and adapted to a broad range of diets including grazing, intermediate feeding, and browsing (Kaiser et al. 2000; Bernor et al. 2003), although *Eurygnathohippus cornelianus*, the form most likely represented in the Daka Member, was a dedicated grazer. *Equus* species inhabit a variety of arid and semiarid niches, but the most

EBSCOhost - printed on 10/28/2022 4:53 AM via . All use subject to https://www.ebsco.com/terms-of-use

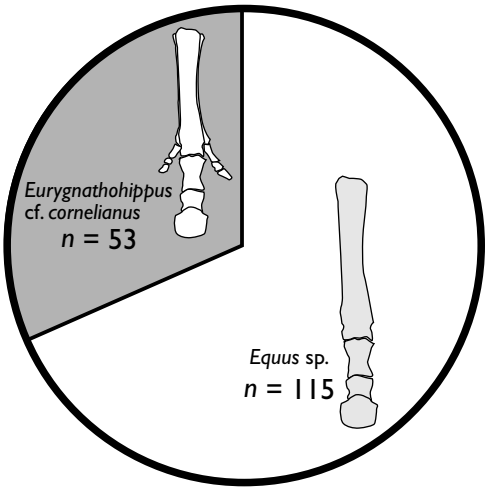

FIGURE 6.21
Relative proportions of *Eurygnathohippus* and *Equus* in the Daka Member based on number of identifiable specimens present for each taxon.

common wild horse, the plains zebra (*E. burchelli*), is widespread across numerous habitat types in Africa. *Equus grevyi* is less water dependent than any other zebra species and is currently restricted to a semiarid zone in Ethiopia, Somalia, and northern Kenya. It is bounded by the ranges of the xeric-adapted *E. asinus* and the more mesic-adapted *E. burchelli* (Kingdon 1979: IIIB). Daka *Equus* sp. is therefore not a precise paleoenvironmental indicator.

EBSCOhost - printed on 10/28/2022 4:53 AM via . All use subject to https://www.ebsco.com/terms-of-use

7

Giraffidae

W. HENRY GILBERT

Giraffids are uncommon in the African Plio-Pleistocene fossil record. As is true for most sites, the Daka Member is not particularly rich in giraffe fossils. Remains of Giraffidae include an immature *Sivatherium* mandible, an immature *Sivatherium* maxilla, a *Sivatherium* upper second premolar, a left *Sivatherium* metatarsal, four *Giraffa* ossicones, and a complete right *Giraffa* metacarpal.

Possible Giraffids first appear in Africa in the early Miocene with genera *Climacoceras, Propalaeoryx*, and *Prolibytherium* (Churcher 1978; Gentry 2000b). Established giraffids appear in the middle and late Miocene, and include *Canthumeryx, Palaeotragus*, *Samotherium*, *Giraffokeryx*, *Helladotherium* (Churcher 1978; Hamilton 1978; Gentry 2000b). These early genera have been placed in the potentially polyphyletic (Geraads 1986) subfamily Paleotraginae (Churcher 1978; Hamilton 1978). Relationships between early and middle Miocene giraffids and the well-documented Plio-Pleistocene sivatherine and giraffine lineages are unclear (Churcher 1978; Hamilton 1978). Giraffinae first appear in the Siwalik Formation of India at around 7 Ma and in Africa at about 6 Ma (Gentry 2000b). Two isolated teeth referred to *Giraffa* are noted in uppermost Miocene deposits from the Adu-Asa Formation of the Middle Awash (Haile-Selassie 2001). As of the beginning of the Pliocene, African giraffids can be discriminated as *Giraffa* or *Sivatherium* (Gentry 2000b).

Giraffa

African early Pliocene specimens of *Giraffa* are known from Kanapoi and Langebaanweg (Churcher 1978). *Okapia* and *Giraffa* are close sister taxa with respect to other Neogene and Quaternary giraffid genera. They are united by ossicone morphology (Janis and Scott 1987) and molarization of the P_3 (Geraads 1986). *Giraffa* species are united by the presence of paired, short ossicones. Modern *G. camelopardalis* exhibits substantial variation in size and morphological characteristics between individuals in different populations (Churcher 1978; Harris 1991b). Two groups within *Giraffa* may be differentiated in the African Plio-Pleistocene: a larger group consisting of *G. camelopardalis* and *G. jumae*, and a smaller group consisting of *G. stillei*, *G. gracilis*, and *G. pygmaeus* (Harris 1991b).

EBSCOhost - printed on 10/28/2022 4:53 AM via . All use subject to https://www.ebsco.com/terms-of-use

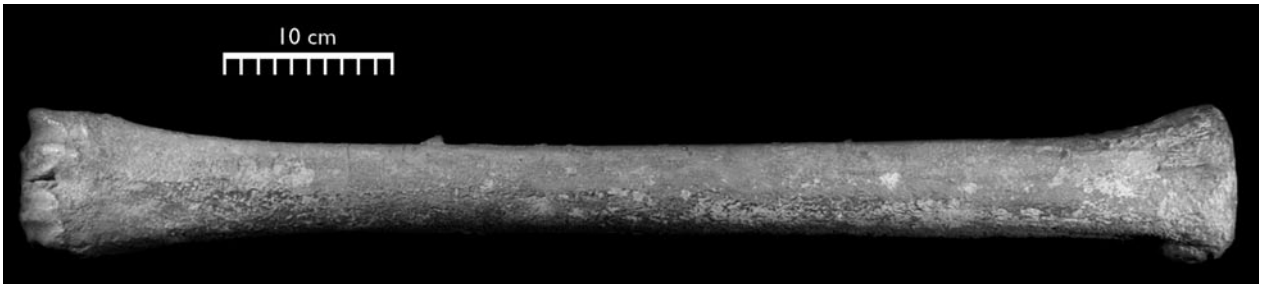

FIGURE 7.1
Daka Member *Giraffa* right metacarpal BOU-VP-25/41, dorsal view.

Detailed systematic analysis has not been undertaken on *Giraffa* below the subgenus level, and relationships among species remain unresolved. Diagnostic features for species within the two size groups are very subtle (Churcher 1978). One potentially useful character is the angular orientation of the ossicones, which does not appear to vary substantially between sexes or conspecific individuals (Harris 1991b). The most consistent difference between *G. camelopardalis* and *G. jumae* is the more anterior insertion and more posteriorly oriented projection of the parietal ossicones in the former (Harris 1991b). Unfortunately, preservation of Daka ossicones is not sufficient for species allocation.

Giraffa Brisson, 1762

GENERIC DIAGNOSIS "Ossicones paired, short, on frontoparietal suture; sometimes with single frontal ossicone between or just behind the level of the orbits; all ossicones variable in form, but usually straight and bluntly ended if paired and rounded or tumescent if single. Exostotic occipital 'horns' may be developed from nuchal crest and azygous 'horns' from the orbital boss. Lower incisors and canines robust; buccal enamel rugose; lower canine occasionally trifid. Cheek teeth variable in size and moderately brachydont; premolars progressively molariform and complex. Basicranial and basipalatal planes not parallel" (Churcher 1978, 518).

DESCRIPTION BOU-VP-25/41 (Figures 7.1 and 7.2, Table 7.1) is a right metacarpal. It measures 704 mm superoinferiorly. Its proximal end is 66.6 mm anteroposteriorly and 98.8 mm mediolaterally, and its distal end is 63.8 mm anteroposteriorly and 98.5 mm mediolaterally. These measurements align the specimen solidly with *Giraffa* as opposed to *Sivatherium* (Harris 1991b).

DISCUSSION Although there is a great deal of intraspecific variation in giraffid ossicones in terms of both their number and shape, they are morphologically diagnostic at the level of genus. Daka Member ossicones (Figure 7.3, Table 7.2) are typical of *Giraffa,* with slightly to moderately ovoid cross sections, an overall columnar appearance, and a ball-like ossified knob distally. While ossicone size places Daka specimens among the larger Plio-Pleistocene *Giraffa,* none of the ossicones retains enough of the base to assess anatomical position or angle of projection, and thus they many not be used for specific allocation.

EBSCOhost - printed on 10/28/2022 4:53 AM via . All use subject to https://www.ebsco.com/terms-of-use

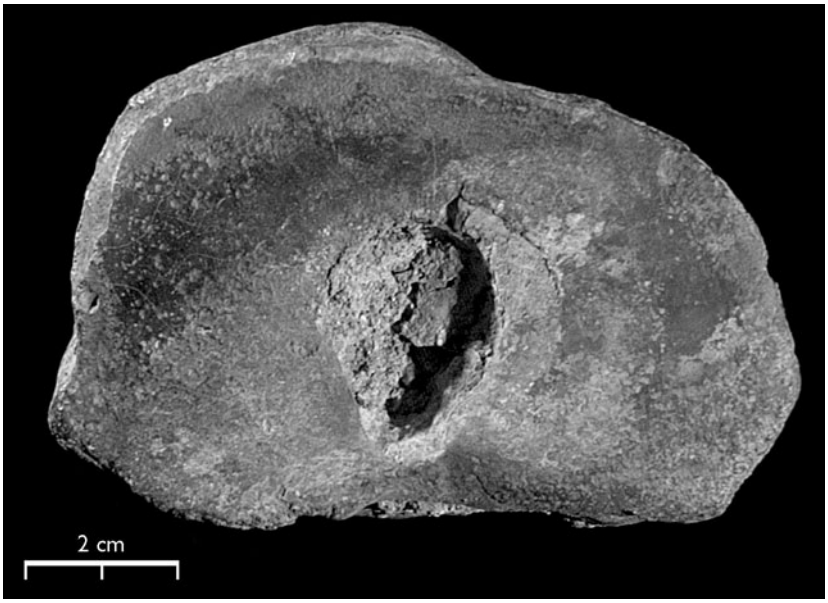

FIGURE 7.2
Daka Member *Giraffa* right metacarpal BOU-VP-25/41, proximal view.

Sivatherium

Sivatheres have a large distribution across the Old World. *Sivatherium,* represented in African and Asian Plio-Pleistocene faunas, survived through the middle Pleistocene (Churcher 1978; Gentry 2000b; Geraads et al. 2004). The earliest record of *Sivatherium* is in late Miocene deposits at Toros-Menalla, Chad (Vignaud et al. 2002). The large ossicones of *Sivatherium* are highly variable in morphology. *Sivatherium maurusium* is the most common species of the genus, but two other species are also recognized, *S. giganteum* from the Asian Pleistocene and *S. hendeyi* from Langebaanweg (Harris 1991b).

TABLE 7.1 Measurements Taken from Daka Member *Giraffa* Metacarpal BOU-VP-25/41

Length	704
Width of proximal facet	97
Depth of proximal facet	66.9
Proximal AP	66.6
Proximal ML	98.8
Minimum shaft AP	39
Minimum shaft ML	52
Distal articular AP	63.8
Distal articular distal ML	95.5

NOTE: AP = anteroposterior; ML = mediolateral.

EBSCOhost - printed on 10/28/2022 4:53 AM via . All use subject to https://www.ebsco.com/terms-of-use

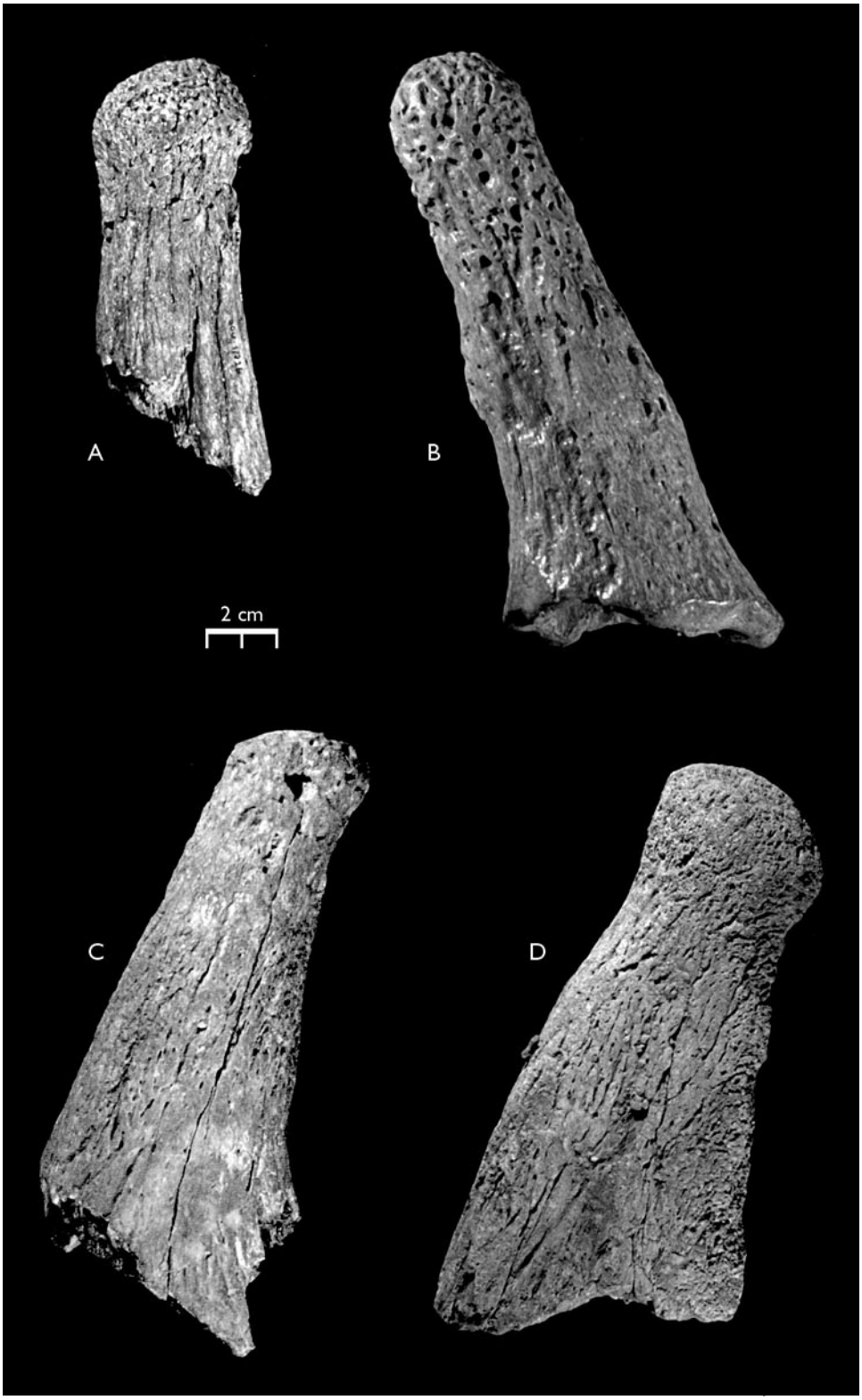

FIGURE 7.3

Daka Member *Giraffa* ossicones. A. BOU-VP-1/226. B. BOU-VP-1/92. C. BOU-VP-19/49. D. BOU-VP-1/54.

EBSCOhost - printed on 10/28/2022 4:53 AM via . All use subject to https://www.ebsco.com/terms-of-use

TABLE 7.2 Measurements Taken from Daka Member *Giraffa* Ossicones

Specimen	*Length*	*AP Base*	*ML Base*	*Distal AP*	*Distal ML*
BOU-VP-1/54	179.2	88.7	50.4	54.8	41.8
BOU-VP-1/92	186.5	69.7	53.5	39.8	39.9
BOU-VP-19/49	166+		53.5	42.5	38.1

NOTE: AP = anteroposterior; ML = mediolateral.

Sivatheres are very large, relatively short-necked giraffids. Two pairs of ossicones are antler-like and spatulate in males, and absent in females (Churcher 1978). The anterior pair is from the frontals, and the larger, planar posterior pair arises from the parietals. The premolars and molars are somewhat hypsodont and display substantial, coarse enamel rugosity. Sivatheres can be differentiated from *Giraffa* based on tooth dimensions, the relative proportions of the cheek tooth row to the whole mandible, absolute size, and ossicone morphology.

Sivatherium Falconer and Cautley, 1832

GENERIC DIAGNOSIS "Gigantic giraffid; skull brachycephalic, face short, nasals retracted. Ossicones in two pairs in males, absent in females; anterior pair arising from frontals and massive palmate posterior pair arising from parietals. Males—frontals broad, flat, or slightly dished; nasals short, convex; sinuses extending throughout main stems of ossicones. Females—skull longer and lower, not markedly broadened, frontals convex. Deep muscular pits in temporal and supraoccipital areas. Facial region relatively short, anterior margin of orbit above M^2. Cranial region deeper than facial, especially in males; basicranial and palatal planes not parallel. Teeth large; enamel coarsely rugose. Body, neck, and limbs heavy, neck and limbs not elongated" (Churcher 1978, 523–524).

REMARKS The Daka Member presents one P^2, a juvenile left mandible with dentition, a juvenile right maxilla with dentition, and a left metatarsal.

DESCRIPTION BOU-VP-1/20 (Figure 7.4; Table 7.3) is a *Sivatherium* mandible with the dp_3 and dp_4 very worn and their roots somewhat resorbed. Permanent premolars bulge beneath the alveolar bone, but do not break the surface. The M_1 and M_2 are partially erupted and in early stages of wear. The dp_3 has the general appearance of an adult premolar. The entoconid, metaconid, and entostylid are fused. Dentin exposed between them is continuous. The protoconid bulges lingually so that its occlusal surface is vesica piscis–shaped. There is only a narrow isthmus of dentin joining the protocone with the bifid paraconid and parastylid. There is an accessory style positioned on the distolingual paraconid that rises approximately 6 cm from the neck of the tooth. The neck of the tooth is tightly constricted, creating an enamel bulge just above it. The hypoconid is large relative to that of an adult premolar and is wider buccolingually than the anterior portion of

EBSCOhost - printed on 10/28/2022 4:53 AM via . All use subject to https://www.ebsco.com/terms-of-use

FIGURE 7.4
BOU-VP-1/20 *Sivatherium* left mandible. A. Occlusal view. B. Lingual view.

the tooth. The cervical margin has a buccal bulge centrally located between the mesial and distal roots.

The dp_4 is trilobate, with the anterior pillar oriented at an angle to the other two so that the buccal valley between the two portions is broad. The dp_4 is very worn, and dentin is continuous between all of the cusps, albeit only barely between the paraconid and parastylid. This slight connection leaves an island of enamel between the mesial and middle pillars. There is no remnant of enamel between the protostylid and paraconid. The junction of the anterior and middle pillars is cleft slightly between the paraconid and metaconid and heavily between the protostylid and protoconid. There are no accessory stylids on the margin of the tooth. The hypoconid is skewed distally so that there is a distal bulge in the hypoconid dentin when viewed from an occlusal perspective. The posterior face of the dp_4 is deeply incised at the interproximal contact facet, and the M_1 enamel is pierced by wear at the contact. The central portion of the tooth and part of its buccal enamel wall are broken away, obscuring some of the morphology of the protoconid.

172

EBSCOhost - printed on 10/28/2022 4:53 AM via . All use subject to https://www.ebsco.com/terms-of-use

TABLE 7.3 Daka Member *Sivatherium* Dental Metrics

Specimen	*Element*	*MD*	*BL*
BOU-VP-1/30	dp^3	38.3	32.2
BOU-VP-1/30	dp^4	39.6	34.8
BOU-VP-1/30	M^1	49.4	45.2
BOU-VP-1/30	M^2	52.4	41.7
BOU-VP-1/30	M^3	52	
BOU-VP-1/20	dp_3	39.1	30.2
BOU-VP-1/20	dp_4	38.5	35.7
BOU-VP-1/20	M_1	54	41.1
BOU-VP-1/20	M_2	52.8	38.3

NOTE: MD = mesiodistal; BL = buccolingual.

The paraconid and metaconid cusps are broken on the M_1, but it is clear that each of the four cusps was isolated from the others by the space between the enamel folds. The parastylid is prominent. A shallow cingulum on the lingual margin of the tooth bears a short, broad metastylid. The entostylid is distinct and discontinuous with the occlusal portion of the entoconid, making the distal hypoconid appear to wrap around the entoconid at its base. The parastylid and entostylid diverge slightly so that together with the metastylid and cingulum they appear to form a W shape. The dentin exposure of the paraconid/metaconid and entoconid is linear rather than crescent shaped. Dentin exposures in the protoconid and hypoconid are crescent shaped. There is a pronounced protostylid tucked under the dp_4, but no other buccal stylids or cingula are visible due to its eruption stage.

The M_2 is grossly similar to the M_1, but there are some differences. The crown is higher due to its early wear stage, and this relative hypsodonty imparts a more vertical aspect to the parastylid and median costa. The hypoconid does not wrap around the entoconid, and the weak entostylid is composed entirely of the latter. The hypoconid is asymmetrical and skewed distally, with a small stylid on its posterolingual surface between the pillars, which would likely produce a bifid enamel pattern when worn. Like the M_1, each of the cusps is isolated. Because the paraconid/metaconid cusp is unbroken, the staggered interfingering of central plicae is apparent. A small protostylid is present on each molar, but any cingulum or hypostylid is obscured by alveolar bone. There is no lingual folding of the cusp tips. The M_3 is barely erupted, only exposing its unworn anterior pillar. The lingual stylids and costa appear to be as parallel as they are on the M_2. The enamel is rugose. The crenulations of enamel are more or less vertical, but project from the lingual median costae like flames, diverging slightly occlusally. The condition on the buccal surface is similar, except for the crenulations converging toward the central pillars and flaring toward the occlusal surface. There are many places on the mandible where juvenile, coarsely woven bone is visible, including the condylar process of the mandibular

EBSCOhost - printed on 10/28/2022 4:53 AM via . All use subject to https://www.ebsco.com/terms-of-use

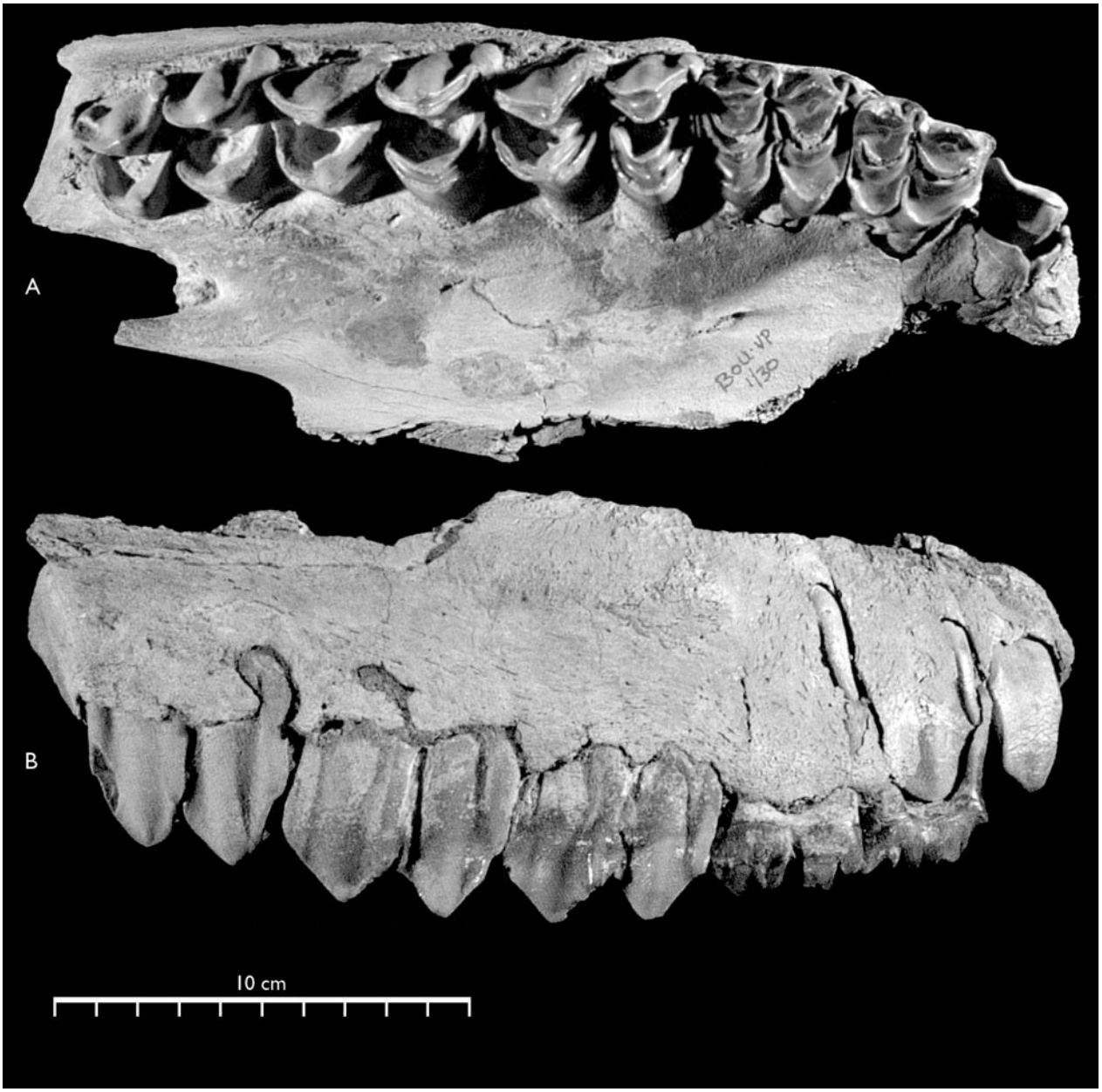

FIGURE 7.5
BOU-VP-1/30 *Sivatherium* right maxilla. A. Occlusal view. B. Buccal view.

ramus and the area approaching the symphysis. The unerupted premolars and incisors bulge under the alveolar bone.

BOU-VP-1/30 (Figure 7.5; Table 7.3) is a partial right maxilla with worn and nearly replaced deciduous premolars (dp^3 and dp^4). On the dp^3 the mesial pillar (protocone and paracone) is substantially broader mesiodistally than the posterior pillar. The base of a prominent hypostyle exposes dentin occlusally to form a somewhat rectangular

174

EBSCOhost - printed on 10/28/2022 4:53 AM via . All use subject to https://www.ebsco.com/terms-of-use

area mesial to the protocone/paracone pillar. A cingulum rises to join the hypostyle base from the mesiolingual surface of the hypocone. The enamel of the protocone and hypocone is compressed to form a mesially oriented plica, and there is a slight cingulum on the mesial hypocone. The bases of these two cusps join into a single, slightly cone-shaped root. The distal pillar is more elongate buccolingually and compressed mesiodistally. The metastyle is mostly absent on the dp^3, but the mesostyle is pronounced even toward the base. The median costa on the metacone is absent, but it is prominent on the parastyle. The dentin exposure is continuous around the margin of the tooth, even barely connecting the protocone and hypocone. Pillars on the dp^4 are more evenly sized than in the dp^3, with the anterior pillar only moderately larger mesiodistally than the posterior. Cingula occur on both the mesial protocone and the distal hypocone. The enamel of the protocone and hypocone does compress centrally on the dp^3, although there is a slight valley formed between them. The metastyle is small and the mesostyle is prominent. There are median costae on both the metacone and paracone; the mesostyle is cone shaped and the parastyle is more columnar. The permanent premolars and molars are not visible. In spite of this, it is clear that the cingula are present on the lingual margin of the M^1 and probably on the M^2. On the M^1, in contrast to the deciduous molars, the mesial pillar is not as mesiodistally broad as the distal. The enamel from the hypocone is entirely separate from the metacone at this early wear stage. That of the protocone barely joins the paracone anteriorly and is otherwise isolated. The anterior half of the protocone is considerably larger than the distal portion and appears as an inverted, lopsided chevron when viewed from an occlusal perspective. The hypocone crescent is less asymmetrical, although the distal half is more rounded and a slight bulge is palpable when the lingual surface of the hypocone is stroked. As with the deciduous teeth, the metastyle is less pronounced than either the mesostyle or the parastyle. The mesostyle has an anterior groove at its occlusal extremity and becomes cone shaped toward the neck. A cingulum is barely visible above the paracone's alveolar margin. The styles and costa of the buccal tooth are more or less parallel. There is less size difference between the anterior and posterior pillars, although the posterior pillar is slightly larger.

The most striking difference between the M^1 and M^2 is in the hypocone. The anterior half of its crescent is straight and runs mesially to just past the level of the mesostyle, coming between it and the posterior portion of the protocone loph. The posterior part of the M^2 hypocone is more rounded than that of the M^1, with a more prominent and palpable bulge that defines a groove on the buccal aspect of the crescent. In this early stage of wear, each of the four cusps is isolated, the metacone and paracone just barely so. A cingulum is barely visible on the anterior protocone just above the alveolar margin. The paracone and metacone of the M^2 are aligned. The M^3 is less erupted than the M^2 or M^1 and entirely unworn. Due to broken alveolar bone, a buccal cingulum is observable. The hypocone's irregular shape, described for the M^1 and M^2, is more pronounced in the M^3 than in the M^1 or M^2, and there is an accessory ridge of enamel that extends from the metastyle, lapping over and joining the hypocone. This feature is also present, but smaller, in the M^2. The rugose crenulations of enamel are more or less vertical, but project from the buccal median costae like flames, diverging slightly occlusally. They converge superiorly lingually.

EBSCOhost - printed on 10/28/2022 4:53 AM via . All use subject to https://www.ebsco.com/terms-of-use

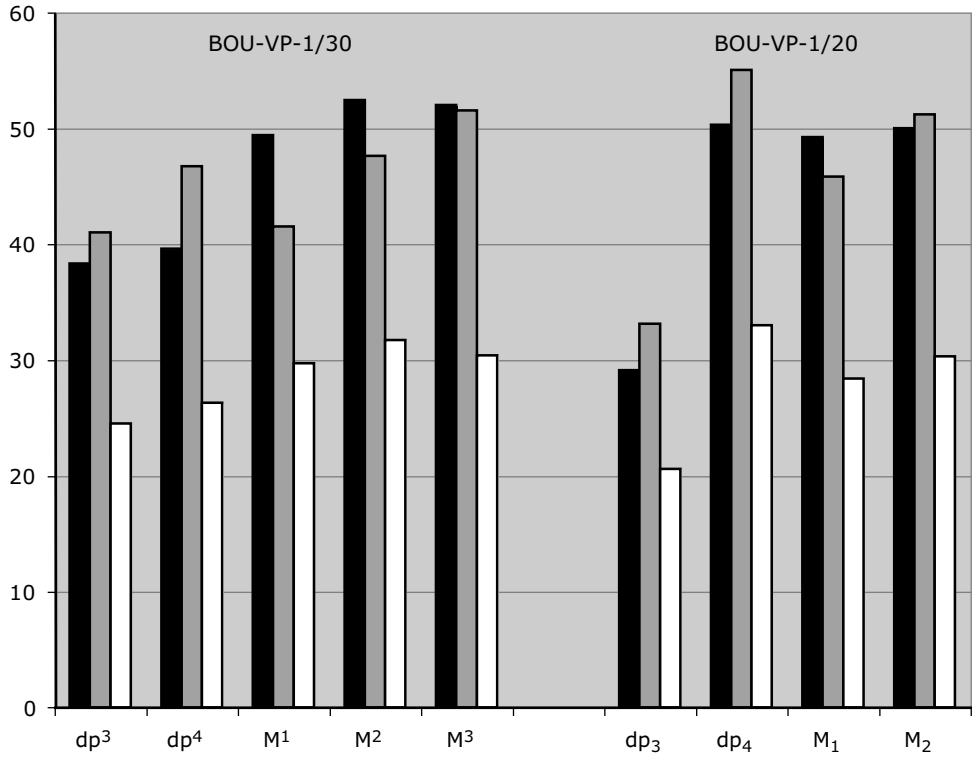

FIGURE 7.6
Daka Member *Sivatherium* (black columns) mesiodistal tooth lengths (BOU-VP-1/20 and BOU-VP-1/30) compared to those of Sivatherinae (gray columns) and *Giraffa* (white columns) reported in Singer and Bone (1960).

The immature bone of the maxilla is coarsely woven and not completely ossified. The maxillary and palatomaxillary sutures are unfused and bone has been resorbed in areas of tooth root formation. Much of the inferior surface of the zygomatic aperture is preserved, as is the nasal aperture. The erupting P^4 protrudes through the alveolar bone. The buccal folding of the occlusal crest of the metacone and paracone, a distinctive feature of sivatheres, is absent in BOU-VP-1/30.

DISCUSSION *Sivatherium* teeth are larger than those of *Giraffa,* and Daka *Sivatherium* dental specimens are assigned to the genus based on dental metrics (see Figure 7.6). Specimens are not identified to species because of the lack of ossicone fossils. Because the mandible and maxilla are both juvenile (different individuals), the relative proportions of cheek tooth row to overall mandible size were not deemed reliable indicators of taxonomy. Juvenile specimens of *Sivatherium* are rare, so the mandible and maxilla specimens are described above in some detail.

The left metatarsal is identified as *Sivatherium* based on its short projected proximodistal length (Figure 7.7). Although the distal end is missing, the overall length can be roughly assessed by the morphology of the shaft, and it would not have been as long as a *Giraffa* metatarsal. The shaft surface is damaged, but the proximal articular surface is well preserved. Measurements for the specimen are in Figure 7.7C. Measurement C1 is 48.9 mm, C2 is 66.2 mm, and C3 is 29.5 mm.

EBSCOhost - printed on 10/28/2022 4:53 AM via . All use subject to https://www.ebsco.com/terms-of-use

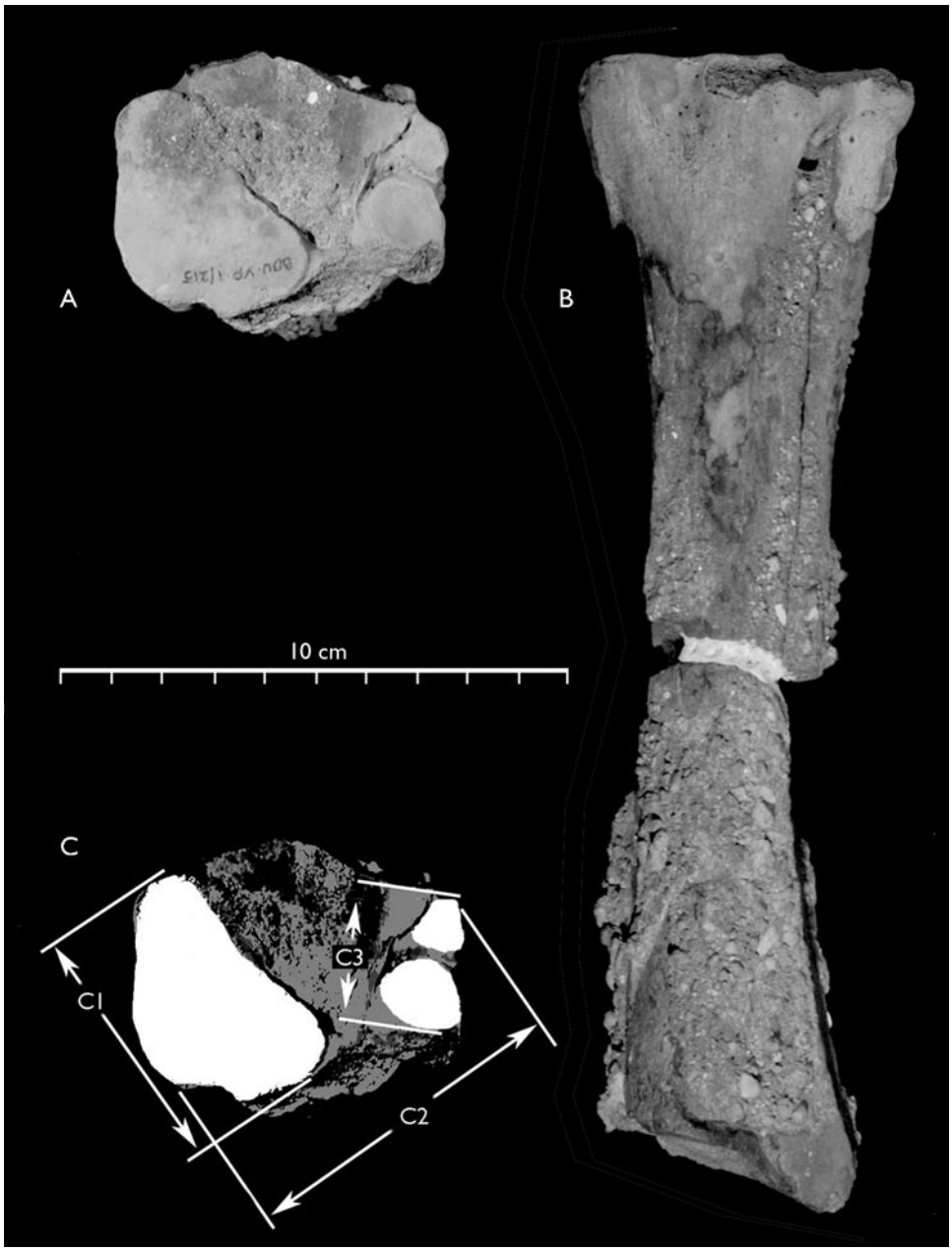

FIGURE 7.7
BOU-VP-1/215 *Sivatherium* left metatarsal. A. Proximal view (anterior is down). B. Anterior view. C. Proximal view (values for C1, C2, and C3 are provided in text). Highly calcified matrix covers much of the shaft in B. This matrix was left in place to prevent damage to the fragile cortex.

Conclusion

The Daka Member contains *Sivatherium* and *Giraffa* fossils, but species assignment is not possible given the relatively small collection. Daka *Sivatherium* dental specimens represent juvenile individuals just prior to eruption of the adult premolars and loss of the third and fourth deciduous premolars. Daka *Giraffa* fossils are of the larger group of Plio-Pleistocene African *Giraffa* species that includes *G. jumae* and *G. camelopardalis*.

EBSCOhost - printed on 10/28/2022 4:53 AM via . All use subject to https://www.ebsco.com/terms-of-use

This Page Left Intentionally Blank

EBSCOhost - printed on 10/28/2022 4:53 AM via . All use subject to https://www.ebsco.com/terms-of-use

8

Hippopotamidae

JEAN-RENAUD BOISSERIE AND W. HENRY GILBERT

The Daka Member has a number of well-preserved hippopotamid fossils (see Figure 8.1). All are assigned here to the genus *Hippopotamus*. The family Hippopotamidae is represented by two living species: *Choeropsis liberiensis* (Liberian hippo), a secretive mammal from western equatorial coasts of Africa; and *Hip. amphibius* (common hippo), known from most sub-Saharan countries, a much larger and better known animal. With only two modern representatives, our knowledge of hippo evolutionary history relies mostly on fossils and morphology. However, molecular methods put hippos at the center of a famous controversy. A substantial diversity of molecular analyses identified Cetacea as a modern sister group of Hippopotamidae, casting serious doubts on the monophyly of the Artiodactyla (see notably Sarich 1985; Irwin and Arnason 1994; Montgelard et al. 1997; Shimamura et al. 1997; Gatesy 1998; Ursing and Arnason 1998; Nikaido et al. 1999; Nomura and Yasue 1999; Amrine-Madsen et al. 2003). Morphologists strongly disagreed with this result, supporting different affinities for Cetacea (Geisler and Luo 1998; O'Leary 1998; O'Leary and Geisler 1999; Geisler 2001). However, recent discoveries of early cetaceans brought conclusive anatomical support to the clade Cetartiodactyla (Artiodactyla + Cetacea) (Gingerich et al. 2001; Thewissen et al. 2001). As a consequence, this debate is now refocusing on infraordinal affinities (Gingerich et al. 2001; Naylor and Adams 2001; Thewissen et al. 2001; Geisler and Uhen 2003). Supporting the previous work of Colbert (1935a, b), Boisserie et al. (2005a, b) indicated recently that hippos probably derived from extinct nonruminant buno-selenodont artiodactyls, the Anthracotheriidae, and that relationships between early cetaceans and anthracotheres should be carefully considered.

Regarding systematics within Hippopotamidae, fossil hippos have been long classified into two genera: *Hexaprotodon* (including the Liberian hippo) and *Hippopotamus*. However, recent authors recognize the paraphyly of *Hexaprotodon,* grouping most African fossil species on plesiomorphic grounds (Stuenes 1989; Harris 1991c; Harrison 1997; Weston 2000, 2003; Boisserie et al. 2003; Boisserie and White 2004). The recent description of several new forms (Gentry 1999; Weston 2000; Boisserie et al. 2003, in press; Boisserie 2004; Boisserie and White 2004) finally led to a revision of hippo phylogeny and taxonomy, focusing on Miocene and Pliocene taxa (Boisserie 2005). Within "traditional" *Hexaprotodon,* several distinct lineages were differentiated at a generic level: *Archaeopotamus* for the narrow-muzzled

EBSCOhost - printed on 10/28/2022 4:53 AM via . All use subject to https://www.ebsco.com/terms-of-use

FIGURE 8.1
An *in situ Hippopotamus* adult mandible from sandy sediments in the Daka Member. Photograph by Tim White, December 1, 2000.

hippos from the late Miocene of eastern Africa and Arabia; *Saotherium* for the early Pliocene Chadian hippos; *Choeropsis* for the modern Liberian hippo; *Hexaprotodon* (abbreviated *Hex*. hereafter) for the mostly Asian lineage. Most of the Plio-Pleistocene hippopotamids of eastern Africa, showing some derived characters similar to those of *Hippopotamus,* are in need of thorough revision. These were provisionally placed under aff. *Hippopotamus*. Finally, *Hippopotamus* was maintained in its most universally accepted meaning.

Hippopotamus

Species of *Hippopotamus* are generally easy to distinguish, particularly based on the morphology of their anterior dentition. The monophyly of *Hippopotamus* has not been recently questioned. However, the accurate number of species and their relationships

EBSCOhost - printed on 10/28/2022 4:53 AM via . All use subject to https://www.ebsco.com/terms-of-use

within the genus are still a matter of debate. Although *Hip. gorgops* is not questioned, its exact range of variation needs to be properly assessed. All or part of the scarce African material attributed to *Hip. kaisensis* Hopwood, 1926 could correspond to various other species (*Hexaprotodon protamphibius*, *Hex. karumensis,* or *Hip. gorgops,* following Gentry 1999) and/or be a synonym of *Hip. amphibius* (see Pavlakis 1990). Some non-African forms are similarly questioned: Mazza (1995) identifies *Hip. incognitus* as a probable synonym of *Hip. amphibius*; the variation range of *Hip. behemoth* is apparently not different from that of *Hip. gorgops* (Martínez-Navarro et al. 2004); *Hip. georgicus* could be, in fact, the most eastern representative of *Hip. antiquus* (Faure 1986); and in general, the status and relationships of most Mediterranean insular hippos remain unclear (for different interpretations, see Faure 1983; Capasso Barbato 1983a, b).

Despite these taxonomic problems and the consequent unresolved phylogeny, the evolutionary history of the genus *Hippopotamus* can be roughly outlined. Its first appearance date (FAD) is uncertain, largely because it depends on very fragmentary remains. Harris et al. (1988a) reported some fossils from the Kataboi member of the Nachukui Formation (West Turkana, Kenya) denoted as *Hip.* cf. *kaisensis*. This member is dated between 4.10 Ma and 3.36 Ma, following Feibel et al. (1989). Faure (1994) attributed to *Hip. kaisensis* some dental and postcranial pieces from the lowest levels of the Nkondo Formation (Western Rift, Uganda), aged about 5.0 Ma. In fact, the genus is well documented in eastern African basins only from 2.5 Ma deposits or younger. It expanded outside Africa around 1.5 Ma, colonizing western Asia and Europe (Mazza 1991; Belmaker et al. 2002). Around or briefly after 1 Ma, it became the only known genus in Africa (*Choeropsis* does not have any fossil record). In Europe, *Hippopotamus* was found as far north as Great Britain and Germany, but, after a series of northern expansions and southern retractions more or less correlated to those of the ice sheets, it finally disappeared after the last interglacial (Mazza 1991, 1995). In the Mediterranean, small insular *Hippopotamus* probably went extinct more or less at the same time (Faure 1983), although *Phanourios minor* is known until the Holocene (Diamond 1992). *Hippopotamus* occurred in western Asia at least until 3,500 B.P. (Horwitz and Tchernov 1990), and withdrew south to the Sahara less than 200 years ago (Manlius 2000).

Hippopotamus Linnaeus, 1758

GENERIC DIAGNOSIS Tetraprotodont, and having the following apomorphies: skull with an elongated muzzle; upper canines with a longitudinal and shallow posterior groove, narrow and covered with enamel; lower canines with strong convergent enamel ridges; deep and widely open notch on the orbital anterior border; limbs short and robust with very large quadri-digitigrade feet. *Hippopotamus* displays many other features that are derived within the family but may be seen in other hippos: antorbital process of the frontal short to absent and a long contact between the maxillary bone and the lacrimal bone; high orbits; short, globular braincase with strong postorbital constriction; mandibular symphysis globular in sagittal section, without incisor alveolar process overhanging frontally; canine processes well developed laterally and frontally; molars high-crowned, compact, and relatively long mesiodistally (after Boisserie 2005).

EBSCOhost - printed on 10/28/2022 4:53 AM via . All use subject to https://www.ebsco.com/terms-of-use

REMARKS It is only recently that major specimens of *Hippopotamus* were collected from the sediments of the Daka Member. To date, the collection includes a perfectly preserved complete cranium, two relatively complete mandibles, 12 other fragmentary craniodental remains (mostly isolated teeth), and a phalanx. Some specimens are still in a preparation phase (notably the mandibles), and further work in the Daka Member will likely see the collection of more specimens.

Hippopotamus cf. *gorgops* Dietrich, 1926

DIAGNOSIS "Large hippopotamus, surpassing the mean for *Hip. amphibius*. Orbits elevated well above the plane of the muzzle with greatly elevated supraoccipital processes bordering a pronounced interorbital depression. Muzzle very elongate and widening anteriorly. Lacrimal tends to disappear from the orbital border and is largely in contact posteriorly with the very enlarged nasal. Auditory foramen low to moderately elevated. Anterior teeth tall and very strongly grooved as in *Hip. amphibius*. Molars tall with simpler tubercles than *Hip. amphibius* and with relatively low cingula. Molars larger than *Hip. amphibius*, particularly the hypoconulid of M_3" (Harris 1991c, 52).

DESCRIPTION In the present study, a modern sample of *Hip. amphibius* was used as a reference for descriptions and comparisons. This sample includes 146 adult individuals housed by the following institutions: Museum für Natuurkunde, Berlin, Germany; Natural History Museum, Berne, Switzerland; Forschunginstitut und Naturmuseum Senkenberg, Frankfurt am Main, Germany; Muséum d'Histoire Naturelle de Fribourg, Switzerland; Muséum d'Histoire Naturelle de la Ville de Genève, Switzerland; Natural History Museum, London, United Kingdom; Musée Guimet d'Histoire Naturelle, Lyon, France; Muséum National d'Histoire Naturelle, Paris, France; Musée Royal d'Afrique Centrale, Tervuren, Belgium.

Cranium The cranium BOU-VP-2/89 (Figure 8.2) was found almost totally buried in a calcrete cemented sandstone matrix, lying on its dorsal side. The posterior part of the basicranium was uncovered, and erosion reduced the occipital condyles to a few fragments and damaged the tympanic bullae. Although some major cracks can be observed, the rest of the cranium shows no distortion and is complete. According to the advanced wear of its M^2 and M^3, this individual was fully mature, even elderly, at death. The cranium is elongate, with a long muzzle that is narrow relative to the massive, wide neurocranium. The premaxillae are relatively small and mediolaterally compressed but protrude strongly anteriorly. They exhibit an anterior interpremaxilla suture and bear two robust incisors. The nasal aperture is rounded in anterior view and largely open dorsally, the nasals showing little anterior extension compared to the premaxillae. The canine processes flare laterally and form short knobs just above the alveoli. The post-canine constriction is particularly long and marked. In lateral view, the nasals are dorsally convex. The dental rows are also curved, being ventrally concave. In ventral view, they are parallel, separated by a relatively narrow flat palate. The palatines extend about 5.0 cm posteriorly to the M^3. Laterally, the facial crests flare strongly from above the contact of M^1 and M^2, posterior and slightly superior to the infraorbital foramen. They show a marked angulation in dorso-ventral view. The lacrimal areas are slightly

EBSCOhost - printed on 10/28/2022 4:53 AM via . All use subject to https://www.ebsco.com/terms-of-use

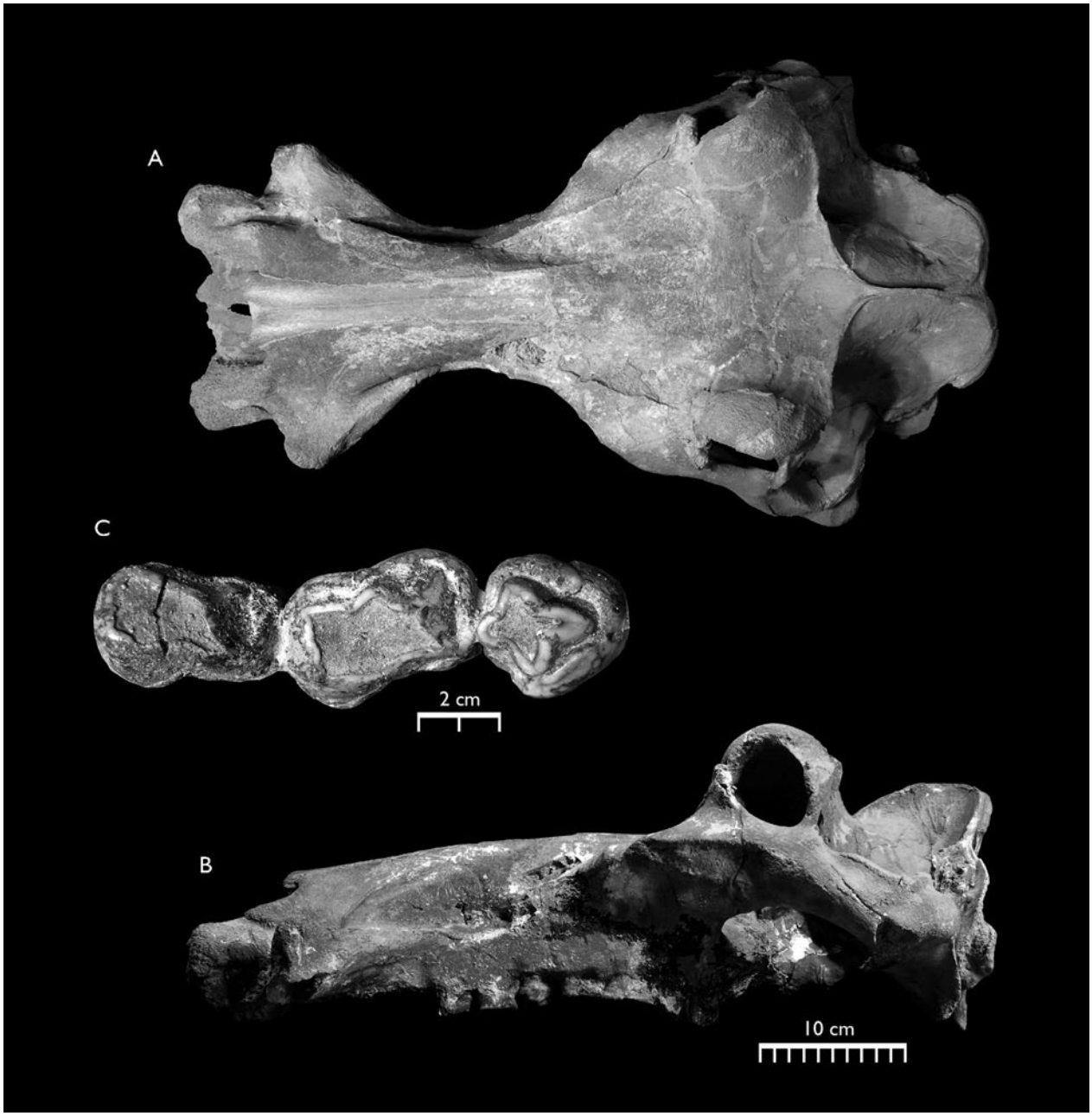

concave and almost horizontal. Due to complete fusion, bone contacts are not visible in these areas. The orbits are particularly high above the braincase, positioned posterior to the M^3. They are dorsoventrally elongate, with a broad, open anterior orbital rim notch. The posterior rim is closed. The supraorbital processes are thick and mostly directed dorsally. The zygomatic arches are robust, positioned high above the dental rows anteriorly, and slope slightly downwards posteriorly. The braincase appears short relative to the muzzle in lateral view. Dorsally, it exhibits a markedly elevated sagittal crest, although the crest is lower

FIGURE 8.2

Hippopotamus cf. *gorgops*. Complete cranium BOU-VP-2/89. A. Dorsal view. B. Left lateral view. C. BOU-VP-2/89, right P^2–P^4, occlusal view. Photograph by Jean-Renaud Boisserie.

EBSCOhost - printed on 10/28/2022 4:53 AM via . All use subject to https://www.ebsco.com/terms-of-use

than the orbits. The braincase itself is moderately inflated. Ventrally, the glenoid processes are wide and marked by knobby lateral extremities. The glenoid fossae are well-developed anteroposteriorly and somewhat reniform in shape (convex anteriorly). The retroglenoid processes are wide and extremely prominent, resulting in an articular surface that is strongly inclined. The tympanic bullae are mostly eroded, but their remnants indicate that they were most probably anteroposteriorly compressed. The tympanic conduit expands laterally and opens at midway up the braincase, below the orbit ventral rims. The narrow basilar part of the basioccipital exhibits two strong and ridged tubercles for muscular insertion. The left paroccipital process (the right is broken) is gracile and anteroposteriorly compressed at its base. Its apex is more ventral than the retroglenoid process. Finally, the occipital plate is wide and relatively flat. The relatively weak supraoccipital tubercle slopes gently laterally; hence, the upper occipital plate outline is more or less rounded.

Upper Dentition The cranium has four incisors. I^1 is larger than I^2, and both teeth are elongated buccolingually. The I^2 is positioned more posteriorly than laterally with respect to I^1. Both exhibit large wear facets truncating the apex, with a marked mesial orientation for I^1. Only the right canine remains. This tooth has a more or less rounded transverse section with a moderate posterior groove and a very extended anterior wear facet.

The first tooth is absent from the premolar row of BOU-VP-2/89 (Figure 8.2), with only a partially closed alveolus visible on the left. The P^2 is a single-cusped elongated tooth, with mesial width significantly larger than distal width. The cingulum is well marked on the lingual and distal sides (Figure 8.2). The P^3 is similar to the P^2, except that it is larger and exhibits a stronger cingulum, attenuated buccally and mesially. The P^4 is also single-cusped. This cusp has four lobes on the right P^4 (Figure 8.2), whereas that of the left P^4 has a simpler shape. Both teeth exhibit a very strong cingulum except on the mesial side.

On the cranium BOU-VP-2/89, M^1 and M^2 are too worn to show cusp morphology, as are P^3–M^1 of maxilla BOU-VP-25/75 (Figure 8.3). On the latter specimen, M^2 is a large subquadrangular tooth that retains a high cingulum, especially on the distal and mesial sides. Styles are present in the transverse valleys and are stronger buccally. Specimen BOU-VP-25/75 shows the wear pattern of M^3 cusps clearly. They appear somewhat more triangular and less trifoliate in shape compared to *Hip. amphibius*. Otherwise, its morphology is similar to that of the M^2. On BOU-VP-2/89 the M^3 differs only by its more pronounced mesiolingual cingulum and by its lack of styles.

Mandible The mandible BOU-VP-1/223 (Figure 8.3) is that of a fully adult individual, as shown by its worn M_3s. It exhibits a symphysis that is particularly massive and robust. It retains four strong procumbent incisors showing little diastemata. The large canines are supported by well-extended canine processes mesially and laterally. In anterior view, the I_2s appear to be inserted higher than the I_1s. The incisor alveolar process is weakly extended anteriorly above large multiple infra-incisive foramina. The dorsal symphyseal plane is large, elongated, and deeply curved transversely between the P_2s. The posterior symphysis is U-shaped in dorsal view and rounded in sagittal section. The horizontal branches are deep and thick. The vertical branches exhibit strong, hook-shaped angular

EBSCOhost - printed on 10/28/2022 4:53 AM via . All use subject to https://www.ebsco.com/terms-of-use

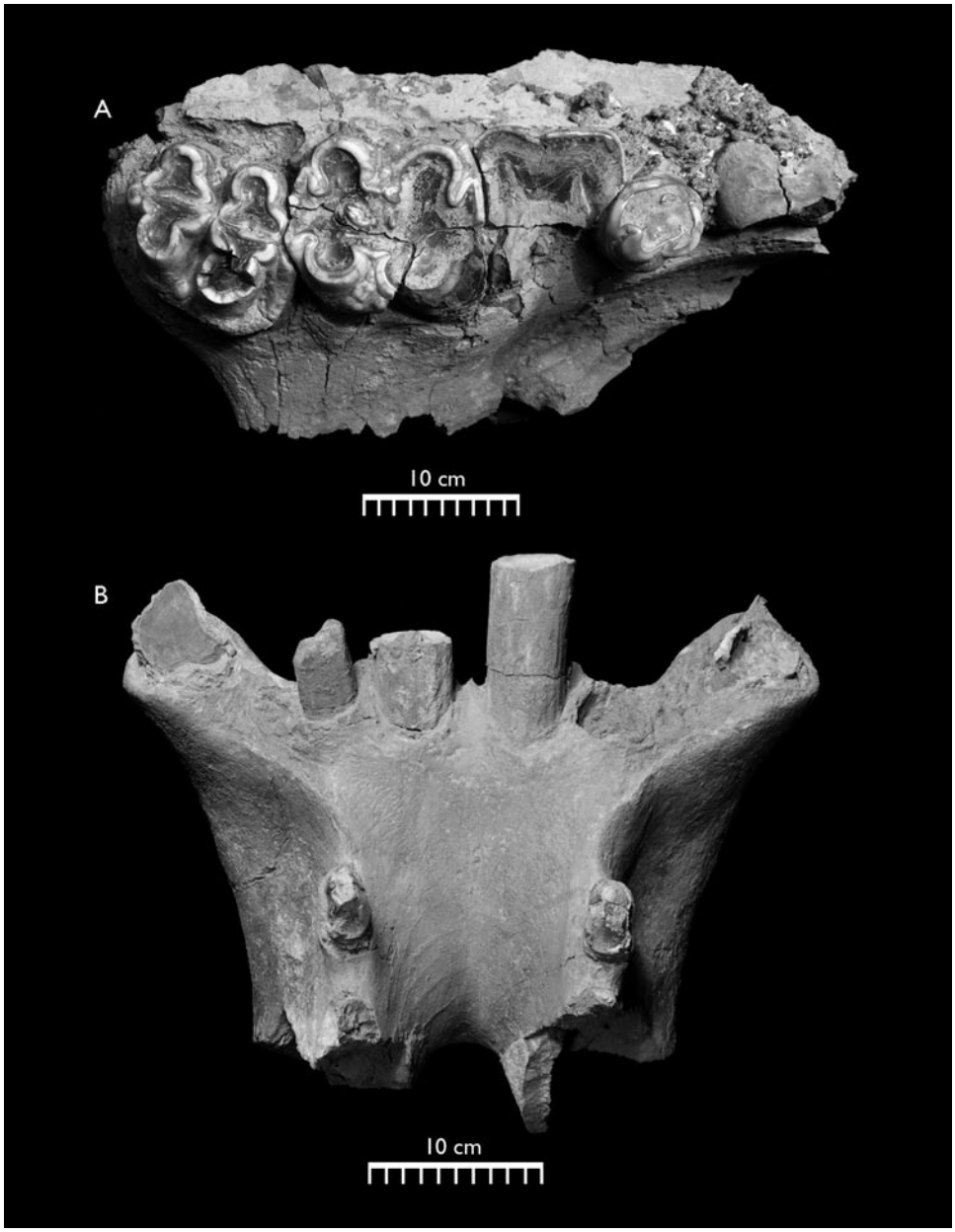

FIGURE 8.3

Hippopotamus cf. *gorgops*. A. Fragmentary maxilla BOU-VP-25/75, with P^4-M^3, occlusal view. B. Mandibular symphysis of mandible BOU-VP-1/223, dorsal view. Photograph by Jean-Renaud Boisserie.

processes that are moderately everted laterally. The coronoid processes are high, strongly crested, and well developed anteroposteriorly.

The second mandible, BOU-VP-1/219, is still partially embedded in its matrix and still needs preparation work. However, one can see that it is much less robust than BOU-VP-1/223, notably in the symphyseal region, although tooth wear clearly indicates that BOU-VP-1/219 was of similar developmental age or older. Tooth dimensions and morphology are similar in both specimens. If these specimens belong to the same species, a hypothesis tentatively favored by the authors, this would probably indicate a very strong

EBSCOhost - printed on 10/28/2022 4:53 AM via . All use subject to https://www.ebsco.com/terms-of-use

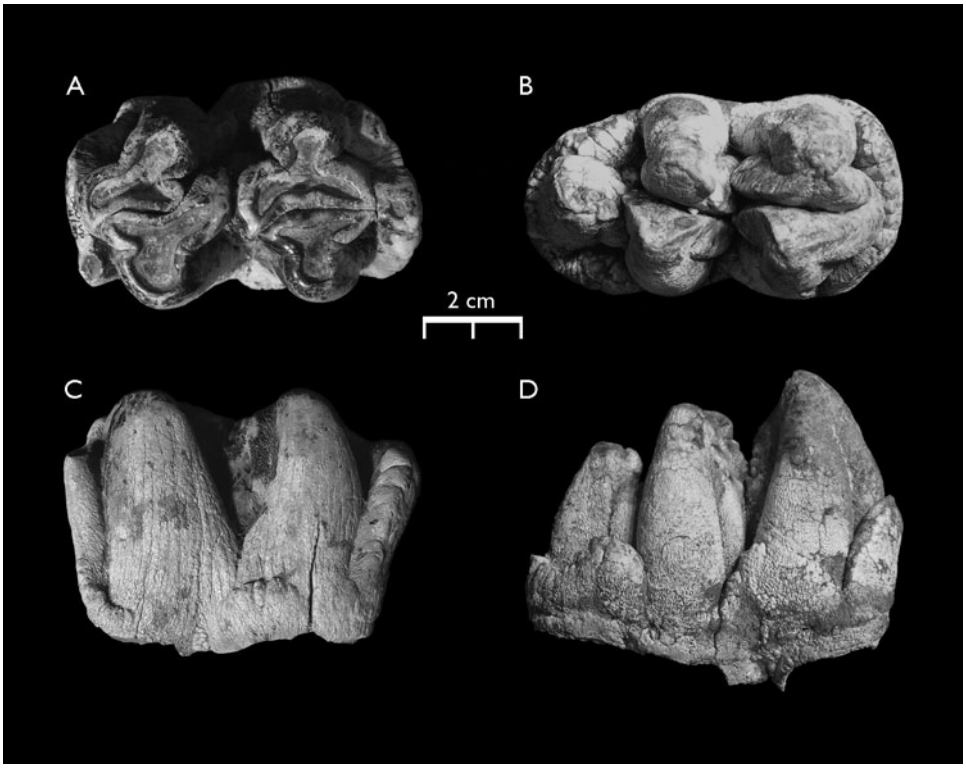

FIGURE 8.4

Hippopotamus cf. *gorgops*. Right M_2 BOU-VP-4/38. A. Lingual view. B. Occlusal view. Left M_3 BOU-VP-19/45. C. Occlusal view. D. Lingual view. Photograph by Jean-Renaud Boisserie.

sexual dimorphism in the Daka hippos. When the preparation and reconstruction of both specimens is achieved, it will be possible to describe their morphology with more detail and test this hypothesis.

Lower Dentition Front teeth are known only for BOU-VP-1/223. They are particularly robust. Notably, I_1 is long and cylindrical, rounded in section at the alveolus and dorsoventrally flattened at their apex. The I_2 is much reduced. The canine enamel is strongly ridged, and some of these ridges are convergent.

First premolars are absent and did not leave any residual alveoli on the mandibles. BOU-VP-1/223 preserved its P_2s. This tooth is moderately elongated, with one simple cusp and a cingulum only present on the mesial and distal sides. It is separated from P_3 by a long diastema. Distal premolars can be observed on the left side of mandible BOU-VP-1/219. However, a supplementary tooth showing abnormal morphology and buccolingual elongation is interposed between P_3 and P_4. The former is a single-cusped tooth similar to the BOU-VP-1/223 P_2 condition. The P_4 appears shorter, with a continuous cingulum that is notably developed lingually. The wear pattern may indicate that this tooth initially bore a lingual accessory cuspid. A small additional accessory cuspid is visible on the distal side.

The morphology of M_1 is not yet known. The M_2, on the other hand, is represented by six relatively complete specimens. It is a large tooth, with a well-marked mesiodistal elongation (Figure 8.4). Cingula are generally well developed and notable in height, occurring on the mesial and distal sides of the tooth. Cingula are absent buccally except on BOU-VP-4/38,

EBSCOhost - printed on 10/28/2022 4:53 AM via . All use subject to https://www.ebsco.com/terms-of-use

which exhibits a reduced buccal cingulum. Ectostylids are present on five of these teeth. Three of them are moderately worn (BOU-VP-4/33, BOU-VP-4/37, BOU-VP-4/38) and show the morphology and relationships of all cuspids. Mesial cuspids exhibit contorted mesial and distal lobes. The mesial lobe of the protoconid is interposed between that of the metaconid and the cingulum, whereas only the distal lobe of the latter is in contact with the mesial lobe of the hypoconid. On all specimens, this cuspid exhibits three well-developed lobes. The entoconid, on the other hand, shows variable development of its mesial and distal lobes. The M_3 (Figure 8.4) has a high and thick cingulum on the mesial side. The cingulum is low and thick distally and absent buccally. Stylids are present in various number and positions, more frequently in the buccal transverse valley and on both sides of the hypoconulid. The protoconid and metaconid show parallel mesial lobes that both touch the cingulum. They exhibit various types of contacts with the distal cuspids. The entoconid varies in shape from a single rounded column to a clearly trilobate cuspid. Two specimens (BOU-VP-19/45, Figure 8.4; and BOU-VP-19/46) are unworn, showing very high crowns. Their respective hypsodonty indices [$h = 100 \times$ (crown height)/(crown maximal width)] are 137 and 122.

Postcrania Regarding the appendicular skeleton, only one phalanx (BOU-VP-25/65) was collected. Its anatomy and maximum length (7.0 cm) indicate it is a proximal phalanx. Being particularly wide and thick (proximal mediolateral width = 5.2 cm; proximal anteroposterior width ≈ 4.0 cm), it belongs to the central digit III or IV. Side and appendage cannot be securely inferred for such an isolated phalanx. The proximal articular surface is large, semicircular, and slightly concave. The distal articular surface, composed of two condyles separated by a barely concave area, is moderately anteroposteriorly compressed (distal anteroposterior width = 2.9 cm) but almost as wide as the proximal one (distal mediolateral width = 4.7 cm).

DISCUSSION The general dimensions and anatomy of these specimens are homogeneous and clearly warrant their attribution to a unique form, except maybe for the mandible BOU-VP-1/219 previously discussed. Features of genus *Hippopotamus* that can be recognized on the specimens include the following: four robust upper incisors; the upper canine rounded in section with a shallow posterior groove associated with an elongated muzzle; high orbits with a deep wide notch on their anterior rim; a flat occipital plate; four enlarged lower incisors separated by small diastemata; and canine processes strongly projected anteriorly and bearing large canines with strong nonparallel ridges. The robustness of the proximal phalanx is also typical of *Hippopotamus*. Outside *Hippopotamus,* only aff. *Hip. karumensis* from Turkana Basin, reported between 2.5 Ma and 1.4 Ma (Harris 1991c), shows such advanced elongated canine processes, high orbits, and a similar overall size. However, this species differs from Daka specimens in retaining the following features: a relatively shorter muzzle; the absence of a deep orbital notch; the retention of only two lower incisors (at least in its more recent occurrences); a particularly wide diastema between its I_1s; and its small canines showing a finely wrinkled enamel with no convergent ridges. Hippopotamid isolated teeth are generally more difficult to differentiate. However, the M_3s from Daka tend to be more hypsodont ($h = 122$ and $h = 137$; see the previous discussion of lower dentition for hypsodonty index formula) than those of aff. *Hip. karumensis* ($98 < h < 123$, average = 108, $n = 7$; data from Harris 1991c). Above all, the molars of the latter have

EBSCOhost - printed on 10/28/2022 4:53 AM via . All use subject to https://www.ebsco.com/terms-of-use

TABLE 8.1 Cheek Tooth Measurement of *Hippopotamus* cf. *gorgops* from the Daka Member Compared to *Hip. gorgops* from Other Localities and Modern *Hip. amphibius*

Tooth	*DAK*	*OLD*	*TUR*	*BUI*	*UB*	*KAI*	*AMP*
P^2n	1	1	1				109
L	37	33	31				32–33
dw	22	24	25–25				21–22
P^3n	1	1	2	1	7	1	130
L	41	37	34–40	38	34–41	27	36–38
dw	28	29	29–30	26	26–34	26	23–25
P^4n	2	1	5		4	1	132
L	30–32	34	32–39		29–33	26	32–33
dw	30–30	40	32–37		23–32	28	32–33
P_2n	1		2		2	3	101
L	41		38–41		33–35	35–38	32–33
dw	24		23–24		19–20	19–22	19–20
M^1n	1	3	7	1	1		139
L		40–52	39–49	55	56		42–43
mw	41	44–51	40–46	44	41		39–40
M^2n	2	4	7	5	3		139
L	50–57	48–61	52–60	56–67	54–68		51–52
mw	53	51–60	52–60	52–60	43–52		48–49
M^3n	2	6	5	6	1	2	127
L	53–60	52–60	56–71	53–63	65	46–46	51–53
mw	53–55	45–57	54–64	50–63	54	39–40	48–50
M_2n	5	3	8	8	1	4	135
L	55–70	57–62	53–64	48–67	54	59–61	54–55
mw	42–48	44–44	35–50	38–48	33	37–39	34–38
M_3n	8	6	8	7	1	2	120
L	70–85	75–85	74–90	70–80	83	73–77	68–70
mw	41–49	39–49	42–50	39–49	47	39–41	39–40

NOTE: Numbers are ranges (min.–max. rounded to millimeters) for the fossil material, confidence intervals ($p = 0.95$) for *Hip. amphibius*. Abbreviations: DAK, *Hip.* cf. *gorgops* from the Daka Member; OLD, *Hip. gorgops* from Olduvai, Tanzania (data from Mazza 1995); TUR, *Hip. gorgops* from Turkana Basin, Kenya (data *pro parte* from Harris 1991c); BUI, *Hip. gorgops* from Buia, Eritrea (data from Martínez-Navarro et al. 2004); UB, *Hip. behemoth* from 'Ubeidiya, Israel (data from Faure 1986); KAI, *Hip. kaisensis,* western Rift (data from Cooke and Coryndon 1970); AMP, *Hip. amphibius*, modern sample from various localities in Africa. L = length, dw = distal width.

cusp(id)s with simpler and shorter lobes, and a lower cingulum is more frequently present on the buccal and lingual sides. Given these features, all isolated dental remains from Daka were also attributed to *Hippopotamus*.

Three species of *Hippopotamus* are documented in the Plio-Pleistocene of Africa. The oldest is *Hip. kaisensis,* defined on fragmentary remains found in the Kaiso Formation, Uganda. The occurrence of this species elsewhere seems unsubstantiated, and its validity is debated (Pavlakis 1990). According to Cooke and Coryndon (1970), who provided an amended diagnosis, descriptions, and measurements of the material from Kaiso, this species differs from the Daka hippopotamid by the following: a smaller size (Tables 8.1 and 8.2); a relatively narrower mandibular symphysis (Table 8.2); the retention of P_1; the small

EBSCOhost - printed on 10/28/2022 4:53 AM via . All use subject to https://www.ebsco.com/terms-of-use

TABLE 8.2 Cranium (Cr) and Mandible (Md) Measurement Ranges of *Hippopotamus* cf. *gorgops* from the Daka Member Compared to Various Hippopotamids

Specimen	*Cr1 (1)*	*Cr2 (2)*	*100 × (1)/(2)*	*Cr3*	*Md1 (3)*	*Md2 (4)*	*100 × (3)/(4)*	*Md3*
Hip. cf. *gorgops* (Daka)	355	239	148.7	448	198	309	64	111
Hip. gorgops (Olduvai)	(390)–(400)	(294)	(133)	432–486				
Hip. gorgops (Turkana)	423	341	123.9	457	(180)	(390)	(46)	
Hip. kaisensis (Kaiso)					(150)–171	(204)–240	(74)–71.3	78–103
Hip. amphibius ($p = 0.95$)	297–308	250–263	116.2–120.5	446–460	162–169	286–296	56.3–58.0	92–99

NOTE: Numbers are ranges (min.–max. in millimeters) for the fossil material, confidence intervals ($p = 0.95$) for *Hip. amphibius*. Abbreviations: Cr1, length between anterior extremity of intermaxilla suture and posterior extremity interpalatine suture; Cr2, width between upper canine alveoli; Cr3, maximal width between lateral extremities of glenoid processes; Md1, sagittal length of symphysis; Md2, width between canine process tips; Md3, height of symphysis. Olduvai specimen data are from Mazza (1995); Kaiso specimens are from Cooke and Coryndon (1970). Measurements in parentheses are estimated.

diastema between P_2 and P_3; a bicuspid P_4; simpler wear pattern of molars; cingulum less attenuated on lateral sides of the teeth. As Pavlakis (1990) also notes, we observed variations for all the aforementioned dental characters in a studied sample of living *Hip. amphibius*. These characters are therefore not conclusive for differentiating species of *Hippopotamus*, except in terms of relative frequencies when large samples are involved. This is not the case for the Daka hippopotamid. However, the observed differences in size and mandibular proportions justify a distinction between the latter and *Hip. kaisensis*.

Gèze (1980) and Harris et al. (1988a) report the occurrence of *Hip. amphibius* in the Turkana Basin at the top of the Shungura Formation (Member L) and the Nachukui Formation (Nariokotome Member), sediments roughly contemporaneous with the Daka Member. The Daka material, however, differs from the living species in several respects. The relative elevation of its orbits and sagittal crest exceed the most frequent pattern seen in *Hip. amphibius*. Most of its dental and cranial dimensions are beyond the confidence intervals of the living hippo (Tables 8.1 and 8.2). In proportion, its muzzle is also more elongated, and its mandibular symphysis is longer (Table 8.2). Finally, the wear pattern of its molars is generally simpler.

Most of these Daka features are found in *Hippopotamus gorgops*, the most frequent early to middle Pleistocene hippo in Africa. The association of extreme orbit elevation and muzzle elongation with relatively simple molar wear pattern is diagnostic of this species (Harris 1991c). The dental dimensions of Daka material (Table 8.1) correspond well to that of *Hip. gorgops* from Olduvai (Mazza 1995), Turkana (Harris 1991c), and Buia (Martínez-Navarro et al. 2004). It must be noted that they also fit those of *Hip. behemoth* from 'Ubeidiya in Israel. In agreement with Martínez-Navarro et al. (2004), we are inclined to see a possible synonym of *Hip. gorgops* in this Levantine species, although this will require further comparisons of postcranial materials to be confirmed. On the other hand, the cranial dimensions of

EBSCOhost - printed on 10/28/2022 4:53 AM via . All use subject to https://www.ebsco.com/terms-of-use

the Daka material seem intermediate between *Hip. gorgops* and *Hip. amphibius* (Table 8.2). Moreover, the muzzle and mandibular symphyses from Daka appear more elongated, with less expansion of the canine processes (Table 8.2). This could be related to normal variation within *Hip. gorgops*, but the variation range of this species is as yet undefined. A review of the existing material, notably a comparison with Olduvai and Turkana specimens, would allow a better assessment of this variation range. Awaiting such work, we prefer to remain cautious and to provisionally attribute the Daka material to *Hip.* cf. *gorgops*.

Conclusion

This chapter constitutes a preliminary account of the hippopotamids from the Daka Member. The collected material, not entirely prepared yet, belongs to the genus *Hippopotamus* and can most probably be assigned to a unique form. Compared to the living *Hip. amphibius*, the advanced features of the skull and the more primitive aspects of the teeth from Daka specimens are similar to *Hip. gorgops*. However, the anterior parts of the skull show proportions narrower than in *Hip. gorgops*. For this reason, the hippo from Daka is provisionally designated *Hip.* cf. *gorgops*.

Daka *Hippopotamus* fossils can potentially bring a lot to the study of African Pleistocene *Hippopotamus*. Fossils from the unit are the best preserved for this genus in the Afar basin and, moreover, are contemporary with a major event in hippo evolutionary history. At approximately 1.0 Ma *Hippopotamus* became the dominant hippopotamid group in Africa, while other lineages went extinct. Although our knowledge of the timing, paleobiogeography, and paleoecology underlying this "hippo turnover" event is limited, it should benefit greatly from new material such as that from the Daka Member. Currently, in contrast with the Mio-Pliocene hippopotamids, no comprehensive study has considered the systematics and phylogeny of the African Pleistocene *Hippopotamus*. In this context, a full understanding of the Daka hippos requires a more general review of related material, notably from Kenya, Tanzania, and South Africa. A full review and analysis of the genus *Hippopotamus* is beyond the scope of this chapter, which is aimed at description and identification of the material from the Daka Member.

Further progress in the study of these remains will provide more accurate identification and affinities and should also deliver some important data on Daka paleoenvironments. Indeed, hippos are a major component of African wetlands, as illustrated by the gregarious *Hip. amphibius*, which may exceed 3,000 kg (Kingdon 1997). This mammal is predominantly a grazer, favoring short fresh grass near water (ponds, swamps, rivers, or lakes), where it usually spends daytimes. Many studies describe the strong impact of this animal on hydrographical network morphology, on vegetation composition, and on water mineral and organic contents, all directly influencing living conditions of ichthyofaunas and surrounding populations of large herbivores (Verheyen 1954; Laws 1968; Lock 1972; Mackie 1976; Kingdon 1979; Ogen-Odoi and Dilworth 1987; Eltringham 1993, 1999; Wolanski and Gereta 1999; Deocampo 2002; Grey and Harper 2002). The fact that the hippopotamid from Daka was even larger than *Hip. amphibius* gives an indication of the ecological pressure that this hippo may have exerted on Afar wetlands 1.0 Ma ago.

EBSCOhost - printed on 10/28/2022 4:53 AM via . All use subject to https://www.ebsco.com/terms-of-use

Finally, some hippo remains were found in association with stone tools in the Daka Member, as well as in the more recent Herto Member of the Bouri Formation (de Heinzelin et al. 2000a). In fact, such an association occurs at many early and middle Pleistocene archeological sites in Africa (e.g., at Olduvai, in the Turkana Basin, at Buia; and also in the Mediterranean). Whatever the exact modalities of this recurring association are, it suggests that hippo paleobiology is somehow correlated with the ecology and behavior of early *Homo*. This prospect reinforces the need for a thorough review of Pleistocene *Hippopotamus,* in which Daka specimens should play an important role.

EBSCOhost - printed on 10/28/2022 4:53 AM via . All use subject to https://www.ebsco.com/terms-of-use

This Page Left Intentionally Blank

EBSCOhost - printed on 10/28/2022 4:53 AM via . All use subject to https://www.ebsco.com/terms-of-use

9

Elephantidae

HARUO SAEGUSA
AND
W. HENRY GILBERT

The Daka Member is very rich in elephant fossils (see Figures 9.1 and 9.2). Two crania of *Elephas recki recki* were excavated from the Daka Member during the 1999 and 2002 field seasons. As the cranium from Haïdal, Djibouti Republic, is currently unavailable for study, the two Daka Member crania are the only specimens that can provide us with a rare chance to study details of the cranial anatomy of advanced *E. recki*. These finds allow revision of ideas concerning the dispersal of palaeoloxodonts from Africa to Eurasia, as well as the taxonomy and spatiotemporal distribution of the Eurasian palaeoloxodont species.

Elephas (Palaeoloxodon) recki is one of the most common faunal elements of the Plio-Pleistocene of eastern Africa. Several evolutionary stages have been recognized in this species (Maglio 1973; Coppens et al. 1978; Beden 1980, 1983, 1987; Todd and Roth 1996). These are distinguished by five evolutionary stages of *E. recki*, to which the following subspecific names were given: *E. r. brumpti*, *E. r. shungurensis*, *E. r. atavus*, *E. r. ileretensis*, *E. r. recki*. These five subspecies have been accepted widely as valid taxonomic units and are frequently employed in discussions of biostratigraphy for Plio-Pleistocene hominid-bearing beds in eastern Africa. However, the validity of these subspecies has been questioned recently by several authors based on evaluations of the variability of dental traits (Ferretti et al. 2003; Todd 2005).

Beyond being important in paleontological and paleoanthropological studies in eastern Africa, *Elephas (Palaeoloxodon) recki* is important as a candidate for ancestry in Eurasian *Palaeoloxodon*. Aguirre (1969a, b, c) first proposed *E. (P.) recki* as the ancestor of Eurasian palaeoloxodont species, and this idea has been accepted by most authors. However, there is no consensus on the timing of the emigration of palaeoloxodont species from Africa. Maglio (1973: 83) argued that *E. namadicus* may have been derived from a form close to *E. ekorensis* or an early evolutionary stage of *E. (P.) recki*. On the one hand, Beden (1983, 1987) argued that subspecies *E. r. atavus* gave rise to the Eurasian species of subgenus *Palaeoloxodon*. On the other hand, some still maintain the classic view that Eurasian palaeoloxodonts were derived from the Indian species *E. planifrons*. This divergence of opinion is due to the lack of *E. recki* crania from eastern Africa and the subsequent inability to confirm characteristic features of the Eurasian species of subgenus *Palaeoloxodon*. Thus, the finding and analysis of new cranial remains is important. However, fossil crania

EBSCOhost - printed on 10/28/2022 4:53 AM via . All use subject to https://www.ebsco.com/terms-of-use

FIGURE 9.1
A. *Elephas (Palaeoloxodon) recki recki* specimen eroding from Daka Member sediments. Photograph by Tim White, December 29, 1992. B. Five years later, the same specimen has slightly deteriorated, but the armor lag has prevented much more actual erosion around the specimen. Photograph by Tim White, December 28, 1997.

of elephants are extremely rare because of the poor preservation potential of their highly pneumatic internal structure. According to Beden (1983, 1987), well-preserved crania of adult *Elephas recki* individuals are known only in two of his five subspecies, *E. r. brumpti* and *E. r. atavus*. Juvenile crania are known in *E. r. shungurensis* and *E. r. ileretensis*, but several important derived characters are undeveloped in juveniles, so they cannot provide us with a clear phylogenetic signal. On the other hand, a nearly complete skeleton of *E. r. recki* has been found in articulation at the Paleolithic site of Haïdal, Djibouti Republic (Chavaillon et al. 1990), but there is no description of this fine skeleton except for very cursory remarks on its molars.

As previously mentioned, the validity of Beden's (1980) five subspecies has been questioned recently by several authors (Ferretti et al. 2003; Todd 2005). These studies suggest that several species, and possibly even genera, may be included in Beden's *Elephas recki* samples. Generally speaking, Eurasian palaeoloxodonts are better known than African, and among Eurasian taxa, *E. (P.) naumanni*, the type species of the subgenus is one of the best-known fossil elephants of Eurasia, as discussed in the section "Notes on *Elephas (Palaeoloxodon) naumanni*" later in this chapter. Thus, study of the phylogenetic relationships of Eurasian palaeoloxodont species will ultimately contribute to solutions of Palaeoloxodon systematic problems involving African taxa.

EBSCOhost - printed on 10/28/2022 4:53 AM via . All use subject to https://www.ebsco.com/terms-of-use

FIGURE 9.2
Excavation of the BOU-VP-25/50 *Elephas (Palaeoloxodon) recki recki* specimen found adjacent to the main water trail between the Awash River to the left (east) and Bouri Village to the right (west). Haruo Saegusa photographs the specimen while Gen Suwa, Awoke Amzay, and Michael Black look on. Photograph by Tim White, December 1, 1999.

Terminology

Many anatomical terms used for mammals are difficult to apply directly to the highly derived cranial remains of elephants. In the following paragraphs we present terms used by Maglio and Ricca (1978), Inuzuka (1977a, b), Beden (1983, 1987), and Saegusa (1993) to define their usage in the subsequent descriptions in this chapter.

Frontoparietal Surface/Region/Plane

The term *sinciput* used by Inuzuka (1977a, b) and Saegusa (1993) corresponds to the terms *cranial vault* and *vertex* used by Beden (1983, 1987). In Elephantoidea (*sensu* Tassy 1988), the area between the nuchal crest and the dorsal margin of the external nares forms a flat surface composed of nasal, frontal, and parietal bones. In adults, the suture between

EBSCOhost - printed on 10/28/2022 4:53 AM via . All use subject to https://www.ebsco.com/terms-of-use

these three bones is diminished so that it is almost impossible to divide the surface along the border between them. Inuzuka (1977a, b) and Saegusa (1993) refer to this surface as sinciput for its relative position in the skull, but Beden (1983: 87) called it a cranial vault and/or vertex, because it is composed of parietal and frontal, which form the cranial vault in other mammals, for instance *Homo*. Hooijer (1955), Maglio (1970, 1973), and Maglio and Ricca (1978) called the same surface the frontoparietal surface, and their usage of the term is followed in this work.

Frontoparietal Crest

The section of the temporal line between the zygomatic process of the frontal and the isthmus frontalis forms a crest, which is called the frontoparietal crest by Maglio (1973). It corresponds to the postorbital crest of Saegusa (1987).

Parietofrontal Crest

This is a headband-like elevation on the upper part of the frontoparietal surface typically seen in *E. (P.) namadicus*. Osborn (1942) and Inuzuka (1977a, b) called this structure a parietofrontal crest, and we employ this name here. This elevation has been variously called the following: supraorbital ridge (Pilgrim 1905), occipitofrontal rugosity (Osborn 1942), frontal torus (Aguirre 1969a, b, c), and frontal crest (Maglio 1973). What is described as the parietal crest in KNM-ER 5711 (Beden 1983) is, however, not homologous with the parietofrontal crest (see the next term).

Parietooccipital Boss

In species of the genus *Elephas*, large swellings are formed on the right and left sides of the occipital and parietal. Inuzuka (1977a, b) called these parietal crests, while Beden (1983) calls them parietooccipital bosses (e.g., Beden 1983: 80, 88, 100). Here the swellings are referred to as the parietooccipital bosses, following Beden (1983: 87).

Post-temporal Crest

A ridge running vertically at the lateral margin of nuchal plane is called the post-temporal crest, following Inuzuka (1977a, b). As has been argued by Beden (1983), strong expansion of the occiput characterizes the genus *Elephas*, but the post-temporal crest distinguishes the subgenus *Palaeoloxodon* from the other members of the genus, giving a rectangular appearance to the upper half of the skull in lateral view.

Premaxillary Fossa

This dorsoventrally elongated fossa is located on the anterior surface of the premaxilla between the right and left jugal alveolaria, and it is called the premaxillary fossa by Maglio and Ricca (1978). It is called the incisive fossa (fossa incisive) by Beden (1983),

EBSCOhost - printed on 10/28/2022 4:53 AM via . All use subject to https://www.ebsco.com/terms-of-use

but the same name is used for other anatomical features found on the hard palate in humans. Inuzuka (1977a) called this depression the intermaxilla median fossa, but the term is not appropriate because the depression is not on the maxilla but rather on the premaxilla.

Nuchal Fossa

A deep depression located at the center of the occiput is referred to as the nuchal fossa here (see Figure 9.6). The nuchal fossa, harboring the nuchal ligament, has an extremely rough surface inferiorly.

Nuchal Plane (Planum Nuchale)

Some authors call this plane the occipital plane or planum occipitale. However, such usage of the term is not appropriate. In most mammals, the superior nuchal line runs along the suture between the occipital and parietal bones. Therefore, they do not have a plane that corresponds to the planum occipitale of human anatomy. The same is true in proboscideans except *Stegodon orientalis*. In this species, the superior nuchal line runs at the midheight of the vertically expanded occiput, and the boundary between occipital and parietal corresponds to the occipital plane or planum occipitale (Saegusa 1993).

Isthmus Frontalis

This is the narrowest part of the parietofrontal surface, where left and right temporal lines come closest to each other. It is referred to as the temporal contraction by Hooijer (1955) and Maglio (1970, 1973).

Methods

Metric procedures applied to proboscidean skulls proposed by previous authors can be classified into two categories. One is to measure distances between landmarks on the skull. The other is to measure the distance or angle between a landmark or surface and a standard plane, often the occlusal plane. The methods proposed by Dubrovo (1960) and revised by Inuzuka (1977a, b) are examples of the latter method. However, specimen incompleteness or damage renders such methods impossible. Additionally, when the occlusal plane is used, measurement is strongly constrained by the wear stage of the molar. Further, these methods are potentially damaging to fragile fossils because the molars must support the invariably heavy cranium when they are applied. In contrast, the metric procedures employed by Beden (1983, 1987) are of the first type and can be applied safely to fossils in various states of preservation. Beyond this, Beden's metric methods are widely employed by various authors, so that comparable data can be readily extracted from the literature. For this reason we employ the metric procedures proposed by Beden. In addition to Beden's methods, we also employ those used by Adam (1986) because they effectively measure some characteristics of the cranium of Eurasian subgenus *Palaeoloxodon* species.

EBSCOhost - printed on 10/28/2022 4:53 AM via . All use subject to https://www.ebsco.com/terms-of-use

Elephas

Palaeoloxodon is here considered a subgenus of *Elephas*, following the conception of Beden (1979, 1980, 1983, 1987). A pair of left and right occipital bosses is present in primitive *Elephas* (Beden 1983, 1987), and this feature can be considered a synapomorphy shared with all of the species of the genus including those allocated to subgenus *Palaeoloxodon*. This and several other cranial features are shared exclusively by species of *Elephas* (Beden 1983, 1987), providing firm morphological justification for its monophyly. The conclusion of Beden (1983, 1987) on the taxonomic status of palaeoloxodont species thus maintains its validity. In previous work, *E. (P.) namadicus* has been referred to as the type species of the subgenus. According to recent studies, however, *E. (P.) naumanni* is the type species of the subgenus (see the later section "Notes on *Elephas (Palaeoloxodon) naumanni*").

Elephas (Palaeoloxodon) recki (Dietrich, 1916)

DIAGNOSIS Very hypsodont *Elephas,* with individuals regularly showing hypsodonty indices higher than 190; enamel thin and strongly folded; enamel folding becoming stronger and more irregular at mid-height, then more regular near the base of the loph(id); lozenge-shaped median expansion (pseudo-loxodont wear pattern) developed weakly on the enamel figure of the lower molars; premaxilla flares strongly; zygomatic arch relatively short; frontoparietal crest long; orbit located at high position on cranium.

DESCRIPTION

Cranium (Figures 9.3 and 9.4, Table 9.2) Cranial materials of *E. (P.) recki* excavated from the Daka Member include BOU-VP-3/131, BOU-VP-25/50, and BOU-VP-4/144. None of these is complete, and they differ in their preserved portions. The developmental age also differs from specimen to specimen.

Cranium BOU-VP-3/131 is one of the largest crania of *Elephas* known. The specimen was found facing downward. Because of the lack of hard concretion protecting the skull from erosion, the posterior portion of the skull is lost and only the facial part is preserved. The left and right tusk sockets were filled with matrix, indicating that the tusks were lost before burial. A nearly complete mandible was found about 4 m from the skull, and it likely belongs to the same individual as the cranium. Except for the mandible, no element that might belong to the same individual as the cranium was found in the surrounding area, though the horizon that produced them is widely exposed. The fossil was removed from a sandy siltstone. The sediment just beneath the skull contains a number of freshwater bivalves, which form a thick concretion. Some handaxes were found in the same layer, but no particular association with the skull is recognized. From this specimen the morphology of the frontoparietal surface, nasal, external nares, anterior rim of orbit including lacrimal process, tusk socket, and premaxillary fossa can be discerned.

In contrast to BOU-VP-3/131, BOU-VP-25/50 was found facing upward. Because of the deep erosion of the bed, most of the superior part of the skull was already exposed high above the ground. The face of BOU-VP-25/50 is missing, with the exception of the central third of the frontoparietal surface. The left and right lateral surfaces of the occiput are also lost. Right

EBSCOhost - printed on 10/28/2022 4:53 AM via . All use subject to https://www.ebsco.com/terms-of-use

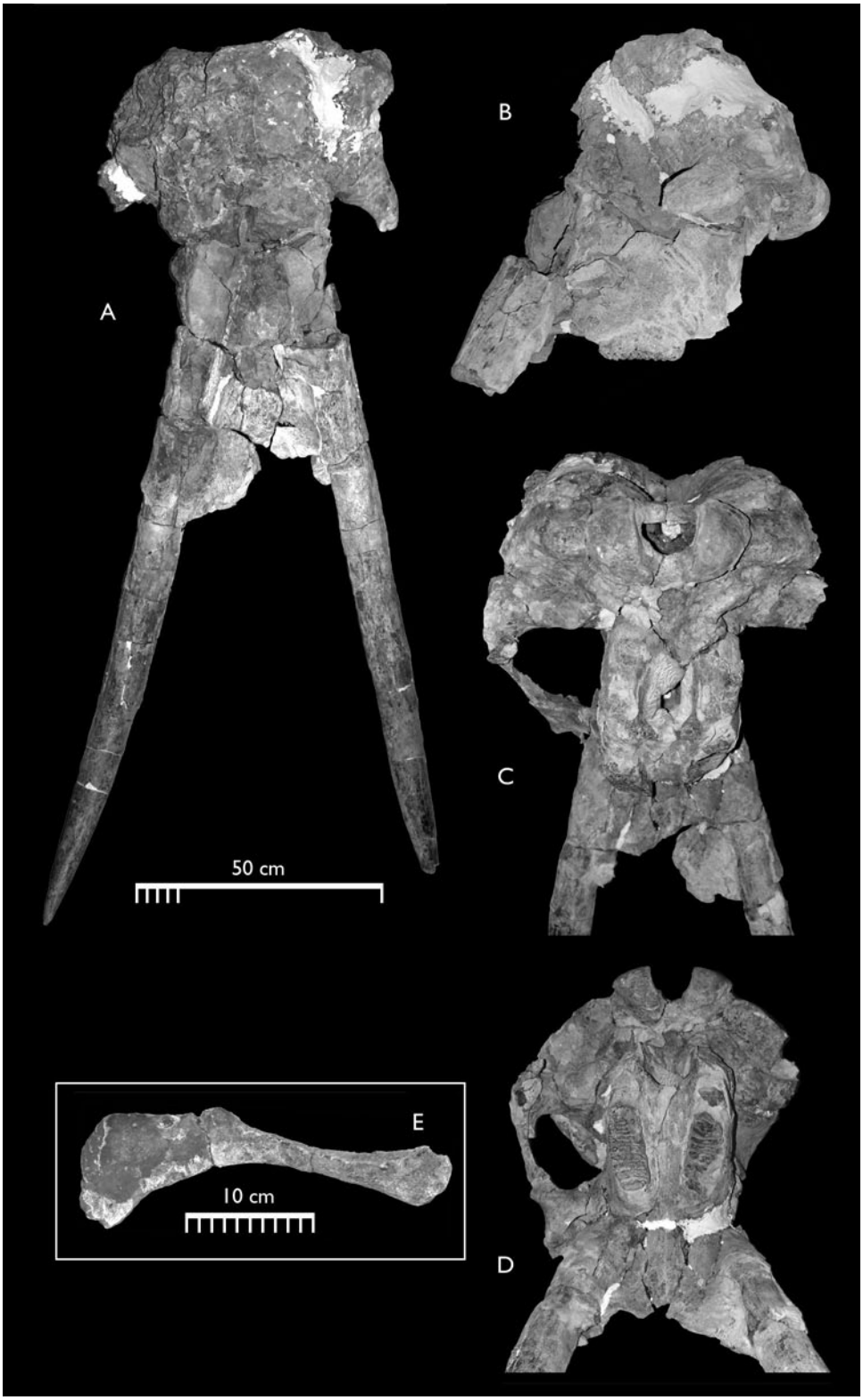

FIGURE 9.3

Elephas (Palaeoloxodon) recki recki cranium BOU-VP-25/50. A. Anterodorsal view. B. Left lateral view. C. Basicranial region. D. Occlusal view. E. Right jugal. Photographs by Haruo Saegusa.

EBSCOhost - printed on 10/28/2022 4:53 AM via . All use subject to https://www.ebsco.com/terms-of-use

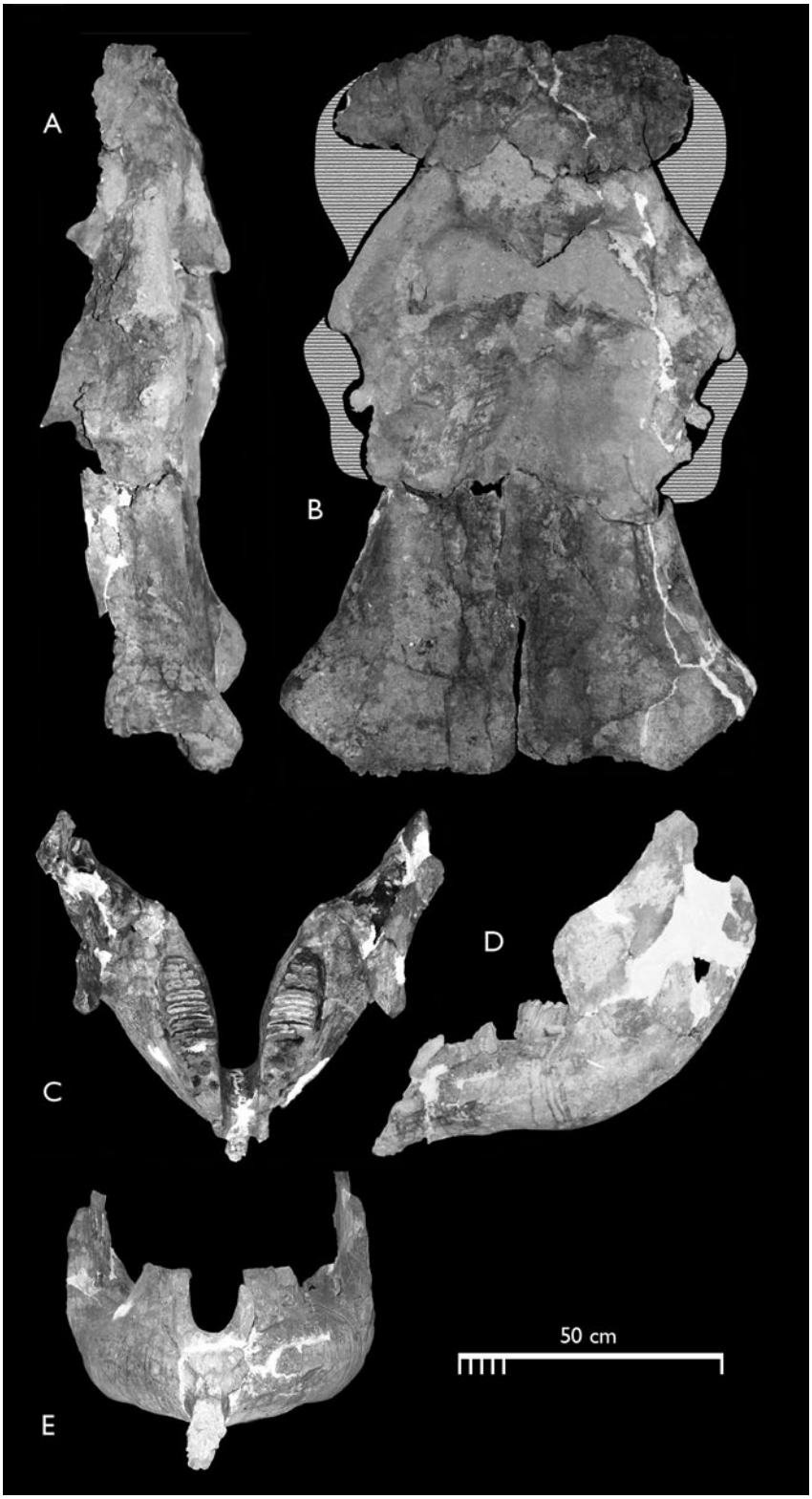

FIGURE 9.4

Elephas (Palaeoloxodon) recki recki cranium and mandible BOU-VP-3/131. Cranium: A. Right lateral view. B. Anterodorsal view. Mandible: C. Occlusal view. D. Left lateral view. E. Anterior view. Photographs by Haruo Saegusa.

EBSCOhost - printed on 10/28/2022 4:53 AM via . All use subject to https://www.ebsco.com/terms-of-use

TABLE 9.1 Mandibular Metrics of Daka Elephants.

Measurement	*BOU VP-3/131*
A	561+ (570 est.)
B	474– (460 est.)
C	
D	
E	493
F	490
G	117
H (Rt)	181
H (Lt)	179
J	65
K (Rt)	80
K (Lt)	
L	192
M	34
N	
Lateral Surface	
A (Rt)	
A (Lt)	246
B	166
C	260 est.
D (Rt)	30
D (Lt)	
E (Rt)	205
E (Lt)	
F (Rt)	168
F (Lt)	167
G (Rt)	
G (Lt)	450+ (500 est.)

NOTE: For measurement points see Beden (1983). A plus sign indicates that the actual specimen measurement is above the reported metric, and a minus sign indicates it is lower. "Est." denotes an estimation.

and left tusks were found in their original anatomical positions in the tusk sockets, and some portions of the tusks outside the sockets are well preserved. The dorsal half of the premaxilla and the basal tusks are mostly missing. Apart from these, the skull of BOU-VP-25/50 is well preserved, including the upper molars, elements lost in BOU-VP-3/131. The basicranium is also preserved very well. Though found detached from the rest of the cranium, both right and left zygomatic arches are completely preserved. The skull seems to have been undamaged before the burial. However, no mandibular or postcranial elements of the individual were found around the skull. Many bivalve and gastropod shells are found in the matrix surrounding the skull.

BOU-VP-4/144 is far more poorly preserved than the other two specimens. It is a fragmentary skull that consists of the anterior half of the maxilla and the posterior half of

EBSCOhost - printed on 10/28/2022 4:53 AM via . All use subject to https://www.ebsco.com/terms-of-use

TABLE 9.2 Mandibular Metrics of Daka Elephants, compared to *Elephas namidicus* (BNHM M3092, BNHM M3093), *Elephas antiquus* (SMNS Nr. 32888), and *Elephas recki atavus* (KNM-ER 5711)

	BOU-VP-3/131	*BOU-VP-25/50*	*BMNH M3092*	*BMNH M3093*	*SMNS Nr. 32888*	*KNM-ER 5711*
Measurement	ORIGINAL	ORIGINAL	ORIGINAL	ORIGINAL	ORIGINAL	BEDEN (1983)
La	1350	846		693+	1235	1350
Lb	429	272+	118+	184+	413	325
Lc (Rt)	326		197		328	260
Lc (Lt)	342		120	152+	352	260
Ld (Rt)	156		131	93	112	210
Ld (Lt)	181		107	94	103	210
Le	874	508 est.		388	772	770
Lf		830				1170
Lg		187		214+	302	265
Lh		297				380
Lj		176				180
Lk (Rt)		258				330
Lk (Lt)		263				330
la	682+	284x2	757		1028+	890
lb	377	286+	513	216x2	534	330
lc	762		616	268x2	821	820
ld	522	335	366	322	670	520
le	620					500
lf	879	441		360+	954	530
lg	155?					110
lh	443		381	313	428	530
lj		63 est.	114		144+	95
lk		245	248			260
ll		102	81			110
lm		404				580
ln		301x2				700
lo		266x2				640
lp		146x2				280
lq		323x2			457x2	820
lr		55		47	69	40
ls		108		73 est.	106 est.	120
lt		215		210 est.	263	300
lu		95			99	
lv	38	31		14	37	
Aa (Rt)						550
Aa (Lt)		341 est.	226		444+	550
Ab (Rt)						490
Ab (Lt)		328			361+	490
Ac (Rt)	236					220
Ac (Lt)				140	207	220
Ad (Rt)						730
Ad (Lt)		470 est.	496	471	638	730
Ae (Rt)						910
Ae (Lt)		504				910
Af (Rt)			514			520

EBSCOhost - printed on 10/28/2022 4:53 AM via . All use subject to https://www.ebsco.com/terms-of-use

TABLE 9.2 *(continued)*

	BOU-VP-3/131	*BOU-VP-25/50*	*BMNH M3092*	*BMNH M3093*	*SMNS Nr. 32888*	*KNM-ER 5711*
Measurement	ORIGINAL	ORIGINAL	ORIGINAL	ORIGINAL	ORIGINAL	BEDEN (1983)
Af (Lt)			525			520
Ag (Rt)			557			800
Ag (Lt)		500+	635			800
Ah (Rt)		339				400
Ah (Lt)		341				400
Aj (Rt)	183	118				
Aj (Lt)				168	216	
Ba		193			188+	280
Bb		172			213−	225
Bc (Rt)		144				135
Bc (Lt)		141				135
Bd (Rt)		125				180
Bd (Lt)		131				180
Be (Rt)						180
Be (Lt)		183				180
Bf (Rt)		143				140?
Bf (Lt)		143				140?
Bg (Rt)		117				100
Bg (Lt)						100
Dap (Rt)	208 est.					
Dap (Lt)						
Dt (Rt)	158				174	135
Dt (Lt)	171				173	135
Ha		509	627			780?
Hb		135	263		148	250?
Hc		165 est.	260			300
1–3					965	
1–4	927				77	
6–7	1355				1275	
8–9	1328				1275	
10–11					1040	
16–17	672		489	204x2	650	
18–19					1010	
Ha/La		0.90	0.83			0.88
Lb/lc	0.56		0.19+		0.50	0.40
Lb/lb	1.14		0.23+		0.77	0.98
lb/lc	0.49		0.83		0.65	0.40
ld/lf	0.59	0.76			0.70	0.98
lh/lc	0.58		0.62		0.52	0.65
lh/ld	0.85		1.04		0.64	1.02

NOTE: For measurement definitions see Beden (1983) and Adam (1986).

EBSCOhost - printed on 10/28/2022 4:53 AM via . All use subject to https://www.ebsco.com/terms-of-use

the premaxilla. It is devoid of molars or incisors. Judging from the size of molar alveoli remaining on the maxilla, it represents a young individual, and it provides unique information on the condition of the tusk socket in young individuals.

Frontal View (Figures 9.3 and 9.4) The distance between right and left tusk alveoli becomes greater toward the anterior extremity of the premaxilla in both BOU-VP-3/131 and BOU-VP-25/50. The anterodorsal surface of the premaxilla gently wraps dorsally at the anterior end. This anterior end of the premaxilla is fringed by a strong rugosity in BOU-VP-3/131.

In BOU-VP-3/131 the premaxillary fossa is very well preserved. Just below the external nares the fossa is narrow and deep, but it becomes rapidly shallow and broad toward the end of the premaxilla. Detail on the premaxillary fossa can be observed only in BOU-VP-3/131, but the preserved surface of the premaxilla on BOU-VP-25/50 suggests that the premaxillary fossa was also broad and shallow. These features are not known in previously described skulls of *E. r. atavus* and *E. r. brumpti*. In these two examples, the right and left tusk alveoli run parallel to each other, and the premaxillary fossa is very narrow and deep. The premaxillary fossa of *Mammuthus* (i.e., Osborn 1942) and early *Elephas* such as *E. r. brumpti*, *E. planifrons,* and *E. hysudircus* is deep and narrow (Beden 1983, 1987), whereas that of *E. ekorensis* is deep and relatively wide (Maglio 1970, 1973). From this comparison, it can be assumed that the depth of the fossa is not the direct consequence of the spacing between the tusk alveoli but rather of the relative position of the alveoli to the anterodorsal surface of the premaxilla. It seems that in the primitive condition, tusk alveoli are located more anterior to the anterodorsal surface of the premaxila relative to derived *E. r. recki* and Eurasian palaeoloxodont species.

The characteristics of the premaxilla seen in BOU-VP-3/131 and BOU-VP-25/50 have never been treated in previous descriptions of *E. recki* from eastern Africa. However, they may be present on the skull of an adult individual of *E. r. recki* found at Haïdalo, Djibouti Republic (Chavaillon et al. 1990). Unfortunately, Chavaillon (1990) did not describe the skeleton. However, judging from the line drawing in Chavaillon (1990), the skull from Haïdalo seems to have a strongly flaring premaxilla as well. The line drawing also shows that the frontoparietal area and occiput of the skull are damaged.

Berthelet (2001) reported the occurrence of a cranium and partial postcranial skeleton of *E. r. ileretensis* from Gobaad, Djibouti Republic, but the skeleton was not described. There is a line drawing in the paper depicting the distribution of the stone artefacts around the skeleton, but the cranial morphology of the skull from the Gobaad specimen cannot be interpreted from the drawing.

Characteristics of the premaxilla observed in BOU-VP-3/131 and BOU-VP-25/50 are also seen in BOU-VP-4/144. BOU-VP-4/144 is a fragment composed of maxilla and premaxilla. It lacks both molars and incisors, but its small dimension indicates that it belongs to a juvenile. Though poorly preserved, the remaining portion of the tusk socket is enough to show that the flaring of the premaxilla is also strong in BOU-VP-4/144. A juvenile skull that preserves the tusk socket, KNM-ER 799, is also known in *E. r. ileretensis* from Koobi Fora (Beden 1983), but the extent of the premaxilla flaring is far less than what is seen in BOU-VP-4/144.

EBSCOhost - printed on 10/28/2022 4:53 AM via . All use subject to https://www.ebsco.com/terms-of-use

The morphology of the external nares can be observed in BOU-VP-3/131. It is very wide transversely and high dorsoventrally. Its lateral margin downcurves gently. The external nares of BOU-VP-3/131 are more primitive than those of Eurasian palaeoloxodont species. In a female *E. namadicus* specimen (BMNH M3092) the lateral margin of the external nares is round and not downcurved. The external nares of SMNS Nr. 32888 are larger than in BMNH M3092, and their lateral margin is downcurved, but they are dorsoventrally narrower than those of BOU-VP-3/131 (Table 9.1). Conversely, the external nares of an adult male *E. r. atavus* (KNM-ER 5711) are larger than those of BOU-VP-3/131, and the lateral margin of the former is downcurved more sharply than that of the Daka Member specimen.

The shape of the external nares changes according to the age and/or sex of the animal. In young individuals of *E. maximus*, the external nares are small and their lateral margins are not downcurved (Inuzuka 1977b). In *E. antiquus* and *E. namadicus* the external nares tend to be degenerated in both juveniles and adults.

The nasal process is as large as that of *E. r. atavus* (KNM-ER 5711) but less pointed than that of the latter. In frontal view, the ventral margin of the nasal process draws ventrally, pointing to a wide opening where the lateral end continues to the highest point of the dorsal margin of external nares without interruption, so the lateral margin of the nasal process cannot be demarcated, and therefore the width of the nasal process cannot be measured. The ventral border of the external nares is located a little higher than the line connecting the left and right zygomatic processes of the frontal. This is a general feature of older males in elephants and stegodons (Inuzuka 1977b; Saegusa 1987; Inuzuka and Takahashi 2004).

The tip of the zygomatic process of the frontal is lost in BOU-VP-25/50, but it can be observed in BOU-VP-3/131. It is very well developed and protrudes strongly laterally. The left and right lacrimal processes are preserved in BOU-VP-3/131, and they are prominent and project strongly laterally from the anterior rim of the orbit.

The morphology of the frontoparietal surface can be observed in BOU-VP-3/131. The frontoparietal surface is higher dorsoventrally and its isthmus frontalis is narrower laterally than in Eurasian paleoloxodont species. In the skull of *E. r. atavus* adult males the frontoparietal surface is also higher and the isthmus frontalis is narrower than in Eurasian paleoloxodont species (Arambourg 1947; Beden 1983, 1987). In SMNS Nr. 32888, which is similar or perhaps larger than BOU-VP-3/131 in the dimension of the whole skull, the frontoparietal area is lower and the isthmus frontalis is wider than in BOU-VP-3/131. Such morphology of the frontoparietal surface is shared widely with Eurasian palaeoloxodont species, except for a skull from Gesher Benot Ya'aqov, which will be discussed below, establishing the derived status of frontoparietal surface morphology observed in SMNS Nr. 32888. Conversely, the condition of the frontoparietal surface seen in BOU-VP-3/131 can be considered a plesiomorphic condition shared with African palaeoloxodont species. In a juvenile skull of *E. r. ileretensis* from Koobi Fora, KNM-ER 799, the isthmus frontalis is wider than that of BOU-VP-3/131, but this is a common condition in juvenile modern African and Asian elephants (Inuzuka 1977b) as well as several fossil proboscidean species, including stegodons (Saegusa 1987).

EBSCOhost - printed on 10/28/2022 4:53 AM via . All use subject to https://www.ebsco.com/terms-of-use

The parietofrontal crest is at least somewhat developed in all Eurasian subgenus *Palaeoloxodon* species. In BOU-VP-3/131, the frontoparietal surface is very flat except for a slight central swelling. This slight swelling is clearly visible in the sagittal cross section and runs from the nasal process to the nuchal crest (Figure 9.6). Similar weak swelling on the central part of frontoparietal surface is frequently seen in *E. maximus*. Therefore, the swelling found on the frontoparietal surface of BOU-VP-3/131 is comparable or homologous with similar swelling in modern Asian elephants rather than with the strong parietofrontal crest developed on the upper half of frontoparietal surface in Eurasian palaeoloxodont species. In BOU-VP-25/5, the frontoparietal surface is largely damaged, but the remaining part of it is completely flat. Judging from this flatness, the parietofrontal crest appears to also be absent in this specimen. In contrast, in an adult male of *E. r. atavus* (KNM-ER 5711), the upper half of the frontoparietal surface is elevated anteriorly and forms a transversally extending elevation. Beden (1983, 1987) considered this swelling in KNM-ER 5711 homologous with the parietofrontal crest widely seen in Eurasian species of subgenus *Palaeoloxodon*. If his identification is correct, *E. r. atavus* is more similar to the Eurasian palaeoloxodont species than to *E. r. recki* from the Daka Member in the development of a parietofrontal crest. However, considering the entire structure of the face, what Beden called a parietal crest appears to be homologous with the swelling found on the frontoparietal surface of *E. maximus* that was discussed earlier rather than the parietofrontal crest of Eurasian palaeoloxodont species. The significance of these features will be discussed further, in conjunction with the derived characters of parietofrontal crest of *E. namadicus*.

Occipital View The occipital can be observed in BOU-VP-25/50. On both sides of the deep nuchal fossa there are well-developed right and left parieto-occipital bosses. The exoccipital protrudes strongly posteriorly. The nuchal plane inclines anteriorly relative to the plane passing through the left and right zygomatic arches. The upper half of the nuchal plane inclines more anteriorly than the lower half of the plane, but not to the extent observed in *E. namadicus*. The lateral margin of the nuchal surface is diminished, but the post-temporal crest appears to have been strongly developed. The frontoparietal surface is heavily damaged, and much of the nuchal crest is missing. However, judging from the remaining part, the distance between the nuchal crest and the dorsal end of the nuchal fossa appears to be moderate. In BOU-VP-3/131 the width of the preserved portion of the occiput measures only approximately 100 mm from the nuchal crest and is strongly flattened by postmortem distortion. Thus, most of the occiput is lost in BOU-VP-3/131, but there is a strong depression accompanied with rugosity at the posteromedial end of the preserved portion. This depression must represent the nuchal fossa and associated rugose attachment surface of the nuchal ligament. If so, the upper end of the nuchal fossa is located very near the nuchal crest in BOU-VP-3/131, contrasting to the morphology of BOU-VP-25/50.

The forward inclination of the upper half of the nuchal surface is weak in BOU-VP-25/50, and the distance between the occipital condyle and the nuchal crest is relatively short. Differing in this aspect of morphology, the upper half of the nuchal plane expands and inclines steeply forward in *E. namadicus*. With this modification, the distance between the occipital condyle and the nuchal crest increases greatly (Hb in Table 9.2). The

EBSCOhost - printed on 10/28/2022 4:53 AM via . All use subject to https://www.ebsco.com/terms-of-use

extreme forward expansion of the nuchal plane decreases the frontoparietal surface (Lc in Table 9.2). In extreme cases seen in the adult males of *E. namadicus*, the frontoparietal surface is obscured by forward expansion of the nuchal plane.

The ratio between the width and height of the occiput of BOU-VP-25/50 is roughly the same as that of *E. r. atavus*. However, in *E. r. atavus* the lower part of the nuchal plane stands nearly vertical or inclines slightly posteriorly with respect to the occlusal plane of the upper molar. That of BOU-VP-25/50 inclines anteriorly. This difference might be due to age or sexual dimorphism rather than taxonomic difference. In *E. maximus* the nuchal plane tends to incline posteriorly or vertically in males, while in females it tends to incline anteriorly or vertically relative to the plane passing through the left and right zygomatic arches (see Osborn 1942: figure 1180). This observation may suggest that the anterior inclination of the nuchal plane in BOU-VP-25/20 is taxonomically insignificant.

Lateral View (Figures 9.3 and 9.4) The temporal fossa can be observed only in BOU-VP-25/50, and even in this specimen the outline of the fossa cannot be clearly delineated because of breakage of anterior and posterior margins of the fossa. However, the remaining part of the rim of the fossa suggests that the outline of the fossa above the crista orbitotemporalis is subrectangular rather than triangular, as is the condition in *E. maximus* and *E. hysudricus*. The dorsal border of the temporal fossa is obscured by heavy damage of the occipitotemporal boss, but it seems to run parallel to the upper half of the nuchal plane, as usual in palaeoloxodont species. The posterior border of the temporal fossa stands nearly perpendicular to the zygomatic arch.

The orbit is located higher than in *E. r. atavus*. The crista orbitotemporalis inclines very steeply in lateral view. Coincidentally, the zygomatic process of maxilla is located higher in BOU-VP-25/50. The right and left jugals of BOU-VP-25/50 were found detached from the zygomatic processes of the maxilla and squamosal, but they are almost completely preserved (Figure 9.3). Minimum dorsoventral height of these is 43.0 mm, and the lengths of right and left sides are 172.0 and 169.0 mm, respectively. Therefore they are thicker dorsoventrally and shorter anteroposteriorly than those of *E. r. atavus*. The frontal process of the jugal is strongly developed at its anterior part. The zygomatic process of squamosal is also thick dorsoventrally. A short and high zygomatic arch is shared with Eurasian species of subgenus *Palaeoloxodon* and *E. r. recki*. These features suggest that the lower half of the skull is shorter and higher than in *E. r. atavus*. This modification must be closely related to the increase of crown height of the molar.

The area surrounding the external nares is deeply excavated by postmortem distortion in BOU-VP-25/50. However, the remaining part of the frontoparietal surface and the premaxilla suggest that the surface surrounding the external nares was gently convex anteriorly in lateral view.

Basicranial View The auditory bulla is high and wide transversely, as is usual in *Elephas*. There is no marked difference between the basicranium of BOU-VP-25/50 and those of *E. r. atavus*. The palate is preserved in BOU-VP-25/50. It has a moderately developed edge along the sagittal suture between the left and right maxilla and palatine. This feature was termed a palatine crest by Beden (1983), but his terminology is not used here.

EBSCOhost - printed on 10/28/2022 4:53 AM via . All use subject to https://www.ebsco.com/terms-of-use

Mandible (Figures 9.4 and 9.5) BOU-VP-3/131 consists of the cranium just described and a nearly complete mandible. In the mandible the dorsal surface of the condyles, the middle part of the ascending ramus, the mesial half of the M_3s, and the alveolar process of the mandible are missing. The mandibular symphysis does not protrude strongly. The corpus of the mandible is robust and high. The upper part of the ascending ramus near the condyles inclines gently medially as is usual in *Elephas*. Though the cranium of *E. r. recki* is markedly different from that of *E. r. atavus* and *E. r. shungurensis*, there are no marked differences observed among the mandibles of *E. r. shungurensis*, *E. r. ileretensis*, or *E. r. recki*.

Incisors The tusk associated with BOU-VP-25/50 is similar to that of *E. antiquus* in being slender and nearly straight. Besides this tusk, a large left tusk from the Daka Member was observed but not collected. It is far larger than the pair of tusks associated with BOU-VP-25/50 (distance between tip and the base of the tusk approximately 1.60 m; the diameter of the tusk at the base is approximately 160.0 mm), and more strongly curved than these. A comparable tusk is associated with a skull reported from Omo (Omo 75.69.3189) by Beden (1987). He did not describe these tusks, but his figures clearly show that the tusks curve outwards, being most closely spaced at about the midlength of the premaxilla. In this respect, the premaxilla and the tusk of Omo 75.69.3189 are somewhat similar to those of *Mammuthus*. It is not clear whether the large uncollected tusk from the Daka Member just mentioned was similarly curved outward, because it was found isolated, but the overall extent of the curvature appears to be comparable with that of Omo 75.69.3189.

Molars (Figure 9.5, Table 9.3) Fifteen molar specimens representing nine individuals have been collected from Daka Member, including those associated with crania and mandibles just described. Molars BOU-VP-1/33, BOU-VP-19/49, BOU-VP-25/58, and BOU-VP-4/5 can be used for evaluation of the hypsodonty of the molar. Specimens BOU-VP-19/49, BOU-VP-25/58, and BOU-VP-4/5 are within the observed range of *E. r. recki* reported by Beden (1979, 1983, 1987), and the first two are comparable with the most hypsodont individuals of *E. r. recki* from Beds III and IV at Olduvai. On the other hand, BOU-VP-1/33 is low crowned, and a comparable hypsodonty index value of it can be found only in the observed range of *E. r. ileretensis* as reported by Beden (1979, 1983, 1987). This specimen was formed atop Daka sediments, but close to the underlying Hata Member disconformity.

Enamel wear patterns show some similarity to *E. r. ileretensis*. In the M^1 of BOU-VP-25/50 the enamel folds sparsely and irregularly at the upper part of the lophid, but folding becomes regular and tighter toward the basal part of the lophid. Some lower molars, such as BOU-VP-4/5 and BOU-VP-4/44, show the same tendencies. In these, the enamel folds irregularly at the upper part of the lophid, but enamel folding becomes regular, dense, and tight toward the basal part of the lophid. Thus, in these molars enamel folding shows some similarity to *E. r. ileretensis* reported by Beden (1979, 1983, 1987).

Conversely, in BOU-VP-3/131, the enamel at the middle height of the lophid is densely folded and regular, and the amplitude of the folding is small. These enamel folding features are the same as those observed in the lectotype of *E. r. recki* from Olduvai. In sum, molars from the Daka Member present features somewhat intermediate between typical *E. r. recki* and *E. r. ileretensis*.

EBSCOhost - printed on 10/28/2022 4:53 AM via . All use subject to https://www.ebsco.com/terms-of-use

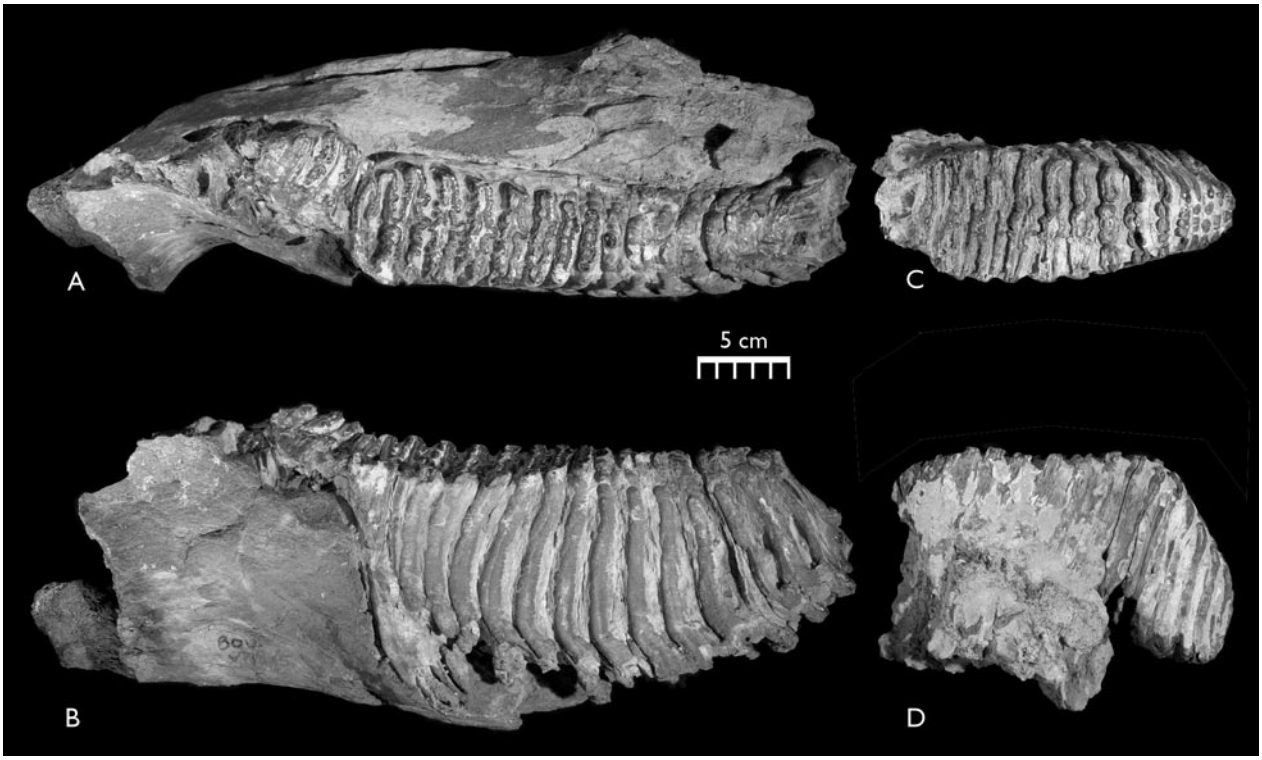

FIGURE 9.5

Elephas (Palaeoloxodon) recki recki mandible and molars. Right mandible with M_2 and M_3 (BOU-VP-4/5). A. Occlusal view. B. Lingual view. Left M^3 (BOU-VP-1/33). C. Occlusal view. D. Lingual view. Left is anterior.

DISCUSSION Cranial features of the elephants from the Daka Member show a number of characters new to eastern African fossil elephants, but their molar features, specifically high hypsodonty and strongly folded enamel, are closely comparable with specimens previously described from this area, especially with those of advanced *E. recki* from Beds III and IV at Olduvai Gorge. The latter taxon has been allocated in *E. r. recki* by Beden (1979, 1983, 1987). However, Beden's scheme of the subspecific classification of *E. recki* is contested (Ferretti et al. 2003; Todd 2005). Todd (2005) suggests that dental samples previously identified as *E. recki* actually contain teeth of several species and that the metric characterization of subspecies of *E. recki* as proposed by Beden is statistically untenable. Ongoing study of the new samples from Konso, Ethiopia, also suggests that the distinction between subspecies *E. (P.) r. atavus* and *E. (P.) r. ileretensis* is not clear (Saegusa, unpublished data). Thus, the scheme proposed by Beden (1979, 1983, 1987) must be revised. However, even in such recent examination of dental features, *E. r. recki* is still clearly distinguished from other subspecies in several metric features (Ferretti et al. 2003; Todd 2005). Examination of the hypsodonty index of selected specimens also suggests that *E. r. recki* is clearly separated from other "*recki*" specimens (Saegusa, unpublished data). Therefore, we consider *E. r. recki*, including the lectotype from Beds III and IV at Olduvai Gorge, a valid taxon.

The sample size of molar materials from the Daka Member is too small to thoroughly address the above problems concerning the validity of Beden's subspecies of *E. recki*. However,

EBSCOhost - printed on 10/28/2022 4:53 AM via . All use subject to https://www.ebsco.com/terms-of-use

TABLE 9.3 Daka Elephant Dental Metrics

Specimen	*Element*	*Side*	*N*	*NF*	*L*	*LF*	*I*	*H*	*e*	*F*	*H/l*
BOU-VP-1/1	M^3	Rt.	−12X	−9	−204	156	79	106	2.7	7	134
BOU-VP-1/1	M^3	Lt.	−15X	−10	−231	167	78	105	2.6	6.6	135
BOU-VP-1/33	M^3	Lt.	X14−	X5	259−	117	88.5	138	3.4	6.4	156
BOU-VP-1/33	M^3	Rt.	X11−	X5	189−	101	89	138	2.9	6.6	155
BOU-VP-19/49	M^3	Lt.	8	0	150.3	0	82	158.9	x	∼.5	194
BOU-VP-25/58	M^3 fragment		x	4	83.5−	39.8	49.4	104.4	2.1	x	211
BOU-VP-25/50	M^1	Rt. and Lt.	X10X	X10X	160	154	72.6	x	2.1	6.2	x
BOU-VP-1/33	M_3	Lt.	X6−	X6−	123−	121	75	111	2.9	6.1	148
BOU-VP-1/33	M_3	Rt.	X15−	X7	308−	130	87	118	2.7	5.8	136
BOU-VP-1/131	M_3	Rt. and Lt.	−7X	−7X	−151	−150	87	x	2.7	5	x
BOU-VP-4/5	M_3	Rt.	X15−	X9	270−	137	75	123	2.6	6	164
BOU-VP-25/37	M_3	Rt.	16	12	325	215	89.9	109.9	3.1	∼.5	122
BOU-VP-4/5	M_2	Rt.	−4	−4	−56	−56	x	x	x	x	x
BOU-VP-4/44	M_2	Rt. and Lt.	X10	X10	185	171.2	69.5	x	2.5∼2.2	x	x
										OR	1.55 − 2.11

NOTE: For measurement points see Beden (1983).

the present sample contains both the molars showing a lower hypsodonty index than *E. recki* from Beds IV and III and those showing a comparable hypsodonty index with the latter. Thus, in dental features, elephants from the Daka Member can be compared with those described from Buia, Eritrea (Ferretti et al. 2003) and from Konso-Gardula, Ethiopia (Saegusa, unpublished data). According to Ferretti et al. (2003), the molar sample from Buia represents an intermediate form between *E. r. recki* and so-called *E. r. ileretensis*, suggesting the presence of the gradually evolving lineage of *E. recki*. Thus, if the foregoing argument is correct, there would be no clear metric boundary between the subspecies of *E. recki*. However, it would not be practical to deny all of the subspecific names because of the continuity of the morphological change through time. We diagnose *E. r. recki* as derived *E. recki* that contains individuals with an M^3 hypsodonty index higher than 190. As mentioned above, the molar sample from the Daka Member contains molars with hypsodonty indices above and below 190. Moreover, Daka Member molars retain marked enamel-folding irregularities. In these features, the sample appears to represent a very early stage of the *E. r. recki* as defined previously.

Distinction between *E. r. atavus*, *E. r. shungurensis*, and *E. r. ileretensis* is not clear from molar characters (Ferretti et al. 2003; Todd 2005), but it does not automatically disqualify *E. r. atavus* as a valid taxon. Crania from Omo (NMNH No. 300; Omo 75.69.3190; Omo 75.70.826; Omo 75.69.3217) and Koobi Fora (KNM-ER 5711) obviously constitute a taxon that shares a suite of unique characters, such as extremely inferiorly positioned orbit, a slender and low zygomatic arch, and a narrow premaxilla. Strong vertical expansion and a box-like appearance of the occiput also characterize these specimens, but these features are also shared with skulls of the elephants from the Daka Member and Eurasian palaeoloxodont species. Therefore, at least the Omo and Koobi Fora crania skulls constitute a

EBSCOhost - printed on 10/28/2022 4:53 AM via . All use subject to https://www.ebsco.com/terms-of-use

single taxon of the subgenus *Palaeoloxodon*, and that includes the historical cranium from Omo described by Arambourg (1947), and the names *E. (P.) r. atavus* or *E. (P.) atavus* are available for them. *E. (P.) r. atavus* proposed by Beden is thus still valid, at least as that composed of the cranial materials allocated in this taxon by Beden (1979). We use *E. (P.) r. atavus* in this sense here.

Revision of *Elephas* Systematics and Paleobiogeography

The type of *E. recki* from Bed IV at Olduvai was first described as a subspecies *E. antiquus recki* by Dietrich (1916). However, in succeeding studies on the eastern African elephant fossils, its generic allocation varied. For instance, Osborn (1942) allocated "*recki*" to subgenus *Palaeoloxodon* together with *E. namadicus*, *E. mnaidrensis*, and several African species such as *E. atlanticus*, based mainly on the similarities in enamel morphology, while Arambourg (1942, 1947) considered *E. recki* to be closely related to *E. meridionalis* and, especially, *E. hysudricus* because of close similarity between crania of *E. recki* from Omo and those of *E. hysudricus* known from the Siwaliks. This view was followed by Vaufrey (1958), Maccagno (1962), and Azzaroli (1966). However, Dietrich (1951) allocated "*recki*" into *Metarchidiskodon*, which is exclusively distributed in Africa and is unrelated to *E. hysudricus*, *E. meridionalis*, or the *E. namadicus/antiquus* group. For him, the similarity between *E. recki* and *E. hysudricus* was convergence.

The idea that African *E. recki* is ancestral to Eurasian *E. namadicus* and *E. antiquus* was revived by Aguirre (1969a, b, c), who first proposed the basic phylogeny of elephants that is widely accepted today. Later hypotheses of elephant phylogeny proposed by Maglio (1973) and Beden (1979, 1983, 1985, 1987) are versions of Aguirre's original idea revised by information obtained from new materials. However, the time of migration from Africa to Eurasia and the morphological features of the first Eurasian palaeoloxodont species have remained unclear until now in spite of intensive sampling of the fossil elephants from the hominid bearing Plio-Pleistocene deposits of eastern Africa.

Maglio (1973) mentioned that the time and place of the origin of Eurasian subgenus *Palaeoloxodon* remain uncertain, but he suggested the possibility that it was derived from a form close to *E. ekorensis* or early *E. recki* (Maglio 1973). Thus he implied an earlier date of the emigration of palaeoloxodonts from Africa than was proposed by Aguirre (1969a, b, c).

In contrast, Beden (1983, 1985, 1987) specified a "morphotype 2" of *E. r. atavus* as the ancestral type of Eurasian subgenus *Palaeoloxodon*. His idea is based on the similarity between his "morphotype 2" of *E. r. atavus* and the *E. antiquus*/*E. namadicus* group in dental features (Beden 1979, 1983, 1985) as well as the geological age of the oldest Eurasian palaeoloxodonts as suggested by Dubrovo (1977). The basis for his argument, however, is somewhat untenable, making it difficult to test. Beden (1979, 1983, 1985, 1987) recognized three morphotypes in the molars of *E. (P.) r. atavus* and suggested that "morphotype 2" of *E. (P.) r. atavus* was ancestral to Eurasian palaeoloxodonts (Beden 1979, 1983, 1985). However, "morphotype 3" depicted in Beden (1983: figure 3.20) appears to correspond to the "second type" (Beden 1983). Therefore, these morphological types are named and used inconsistently in his paper.

EBSCOhost - printed on 10/28/2022 4:53 AM via . All use subject to https://www.ebsco.com/terms-of-use

This inconsistency first appeared in his unpublished doctoral thesis (Beden 1979) and was repeated in succeeding papers (Beden 1983, 1985, 1987) without correction. Because of this inconsistency, it is not clear whether "morphotype 2" described as ancestral to Eurasian palaeoloxodont species in Beden (1979, 1983, 1985) corresponds to "morphotype 2" or "second type" on the other pages of these papers. As he passed away more than two decades ago, it is impossible to be sure exactly which type he considered ancestral to Eurasian palaeoloxodonts, but judging from the context of the sentences and figures of his paper, "3 ème type" described in Beden (1979, 1987) and "third type" (Beden 1983: 85) appear to correspond to "morphotype 2," which is described as the ancestral type of Eurasian subgenus *Palaeoloxodon* in Beden (1979, 1983, 1985). On the other hand, the above "morphotype 2" appears to correspond to "morphotype 1" in figure 3.20 of Beden (1983) and corresponding figures in Beden (1979, 1987). He characterizes this type by thin and strongly folded enamel. However, there is a strong possibility that such features are solely found on upper molars. Enamel morphology depicted as "morphotype 1" in figure 3.20 of Beden (1983) corresponds to that of KNM-ER 4305 in figure 3.18 of the same paper. Though KNM-ER 4305 is described as an M_3, in both the caption of the figure and the text of Beden (1979, 1983), the specimen depicted is in fact an M^3. Specimen KNM-ER 4305 is composed of two M^3s, one of which was described erroneously as an M_3, and a fragment of a genuine M_3 that shows irregular enamel folding. Beden stressed that such irregular enamel folding was inherited exclusively by consecutive subspecies *E. r. ilereten-sis* and *E. r. recki*. "Irregularity" of the enamel folding mentioned here is the condition of many weak folds intermingled with a few strong enamel folds that are as deep as or deeper than the median sinus. However, such "irregularity" of the enamel folding can be still observed in some specimens of Eurasian palaeoloxodont species even though the frequency of such "irregular folding" is greatly reduced by the mesiodistal compression of loph(ids) in Eurasian palaeoloxodont species.

The second basis of Beden's idea on the ancestry of Eurasian palaeoloxodonts is the early Pleistocene date of the oldest subgenus *Palaeoloxodon* species from Eurasia. Dubrovo (1977) noted that the oldest representatives of the genus are from the early Pleistocene of China (Nihewan) and Japan (Osaka group and Umegase Formation). However, her idea is based on erroneous identification of primitive *Mammuthus* from eastern Asia.

Subgenus *Palaeoloxodon* has been reported from the late Pliocene and early Pleistocene of China (Zhang et al. 1983; Takahashi and Namatsu 2000), but recent revision revealed that the designated specimens belong instead to the genus *Mammuthus*. Those purported to have been collected from the Nihewan beds are actually from younger terrace deposits and are more correctly allocated to earliest *M. trogontherii* (Wei et al. 2003). Those collected from late Pliocene beds in northern China are best assigned to *M. meridionalis* or *M. rumanus*, rather than early subgenus *Palaeoloxodon* (Lister et al. 2005), including "*P. tokunagai*" described from Yushe Basin by Teilhard de Chardin and Trassaert (1937). A cranium (IVPP V.4443) correctly assigned to subgenus *Palaeoloxodon* has been described from the early Pleistocene Nihewan beds (Wei 1976). However, the specimen was actually excavated from deposits younger than the middle Pleistocene (Qi 1999; Takahashi and Namatsu 2000). Thus, no specimen of subgenus *Palaeoloxodon* has been found from deposits older than the middle Pleistocene in China.

EBSCOhost - printed on 10/28/2022 4:53 AM via . All use subject to https://www.ebsco.com/terms-of-use

Osborn (1942) and Maglio (1973) allocated all of the elephantid specimens from the Japanese Pleistocene into *(P.) namadicus*. Dubrovo (1981) admitted the validity of *E. (P.) naumanni* but allocated all of the Pleistocene elephants from Japan into this species. On this basis she argued that the range of Japanese subgenus *Palaeoloxodon* extends to the early Pleistocene. However, elephants from the early Pleistocene of Japan are more correctly allocated to *Mammuthus protomammonteus* rather than *E. (P.) naumanni* (Takahashi and Namatsu 2000; Lister et al. 2005; the section "Notes on *Elephas (Palaeoloxodon) naumanni*" of this chapter).

The idea that subgenus *Palaeoloxodon* originated from *E. planifrons* was held by several Russian and Chinese students such as Dubrovo (1960, 1977) and Zhang et al. (1983). Their arguments are, however, no longer tenable because the crania from the Daka Member presented here provide a concrete link between Eurasian palaeoloxodonts and African *E. (P.) recki* as discussed subsequently.

Biogeography

The earliest reliable record of Eurasian subgenus *Palaeoloxodon* species is obtained from Soleilhac, France, where a complete straight tusk and molars, definitely showing characteristic features of subgenus *Palaeoloxodon*, have been recovered from beds dating to 0.93 Ma together with *Mammuthus meridionalis* (Bonifay 1996; Aouadi 2001). A mandible with fairly complete molars from Huescar 1, Spain, has also been reported as an early representative of Eurasian subgenus *Palaeoloxodon* (Mazo 1989), but its molars suggest affinities to *Mammuthus* rather than subgenus *Palaeoloxodon* in having a weakly folded enamel layer and parallel-sided enamel loops. An isolated molar from Silvia, Italy, represents the earliest palaeoloxodont of the area, and its date is bracketed between 1.1 and 0.6 Ma (Palombo and Ferretti 2005).

Thus, the date of the first Eurasian appearance of subgenus *Palaeoloxodon* roughly corresponds to the earliest middle Pleistocene, almost contemporaneous with the Daka elephants, the first African palaeoloxodont. Specimens from the Daka Member present some derived features previously known only in Eurasian palaeoloxodont species such as a strongly flared premaxilla (see next section). Such coincidence suggests that the dispersal of the subgenus out of Africa took place at around 1.0 Ma, just after the aquisition of the derived features shared with Daka Member elephants and Eurasian palaeoloxodont species. This timing of emigration of the subgenus from Africa to Eurasia may correspond to the onset of the intense fluctuation of the glacial and interglacial climatic regimes, which would have forced some elements of the mammalian fauna to adapt to cooler and more open habitats (van der Made and Mazo 2001, 2003). An adaptive shift of *Mammuthus* towards the cooler and more open habitat appears to have allowed palaeoloxodont species to intrude into the habitat that had been occupied by *M. meridonalis* before the middle Pleistocene.

Eurasian and African Subgenus *Palaeoloxodon*

See Figures 9.6, 9.7, 9.8, 9.9, and Table 9.4. The idea on the time and place of the origin of the Eurasian subgenus *Palaeoloxodon* proposed here is very similar to that proposed

EBSCOhost - printed on 10/28/2022 4:53 AM via . All use subject to https://www.ebsco.com/terms-of-use

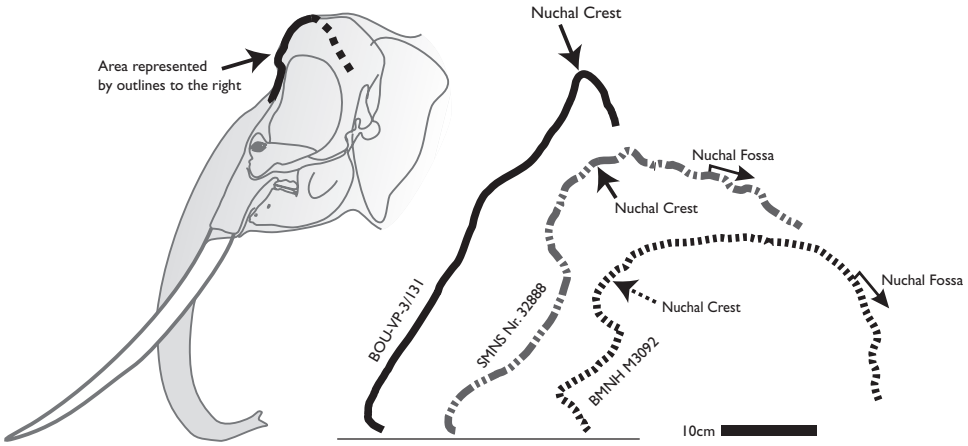

FIGURE 9.6

Sagittal sections of the cranial vault. Anterior is to the left, and upper is to the top of the page. BOU-VP-3/131, *Elephas (Palaeoloxodon) recki recki*; SMNS Nr. 32888, "*Elephas antiquus*"; BMNH M3092, *Elephas namadicus*. The anterior margin of the nuchal plane corresponds to the nuchal crest. Note that the extreme shortening of the frontoparietal surface is caused by the anteroventral displacement of the nuchal crest. Its most extreme state can be seen in *E. namadicus*, where the upper half of the nuchal plane faces anteriorly.

by Aguirre (1969a, b, c), who argued for the first time that Eurasian palaeoloxodonts appeared at the beginning of the middle Pleistocene as a descendant of African *(Palaeoloxodon) recki*. Our conclusion is derived from two lines of evidence. One is that the most reliable date of the earliest Eurasian palaeoloxodont species is recorded from Soleilhac, France, as just mentioned. Another line of the evidence is the date and morphology of skulls from the Daka Member presented here.

Advanced *E. (P.) recki* (referred to here as *E. [P.] r. recki*) from the Daka Member described in this work fill the morphological gap between *E. (P.) r. atavus* and Eurasian subgenus *Palaeoloxodon*. They confirm that *E. r. atavus* and *E. r. recki* belong to a monophyletic subgenus *Palaeoloxodon* (Figure 9.9). The characters shared with *E. r. atavus*, *E. (P.) r. recki* from Daka, and Eurasian palaeoloxodont species are related to the unique manner of the expansion of the occiput and cranial vault and the steep frontoparietal plane.

Paired left and right occipital bosses, emergent from expansions of the occiput associated with a mid-sagittal depression in frontal view, is a synapomorphy of *Elephas*, including primitive species of the genus, *E. planifrons*, *E. ekorensis*, and "*E. r. brumpti*" (Maglio 1973; Beden 1979, 1983, 1987), but the formation of the post-temporal crest by way of vertical heightening of the occiput is unique to *E. (P.) r. atavus*, *E. (P.) r. recki*, and Eurasian subgenus *Palaeoloxodon* species. In these forms the frontoparietal plane is positioned more dorsoanteriorly and is more vertical (Figures 9.4, 9.6, and 9.7). The temporal fossa also extends vertically to become rectangular or oblong. The dorsal margin of the temporal line runs nearly parallel with the occlusal plane in these forms. These specializations give the upper half of the cranium of subgenus *Palaeoloxodon* species a boxlike appearance. These features are exclusively shared with *E. (P.) r. atavus*, *E. (P.) r. recki*, and all Eurasian palaeoloxodont species, including *E. (P.) naumanni*, the type species of the subgenus. The skull of *E. hysudricus* from the Pleistocene of India has been frequently compared with *E. (P.) r. atavus*, and a close relationship between them has been inferred (Arambourg 1942, 1947; Vaufrey 1958; Azzaroli 1966). However, in *E. hysudricus* and *Mammuthus*, the derived features of subgenus *Palaeoloxodon* explained above are not present. The skull of "*E. r. brumpti*" from Omo described by Beden (1987) also lacks these derived traits of

EBSCOhost - printed on 10/28/2022 4:53 AM via . All use subject to https://www.ebsco.com/terms-of-use

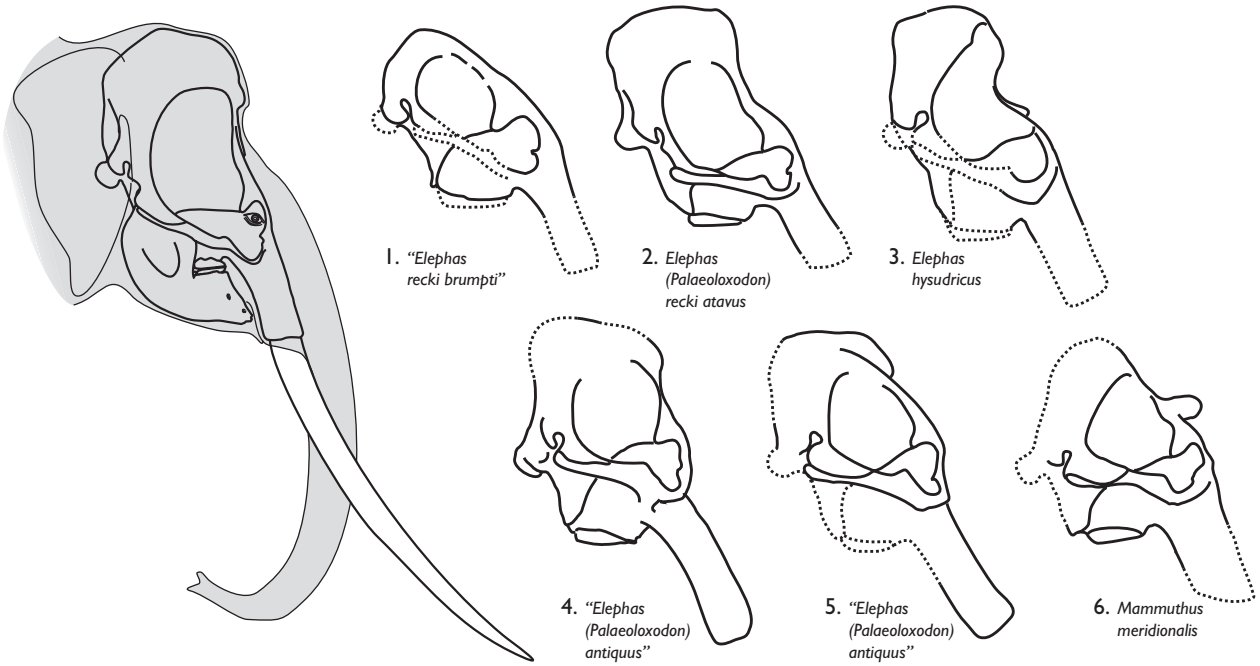

FIGURE 9.7

Lateral view of crania from various elephants. Anterior is to the right, and dorsal is to the top of the page. Not to scale. 1. "*Elephas recki brumpti*," ENM L.1.70, Shungura, Omo, Ethiopia (after Beden 1987). 2. *E. (Palaeoloxodon) r. atavus*, MNHN No. 300, Shungura, Omo, Ethiopia. 3. *E. hysudricus*, BMNH M. 3109, Siwalik. 4. "*E. (Palaeoloxodon) antiquus*", Pian dell'Olmo, Italy (after Maccagno 1962). 5. "*E. (Palaeoloxodon) antiquus*", SMNS. Nr. 15930, Steinheim, Germany (after Osborn 1942). 6. *Mammuthus meridionalis*, Chilhac, France (after Boeuf 1990, reversed).

the cranial vault and occiput. The species also lacks the pseudoloxodont plica (median expansions of enamel loops similar to those of *Loxodonta*), which can be seen in *E. r. atavus* and other later species of subgenus *Palaeoloxodon*, including Daka Member specimens. Therefore, there is presently no supporting evidence for the allocation of "*E. r. brumpti*" to subgenus *Palaeoloxodon*.

The premaxilla flares strongly and the premaxillary fossa is shallow and wide in all Eurasian subgenus *Palaeoloxodon*. This is one of the most peculiar characters of Eurasian palaeoloxodonts, but in *Elephas (P.) recki atavus* the premaxillary fossa is deep and narrow and the alveoli of the tusks do not flare (Figure 9.8). Thus, *E. r. atavus* shares primitive characters with "*E. r. brumpti*," *E. hysudricus*, and *Mammuthus*. On the other hand, *E. r. recki* from the Daka Member shows the type of premaxilla that characterizes Eurasian subgenus *Palaeoloxodon* (Figure 9.8). Steeper inclination of the crista orbitotemporalis, a higher position of the orbit, and the shorter and stockier zygomatic arch are also the derived characters shared with Eurasian palaeoloxodonts and Daka Member specimens (Figures 9.6 and 9.7). These features appear to have developed before the emigration of palaeoloxodonts from Africa.

Conversely, the modification of the frontoparietal surface, including the formation of a distinct parietofrontal crest, appears to have occurred after the immigration of subgenus *Palaeoloxodon* into Eurasia. A cranium from Gesher Benot Ya'aqov, Israel (Goren-Inbar et al. 1994) suggests this scenario. Based on magnetostratigraphy and biochronology, the geological age of the Gesher Benot Ya'aqov is estimated as approximately 0.78 Ma (Goren-Inbar et al. 2000). Only the facial part of skull is preserved, but it is enough to show that the premaxilla flares strongly. Goren-Inbar et al. (1994) identified this skull as *(P.)*

EBSCOhost - printed on 10/28/2022 4:53 AM via . All use subject to https://www.ebsco.com/terms-of-use

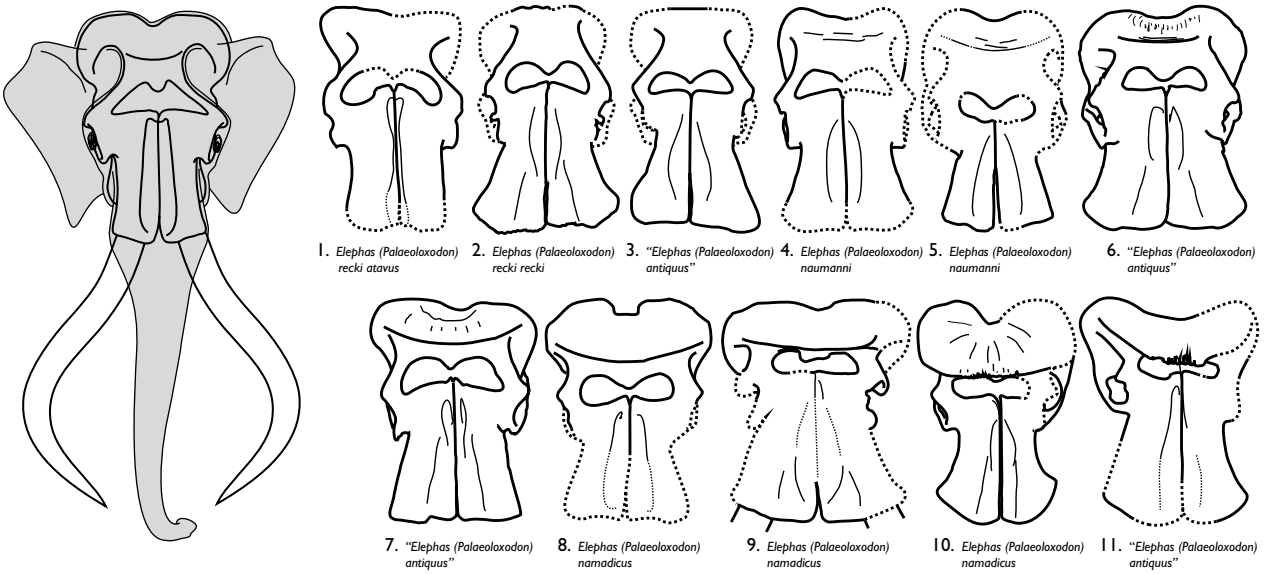

FIGURE 9.8

Anterior view of the crania of *Palaeoloxodon*. Not to scale. 1. *Elephas (P.) recki atavus*, MNHN No. 300, Shungura, Omo, Ethiopia. 2. *E. r. recki*, BOU-VP-1/131, Bouri, Ethiopia. 3. "*E. (P.) antiquus*," Gesher Benot Ya 'aqov, Israel (after Goren-Inbar et al. 1994). 4. *E. (P.) naumanni*, male NSM PV18700, Chiba, Japan (after Inuzuka 1977a,b). 5. *E. (P.) naumanni*, female Tokyo, Japan (after Inuzuka 1991a,b). 6. *E. antiquus*, SMNS Nr. 32888, Stuttgart, Germany. 7. "*E. (P.) antiquus*," Pian dell'Olmo, Italy (after Maccagno 1962). 8. *E. (P.) namadicus*. female, BMNH M. 3092, Nebada, India. 9. *E. (P.) namadicus*, male, Godavari, India (after Pilgrim 1905). 10. *E. (P.) namadicus*, IVPP. V.4443, Nihewan, China (after Wei 1976). 11. "*E. (P.) antiquus*," La Polledrara di Cecanibbio, Rome, Italy (after Palombo et al. 2003).

antiquus. A flared premaxilla is a characteristic feature of Eurasian subgenus *Palaeoloxodon*, and this character is present in the type species of the subgenus *(P.) naumanni* (Inuzuka 1977a; Inuzuka and Takahashi 2004). Thus, the presence of this character in the cranium from Gesher Benot Ya'aqov supports the generic identification of the specimen. It presents some primitive characters not seen in other Eurasian species of subgenus *Palaeoloxodon*. Goren-Inbar et al. (1994) note that the parietofrontal crest is very weak in the cranium from Gesher Benot Ya'aqov, and suggest that this is because it is a female or juvenile male, but the parietofrontal crest figured in this publication looks even weaker than that of a female of *E. (P.) naumanni* from Tokyo, Japan. Therefore, the weak development of the parietofrontal crest in the skull from Gesher Benot Ya'aqov is more likely a primitive character than a result of sexual dimorphism or young individual age. The figures presented in Goren-Inbar et al. (1994) clearly show that the frontoparietal area is high dorsoventrally and that the isthmus frontalis is narrower than the other Eurasian species of subgenus *Palaeoloxodon*. The narrowness of the isthmus frontalis cannot be explained by sexual dimorphism or juvenility, because this isthmus becomes narrower in older modern *E. maximus* individuals (Inuzuka 1977b; Inuzuka and Takahashi 2004). Furthermore, the isthmus frontalis of females of *E. (P.) naumanni* is not narrower than that of males (Figure 9.8). Therefore, the combination of an extremely weak parietofrontal crest, a high frontoparietal region, and a narrow isthmus frontalis cannot be entirely explained by sexual dimorphism or young individual age. In having these characters, the Gesher Benot Ya'aqov cranium is markedly different from those of other Eurasian palaeoloxodont species. These features are primitive characters shared with Daka Member specimens, suggesting that the Gesher Benot Ya'aqov cranium belongs to the same species, *E. (P.) recki*, rather than *E. (P.) antiquus*. At a minimum, it suggests that the skulls of the earliest Eurasian palaeoloxodonts from the early middle Pleistocene were not especially different from *E. r. recki*.

The parietofrontal crest of *Elephas (Palaeoloxodon) recki recki* and the cranium from Gesher Benot Ya'aqov are weaker or equivalent in presentation to those in *E. r. atavus*

EBSCOhost - printed on 10/28/2022 4:53 AM via . All use subject to https://www.ebsco.com/terms-of-use

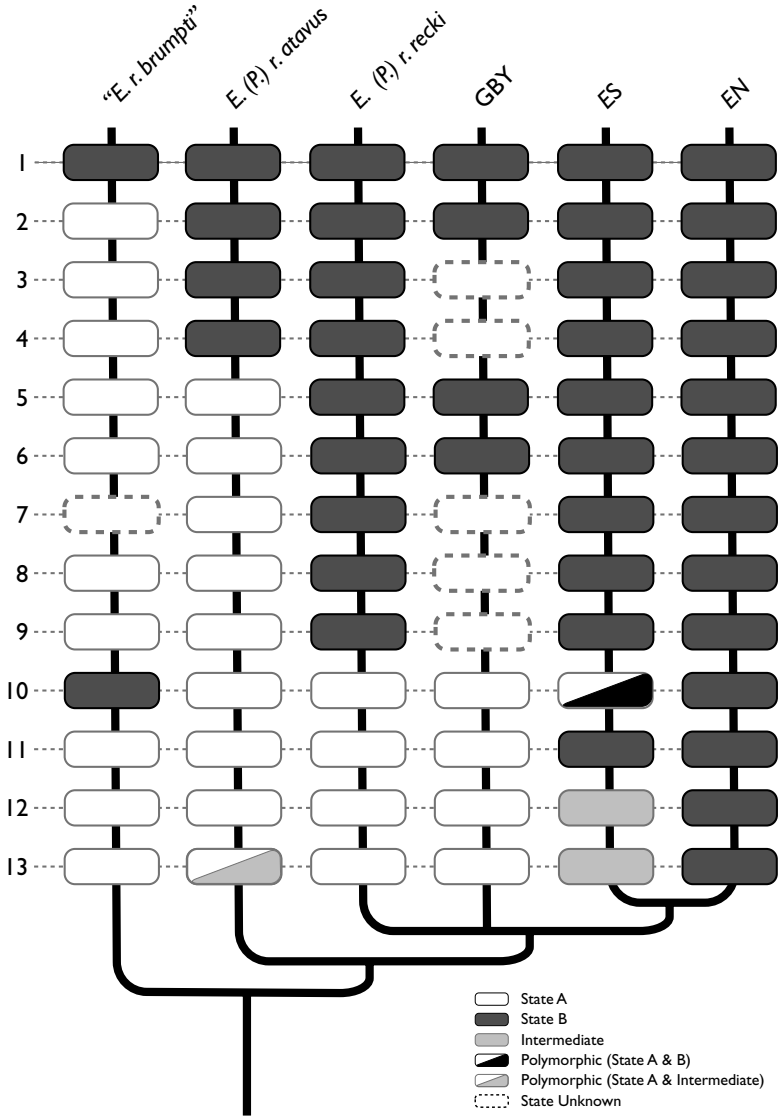

FIGURE 9.9

Suggested relationship among *Palaeoloxodon* and *Elephas*. (GBY): *"E. (P.) antiquus"* from Gesher Benot Ya'aqov, Israel; (ES): Stuttgart morph; (EN): *namadicus* morph.

(Figure 9.8). Thus, the parietofrontal crest appears to have developed homoplastically in later palaeoloxodont species. This reversal of the parietofrontal crest may be explained by the transformation of the frontoparietal plane. As explained above, the frontoparietal plane of *E. r. atavus* lies on nearly the same plane as the dorsoanterior surface of the premaxilla (Figure 9.7). However, compared to Eurasian subgenus *Palaeoloxodon* species and elephants from the Daka Member, the frontoparietal plane of *E. r. atavus* lies more posteroventrally and inclines more gently. Because of this arrangement, the lower half of the frontoparietal plane forms a depression between its upper half and the anterodorsal surface of the premaxilla. This arrangement gives the impression that the upper half of

EBSCOhost - printed on 10/28/2022 4:53 AM via . All use subject to https://www.ebsco.com/terms-of-use

TABLE 9.4 *Elephas* Cranial Characters

Character	*State A*	*State B*
1. Occiput expands to form left and right occipital boss	No	Yes
2. Frontoparietal surface and dorsal surface of premaxilla	Strongly angled	Slightly or not angled
3. Occiput rectangular in lateral view	No	Yes
4. Lateral view of temporal fossa	Triangular	Oblong or rectangular
5. Premaxilla	Parallel sided	Flare strongly
6. Premaxillary fossa	Deep narrow	Shallow wide
7. Zygomatic arch	Long, slender	Short, stocky
8. Position of the orbit	Low	High
9. Inclination of the crista orbito temporalis	Gentle	Steep
10. External naris in male	Lateral margin down turned	Lateral margin round
11. Isthmus frontalis	Narrow	Wide
12. Postorbital crest	Long	Extremely short
13. Parietofrontal crest	Absent	Extremely developed

NOTE: The primitive states are sympleisiomorphic for *Elephas*, and the derived states are synapomorphic for subgenus *Palaeoloxodon*. See also Figure 9.9.

the frontoparietal plane projects anteriorly. Associated with the anterodorsal displacement of the orbit in *E. r. recki*, the frontoparietal plane is also displaced more anterodorsally and comes to the same plane as the anterodorsal surface of the premaxilla. Because of this modification, the depression between the anterodorsal surface of the premaxilla and the upper half of the frontoparietal plane is absent. In other words, the parietofrontal crest (= anterior projecton of upper half of frontoparietal plane) is not present. In later Eurasian palaeoloxodont species, the parietofrontal crest formed again by means of the further anterior expansion of the upper half of the nuchal and frontoparietal plane beyond the plane passing through the anterodorsal surface of the premaxilla.

Strong anterior projection of the parietal in *Elephas hysudricus* also appears to result from a combination of a gently sloped, low frontoparietal plane and strong expansion of the occipital bosses (Figure 9.7). On the upper part of the frontoparietal surface of crania of this species there is strong swelling similar to that of *E. r. atavus*, repesented well by MNHN No. 300 from Omo. Arambourg (1947) compares this cranium with *E. hysudricus*, wherein the extent of the development of the swelling on the frontoparietal surface is greater. However, this swelling appears to be the result of a combination of a strong expansion of the occiput and a posterior inclination of the lower part of the frontoparietal surface, derived and primitive characters respectively. As explained above, the same combination of derived and primitive characters of the face likely caused the anterior projection of frontoparietal surface in MNHN No. 300.

Except for subgenus *Palaeoloxodon* from Gesher Benot Ya'aqov, Israel, all known crania of Eurasian palaeoloxodonts share a distinct parietofrontal crest, a shortened frontoparietal crest, and forward expansion of the upper half of the nuchal plane. Subgenus *Palaeoloxodon* species sharing these derived features can be separated into two cranial morphotypes.

EBSCOhost - printed on 10/28/2022 4:53 AM via . All use subject to https://www.ebsco.com/terms-of-use

The first morphotype is characterized by weak development of the parietofrontal crest, as is presented well in cranium SMNS Nr. 32888 from the travertine in Bad Cannstatt, Stuttgart, Germany (Adam 1986). The other type is represented by crania of *Elephas namadicus* from the Indian Pleistocene (Falconer and Cautley 1846; Pilgrim 1905) that show extreme development of parietofrontal crest (Figure 9.8). For the convenience of discussion, the latter and the former are dubbed here "Stuttgart morph" and "*namadicus* morph" respectively. Both morphotypes are seen also in several island endemics such as *E. (Palaeoloxodon) mnaidrensis* from Sicily and *E. (P.) naumanni* from Japan.

The "*namadicus* morph" is further characterized by a round lateral margin of the external nares. In contrast, the lateral margin of the external nares is downcurved in the "Stuttgart morph" and African and Israeli forms. The latter state is apparently primitive, because it can be seen widely in Elephantoidea. The "Stuttgart morph" may also be distinguished from the "*namadicus* morph" in the inclination of the facial-parietal plane and anterodorsal plane of premaxilla. Unfortunately, the inclination of the face is apt to be altered drastically by postmortem distortion, so, not yet having been carefully examined on original specimens, this character is not employed in this analysis.

There appears to be some sexual dimorphism in the "*namadicus* morph" (Figure 9.8). In a cranium described by Falconer and Cautley (1846), the overhang of the parietofrontal crest is weaker than what is seen in the cranium from Godavari, India (Pilgrim 1905). As the tusk of the former skull is considerably smaller than that of the latter, it is likely a female, while the latter is probably a male. Thus, the difference observed between the two is likely the result of sexual dimorphism. However, the morphology of the parietofrontal crest in the female is fundamentally similar to that of the male. In both of them, a strongly expanded anterior surface of the nuchal plane can be seen in frontal view, and a superior nuchal crest runs along the ventral margin of the strongly overhanging parietofrontal crest. Strong rugosity along the middle part of the nuchal crest possibly represents the attachment surface of nuchal muscles rather than muscles of proboscis, contra Palombo et al. (2003). A similar rugosity is present on the "Stuttgart morph" cranium, but it is located more dorsally (Figure 9.8). Consequently, in this morph, the nuchal plane cannot be seen in frontal view of the skull. Sexual dimorphism in the "Stuttgart morph" is best observed in *Elephas naumanni*.

Though the cranial morphology of the "Stuttgart morph" and the "*namadicus* morph" can be distinguished from each other, at present no distinguishing character has been found in their dentitions. In the section that follows, distribution of these morphs is examined through the revision of previously described cranial materials from Eurasia.

Spatiotemporal Distribution and Evolutionary History of Subgenus *Palaeoloxodon* in Eurasia

As discussed previously, the most primitive morphology of Eurasian subgenus *Palaeoloxodon* is currently known from the Gesher Benot Ya'aqov cranium. The "Stuttgart morph" and the "*namadicus* morph" are known from several crania at various localities.

In Europe, both the "Stuttgart morph" and the "*namadicus* morph" are found. A cranium (SMNS Nr. 32888) from the travertine in Bad Cannstatt, Stuttgart, Germany

EBSCOhost - printed on 10/28/2022 4:53 AM via . All use subject to https://www.ebsco.com/terms-of-use

(Figure 9.8) presents the weak development of the parietofrontal crest associated with the "Stuttgart morph" of the skull of Eurasian *Palaeoloxodon*. The travertine of the Bad Cannstatt, Stuttgart, has been correlated with the Holsteinian (Reiff 1986), which, according to recent revisions on the chronostratigraphy of the middle Pleistocene of central Europe, can be correlated with marine isotopic stage (MIS) 11 (Turner 1998; de Beaulieu et al. 2001). Therefore, SMNS Nr. 32888 is the oldest well-preserved skull of the subgenus *Palaeoloxodon* from Europe currently available for study. Two well-preserved crania (SMNS Nrs. 15930 and 15344; Figure 9.7) with the same morphology are known from Steinheim am der Murr, Germany, and were housed in Württembergische Naturaliensamlung, Staatliches Museum für Naturkunde, Stuttgart (Osborn 1942). These were originally reffered to as *Palaeoloxodon antiquus germanicus* by Osborn (1942). The layer that yielded these is also attributed to the Holsteinian (Adam 1985; Schreve and Bridgland 2002). Unfortunately, these specimens were all but destroyed during World War II bombings, and all that remain today in SMN are a few charcoaled cranial fragments and the upper molars. Judging from illustrations and the remaining part of the right margin of the parietofrontal surface, there was no developed parietofrontal crest overhanging the external nares.

Fairly complete crania of subgenus *Palaeoloxodon* have also been found from Italian middle Pleistocene beds. Among them, the La Polledrara di Cecanibbio is outstanding (Figure 9.8). Complete crania of elephants associated with numerous animal bones and artifacts are found at this locality from a bed correlated to MIS 9 (Palombo et al. 2003). The crania are still not described in detail, but they are identified as *(P.) antiquus* (Palombo et al. 2003). They are almost identical to a male skull (Figure 9.8) described by Pilgrim (1905) as *(P.) antiquus (namadicus)* from Godavari, India, in their extremely developed parietofrontal crest, which overhangs the external nares. The same specialization marks a cranium from Fonte Campanile (Viterbo), Italy (Trevisan 1947). This specimen is the part of a complete skeleton of "*Elephas antiquus*" and shows extreme shortening of the frontoparietal region and an associated strong development of the parietofrontal crest. In a cranium from Pian dell'Olmo, Italy (Figure 9.7), the parietofrontal crest is less developed than in the two examples, but its nuchal plane can be seen in anterior view to be similar to these two examples (Maccagno 1962). Pian dell'Olmo is also correlated to MIS 9 (Palombo et al. 2003). Most of the Mediterranean island dwarf elephants derive from palaeoloxodont species from the mainland (Palombo 2004). *Elephas (P.) "mnaidriensis"* from Sicily is known from a considerable collection of skeletal materials, including complete crania (Palombo 2004). Though the species is about 30–40 percent smaller than the mainland form in linear measurements (Palombo and Ferretti 2005), its skull is very similar in showing strong development of the parietofrontal crest. Thus it can be also grouped into the "*namadicus* morph."

Thus, Italian "*Elephas antiquus*" is characterized by a highly developed parietofrontal crest and extreme shortening of the frontoparietal surface (Palombo et al. 2003). However, different authors interpret the taxonomic implications of these features differently. Based on the comparison with the skull of *E. "mnaidrensis"* from Sicily, Pilgrim (1905) assumed that a complete skull of "*E. antiquus*," which was not known at that time, would be similar to that of *E. namadicus* from India. Based on this assumption, he suggested that "*E.*

EBSCOhost - printed on 10/28/2022 4:53 AM via . All use subject to https://www.ebsco.com/terms-of-use

antiquus" was conspecific with *E. namadicus* and allocated his new specimen from Godavari to *E. antiquus (namadicus)*. For him the Indian form was a subspecies of "*E. antiquus*" though the description of "*E. antiquus*" postdated to that of *E. namadicus*. Azzaroli (1966) did not consider *E. namadicus* to be conspecific with "*E. antiquus*," though he admitted a close similarity between them in cranial morphology. Maglio (1973) suggested a close relationship between the Indian *E. namadicus* and an "undescribed" cranium from Pian dell'Olmo, Italy (Maglio missed that the skull had already been described by Maccagno in 1962), and argued that "*E. antiquus*" should become a junior synonym of *E. namadicus*. Recently Palombo et al. (2003) rebutted this idea based on the difference between European and Asian subgenus *Palaeoloxodon* species in molar features and presumed migration routes from Africa, but they do not provide sufficient empirical evidence for their argument.

Conversely, almost all *Palaeoloxodon* from India have been allocated to *Elephas (P.) namadicus*, though both "Stuttgart" and "*namadicus*" morphs have been found from the Indian subcontinent. As previously mentioned, Pilgrim (1905) allocated the specimen from Godavari to *E. antiquus (namadicus)*. However, he correctly suggested that this specimen shared some characteristics with the type cranium of *E. namadicus* (BMNH M3092) described by Falconer and Cautley (1846). Both present a strong parietofrontal crest, falling into the "*namadicus* morph." The parietofrontal crest of BMNH M3093, which is also described in Falconer and Cautley (1846), is weak, but it could be due to its young individual age. However, the cranium (No. G/336) from Hoshangabad, depicted in Sahni and Khan (1988: figures 85 and 86), appears to be an old individual, though its parietofrontal crest is very weak. Thus the "Stuttgart morph" appears to also have existed on the Indian subcontinent. Unfortunately we do not know their detailed stratigraphic level.

Dubrovo (1960) described a new species *(Palaeoloxodon) turkmenicus* based on cranial remains associated with a partial skeleton from Turkmenistan. The mid-facial part of the skull was badly damaged during the excavation, but it is clear that the parietofrontal crest is not strong. The skull of *(P.) turkmenicus* obviously belongs to the "Stuttgart morph."

Wei (1976) reported a fine cranium of *(Palaeoloxodon) namadicus* from Nihewan, Hebei Province, China (IVPP V.4443). It is very similar to *(P.) antiquus* from the middle Pleistocene site La Polledrara di Cecanibbio, Rome, Italy (Palombo et al. 2003) and those of *(P.) namadicus* from India (Falconer and Cautley 1846; Pilgrim 1905). The cranium from Nihewan suggests that the "*namadicus* morph" enjoyed a wide distribution in Eurasia. This specimen was originally said to have been excavated from the early Pleistocene Nihewan Beds (Wei 1976), but the specimen is now believed to have been found from the late Pleistocene terrace deposits of the area (Qi 1999; Takahashi and Namatsu 2000). Besides this cranium, none of the palaeoloxodont crania known from China have the upper half of the facial part of the skull preserved. However, the former presence of the "Stuttgart morph" in East Asia can be inferred from *Elephas (P.) naumanni* from Japan. Though some authors doubt its specific status (e.g., Osborn 1942; Maglio 1973), *E. (P.) naumanni* is a bona fide species diagnosed by several derived features (see the following section). The parietofrontal crest is weak, and therefore *E. (P.) naumanni* can be classified as belonging to the "Stuttgart morph." In Japan, *E. naumanni* has been known from a horizon younger than MIS11, and the ancestor of *E. naumanni* appears to have emigrated from the mainland to Japan prior

EBSCOhost - printed on 10/28/2022 4:53 AM via . All use subject to https://www.ebsco.com/terms-of-use

to MIS 12 (Konishi and Yoshikawa 1999). Therefore, cranial morphology of *E. naumanni* suggests the former presence of the "Stuttgart morph" and the "*namadicus* morph" on the mainland of eastern Asia prior to MIS 12.

Examination of the examples of subgenus *Palaeoloxodon* crania from Eurasia presented above suggests that both "Stuttgart" and "*namadicus*" morphs were widely distributed throughout Eurasia. There are three scenarios that could explain the distribution pattern of these two morphotypes. The first is that they merely reflect individual, sexual, or ontogenetic variation seen in a species. Maglio (1973) has suggested that all the palaeoloxodont species from Eurasia belong to single species *Elephas (P.) namadicus*. The second scenario is that "Stuttgart" and "*namadicus*" morphs may represent two distinct taxa. Under this scenario, the "*namadicus* morph" would have been derived from the "Stuttgart morph" and would have subsequently replaced it nearly completely, except for populations isolated on islands like Japan. The third possibility is again that the "Stuttgart" and "*namadicus*" morphs represent two taxa, but that the "*namadicus* morph" was derived from the "Stuttgart morph" but failed to replace it completely. The latter mainly occupy the southern half of the whole distributional area of palaeoloxodonts in Eurasia.

The first hypothesis is the least plausible considering the great morphological difference between the two morphotypes. Such differences cannot be entirely attributed to either sexual dimorphism or ontogenetic change because both morphs are known from crania of matured males and females. The extent of the sexual dimorphism in the parietofrontal crest in the "Stuttgart morph" can be examined in a pair of female and male skulls of *(Palaeoloxodon) naumanni* from Japan. They are not known from the same locality, but the chronological interval between them is short enough to allocate them to the same group (see the following section). The sexual dimorphism of the parietofrontal crest observed in them is far weaker than differences between the "Stuttgart" and "*namadicus*" morphs. Therefore, taxonomic distinction seems to be warranted for these two morphotypes.

If the difference observed between the two morphotypes is enough to warrant specific distinction, then when and how did they differentiate into two separate taxa? A male cranium from Pian dell'Olmo, Italy, may elucidate this transition. In this cranium, the upper and anterior portion of the nuchal plane can be observed in frontal view, but the extent of the overhanging of its parietofrontal crest is weaker than in the crania from La Polledrara di Cecanibbio (Palombo et al. 2003), Godavari (Pilgrim 1905), and Nihewan (Wei 1976). Thus it may represent an early member of the "*namadicus* morph." If this is the case, the "*namadicus* morph" diverged from the "Stuttgart morph" during or slightly before the MIS 9. Crania from Steinheim and Stuttgart, Germany, comply with this speculation because they show a weak parietofrontal crest and date to MIS 11.

As explained, there are two possibilities for what happened after the speciation of the "*namadicus* morph" (or *Elephas [Palaeoloxodon] namadicus*). One is that derived *E. (P.) namadicus* replaced the "Stuttgart morph" completely. If this speculation is correct, palaeoloxodonts older than MIS 10 should be allocated to *E. (P.) antiquus* and those younger than MIS 10 to *E. (P.) namadicus*, irrespective of their geographic location. The likelihood of this scenario is inferred from a "*namadicus* morph" skull from Nihewan, Northern China. As mentioned, this cranium

EBSCOhost - printed on 10/28/2022 4:53 AM via . All use subject to https://www.ebsco.com/terms-of-use

is now considered to have come from late Pleistocene terrace deposits (Wei 1976), which would suggest a wide distribution of the "*namadicus* morph" during the late Pleistocene.

Younger dates for *Elephas (Palaeoloxodon) naumanni* (see the following section), which belongs to the "Stuttgart morph," may contradict this, but it can be addressed by their probable emigration to Japan before the speciation and dispersal of *E. (P.) namadicus*, where they would have been protected from subsequent replacement by isolation. This idea would also explain the contemporaneous existence of the *namadicus* morph in the late Pleistocene of North China (Wei 1976). Isolation of the subgenus *Palaeoloxodon* population is highly plausible because other mammalian fossils of the age suggest that Japanese fauna was isolated from the mainland during most of the late Pleistocene (Kawamura 1998). The only contradicting evidence against this explanation is the report of occurrences of molars of *E. (P.) naumanni* from the late Pleistocene of North China. Final word on this awaits detailed work on the taxonomy and chronology of these specimens (Takahashi and Namatsu 2000).

In a third possible scenario, ancestral "Stuttgart morph" and "*namadicus* morph" *(Elephas [Palaeoloxodon] namadicus)* coexisted but were distributed in different areas. This type of coexistence has recently been recognized in *Mammuthus* evolution (Lister et al. 2005). As the evidence currently available is very sparsely distributed across Eurasia, it is impossible to completely rule out the possibility of the contemporaneous existence of these two forms.

Given the currently published morphological and geological evidence, it is hard to judge which of these two contradictory hypothesis is the more viable. However, undescribed material that might address these issues does exist. Recently, fairly complete skeletons of *(Palaeoloxodon) antiquus*, including intact crania, have been recovered from Gröbern and Neumark Nord, Germany (Fischer 2004). Gröbern and Nuemark Nord are correlated to MIS 5 and MIS 7 respectively (Brühl and Mania 2003; Fischer 2004). These sites are geologically younger than Italian sites with crania of the "*namadicus* morph." Detailed description of these remains from Germany is still in progress. Once it is completed, we should know a great deal more about cranial morphology of European palaeoloxodonts younger than the MIS 9, as well as the individual variation of the skull. If they are of the "Stuttgart morph," the second scenario mentioned above—the complete replacement of "Stuttgart" by "*namadicus*"—will be completely rejected.

Notes on *Elephas (Palaeoloxodon) naumanni*

Osborn (1942) and Maglio (1973) allocated all of the elephantid specimens from the Japanese Pleistocene into *(Palaeoloxodon) namadicus*. Dubrovo (1981) admitted the validity of *(P.) naumanni*, but she allocated all of the elephantids' specimens from Japan into this species, and on this basis she argued that the range of Japanese subgenus *Palaeoloxodon* extends to the early Pleistocene. It was legitimate to synonymize all of the Japanese Pleistocene elephants into a single species given the previous confusion of the classification of Japanese fossil elephants. During the 1920s and 1930s numerous species and subspecies were erected based on single and occasionally rather fragmentary specimens. However, since the early 1970s, Japanese fossil

EBSCOhost - printed on 10/28/2022 4:53 AM via . All use subject to https://www.ebsco.com/terms-of-use

elephants from the Seto Inner Sea and from Nojiri-ko have been revised on the basis of dental variability (Kamei and Taruno 1972; Takahashi and Mazima 1991). Male and female crania recovered from downtown Tokyo have also been analyzed (Inuzuka 1977a, b; Hamacho Naumannzou Kennkyu Gurupu 1978). As a result of these revisions and descriptions, all of the middle and late Pleistocene elephants of Japan are now grouped into *E. (P.) naumanni* (Makiyama 1924).

On the other hand, elephants from the early Pleistocene of Japan are best allocated to *Mammuthus protomammonteus* (Matsumoto 1924) rather than *(Palaeoloxodon) naumanni* (Takahashi and Namatsu 2000; Lister et al. 2005). The taxon *M. protomammonteus* is an endemic species of *Mammuthus* characterized by relatively small overall dimensions and a narrow width of the crown (Matsumoto 1924; Takahashi and Namatsu 2000; Lister et al. 2005).

Anatomical features and chronostratigraphic distribution of *Elephas (P.) naumanni* are fairly well known. *E. (Palaeoloxodon) naumanni* is a legitimate species diagnosed by several derived features, including smaller body size compared to mainland forms, an extremely shortened symphysis, and twisted tusks (Hasegawa 1972; Inuzuka 1977a, b; Dubrovo 1981; Inuzuka 1991a, b; Takahashi et al. 1991; Takahashi and Namatsu 2000). *E. naumanni* is further diagnosed by the angulus of the posterior ramus of the stylohyoid (Inuzuka et al. 1975), a feature not shared with subgenus *Palaeoloxodon* from Gesher Benot Ya'aqov (Shoshani et al. 2001) and Bad Cannstatt, Stuttgart. The parietofrontal crest of *E. naumanni* is weak, and therefore the skull of *E. (P.) naumanni* can be classified as belonging to the "Stuttgart morph" established in this chapter.

The holotype of *(Palaeoloxodon) naumanni* was excavated from the Sahama Mudstone Member of the Hamamatsu Formation, which is assigned to the later half of MIS 7 (Sugiyama 1991). Crania from males and females of this species are known from the upper part of the Kamiizumi Formation in Saruyama, Chiba, and the lower part of the Tokyo Formation in downtown of Tokyo, respectively (Omori et al. 1971; Hamacho Naumannzou Kennkyu Gurupu 1978; Nakazato 1993; Port of Tokyo Geological Research Group 2000a). The lower part of the Tokyo Formation can be correlated to the interval between MIS 7.5 and 7.4, while the upper part of the Kamiizumi Formation correlates to the interval between MIS 8 and 7.5 (Port of Tokyo Geological Research Group 2000b; Nakazato 2001; Nakazawa et al. 2003). Therefore, these crania are penecontemporaneous with the holotype of the species. Besides these sites with more complete specimens, *Elephas naumanni* has been reported from nearly every corner of the Japanese Island, including the most northern island Hokkaido, and all of the findings are confined to the interval between MIS 10 and MIS 2. The ancestor of *E. naumanni* appears to have emigrated from the mainland to Japan before MIS 12 (Konishi and Yoshikawa 1999). Though the presence of *E. naumanni* in northern China has been suggested, genuine *E. naumanni* have only been reported from Japan.

Elephas (Palaeoloxodon) namadicus has been referred to as the type species of subgenus *Palaeoloxodon* in previous works (Aguirre 1969c; Beden 1979, 1983, 1987) because *(P.) naumanni* has been restricted to the status of junior synonym to *E. (P.) namadicus* (Aguirre 1969c; Maglio 1973; Beden 1979, 1983, 1987). However, such reference to the type species of subgenus *Palaeoloxodon* is no longer valid, since the specific status of *E. (P.) naumanni* is now confirmed. The species *E. (P.) naumanni* is an appropriate representative

EBSCOhost - printed on 10/28/2022 4:53 AM via . All use subject to https://www.ebsco.com/terms-of-use

of the clade *Palaeoloxodon* because its anatomical features are very well known. The only difficulty in using *P. naumanni* as the specifier of the stem-based clade *Palaeoloxodon* is that most of the publications on this species are written in Japanese and have not been translated into more universally understood communication formats. Thus, the stem-based taxon name *Palaeoloxodon* can be defined as *E. (P.) naumanni* and all taxa sharing a more recent common ancestor with *E. (P.) naumanni* than with *E. maximus*.

Later African *Palaeoloxodon*

In the foregoing discussion we concentrated mostly on the problems of Eurasian subgenus *Palaeoloxodon*. However, the problem of Eurasian palaeoloxodonts must be closely linked to the validity of *Elephas iolensis* and *E. zulu* and also to the demise of palaeoloxodont species in Africa.

Some elephant fossils retrieved from the beds younger than the early Pleistocene have been attributed to *Elephas iolensis* and *E. zulu* or other species of *Palaeoloxodon* (Beden 1979, 1983, 1987; Todd and Roth 1996). They are said to be distinct from *E. recki recki* in more derived dental traits, but they have never been meticulously compared with Eurasian subgenus *Palaeoloxodon* species. There remains some possibility that so-called *E. iolensis* and *E. zulu* are actually conspecific with some Eurasian palaeoloxodont species. This naturally leads to the question of the date of the last palaeoloxodont specimens in Africa. In Europe, subgenus *Palaeoloxodon* is extinct before ca. 20 Ka (Stuart 2005), while in Japan *E. (P.) naumanni* became extinct during the last glacial maximum (Konishi and Yoshikawa 1999). If African and Eurasian populations were continuous, the extinction of palaeoloxodonts might also be later in Africa, possibly during the late Pleistocene. These issues are closely connected to the phylogeography of the African elephant, which is the subject of recent debate (Roca et al. 2001; Eggert et al. 2002; Debruyne 2005). Migration and differentiation of the African elephant might be connected with the extinction of *E. recki* or a related form, which occupied the open habitat where *Loxodonta africana* dominates today.

Conclusions

The sample of elephant molars from the Daka Member is small, but it is sufficient to suggest that they belong to the derived group of *Elephas recki*, which includes the type of *E. r. recki* of Beden (1983). *Elephas* from the Daka Member is identified as an early representative of *E. r. recki*. The finding of cranial materials of *E. recki* from Daka sheds new light on the origin and emigration of palaeoloxodonts to Eurasia, contradicting ideas on the timing of the dispersal of palaeoloxodont species from Africa to Europe proposed by Maglio (1973) and Beden (1983, 1987). Cranial remains from the Daka Member show several derived features previously known exclusively from Eurasian palaeoloxodonts. This, coupled with the early geological age of the Daka Member (this being the earliest specimen of Eurasian subgenus *Palaeoloxodons*), suggests that the immigration of palaeoloxodonts from Africa to Eurasia took place at around 1.0 Ma. Cranial remains from the Daka Member represent the immediate outgroup of Eurasian palaeoloxodonts.

EBSCOhost - printed on 10/28/2022 4:53 AM via . All use subject to https://www.ebsco.com/terms-of-use

Comparison of cranial materials from Eurasia suggests the derivation of *E. (P.) namadicus* from the palaeoloxodonts represented by a cranium from Stuttgart (Stuttgart morph). European palaeoloxodonts have been attributed to "*E. (P.) antiquus*," but they appear to be a mixture of *E. (P.) namadicus* and "Stuttgart morph" palaeoloxodonts.

EBSCOhost - printed on 10/28/2022 4:53 AM via . All use subject to https://www.ebsco.com/terms-of-use

10

Rhinocerotidae

W. HENRY GILBERT

Living rhinos are extremely rare and threatened with extinction, but they are the survivors of a once broadly distributed and extremely diverse clade. Rhinos are known from North America and the Old World and have a well-documented fossil record (Prothero et al. 1989). Rhinocerotidae is first reported from the Eocene, and representatives of the family persist through the remaining Cenozoic. Different rhino taxa occupied many different niches. Taxa included small, cursorial forms as well as giraffe-like canopy browsers (Prothero et al. 1989). Modern genera have not changed dramatically since their first appearances in the Pliocene. Daka Member rhinos are attributed to *Ceratotherium* (the white rhino) and *Diceros* (the black rhino).

Tougard et al. (2001) estimate the divergence of Rhinocerotidae from other Perissodactyla to have occurred around 29.0 Ma based on analysis of mitochondrial cytochrome *b* and 12S rRNA genes. The earliest known fossil rhinos, genus *Teletaceras*, occur in the early Eocene of North America and, debatably, Asia (Cerdeño 1998). This genus is present in Asia by later Eocene times. Numerous genera appear in the Oligocene of North America and Eurasia. The first African rhinos occur in the early Miocene, and the lineage that would eventually lead to the modern African genera is first recorded in the middle Miocene with the genus *Paradiceros*. The two modern African lineages, genera *Diceros* and *Ceratotherium*, are first reported from the late Miocene, and they are suggested to have diverged close to this time (Geraads 1988, 2005). The modern species may have already been established in the Pliocene (Cerdeño 1998).

There are five modern rhino species. The grazing, square-lipped "white" *(Ceratotherium simum)* and the browsing, pointed-lipped "black" *(Diceros bicornis)* rhinoceroses are African. The Indian *(Rhinoceros unicornis)*, Javan *(R. sondaicus)*, and Sumatran *(Dicerorhinus sumatrensis)* rhinoceroses are Asian. Molecular phylogenetic analyses indicate that the African rhinos are more closely related to each other than either is to Asian genera (Tougard et al. 2001), a claim supported by morphological data (Hooijer 1969).

Ceratotherium and *Diceros*

The first appearance of *Ceratotherium* is in the upper Miocene of Pikermi, Greece (Geraads 1988, 2005). The earliest African *Ceratotherium* is *C. neumayri* from Sahabi (Bernor et al. 1987). *Ceratotherium* is the sole grazer among living rhinos. Morphological differences

EBSCOhost - printed on 10/28/2022 4:53 AM via . All use subject to https://www.ebsco.com/terms-of-use

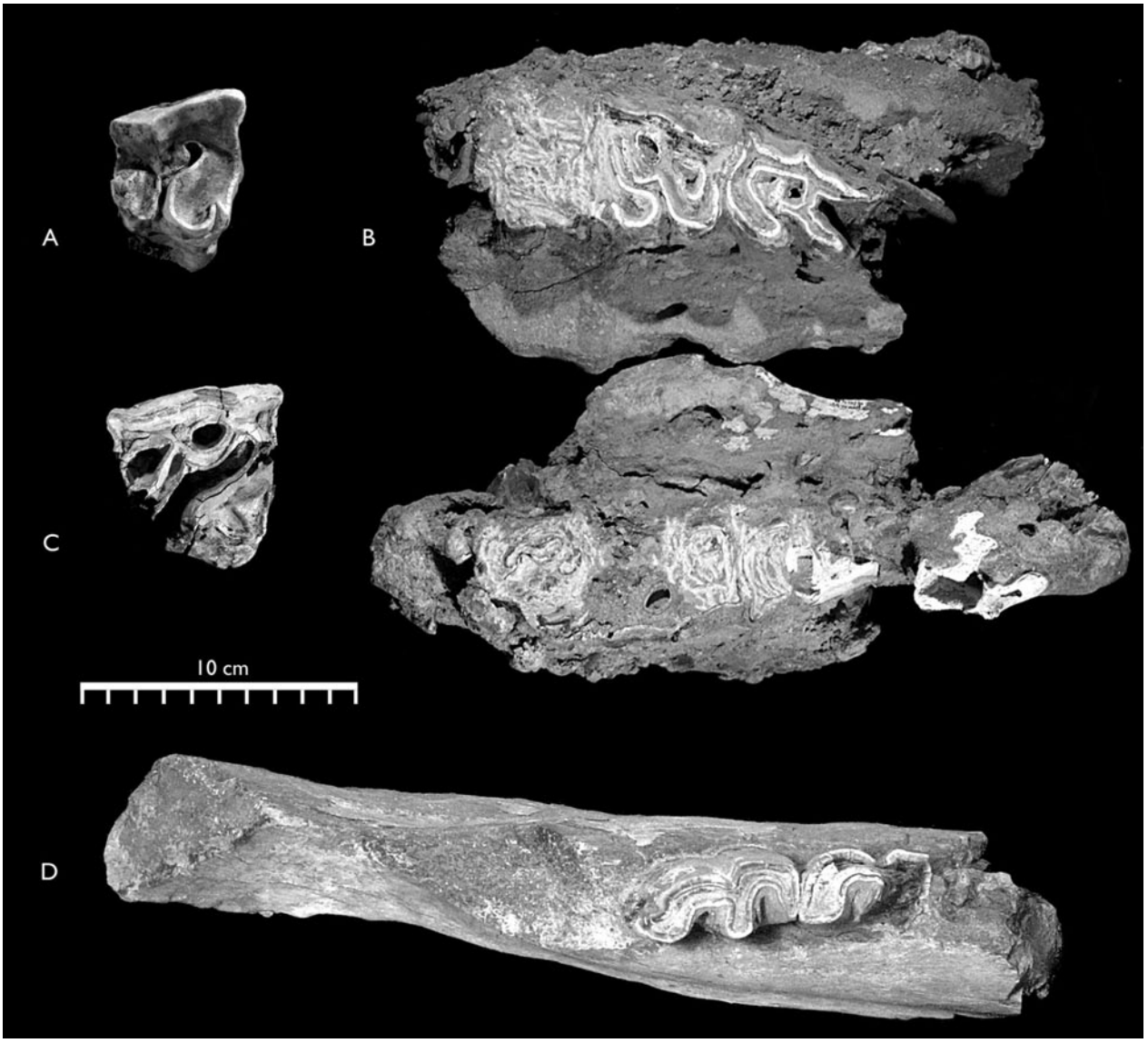

FIGURE 10.1

Daka Rhinocerotidae. A. BOU-VP-4/36, *Diceros* sp. RM^1 or RM^2. B. BOU-VP-4/55, *Ceratotherium simum* maxilla with R dp^4–M^3 and L dp^4–M^2 (exposed LM^1 or LM^2). C. BOU-VP-1/89. *C. simum* RM^2. D. BOU-VP-1/116, *C. simum* left mandible with M_2 and M_3.

between it and *Diceros* have been associated with its unique ecology (Kingdon 1989a). *Ceratotherium* has a broad, less prehensile lip, a wide mouth, a longer head, and more hypsodont teeth. *Ceratotherium* further differs from *Diceros* in the following dental features: The first upper premolar is shed early and is not present in mature individuals; upper premolars differ strikingly from upper molars; the premolar medivallum is rapidly enclosed with wear by fusion of the protocone and hypocone; premolar protoloph is arcuate and curved posteriorly; the parastyle is more pointed and not apparently grooved; the postfossette becomes isolated with wear; and the metaflexid is persistent through wear (Cooke 1950).

One *Ceratotherium simum* (KNM-ER 2320) is first recognized in the sub-KBS units at Koobi Fora (Harris 1983). It is distinguished from its closest sister species, *C. praecox*,

EBSCOhost - printed on 10/28/2022 4:53 AM via . All use subject to https://www.ebsco.com/terms-of-use

TABLE 10.1 Daka Rhino Dental Metrics

Specimen	*Element*	*Wear (1–5)*	*Anterior Labiolingual Breadth*	*Mesiodistal Length*	*Ectoloph Height*	*Posterior Labiolingual Breadth*
BOU-VP-4/36	M.[1 or 2]	4 1/2	61.3	52.2	32.5	49.7
BOU-VP-4/55	R. dP^4	5	37.4e	51.5e		50.8e
BOU-VP-4/55	R. M^1	2	42.7e	44.6	49.3e	30.3
BOU-VP-4/55	R. M^2	2	33.8	47.4	62.3e	22.9
BOU-VP-4/55	R. M^3	1	22.8			
BOU-VP-4/55	L. dP^4	5	54.6	41.4		41.8e
BOU-VP-4/55	L. M^1	2	43.1	44	48.2e	32.6
BOU-VP-4/55	L. M^2	2	32	48.4e	61e	26.8
BOU-VP-1/89	R. M^2	2	57.9	66.8	70.6e	44.1e
BOU-VP-1/89	R. M^3	2	37.4	44.4	85.4e	
BOU-VP-1/72	L. M_3	2	23.8	57.4		
BOU-VP-1/116	L. M_3	2	21.2	52.7		

NOTE: Metrics are in millimeters. e = estimate.

by the following features: presence of medifossettes, rounded corners of upper teeth, no fossettids in the lower dentition, less hypsodont cheek teeth, and variable internal cingula on uppers (Hooijer and Patterson 1972). Four subspecies of *C. simum* have been named. Two are prehistoric: *C. s. germanoafricanum* from eastern and southern Africa, and *C. s. mauritanicum* from the Maghreb. Two subspecies are extant, *C. s. cottoni* of central Africa and *C. s. simum* of southern Africa (Prothero et al. 1989).

Ceratotherium simum (Burchell, 1817)

DIAGNOSIS "Skull markedly dolichocranial, with backwards leaning occipital crest; no incisors or canines; jaws abbreviated in front; mandibular symphysis broad, spatulate; nasal bones broad, short, high; ascending ramus of mandible backwards-leaning; no marked angulation at gonion. Cheek teeth hypsodont; protoloph and metaloph strongly curved back, showing early fusion with wear; much cement on crown" (Harris 1983, 132).

DESCRIPTION Nonjoining right and left halves of maxilla BOU-VP-4/55 (Figure 10.1 B) preserve dp^4–M^3 on the right and dp^4–M^2 on the left. Alveolar and palatal bone is preserved on both sides, and unerupted premolars are detectable below the broken alveoli. Partial mandible BOU-VP-1/116 (Figure 10.1D) preserves the M_3, part of the M_2, and much of the corpus. Dental specimen BOU-VP-1/89 (Figure 10.1C) consists of associated right and left upper molars. Other specimens are isolated teeth.

DISCUSSION These specimens are placed in *Ceratotherium* because of their isolated postfossettes, enclosed medivalli, pronounced metaflexids, and overall morphological similarity to the modern form. They are placed in *C. simum* based on the presence of medifossettes and rounded corners in upper molars and premolars. Dental metrics (Table 10.1) are similar to those reported for Koobi Fora *C. s. germanoafricanum* and recent *C. simum* (Harris 1983). Morphological features diagnosing *C. simum* subspecies, many of which pertain to cranial vault metrics (Harris 1983), are not preserved in the small Daka sample.

EBSCOhost - printed on 10/28/2022 4:53 AM via . All use subject to https://www.ebsco.com/terms-of-use

Diceros Gray, 1821

GENERIC DIAGNOSIS "Premaxilla absent or vestigial; cranium short and relatively broad; neurocranium tilted anterodorsally relative to splanchnocranium, resulting in more vertically oriented occipital plane or even one inclined anterodorsally, nuchal crest less expanded posteriorly, more deeply concave cranial profile, basioccipital angled relative to basisphenoid, shortened face with orbits more anteriorly positioned and closer to nasal notch, and often nasolacrimal contact" (Geraads 2005).

Diceros sp.

Diceros upper molars and premolars differ from those of *Ceratotherium* in being less hypsodont. *Diceros* protolophs and metalophs do not join lingually, even in late stages of wear. The prefossette, medifossette, and medivallum are connected, opening lingually. The metacone forms a posterior projection that makes no lingual connection with the hypocone, as occurs with moderate wear in *Ceratotherium*. The *Diceros* occlusal outline of the protoloph, ectoloph, and metaloph presents a pattern similar to the Greek letter pi. Upper third molars are less mesiodistally elongate than in *Ceratotherium*.

Only one specimen from the Daka Member is referred to *Diceros*. Upper molar BOU-VP-4/36 (Figure 10.1A) is very highly worn. It has a separated protoloph and metaloph with prefossette, medifossette, and medivallum that open lingually. These characters are typical for *Diceros*.

Conclusion

Ceratotherium simum, a grazer, and *Diceros bicornis*, a browser, are both present in the Daka Member. *Ceratotherium simum* is represented by a mandible, a maxilla, and several dental specimens and is not demonstrably different from Pleistocene and recent *C. simum*. Daka Member *Diceros* is represented by a single upper molar.

EBSCOhost - printed on 10/28/2022 4:53 AM via . All use subject to https://www.ebsco.com/terms-of-use

11

Suidae

W. HENRY GILBERT

The Daka Member presents an important assemblage of African suid fossils from approximately 1 Ma. With three nearly complete crania, several more fragmentary crania, and numerous dental specimens, it is one of the best samples of *Kolpochoerus majus* in the world. It also comprises a moderate sample of *K. olduvaiensis* and includes one of the only known complete crania of the taxon (Figures 11.1 and 11.2). *Metridiochoerus* (including *M. modestus*) is also present. Daka sediments also contain early *Phacochoerus*. The co-occurrence of *M. modestus* and *Phacochoerus* supports their taxonomic separation.

The taxonomic group Suina includes Suidae (pigs) and Tayassuidae (peccaries). Recent phylogenetic work has eliminated Hippopotamidae as a close relative to this group but has supported the sister-clade status of suids and tayassuids (Montgelard et al. 1998; Boisserie et al. 2005b). Ancestors of Suidae and Tayassuidae first appear in the Oligocene (Cooke and Wilkenson 1978). Endemic suids are restricted to the Old World. It has traditionally been thought that Tayassuids are endemic to the New World, but more recent discoveries suggest their presence in Asia (Ducrocq 1994).

Suidae

There are five living genera of suids: *Sus*, *Potamochoerus*, *Hylochoerus*, *Phacochoerus*, and *Babyrousa* (Nowak 1991). *Sus* includes *S. scrofa* (the domestic pigs and the widespread wild boar), *S. barbatus* (the bearded pig of the Malay Peninsula, Borneo, Indonesia, and the Philippines), *S. celebensis* (the Celebes wild boar of Sulawesi), and *S. verrucosus* (the Javan pig). *Potamochoerus* has one modern species, the bushpig *(P. porcus)* of central Africa. *Hylochoerus*, the giant forest hog, has a single species, *H. meinertzhageni*, and is found in central Africa. *Phacochoerus* is represented by *P. aethiopicus*, the warthog. It ranges throughout sub-Saharan Africa. Finally, the unique *B. babyrousa* occurs on Sulawesi and nearby islands (Nowak 1991).

The first well-established suids are present in Eurasia by the early Miocene (van der Made 1990). Numerous forms are known from the Miocene, among them Tetraconodontinae and Suinae (van der Made 1990). Tetraconodontinae includes the *Nyanzachoerus*/*Notochoerus* group of Plio-Pleistocene Africa. *Nyanzachoerus* appears in Africa by 11.0 Ma and gives rise

EBSCOhost - printed on 10/28/2022 4:53 AM via . All use subject to https://www.ebsco.com/terms-of-use

FIGURE 11.1

Leslea Hlusko with *Kolpochoerus olduvaiensis* subadult cranium BOU-VP-3/150, eroding in situ from Daka Member sediments. View to the west is of the Bouri Ridge forming the horizon. Photographs by Tim White, December 1, 1999.

EBSCOhost - printed on 10/28/2022 4:53 AM via . All use subject to https://www.ebsco.com/terms-of-use

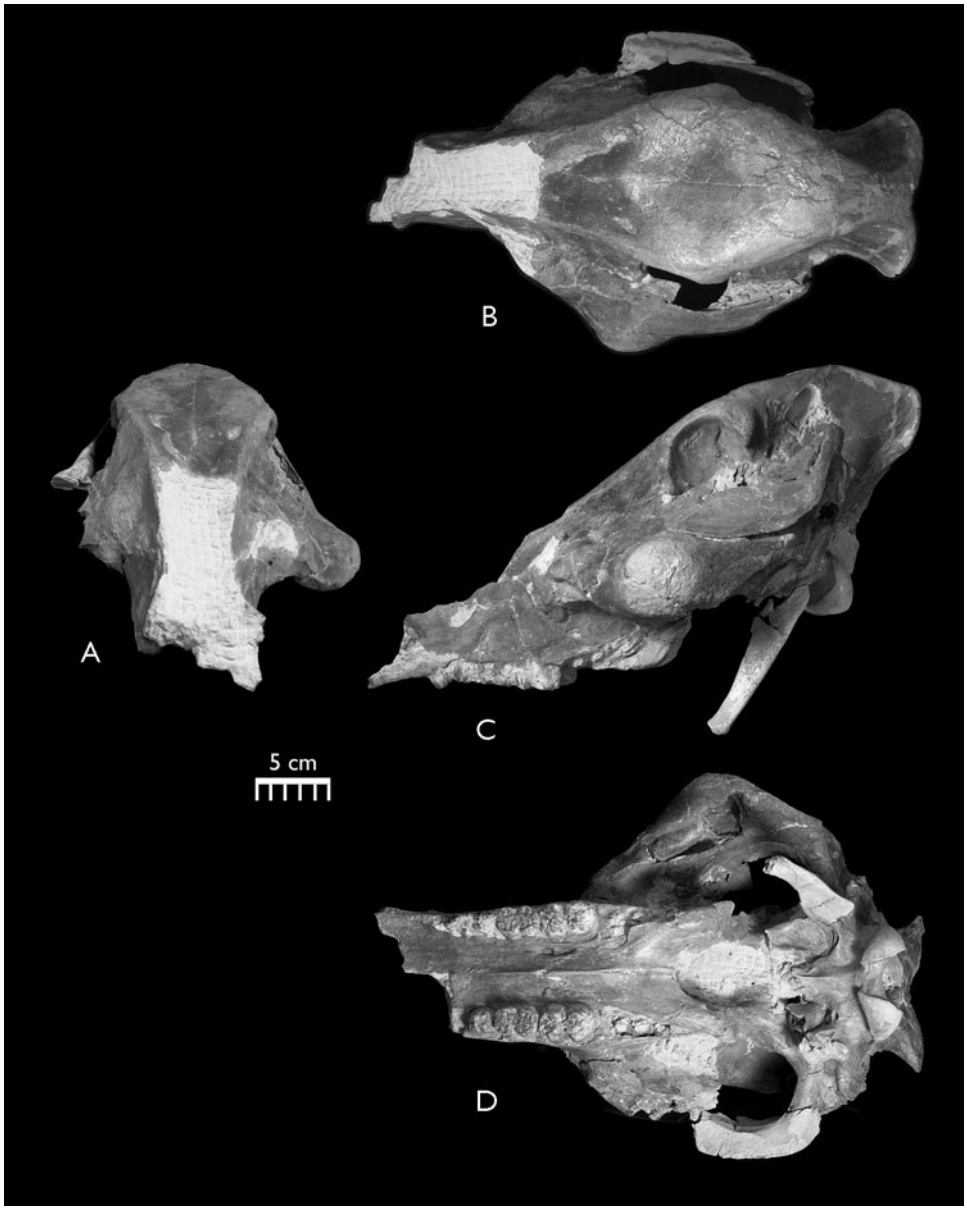

FIGURE 11.2
BOU-VP-3/150 *Kolpochoerus olduvaiensis* cranium. A. Anterior view. B. Dorsal view. C. Left lateral view. D. Basal view.

to the genus *Notochoerus* at about 3.5 Ma (White 1995). The latest *Notochoerus* representatives are found in Africa at the end of the Pliocene.

Suinae likely immigrated to Africa from Asia in or before the lower Pliocene (Brunet and White 2001). It is diagnosed by the development of a prezygomatic shelf and a flange, separating muscles of mastication from the proboscis musculature, that is likely associated with well-developed rooting behavior (Cooke and Wilkenson 1978; Kingdon 1979). This group includes all of the modern suid genera and, in Africa, the extinct genera *Metridiochoerus* and *Kolpochoerus*. After arriving in Africa in the Neogene, *Metridiochoerus*

EBSCOhost - printed on 10/28/2022 4:53 AM via . All use subject to https://www.ebsco.com/terms-of-use

and *Kolpochoerus* radiated during the Pliocene and early Pleistocene. Many taxa in these clades became extinct during the middle Pleistocene, but derived descendants of both lineages still exist. *Hylochoerus* is a probable *Kolpochoerus* descendant, and *Phacochoerus* is widely accepted as being derived from *Metridiochoerus* (Geraads 1993; White 1995; Cooke 1997).

Kolpochoerus

The diminutive early Pliocene *Kolpochoerus deheinzelini* is the earliest species of the genus and is found in both Chad and Ethiopia (Brunet and White 2001). Brunet and White suggest a possible relationship to the Miocene Asian genus *Propotamochoerus. Kolpochoerus deheinzelini* is the sole known representative of the genus in Africa for over 1 million years.

Kolpochoerus is well represented in Africa during the Pliocene and early Pleistocene. *Kolpochoerus afarensis*, the descendant of *K. deheinzelini*, is present during the middle and late Pliocene, and *K. cookei* is known from the late Pliocene at Omo (Brunet and White 2001). *Kolpochoerus limnetes* is present in the Pliocene and earliest Pleistocene of eastern and southern Africa. It is distinguished from its derived daughter taxon, *K. olduvaiensis,* by its shorter M3s. Konso-Gardula, Ethiopia, presents the best record of this transition (Suwa et al. 2003). *Kolpochoerus limnetes* occurs in interval 1 of Konso and is similar in morphology during this interval to *K. limnetes* of the upper Burgi Member of Koobi Fora and Omo Member G. *Kolpochoerus limnetes* is more advanced in Konso intervals 3, 4, and 5, and its morphology is intermediate between earlier *K. limnetes* and later *K. olduvaiensis*. *Kolpochoerus phacochoeroides* is the Plio-Pleistocene northern African sister taxon of *K. olduvaiensis*. Neither *K. phacochoeroides* nor *K. olduvaiensis* are represented after approximately 0.8 Ma. *Kolpochoerus majus* first appears at approximately 1.9 Ma at Konso and continues into the middle Pleistocene at numerous eastern African localities (White 1995; Suwa et al. 2003).

The following features diagnose *Kolpochoerus*: a mandibular body that bulges on its lateral margins, a developed protocone on upper premolars, and rooted, low crowned molars (Harris and White 1979). Two *Kolpochoerus* species occur in the Daka Member: *K. majus* and *K. olduvaiensis*.

Kolpochoerus olduvaiensis (Leakey, 1942)

DIAGNOSIS "A *Mesochoerus* in which the third lower molars have five pairs of lateral pillars instead of four and in which the second lower molars have only the most rudimentary of medial pillars in front of the anterior pair of lateral pillars. The enamel is covered with cement. The crowns of unworn molars are low, compared with those of the genotype, and average about 24 mm instead of 30 mm" (Leakey 1942, 179).

DESCRIPTION An immature, but very well-preserved *K. olduvaiensis* cranium, BOU-VP-3/150 (Figure 11.2), preserves nearly the whole cranium posterior to the canines. This cranium is described in great detail here because of its rareness. The canines, premaxilla, and nasals are missing, and there is some plastic deformation due to postdepositional distortion. The cortical bone is immature, presenting a woven texture in many areas.

EBSCOhost - printed on 10/28/2022 4:53 AM via . All use subject to https://www.ebsco.com/terms-of-use

A small portion of the posterior margin of the left canine socket is visible in BOU-VP-3/150. The broken root of the RP^2 is in line coronally with this posterior margin, and there is no trace of a P^1. Immediately behind the most posterior extent of the canine socket is a short, linear depression. It is approximately 2 cm in length and terminates beneath the anteroinferior extent of the infraorbital foramen. The foramen itself is an elongate oval, also about 2 cm long, and is oriented obliquely at an angle of approximately 45 degrees with the horizontal, with the anterior extremity inferior to the posterior. The nasals and frontal are broken above the foramen, and it is not possible to tell whether there is a *K. majus*–like maxillary concavity between it and the zygomatic root. The zygomatic root extends anteriorly in the area of the origin of the dilator naris lateralis muscle and levator rostri muscle farther than seen in *K. majus*, and the point where it begins to flare laterally is at approximately the coronal level of the anterior M^2.

The zygomatic arch between the knob and the maxilla is visor-like, with an extensive, planar anterior portion that faces anterolaterally and mostly superiorly. The zygomaticomaxillary suture is raised where the bone has knit together, and there is a pyramid-like projection on its anteroinferior extent. Viewed from an inferior perspective the suture extends posterolaterally and arcs posteriorly, defining the inferior zygomatic root for approximately 4 cm before crossing to the internal face of the zygomatic. A crest also extends almost directly lateral from the base of the previously discussed pyramid, then arches posterior to define the anterior edge of the zygomatic root when viewed from an inferior perspective. The two discussed arches are more or less parallel. The groove formed between the two is deeper along its anterior margin, and there is a slightly raised escarpment that runs anteroposteriorly when viewed from an inferior perspective. The escarpment separates the described sutural pyramid medially from the depths of the groove. From an anterior perspective the anterior crest extends laterally and then inferolaterally, disappearing from view under the medial portion of the zygomatic knob.

The portion of the zygomatic root along the superior portion of the anterior zygomaticomaxillary suture is inflated superior to the pyramid described in the previous paragraph, defining a broad depression between it and the more vertical portion of the maxillary wall. There is some distortion in this area on both the left and right sides. Viewed from a superior perspective the anterior margin of the zygomatic process is linear except for the area proximal to the pyramid, making an angle of approximately 45 degrees from the sagittal plane as it approaches the lateral tip of the zygomatic knob. The lateral extent of the knob is anterior to the forward extent of the zygomatic process of the temporal. Posterior to this point the lateral margin of the zygomatic bone turns slightly medial, becoming invisible from a superior perspective at the coronal level of the lower postorbital process. A substantial portion of the anterior zygomatic root forms a ceiling over the sagittally oriented maxilla adjacent to the M^2, although this portion of the bone is very damaged. There is a large sinus in the zygomatic, bounded superiorly by the jugal. The suture between the jugal and zygomatic is well separated in the specimen, although this is certainly affected by the young age of the individual.

The anterior margin of the orbit is oriented vertically when viewed from a lateral perspective and is entirely posterior to the unerupted M^3. There is a groove at the base of this vertical portion that separates it from the portion of the orbit bounded by the postorbital

EBSCOhost - printed on 10/28/2022 4:53 AM via . All use subject to https://www.ebsco.com/terms-of-use

process and a small bony eminence on the orbital rim superior to the groove. The lacrimal foramen is approximately 1 cm anterior of, and slightly superior to, this eminence. Another smaller groove separates the vertical portion from the even, horizontal arch of the superior orbit. The superior border of the inferior postorbital process is flat and makes an angle of approximately 30–40 degrees from the horizontal when viewed from a lateral perspective, rising posteriorly. It is very flat and thin in the oblique plane defined by the anterior surface of the zygomatic, although it is thicker toward the superior border than the posterior. The posterior border is also linear, the superior portion slightly more posterior than the inferior. The superior surface of the jugal makes an acute notch with the posterior border of the postorbital spike. Both come to a sharp crest along their margins. From the depth of this notch the anterosuperior portion of the zygomatic-temporal suture extends anterolaterally toward the superolateral margin of the zygomatic knob. The superior margin of the zygomatic process of the temporal arcs posterosuperiorly in a shallower curve than in the *K. majus* condition. Its posterior extremity comes to a point superiorly, projecting approximately 1 cm superior to the opening of the auditory meatus.

There are two large foramina in the frontal that occur in a plane slightly anterior to the vertical portion of the orbital margin. They are oval shaped, approximately 7 mm by 15 mm, and oriented so that the anterior portion is more medial than the posterior. Lines extending from the long axes of the pair of foramina would intersect at the midline approximately 25 mm anterior to their anteroposterior median. Two deep but gently concave grooves extend from the anterior portions of the foramina and arch anteriorly to become almost parallel where they cross the broken margin of the anterior frontal. Between the two foramina the frontal bulges along the midline, and posterior to this bulge the frontal is broadly and shallowly concave between the orbits. A distinct metopic suture spans the frontal, terminating at the coronal suture approximately 45 mm posterior to a coronal section through the superior postorbital process. The posterior aspect of the superior postorbital process is crested. This crest defines a broad groove between it and the sagittally oriented portion of the coronal suture in the temporal fossa of the frontal. The temporal lines are distinct, originating posterior to the previously described groove behind the orbit. Viewed from a superior perspective they converge posteriorly and are slightly more sagittally oriented than the coronal sutures. In a coronal plane in line with the auditory meati, the temporal lines arch posteriorly. The two temporal lines are approximately 37 mm apart at the anterior point where they become parallel. Posterior to this point the temporal lines flare slightly laterally. There is a distinct angle in each temporal line as it transitions into the nuchal crest.

The nuchal crest continues laterally, curving inferiorly and then medially again. The nuchal crest becomes broader inferior and subtly bifurcates, its anterior border projecting a narrow crest to the medial margin of the auditory meatus. This crest demarcates the posteroinferior border of the temporal fossa. The anterosuperior surface of the zygomatic process of the temporal is concave mediolaterally and is not as broad in this dimension as in *K. majus*. The occipital is concave superiorly between two bony alae defined by the nuchal crest. The posterolateral aspects of these alae are roughened where the semispinalis capitis muscle originates. The nuchal crest, as previously mentioned, bifurcates, and the posterior projection extends inferiorly and joins the lambdoidal suture. Inferior to a temporal plane through the meatus openings the lambdoidal suture runs inferiorly and somewhat

EBSCOhost - printed on 10/28/2022 4:53 AM via . All use subject to https://www.ebsco.com/terms-of-use

medially toward the lateral border of the foramen magnum. After approximately 20 mm it turns abruptly laterally, runs laterally and somewhat inferiorly for approximately 28 mm, then arcs inferiorly and medially toward the base of the paramastoid process.

The superior opening of the external auditory meatus is approximately 15 mm inferior to the superior projection of the zygomatic process of the temporal. A crest projects inferiorly and slightly laterally from its lateral margin, then arches medially toward the paramastoid process, nearly converging with the lambdoidal suture in a coronal plane at the level of the superior occipital condyle. The crest smooths in this area then flares laterally again, forming a spatulate hood on the temporal bone anterior and lateral to the base of the paramastoid process. The tympanic bone is separated from the rest of the temporal by a groove, which is narrow superiorly. A second crest demarcates the anterior margin of the superior half of the groove. This second crest is strongest inferiorly, and inferior to it the groove opens into a broad and shallow triangular fossa. The horizontal, column-like inferior border of the zygomatic process of the temporal defines the base of this fossa. The superomedial margin of the fossa is formed by the groove under the tympanic bone, which continues to the base of the mastoid process.

A crest coincides with the lambdoidal suture lateral to the superior half of the occipital condyle. This crest is crossed by a small groove at the posterior base of the paramastoid process and then continues up the posterior aspect of the paramastoid process, becoming smoother and rounder toward its tip. There is a knob at the tip of the process that is not completely ossified. The paramastoid process has a lenticular cross section, being more convex laterally. A longitudinal crest divides the base of the medial surface of the paramastoid process into anterior and posterior halves. This crest turns anteromedially superior to the paramastoid base, defining the lateral edge of the basilar portion of the occipital as it wraps around the mastoid process. Just superior to the base of the paramastoid process an ovoid foramen opens into the crest. Posterior to this crest a depression is formed, defined by the condylar bases posterior and the midline basilar torus medially. The midline of the basilar portion of the occipital is crested anterior to a coronal plane transecting the previously described foramina.

Viewed from an inferior perspective the angle formed between the medial margins of the occipital condyles measures approximately 30 degrees, similar to the condition seen in *Phacochoerus*. The anteroinferior border of each condyle is linear and nearly coronal in orientation, although the medial edge of the linear portion is slightly anterior. Viewed from a lateral perspective, the condyle is an asymmetrical crescent that opens anteriorly. Its superolateral tip is posterior to the inferomedial tip. The condyle is not as separated into two faces as is seen in *K. majus*, although the condylar surface does correspond to different tangent angles superiorly and inferiorly. The superior portions of the condyles face more posteriorly than in the *K. majus* condition. Viewed from an inferior perspective the posterior third of the foramen magnum is posterior to the condyles. This border is composed of two crests extending posterosuperiorly from under the posterosuperior condylar face. These crests curve medially toward one another, then superiorly before converging, although the notch in the posterior foramen magnum is not as pronounced, lacking as sharp a separation from the rest of the foramen magnum. The external surface of the occipital does not project posteriorly along the midline and becomes concave as it is traced superiorly.

EBSCOhost - printed on 10/28/2022 4:53 AM via . All use subject to https://www.ebsco.com/terms-of-use

The medial surface of the spatulate mastoid process is flattened, and it comes to a sharp point anteroinferiorly. The inferior border of the mastoid process is concave and comes to a second, more rounded, less inferior point posteriorly, anterior to a fissure between the mastoid and paramastoid processes. The mastoid broadens superiorly and posteriorly, and its anterolateral surface is convex. The right mastoid process is broken, exposing numerous air cells. Fissures separate the mastoid processes from the sphenoid. Beneath the fissure, the base of the column of bone that rises to become the pterygoid plate is parallel with the anterosuperior border of the mastoid process, and it is parallel all the way along its course toward the palate. A flange extends laterally from the obliquely oriented portion of the pterygoid base. A groove is formed between this flange and the column-like base of the pterygoid. Posterior projections of the palatines cap the inferior pterygoid so that the most inferior extent of the pterygoid plates is in approximately the same transverse plane as the floor of the posterior nasal aperture. When viewed posteriorly, the palatine and sphenoid are separated by a suture that begins inferolaterally at the transverse level of the posterior nasal aperture and climbs superomedially, making an angle of approximately 45 degrees with the horizontal plane. Inferomedial to this suture, on the medial face of the posterior projections of the maxilla, there are paired, oval-shaped exposures of sutural bone. The distal third of the unerupted M^3 is beneath the pterygoid projection, and the mesial two-thirds are beneath the posterior projections of the palatines. A groove separates these posterior projections from the thin, broken alveolar bone covering the unerupted M^3.

The posterior opening of the nasal aperture is filled with matrix, but its inferior border is observable. It is sharply crested, as is the case for *Phacochoerus*, but relatively broader, with two troughs on either side of the nasal septum that ramp up onto it when viewed posteriorly. A grooved midline keel extends from the posteroinferior nasal septum, following this ramp toward the palate. The keel would be vertical at its origin around the septum, follows a weakening curve toward the horizontal palate's midline. The midline crest flattens into an interfingered suture on the ramped portion of the palate and then becomes a sharp, ungrooved crest in line with the mesial M^3. The crest is most prominent between the M^2 and M^1, becoming flatter in line with the P^3. The palate is broken anterior to the P^2 root. A deep ovoid foramen lies just medial to the mesial portion of the M^2, extending anteroposteriorly from the mesial margin of the M^2 to just posterior to the fissure between the mesial and distal lingual pillars of the M^2. The palatine suture extends anteromedially from the posterior aspect of the palatine foramen and meets the midline in a coronal plane at the plane of the anterior foramen.

DISCUSSION Referred fossils are placed in *Kolpochoerus* based on their well-rooted, low-crowned teeth and the lateral inflation of the mandibular body below the molars. Fossils were assigned more specifically to *K. olduvaiensis* based on molar morphology. Daka *K. olduvaiensis* teeth are elongated mesiodistally with respect to *K. limnetes*, possessing four to five pairs of major enamel pillars. Two triangular median pillars with abutting bases form the junction of the talonid and trigonid in these teeth.

Daka *K. olduvaiensis* M^3 and M_3 are very similar both morphologically and metrically to those of members of the taxon from upper levels at Olduvai Gorge (Harris and

EBSCOhost - printed on 10/28/2022 4:53 AM via . All use subject to https://www.ebsco.com/terms-of-use

TABLE 11.1 Average Third Molar Metrics of Daka Suidae Taxa Compared to Non-Daka Conspecifics

	n	M_3 *length*	*n*	M_3 *height*	*n*	M^3 *length*	*n*	M^3 *height*
Kolpochoerus olduvaiensis								
Daka	12	68.5			4	63.0		
Omo L	1	72.0			1	69.0		
Olduvai Bed IV	1	73.0			2	62.0		
Koobi Fora Okote	16	59.6			12	58.7		
Olduvai bed II	7	63.0			4	58.0		
Kolpochoerus majus								
Daka	9	46.5			5	41.9		
Bodo	4	43.0			1	42.7		
Harris and White (1979)	10	43.8			6	42.7		
Metridiochoerus compactus								
Daka					4	76.7	7	59.2
Harris and White (1979)					15	80.4	16	73.0
Metridiochoerus modestus								
Daka	3	45.9	4	37.5	2	46.3	4	38.3
Harris and White (1979)	10	47.6	4	35.6	4	46.2	3	37.6

White 1979) (Table 11.1). M3s of representatives from earlier deposits at Koobi Fora and Olduvai are mesiodistally shorter. These differences reflect the progressive elongation of M3s in the *K. limnetes* to *K. olduvaiensis* lineage over the early Pleistocene. This lineage thus has high value as a biochronological tool.

Kolpochoerus majus (Hopwood, 1934)

DIAGNOSIS "A species of *Mesochoerus* of moderate size. M3 morphology comparable to the least progressive examples of *Mes. limnetes* but the cheek teeth differ from the latter by being more hypsodont, with more strongly crenulated enamel (thicker cementum cover) and by a strong lateral bulge of crown elements above the enamel line" (Harris and White 1979, 37).

DESCRIPTION Because the Daka Member represents one of the largest samples of *K. majus* and provides exceptional insight into sexual dimorphism, several specimens are described in great detail. Two reasonably complete and two partial *K. majus* crania have been recovered from the Daka Member. The most complete, BOU-VP-25/107 (Figure 11.3), is likely a male. This specimen preserves the maxilla and premaxilla in their entirety and has a complete upper dentition. The left zygomatic is present, as is the complete basicranium. Most of the frontal and parietals are missing. Little surface detail is preserved on BOU-VP-25/107.

BOU-VP-1/7 (Figure 11.4) is more gracile than BOU-VP-25/107, with markedly smaller canine roots and zygomatic knobs. It preserves the maxilla and premaxilla, as well as the right zygomatic and basicranium. As in BOU-VP-25/107, most of the frontal and parietals are missing.

BOU-VP-3/10 (Figure 11.5) is small, like BOU-VP-1/7, and is more fragmentary than both aforementioned crania. Much of the premaxilla is missing, as are the frontal,

EBSCOhost - printed on 10/28/2022 4:53 AM via . All use subject to https://www.ebsco.com/terms-of-use

FIGURE 11.3
BOU-VP-25/107
Kolpochoerus majus
cranium.
A. Superior view. B. Basal view. C. Left lateral view. D. Anterior view.

EBSCOhost - printed on 10/28/2022 4:53 AM via . All use subject to https://www.ebsco.com/terms-of-use

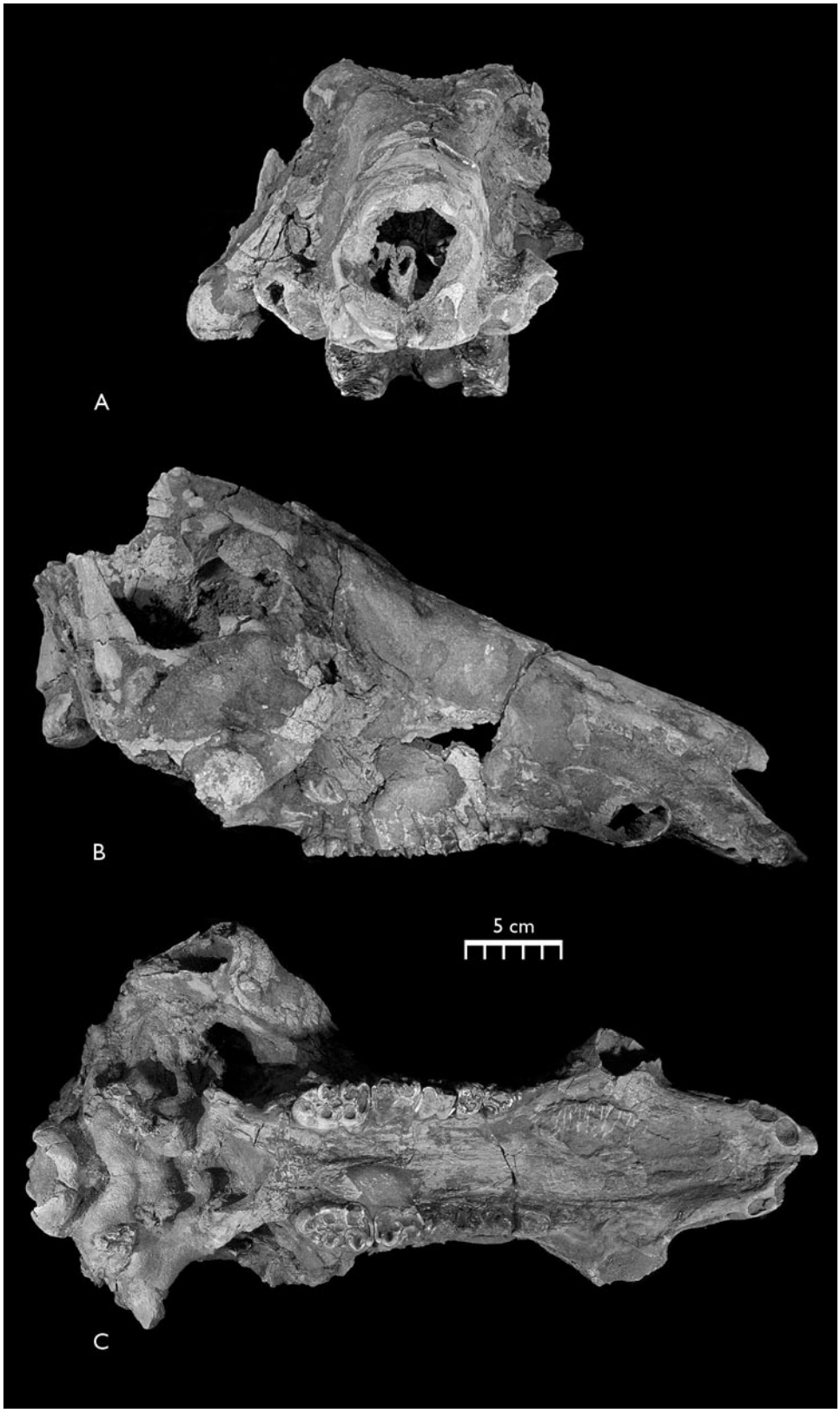

FIGURE 11.4

BOU-VP-1/7 *Kolpochoerus majus* cranium. A. Anterior view. B. Right lateral view. C. Basal view.

EBSCOhost - printed on 10/28/2022 4:53 AM via . All use subject to https://www.ebsco.com/terms-of-use

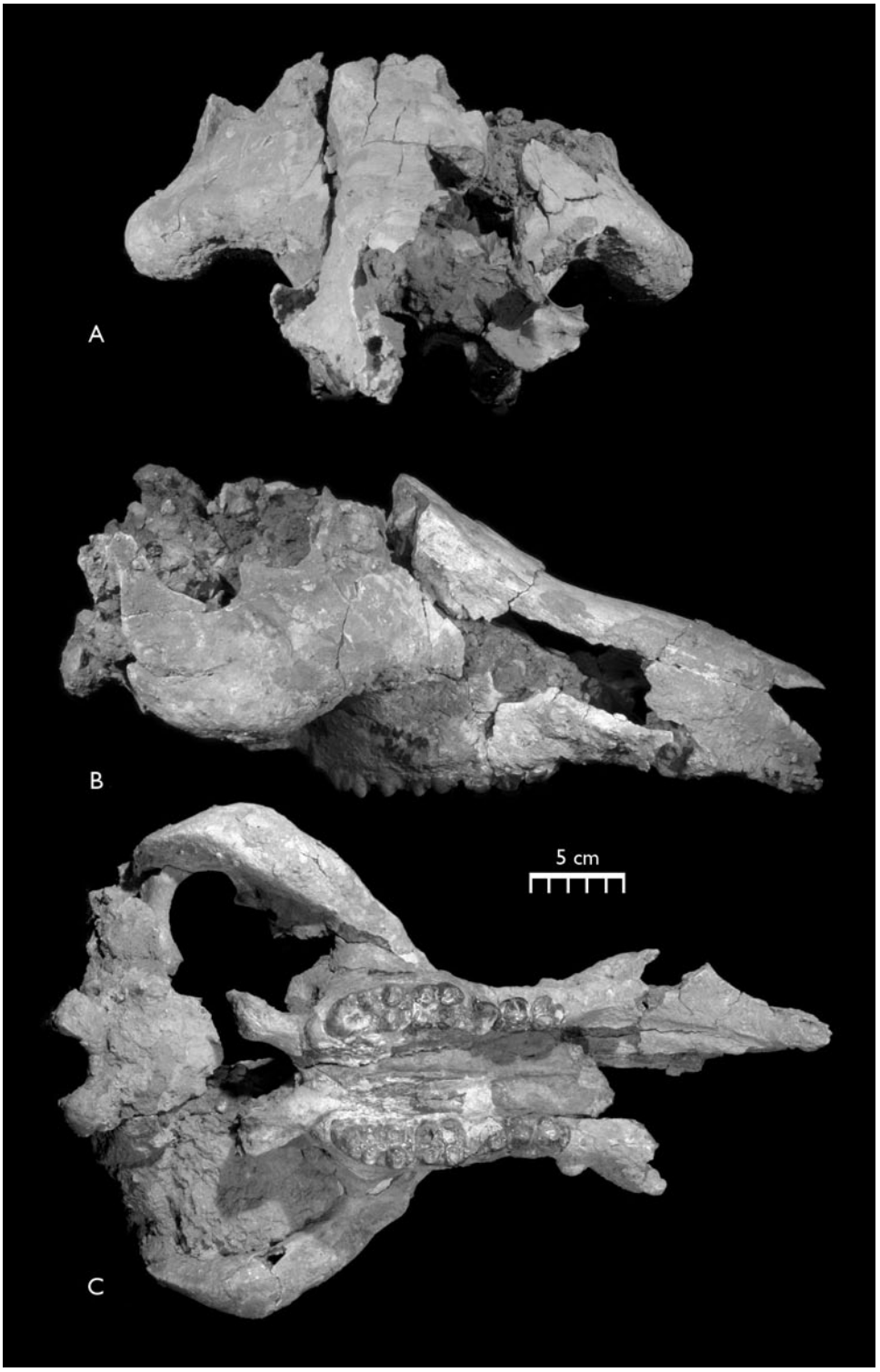

FIGURE 11.5
BOU-VP-3/10
Kolpochoerus majus
cranium. A. Anterior view.
B. Right lateral view.
C. Basal view.

EBSCOhost - printed on 10/28/2022 4:53 AM via . All use subject to https://www.ebsco.com/terms-of-use

parietals, and much of the basicranium. Both zygomatic processes are present, as is most of the postcanine dentition.

BOU-VP-25/98 comprises a large right maxilla, premaxilla, and nasal. The two more complete crania are described in detail in the following sections. Discussions of sexual dimorphism follow and include the less complete crania.

BOU-VP-25/107

BOU-VP-25/107 (Figure 11.4) is very large and probably a male. The alveolar margin of the I^2 projects a crest posteriorly and somewhat superiorly from above the second incisors. This crest runs linearly toward the middle of the canine alveolus, smoothing just anterior to the lateral projection of the anterior canine socket. Viewed laterally, this crest makes an acute angle with the inferior palate, forming a triangular depression beneath it. The lateral borders of the nasal aperture are crested anteriorly along the premaxillary portion. Medial to the crest is a rounded plateau of bone that extends medially about 1 cm before dropping off to the depths of the plateau. This bulgelike plateau smoothes posteriorly into the inner wall of the nasal aperture in the coronal section defined by the posterior margin of the aperture. This shelf converges anteriorly with the lateral crest of the nasal aperture margin, ending above the middle of the first incisor. Alae project superolaterally from a raised, sagittally oriented bony septum that spans the observable midline of the nasal aperture floor.

The medial walls of the nasal conchae are vertical to the point where they curl laterally. The premaxilla projects anteriorly medial to this point so that a sill of bone overhangs the mesial portion of the second incisors. The nasal bones are broken anteriorly, but it is clear that they would have projected some distance beyond the most posterior point on the nasal aperture. The anterior portion of the preserved nasals is slightly depressed at the midline, becoming gently convex laterally so that, overall, the anterior nasals bulge slightly superiorly. The lateral margin of the nasals is depressed so that a groove is palpable along the suture with the maxilla. Just lateral to this, along the middle third of the snout, the maxilla is ridged at its transition from transverse to sagittal orientation, making the proboscis above the canine sockets appear flattened. When observing the cranium from a superior perspective, lateral margins of the snout appear parallel for their entire length, from the middle of the canine socket to the coronal section of the anterior zygomatic root.

The canine socket is long anteroposteriorly, extending posteriorly to above the P^4. Its posterior border is oriented almost coronally when observed from a superior perspective, with only a slight lateral tendency where it contacts the sagittally oriented maxilla. The pedestal's lateral border is oriented sagittally for its posterior half, behind the canine socket, when viewed from the same perspective. A sagittal crest defines this lateral margin and extends anteriorly across the canine socket for the entire length of the pedestal. A deep, rounded groove separates the lateral margin of the pedestal from the vertical wall of the anterior maxilla and premaxilla surrounding the nasal aperture. The inferior surface of the canine socket curves smoothly around the canine root, with the exception of a slightly roughened surface between the P^1 and the distal canine. The bone surface in this area is weathered.

The infraorbital foramen opens at the posterior root of the canine socket. The sagittally oriented portion of the maxilla above the first and second molars is concave anterior

EBSCOhost - printed on 10/28/2022 4:53 AM via . All use subject to https://www.ebsco.com/terms-of-use

and inferior to the maxillary zygomatic root. The anterior projections of the frontal arise from the superolateral edge of the snout, collinear in the coronal plane with the posterior margin of the infraorbital foramen. These projections overhang the concave portion of the sagittal maxilla described previously, creating a groove that extends posteriorly toward the orbit. This groove broadens into a spoonlike fossa anterior to the orbit. Viewed from a lateral perspective, the superior surface of the anterior projections of the frontal is more coronally inclined than the surface of the snout anterior to it. This change is abrupt. The frontal is broken above the transverse level of the mid-orbit.

The anterior border of the orbit is above the M^3 talon. The inferior zygomatic is buttressed by a column of maxillary bone extending above the M^3 paracone. This column arcs laterally, approaching horizontal beneath the anterior zygomatic and bending posteriorly so that it is parallel to the anterior face of the zygomatic when viewed from an inferior perspective. The posterior face of this anterior zygomatic root is grooved along the zygomatic/maxilla transition between this buttress and the inferior lip of the orbital depression, producing another column-like feature between it and the posterior opening for the trigeminal nerve. Inferior to this opening and posterior to the buttress, the posterior aspect of the maxilla wraps slightly medially around the M^3 roots and creates a gently curved trough between the M^3 and the lateral pterygoid plate when viewed from an inferior perspective. The anterior aspect of the orbit is matrix-filled but is detectably concave. Its anterior wall is impressed forward beyond the anterior orbital margin and likely possesses an impression like the one described for the female cranium in the paragraphs that follow.

The superior border of the inferior postorbital spike is horizontal, and the spike itself does not project as a posterior overhang. Beneath its horizontal superior margin is a pronounced bulge that is slightly broader anteriorly. Inferior to the anterior projection of the frontal, and posterior to its anterior margin, the zygomatic root is concave on its anterosuperior face. A crest runs anteriorly from the tip of the postorbital process across the posterior margin of the lacrimal, dipping inferiorly as it passes to the frontal, and bounding the concave inferior border of the orbital fossa. The inferolateral external orbital margin is grooved above the horizontal portion of the postorbital spike.

Viewed from a superior perspective, the anterior root of the zygomatic has a skewed sigmoid outline, curving laterally from the sagittally inclined portion of the maxilla and becoming nearly tangent to the coronal plane before curving gently posteriorly around the zygomatic knob. The zygomatic knob is very large. Viewed from an anterior perspective, the line that best fits the central tendency of the zygomatic projection makes an angle of approximately 35–40 degrees from horizontal. The zygomatic knob projects inferiorly when viewed from an anterior perspective, giving it a compressed neck and the general outline of an asymmetrical teardrop. The most inferior point on the zygomatic knob is located posteromedially on its underside. A rounded crest extends from it posteriorly and superiorly and is interrupted by the zygomatic-temporal suture but is in line with the posterior margin of the jugal bone. The anterior jugal covers the posteromedial quarter of the zygomatic knob when it is viewed from a superior perspective. Its anterior and lateral borders are convex from this perspective. The anterior tangent of this convexity defines a coronal section coplanar with the middle of the horizontal portion of the postorbital process. The posterolateral quarter of the superior surface of the zygomatic portion of the knob forms a half-crescent that wraps medially around the portion of the knob

EBSCOhost - printed on 10/28/2022 4:53 AM via . All use subject to https://www.ebsco.com/terms-of-use

covered by the jugal. There is a crest on the medial aspect of the zygomatic knob on the inner wall of the zygomatic bar, along its suture with the jugal.

The posterior aspect of the postorbital process is oriented at an angle of approximately 70–75 degrees from horizontal so that there is no posterior overhang of the projection. A crest marks this superior margin of the zygomatic arch for its length. When viewed laterally it descends the postorbital bar, dips into a trough with a somewhat flattened bottom along the anterior jugal, climbs the superior border of the posterior jugal, and continues onto the lateral temporal. Between this and the posterior margin of the jugal, this bone is flattened in a sagittally oriented plane, and this flattened face continues on the lateral temporal bone. When viewed from a lateral perspective this sagittal surface comes to a slightly posteriorly skewed superior point. Its tip is the most superior point on the zygomatic arch, but this feature does not appear to project a process superiorly, although it is heavily weathered. Being incompletely fused, the suture between the jugal and the temporal is easily distinguished. There is a ridge of bone straddling this suture along the inferior half of its oval cross section that is easily palpable with a finger passed laterally across the inferior border of the zygomatic process of the temporal and medial jugal.

The zygomatic process of the temporal is smooth along its anterosuperior face from the squama to the superior crest of the jugal, not noticeably undulating over the auditory meatus. The meatus opens slightly lateral to the middle of the superior border of the zygomatic process of the temporal. Projecting inferiorly from the lateral margin of the external auditory meatus, a crest courses first vertically, then gently arcs toward the superolateral edge of the occipital condyle. This crest turns again inferiorly as it crosses the lambdoidal suture, which it follows for its length all the way to the posterior margin of the paramastoid process. Lateral to the vertical portion of this crest and medial to the crest along the posterior jugal/lateral temporal is a trough. Viewed from a superior perspective the trough opens posteriorly and only slightly laterally. It does not open fully laterally as it does in *Phacochoerus*. Inferior to this the trough wraps medially and continues inferomedially toward the base of the paramastoid. The trough is deep and is matrix filled in this area. This trough ends at the lateral base of the paramastoid process. The crest following the auditory meatus does not fold anteriorly over the depth of the trough and no crest is palpable as it overlaps the paramastoid process. At the medial end of this trough, on the lateral base of the paramastoid process, is a pronounced tubercle with its surface eroded. It is taller than it is wide, approximately 1.7 cm superoinferior by 1.2 cm mediolaterally.

Viewed from an inferior perspective the angle formed between the medial margins of the occipital condyles is approximately 45 degrees, much more obtuse than the phacochoere condition. The anterior border of both condyles defines a broad parabola when viewed from an inferior perspective, the medial tips separated by approximately 10 mm. Viewed from a lateral perspective, the condyle is a slightly asymmetrical crescent that opens anteriorly, its superolateral tip extending anteriorly beyond the inferomedial one. Each condyle has two faces separated by a more convex area. One face is oriented inferolaterally and one posterosuperiorly. Each face has a more or less equal area. Viewed from an inferior perspective, the posterior border of the foramen magnum projects posteriorly beyond the posterior extent of the condyles. This border is composed of two crests extending posterosuperiorly from the middle of the nonarticular, superomedial portion of the

EBSCOhost - printed on 10/28/2022 4:53 AM via . All use subject to https://www.ebsco.com/terms-of-use

posterior condyle projection. These crests curve medially toward one another, then climb almost perpendicularly for more than a centimeter before converging, such that the foramen magnum has a projection from its posterior border. The midline of the occipital projects posteriorly so that the occipital is concave on either side of it, superolateral to the foramen magnum's tubercle. The superior portion of the occipital is missing.

Both paramastoid processes are broken, and the base of the paramastoid measures approximately 2 cm anteroposteriorly and 1 cm mediolaterally. Anterior to the paramastoid process, the mastoid processes project anteriorly, coming to a point at its anterior tip when viewed from an inferior perspective. The surface of the processes is eroded, exposing numerous mastoid air cells. Although it is matrix filled, a deep fissure can be detected that extends posterosuperiorly under the mastoid processes, separating them from the sphenoid. Beneath the fissure the base of the column of bone that rises to become the pterygoid plates is parallel with the anterosuperior border of the mastoid process. At the transverse level of the opening of the fissure it turns abruptly inferiorly so that the depth of the fissure dividing the medial and lateral pterygoid plates is vertically oriented. A flange extends laterally from the obliquely oriented portion of the pterygoid base, but it is broken, its lateral extent obscured.

Although they are very worn, some details of the pterygoid plates are visible. A crest marks the posterior border of the lateral pterygoid plate, smoothly arching laterally and inferiorly to approximately two-thirds of the way down the vertical portion of the pterygoid column, then twisting anteriorly and medially toward the palate. A crest also follows the posterior border of the medial pterygoid plate almost directly inferiorly so that the arch of the lateral pterygoid plate diverges from it laterally. The crest of the medial plate bifurcates approximately two-thirds of the way down the vertical portion of the pterygoid column. The lateral branch of this bifurcation turns sharply laterally, then twists anteriorly and curls back around to connect with the lateral pterygoid crest. The medial branch of the bifurcation continues along the inferior course of the more superior part of the medial pterygoid plate, then turns sharply anteriorly and approaches the palate horizontally. On the lateral side of the medial branch of the crest, at the point that it makes a right angle, there is a small bony projection.

The posterior opening of the nasal aperture is filled with matrix, but its inferior border is observable. It is not sharply crested, as is the case for *Phacochoerus*. The distance between the medial pterygoid plates is more than half of the distance between the lateral plates. Alveolar bone continues posteriorly and medially beyond the M^3 and forms a small ridge and retromolar sulcus parallel to the medial border of the M^3 talon. Another sulcus exists posterior and slightly lateral to the alveolar extension just described, separating it from the anterior extensions of the pterygoid crests. A prominent midline keel follows the palate all the way to the incisive foramen, flattening somewhat between the canines. Two grooves extend posteriorly from the incisive foramina, ending beneath the canines. The lateral border of the alveolar bone covering the canines does not retreat medially where it is continuous with the palate, as it does in *Phacochoerus*. Rather, it defines an anterolaterally opening arch when viewed from an inferior perspective. The maxilla extends to be anterior to the canine socket. Its suture with the premaxilla projects posterolaterally from the posterior portion of the incisive foramen, making an angle of approximately 45 degrees with the sagittal plane, wrapping around the smooth lateral margin of this part of the palate. The

EBSCOhost - printed on 10/28/2022 4:53 AM via . All use subject to https://www.ebsco.com/terms-of-use

crest between the canine and I^2 just described does not mark the transition from the horizontal palate to the perpendicular portion of the anterior maxilla and premaxilla. Rather, this crest is superior to the transition.

BOU-VP-1/7

Cranium BOU-VP-1/7 (Figure 11.4) is more gracile than BOU-VP-25/107 (Figure 11.3) and almost certainly represents a female. The alveolar margin of the I^2 projects a crest posteriorly and superiorly from the posterior sockets of the second incisors. It runs linearly toward the anterior corner of the rounded triangular cross section of the canine. Viewed from a lateral perspective this crest is parallel to the inferior border of the premaxilla, which changes inclination abruptly from horizontal to an angle of approximately 40 degrees from horizontal as it passes beneath the canine sockets. The lateral borders of the nasal aperture possess anterior crests along the premaxillary portion of the aperture's margin. The plateau of bone medial to this crest itself has a crest. The two converge anteriorly to produce a V-shaped groove, the united crest of which continues anteriorly and then arches toward the midline. It becomes the most anterior point on the premaxilla, extending well beyond the incisor sockets. Alae project superolaterally from a raised, anteroposteriorly oriented bony septum that spans the observable midline of the nasal aperture floor. The medial wall of the nasal concha is slightly more rounded than in BOU-VP-25/107. The anterior portions of the nasal bones are broken, but remaining portions project some distance anterior to the most posterior point on the nasal aperture. The anterior portions of the preserved nasals are slightly depressed at the midline, becoming somewhat more convex than BOU-VP-25/107 laterally, so that the anterior nasals bulge slightly superiorly.

The lateral margin of the nasals is depressed and a groove is palpable along the suture with the maxilla. Just lateral to this, along the middle third of the snout, the maxilla is ridged at its transition from transverse to sagittal orientation, although not so much as in BOU-VP-25/107. The anterior portion of the snout does not appear flattened on its superior surface. When the cranium is observed from a superior perspective, lateral margins of the snout appear more or less parallel, although they converge slightly posterior to the canine socket. The superior portion of a coronal section of the snout would have been convex in BOU-VP-1/7 rather than flattened as in BOU-VP-25/107, but the second female, BOU-VP-3/10, more closely approximates the male condition in this respect.

The canine socket is not nearly so anteroposteriorly elongate as in BOU-VP-25/107, extending posteriorly only to above the P^2. Its posterior border is oriented closer to sagittal than coronal and continues in an oblique, anterolateral direction all the way to the posterior border of the canine socket. A sagittal crest extends anterior from the middle of this oblique surface when viewed from a superior perspective and continues to the anterior border of the pedestal. A deep, rounded groove separates this crest from the vertical wall of the anterior maxilla and premaxilla surrounding the nasal aperture. This groove is narrower mediolaterally than it is in BOU-VP-25/107. The inferior surface of the canine socket curves smoothly around the anterior portion of the canine root, but a crest joins the mesial P^2 alveolar margin with the posterior canine root. There is no P^1. A groove bounds this crest medially.

The infraorbital foramen opens superior to the posterior margin of the canine socket. The sagittally oriented portion of the maxilla above the first and second molar is concave

EBSCOhost - printed on 10/28/2022 4:53 AM via . All use subject to https://www.ebsco.com/terms-of-use

anterior and inferior to the maxillary zygomatic root. The anterior projections of the frontal arise from the lateral edge of the snout posterior to a coronal plane through the infraorbital foramen. A groove defines the frontonasal suture and follows it as it wraps around to the sagittally oriented part of the snout. Although this groove is probably present on BOU-VP-25/107 (the area is matrix filled), it does not follow the suture over the snout's lateral margin, which is less rounded than in the male specimen. These projections overhang the concave portion of the sagittal maxilla only slightly, creating a depression that extends posteriorly toward the orbit. Viewed from a lateral perspective, the superior surfaces of anterior projections of the frontal are only slightly more coronally oriented than the anterior surface of the snout. The frontal is broken above the orbit, and a superior postorbital spike extending from the frontal is present on the right side.

The anterior border of the orbit is above the M^3 talon. A less pronounced column of maxillary bone than seen on BOU-VP-25/107 buttresses the inferior zygomatic. This column arches laterally toward horizontal beneath the anterior zygomatic, bending posteriorly as it does, so that it is parallel to the anterior face of the zygomatic when viewed from an inferior perspective. The posterior face of this anterior zygomatic root is not so deeply grooved along the inferior portion of the zygomatic/maxilla suture but is so deeply grooved on the superior portion. This groove extends toward the inferolateral margin of the orbit and bisects the otherwise continuous crest along the posteroinferior orbital rim of the posterior face of the anterior zygomatic root. The feature produced between the groove and the posterior opening for the trigeminal nerve is less columnar and more cone-shaped, opening superiorly. Inferior to this opening and posterior to the buttress, the posterior aspect of the maxilla wraps slightly medially around the M^3 roots and creates a concave depression between the lateral pterygoid plate and the alveolar bone over the posterior root of the M^3 trigon. This depression comes to a rounded anteroinferior point between the roots of the M^3 trigon and talon.

The anterior aspect of the orbital socket is not as matrix-filled as it is in the male cranium. There is a depression with a rounded trough extending inferomedially from the anteroinferior orbital rim. The groove on the posterior aspect of the anterior zygomatic root continues superiorly and defines a crest along the inferolateral margin of the rounded depression above it. The superior border of the inferior postorbital bar is horizontal, the anterior aspect of its horizontal portion bounded by the aforementioned groove. Although the posterior portion of the bar is broken in BOU-VP-25/107, it projects slightly posteriorly in female specimen BOU-VP-3/10. Beneath its horizontal superior margin there is not such a pronounced bulge as the one seen in BOU-VP-25/107. Anterior to this bulge, inferior to the anterior projection of the frontal, and posterior to the anterior extent of the frontals, the lacrimal area is concave along its anterosuperior surface. The crest that runs anteriorly from the tip of the postorbital process across the posterior margin of the lacrimal in BOU-VP-25/107 is not present in the female.

Viewed from a superior perspective, the anterior root of the zygomatic is less sigmoid than in the male, the middle of its anterolateral face being somewhat obliquely linear. There is only mild expansion of the lateral zygomatic. The extreme lateral portion of the zygomatic is broken, with a sinus inside. Viewed from an anterior perspective the line that best fits the central tendency of the zygomatic projection makes an angle of approximately

EBSCOhost - printed on 10/28/2022 4:53 AM via . All use subject to https://www.ebsco.com/terms-of-use

55–60 degrees from horizontal. The zygomatic knob does not project so far inferiorly when viewed from this perspective. The most inferior point on the zygomatic knob is located anteromedially. A rounded crest is present above the broken base of the zygomatic along its posterior border. It is interrupted by the zygomaticotemporal suture but is in line with the posterior margin of the jugal bone. It does not cover much of the expanded zygomatic.

Although the exact lateral extent of the jugal cannot be judged in BOU-VP-1/7 (Figure 11.4) because of a matrix covering, in female specimen BOU-VP-3/10 (Figure 11.5) it is not very laterally convex when viewed from a superior perspective. Its anterior and lateral borders are convex from this perspective, the anterior coronal tangent defining a section in line with the middle of the horizontal portion of the inferior postorbital spike. The posterolateral quarter of the superior surface of the zygomatic portion of the knob forms a half-crescent that wraps medially around the portion of the knob covered by the jugal. There is a crest on the medial aspect of the zygomatic knob, on the inner wall of the zygomatic bar along its suture with the jugal. The posterior aspect of the postorbital process, as mentioned before, is missing but can be seen to project posteriorly in BOU-VP-3/10. A crest marks this superior margin of the zygomatic arch for its length. Viewed laterally, it descends the postorbital bar, dips into a trough with a somewhat flattened bottom along the anterior jugal, climbs the superior border of the posterior jugal and continues onto the lateral temporal. Between this and the posterior margin of the jugal, this bone is flattened in the sagittal plane, and this flattened surface continues onto the lateral temporal bone. When viewed laterally, the sagittal surface does not come to a point superiorly as in BOU-VP-1/7, although it does in the BOU-VP-3/10. The superior margin of the zygomatic arch is broken in both female specimens. The suture between the jugal and the temporal is only visible as a slightly raised surface on the superior end of the crest along the posterior jugal.

The zygomatic process of the temporal is smooth along its anterosuperior face from the squama to the superior crest of the jugal, with a slight groove palpable medial to the superior end of the auditory meatus. Projecting inferiorly from the lateral margin of the external auditory meatus a crest courses first vertically, then gently arcs in an inferolateral direction. This crest turns again inferiorly and slightly laterally as it crosses the transverse level of the superior margin of the occipital condyle. Lateral to the vertical portion of this crest is a shallow trough that is much less concave than the one in the male. Viewed from a superior perspective the trough opens posteriorly and only slightly laterally. Inferiorly, this trough wraps medially and becomes deeper anteriorly so that the portion of the groove beneath the oblique margin of the crest of the tympanic bone is easily distinguished, existing as an isolated shelf. It continues inferomedially, twisting anteriorly toward the base of the mastoid process, differentiating it from the male condition. Further differentiating this specimen from the male condition, the groove continues anteriorly past the base of the paramastoid process, making a groove on the medial margin of the otherwise columnar posterior zygomatic buttress. The crest following the auditory meatus does not fold anteriorly over the depth of the trough, although it does twist laterally. There is no tubercle at the lateral base of the paramastoid process. It is not as anteroposteriorly elongate as in the male condition, and it has a slight groove separating it from the mastoid.

Viewed from an inferior perspective the angle formed between the medial margins of the occipital condyles is greater than 45 degrees. The anterior border of both condyles defines a

EBSCOhost - printed on 10/28/2022 4:53 AM via . All use subject to https://www.ebsco.com/terms-of-use

broad parabola when viewed from the same perspective. The medial tips of the condyles are separated by approximately 10 mm. The superolateral tip of each condyle extends anterior to the same coronal level as the inferomedial one. The condyles are more evenly curved in both probable females, without distinguishable faces. The superior portion of the articular surface becomes almost transversely oriented and there is a groove in the occipital just superior to it. The posterior border of the foramen magnum bears two crests extending posterosuperiorly from the posterior aspect of the nonarticular, superomedial portion of the posterior condylar projection. These crests curve medially toward one another, then climb almost perpendicularly for more than a centimeter. They then diverge to create a superior opening, a cone-like depression extending superior to the tubercle of the posterior border of the foramen magnum. This depression and the groove just superior to the occipital condyle define a cone-shaped bony plateau that comes to a point where the crest of the posterior foramen magnum turns into the tubercle. The superior portion of the occipital is missing.

Both paramastoid processes are broken, and the base of the paramastoid is not as absolutely long anteroposteriorly as it is in the male. Anterior to the paramastoid processes the mastoid processes project anteriorly, coming to a point at the anterior tip when viewed from an inferior perspective. The surfaces of the processes are not as eroded as in the male, and they come to a pronounced anterior point. Although matrix-filled, deep fissures can be detected that extend posterosuperiorly under the mastoid processes, separating them from the sphenoid.

Beneath the fissure, the base of the column of bone that rises to become the pterygoid plates is angled more vertically than the superior border of the mastoid, and there is no direction change in the posterior pterygoid column as is seen in the probable male. A flange extends laterally from the pterygoid base above the mastoid. This crest becomes gradually reduced inferiorly until again twisting laterally on the lateral pterygoid plate. The posterior-facing trough between the medial and lateral pterygoid plates thus has an isthmus on its inferior aspect not seen in *Phacochoerus*. The inferior portions of the pterygoid plates are not as worn as those in the male but have a very similar morphology. A crest marks the posterior border of the lateral pterygoid plate, smoothly arching in a lateral and inferior direction to approximately two-thirds of the way down the portion of the pterygoid column inferior to the mastoid. It then twists anteriorly and medially toward the palate. At the corner where it twists anteriorly there is a small horizontal bar of bone that joins it. This bar is probably also present, but eroded, in the male. A crest also follows the posterior border of the medial pterygoid plate almost directly inferior so that the arch of the lateral pterygoid plate diverges from it laterally. The crest of the medial plate bifurcates approximately two-thirds of the way down the portion of the crest inferior to the mastoid. The lateral branch of this bifurcation turns sharply laterally, then twists anteriorly and curls back around to connect with the lateral pterygoid crest as it approaches the palate. The medial branch of the bifurcation continues along the inferior course of the medial pterygoid plate, then makes a sharp anterior turn and approaches the palate horizontally. On the lateral side of the medial branch of the crest, exactly at the point where it makes a right angle, there is a small bony projection, as with the male.

The posterior opening of the nasal aperture is filled with matrix. The distance between the medial pterygoid plates is more than half of the distance between the lateral plates.

EBSCOhost - printed on 10/28/2022 4:53 AM via . All use subject to https://www.ebsco.com/terms-of-use

Alveolar bone does not continue posteriorly and medially beyond the M^3, although it does in the second female. A prominent midline keel follows the palate only to the coronal level of the P^4. It continues farther anterior in the second female (BOU-VP-3/10) but the posterior portion of the keel is heavily emphasized, making a high crest. Two grooves extend posteriorly from the incisive foramina, ending at the coronal level of the middle of the M^1. Most of this area is broken in the second female, although it does appear on the preserved portion of palate behind the premolars. The lateral border of the alveolar bone covering the canines retreats slightly medially, but not nearly to the degree that it does in *Phacochoerus*. The maxilla extends anterior to the canine socket, and its suture with the premaxilla projects posterolaterally from the posterior portion of the incisive foramen, making an angle of approximately 60 degrees with the sagittal plane, although it is not well defined. The crest between the canine and I^2 described in the first paragraph does not mark the transition from the horizontal palate to the perpendicular portion of the anterior maxilla and premaxilla. Rather, this crest is superior to the transition. The inferior surface of the palate is much more concave anteroposteriorly in the females, making a sharp inferior turn anterior to the premolars. Although the overall shape is not likely to vary so much, surface details on the palate seem to be subject to individual variation.

Dentition Male and female *K. majus* are quite similar in tooth morphology in the Daka sample. Occlusal wear patterns, however, appear to be different. In the females, there is a zone of decreased wear that separates the molar occlusal surfaces from those of the premolars, especially buccally. Wear on the M^1 hypocones is excessive in the females, much more pronounced than that of the males. This produces a parabolic best fit to the line defining the buccal and mesial margin of the molar portion of occlusal wear in females when it is viewed from a superior perspective. In the males observed there is no distinction between the occlusal wear of the premolars and molars. The buccal margins of the M^2s extend laterally substantially beyond the buccal margin of the M^1 in females. They do not extend like this in males. This makes the buccal margin of the arcade bottleneck at around the parabolic wear outline in females, augmenting its perceptibility. Therefore, if these observations were to be made in other samples, isolated M^1s and M^2s might sometimes be sexed. The overall wear on the male M^2s is troughlike, such that the lingual margin of the protocone and hypocone is less worn than the buccal portion of these pillars. A coronal section of the occlusal margin is concave in males. In females the lingual margin of the protocones is the most worn, and a coronal section of the anterior tooth would not form a trough. As mentioned previously, the hypocone of the M^1 in females is most worn. The paracone is the least worn in females. This orients the wear obliquely, so that the plane of wear faces distally and lingually. In males the protocone and hypocone are more or less evenly worn, as are the paracone and metacone, so that the plane of wear faces lingually. These differences in occlusion are likely the effect of the downturned snout anterior to the premolars in females, a feature absent in males. This morphological difference arises from the impact of canine sexual dimorphism on surrounding structures. Both males observed have retained P^1s, and neither female does.

Although there are no intact female canines, the sexually dimorphic nature of canine size is apparent when comparing the tooth's socket. The cross section of the female canine is somewhat heart-shaped, with a rounded bottom and a depression superiorly. The cross section of the male canine at the socket is closer to kidney shaped and opens more laterally

EBSCOhost - printed on 10/28/2022 4:53 AM via . All use subject to https://www.ebsco.com/terms-of-use

than the females'. The rest of the description applies only to the male canines. Canine basal projection is oriented about 30 degrees anterior of the sagittal plane prior to curving. Viewed from a superior perspective, the tooth curves evenly in a posterior crescent, its posterolateral border even with the posterior margin of the canine socket. Most of the enamel is crenulated in parallel bands that follow the posterior curve of the tooth. They average about 1 mm in width, but their width is irregular. Enamel is absent on an approximately 1.0 cm wide crescent of the superior surface of the tooth where the cross section is depressed. Another, narrower crescent of exposed dentin is present on the posteroinferior aspect of the tooth. There is a large contact facet for the lower canine on the anterolateral third of the tooth.

DISCUSSION Crania BOU-VP-3/10 (Figure 11.5) and BOU-VP-1/7 (Figure 11.4) have moderately sized canines, canine flanges, and zygomas, while in cranium BOU-VP-25/107 they are pronounced. This exemplifies the high degree of sexual dimorphism detailed above in the sample. The upper premolars of BOU-VP-1/7, 3/10, 25/107, 3/33, and 25/71 are large. Molars in all specimens are rooted and low crowned. The gonial angle in BOU-VP-3/50 is everted (*K. majus* mandibular metrics are given in Table 11.5). M3s are short and low crowned, similar in overall appearance to those of early *K. limnetes*. Teeth of these cranial specimens, and many other isolated teeth, have thick cementum and show strongly crenulated enamel. Further aligning the material with *K. majus*, molars and premolars bulge buccolingually in the coronal plane just above the cementoenamel junction. M3 metrics are comparable to those of *K. majus* reported for the taxon by Harris and White (1979) (Tables 11.1 and 11.2).

Metridiochoerus and *Phacochoerus*

Metridiochoerus andrewsi first appears in Omo's Usno Formation at around 3.4 Ma (White et al. 2006) and is a possible Asian immigrant (White 1995). Other *Metridiochoerus* species, *M. compactus*, *M. hopwoodi*, and *M. modestus*, are derived from this parent taxon and appear in the early Pleistocene. These three taxa last appear in Olduvai Bed IV (White 1995). The origins of *Phacochoerus* are not well documented, but there is agreement over its derivation from *Metridiochoerus* (Harris and White 1979; Cooke 1982). *Metridiochoerus compactus*, *M. modestus*, and *Phacochoerus* occur in the Daka Member.

Metridiochoerus taxa are united by extremely hypsodont M3s with delayed root fusion. Occlusal relief is extremely low, and, after initial wear, M3 transverse-section morphology is relatively stable along the superoinferior axis of the tooth (Harris and White 1979). *Metridiochoerus* species exhibit pronounced sexual dimorphism, and males tend to have very enlarged canines. Table 11.4 provides dental metrics.

Metridiochoerus compactus (Van Hoepen and Van Hoepen, 1932)

DIAGNOSIS "A large and progressive species of *Metridiochoerus*. Upper canine large, oval to triangular in cross section, incipiently bilobate, lacking enamel, and with a core of cellular osteodentine. Lower canines are large, oval, or modified verrucose but lacking enamel. Premolar row reduced and all but M3 shed in fully mature adults. M3s large, but variable in size, extremely hypsodont with delayed root fusion as in *Phacochoerus*. Major paired pillars Y-shaped and contiguous so that worn specimens surrounded by solid outer rim of enamel (as advanced *Met. andrewsi* but cf. *Met. hopwoodi*)" (Harris and White 1979, 50).

EBSCOhost - printed on 10/28/2022 4:53 AM via . All use subject to https://www.ebsco.com/terms-of-use

TABLE 11.2 Daka Member *Kolpochoerus majus* Dental Metrics

Specimen	*Taxon*	*Element*	*Basal Length*		*Maximum Breadth*		*Talon (id)*		*Crown Height*		*Crown Center Length*
BOU-VP-1/7	*K. majus*	LM^3	41.2		26.1		31.4				
BOU-VP-1/7	*K. majus*	RM^3	40.6		25.7		31.6				
BOU-VP-1/7	*K. majus*	LM^2	27.4	e	23.8						
BOU-VP-1/7	*K. majus*	RM^2	27.2								
BOU-VP-1/7	*K. majus*	RM^1	18.6	e	12.5						
BOU-VP-1/7	*K. majus*	RP^4	15.5		19.6						
BOU-VP-1/7	*K. majus*	RP^3	16.5		19.7						
BOU-VP-1/53	*K. majus*	RM_3			20.6						
BOU-VP-1/58	*K. majus*	RM_2	22.0		21.0						
BOU-VP-1/58	*K. majus*	RM_3	37.5		25.5		26.2		15.1		40.8
BOU-VP-1/59	*K. majus*	LM_1	20.7		16.2						
BOU-VP-1/59	*K. majus*	LM_2	* 21.2		19.5						
BOU-VP-1/59	*K. majus*	LM_3	38.7		20.9		27.8		7.8		38.1
BOU-VP-2/27	*K. majus*	RM^3	e 52.3		22.9			+	19.0		
BOU-VP-3/10	*K. majus*	LM_3			24.6		29.2				49.1
BOU-VP-3/10	*K. majus*	LM^1	* 18.8	e	19.6						
BOU-VP-3/10	*K. majus*	LM^2	26.3		24.8						
BOU-VP-3/10	*K. majus*	LM^3			26.2	*	29.4		16.9	*	40.4
BOU-VP-3/10	*K. majus*	LP^3	19.1		18.6						
BOU-VP-3/10	*K. majus*	LP^4	14.5		17.7						
BOU-VP-3/10	*K. majus*	RM_3			24.1		29.2				50.2
BOU-VP-3/10	*K. majus*	RM^1	* 18.2	e	19.7						
BOU-VP-3/10	*K. majus*	RM^2	* 25.9		26.8						
BOU-VP-3/10	*K. majus*	RM^3		*	26.8		27.5	+	16.7	*	43.4
BOU-VP-3/10	*K. majus*	RP^3	* 18.0		18.0						
BOU-VP-3/10	*K. majus*	RP^4	* 17.0	*	17.8						
BOU-VP-3/33	*K. majus*	LM_2	26.7	*	26.4						
BOU-VP-3/33	*K. majus*	LM_3			28.1	*	30.7	+	15.8	*	40.7
BOU-VP-3/33	*K. majus*	RM^1	e 18.1	e	20.2						
BOU-VP-3/33	*K. majus*	RM^2	* 27.9	*	27.1						
BOU-VP-3/33	*K. majus*	RM^3		*	25.6	*	31.0	+	11.7	*	41.3
BOU-VP-3/33	*K. majus*	RP^1									
BOU-VP-3/33	*K. majus*	RP^2	* 16.0	*	10.6						
BOU-VP-3/33	*K. majus*	RP^3	* 16.3	*	18.5						
BOU-VP-3/33	*K. majus*	RP^4	14.3		20.5						
BOU-VP-3/50	*K. majus*	RM_1	19.7		14.8						
BOU-VP-3/50	*K. majus*	RM_2	* 31.5		20.4						
BOU-VP-3/50	*K. majus*	RM_3	* 42.7		22.3		26.4		23.0		41.8
BOU-VP-3/50	*K. majus*	RP_3	* 13.0	*	9.7						
BOU-VP-3/50	*K. majus*	RP_4	17.1		12.6						
BOU-VP-3/67	*K. majus*	LP^2	* 11.1	*	10.6						
BOU-VP-3/67	*K. majus*	LP^3	15.1		15.8						
BOU-VP-3/67	*K. majus*	LP^4	16.2		17.4						
BOU-VP-3/67	*K. majus*	RM^1	19.4		22.8						
BOU-VP-3/67	*K. majus*	RM^2	23.7	*	24.8						
BOU-VP-3/67	*K. majus*	RP^2	* 7.5		8.5						
BOU-VP-3/67	*K. majus*	RP^3	15.2		15.9						
BOU-VP-3/67	*K. majus*	RP^4	16.4		17.8						

EBSCOhost - printed on 10/28/2022 4:53 AM via . All use subject to https://www.ebsco.com/terms-of-use

TABLE 11.2 *(continued)*

Specimen	*Taxon*	*Element*		*Basal Length*		*Maximum Breadth*		*Talon (id)*		*Crown Height*		*Crown Center Length*
BOU-VP-3/72	*K. majus*	LM_1	e	21.3	e	18.9						
BOU-VP-3/72	*K. majus*	LM_2	e	29.6		22.7						
BOU-VP-3/72	*K. majus*	LM_3	e	54.9		25.2						
BOU-VP-3/114	*K. majus*	RM_3		55.3		22.1		33.5		22.6		
BOU-VP-3/127	*K. majus*	RM_2		30.0		21.9						
BOU-VP-3/127	*K. majus*	RM_3	*	48.3		22.7		31.5		27.7	*	43.5
BOU-VP-4/1	*K. majus*	LM_1	*	21.1	*	18.8						
BOU-VP-4/1	*K. majus*	LM_2	*	28.1		21.5						
BOU-VP-4/1	*K. majus*	LM_3				22.3		31.2	+	18.5	*	45.1
BOU-VP-4/1	*K. majus*	LP_2		20.1		14.8						
BOU-VP-4/1	*K. majus*	LP_3	*	16.4	e	13.1	*	10.7	e	8.7		
BOU-VP-4/4	*K. majus*	LM^2	*	31.3	*	27.0						
BOU-VP-4/4	*K. majus*	LM^3		49.6		24.1		29.8	+	12.0		51.8
BOU-VP-4/9	*K. majus*	LM_3		45.6		25.2		36.6	+	20.9		
BOU-VP-4/17	*K. majus*	LM_3			*	22.3				20.3		
BOU-VP-4/17	*K. majus*	LM^3		43.4		25.7	*	29.9	+	20.4		
BOU-VP-19/3	*K. majus*	RM_2	*	28.7		20.6						
BOU-VP-19/3	*K. majus*	RM_3	*	47.5		20.8		29.4		20.2		
BOU-VP-19/50	*K. majus*	LP_3		20.9		15.5				19.9		56.3
BOU-VP-19/50	*K. majus*	LM_1		25.1		16.9			+	15.5		23.5
BOU-VP-19/50	*K. majus*	LM_2	*	33.0		21.7						
BOU-VP-19/50	*K. majus*	LM_3			*	22.3				32.6		
BOU-VP-25/28	*K. majus*	LM_3		48.3		22.4		26.9	+	18.9		
BOU-VP-25/71	*K. majus*	LM^2	*	51.6		27.2		36.0	+	20.4		
BOU-VP-25/71	*K. majus*	LM^3		24.3		25.1						
BOU-VP-25/98	*K. majus*	RM^1	*	26.2		24.8						
BOU-VP-25/98	*K. majus*	RM^2	*	31.1		28.7						
BOU-VP-25/98	*K. majus*	LP^2	*	17.4		12.9						
BOU-VP-25/98	*K. majus*	LP^3		20.0		21.0						
BOU-VP-25/98	*K. majus*	LP^4		19.0		24.5						
BOU-VP-25/107	*K. majus*	LM^1	*	21.3	*	21.1						
BOU-VP-25/107	*K. majus*	LM^2	*	27.3	*	22.9						
BOU-VP-25/107	*K. majus*	LM^3				25.4		33.6	+	16.3		42.2
BOU-VP-25/107	*K. majus*	LP^1	*	11.9								
BOU-VP-25/107	*K. majus*	LP^2	*	17.1		12.9						
BOU-VP-25/107	*K. majus*	LP^3	*	17.5		16.8						
BOU-VP-25/107	*K. majus*	LP^4	*	17.6		20.6						
BOU-VP-25/107	*K. majus*	RM^1	*	22.5								
BOU-VP-25/107	*K. majus*	RM^2	*	27.7	*	23.2						
BOU-VP-25/107	*K. majus*	RM^3				25.5		32.9		19.1		40.9
BOU-VP-25/107	*K. majus*	RP^2		16.9	*	11.6						
BOU-VP-25/107	*K. majus*	RP^2	*	11.7								
BOU-VP-25/107	*K. majus*	RP^3		20.5	*	16.4						
BOU-VP-25/107	*K. majus*	RP^4	*	21.6	*	19						

NOTE: + marks indicate that the crown height of the specimen would have been higher if unworn. * marks denote measurements rendered slightly off due to damaged or obscuring matrix. e refers to estimated (± 3 mm) measurements.

EBSCOhost - printed on 10/28/2022 4:53 AM via . All use subject to https://www.ebsco.com/terms-of-use

TABLE 11.3 Daka Member *Kolpochoerus olduvaiensis* Dental Metrics

Specimen	*Taxon*	*Element*		*Basal Length*		*Maximum Breadth*		*Talon (id)*		*Crown Height*	*Crown Center Length*
BOU-VP-3/77	*K.* cf. *olduvaiensis*	LM_3								37.7	54.1
BOU-VP-1/16	*K. olduvaiensis*	LM_2		27.7		18.1					
BOU-VP-1/16	*K. olduvaiensis*	LM_3	e	50.9		19.9		26.1	+	20.5	
BOU-VP-1/27	*K. olduvaiensis*	LM^3		56.5		28.3			+	10.3	60.1
BOU-VP-1/46	*K. olduvaiensis*	RM_3				26.3		32.3	+	14.9	
BOU-VP-1/96	*K. olduvaiensis*	LM_3		63.0	*	23.2	e	24.6	+	19.8	61.1
BOU-VP-1/110	*K. olduvaiensis*	LM_3	e	64.1		19.5		26.6		26.6	60.1
BOU-VP-1/110	*K. olduvaiensis*	RM_3	e	58.2		18.3		27.1	+	16.0	79.9
BOU-VP-2/17	*K. olduvaiensis*	RM^3		59.4		22.8		24.9		31.2	76.1
BOU-VP-2/22	*K. olduvaiensis*	LM_2		28.0		22.3			+	12.3	28.6
BOU-VP-2/22	*K. olduvaiensis*	LM_3		78.6		27.8		31.1	+	13.7	78.6
BOU-VP-3/7	*K. olduvaiensis*	LM^3	*	75.3	*	31.9		32.1	+	10.8	74.6
BOU-VP-3/42	*K. olduvaiensis*	LM_3				23.0				20.4	
BOU-VP-3/62	*K. olduvaiensis*	LM_3				22.0				23.8	
BOU-VP-3/65	*K. olduvaiensis*	LM_1		19.1		17.3		17.3			
BOU-VP-3/65	*K. olduvaiensis*	LM_2		28.5		22.3					
BOU-VP-3/65	*K. olduvaiensis*	LM_3				24.8		31.9	+	12.8	
BOU-VP-3/65	*K. olduvaiensis*	LP_4		18.3		14.3					
BOU-VP-3/69	*K. olduvaiensis*	RM_3	*	81.6		28.6		32.8	+	14.5	75.9
BOU-VP-3/100	*K. olduvaiensis*	RM_3	*	82.3		27.4		32.9	+	12.9	
BOU-VP-3/122	*K. olduvaiensis*	RM_3			e	20.4			+	17.8	80.7
BOU-VP-3/124	*K. olduvaiensis*	LM_3		82.4		25.7		32.7	+	25.8	80.9
BOU-VP-19/51	*K. olduvaiensis*	RM_3	*	64.1		20.0		28.1		20.4	57.5
BOU-VP-25/14	*K. olduvaiensis*	RM_3			e	19.3				28.2	
BOU-VP-25/69	*K. olduvaiensis*	LM^3		60.9		23.6		25.6	+	25.3	86.7
BOU-VP-25/103	*K. olduvaiensis*	RM_3	*	67.8		23.2		26.1		29.6	63.7
BOU-VP-3/140	*K. olduvaiensis*	RM_3		52.7		22.6		23.4			53.9

NOTE: + marks indicate that the crown height of the specimen would have been higher if unworn. * marks denote measurements rendered slightly off due to damaged or obscuring matrix. e refers to estimated (± 3 mm) measurements.

DISCUSSION Daka *M. compactus* M3s are extremely hypsodont. None exhibit root fusion. Relatively symmetrical pillars are H, Y, and T shaped; the portion of their enamel farthest from the midline of the tooth is mesiodistally elongate. Enamel pillars are fused or nearly fused in specimens at advanced wear stages. The two complete M3s found have five and six pairs of pillars. The upper canine is large, gently curved, oval in cross section, and lacks enamel. Daka *M. compactus* M^3 lengths are well within the range for the species reported by Harris and White (1979) (Table 11.1). Crown height falls outside Harris and White's (1979) reported range (63.4–90 mm) in many of the Daka specimens (39–80 mm). Daka *M. compactus* appears in Figure 11.6.

Metridiochoerus cf. *hopwoodi* (Leakey, 1958)

Metridiochoerus hopwoodi and *M. modestus* co-occur at Konso-Gardula throughout levels 4 and 5. In the Konso assemblage, *M. hopwoodi* M3s are larger overall, have

EBSCOhost - printed on 10/28/2022 4:53 AM via . All use subject to https://www.ebsco.com/terms-of-use

TABLE 11.4 Daka Member Metridiochoerine Dental Metrics

Specimen	*Taxon*	*Element*		*Basal Length*		*Maximum Breadth*	*Talon (id)*		*Crown Height*	*Crown. Center Length*
BOU-VP-1/76	*M.* cf. *compactus*					18.6				50.8
BOU-VP-1/76	*M.* cf. *compactus*			27.5		20.0				
BOU-VP-1/4	*M. compactus*	RM^3			*	21.8			66.0	
BOU-VP-1/90	*M. compactus*	LM^3				25.9			39.9	
BOU-VP-1/117	*M. compactus*	LM^3		88.1		24.4			56.3	
BOU-VP-1/120	*M. compactus*	LM^3		63.7		24.8		*	66.1	
BOU-VP-1/151	*M. compactus*	RM^3			*	25.6			54.4	
BOU-VP-1/156	*M. compactus*	LM^3				20.8		+	47.7	
BOU-VP-1/170	*M. compactus*	RM^3			e	26.8			51.8	
BOU-VP-1/172	*M. compactus*	RM^3		80.4		23.3			80.0	
BOU-VP-1/191	*M. compactus*	RM_3				21.8				
BOU-VP-1/237	*M. compactus*	RM^3	*	74.6		20.1			66.3	
BOU-VP-1/237	*M. compactus*	RM^2		27.4		19.4				
BOU-VP-4/12	*M. compactus*	RM^3			e	22.0		+	52.5	
BOU-VP-2/14	*M.* cf. *hopwoodi*	RM^3		57.6		16.6			33.4	
BOU-VP-1/66	*M.* ?*modestus*/?*hopwoodi*	LM^3				18.2			42.6	
BOU-VP-1/185	*M.* ?*modestus*/?*hopwoodi*	RM^3			*	15.0		+	29.2	
BOU-VP-19/13	*M.* ?*modestus*/?*hopwoodi*	LM_2		18.9		12.9			39.1	
BOU-VP-19/13	*M.* ?*modestus*/?*hopwoodi*	LM_3				15.7				
BOU-VP-1/181	*M. modestus*	LM^3			*	13.7			37.9	
BOU-VP-1/186	*M. modestus*	RM^3			*	14.1		+	22.9	46.8
BOU-VP-1/194	*M. modestus*	LM^3				13.5			43.4	41.1
BOU-VP-2/68	*M. modestus*	RM^3				12.5		+	24.7	
BOU-VP-4/7	*M. modestus*	LM^3				14.1		*	30.2	
BOU-VP-19/6	*M. modestus*	RM_3		38.6		11.8			27.7	
BOU-VP-19/35	*M. modestus*	RM_3	*	50.1		13.0			38.5	38.8
BOU-VP-25/15	*M. modestus*	RM_3			*	11.8			40.5	
BOU-VP-25/21	*M. modestus*	RM_3				11.6		+	31.8	44.6
BOU-VP-25/51	*M. modestus*	RM_3	*	44.7		13.1			41.1	
BOU-VP-25/101	*M. modestus*	LM^3		47.8		15.1			34.5	50.2
BOU-VP-26/8	*M. modestus*	LM_3		49.0	*	14.5			43.3	
BOU-VP-26/23	*M. modestus*	LM^3				14.9			47.2	42.6
BOU-VP-2/67	*M.* ?*modestus*/?*Phacochoerus*	LM_3			*	11.5			30.2	
BOU-VP-2/67	*M.* ?*modestus*/?*Phacochoerus*	RM_3			*	12.1			36.9	37.6
BOU-VP-1/124	*Phacochoerus*	RM_3	e	43.4		13.9		+	14.3	
BOU-VP-19/14	*Phacochoerus*	$L?M_3$				11.0		+	27.7	40.1
BOU-VP-19/55	*Phacochoerus*	RM_3				10.6			35.4	43.6

NOTE: + marks indicate that the crown height of the specimen would have been higher if unworn. * marks denote measurements rendered slightly off due to damaged or obscuring matrix. e refers to estimated (± 3 mm) measurements.

more complicated enamel pillar outlines, especially laterally where they are sometimes bilobate, and have pillars that merge earlier in wear than contemporary *M. modestus*. Maxilla BOU-VP-2/14 exhibits these features and is provisionally assigned to *M. hopwoodi*.

EBSCOhost - printed on 10/28/2022 4:53 AM via . All use subject to https://www.ebsco.com/terms-of-use

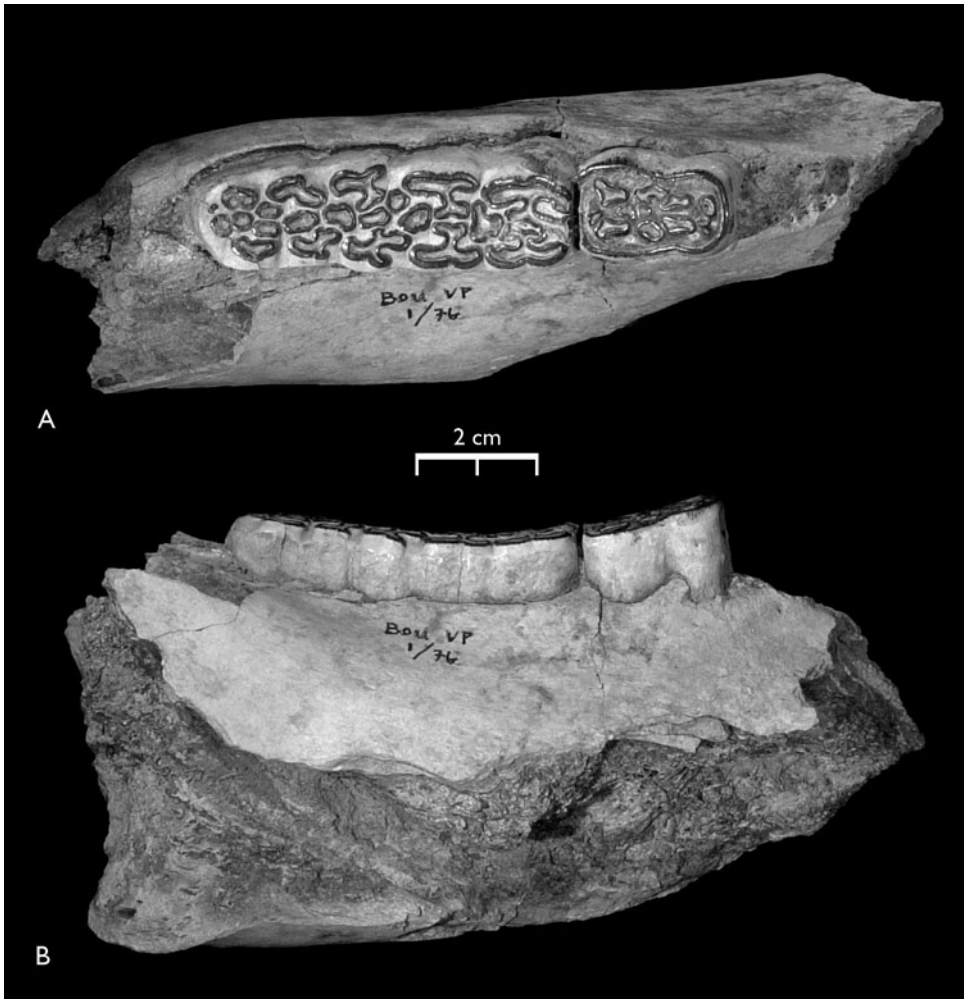

FIGURE 11.6
BOU-VP-1/76 *Metridiochoerus compactus* right mandible. A. Occlusal view. B. Lateral view. Left of photo is caudal.

Metridiochoerus modestus (Van Hoepen and Van Hoepen, 1932)

DIAGNOSIS "Species of *Metridiochoerus* of small size. Cranium, mandible, and canines strongly resemble those of *Phacochoerus*. Third molar very hypsodont but constituent elements aligned as in *Metridiochoerus* rather than *Phacochoerus*" (Harris and White 1979, 49).

TABLE 11.5 *Kolpochoerus majus* Mandibular Measurements

Measurement	*BOU-VP-3/10*	*BOU-VP-1/58*	*BOU-VP-4/1*	*BOU-VP-3/50*
Mandibular length	37.5e		37	
Mandibular height	24.2			19.7
Mandibular symphysis breadth	13.9	10.38	13.24	
Mandibular symphysis length	14.19	11.66	13.76	
Postcanine constriction	10.5	8.15	10.44	
Molar series length			9.43	
Premolar series length			5.05	

EBSCOhost - printed on 10/28/2022 4:53 AM via . All use subject to https://www.ebsco.com/terms-of-use

FIGURE 11.7
BOU-VP-1/124 *Phacochoerus* mandible.
A. Anterior view.
B. Right lateral view.
C. Occlusal view.

DISCUSSION Dental material assigned to *M. modestus* is similar in size to some modern *Phacochoerus africanus*. Lateral pillars in Daka *M. modestus* are more mesiodistally elongate than the enamel pillars of most modern *Phacochoerus*. This morphology aligns them with *Metridiochoerus*, although modern *Phacochoerus* has variable M3 morphology (Ewer 1958). Unlike many modern warthog M3s, the Daka buccal and lingual M3 pillars are relatively symmetrical across the crown, even in early wear stages. Both M^3 and M_3 lengths in Daka *M. modestus* overlap with those reported for the taxon in Harris and White (1979), while Daka specimens are, on average, narrower buccolingually. Daka *M. modestus* has a typical *Metridiochoerus* enamel pattern and flaring trigon roots characteristic of the genus.

EBSCOhost - printed on 10/28/2022 4:53 AM via . All use subject to https://www.ebsco.com/terms-of-use

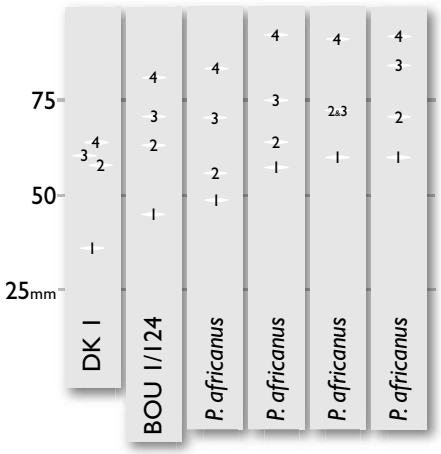

FIGURE 11.8
Metridiochoerus modestus and *Phacochoerus* mandibular measurements. BOU-VP-1/124 *Phacochoerus*, recent *P. africanus* specimens collected from the Middle Awash study area in the Afar Rift of Ethiopia, and the DK 1 *M. modestus* skull from Bed 1 of Olduvai Gorge, Tanzania. Measurements: 1. Minimum breadth of the lateral margins of the mandibular corpus posterior to the canines. 2. Chord from posterior border of canine socket to anterior margin of M_1 alveolus measured along the alveolar crest. 3. Chord from alveolare to anterior margin of M_1 alveolus. 4. Anteroposterior length of the symphysis. Measurements on the DK 1 skull for measurements 2 and 3 were taken from photographs in Cooke (1984).

Cooke (1984) places *modestus* in *Phacochoerus* in his description of cranium DK I but did not engage in differential description that included both *Metridiochoerus* and *Phacochoerus*, preferring to use the latter and *Sus* as reference points. Harris and White (1979) assign the species to *Metridiochoerus* based on dental morphology. Cooke (1982) does note the clear resemblance of *M. modestus* to *Metridiochoerus* in his discussion, if not in his description, and suggests it has a close relationship with *M. andrewsi*. Harris and White (1979) note tooth size similarities between *M. modestus* and *M. andrewsi*. Noting clear differences between dental specimens assigned to this genus and *Phacochoerus* in the assemblage, we follow Harris and White (1979).

Phacochoerus Cuvier, 1817

DIAGNOSIS "A sexually dimorphic genus of Suidae of small to moderate size. Cranium with broad zygomatic arches lacking distinct knobs, elevated orbits and short cranial region. Upper incisors reduced to one pair. Upper canines lacking enamel except at tips. Premolars reduced and commonly shed in adults. Molars hypsodont, formed of closely packed columnar elements and well cemented; lateral pillars flattened externally, elongate and oval to subtriangular in shape" (Harris and White 1979, 65).

DISCUSSION Both Cooke (1984) and Harris and White (1979) agree that the origin of modern *Phacochoerus* is unresolved with respect to *Metridiochoerus modestus*. White and Harris (1979) point to contemporaneous *M. modestus* and *Phacochoerus* from Olduvai Beds IV as evidence that there is no clear anagenetic lineage between the two taxa. Their coexistence in the Daka Member further supports this conclusion. We agree with Cooke (1984) that more cranial material is necessary for any definitive statement to be made regarding the origin of *Phacochoerus*.

One of the problems in *Phacochoerus* systematic work noted by several authors (Harris and White 1979; Cooke 1984; White 1995) is the tendency for modern warthog teeth to take on a fossilized appearance after a geologically brief period. This renders many supposedly prehistoric warthog teeth collected from the surface of suspect antiquity. Fortunately, one of the best *Phacochoerus* specimens from the Daka Member was found in

EBSCOhost - printed on 10/28/2022 4:53 AM via . All use subject to https://www.ebsco.com/terms-of-use

TABLE 11.6 Daka Member Suid Cranial Metrics

Measurement	*BOU-VP-3/150*	*BOU-VP-7/2*	*BOU-VP-1/7*
Basilar length		43.1	40.5
Bizygomatic breadth	26.6	35.6	26.4
Occipital Height	17.4		
Parietal constriction	3.7		
Frontal breadth	14		17.7
Muzzle breadth	5.2e	6.09	5.6
Palate length		31.45	28.8
Lateral maximum M\3-M\3 breadth	7.2e	9.55	9.1
Medial minimum M\3-M\3 breadth		4.2	3.5
Maximum premax breadth		7.64	9.1
Anterior muzzle (including-anterior can.)		8.7	7.31
Molar series length		93.7	85.8
Premolar series length		49.7	47

situ. This specimen, mandible BOU-VP-1/124, presents an anteriorly arched, projecting incisor alveolar margin like that found in *Phacochoerus* rather than a flat, spatulate margin like that seen in *Metridiochoerus*, including *M. modestus* (Figure 11.7). This specimen also presents metrics aligning it with *Phacochoerus*, most relating to a relatively longer snout than is found in *M. modestus* (Figure 11.8, Table 11.6).

Conclusion

Daka pigs provide important systematic data. Until recently, *Kolpochoerus majus* was not well known. Recent discoveries have improved its record substantially, and the past decade has seen an increased interest in *Kolpochoerus* (Geraads 1993; Cooke 1997; Brunet and White 2001; Suwa et al. 2003). Metrics of Daka *K. majus* overlap with those reported in Harris and White (1979). Patterns of sexual dimorphism in this taxon are well documented by Daka material. With Bodo, Gona, Konso, and Daka material, this previously ill-defined taxon now has a rich eastern African record. *Kolpochoerus olduvaiensis* is well represented in the Daka Member and further demonstrates the gradual elongation of M3 talons and talonids in this lineage during the early Pleistocene. Daka specimens substantially improve the quality of *K. olduvaiensis* as a biochronological indicator. Daka *Metridiochoerus modestus* co-occurs with distinctive *Phacochoerus*. This provides further evidence supporting the metridiochoere status of the former and represents the earliest well-established record of the latter.

The Daka Member is the best dated sample of African suids known from the 1.0 Ma horizon. It contributes a solid reference for both biochronological and phylogenetic studies. Additionally, Daka Member suids provide data relevant to local paleoecology and global paleoclimate and are discussed in this regard in Chapter 17.

EBSCOhost - printed on 10/28/2022 4:53 AM via . All use subject to https://www.ebsco.com/terms-of-use

12

Rare Taxa

W. HENRY GILBERT
AND
THOMAS STIDHAM

While preservation of large mammals in the Daka Member is very good, there are few micromammals and birds preserved. These phylogenetically disparate fossils include a possible stork, a grass rat, and a fish.

Aves

Relatively few Pleistocene avian fossils have been described from Ethiopia (Brodkorb 1980; Brodkorb and Mourer-Chauviré 1982). This contrasts with the better-known avifaunas elsewhere in Africa, including those from Olduvai, Die Kelders Cave, and other assemblages. Despite this rarity of data on Ethiopia, the avifauna of Ethiopia's recent past should be quite interesting, because the modern avifauna of Ethiopia is composed of many rare, endangered, and endemic birds, including such species as Stresemann's bushcrow *(Zavattariornis stresemanni)*. The fossil from the Daka Member does not belong to any of the previously described taxa from the Pleistocene of Ethiopia and thus represents an additional species on the avifaunal list of Ethiopia's past.

aff. Ciconiiformes Bonaparte, 1854

Specimen BOU-VP-3/138 (Figure 12.1) is a fragment of the distal end of a right carpometacarpus from a large-sized bird. Most of the fragment is of the major metacarpal (with the articular surface for digit II preserved), and some is of the interosseus bone, which connected the major metacarpal with the minor metacarpal. The proximal end of the fragment is only slightly proximal to the proximal end of the interosseus bone.

DESCRIPTION On the dorsal side of the major metacarpal is a large pneumatic pocket. The anterodorsal edge of the major metacarpal has an undulating edge with a slightly raised area at about the midpoint of the specimen and a raised tuber adjacent to the phalangeal articulation. These are next to a tendinal groove. The anterior face of the major metacarpal is relatively flat but has a groove on the ventral side of the distal end. The phalangeal articular facet is asymmetrical in distal view, with the dorsal portion of the facet extending anterior to the ventral portion. A smaller tubercle is present posterior to

EBSCOhost - printed on 10/28/2022 4:53 AM via . All use subject to https://www.ebsco.com/terms-of-use

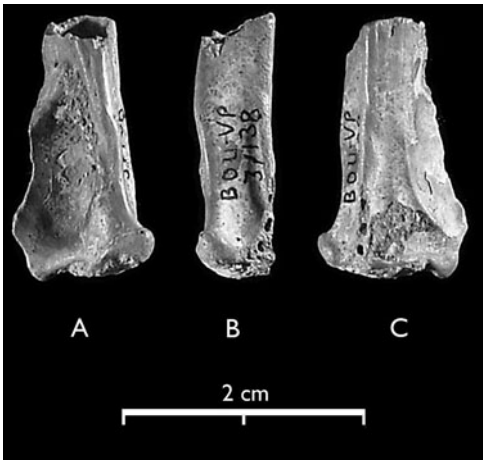

FIGURE 12.1
Right carpometacarpus of aff. Ciconiiformes. A. Dorsal view. B. Anterior view. C. Ventral view.

the asymmetrical part. The ventral face is relatively flat, but the posterior edge is scalloped (ventral to the pneumatic pocket).

DISCUSSION The carpometacarpus fragment is from a large bird. Accipitrids lack the deep pneumatic pocket seen in the Daka specimen. *Bucorvus* (Bucerotidae) also lacks the pocket, and, in addition, the major metacarpal is very inflated in comparison to the fossil. Comparisons with Ardeidae, Pelecaniformes, Gruidae, Numididae, Anatidae, Columbidae, Laridae, and other large to medium-sized taxa appear to rule out allocation of the fossil to any of those clades. The fossil is possibly a taxon within the Ciconiiformes. Order Ciconiiformes is composed of large wading birds, including herons, egrets, and storks.

Murinae

Murine rodents (rats, mice, and relatives) possibly originated in southeast Asia and diversified during the middle and late Miocene across the Old World (Steppan et al. 2004, 2005). Multiple migrations of the subfamily into Africa from Eurasia are plausible (Steppan et al. 2005). African otomyines and arvicanthines diverged in the latest Miocene (Steppan et al. 2004, 2005). The first appearance of *Arvicanthis*, the unstriped grass mouse or grass rat, in the fossil record is in the Omo Shungura Formation (upper Member G and upper Member B) and dates to approximately 3 Ma (Wesselman 1984; Feibel et al. 1989). Modern members of *Arvicanthis* are highly variable in size and other morphological features, and distinction of species within living *Arvicanthis* is controversial (Wesselman 1984; Ducroz et al. 1998). The Daka specimen is identified only to genus.

Arvicanthis Lesson, 1842

GENERIC DIAGNOSIS The teeth of *Arvicanthis* show laminization even when unworn. Laminization is more pronounced, cones are more robust, and crests are broader between the cones than in its close sisters *Aethomys*, *Lemniscomys*, and *Pelomys*. *Lemniscomys* and *Pelomys* have well-isolated cones joined by thinner crests and laminization that occurs

EBSCOhost - printed on 10/28/2022 4:53 AM via . All use subject to https://www.ebsco.com/terms-of-use

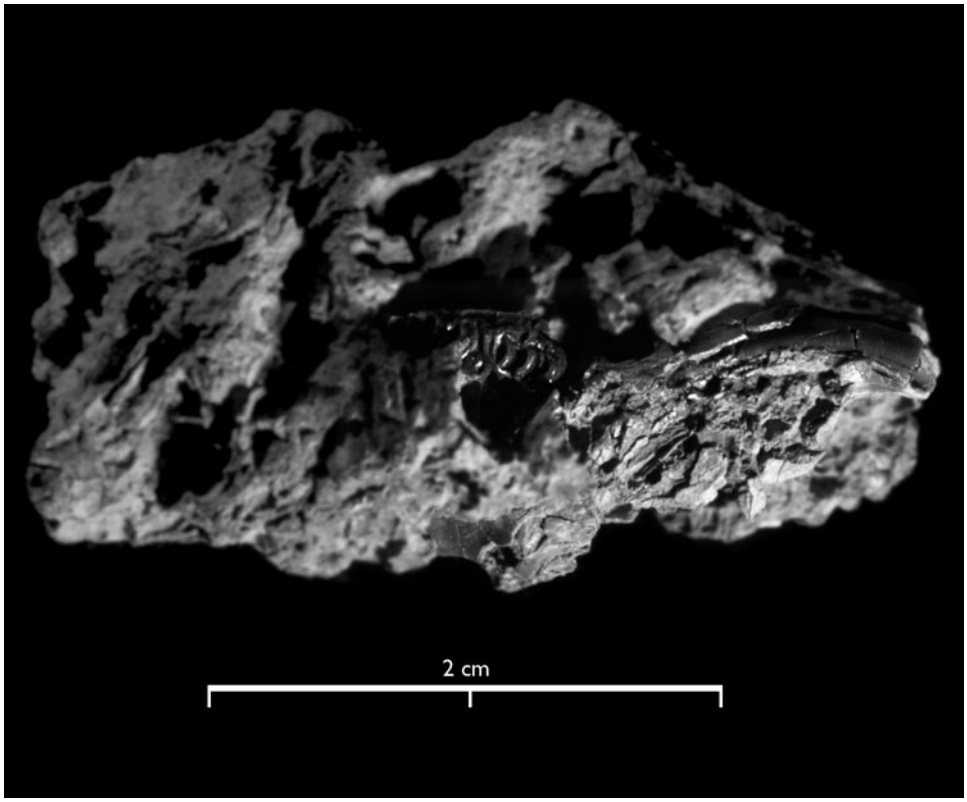

FIGURE 12.2
Arvicanthis cranium showing right upper incisor, M^1, and part of the M^2.

later in wear relative to both *Arvicanthis* and *Aethomys*. The cones of *Arvicanthis* teeth are buccolingually collinear. This is especially true of the lowers, which present linear lamina between cones and lack the characteristic chevron shape of close sister taxa. The talon of the M^3 in *Arvicanthis* is narrow and mesiodistally elongate relative to *Aethomys*. There are no outer cingular conules in the lower dentition (see Misonne 1969).

REMARKS Specimen BOU-VP-25/95 (Figure 12.2) is a cranium embedded in matrix that exposes the right incisor, M^1, and part of the M^2. Its identification to Murinae is straightforward based on overall morphology. The unworn occlusal surfaces of the M^1 and M^2 are laminar, with no outer cingular conules, confirming the specimen as *Arvicanthis*. This specimen is not identified to species.

Siluriformes

Siluriformes, the catfish order, comprises 35 families, 446 genera, and nearly 3,000 species (Nelson 2006). Taxa in Siluriformes are common elements of African waterways. Nine siluriform families are known from Africa: Amphilidae (66 species in Africa), Mochokidae (179 species in Africa), Malapteruridae (19 species in Africa), Auchenoglanididae (28 species in Africa), Clariidae (90 species in Africa and Asia), Austroglanidae (3 species in Africa), Claroteidae (59 species in Africa), Schilbeidae (56 species in Africa and Asia), and Bagridae (170 species in Africa and Asia).

EBSCOhost - printed on 10/28/2022 4:53 AM via . All use subject to https://www.ebsco.com/terms-of-use

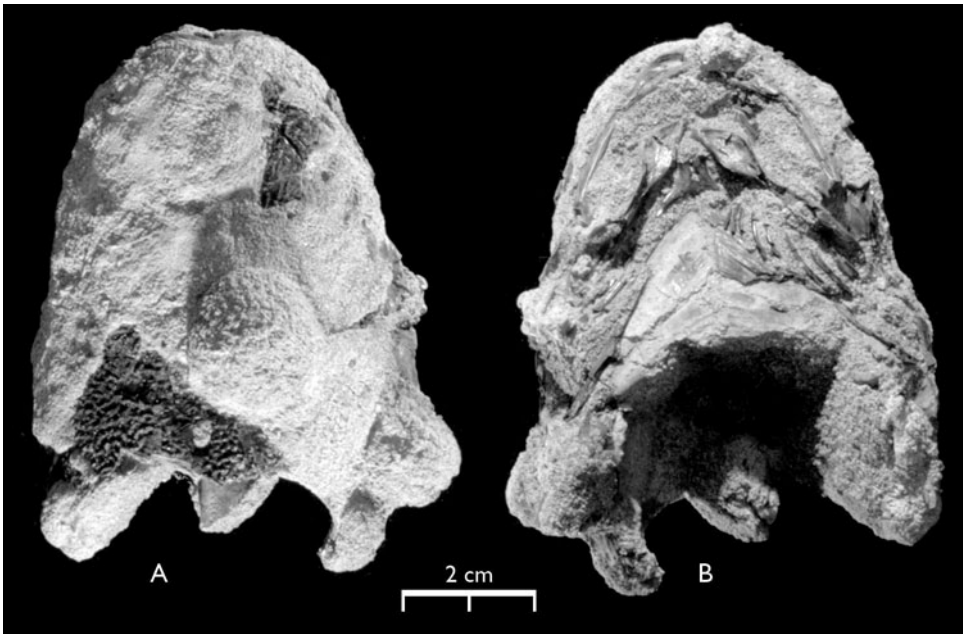

FIGURE 12.3
Siluriformes cranium.
A. Dorsal view.
B. Ventral view.

Specimen BOU-VP-3/91 (Figure 12.3) is the cranium of a member of Siluriformes. While the cranium is complete, it is encased in matrix. Only small parts of the cranial surface of the neurocranium and the ventral surfaces of the mandibular arch, palatoquadrate, hyoid arch, branchial arches, opercular, and pectoral girdle are visible through the matrix. Further cleaning and analysis will certainly allow refinement of its taxonomic assignment.

Conclusions

Micromammals and birds are very rare in the Daka Member. Part of this phenomenon relates to collection procedures (isolated fish bones, crocodile teeth, and crocodile scutes were not collected), but much of it is related to the site's preservation. There are no known areas in the Daka Member with concentrations of micromammals, and there are no bird fossils beyond the single one described in this chapter.

EBSCOhost - printed on 10/28/2022 4:53 AM via . All use subject to https://www.ebsco.com/terms-of-use

13

Homo erectus Cranial Anatomy

BERHANE ASFAW,
W. HENRY GILBERT,
AND
GARY D. RICHARDS

This chapter, the first of four discussing Daka hominid material, presents a detailed ectocranial description of the Daka calvaria (BOU-VP-2/66) and a presentation of other cranial and mandibular specimens from the Daka Member. The other chapters on Daka hominids assess endocranial and internal features (Chapter 14), the systematic placement of the Daka calvaria (Chapter 15), and hominid postcranial remains (Chapter 16).

Recovery, Cleaning, and Restoration

The first hominid fossils found at Bouri were recovered in 1992 from Daka Member sediments. These remains were femoral specimens and are described in Chapter 16. The first cranial remains were found the following year but were highly fragmentary and not diagnostic (see the section on "Additional Cranial and Mandibular Specimens," later in this chapter). Late in the 1997 field season, while the paleontology team was resting after lunch at BOU-VP-2, one of the authors (WHG) was surveying a pebble lag–covered slope near the drainage divide between BOU-VP-2 and BOU-VP-3. High on the slope the top of a hominid calvaria was emerging from the armored, slowly eroding sediments (Figure 13.1).

After the rest of the crew was alerted, a photo and video documentation was completed prior to any disturbance of the specimen. A perimeter around the in-situ calvaria was protected from foot traffic, and only the discoverer (WHG), a photographer, and an excavator (TW) moved within that c. 50-square-meter area for the duration of the afternoon and evening (Figure 13.2). There are large numbers of domestic and wild animals in this area of the Bouri Peninsula, with porcupines, jackals, hyaenas, lions, and a variety of ungulates regularly passing nocturnally across the outcrops. Furthermore, the project's previous experience with the application of solvent-based preservatives (Vinac dissolved in acetone) has shown that carnivores are able to smell freshly hardened specimens from great distances and are highly attracted to any fossil left overnight in the field.

Given the lateness of the hour, it was immediately decided to delay the sieving of the slope to recover any small vault pieces that had been washed or trampled away from the main specimen. Rather, focus was on extraction of the in-situ cranial vault and base. First, all loose vault

EBSCOhost - printed on 10/28/2022 4:53 AM via . All use subject to https://www.ebsco.com/terms-of-use

FIGURE 13.1

Henry Gilbert at the discovery site of the Daka calvaria BOU-VP-2/66 on the day of its discovery in 1997. The broken occipital profile is to the left, below the broken superior vault profile. Pieces of the vault had scattered downslope during the erosional process, but the remainder of the calvaria was locked into place by the desert pavement that surrounds the fossil. Photograph by Tim White, December 27, 1997.

pieces that had dropped into the calvaria were collected, as well as any pieces embedded in the adjacent desert pavement. Upon close inspection of the in-situ specimen it was apparent that it was exceedingly well fossilized, and many of the broken pieces were still coated with a tightly adhering layer of calcium carbonate. The specimen was oriented in roughly anatomical position, and any facial skeleton and cranial base would have projected below the level of the adjacent desert pavement marking the erosional plane. The specimen had been found at an ideal time in its exposure: Longer exposure to the elements would have further broken and scattered the pieces, and orientation of the specimen helped to secure its anatomy.

Using knives and rock hammers, a deep trench was cut into the original matrix encapsulating the specimen's base, to a level well below the extension of any possible face and/or mandible (Figure 13.3). The top of the specimen was covered with wet tissue, and then plaster medical bandages were applied to the top half of the specimen down to a level near the bottom of the trench. Steel tent pegs were then driven into the base of the trench, and the cranium was rocked free. At this stage of the extraction, completed well after sunset, the jacketed specimen in matrix weighed about 50 kg.

Prior to transport of the specimen from the field to camp at Esa Dibo on the Bouri ridge, the base of the jacketed specimen was further bandaged, completely encasing the removed fossil and embedding matrix. Upon arrival at the National Museum of Ethiopia, the plaster jacket was cut away from the specimen, exposing it approximately as it had been found in the field (Figure 13.4). Matrix around the specimen was differentially indurated, and the softer parts could be brushed away. Harder parts were removed by dental pick (Figure 13.5) and by porcupine quill when working close to bone surface that was not protected by the adhering calcium carbonate matrix. This operation revealed the presence of a dense, reticulate network of calcified rootcasts across the top of the vault

EBSCOhost - printed on 10/28/2022 4:53 AM via . All use subject to https://www.ebsco.com/terms-of-use

FIGURE 13.2

Excavation of the Daka calvaria BOU-VP-2/66 on the day of discovery. The low hills on the skyline are the Dulu Ali basalts and sediments, and the site of Aramis lies beyond these hills. Daka Member sediments are exposed in the rays of the setting sun in the middle distance, with the trees on the right horizon marking the main channel of the Awash River flowing to the north. Photograph taken December 27, 1997.

(Figure 13.6). Loose pieces along the sides of the vault were removed during this operation for later refitting.

As excavation proceeded in the laboratory, it became disappointingly evident that there was no face attached. The endocranial matrix was left in the vault as it was removed from the remaining matrix in the jacket (Figure 13.7). The basicranium was more poorly preserved than the vault pieces, and most of it lacked the thin layer of protective calcite and calcium carbonate matrix. It was penetrated in many places by roots, as indicated by fossilized rootcasts (Figure 13.8), probably of papyrus (see also Plate 14.8). Cleaning of the basicranium took place under a binocular microscope, and consolidation of the fragile bone was done as the cleaning proceeded millimeter by millimeter.

The endocranial matrix was removed last, and the vault pieces were then reattached after the skin of strongly indurated, tightly adherent matrix had been removed by air scribe. The latter operation was also accomplished under a binocular microscope, and some matrix adhering to the postmortem, prefossilization damage on the ectocranial surface (carnivore modifications, see the discussion of the frontal bone later in this chapter and Figure 13.16) was left in place to show the antiquity of these marks.

EBSCOhost - printed on 10/28/2022 4:53 AM via . All use subject to https://www.ebsco.com/terms-of-use

FIGURE 13.3
Henry Gilbert examines the pedestaled Daka calvaria BOU-VP-2/66 after the loose pieces had been collected and prior to jacketing for removal of the specimen. The supraorbitals are directed into the bank nearest the photographer. At this point it was unknown whether the specimen represented a skull, cranium, or calvaria. After this photograph was taken, the calvaria and its pedestal were removed within a plaster jacket and transported to the National Museum of Ethiopia for cleaning. Photograph by Tim White, December 27, 1997.

After cleaning of all the individual pieces, the vault was restored with acetone-soluble Vinac glue. Photography (Figures 13.9–13.11) was completed prior to molding of the carnivore marks for scanning electron microscope (SEM) analysis. A full Silastic E production mold was made of the specimen by Alemu Ademassu. After that documentation was completed, the specimen was measured and analyzed as described in the following sections.

Introduction to Descriptions

Any description or characterization of cranial anatomy is historically embedded. Furthermore, some features, for example the bony circumference of the auditory meatus, are bound functionally and thereby stand out as discrete features warranting description as units. Others, such as the angular torus, are features that emerge by their possession of morphology that triggers human perception to view them as a unit. Many such features are more likely to result from adventitious interaction of morphogenetic developmental fields rather than developmental canalization via selection on an integrated functional unit. For systematics the latter type of feature is useful whereas the former is not. Phylogenetically informative characters should be functionally independent and part of a developmental process with a detectable genetic influence. Unfortunately, this goal is difficult to meet in practice. Most ectocranial features are poorly understood from an evolutionary developmental perspective. This means that these features are of questionable phylogenetic importance and are very likely legacies of descriptive history or human perception rather than a genetic substrate.

The following description of the Daka cranium, like most other descriptions of fossil hominids of this antiquity, was profoundly influenced by Weidenreich (1943),

EBSCOhost - printed on 10/28/2022 4:53 AM via . All use subject to https://www.ebsco.com/terms-of-use

FIGURE 13.4

Removal of the protective plaster jacket at the National Museum of Ethiopia. Tim White is removing the top of the jacket. Left to right: Professor Henry de Lumley, Alban Defleur, John Yellen, Yonas Beyene, Muluneh Gebre-Mariam, and Henry Gilbert. Photograph courtesy of David Brill, October 1998.

FIGURE 13.5

Cleaning matrix from the Daka calvaria by means of a dental pick. At this stage in the preparation it was still not possible to determine whether a face was attached to the vault. Photograph by Tim White, October 1998.

EBSCOhost - printed on 10/28/2022 4:53 AM via . All use subject to https://www.ebsco.com/terms-of-use

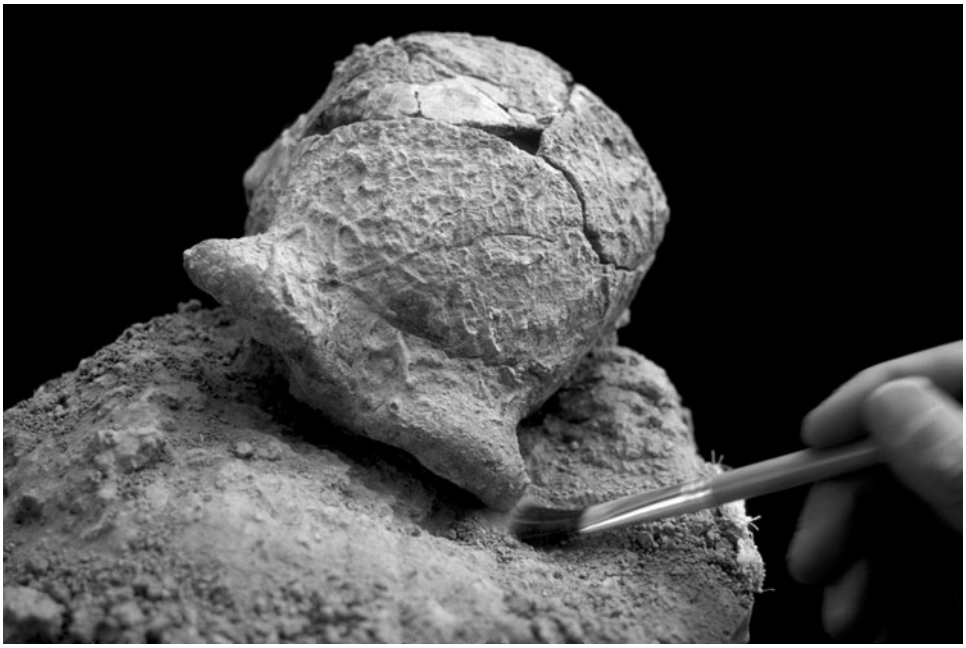

FIGURE 13.6

The Daka calvaria emerges from the rootcast matrix surrounding its lower surface. Note the reticulate network of fossilized papyrus rootcasts covering the ectocranial surface. The right parietal emerged first from the sediment, broken from the specimen and moved downslope as a separate piece. By the time of discovery this fragment had already shed its calcium carbonate matrix. The remaining matrix was tightly cemented to the bone and had to be cleaned with an air scribe after the fragile base of the cranium had been solidified by the application of polyvinyl acetate preservative. Photograph by Tim White, October 1998.

who was himself influenced by Schwalbe (1899, 1902, 1907). These workers chose to describe the traits that impressed them as different from modern apes and humans, and these traits were often chosen for being conspicuous rather than being developmentally or functionally correlated. This is an important consideration, because features such as the angular torus, the postglenoid process, and glabellar inflexion described here have a large influence on interpretation of evolutionary relationships, as discussed in Chapter 15.

Descriptions of *Homo erectus* vary considerably in length. Some are short, such as the seven monograph pages allotted to KNM-ER 3733 (Wood 1991). Others, such as the description of the Zhoukoudian (ZKD) crania (Weidenreich 1943), are much longer. We have chosen thoroughness in preference to brevity for this description. We address features considered by other authors and add some of our own observations with reference to osteological and systematics literature. Our goal is the provision of a written comparative archive of the morphology of the Daka calvaria.

In developing the description we extracted characters and features from many published descriptions and phylogenetic analyses of early *Homo* crania (Martin 1928; Weidenreich 1943; Howells 1980, 1989; Murrill 1981; Rak 1983; Andrews 1984; Stringer 1984; Wood 1984, 1991; Turner and Chamberlain 1989; Kennedy 1991; Pope 1991; Tobias 1991; Frayer et al. 1993; Wu and Bräuer 1993; Lieberman 1995; Lahr 1996; Schwartz and Tattersall 1996; Arsuaga et al. 1997, 1999; Bermúdez de Castro et al. 1997; Martínez and Arsuaga 1997; Seidler et al. 1997; Abbate et al. 1998; Bräuer and Broeg 1998; Dean et al. 1998; Hublin 1998b; Gabunia et al. 2000; Delson et al. 2001; Kramer et al. 2001; Manzi et al. 2001; Rightmire 2001; de Lumley et al. 2006; Rightmire et al. 2006). We added these features to those enumerated for cranial vault bones by White and Folkens (2005).

EBSCOhost - printed on 10/28/2022 4:53 AM via . All use subject to https://www.ebsco.com/terms-of-use

FIGURE 13.7

The uncleaned endocranial cavity of the Daka calvaria. Note the right petrous portion with the fossilized rootcast. Photograph by Tim White, January 1999.

Some of these features were addressed cladistically in the Asfaw et al. (2002) announcement of the Daka calvaria (and see Chapter 15). As pointed out by White et al. (2001), effective descriptions should be comparative. Effort was made to describe the Daka calvaria relative to other pertinent specimens. This description is organized by anatomical region to facilitate efficient use.

The Daka calvaria was compared to casts, published descriptions, and illustrations of an array of Pleistocene *Homo* crania. We did not include European middle Pleistocene hominids, such as the Sima de los Huesos specimens, Arago, Petralona, or Steinheim, which, with the exception of Ceprano (which we did include), are likely early members of the Neanderthal lineage (Arsuaga et al. 1997). Additionally, we did not include KNM-WT 15,000 because of its juvenile status. Our primary in-house comparative sample included Dmanisi D 2280 and D 2282; KNM-ER 3733; KNM-ER 3883; OH 9; OH 12; Sangiran 2, 4, and 17; Trinil 2; Sambungmacan 1 and 3; Ngandong 6, 7, 11, and 12; ZKD 3, 5, 10, 11, and 12; Kabwe; Bodo; Ceprano; Mapa; and Saldanha. Features were compared for specimens Dmanisi D 2700, BOD-VP-1/1, Sambungmacan 4, Hexian, Dali, and Buia using published descriptions (Asfaw 1983; Wu and Poirier 1995; Abbate et al. 1998; Vekua et al. 2002; Baba et al. 2003; Rightmire et al. 2006). Many observations of discrete features described here were made on casts, but distortion inherent to molding and casting materials and procedures renders physical replicas of fossils less effective than original specimens for accurate measurement (Clarke and Howell 1972; White 2000). Frequently, missing anatomy, fossil preservation, published description depth, or cast quality precluded accurate assessment of particular features. After this chapter was written, a fourth cranium from Dmanisi was described (D 3444; Lordkipanidze et al. 2005, Lordkipanidze et al. 2006). Neither this

EBSCOhost - printed on 10/28/2022 4:53 AM via . All use subject to https://www.ebsco.com/terms-of-use

FIGURE 13.8

Close-up of the right petrous and the network of fossilized rootcasts within the uncleaned endocranial cavity. Photograph by Tim White, January 1999.

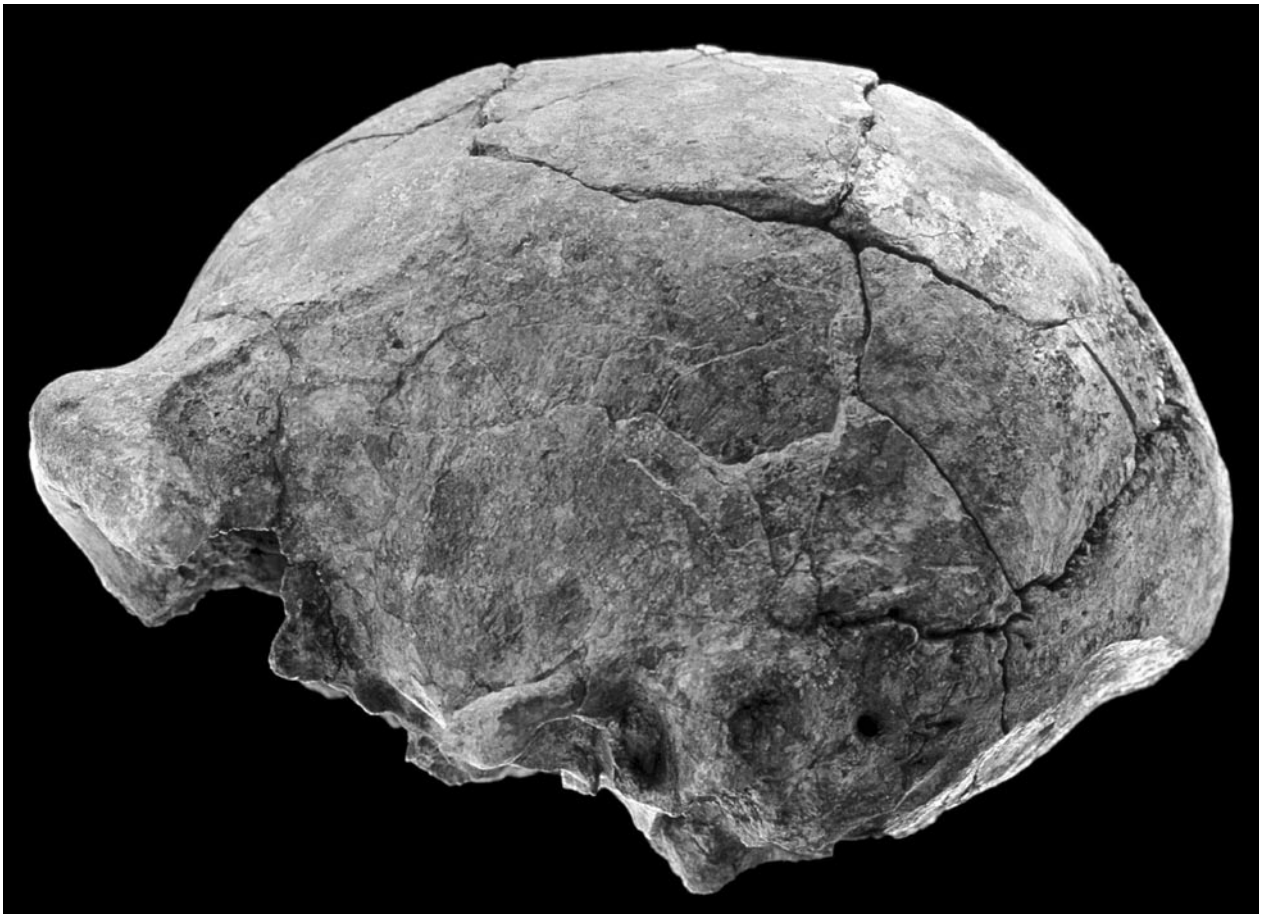

FIGURE 13.9

Left lateral view of Daka *Homo erectus* calvaria, BOU-VP-2/66. Photograph courtesy of David Brill.

EBSCOhost - printed on 10/28/2022 4:53 AM via . All use subject to https://www.ebsco.com/terms-of-use

FIGURE 13.10

View of Daka *Homo erectus* calvaria, BOU-VP-2/66, in approximated Frankfurt horizontal. Photograph courtesy of David Brill.

specimen nor another important one from the same site are included in our comparative analysis.

Many of Daka's features, such as smaller cranial capacity, are primitive. Conversely, many features, such as elevated cranial vault thickness and massiveness of the supraorbital tori, are derived relative to earlier hominids, even though these have traditionally been interpreted as primitive relative to later *Homo sapiens*. However, speculation that these and several other features could be used to define a monophyletic group has been offered for decades (Leakey 1934) and advanced more recently

EBSCOhost - printed on 10/28/2022 4:53 AM via . All use subject to https://www.ebsco.com/terms-of-use

FIGURE 13.11
Oblique view of Daka *Homo erectus* calvaria, BOU-VP-2/66. Photograph courtesy of David Brill.

through more formal cladistic analysis (Andrews 1984). These characters of cranial robusticity, particularly pronounced in Pleistocene *Homo*, are today often viewed as autapomorphies (uniquely derived characters), but this contrasts with substantial evidence for a consistent, accelerating increase in cranial capacity in Pleistocene *Homo* through time and across the noninsular Old World (Rightmire 2004). The hypothesis that these features were acquired and later lost, with *H. erectus* occupying a broadly ancestral status to *H. sapiens*, therefore continues to be widely accepted among active paleoanthropologists.

One obstacle to providing a thorough comparative description for Pleistocene *Homo* crania is the inconsistent reporting of cranial metrics by describers. For this reason we compiled a comprehensive list of measurements made on Pleistocene *Homo* crania using multiple published sources (Appendix 13.1). This appendix presents Daka measurements and indices for over 200 published metrics. Most of these measurements were made using the original specimen; some are derived from CT and microscribe

EBSCOhost - printed on 10/28/2022 4:53 AM via . All use subject to https://www.ebsco.com/terms-of-use

data. Values for the Daka calvaria are in relative agreement where measurements were taken with multiple methods. Measurements of the bony labyrinth of the petrous and several vault thickness measurements from nonstandard locations on the calvaria are presented in Chapter 14 and do not appear in Appendix 13.1. Note that we did not include metrics that required the establishment of Frankfurt Horizontal. Without knowing the height of the orbits, this estimation would lead to measurements with lessened comparative value relative to other specimens in the *H. erectus* hypodigm. However, we have made every effort to approximate correct orientation in the visual comparisons here.

Daka Calvaria: Overall Size, Shape, and Proportions

The Daka calvaria is described here from six standard views. Each view is treated separately, and emergent patterns of calvaria morphology are discussed within each. Features expressed over more than one vault bone (e.g., the temporal lines) are described in these views, whereas features that are restricted to individual bones are treated in the section on individual bones of the calvaria.

Frontal View (Plate 13.1)

Preservation and Distortion

All the facial elements below nasion are missing. The frontal is complete and presents minimal distortion. The supraorbital tori are fully preserved, with intact frontal halves of the frontozygomatic sutures bilaterally. In frontal view, the greater wings of the sphenoid are visible along the anterior connection to the zygomatic process of the frontal. The superior surface of the right supraorbital torus lateral to the supraorbital foramen is depressed, by less than 1.0 mm, as a result of a fracture that bisects the torus. The remainder of the frontal bone is free from any distortion visible in this view. Details on fragments and cracks are presented in the next section on individual bones of the calvaria.

Overall Outline and Proportions

In frontal view, the Daka calvaria presents massive, individually arching supraorbital tori and a frontal squama that is separated from these tori by a deep and wide supratoral sulcus. The supraorbital tori project anteriorly (including the glabellar region) in a continuous bony torus. The maximum frontal breadth of the Daka calvaria is narrower than the overall maximum cranial breadth (see Appendix 13.1). The maximum breadth of the calvaria occurs in the mastoid/supramastoid region, a condition typically seen in African and Asian *Homo erectus*. A very weak keel extends from the sagittal midpoint of the frontal into the bregma region. This keel is interrupted by the loss of a fragment of the right parietal in the bregma region.

Viewed from the front, the Daka calvaria's combination of relatively flat sides and gently sloping parietals between the bosses and the sagittal suture results in a sharp angle above the temporals (see Chapter 15, Figure 15.1). Weidenreich (1943) refers to the pronounced bosses resulting from this vault configuration as parietal tuberosities

EBSCOhost - printed on 10/28/2022 4:53 AM via . All use subject to https://www.ebsco.com/terms-of-use

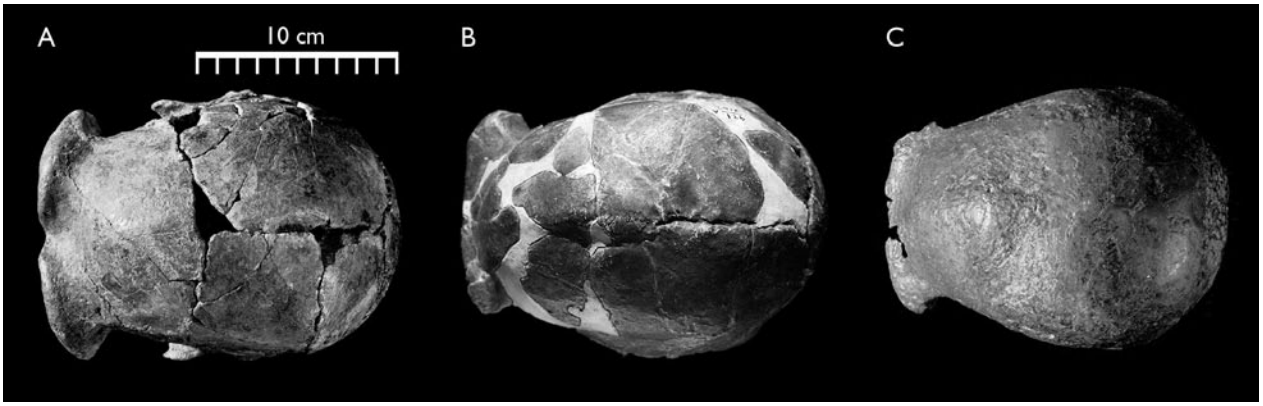

FIGURE 13.12
Superior views. A. Daka calvaria. B. ZKD 10. C. Trinil 2. Photograph by Tim White.

for the Zhoukoudian crania, and we follow this convention. The Daka calvaria differs from the Zhoukoudian specimens in that the vault is more vertical-sided inferior to the tuberosities.

Superior View (Plate 13.2)

Preservation and Distortion

Details on fragments and cracks are presented in sections on individual vault bones. The distortion most observable in superior view is a medial compression of the left parietal wall between the coronal suture and the parietal tuberosity. A small portion of the right parietal along the coronal suture just superomedial to the temporal line is uplifted, resulting in artificial opening of the suture.

Overall Outline and Proportions

In superior view, the calvaria outline presents an elongate, asymmetrical ellipsoid, narrower anteriorly than posteriorly. The narrower anterior vault contrasts with the lateral flare of the supraorbital torus. The anterior margin of the Daka supraorbital torus is broadly similar to that of KNM-ER 3733, but it is relatively longer anteroposteriorly. The anterior margin of the supraorbital torus is also convex, curving posteriorly from the margin of the glabellar notch as it trends laterally. The anterior aspect of each orbit's torus is convex. The most anterior point on each torus lies at the lateral margin of the glabellar notch. Kabwe, Hexian, Dmanisi D 2700, Saldanha, Dali, KNM-ER 3733, and KNM-ER 3883 are similar to the Daka calvaria, both in the medial positioning of the most anterior point on the torus, and in the transverse occipital profile convexity at the rear of the cranium in this view.

In contrast, Buia, Ceprano, Sangiran 17, Sambungmacan 1, Sambungmacan 4, and Bodo present the most anterior point of the anterior margin in this view at the midline and distinctively recede posteriorly as they extend laterally from this point. The individual tori, however, are not so convex, with each torus being somewhat flattened anteriorly. Other specimens such as Trinil 2, Sambungmacan 3, and especially the Zhoukoudian and Ngandong specimens, do not recede so markedly posteriorly in their lateral course (Figure 13.12). Rather, the anterior aspects of the tori define flat, nearly parallel lines.

EBSCOhost - printed on 10/28/2022 4:53 AM via . All use subject to https://www.ebsco.com/terms-of-use

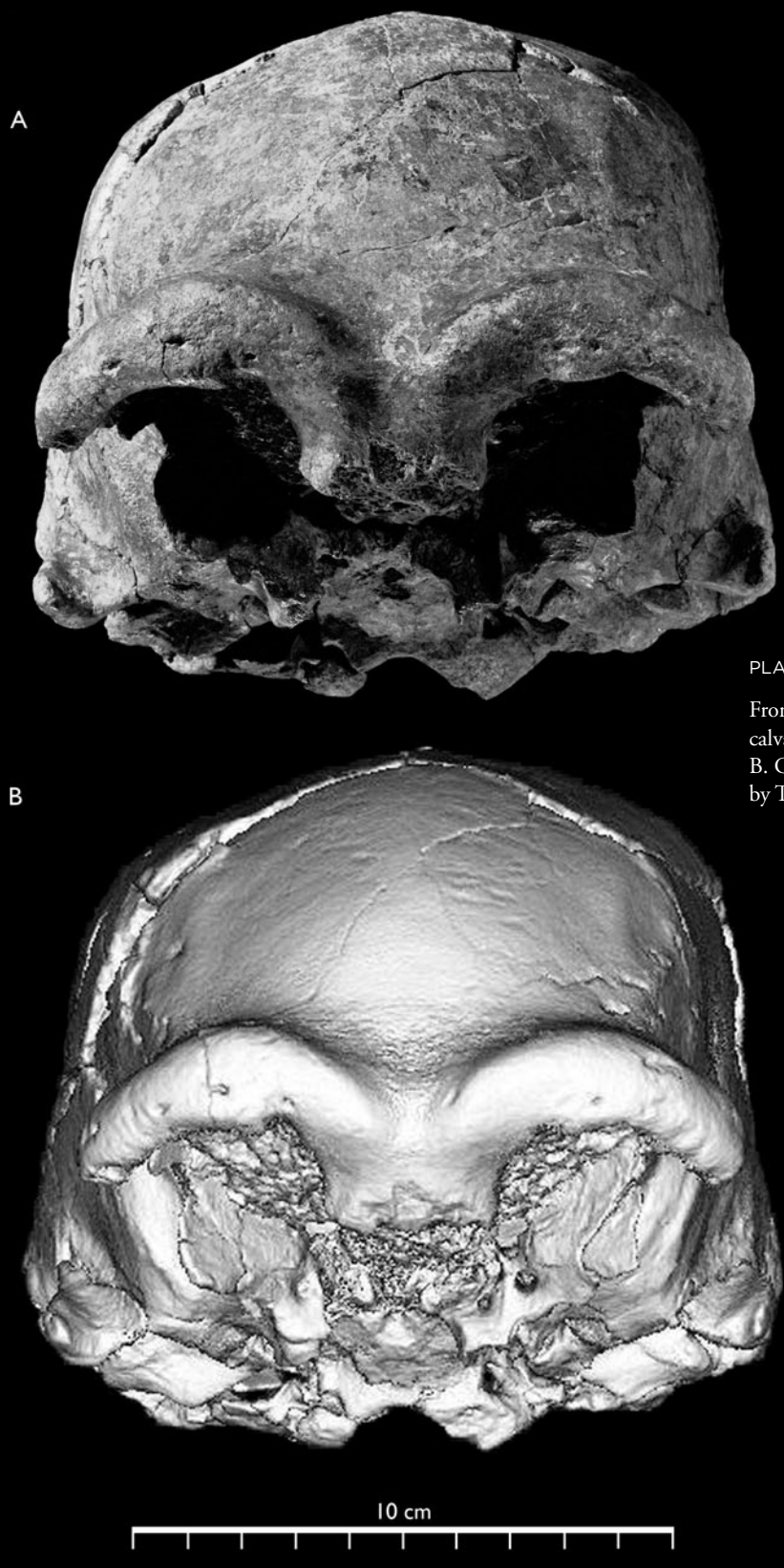

PLATE 13.1

Frontal views of Daka calvaria. A. Photograph. B. CT image. Photograph by Tim White.

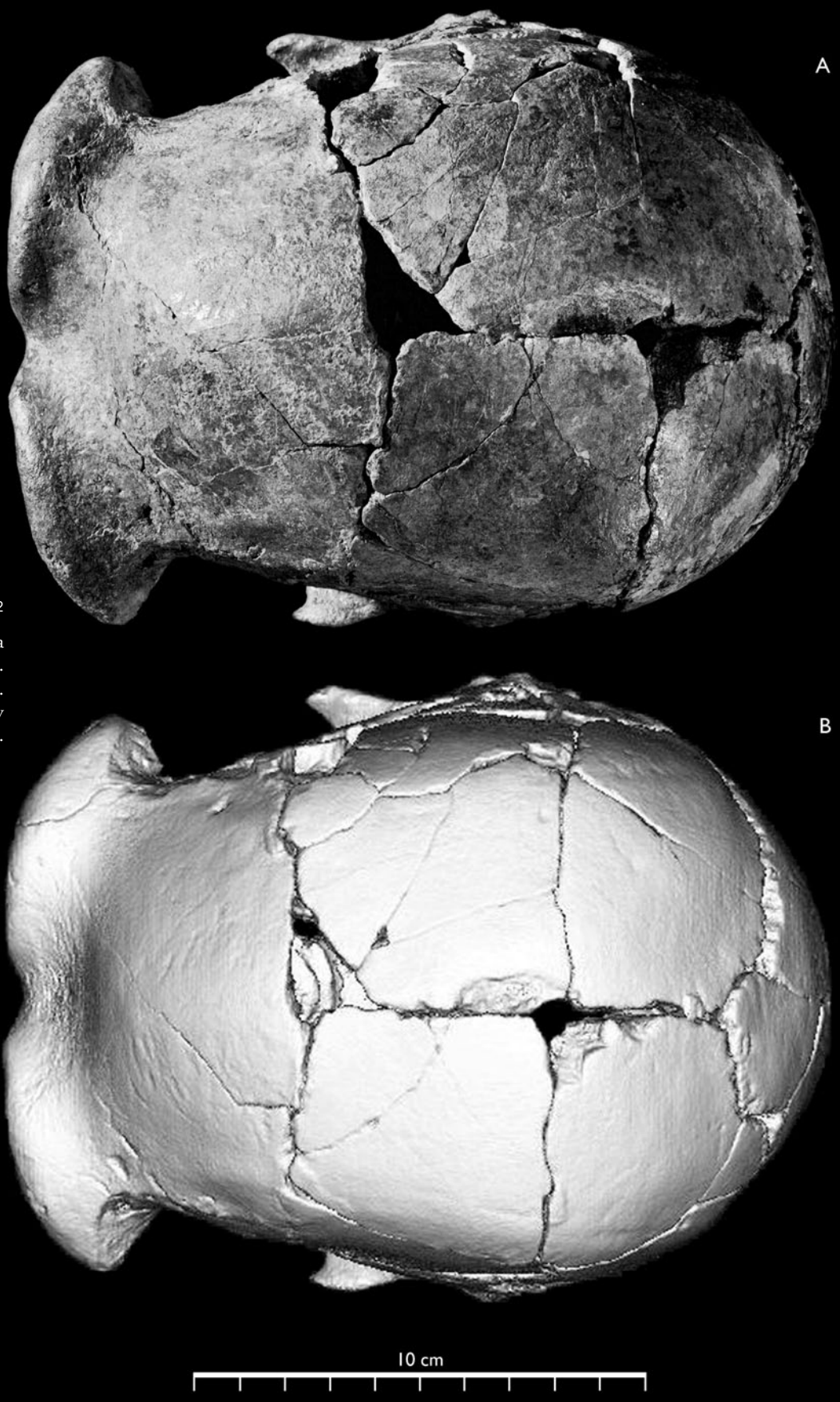

PLATE 13.2

Superior views of Daka calvaria. A. Photograph. B. CT image. Photograph by Tim White.

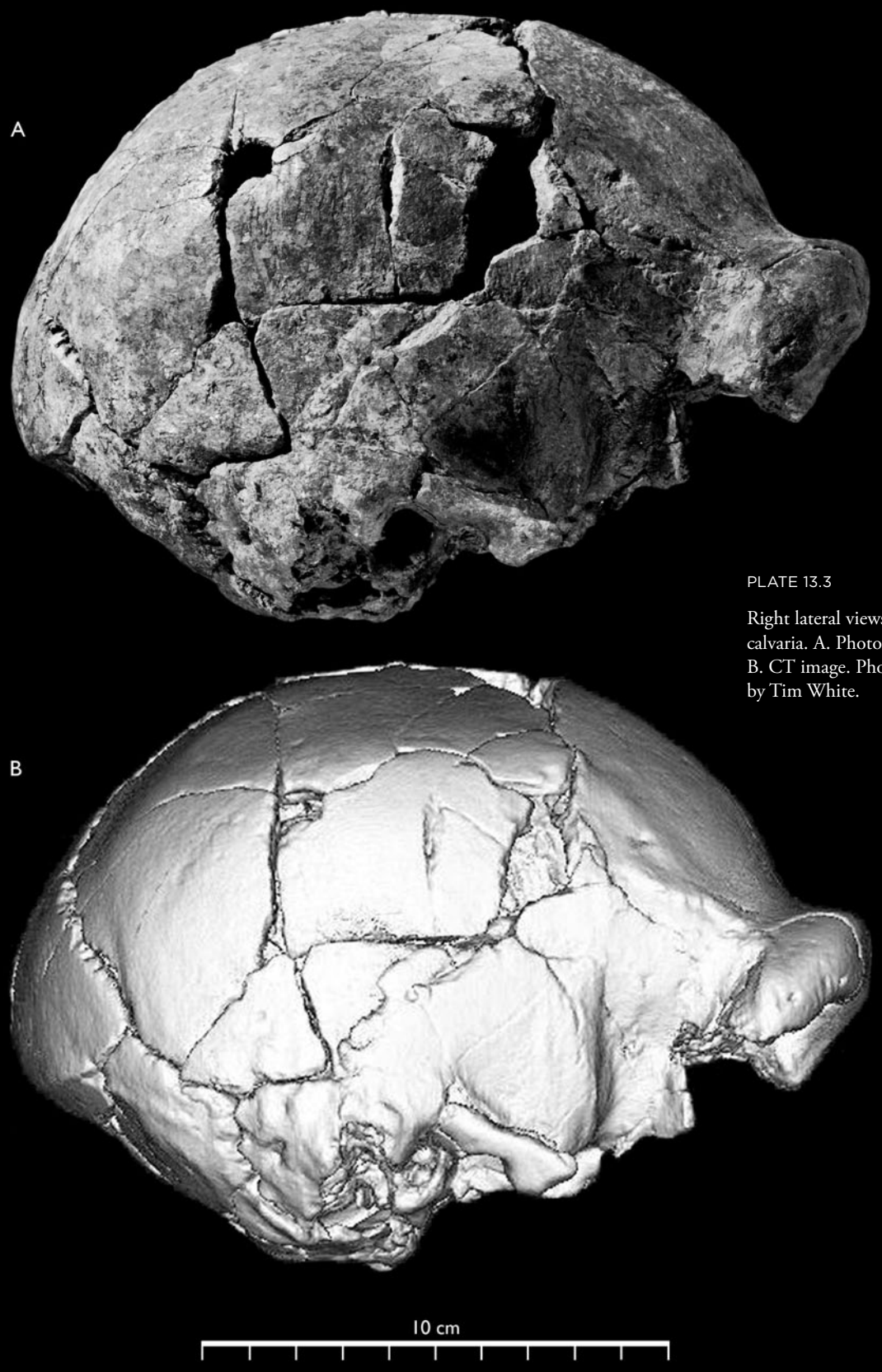

PLATE 13.3

Right lateral views of Daka calvaria. A. Photograph B. CT image. Photograph by Tim White.

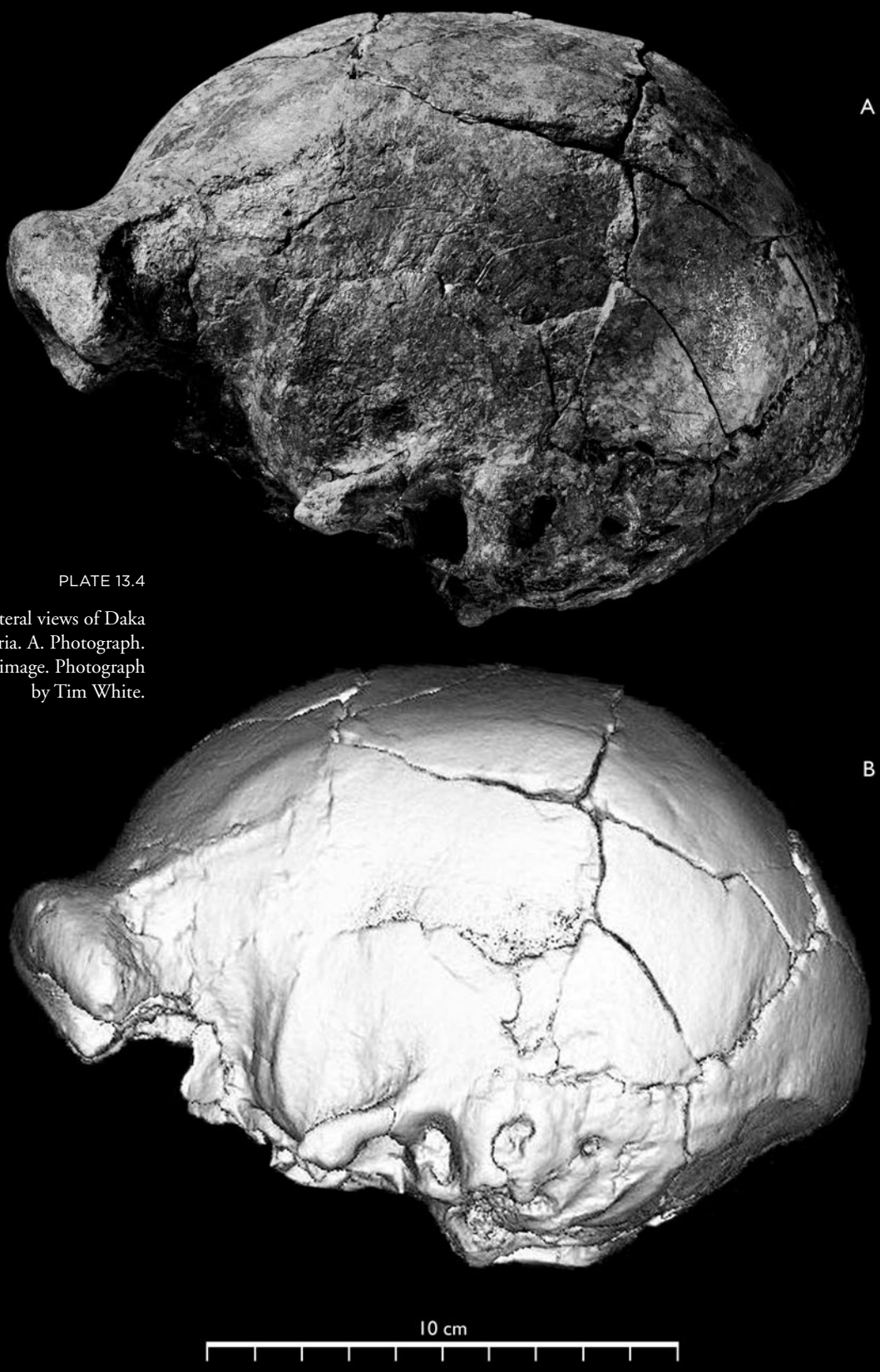

PLATE 13.4

Left lateral views of Daka calvaria. A. Photograph. B. CT image. Photograph by Tim White.

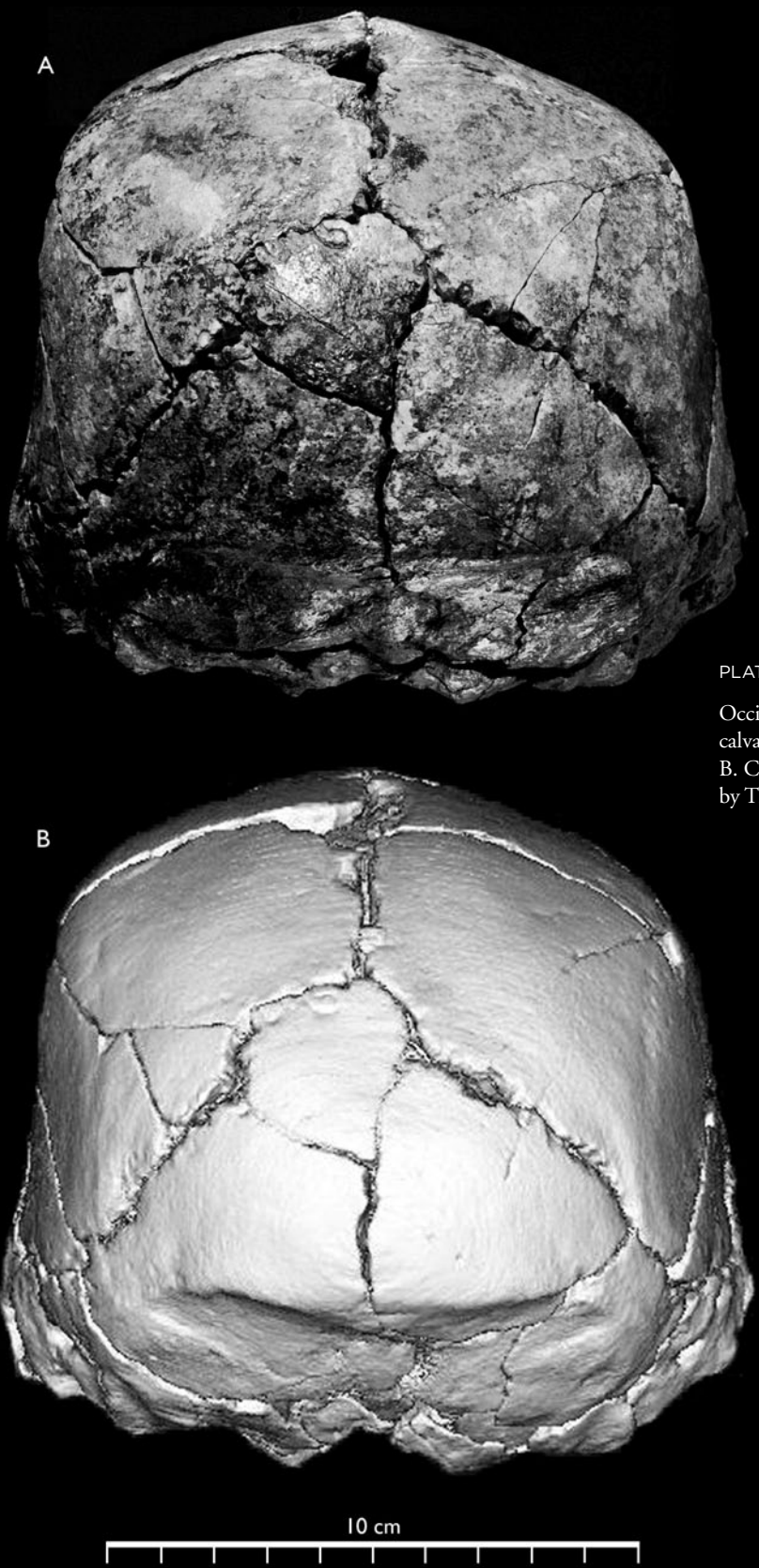

PLATE 13.5

Occipital view of Daka calvaria. A. Photograph. B. CT image. Photograph by Tim White.

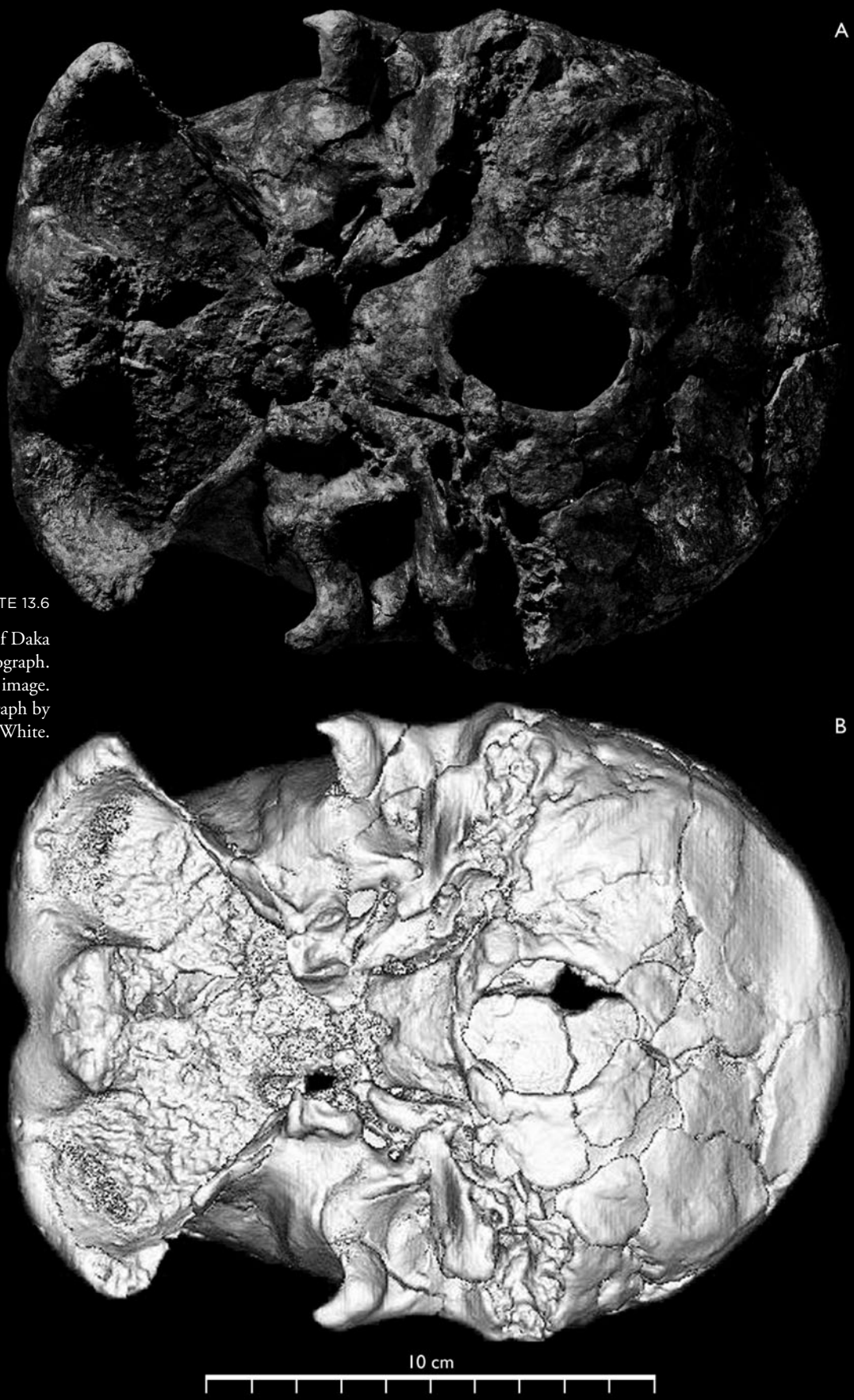

PLATE 13.6

Basal view of Daka calvaria. A. Photograph. B. CT image. Photograph by Tim White.

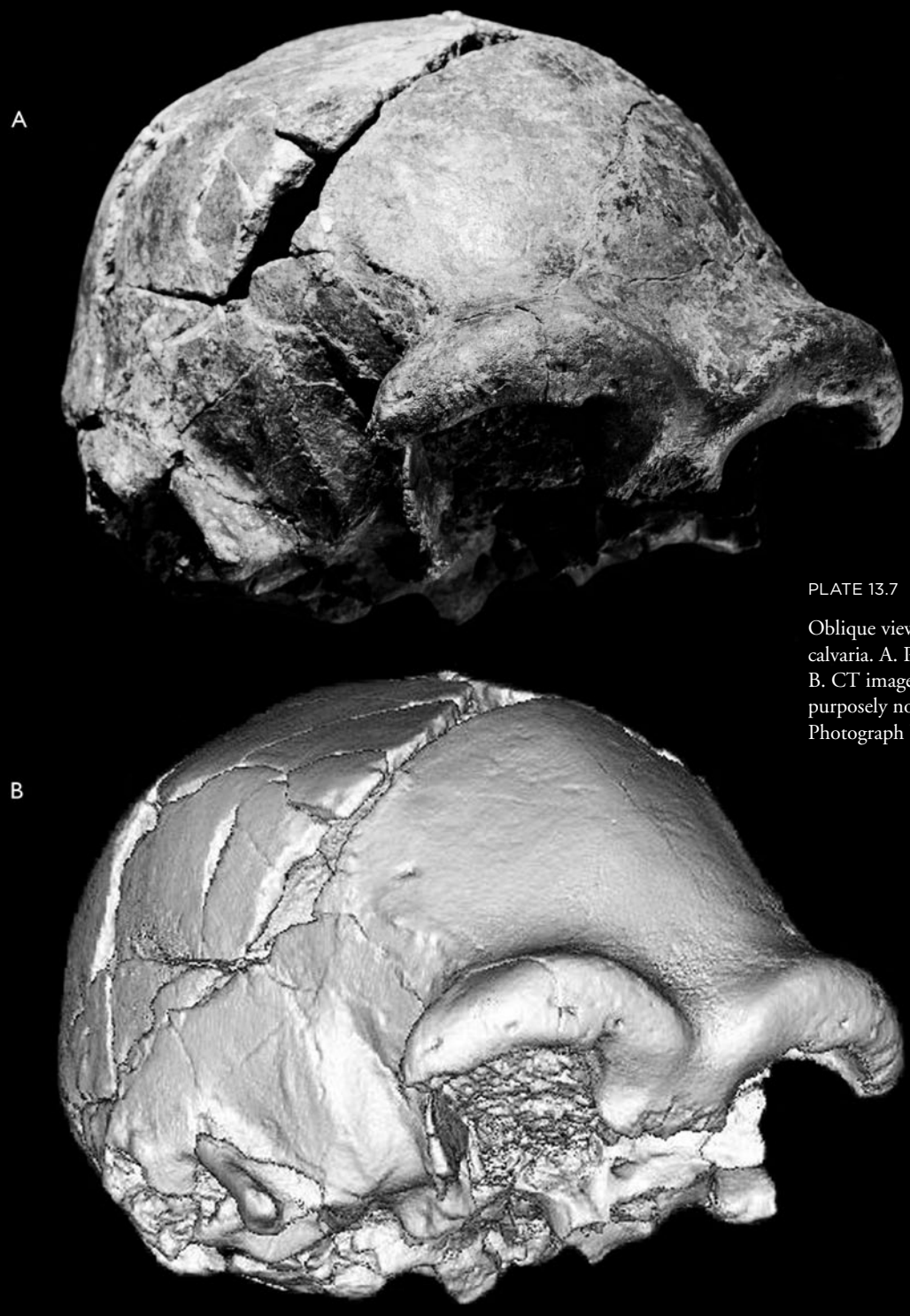

PLATE 13.7

Oblique view of Daka calvaria. A. Photograph. B. CT image. (Scale purposely not included.) Photograph by Tim White.

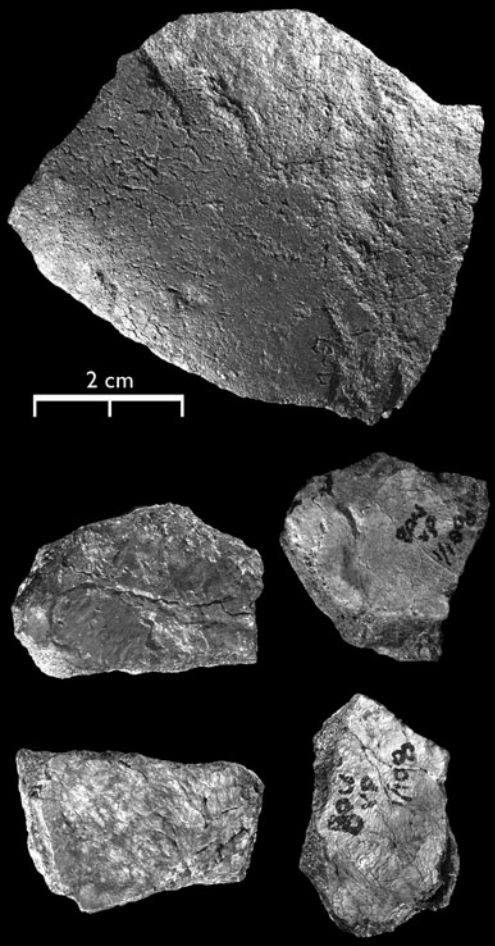

PLATE 13.8

BOU-VP-1/108.

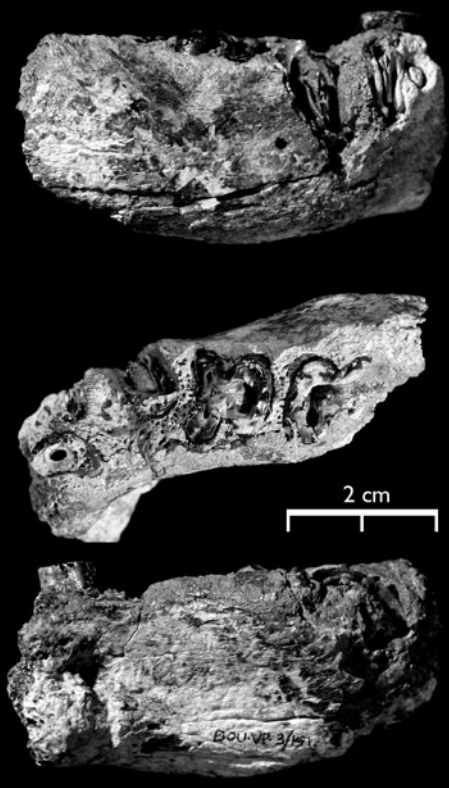

PLATE 13.10

BOU-VP-3/154.

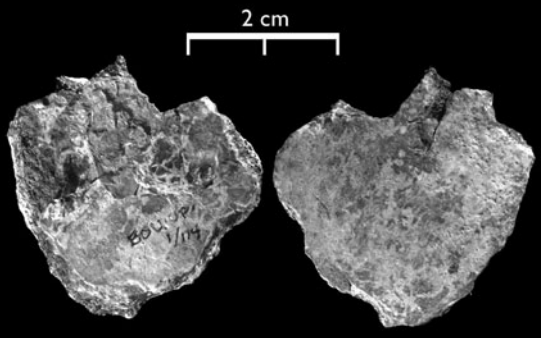

PLATE 13.9

BOU-VP-1/114.

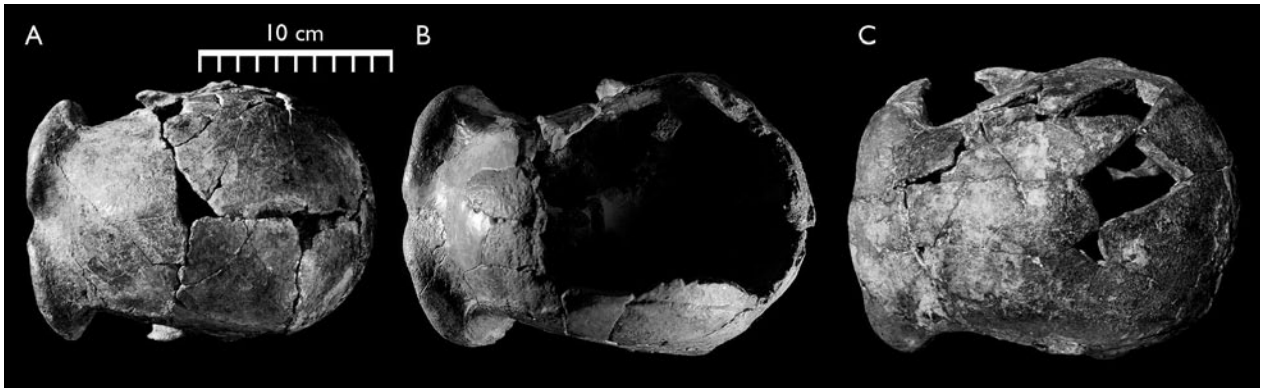

FIGURE 13.13
Superior views. A. Daka calvaria. B. OH 9. C. Sangiran 17. Photographs by Tim White.

The condition is especially prominent in ZKD 11, which exhibits strikingly different morphology from that presented in the Daka calvaria.

Perception of postorbital constriction is often influenced by the robusticity of the supraorbital tori. When the tori are very pronounced, the apparent constriction is greater. To address this perception problem we assessed the postorbital constriction relative to the maximum cranial breadth (see Appendix 13.1, note). The Daka calvaria presents moderate constriction relative to other Pleistocene *Homo* crania when assessed in this manner (and also when assessed by comparing minimum frontal breadth to biorbital breadth). Specimens KNM-ER 3883, Dmanisi D 2280, ZKD 5, Trinil 2, Sangiran 2, and Sangiran 17 have more pronounced postorbital constriction (minimum frontal breadth vs. maximum cranial breadth). Reduced constriction is present in Kabwe, Bodo, the Ngandong specimens, and Sambungmacan 3. The Daka calvaria is most similar to ZKD 3, ZKD 10, ZKD 11, ZKD 12, OH 9, Ceprano, and Sambungmacan 1, which also present moderate constriction (see Figures 13.12, 13.13, and 13.14).

The temporal lines are strongly marked on the frontal bone but diminish as they cross the coronal suture onto the parietals. The temporal lines curve laterally as they course anteriorly across the temporal fossae toward the zygomatic processes of the frontal. As a result of this acute lateral turn, the lateral thirds of the supraorbital tori form wide triangles. The temporal lines of the Daka calvaria form the boundary between the vertical temporal fossae and the more horizontal portion of the frontal squama. This creates a moderately angled coronal cross section through the frontotemporale in Daka. Ceprano, Kabwe, Sangiran 17, the Ngandong crania, the Sambungmacan crania, and Mapa are less angled, whereas specimens KNM-ER 3733 and OH 9 are more angled, and the Dmanisi crania are still more angled. The Daka calvaria is most similar in cross section to KNM-ER 3883, the Zhoukoudian crania, Bodo, and Sangiran 2 across this region.

Each temporal line diverges into superior and inferior lines just posterior to the frontotemporale. Each inferior temporal line forms a strong, rugose ridge on the superior part of the lateral wall of the temporal fossa between the zygomatic process of the frontal and its coronal border. The superior temporal lines are subdued, presenting smoothly rounded, torus-like apices rather than crests as they course toward the coronal border. Both are also distinct on the parietals, but the crestlike inferior temporal lines transform to weak ridges

EBSCOhost - printed on 10/28/2022 4:53 AM via . All use subject to https://www.ebsco.com/terms-of-use

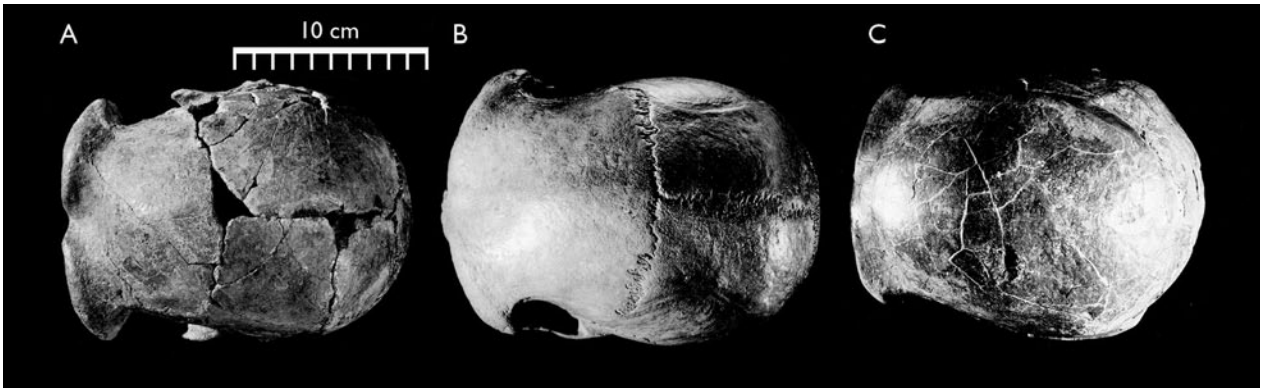

FIGURE 13.14
Superior views. A. Daka calvaria. B. Kabwe. C. Ngandong 6. Photographs by Tim White.

as they cross the coronal suture posteriorly. The temporal lines are more strongly developed and better preserved on the left side. Placement of the minimum distance between the superior temporal lines differs among Pleistocene *Homo* specimens. In some specimens it occurs on the anterior frontal, and in others near the coronal suture, or at mid-parietal. The position of the minimum distance between the superior temporal lines on the Daka calvaria occurs approximately on the coronal suture, as it does with Sangiran 17. This condition is similar to Dmanisi D 2282, KNM-ER 3733, Sangiran 2, and Sambungmacan 1, in which the lines most closely converge on the anterior parietal. Kabwe has temporal lines that come closest together on the anterior half of the parietal, and it presents a unique, hourglass-like constriction of the lines, which are well-separated on the coronal suture (see Figure 13.14). Dmanisi D 2280 and probably OH 9 have a minimum distance more posterior on the parietal, near-midway between coronal planes running through bregma and lambda. The temporal lines appear to be closest on the anterior frontal near frontotemporale in the Ngandong specimens, the Zhoukoudian specimens, and Ceprano.

Posteriorly, the superior temporal lines of the Daka calvaria diverge from each other as they traverse the parietal and descend close to its lambdoidal border. The two temporal lines are faint as they course along the superior part of the lateral wall of the parietal, similar to the Zhoukoudian specimens, Bodo, and Sambungmacan 3. This is different from the robust presentation of the temporal lines seen in KNM-ER 3733, OH 9, the Dmanisi crania, Kabwe, and Sambungmacan 1. The Ngandong specimens, Sangiran 17, and Ceprano present moderately pronounced temporal lines. The Daka calvaria is unique in possessing distinct superior and inferior temporal lines on the frontal.

The transverse posterior occipital profile of the Daka calvaria viewed in superior view is overall similar to KNM-ER 3733, Hexian, Sangiran 17, Saldanha, and the Ngandong crania in being more parabolic than evenly rounded (see Figures 13.12, 13.13, and 13.14). This transverse profile narrows gently in a continuous arch from the lateral walls of the parietal/temporal region to opisthocranion. The condition present in KNM-ER 3883, Sangiran 2, Sangiran 4, Buia, and Kabwe is somewhat different, being a more rounded occipital profile compared to Daka. The Zhoukoudian crania, Dmanisi D 2280, D 2282, and D 2700, Ceprano, Sambungmacan 3, Sambungmacan 4, and OH 9 are even more parabolic than Daka, with a subtle flattening posteriorly that effects a slightly polygonal shape.

EBSCOhost - printed on 10/28/2022 4:53 AM via . All use subject to https://www.ebsco.com/terms-of-use

Sutures

None of the sutures visible in superior view are completely fused. Fusion of the coronal suture is incipient inferior to the temporal lines, but the medial portion between the two temporal lines remains entirely unfused. The preserved parts of the sagittal suture are incompletely fused. The lambdoidal suture, which is very well preserved, is unfused and visible over its entire course. The low degree of ectocranial suture fusion suggests that the individual was a young adult at the time of death.

Lateral View (Plates 13.3 and 13.4)

Preservation and Distortion

Details on fragments and cracks are presented in the section on individual bones of the calvaria. Little overall distortion is apparent in left lateral view. In right lateral view some overall distortion in vault outline occurs along the nuchal plane inferior to the occipital torus, where the nuchal plane of the occipital is compressed approximately 3.0 mm just inferior to inion.

Overall Outline and Proportions

In lateral view the Daka vault is somewhat long and low relative to *Homo sapiens*, but higher relative to its length compared to other Pleistocene *Homo*. In another similarity with *H. sapiens*, the lateral parietal walls are nearly vertical. This also distinguishes the Daka calvaria from any of the specimens to which it has been compared, even Kabwe, Ceprano, and the Ngandong specimens, which present more vertically oriented parietal walls than the other comparative specimens. The Daka calvaria is comparable to the more vertically sided Buia cranium in this feature (see Chapter 15, Figure 15.1).

The plane of maximum cranial length in the Daka calvaria is positioned vertically at the approximate level of the superior aspect of the temporal squama border. This plane divides the calvaria into roughly equal upper and lower halves. This condition is different from that of *Homo sapiens*, where this plane is more inferiorly positioned, passing about one-fourth of the way down the temporal squama. This results in the majority of cranial volume being above this line in *H. sapiens*. The Daka condition is similar to all known *H. erectus* (see Chapter 15, Figure 15.6). The superior outline of the calvaria posterior to the glabella and the supraorbital sulcus rises steeply along the frontal. The frontal rises in a steep, posteriorly curving arch to midfrontal, then curves posteriorly, giving the midline of the frontal a gentle convexity between metopion and bregma. Just posterior to bregma the vault outline slopes gently to become almost flat. This somewhat horizontal portion of the outline continues for about 15.0 mm and then gently drops toward the occipital region. This results in a substantially curved parietal along the sagittal suture. This differentiates the Daka calvaria from many Pleistocene *Homo* crania that present sagittal suture profiles that are nearly flat or only gently curved, such as KNM-ER 3733, the Zhoukoudian crania, Sangiran 2, Sangiran 17, and the Ngandong crania. The Daka calvaria is also different from some of the crania with moderate curvature, including Ceprano, Saldanha, and Dmanisi D 2280 and D 2700. Daka is most similar

EBSCOhost - printed on 10/28/2022 4:53 AM via . All use subject to https://www.ebsco.com/terms-of-use

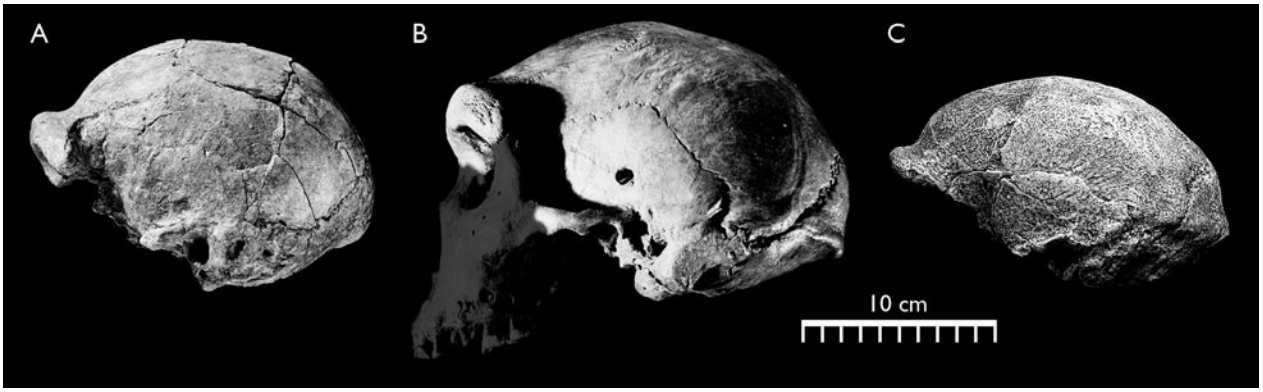

FIGURE 13.15
Lateral views. A. Daka calvaria. B. Kabwe. C. ZKD 3. Photographs by Tim White.

to KNM-ER 3883, Kabwe, Buia, Trinil 2, Sambungmacan 1, Sambungmacan 3, and Sambungmacan 4, which display tight curvature (see Figure 13.15).

Occipital angulation, the angle between the nuchal and the occipital planes, varies among Pleistocene *Homo* specimens. Some have relatively narrow occipital angles (under 100 degrees), including ZKD 5, the Sangiran specimens, and the Ngandong specimens. Those with wider occipital angles (between 100 degrees and 110 degrees) include KNM-ER 3733, KNM-ER 3883, Daka, Dmanisi D 2280, ZKD 11, ZKD 12, and Sambungmacan 3, which had the widest occipital angle of compared specimens.

Sutures

Unfused sutures visible in lateral view include the parietomastoid, the lambdoidal, the squamosal, and the superior part of the coronal suture. Sutures of the pterionic region are completely fused but still detectable. The most obliterated suture of this region is the sphenotemporal suture, which is very subtle. The sphenofrontal suture, though completely fused, is detectable over its entire course. The frontal half of the frontozygomatic suture is preserved, although the zygomatic is not present.

Bregma in the Daka calvaria is only indirectly observable in left lateral view via extrapolation from the orientation of the surrounding bone. No noticeable bregmatic eminence is preserved. Keeling among the Pleistocene *Homo* crania compared is highly variable in intensity and position along the midline. It is sometimes present on the coronal suture. The sagittal keel of the Daka calvaria is very weak on the sagittal suture but more pronounced in the metopic region of the frontal. It is visible as a subtle ridge on both parietals along either side of the preserved portion of the sagittal suture, especially anteriorly. In lateral view of the Daka calvaria a significantly raised bony plateau is visible at bregma. Sagittal keeling in KNM-ER 3733 is present on the metopic region of the frontal, especially near bregma. Specimen KNM-ER 3883 presents a very slight keel that is localized on the sagittal suture midway between bregma and lambda. Both Dmanisi D 2280 and D 2282 present moderate keeling along the coronal suture, the metopic region, and along the sagittal suture. Sagittal keeling is consistently found in Zhoukoudian specimens and is described in detail by Weidenreich (1943). It is also present in the metopic regions of the Zhoukoudian specimens. Kabwe is keeled in the metopic region. Bodo has a weak sagittal keel along the preserved sagittal suture that is most prominent near bregma. Trinil 2 has

EBSCOhost - printed on 10/28/2022 4:53 AM via . All use subject to https://www.ebsco.com/terms-of-use

a metopic keel and keeling around bregma. Sangiran 2 presents keeling on the anterior part of the sagittal, and Sangiran 4 possesses a sagittal keel. Ngandong 6, 7, and 11 have metopic and sagittal keeling, whereas in Ngandong 12 keeling is restricted to the sagittal suture. Sambungmacan 1, 3, and 4 and Sangiran 17 have both metopic and sagittal keeling. The Ceprano cranium does not have keeling. It is important to note that sutural keeling, especially on the sagittal suture, occurs regularly in *H. sapiens* (Etler 1994).

Occipital View (Plate 13.5)

Preservation and Distortion

Because of the noticeable compression of the left and right parietals, the Daka calvaria presents a slight skew to the left in occipital view. The right parietal tuberosity region is inferiorly and medially displaced relative to its analog on the left. Inferior displacement of the right rim of the foramen magnum is apparent. This displacement is more visible in computed tomography scans than ectocranially and is discussed more fully in Chapter 14.

Overall Outline and Proportions

The profile of the Daka calvaria in occipital view is similar to that of other *Homo erectus* specimens from Asia and Africa. There is significant parietal bossing associated with the relatively vertical sides of the calvaria. Despite this marked bossing, the Daka calvaria has maintained the tent-shaped profile observed in other *H. erectus* specimens, even though the parietal walls inferior to the parietal tuberosities are relatively vertical. The Daka calvaria possesses a distinctive parietal tuberosity similar to Ceprano. The cranial breadth at the parietal bossing is significantly less than the maximum width of the cranium, which occurs on the mastoid crest. This is the typical condition in *H. erectus*. Below the transverse biauricular plane the Daka calvaria has a slight medial taper due to the medial inflection of the mastoid processes.

Sutures

A striking feature of the Daka calvaria in occipital view is the shape of the lambdoidal suture. In most of the Pleistocene crania compared, the lambdoidal suture forms an obtuse, sometimes flattened or rounded angle at lambda. Specimens KNM-ER 3733, the Dmanisi crania, the Zhoukoudian crania, Kabwe, Trinil 2, the Sangiran crania, and the Ngandong crania present obtuse lambdoidal angles. In KNM-ER 3883 the suture is flattened across lambda, and in the Sambungmacan crania it is rounded. While still presenting obtuse angles, both Ceprano and Saldanha have more angular lambdoidal sutures at lambda. In Daka, the lambdoidal suture forms an acute angle at lambda and is distinctly triangle-shaped, very different from compared Pleistocene *Homo* specimens. The Daka calvaria's condition is more like that observed in *H. sapiens*.

The Daka calvaria's lambdoidal suture is asymmetrical in the area of lambda. The suture for the first 1.5 cm to the left of lambda runs more laterally than inferiorly, makes a relatively sharp angle to change direction to almost directly superoinferior for about 1.0 cm, and then makes another relatively sharp turn to become parallel once again with the first portion. It follows this course for the rest of its length toward asterion. The portion of the lambdoidal suture

EBSCOhost - printed on 10/28/2022 4:53 AM via . All use subject to https://www.ebsco.com/terms-of-use

extending to the right of lambda is more inferiorly than laterally inclined for its first 1.5 cm. It then changes direction to more lateral as it extends toward asterion. The whole course of the lambdoidal suture is visible in occipital view. This suture is relatively simple and lacks extensive or complicated interfingering in its lateral portions, although some interfingering is noticeable near lambda. No extrasutural bones are present along the lambdoidal suture.

In posterior view, the midsagittal region is raised into a very weak sagittal keel at the highest point (vertex) of the calvaria. Parasagittal depressions are visible on either side of the sagittal suture just superior to lambda. The right depression is more pronounced and extends inferolaterally for about 20.0 mm along the lambdoidal suture. The parasagittal depression on the left is less pronounced. Just inferior to lambda the occipital shows a mild flattening. Asymmetry of the parasagittal depressions is associated with the asymmetry of the lambdoidal suture discussed in the preceding paragraph. The upper scale of the occipital inferior to this depressed area is strongly sagittally and transversely convex. This vaulting is present over the entire upper scale.

Basal View (Plate 13.6)

Preservation and Distortion

Cracks visible in basal view are discussed under the individual bone sections. Some distortion is visible in basal view. The foramen magnum is visibly asymmetrical. This asymmetry is created by several cracks through the occipital. The major component of this distortion—the inferior displacement of the left rim of the foramen magnum—is not readily visible externally, but it is visible using computed tomography (see Chapter 14).

Overall Outline and Proportions

Much of the overall outline of the calvaria visible in this view has been detailed in the discussion of superior view. In light of this, this section focuses on the relationships of various features of the basicranium. Detailed description of these features may be found in the discussions of individual bones. Both the right and the left foramen ovale and spinosum are well preserved, and the left foramen ovale is bigger than the right. Foramina lacera are not expressed in the Daka calvaria as large openings at the tips of the petrous pyramids. This area is not often preserved in Pleistocene *Homo* specimens, but the Daka condition is similar to that presented in Bodo, where the petrous apices articulate with the sphenoid. The sphenopetrous fissures and the grooves for the cartilaginous portions of the auditory tubes are well preserved in Daka. The petrous pyramids are strongly angled, changing from having coronal to sagittal orientation in the region of the carotid canals. These sagittally oriented portions of the petrous bones parallel the length of the basioccipital. The basioccipital segment is strongly angled posteroinferiorly, and the anterior aspect of the foramen magnum's margin parallels the plane of the basilar portion of the occipital. The distance from the base of the lateral pterygoid plate to the margin of the glenoid fossa is moderate in Daka relative to other specimens. The distance is markedly lower in KNM-ER 3733 than in Daka. Dmanisi D 2280, ZKD 11, Kabwe, Ceprano, and Sangiran 4 have slightly greater measures for this feature than Daka, whereas Ngandong 7 and 11 are substantially broader.

EBSCOhost - printed on 10/28/2022 4:53 AM via . All use subject to https://www.ebsco.com/terms-of-use

Sutures

The sphenooccipital synchondrosis is completely fused, indicating the fully adult status of the Daka hominid. The most clearly observable sutures in basal view are the sphenotemporal sutures. These sutures show some degree of fusion but are still visible on the right side. The frontonasal and the frontozygomatic sutures are visible on the frontal bone. Portions of the occipitomastoid sutures are also visible in basal view, especially on the right side.

Individual Bones of the Calvaria

Frontal

Preservation and Distortion

The frontal of the Daka calvaria is fully preserved. Most of the borders of the frontal are intact. The posterior portion of the orbital roof was left covered with matrix to prevent damage to this thin, fragile area. The right supraorbital torus is cracked on the lateral margin of the supraorbital foramen, dividing the anterior face of the right torus into nearly equal right and left portions. This crack extends posteriorly, projecting nearly parasagittaly from the anterior part of the supraorbital torus and then bending sharply toward the temporal notch. This crack crosses the temporal notch at frontotemporale and extends toward the coronal suture. Very minor offset on this crack shifts the lateral portion of the supraorbital torus slightly inferiorly with respect to the medial portion. None of the several other cracks that traverse the frontal squama cause any displacement of the bone. The only place where part of the frontal squama has been lost is along the coronal suture. This minor bone loss along the coronal suture extends approximately 3.0 cm to the right from bregma. Just posterior to this there is a major crack that extends from the frontal squama down toward the lateral orbital wall. The external bone surface of this region has suffered minor exfoliation along these cracks in at least two places. The border between the frontal and the sphenoid is very well preserved on both sides.

The Daka calvaria possesses an array of shallow parallel perimortem grooves and striae located to the left of the midline on the frontal squama and bregmatic corner of the left parietal (Figure 13.16A). Some of the more medial grooves closer to the coronal border pass to the right half of the squama, but most are restricted to the left. The morphology of the grooves, while not definitive, is inconsistent with hominid-induced defleshing or rodent gnawing and is more consistent with carnivore gnawing. On the left half of the supraorbital torus and frontal squama are two depressions (Figure 13.16B). These depressions, one above the temporal line and one below the temporal line, may also be the result of carnivore activity. These depressions are also discussed in Chapter 14. There are two depressions on the anterior face of the left supraorbital torus that may also be related to carnivore activity (Figure 13.16C) but are more ambiguous.

Features

GLABELLAR INFLEXION Glabellar inflexion, or the presence of a groove between the right and left tori, is variable in Pleistocene *Homo* (Figures 13.12, 13.13, and 13.14). Some specimens, such as Dmanisi D 2280, ZKD 10, and ZKD 11, present no groove at all.

EBSCOhost - printed on 10/28/2022 4:53 AM via . All use subject to https://www.ebsco.com/terms-of-use

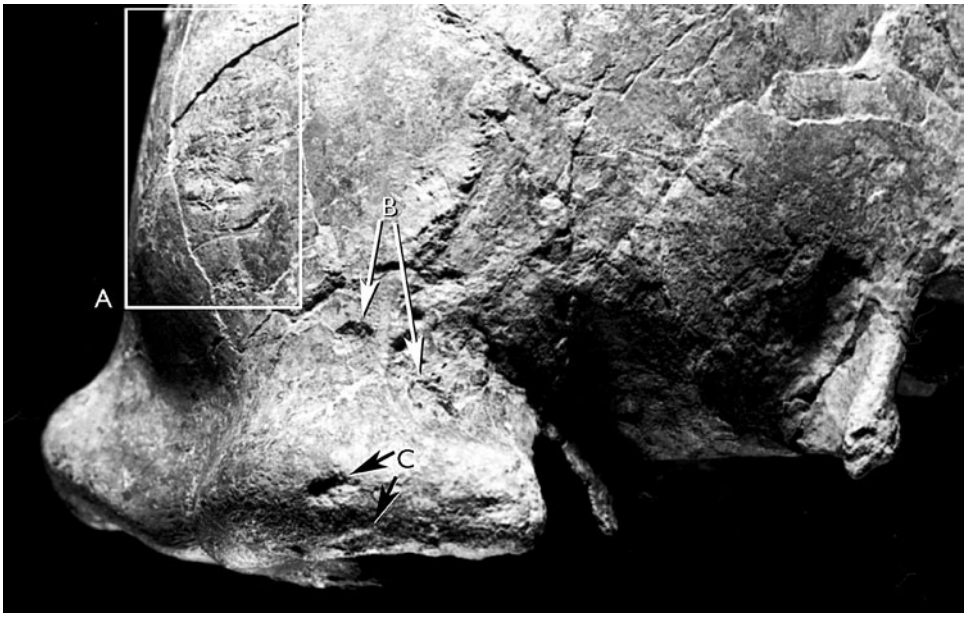

FIGURE 13.16

Daka calvaria frontal showing possible carnivore activity. A. Array of shallow parallel grooves on left frontal. B. Possible bite marks. C. Possible bite marks. Photograph by Tim White.

Other specimens, such as KNM-ER 3733, KNM-ER 3883, ZKD 3, ZKD 5, ZKD 12, Kabwe, Bodo, and Sangiran 17, have a diminished groove between the tori. Ceprano, Hexian, the Ngandong crania, and Sambungmacan 3 and 4 all have relatively strong intertoral grooves. Glabella in the Daka calvaria is positioned in a very strong intertoral groove relative to all of these specimens, comparable in depth only to OH 9. Nasion is positioned noticeably posteroinferior to glabella, and a shallow superoinferiorly oriented sulcus connects the upper nasal and glabellar regions.

ORBITS The orbital plates of the Daka calvaria are only partially exposed, with the majority of these surfaces still covered by matrix intentionally left to protect the specimen. In spite of this, morphology of the orbital plates can be assessed from the exposed areas, and they are not flattened as in the Zhoukoudian crania, Dmanisi D 2280, OH 9, Ceprano, Kabwe, or Bodo. Rather, the Daka orbital plates are curved and cuplike and are more similar to Sangiran 17, Sambungmacan 3, Mapa, and the Ngandong crania in this regard. The sphenoid aspects of the infraorbital fissures and foramina rotunda are visible on the Daka calvaria.

SUPRAORBITAL TORI The Daka supraorbital tori arch independently, but this is not always the case in Pleistocene *Homo*. The Ngandong crania all have flat, parallel supraorbital tori. Specimens ZKD 5 and 11 are also relatively flat and parallel, whereas ZKD 3, ZKD 10, and ZKD 12 are slightly arched. Moderately arched specimens include KNM-ER 3883, Ceprano, OH 9, Bodo, and Sangiran 17. The Daka calvaria, KNM-ER 3733, Kabwe, and Saldanha present extremely arched supraorbital tori (see Figure 13.17). Interorbital breadth varies considerably in Pleistocene *Homo*, but it is generally wider than in *H. sapiens*. Some breadths are especially large, as in Ceprano and OH 9. Ngandong 12,

EBSCOhost - printed on 10/28/2022 4:53 AM via . All use subject to https://www.ebsco.com/terms-of-use

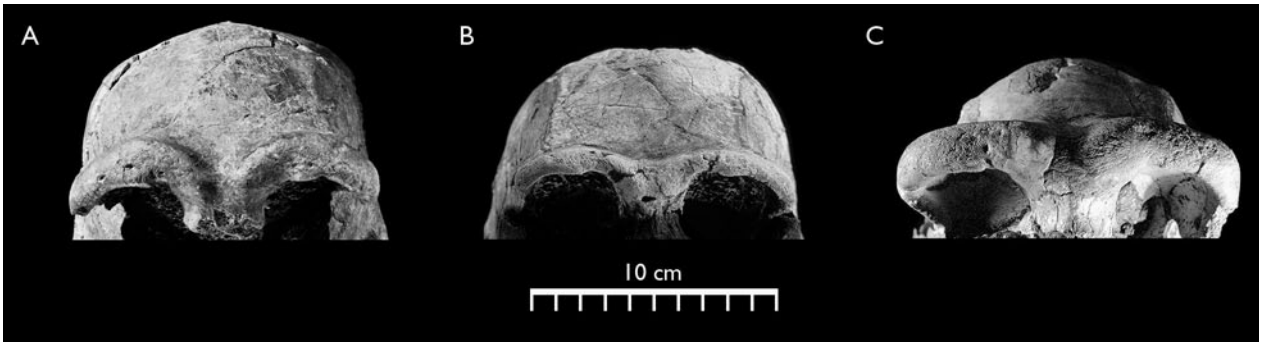

FIGURE 13.17

Frontal views. A. Daka calvaria. B. KNM-ER 3733. C. OH 9. Photographs by Tim White.

Bodo, and Dmanisi D 2700 have relatively broad interorbital breadths. The interorbital breadth of the Daka calvaria is moderate with respect to other Pleistocene *Homo* and is similar to ZKD 3, Sangiran 17, and Ngandong 7.

In some Pleistocene *Homo* specimens the superior and inferior boundaries of the supraorbital tori are parallel. In others the inferior supraorbital margin is more arched than the flatter superior margin. Both the squamal and orbital margins of each half of the supraorbital torus of the Daka calvaria are arched and relatively parallel. This condition is present in KNM-ER 3733, KNM-ER 3883, Dmanisi D 2280, Kabwe, Sangiran 17, and Saldanha. In OH 9, the Zhoukoudian crania, and the Ngandong crania, where the inferior border is more arched than the top (see Figure 13.17). Ceprano is unique in having a superior margin that is more arched than the inferior margin.

FRONTAL SQUAMA The supraglabellar surface in the Daka calvaria has a marked depression relative to the individually arched supraorbital tori. The supraorbital sulcus is deepest posterior to glabella at ophelion. Laterally the sulcus widens, but is not as deep. The frontal squama of the Daka calvaria just posterior to the supraorbital torus is very narrow mediolaterally, and this narrowness is accentuated by rapid widening toward the coronal suture. Postorbital constriction is discussed under superior view. Frontal squamae of Pleistocene *Homo* specimens tend to be flatter sagittally and transversely than in *H. sapiens*. The frontal squama of the Daka calvaria is flat relative to *H. sapiens*, but it is nonetheless gently vaulted transversely and sagittally. It is not so flattened in these dimensions as are Sangiran 17, Sangiran 2, Trinil 2, Ngandong 6, Ngandong 11, Ngandong 12, Sambungmacan 1, Dmanisi D 2280, D 2282, and D 2700, Bodo, Kabwe, and KNM-ER 3883. The Daka calvaria is more similar to KNM-ER 3733, Ngandong 7, Sambungmacan 3, and the Zhoukoudian specimens in this regard.

The Daka calvaria's deep supratoral sulcus follows the arched supraorbital tori and forms a relatively deep, symmetrical rhomboid (kite-shaped) depression superior to glabella. This depressed area is most closely approximated in KNM-ER 3733, although it is less pronounced, owing to the more gracile supraorbital tori of that fossil. The Zhoukoudian specimens are also similar to Daka in this feature, but the rhomboid depression is more mediolaterally elongate than in Daka. Although much of the frontal is broken in OH 9, it likely would have also had a relatively deep frontal trigon. Sangiran 17, Dmanisi D 2282, Ceprano, and Saldanha also present frontal trigons, but they are not so deep as in Daka. Specimens Dmanisi D 2282,

EBSCOhost - printed on 10/28/2022 4:53 AM via . All use subject to https://www.ebsco.com/terms-of-use

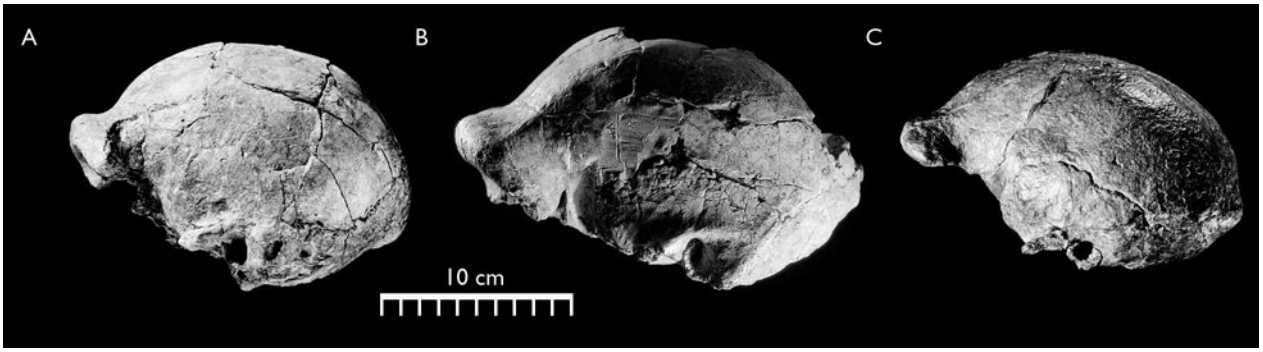

FIGURE 13.18
Lateral views. A. Daka calvaria. B. OH 9. C. Sangiran 2. Photographs by Tim White.

KNM-ER 3883, Kabwe, Bodo, the Ngandong crania, and Sambungmacan 3 are relatively flat across supraglabellare and do not possess concave frontal trigons.

The Daka frontal reveals a convexity along its median sagittal profile between the supratoral sulcus and bregma. Specimens presenting a similar convexity include KNM-ER 3733, the Zhoukoudian crania, Ceprano, Ngandong 7, Dmanisi D 2282, and Sambungmacan 1 and 4. Many other specimens compared were more flattened sagittally (see Figures 13.15 and 13.18).

Parietals

Preservation and Distortion

A triangular piece of the anteromedial corner of the right parietal is missing near bregma. Its anterior side is bounded by the frontal along the coronal suture, and its medial side is bounded by the left parietal along the sagittal suture. The coronal side of this missing triangle measures approximately 30.0 mm, the sagittal side measures approximately 19.0 mm, and the third side measures approximately 32.0 mm. A fragment adjacent to the coronal suture at and below the temporal line (approximately 32.0 mm by 14.0 mm) is also missing. Most of the bone loss is on the parietal, but some fragmentation and crushing of the frontal are present. Just superior to this bone loss a fragment of the parietal (approximately 24.0 mm by 20.0 mm) is uplifted approximately 3.0 mm with respect to the adjacent frontal. A small fragment (approximately 10.0 mm by 8.0 mm) is missing from the right parietal tuberosity just inferior to the superior temporal line. The ectocranial surface of the right parietal is missing over a surface of approximately 30.0 mm long by 10.0 mm wide adjacent to the sagittal suture near the calvaria's apex. The posterior portion of this exfoliation abuts a missing triangular fragment on the left parietal. The sagittal length of this region of bone loss is approximately 10.0 mm, and the coronal dimension is approximately 5.0 mm. The posterior margin of this small opening is beveled, exposing the diploe and internal cortical plate. Posterior to the triangular hole, the ectocranial part of the sagittal suture is damaged for a length of 16.0 mm.

Two major coronal cracks that divide both parietals into anterior and posterior halves radiate from the triangular hole just described. The coronal crack in the left parietal opens approximately 2.0 mm, crosses a major anteroposterior crack at the parietal tuberosity, and continues inferiorly on the lateral vault toward the posterior aspect of the temporal

EBSCOhost - printed on 10/28/2022 4:53 AM via . All use subject to https://www.ebsco.com/terms-of-use

squama and into the apex of the parietal notch. The anteroposterior crack is approximately 2.0 mm wide and originates from the coronal suture at stephanion, extending posteriorly to the lambdoidal suture. Anteroinferior to the intersection of these two major cracks, a large rectangular fragment of the left parietal is compressed medially approximately 3.0 mm. An accessory crack that is approximately 0.5 mm wide projects posteroinferiorly from the major coronal crack midway between the parietal tuberosity and the parietal notch and crosses onto the occipitals just posteromedial to asterion, continuing onto the nuchal surface. A second accessory crack extends anteroinferiorly from the same point to terminate along the posterior aspect of the temporal squama. Shearing offset along this crack is associated with the depressed fragment of parietal just described. Several other small cracks with no offset are present across the surface of the left parietal.

The coronal crack emanating from the triangular hole and projecting onto the right parietal extends laterally without causing distortion. It is intercepted by the missing fragment of parietal bone at the parietal tuberosity described in the first paragraph of this section and also by a major anteroposterior crack (approximately 1.0 mm wide). The anteroposterior crack extends from the uplifted fragment of parietal described in the first paragraph of this section, crosses the missing fragment at the parietal tuberosity, and continues posteromedially toward the lambdoidal suture. The coronal crack continues posteroinferiorly lateral to this anteroposterior crack and widens to approximately 1.5 mm until it intercepts a second, anteroposteriorly oriented crack that extends from the apex of the temporal squama to asterion. This second anteroposterior crack is not open, but there is slight shearing offset. Superior to the second anteroposterior crack and anterior to the coronal crack, a rectangular fragment of the lateral wall of the parietal is medially compressed by approximately 3.0 mm at its posteroinferior corner. Below the crack intersection just described, the coronal crack, still about 1.5 mm wide, continues, terminating at the parietal notch. Several other small cracks with no offset are present across the surface of the right parietal.

Features

The parietal bones of the Daka calvaria are similar to those of other *Homo erectus* in having a relatively rectangular shape. The distance along the inferior border of the parietal (asterion–pterion) is nearly equal to the distance along its superior border from lambda to bregma. The squamosal border of the Daka parietal is not visible because of the presence of the articulated and overlapping temporal bone. Parietal striae are well preserved and distinct along the left superior squamosal border. These striae are long, extending onto the parietal squama approximately 20.0 mm above the preserved superior border of the temporal.

SPHENOIDAL ANGLE The sphenoid angle of the Daka parietals is very obtuse. Most of the specimens are more moderately obtuse, including KNM-ER 3733, the Dmanisi specimens, the Zhoukoudian specimens, Sangiran 2, Sangiran 17, the Ngandong specimens, and Sambungmacan 3. Bodo displays a less obtuse sphenoidal angle than these specimens, and Kabwe has a morphology similar to *Homo sapiens*. Inferior to the sphenoid angle, the temporosphenoid crest on the left side of the Daka calvaria is very well marked and is continuous inferiorly with the sphenotemporal suture. On the right side, crest development differs in that it is split into two distinct short crests. Specimens KNM-ER 3733,

EBSCOhost - printed on 10/28/2022 4:53 AM via . All use subject to https://www.ebsco.com/terms-of-use

KNM-ER 3883, Sambungmacan 1, ZKD 11, ZKD 3, and Kabwe have well-defined sphenotemporal crests. Dmanisi D 2280, Sangiran 17, the Ngandong crania, and Bodo do not. Ceprano has a torus-like raised area near the sphenotemporal crest. The right sphenotemporal suture on Daka is visible in its entire extent.

CORONAL SUTURE The trend of the coronal suture between right and left stephanion in Daka is only very slightly anteriorly concave when viewed superiorly, corresponding closely to a single coronal plane. Crania similar to the Daka calvaria include KNM-ER 3733, the Zhoukoudian crania, Saldanha, Kabwe, Trinil 2, and the Sambungmacan crania. The Ngandong crania are extremely flat along the coronal suture between right and left stephanion. Bodo and Dmanisi D 2282 are more like *Homo sapiens* in this regard, with bregma occurring markedly posterior to stephanion.

As previously mentioned, preserved anatomy indicates that the Daka hominid possessed a well-developed sphenoid angle of the parietal. The sphenoparietal sulcus (Schwalbe 1907), characteristic of *Homo sapiens*, is not present on the Daka calvaria. Although cast quality rendered it difficult to assess this feature in many specimens, it appears absent in Dmanisi D 2280, the Zhoukoudian specimens, Kabwe, Ngandong 12, and Sambungmacan 3. Ceprano possesses a slight concavity in the region.

Although the coronal suture profile of the Daka calvaria is very similar to what is seen in the Zhoukoudian specimens and KNM-ER 3733, the lambdoidal suture profile differs. The Daka condition is similar to that present in *Homo sapiens*. From lambda, the parietal borders drop sharply inferolaterally toward asterion and take an anteriorly arching course along the mastoid border and the parietal notch. The Daka occipital borders of the parietals differ from those in the Zhoukoudian specimens, which follow a "rather strict frontal plane with no tendency to deviate in an anterior direction" (Weidenreich 1943, 33). Suture morphology is detailed in the discussion of occipital view. The occipital angle of the Daka parietal is more obtuse on the right side than the left. This asymmetry is discussed more fully in the discussion of occipital view.

TEMPORAL LINES AND ANGULAR TORUS Because the temporal lines are present on both the frontal and parietal, they are also discussed under superior view. The superior and inferior temporal lines are not as easily distinguished from each other on the parietal as they are on the frontal. At the coronal suture the left superior and inferior temporal lines are separated by 15.0 mm. The crestlike inferior temporal line on the left frontal curves superiorly, however, to merge with the superior temporal line just posterior to the coronal suture. The temporal lines of the Daka calvaria are subtle over their parietal courses. The minimum distance between the superior temporal lines on the parietals occurs at the level of the coronal suture, and the lines slowly diverge posterior to this. At their posterior extent they turn to follow the border of the lambdoidal suture to approximately 20.0 mm superior to asterion.

The temporal lines are well marked in the region around asterion. The thickening that they form in this area is positioned similarly to the angular torus described for the Zhoukoudian specimens (Weidenreich 1943), but it is less pronounced and does not stand out as an isolated bulge (see Figures 13.15 and 13.18). Angular tori, defined as isolated raised thickenings at the posterior end of the temporal lines near the lambdoidal suture,

EBSCOhost - printed on 10/28/2022 4:53 AM via . All use subject to https://www.ebsco.com/terms-of-use

are variably expressed in Pleistocene *Homo*. For some specimens, such as KNM-ER 3733, Sangiran 2, Kabwe, Ngandong 7, and Sambungmacan 3, there are no discernible angular tori. For others, Dmanisi D 2280, Ceprano, Sangiran 4, Sangiran 17, Ngandong 6, Ngandong 12, Sambungmacan 1, BOD-VP-1/1 and, of course, the Zhoukoudian crania, the enlargement of the temporal line is discernible as an angular torus. The posterior descent of the temporal lines in the Daka calvaria borders the lambdoidal margin near asterion. This positioning of the posterior attachment of the temporalis muscle creates a mild thickening of the parietal, which is associated with the weak projection in the region where one would expect an angular torus.

PARIETAL FORAMINA Parietal foramina are absent in the Daka calvaria. Often Pleistocene early *Homo* and *H. sapiens* present a flattening in the area around obelion. Daka presents some flattening in this region (also discussed under occipital view). Other crania that exhibit flattening include KNM-ER 3733, Kabwe, and Sambungmacan 1, 3, and 4. More moderately flattened specimens include the Zhoukoudian crania, Saldanha, Sangiran 17, and the Ngandong crania.

Temporals

Preservation and Distortion

The temporal bones of the Daka calvaria are well preserved, particularly the basal parts, with the exception of the damage to the mastoid processes. The temporal squama is better preserved on the left than on the right side. The left temporal is cracked along its posterosuperior margin, allowing the slight depression of a rectangular fragment (approximately 26.0 mm by 6.0 mm) along the descending squama. The superior part of the right temporal squama is missing along its posterior half, and there is some crushing of the superior squama. The anterior portions of the zygomatic processes are missing just anterior to the articular eminences. The roots of the zygomatic processes on both sides of the temporal are preserved. A crack bisects the left glenoid fossa, running from the anterolateral edge of the auditory meatus to the sphenotemporal suture approximately 10.0 mm lateral to foramen ovale. The temporal medial to this crack is compressed by approximately 1.5 mm. Another crack separates the left zygomatic root from the rest of the temporal. It does not result in any major offset. A similar single crack on the right side that runs anteroposteriorly is also visible and also does not contribute to substantial distortion.

Damage occurs in the regions of the left and right mastoid processes. The right mastoid is mostly missing, and the adjacent region shows a V-shaped depression that exposes the trabecular bone and mastoid air cells. Damage has resulted in the loss of a major portion of the anterior (auditory) border. Bone loss extends posteriorly to encompass most of the length of the digastric fossa and medially to the stylomastoid foramen and occipitomastoid suture. The left mastoid is not as extensively damaged, and bone loss is restricted to fracturing and loss of the jugular process of the occipital. Most of the bone loss, which exposes the underlying trabeculae, is restricted to an approximately 5.0 mm wide region. However, instead of continuing posteriorly, the damage runs a straight course laterally to include the tip of the mastoid process and the anterior digastric fossa.

EBSCOhost - printed on 10/28/2022 4:53 AM via . All use subject to https://www.ebsco.com/terms-of-use

Features

TEMPORAL SQUAMA The high, arched profile of the temporal squama of the Daka calvaria differs from the condition of many of the comparative specimens (see Figures 13.15, 13.18, and Chapter 15, Figure 15.6). Most of the specimens, including KNM-ER 3733, KNM-ER 3883, OH 9, the Dmanisi crania, the Zhoukoudian crania, the Sangiran crania, the Ngandong crania, and the Sambungmacan crania, have lower, anteroposteriorly longer, and flatter squamosal borders than the Daka calvaria. The high, arched condition of Daka is also present in Ceprano, Kabwe, and Bodo. The Daka sphenotemporal border, which is fully preserved in its superoinferior extent, is completely fused on the left side and forms a crest along its boundary. The right sphenotemporal suture is less completely fused and it is still visible, especially superiorly. Posterior to the sphenotemporal suture on the right side, a low ridge is formed on the temporal squama that runs parallel to it for a short distance. On the left side, this parallel ridge is not visible.

The transition to the squama above the meatus displays less relief on the Daka calvaria than in comparable *Homo erectus* specimens. There is no supramastoid crest. The Daka temporal squama, from the roots of the zygomatics to the apex of the squama, is very smooth on the better-preserved left side.

ZYGOMATIC PROCESS The root of the zygomatic process of the Daka temporal is rounded superiorly on its posterolateral margin, lacking a sharp crest. This is similar to the condition observed in Sangiran 4, Sangiran 17, and Ngandong 6. Specimens KNM-ER 3733, KNM-ER 3883, Dmanisi D 2280 and D 2282, ZKD 10, ZKD 11, ZKD 12, and Ngandong 12 have crested posterolateral zygomatic root margins. Specimens OH 9, ZKD 3, Ceprano, Kabwe, and Ngandong 12 have a morphology intermediate between crested and rounded. In the Daka calvaria a deep trough is formed between the temporal squama and lateral border of the zygomatic. This is similar to KNM-ER 3883, Sangiran 2, and Ngandong 6. Specimens KNM-ER 3733, OH 9, Dmanisi D 2282, Kabwe, and Sangiran 17 have shallower zygomatic root troughs. Specimens Ngandong 11 and 12 are intermediate in this morphology.

The mediolateral breadth of the anterior margin of the zygomatic trough is broad in the Daka calvaria, comparable to Sangiran 17, OH 9, and the Ngandong specimens. Other crania are more moderate in this dimension, including KNM-ER 3733, KNM-ER 3883, Dmanisi D 2282, Ceprano, and Sangiran 2. Kabwe presents a markedly narrower anterior zygomatic trough than the others and is more similar to *Homo sapiens* in this feature.

The anteroposterior dimension of the superior aspect of the zygomatic root adjacent to the squama is relatively long in the Daka calvaria. Ngandong 6 and KNM-ER 3883 are similar in dimension, and OH 9, the Dmanisi crania, and Ngandong 12 are only slightly shorter. The medial zygomatic trough lengths for KNM-ER 3733, Sangiran 17, and Ngandong 12 are intermediate, whereas the dimensions in ZKD 3, Ceprano, Kabwe, Sangiran 2, and Sambungmacan 1 are short.

Viewed laterally, the crest of the zygomatic root varies in inclination among Pleistocene *Homo* from being close to horizontal to being significantly oblique, with the anterior root positioned inferiorly relative to the posterior root. The zygomatic roots of Ceprano, Kabwe, and Dmanisi D 2282 are less oblique and are close to horizontal. The Ngandong

EBSCOhost - printed on 10/28/2022 4:53 AM via . All use subject to https://www.ebsco.com/terms-of-use

crania and OH 9 present strongly oblique zygomatic roots. The Daka calvaria is moderate in this regard, as are KNM-ER 3733, KNM-ER 3883, and Sangiran 17.

AUDITORY MEATUS The auditory meatus in the Daka calvaria is oval in shape, longer superoinferiorly and narrower anteroposteriorly. It is nearly vertically inclined with respect to an approximated Frankfurt Horizontal plane but has a slight posteroinferior slope. It is similar to KNM-ER 3733, ZKD 5, and Sangiran 4. Auditory meati for Dmanisi D 2280, Ngandong 6, and Ngandong 7 are less vertically elongate ovals, whereas KNM-ER 3883 and OH 9 present even more vertically elongate ovals. Other specimens have more circular meati, including ZKD 3, ZKD 10, ZKD 11, Sangiran 2, Sangiran 17, Ngandong 11, Ngandong 12, and the Sambungmacan specimens. Cranium ZKD 12 is unique in possessing a horizontally ovoid auditory meatus.

The morphology of the tympanic bone encircling the external auditory meatus varies in Pleistocene *Homo*. In some specimens the tympanic bone is restricted to the inferior border of the meatus, whereas in some specimens it wraps to encircle more of the meatus. The tympanic bone of the Daka calvaria is restricted to the inferior border of the meatus.

The superior border of the Daka auditory meatus is not shelved by a continuous zygomatic root and mastoid crest. As a result, porion and auriculare are not widely separated in the Daka calvaria. Specimens OH 9, Sangiran 17, Ceprano, and Dmanisi D 2280 and D2700 are intermediate, whereas Ngandong specimens, Bodo, Zhoukoudian specimens, Sambungmacan specimens, and Sangiran 4 exhibit a larger separation of porion from the lateral margin of the suprameatal crest. Crania KNM-ER 3733, KNM-ER 3883, Kabwe, and Sangiran 2 are similar to the Daka calvaria in presenting low degrees of separation between porion and auriculare.

PETROUS PORTION The petrous pyramids and the tympanic bones of the Daka calvaria are very well preserved. In inferior view the lateral half of the petrous bone is oriented slightly more coronally than it is in Bodo. The medial half of the petrous has a more nearly parasagittal orientation. This is similar to what is seen in Zhoukoudian specimens. The angular orientation of the tympanic plate in the Daka calvaria is somewhere between apes, where the petrous takes a nearly coronal orientation, and *Homo sapiens*, whose tympanic plates generally present orientations of about 45 degrees between sagittal and coronal. This is the condition of all compared crania that preserve the region except Kabwe, which is more similar to *H. sapiens* in this respect (see Figure 13.15).

The anteromedial apex of the Daka petrous pyramid articulates with the sphenoid, filling the space denoted as the foramen lacerum in *Homo sapiens*. As discussed previously, this area is not commonly preserved in *H. erectus* crania, and where it is, cast imperfections regularly obscure the area. Fortunately, Weidenreich (1943) describes this feature for the Zhoukoudian crania, and the Daka condition is similar to his description. Kabwe has a distinct foramen lacerum more similar to that of *H. sapiens* (see Figure 13.19).

TYMPANIC The crista petrosa, as described by Weidenreich (1943: 59) for Zhoukoudian specimens, "rises immediately medialward from the porus to a huge spine and forms beyond it a ledge-like margin toward the jugular incisure and the carotid canal." Weidenreich also

EBSCOhost - printed on 10/28/2022 4:53 AM via . All use subject to https://www.ebsco.com/terms-of-use

FIGURE 13.19

Basal views. A. Daka calvaria. B. Kabwe. C. ZKD. Photographs by Tim White.

notes that this condition differs from that of *Homo sapiens*, where the tympanic plate is flattened to form a "thin blade-like edge, which begins near the porus and ends near the anterior margin of the carotid canal, retaining its thickness the entire way." In the Daka calvaria the crista petrosa arises as a moderately thickened plate medial to the lateral edge of the tympanic plate. From this point it rises sharply to form a slightly thickened spine and then continues as a bladelike edge, terminating at the anterior border of the carotid canal.

In the Daka calvaria the crista petrosa divides into two low crests, which encircle the processus supratubalis. This terminal aspect of the tympanic plate is slightly more flattened on the left side relative to the more tubular right side. This is due to a larger, more rugose processus supratubalis on the left side. The crista petrosa in the Daka calvaria is slightly thinner anteroposteriorly than in the Zhoukoudian specimens (Weidenreich 1943). The spine of a crista petrosa is visible as a weak projection on the Daka calvaria, medial to the lateral border of the petrous, that rises steeply to form an inferiorly projecting spine. The most inferior projection of this spine occurs at the midpoint of the stylomastoid foramen. The crista petrosa angles superomedially from this foramen, but it remains a distinct spine until it passes the styloid pit medially. This "spina crista petrosa" in the Daka calvaria differs from that of ZKD 3 in being less robust. Two closely spaced features are preserved just posterior to the crista petrosa: the styloid pit and the stylomastoid foramen. Both foramina are completely preserved on the right side, whereas on the left side the posterior aspect of the stylomastoid foramen is missing. The crista petrosa of Weidenreich (1943) is not the same as the "petrous crest" of Aiello and Dean (1990), where the term is used to refer to the sharp endocranial edge of the petrous that forms the boundary between the middle and posterior cranial fossae.

Another striking feature of the Daka temporal is the pronounced cortical thickness of the tympanic plate. It is similar in thickness to KNM-ER 3733, OH 9, ZKD 5 and 10, and the Ngandong specimens. Specimens Dmanisi D 2280, ZKD 3 and 11, and the Sangiran crania are intermediate in tympanic cortical thickness, and tympanic cortices of KNM-ER 3883, Kabwe, and Sambungmacan are thinner. The tympanic cortices in all compared crania are thicker than those of most *Homo sapiens*. The tympanics of the

EBSCOhost - printed on 10/28/2022 4:53 AM via . All use subject to https://www.ebsco.com/terms-of-use

Daka calvaria do not separate into a "labium anterior tympanic" and a "labium posterior tympanic," as is described by Weidenreich (1943) for some Zhoukoudian specimens. This structure in the Daka calvaria is a single unit with no intervening groove, similar to all except ZKD 3 and ZKD 11.

The lateral part of the articular eminence is well developed in the Daka calvaria. A postglenoid process is present in Daka and extends in a sweeping arch from the lateral border of the glenoid fossa to approximately mid-fossa. The process itself projects similarly to others, including KNM-ER 3733, OH 9, ZKD 3, Sangiran 2, Ngandong 6, and Sambungmacan 1. Daka postglenoid processes are much less projecting than those of Kabwe and Bodo, and they are somewhat less projecting than those of KNM-ER 3883, Dmanisi D 2280, ZKD 5, ZKD 12, Sangiran 4, and Sangiran 17.

GLENOID FOSSA/ARTICULAR EMINENCE The glenoid cavity is mediolaterally narrow and deep in the Daka calvaria. The anterior aspect of the articular surface extends a short distance anterior to the articular eminence. This area is more clearly demarcated on the left side and does not appear to extend as far anteriorly on the right. The area covered by the articular joint capsule in the Daka calvaria is well delineated from the facies infratemporalis of the sphenoid and the adjacent temporal margin, similar to the condition seen in OH 9, the Zhoukoudian crania, Sangiran 4 and 17, Ngandong 6, 7, and 12, and Sambungmacan 3. In KNM-ER 3733 and Sangiran 2 the two surfaces gently merge with only limited delineation. Specimens KNM-ER 3883, Dmanisi D 2280, Ceprano, Kabwe, and Ngandong 11 are intermediate in this feature. Viewed from an inferior perspective, the anterior margins of the Daka glenoid fossae are markedly concave, similar to Dmanisi D 2280, ZKD 3, ZKD 11, Ceprano, Sangiran 4, and the Sambungmacan crania. In KNM-ER 3733, KNM-ER 3883, OH 9, Kabwe, Sangiran 2, Sangiran 17, and the Ngandong crania, the anterior glenoid is less concave.

The posteromedial margin of the Daka calvaria's glenoid fossa is a sharply pointed sphenoid spine. The sphenoid spine is prominent on both the right and left sides, forming a tongue-like projection that bends inferiorly away from the adjacent tympanic bone. The spines are thus separated from the tympanic at their termini by petrotympanic fissures. The narrow edge of the entoglenoid, the only parts of the glenoid composed of sphenoid, laps over the tympanic plate, which courses medially and laterally underneath the spine. This is visible on both right and left glenoid regions of the Daka calvaria but is especially pronounced on the left. Many specimens, including KNM-ER 3733, KNM-ER 3883, OH 9, Dmanisi D 2280, and Sangiran 2, differ dramatically from the Daka calvaria and present tympanic plates separated from the entoglenoid processes by wide gaps. Other crania, including ZKD 3, ZKD 5, ZKD 11, Kabwe, Sangiran 4, the Ngandong crania, and the Sambungmacan crania, have a narrower separation between the two elements.

Although the Daka entoglenoid process projects posteriorly more than in the other comparative specimens, it is mediolaterally thin, like those of Kabwe, Sangiran 4, and Ngandong 12. Specimens KNM-ER 3733, KNM-ER 3883, the Dmanisi crania, ZKD 5, ZKD 11, Ceprano, Sangiran 2, Sangiran 17, and Sambungmacan 1 present relatively thick entoglenoid processes, and ZKD 3, Ngandong 7, and Sambungmacan 3 have intermediate mediolateral thicknesses of the entoglenoid processes.

EBSCOhost - printed on 10/28/2022 4:53 AM via . All use subject to https://www.ebsco.com/terms-of-use

The anterior wall of the Daka glenoid fossa is vertical, similar to OH 9, Dmanisi D 2280, ZKD 3, ZKD 5, Sangiran 4, the Ngandong crania, and Sambungmacan 3. The anterior glenoid walls of KNM-ER 3733, Ceprano, and Kabwe are much less vertical. Specimens KNM-ER 3883, ZKD 11, ZKD 12, and Sangiran 17 are intermediate with respect to this feature. The shape of the lateral surface of the entoglenoid process, the medial wall of the glenoid fossa, varies in Pleistocene *Homo*. In some specimens, the posterior projection of the process twists medially, making the lateral surface convex. Several of the specimens compared had convex lateral entoglenoid walls: KNM-ER 3733, KNM-ER 3883, Dmanisi D 2280, the Zhoukoudian crania, Sangiran 2, Sangiran 17, Ngandong 6, Ngandong 12, and Sambungmacan 1. In others, the lateral surface is concave, continuing the trend of the anterior glenoid margin. The Daka calvaria and Sambungmacan 3 exhibit this morphology. Some specimens, including OH 9, Kabwe, Sangiran 4, and Ngandong 7, are intermediate.

The Daka tympanic plate forms the entire posterior wall of the glenoid cavity medially, without a significant contribution from the postglenoid process, which is more prominent laterally. This is similar to the condition seen in OH 9, Dmanisi D 2280, ZKD 5, Sangiran 2, Sangiran 4, the Ngandong crania, and the Sambungmacan crania. Specimens KNM-ER 3733, KNM-ER 3883, Dmanisi D 2282, ZKD 3, ZKD 10, ZKD 11, ZKD 12, Ceprano, and Kabwe all exhibit posteromedial glenoid walls with some contribution from the postglenoid process. In the Daka calvaria the tympanic plate inclines strongly posteriorly from vertical, and the posteriorly concave articular eminence inclines anteroinferiorly from the depth of the glenoid, giving the fossa a wide inferior part and a narrow apex when viewed laterally in approximated Frankfurt Horizontal plane. The central portion of the Daka glenoid fossa occurs in a deep recess bounded anteriorly by the articular eminence and posteriorly by the tympanic plate. In this regard it is similar to OH 9, ZKD 5, the Ngandong crania, and Sambungmacan 3. Other crania, such as KNM-ER 3733, Kabwe, and Sangiran 2, have central glenoid fossae that appear shallow due to more gently sloping anterior walls. However, when the depth of the glenoid fossa is observed laterally, between the postglenoid process and the lateral portion of the articular eminence, the Daka calvaria presents a more moderate glenoid fossa depth, similar to KNM-ER 3733. In this aspect, KNM-ER 3883, OH 9, ZKD 3, ZKD 5, ZKD 11, Kabwe, Sangiran 4, Ngandong 6, and Ngandong 12 all have deeper glenoid fossae, whereas those of Dmanisi D 2280 and Sangiran 2 are shallower.

The lateral edge of the right articular eminence in the Daka calvaria projects inferiorly as a knob-like eminence. This prominence is accentuated by the concavity of the anterior articular eminence along the border of the glenoid. The root of the zygomatic posterior to the lateral articular eminence is reduced in superoinferior thickness to give the eminence a distinctive, bulging lateral profile. Other crania that have knob-like lateral articular eminences include KNM-ER 3733, Sangiran 17, Ngandong 11, and Ngandong 12.

MASTOID REGION Both the right and left mastoid processes are damaged, but the mastoid crest is present as a slightly raised bulge on the left side. It does not extend posteriorly from the mastoid toward asterion. All of the crania observable for the region have more pronounced mastoid crests than the Daka calvaria.

EBSCOhost - printed on 10/28/2022 4:53 AM via . All use subject to https://www.ebsco.com/terms-of-use

The supramastoid regions of the Daka calvaria project noticeably where the vault widens inferiorly, and the roots of the zygomatics project laterally anterior to porion, but the suprameatal shelf is reduced above porion. This condition is similar in Ceprano, Sangiran 2, and Kabwe. Specimens Dmanisi D 2280 and D 2700, KNM-ER 3733, KNM-ER 3883, and the Ngandong crania have shelves that project moderately over porion. Some specimens have pronounced shelves, such as OH 9, the Zhoukoudian crania, Sangiran 17, and the Sambungmacan crania.

In *Homo sapiens* the supramastoid crest projects posteriorly as a continuation of the suprameatal line and the zygomatic root. It is distinct from the more inferiorly placed mastoid crest, which often projects posteriorly toward, and is sometimes continuous with, the posteroinferior extremity of the temporal line. A supramastoid crest extension onto the posterior aspect of the parietal is seen in the Zhoukoudian crania, OH 9, KNM-ER 3733, Sangiran 2, Sangiran 17, the Sambungmacan crania, Dmanisi D 2282, and Kabwe, but the Daka calvaria does not show this feature. The mastoid crest and supramastoid crest are generally somewhat parallel. The two tend to converge posteriorly rather than being subparallel in the Pleistocene *Homo* specimens compared. In specimens KNM-ER 3733, KNM-ER 3883, Sangiran 17, the Sambungmacan crania, the Ngandong crania, ZKD 10, ZKD 3, ZKD 5, Kabwe, and Ceprano, the mastoid crests converge posteriorly but stay separate for their lengths. In Dmanisi D 2280 and ZKD 11 the two lines converge and eventually join each other posteriorly. Sangiran 2 lacks a distinctive mastoid crest. Although the Daka calvaria is damaged in the mastoid crest region, it appears to be most similar to Sangiran 2 in morphology.

Mastoid crest development in KNM-ER 3733 can be viewed only from the superior part of the mastoid region due to damage to the inferior part. It is visible as a crest and extends toward the parietal angular torus area. In KNM-ER 3883 a well-developed mastoid crest is present. In comparison with the Daka calvaria this crest is significantly more inferiorly placed, with the Daka crest being near the superior aspect of the external meatus. Specimen KNM-ER 3733 is similar to the Daka calvaria in this regard, whereas KNM-ER 3883, Dmanisi D 2282, and Sambungmacan 1 differ. In summary, the Daka calvaria lacks strong supramastoid crests, a supratoral sulcus, and strong mastoid crests like those visible in OH 9, KNM-ER 3733, and the Zhoukoudian crania.

The Daka calvaria possesses a relatively small mastoid processes. Although the inferiormost tip of the left mastoid is not preserved, it is possible to adequately approximate the orientation of the mastoid process. Its axis is inferomedially oriented rather than vertically oriented as it is in *Homo sapiens*. Medial deflection of the mastoid process is also observed in all specimens compared except Kabwe. Most specimens that preserve the area (Dmanisi D 2280, KNM-ER 3733, OH 9, Sangiran 2 and 17, Sambungmacan 1 and 3, and the Zhoukoudian specimens) present mastoid processes similar to Daka in exhibiting little inferior projection. The Ngandong specimens, KNM-ER 3883, and Sangiran 4 have mastoid processes that project substantially inferiorly. Kabwe and Ceprano possess mastoid processes that are moderate in inferior projection. The Daka mastoid processes, as can be deduced from the better-preserved left side, would not have projected substantially inferiorly.

The short and broad mastoid processes are highly pneumatized. Mastoid air cells are visible on the fractured surfaces of both sides. Internal aspects of the mastoid processes are

EBSCOhost - printed on 10/28/2022 4:53 AM via . All use subject to https://www.ebsco.com/terms-of-use

discussed in further detail in Chapter 14. Aspects of the articulation between the tympanic plates and mastoid processes can be viewed along the partially preserved anterior portions of the mastoids. Daka's left tympanic plate laps over the mastoid without a deep mastoid fissure intervening. It is possible that a mediolaterally short fissure was present at the most lateral aspect of the tympanic plate, but because of breakage, this is unclear.

The mastoid foramina of the Daka calvaria are very large and have broad openings. The right side has a second, smaller foramen superior to the mastoid foramen that is positioned midway between asterion and the parietal notch. The left side does not have a second foramen. The digastric groove is well preserved on the left side, where it is shallow and wide. It is similar to Dmanisi D 2280 and D 2282, and Sangiran 2 in being shallow. It differs from KNM-ER 3733, Kabwe, Sangiran 4, Ngandong 7, Ngandong 12, Sambungmacan 3, and Ceprano, where the feature is deeper and narrower.

The Daka calvaria's left side reveals two crests/eminences in the region of the mastoid and the occipitomastoid suture. The first, the occipitomastoid crest, is prominent and runs along the occipitomastoid border. The second, smaller eminence, the juxtamastoid eminence (see discussion of nomenclature in Martínez and Arsuaga 1997), forms the posteromedial border of the digastric, running almost parallel to the occipitomastoid crest, and is exclusively on the temporal. Between these two crests/eminences is a sulcus that is narrower anteroinferiorly and broader posterosuperiorly. This shallow groove represents the passage for the occipital artery (Aiello and Dean 1990; Walensky 1964). The mastoid foramen is located at its anterosuperior edge and is linked to the larger groove by a short, shallow vascular groove.

JUGULAR NOTCH The space defined by the external opening of the jugular notch in the Daka calvaria is less bulbous than it is in most *Homo sapiens*. The right opening in Daka is narrower than the left. The carotid canals of the Daka calvaria are similar to each other in size and occur superomedial to the jugular notches and are separated from them by thin septa, similar to ZKD 3 (although the Zhoukoudian carotid canals are located more directly anterior to the jugular notch). Kabwe, KNM-ER 3883, Sangiran 17, Ngandong 7, and Ngandong 12 also have thin septa separating the carotid canals from the jugular notches, whereas Sangiran 4 presents a thicker septum.

Occipital

Preservation and Distortion

The Daka occipital is fragmented by major cracks. The first fragment is bounded by a crack that originates on the lambdoidal suture approximately 18.0 mm lateral to lambda. This crack extends inferiorly to inion and then turns laterally, eventually terminating at the lambdoidal suture approximately 28.0 mm superomedial to asterion. This crack is relatively wide, averaging about 2.0 mm along its course. The nuchal plane inferior to this first fragment is compressed by approximately 3.0 mm endocranially. The second major fragment of the upper scale is roughly heart-shaped and measures approximately 37.0 mm by 37.0 mm. It is positioned adjacent to lambda, bounded superiorly by the lambdoidal suture, and extends to either side of lambda. On the right it is bounded by

EBSCOhost - printed on 10/28/2022 4:53 AM via . All use subject to https://www.ebsco.com/terms-of-use

the crack just described, and inferiorly it is bounded by a second crack reaching from the lambdoidal suture approximately 35.0 mm left of lambda and terminating in the first major crack approximately 29.0 mm inferior to the lambdoidal suture. It is approximately 2.0 mm wide. The third piece of occipital bone measures approximately 87.0 mm wide by 79.0 mm long. It is located to the left of the first fragment and inferior to the second fragment. It covers most of the left occipital scale, much of the posterior left nuchal scale, and crosses onto the right nuchal scale. It is bounded inferiorly by a crack that originates at left asterion, passes approximately 7.0 mm posterior to the foramen magnum, and terminates at the occipitomastoid suture approximately 23.0 mm inferior to asterion. This crack averages approximately 1.5 mm in width and incorporates two areas of bone loss on either side of the median nuchal crest. That on the left is roughly triangular and measures approximately 16.0 mm by 15.0 mm. That on the right is rectangular and measures approximately 23.0 mm by 6.0 mm. Posterolateral to this area of bone loss is the fourth major fragment of occipital. It measures approximately 37.0 mm long by 35.0 mm wide. It is bounded on the right by the lambdoidal and occipitomastoid sutures, superiorly by the first major crack described in this paragraph, and medially by a smaller crack that extends from the first crack to the rectangular area of bone loss just described.

A fifth fragment of occipital is immediately anterior to the fourth and is much smaller, measuring approximately 21.0 mm by 23.0 mm. The nuchal surface of the occipital posterolateral to the right jugular notch has lost a small part of the bordering bone. Posteromedial to this area of bone loss is a sixth fragment of occipital, which includes the right margin of the foramen magnum. It is separated anteriorly from the basilar region by a significant crack approximately 2.0 mm wide. Offset produced by this crack is discussed in Chapter 14. The seventh major fragment of occipital includes the basilar portion and the left anterior nuchal plane. This area is bounded posteriorly by a crack already described, and it is bounded anteriorly by the left temporal and sphenoid bones. The right occipital condyle is damaged and retains no articular surface, but the left preserves the posterior one-third of the condyle.

Features

UPPER AND LOWER SCALES The upper scale (the midline region of the occipital between lambda and inion) of the Daka occipital is convex, giving it a sagittally-convex, vaulted profile. The Dmanisi crania, Ceprano, and Saldanha are similarly convex sagittally. The Ngandong crania and Sambungmacan 4 are also sagittally convex, but the convexity is somewhat occluded by the pronounced occipital tori of these crania. Specimens KNM-ER 3733, KNM-ER 3883, the Zhoukoudian specimens, the Sangiran specimens, and Sambungmacan 1 and 3 have flatter sagittal profiles of the upper scale.

The arc length of the Daka calvaria's occipital is greater than most of the crania compared. Only Sangiran 17, Ngandong 6, Ngandong 11, and Ngandong 12 are as large or larger. The occipital angle of the Daka calvaria is relatively wide. It is comparable to Dmanisi D 2280, Ngandong 7, ZKD 3, ZKD 11, and ZKD 10. Although the range of variation is small, the occipitals of Ngandong 11, Ngandong 12, ZKD 12, KNM-ER 3733, and KNM-ER 3883 are all more acutely angled. The chord length of the upper scale of the Daka calvaria is close to the average of crania compared.

EBSCOhost - printed on 10/28/2022 4:53 AM via . All use subject to https://www.ebsco.com/terms-of-use

The lower scale (midline region of the occipital between inion and opisthion) of the Daka calvaria is curved in its sagittal profile and is short compared to the upper scale length. This differs from what is seen in most Zhoukoudian specimens, where the upper scale is generally shorter than the lower scale (although ZKD 3 has upper and lower scales of equal length). In KNM-ER 3733, the absolute length of the lower scale is not very different from the condition in the Daka calvaria, but the lower scale is longer than the upper scale.

NUCHAL PLANUM/FORAMEN MAGNUM The mediolateral profile of the nuchal planum reveals shallow concavities on either side of the external occipital crest. Lateral to these concave areas there are two convex areas corresponding to rectus capitis posterior minor muscle attachments. More information on nuchal planum morphology is presented in the subsequent discussion of nuchal muscle attachments.

Foramina magna in Pleistocene *Homo* vary in shape from circular to anteroposteriorly elongate ovoids. Specimens KNM-ER 3733 and KNM-ER 3883 present more circular openings. The Daka foramen is more elongate, similar to Kabwe, Sangiran 17, Sambungmacan 4, and Ngandong 7. Sangiran 4 and Ngandong 12 have extremely elongate foramina magna. Angular change in the Daka foramen magnum's sagittal profile occurs just posterior to the occipital condyles, with the posterior aspect of the foramen angling posterosuperiorly. This gives an anterior-posterior convexity to the margin of the Daka foramen magnum when viewed laterally, similar to Ngandong 7 and 12. It differs from the more planar nature of the feature in KNM-ER 3883, Kabwe, Sangiran 4, Sangiran 17, and Trinil 2. The rim of the Daka foramen magnum smoothly transitions into the surrounding nuchal planum of the occipital with only a slight elevation. The margin in KNM-ER 3733 is elevated and slightly crested. The margins of the foramina magna of Ngandong 7 and Ngandong 12 are raised, but not crested, with a more torus-like transition into the nuchal planum.

Cracks surrounding the nuchal planum on the Daka calvaria, especially the one that traverses the occipital on the right side of the occipital crest, obscure observation of the relationship of the external occipital crest to the surrounding bone surface. However, the weak nature of this crest can easily be discerned on the Daka calvaria. The external occipital crests of Dmanisi D 2280, ZKD 3, ZKD 12, Sangiran 2, and the Sambungmacan crania are also relatively weak. External occipital crests are more strongly marked on KNM-ER 3733, OH 9, Kabwe, Sangiran 4, Sangiran 17, and the Ngandong crania. The parasagittal depression extending from the better preserved left side of the Daka external occipital crest is visible, and, while shallow in some areas, it extends all the way to the base of the occipital torus. The portion of the Daka calvaria's external occipital crest superior to the inferior nuchal lines is very faint.

The hypoglossal canal is intact anterolateral to the left occipital condyle. The right side is damaged. Although the canal was not measured internally, the size of the external aspect of the hypoglossal canal of the Daka calvaria is very large relative to cranial size. In the Daka calvaria the hypoglossal canals are located on the lateral edge of the basilar portion and are enclosed by extensions from its lateral surface.

There is a shallow condylar fossa posterior to the left occipital condyle. In the Daka calvaria, Kabwe, Sangiran 4, and Ngandong 7 the occipital condyles are the most inferior points on the occipital, whereas in Sangiran 17 and KNM-ER 3733 the condyles are

EBSCOhost - printed on 10/28/2022 4:53 AM via . All use subject to https://www.ebsco.com/terms-of-use

positioned superior to opisthion (the preserved occipital condyles are situated superior to opisthion, but below the posterior portion of the nuchal planum in KNM-ER 3733).

In some Pleistocene *Homo* specimens (for example, Kabwe and Sangiran 17), the nuchal planum is nearly horizontal, whereas in others it is oblique. The Daka calvaria has an oblique nuchal planum, similar to KNM-ER 3733, Dmanisi D 2280 and D 2700, Ceprano, Saldanha, the Ngandong crania, and the Sambungmacan crania. Moderately oblique nuchal planes are also seen in OH 9, the Zhoukoudian crania, Sangiran 2, and Sangiran 4.

NUCHAL MUSCLE ATTACHMENTS Musculotendonous attachments on the nuchal planum of the Daka calvaria are well delineated, with the left side revealing more detail than the right. Comparisons are limited here to *Homo sapiens*, Sangiran 17, KNM-ER 3733, Sambungmacan 3, and Kabwe because of the difficulty of delineating these subtle features on other Pleistocene *Homo* crania. Starting from the midline and working laterally, the depression corresponding to the attachment of the semispinalis capitis muscle is bounded superiorly by the arch-shaped superior nuchal line, which curves laterally from inion to about 16.0 mm posterior to asterion. The shape of the arch is similar to Kabwe and Sangiran 17. It is less tightly arched than in Sambungmacan 3 and more tightly arched than in KNM-ER 3733 or *H. sapiens*. The superior nuchal line continues anteriorly toward the mastoid foramen, beyond the point where the attachment of the semispinalis capitis muscle ends. The anteroinferior border of this depression is triangular, and the anterior apex of this triangle lies just lateral to the median sagittal plane, similar to Sambungmacan 4. The long side of this triangle runs laterally toward the nuchal crest 16.0 mm posterior to asterion, and the short side runs toward inion. The overall area of the semispinalis capitis muscle attachment is greater than in *H. sapiens* or Sambungmacan 3, but less than that of Kabwe and Sangiran 17. It is similar to that of KNM-ER 3733. A crescent-shaped eminence (with the crescent opening anteromedially) lies anterolateral to the long side of the triangle just described. This eminence, which corresponds to the attachment of the superior oblique muscle, is different from all of the specimens compared. In Kabwe, Sangiran 17, and Sambungmacan 3 the eminence is more knob-like, and in *H. sapiens* it is only slightly raised. It is not discernible in KNM-ER 3733. The inferior tip of this raised area in Daka extends as a crest that parallels the occipitomastoid crest. The superior oblique muscle originates via tendonous fibers on the transverse process of the atlas vertebrae. This tendonous bundle corresponds to a smooth groove that occurs lateral and parallel to the linear extension just described and medial to the occipitomastoid crest. This groove is substantially less pronounced in Kabwe and Sambungmacan 3. It is broad and shallow in Sangiran 17, and is impossible to distinguish in KNM-ER 3733. The anteroinferior end of the linear crest lateral to the groove for the superior capitis oblique muscle described above terminates in a rugose ledge that corresponds to the lateral extension of the inferior nuchal line. Anterior and medial to this ledge is a depressed area bounded medially by the posterolateral border of the foramen magnum and anteriorly by a subtle crest posterior to the occipital condyle that courses from anterolateral to posteromedial. The rugose, arch-shaped anterior ledge of the lateral extension of the inferior nuchal line bounds this depressed area posteriorly and laterally. This depressed area corresponds to the attachment of the rectus capitis posterior major muscle. The area of this attachment

EBSCOhost - printed on 10/28/2022 4:53 AM via . All use subject to https://www.ebsco.com/terms-of-use

is smaller in Daka than it is in Kabwe, but larger than in Sangiran 17 and in *H. sapiens*. It is similar in area to KNM-ER 3733. The medial portion of the inferior nuchal line, the median nuchal crest, the posterior margin of the foramen magnum, and the rectus posterior capitis major attachment bound a rhomboidal depression that corresponds to the insertion of the rectus capitis posterior minor muscle. This attachment area is larger in Kabwe, but similar in extent in Daka in KNM-ER 3733 and Sangiran 17.

OCCIPITAL TORUS Occipital tori of Pleistocene *Homo* crania tend to be pronounced (see Figure 15.6). They are, however, variable in morphology. Some are barlike, extending across the entire posterior occipital. Some are more pronounced medially but become reduced laterally. Some are well defined inferiorly, overhanging the nuchal planum with a deep subtoral concavity, but are less defined superiorly. In the analysis presented in Chapter 15, an occipital torus is defined by the presence or absence of a supratoral sulcus and scored as minimal, moderate, or pronounced, but this definition does not capture the range of morphology present in Pleistocene *Homo*. Occipital torus morphology is frequently similar among crania from the same site. For example, the robust double arches of the Ngandong occipital tori are unique among Pleistocene *Homo* but occur in all of the Ngandong crania. The Ngandong occipital tori have strong supratoral and subtoral sulci. Many Pleistocene *Homo* crania have occipital tori that are barlike and relatively continuous across the occipital, including Dmanisi D 2280, the Zhoukoudian crania, Trinil 2, Ceprano, and Sangiran 2. Some have tori that are more pronounced medially, including KNM-ER 3733, KNM-ER 3883, OH 9, Saldanha, Sangiran 4, Sangiran 17, and Sambungmacan 1. Sambungmacan 3 and 4 have tori that are mediolaterally continuous, but double arched rather than linear. The Daka occipital torus is extremely subtle relative to other Pleistocene *Homo* except Dmanisi D 2282 and D 2700. It is narrow and crestlike laterally and is discernible medially only as a result of a subtoral sulcus. There is no supratoral sulcus medially. The torus does not cross onto the mastoid but rather terminates at the border of the occipital and temporal. There are slight supratoral sulci superior to the lateral parts of the occipital torus. The slight occipital torus of Daka is more prominent on the left side.

The Daka calvaria exhibits a transversely and sagittally rounded area surrounding opisthocranion. Inion, the projecting attachment point for the nuchal ligament, is anteroinferiorly separated from opisthocranion by about 12.0 mm. This relatively pronounced separation is similar to what is seen in Sangiran 4 and in the Ngandong crania. In many Pleistocene *Homo* crania, such as Dmanisi D 2280, KNM-ER 3733, OH 9, the Zhoukoudian crania, Sangiran 17, and the Sambungmacan crania, these points are relatively close together or nearly coincident.

Sphenoid

Preservation and Distortion

The sphenoid of the Daka calvaria is relatively well preserved, but it is missing small parts of the lateral portions of the orbital plates of the greater wings, major portions of the pterygoid processes, and the anterior body and sphenoidal crest. The superior base of the left

EBSCOhost - printed on 10/28/2022 4:53 AM via . All use subject to https://www.ebsco.com/terms-of-use

medial and lateral pterygoid plates is preserved, as is the superior aspect of the pterygoid fossa. On the right side, only the base of the pterygoid processes is preserved. The external surface of the sphenoid, from approximately 10.0 mm anterior to the sphenoccipital synchondrosis along the orbital plates and into the supraorbital region, was intentionally left in a matrix-covered state to protect the specimen. Details on this matrix-obscured region are visible using computed tomography and are presented in Chapter 14.

No sign of distortion of the sphenoid is visible on the right side, but the left side shows minor distortion resulting in displacement created by a crack that runs from the glenoid cavity sagittally and bisects the base of the infraorbital plate. The left greater wing medial to this crack is deflected superiorly by less than a millimeter.

Features

The profile of the temporal and infratemporal surfaces of the sphenoid has been discussed in connection with the lateral view. The temporal surface of the Daka greater wing trends medially as it drops inferiorly. The transition from the temporal surface to the infratemporal surface of the Daka sphenoid is similar to that in Zhoukoudian specimens, described by Weidenreich (1943) as a gentle, smooth curve without any sharp crest or line (infratemporal crest) dividing the two surfaces. This smooth condition is also present in Sangiran 17, KNM-ER 3733, and Ceprano. Specimens with a crest-like transition include KNM-ER 3883, Dmanisi D 2280, Kabwe, Ngandong 7, Ngandong 12, and Sambungmacan 3. The superior borders of the Daka greater wings have maximum anteroposterior widths of approximately 30.0 mm where they articulate with the frontal and the parietals. The minimum anteroposterior widths of the greater wings, which occur on the infratemporal boundary, are about half of the superior widths (~16.0 mm). The Daka greater wings are very strongly concave in the transverse plane, resulting in a deep, narrow temporal fossa over the entire greater wing, similar to KNM-ER 3733, KNM-ER 3883, OH 9, and Dmanisi D 2280. The greater wings of Kabwe are more strongly concave and define deeper, narrower channels. The Ceprano greater wings are only moderately narrow and deep. The preserved greater wing of Bodo has a deep, but broad trough. Finally, the Ngandong crania have greater wings that are broader, with shallower troughs.

The area of the Daka calvaria where one would expect to find an infratemporal crest shows neither crest development nor the development of a spine. The transition from the infratemporal surface to the orbital fissure in the Daka calvaria is marked by a thin lamina of bone. This inferior border of the sphenomaxillary crest curls posterolaterally along the medial third of the plate and inclines strongly posteroinferiorly. The zygomatic margin is also crested and fully preserved. The majority of the orbital crest region is missing on the Daka calvaria, but there is a small projection in the transition from the zygomatic margin into the sphenomaxillary crest. Its position is in nearly the same horizontal plane as the apex of the transition between the temporal surface and infratemporal surface of the greater wing of the sphenoid. The curled crest that borders the infratemporal surface along the infraorbital fissure connects to the orbital crest with a slight sigmoid twist. The lateral walls of the temporal fossae deflect medially as they descend. This medial deflection is more pronounced in KNM-ER 3733, KNM-ER 3883, ZKD 3, the Ngandong crania, and OH 9 than in the Daka calvaria, but it is less pronounced in Bodo, Kabwe, and Ceprano.

EBSCOhost - printed on 10/28/2022 4:53 AM via . All use subject to https://www.ebsco.com/terms-of-use

The infratemporal surfaces in Pleistocene *Homo* vary in orientation from nearly horizontal to oblique and more vertical. The infratemporal surface of the Daka calvaria is horizontal, similar to the condition in OH 9, Kabwe, Dmanisi D 2280, Sangiran 4, Ngandong 7, Ngandong 12, and Sambungmacan 3. Specimens with infratemporal surfaces that are moderately oblique include ZKD 3, ZKD 11, Ceprano, Sangiran 2, and Sangiran 17. The most obliquely oriented infratemporal surfaces include KNM-ER 3733 and especially Bodo.

The orbital crest and the sphenomaxillary crest are distinct and laminar. They are well preserved on the left side and partially preserved on the right side of the Daka calvaria. These structures are thick (approximately 1.75 mm) relative to the condition in *Homo sapiens*. The laminae of the sphenomaxillary crests are posterolaterally flared and curl slightly to project over the infratemporal surface. They form deep sulci along the anterior margins of the infratemporal surfaces, then merge into the base of the pterygoid. These structures are better preserved on the left side than on the right. The Daka sphenomaxillary crest is inferior to the infratemporal crest region, a condition also seen in Dmanisi D 2280, Ceprano, Kabwe, Bodo, and Ngandong 12. Weidenreich (1943) notes that in apes the temporal surface of the sphenoid extends more inferiorly than the lower border of the orbital fissure so that the infratemporal crest region is inferior to the sphenomaxillary crest. According to Weidenreich (1943), the ape condition is similar to that of Zhoukoudian specimens, and our observations of ZKD 3 corroborate this. At the medial extent of the Daka orbital crests, the foramina rotunda are both preserved, as are the pterygoid canals. Foramina spinosa, foramina ovale, and foramina lacera have been discussed in the lateral view discussion. The anteroposterior dimension of the pterygoid base, as measured between foramen ovale and the anterior opening of the foramen rotundum, is similar in the Daka calvaria and *H. sapiens*.

The pterygoid roots, which are preserved only on the left side, reveal thick medial and lateral bases for pterygoid plates on the Daka sphenoid. The right side of the sphenoid is damaged at the pterygoid bases and has exposed a large lateral sphenoidal sinus. Sinus development is less than what is seen in the highly inflated Bodo lateral sphenoidal sinuses, which extend laterally to the temporal walls of the greater wing. Sphenoidal sinus development is discussed more extensively in Chapter 14. The pterygoid fossa, which can be seen on the left side, is deep. The external mediolateral dimension between the medial and lateral pterygoid plates is approximately 14.0 mm. The Daka sphenooccipital suture is completely fused.

Additional Cranial and Mandibular Specimens

Two additional hominid cranial vault specimens and one mandibular specimen derive from the Daka Member. Specimen BOU-VP-1/108 consists of five vault fragments (Plate 13.8). The largest, a fragment of right frontal and parietal, covers approximately 25.0 cm^2 of the vault. The coronal suture is present on this specimen, separating parietal from frontal. The specimen is roughly square-shaped, and the suture separates a strip of parietal that is approximately 4.5 cm by 1.0 cm. The temporal line is present across the whole fragment, continuing over the parietal portion. It is well defined and rugose anteriorly. This fragment presents a relatively uniform 0.85 cm vault thickness. The

EBSCOhost - printed on 10/28/2022 4:53 AM via . All use subject to https://www.ebsco.com/terms-of-use

other four fragments of BOU-VP-1/108 are much smaller, each with an area of about 6.0 cm^2. One of these smaller pieces is identifiable as a fragment of parietal, but the others are not clearly identifiable to element. All are relatively thick, with thicknesses between 0.8 and 1.0 cm. The smaller fragments cannot be effectively sided. Specimen BOU-VP-1/114 (Plate 13.9) is a small hominid cranial vault fragment, with a preserved ectocranial surface area of approximately 9.0 cm^2. Its vault thickness is less than that of any of the BOU-VP-1/108 fragments, measuring approximately 0.65 cm.

Specimen BOU-VP-3/154 (Plate 13.10) is a fragment of a right hominid mandible. It preserves the mandibular body from the I_2 alveolus anteriorly to just distal to the alveolus for the M_2 distal root. No tooth crowns remain, but the roots for the canine and M_1 are fully preserved, and those for the premolars and M_2 are partially preserved. A partial alveolus for the I_2 is present, as is a small portion of the apex of the I_1 alveolus. The specimen was recovered very recently, and detailed description awaits work on stratigraphy and provenience.

Conclusion

One of the most striking perspectives offered by the preceding description is that ectocranial features are distributed in a complex mosaic across Pleistocene *Homo* specimens in Africa and Eurasia. Features that are geographically circumscribed are rare outside of groups from single sites. While there is a great deal of similarity in homologous features among specimens from single sites, as with the unique occipital torus morphology of the Ngandong crania or the unique angular torus morphology of the Zhoukoudian crania, general associations of morphology with geographic regions above the scale of a single site are impossible to make. This phenomenon is especially relevant when contemplating phylogeny. It is impossible to form an argument for regional homogeneity whenever more than a few features are considered simultaneously. The phylogenetic analysis presented in Chapter 15 further investigates this phenomenon.

As more Pleistocene *Homo* crania become available, the reality of the substantial morphological variation they present is becoming more apparent. The implications of biological variation have been appreciated in extant mammalian skeletal biology, including that of humans, for over a century (Bowler 2005), but disclosures of variation's confounding effects on phylogenetic reconstruction have traditionally been superseded by the simplicity and appeal of evolutionary arguments based on sparse fossils and few or developmentally linked morphological features. Considering the variation now observable in the Pleistocene hominid record and the outcome of studies of evolutionary developmental biology (Lovejoy et al. 1999), there is no longer any basis for simplistic phylogenetic reconstructions that are based on subtle osteomorphological characters and inadequate samples.

EBSCOhost - printed on 10/28/2022 4:53 AM via . All use subject to https://www.ebsco.com/terms-of-use

APPENDIX 13.1 Daka Cranial Metrics

Measurement			*References*			
	Measurement Type	*Notes*	*Weidenreich (1943)*	*Wood (1991)*	*Martin (1928)*	*Other Authors*
Auriculo-bregmatic arc (po-po [b])	A		t.19, no.51		no.24	
Biasterionic arc (ast-ast)	A			no.42		
Bregma-pterion arc (b-sphn)	A			no.22		
Bregma-asterion arc	A			no.34		
Bregma-opisthion arc	A					G
Frontal torus arc	A			no.67		
Glabella-bregma arc	A		t.19, no.55	no.18		
Inion-opisthion arc	A			no.38		
Lambda-inion arc	A			no.36		
Lambda-opisthocranion [inion] arc (l-op [i])	A		t.19, no.70		no.28(1)	
Mandibular fossa longitudinal arc	A			no.81		
Mandibular fossa transverse arc	A			no.83		
Median sagittal arc I (n-op)	A		t.19, no.52		no.25a	
Median sagittal arc II (n-o)	A		t.19, no.53		no.25	
Nasion-bregma, Frontal sagittal arc	A		t.19, no.54		no.26	
Occipital sagittal arc, Lambda-opisthion arc (l-o)	A		t.19, no.60	no.40	no.28	
Opisthocranion-opisthion arc	A		t.19, no.72		no.28(2)	
Parietal coronal arc (b-sphn)	A			no.30		
Parietal lambdoid arc, Lambda-asterion arc (l-ast)	A		t.19, no.68	no.32	no.27(3)	
Parietal sagittal arc length, Bregma-lambda arc	A		t.19, no.58	no.26	no.27	
Parietal temporal arc (sphn-ast)	A			no.28		
Postglabellar sulcus-bregma arc	A			no.20		
Sagittal arc-pars glabellaris frontalis (n-sg)	A		t.19, no.62		no.26(1)	
Sagittal arc-pars glabellaris frontalis (sg-b)	A		t.19, no.64		no.26(2)	
Sphenion-asterion arc (sph-ast)	A				no.27(1)	
Cranial base angle (ba-n-o)	An		t.20, no.14			
Frontal angle	An				no.32(5)	
Frontal curvature (m-n-b)	An		t.20, no.6			
Frontal inclination angle I (b-n-op[i])	An		t.20, no.2		no.32(1)	
Frontal inclination angle II (b-n-o)	An		t.20, no.11			
Frontal profile angle (m-g-op[i])	An		t.20, no.1		no.32a	
Inclination of occipital foramen (n-ba-o)	An		t.20, no.15			
Inclination of pars cerebralis (sg-b ∠ n-op[i])	An		t.20, no.5		no.32(4)	

EBSCOhost - printed on 10/28/2022 4:53 AM via . All use subject to https://www.ebsco.com/terms-of-use

Best Daka Measurement					*Right or Midline*			*Left*		
Midline	*Right*	*Left*	*Error*	*Source*	*Original*	*Microscribe*	*CT*	*Original*	*Microscribe*	*CT*
269.0			**±2**	**o**	269.0					
143.0			**±1**	**o**	143.0					
	99.0	**98.0**	**±2**	**o**	99.0			98.0		
	150.0	**146.0**	**±2**	**o**	150.0			146.0		
218.0			**±2**	**o**	218.0					
150.0			**±2**	**o**	150.0					
101.0			**±1**	**o**	101.0					
48.0			**±2**	**o**	48.0					
75.0			±1	**o**	75.0					
52.0			**±2**	**o**	52.0					
	34.0	**31.0**	**±1**	**o**	34.0			31.0		
	32.0	**33.0**	**±1**	**o**	32.0			33.0		
282.0			**±2**	**ct**			282.0			
336.0			**±1**	**ct**			335.9			
116.0			**±1**	**o**	116.0					
120.0			**±1**	**o**	120.0					
63.0			**±2**	**o**	63.0					
		94.0	**±1**	**o**				94.0		
	103.0	**97.0**	**±1**	**o**	103.0			97.0		
99.0			**±1**	**o**	99.0					
		94.0	**±1**	**o**				94.0		
80.0			**±2**	**o**	80.0					
36.0			**±2**	**o**	36.0					
85.0			**±2**	**o**	85.0					
	91.0	**81.0**	**±1**	**o**	91.0			81.0		
7.4			**±1**	**ct**			7.4			
141.0			**±1**	**ct**			141.0			
17.0			**±1**	**ct**			17.4			
55.0			**±1**	**ct**			55.0			
70.0			**±1**	**ct**			70.0			
65.0			**±1**	**ct**			65.0			
154.0			**±1**	**ct**			154.0			
46.0			**±1**	**ct**			46.0			

EBSCOhost - printed on 10/28/2022 4:53 AM via . All use subject to https://www.ebsco.com/terms-of-use

APPENDIX 13.1 *(continued)*

Measurement			*References*			
	Measurement Type	*Notes*	*Weidenreich (1943)*	*Wood (1991)*	*Martin (1928)*	*Other Authors*
Inclination of pars glabellaris (sg-n-op[i])	An		t.20, no.4		no.32(3)	
Inclination of whole occipital (l-o-n)	An		t.20, no.12			
Inclinaton of frontal squama (b-g-op[i])	An		t.20, no.3		no.32(2)	
Mandibular fossa angle	An	3		no.139		
Occipital angle I	An					G, V
Occipital angle II	An					H
Occipital curvature (l-op[i] ∠ op[i]-o)	An		t.20, no.10		no.33(4)	
Occipital inclination I (l-op[i] ∠ op[i]-n)	An		t.20, no.7		no.33(1a)	
Occipital inclination II (l-op[i] ∠ op[i]-g)	An		t.20, no.8		no.33(1b)	
Opisthion-opisthocranion-nasion (o-op[i] ∠ op[i]-n)	An		t.20, no.9		no.33(2a)	
Parietal angle	An					H
Petromedian angle	An	4	t.8	no.137		
Tympanomedian angle	An	4	t.8	no.138		
Foramen magnum area	Ar			(no.76 ÷ 2) × (no.77 ÷ 2pi)		
Average 'maximum'	B	5	t.19, no.20		no.8*	
Biasterionic breadth (ast-ast)	B		t.19, no.27	no.14	no.12	
Biauricular breadth	B		t.19, no.26		no.11	
Biforamen ovale breadth	B					W/L
Bifrontal breadth (fma-fma)	B					H
Biporionic breadth, Interporial (po-po)	B		t.19, no.29	no.11		
Bistephanic breadth (st-st)	B		t.19, no.25		no.10b	
Entoglenoid breadth	B			no.16		
Foramen magnum maximum width	B			no.77	no.16	
Greatest frontal (co-co), Maximum frontal breadth	B		t.19, no.24		no.10	
Inner orbital breadth (fmo-fmo)	B				no.43(1)	
Inner skull breadth	B		t.19, no.21		no.8(2)	
Interentoglenoid breadth	B			no.15		
Interorbital breadth	B				no.49a	
Lateral interglenoidal	B		t.19, no.30			
Maximum cranial breadth (eu-eu)	B				no.8	
Maximum parietal breadth	B			no.9		
Maximum supramastoid, Maximum intercrestal breadth	B		t.19, no.19	no.12		
Maximum temporal breadth	B			no.10		

EBSCOhost - printed on 10/28/2022 4:53 AM via . All use subject to https://www.ebsco.com/terms-of-use

Best Daka Measurement					*Right or Midline*			*Left*		
Midline	*Right*	*Left*	*Error*	*Source*	*Original*	*Microscribe*	*CT*	*Original*	*Microscribe*	*CT*
80.0			**±1**	**ct**			80.0			
92.0			**±1**	**ct**			92.0			
52.0			**±1**	**ct**			52.0			
	100.0	**105.0**	**±3**	**ct**			100.0			105.0
107.0			**±1**	**ct**			107.0			
107.0			**±1**	**ct**			107.0			
107.0			**±1**	**ct**			107.0			
72.0			**±1**	**ct**			72.0			
68.0			**±1**	**ct**			68.0			
37.0			**±1**	**ct**			37.0			
147.0			**±1**	**ct**			147.0			
	40.0	**41.0**	**±2**	**ct**			40.0			41.0
	82.0	**78.0**	**±2**	**ct**			82.0			78.0
828.4				**calc.**						
128.5				**calc.**						
116.0			**±2**	**o**	116.0					
130.0			**±1**	**o**	130.0	129.3	129.6			
47.4			**±1**	**o**	47.4					
117.0			**±2**	**o**	117.0	119.9	117.9			
123.0			**±1**	**o**	128.0					
101.0			**±2**	**o**	101.0	102.7				
66.1			**±2**	**o**	66.1					
29.3			**±1**	**o**	29.3					
105.0			**±2**	**o**	105.0					
111.2			**±1**	**o**	111.2	110.1	109.9			
112.3			**±1**	**ct**			112.3			
70.4			**±1**	**o**	70.4	69.8				
31.5			**±1**	**o**	31.5	29.9				
121.5			**±1**	**o**	121.5	122.9				
133.0			**±2**	**o**	133.0					
129.0			**±1**	**o**	129.0					
139.5			**±1**	**ct**			139.5			
141.0			**±2**	**o**	141.0					

EBSCOhost - printed on 10/28/2022 4:53 AM via . All use subject to https://www.ebsco.com/terms-of-use

APPENDIX 13.1 *(continued)*

Measurement			*References*			
	Measurement Type	*Notes*	*Weidenreich (1943)*	*Wood (1991)*	*Martin (1928)*	*Other Authors*
Medial interglenoidal	B		t.19, no.31			
Minimum cranial breadth	B				no.14	
Minimum frontal breadth, Least frontal (ft-ft)	B		t.19, no.22	no.8	no.9	
Postorbital breadth	B		t.19, no.23		no.9(1)	
Stylo-mastoid breadth	B		t.19, no.32			
Superior facial breadth (fmt-fmt), External biorbital breadth	B			no.49	no.43	
Temporoparietal breadth	B		t.19, no.17		no.8c	
Torus angularis breadth, Black's maximum parietal breadth	B		t.19, no.18			
Width temporal gutter	B			no.61		
Biasterionic chord (ast-ast)	C			no.41		
Bregma pterion chord (b-sphn)	C			no.21		
Bregma-asterion chord	C			no.33		
Chord-pars glabellaris frontalis (n-sg)	C		t.19, no.63		no.29(1)	
Chord-pars glabellaris frontalis (sg-b)	C		t.19, no.65		no.29(2)	
Frontal torus chord	C			no.66		
Glabella-bregma chord	C		t.19, no.57	no.17		
Inion-opisthion chord	C			no.37		
Lambda-inion chord	C			no.35		
Lambda-opisthocranion [inion] chord (l-op [i])	C		t.19, no.71		no.31(1)	
Mandibular fossa breadth chord	C			no.82		
Mandibular fossa length chord	C			no.80		
Nasion-bregma, Frontal sagittal chord	C		t.19, no.56		no.29	
Occipital sagittal chord, Lambda-opisthion chord (l-o)	C		t.19, no.61	no.39	no.31	
Opisthocranion-opisthion chord	C		t.19, no.73		no.31(2)	
Parietal coronal chord (b-sphn)	C			no.29		
Parietal sagittal, Bregma-lambda chord	C		t.19, no.59	no.25	no.30	
Parietal-lambdoid, Lambda-asterion chord (l-ast)	C		t.19, no.69	no.31	no.30(3)	
Postglabellar sulcus-bregma chord	C			no.19		
Sphenion-asterion, Parietal temporal chord (sph-ast)	C		t.19, no.67	no.27	no.30(2)	
Cranial capacity	V	1	t.19, no.74			
Horizontal circumference (on-on [op])	Cir		t.19, no.49		no.23a	
Maximum horizontal circumference (g-g[op])	Cir	2	t.19, no.50		no.23	

EBSCOhost - printed on 10/28/2022 4:53 AM via . All use subject to https://www.ebsco.com/terms-of-use

Best Daka Measurement					*Right or Midline*			*Left*		
Midline	*Right*	*Left*	*Error*	*Source*	*Original*	*Microscribe*	*CT*	*Original*	*Microscribe*	*CT*
72.3			**±2**	**o**	72.3					
70.0			**±1**	**o**	70.0					
89.0			**±1**	**o**	89.0	89.7				
95.0			**±1**	**o**	95.0					
84.5			**±1**	**o**	84.5					
124.0			**±1**	**o**	124.0					
125.0			**±2**	**ct**			125.0			
121.0			**±1**	**o**	121.0					
	20.2	**20.0**	**±1**	**o**	20.2		19.3	20.0		18.5
113.0			**±1**	**o**	113.0					
	78.0	**79.0**	**±1**	**o**	78.0	81.4		79.0	79.5	
	124.0	**123.3**	**±2**	**o**	124.0			123.3		
26.5			**±2**	**o**	26.5					
75.0			**±2**	**o**	75.0		74.2			
121.4			**±1**	**o**	121.4					
97.0			**±1**	**o**	97.0	94.8	96.0			
47.0			**±2**	**o**	47.0	43.0	44.0			
65.0			**±1**	**o**	65.0	66.3	65.3			
51.1			**±2**	**o**	51.1	51.4	52.1			
	27.9	**27.0**	**±1**	**o**	27.9			27.0		
	21.7	**20.1**	**±1**	**o**	21.7			20.1		
101.0			**±2**	**o**	101.0	100.3	99.2			
95.0			**±2**	**o**	95.0	92.1	92.6			
60.8			**±2**	**o**	60.8	63.1	62.1			
		79.0	**±1**	**o**				79.0		
94.0			**±1**	**o**	94.0	96.2				
	90.7	**85.1**	**±1**	**o**	90.7			85.1		
75.0			**±2**	**o**	75.0		74.5			
	81.1	**76.8**	**±1**	**o**	81.1			76.8		
986.0			**see notes**	**ct**	995.0		986.0			
480.0			**±4**	**o**	480.0					
560.0			**±4**	**o**	560.0					

EBSCOhost - printed on 10/28/2022 4:53 AM via . All use subject to https://www.ebsco.com/terms-of-use

APPENDIX 13.1 *(continued)*

Measurement			*References*			
	Measurement Type	*Notes*	*Weidenreich (1943)*	*Wood (1991)*	*Martin (1928)*	*Other Authors*
Mandibular fossa depth	D			no.84		
Bregma-subtense fraction	F					H
Lambda-subtense fraction	F					H
Nasion subtense fraction	F					H
Nasion subtense fraction	F					H
Auricular-bregmatic height	H		t.19, no.36		no.20	
Auriculo-lambda height	H		t.19, no.38			
Bregma height above g-op [i]	H		t.19, no.40			
Bregma height above n-o	H		t.19, no.44			
Calvarial height above g-l	H		t.19, no.43		no.22b	
Calvarial height above g-op [i]	H		t.19, no.41		no.22a	
Calvarial height above n-op [i]	H		t.19, no.42		no.22	
Inion above n-o	H		t.19, no.48			
Lambda height above n-o	H		t.19, no.46			
Maximum squamous height	H				no.19d	
Opisthocranion height above n-o	H		t.19, no.47			
Altitudinal index (ba-b/g-op)	I			no.4 ÷ no.1		
Anteroposterior supraorbital torus chord/arc index	I			no.63 ÷ no.64		
Basi-bregmatic height-length index	I				no.17 ÷ no.1	
Biasterionic chord/arc breadth index	I			no.41 ÷ no.42		
Breadth-height index	I	5	t.21, no.6		no.17 ÷ no.8*	
Bregma height above (g-op [i]) index	I		t.21, no.8			
Bregma height above (n-o) index	I		t.21, no.11			
Bregma position above (n-o) index	I		t.21, no.16			
Bregma pterion chord/arc index	I			no.21 ÷ no.22		
Bregma-asterion chord/arc index	I			no.33 ÷ no.34		
Calvarial height above (g-op [i]) index	I		t.21, no.9		no.22a ÷ no.1(2)	
Calvarial height above	I		t.21, no.10		no.22 ÷ no.1d	
Cerebral curvature index (n-op [i]) index	I		t.21, no.37		no.29(2) ÷ no.26(2)	
Coronal chord/arc index	I			no.29 ÷ no.30		
Cranial breadth-basi-bregmatic height-length index	I				no. 8− no.17 ÷ no.1	

EBSCOhost - printed on 10/28/2022 4:53 AM via . All use subject to https://www.ebsco.com/terms-of-use

Best Daka Measurement					*Right or Midline*			*Left*		
Midline	*Right*	*Left*	*Error*	*Source*	*Original*	*Microscribe*	*CT*	*Original*	*Microscribe*	*CT*
	4.5	**5.4**	**±1**	**ct**			4.5			5.4
49.0			**±2**	**o**	49.0		53.6			
50.0			**±2**	**o**	50.0		48.5			
55.0			**±2**	**o**	55.0		53.0			
55.0			**±3**	**o**	55.0		53.0			
101.0			**±2**	**ct**			101.0			
98.0			**±2**	**ct**			98.0			
73.0			**±1**	**ct**			73.0			
92.0			**±1**	**ct**			92.0			
51.0			**±1**	**ct**			51.0			
73.0			**±1**	**ct**			73.0			
80.0			**±1**	**ct**			80.0			
33.0			**±2**	**ct**			33.0			
93.0			**±1**	**ct**			93.0			
	43.0		**±1**	**o**	43.0					
43.0			**±2**	**ct**			43.0			
67.3				**calc.**						
72.0				**calc.**						
67.3				**calc.**						
79.0				**calc.**						
94.2				**calc.**						
40.6				**calc.**						
69.7				**calc.**						
22.1				**calc.**						
	78.8	**80.6**		**calc.**						
	81.6	**82.2**		**calc.**						
41.3				**calc.**						
45.9				**calc.**						
88.2				**calc.**						
	75.1	**78.9**		**calc.**						
6.7				**calc.**						

EBSCOhost - printed on 10/28/2022 4:53 AM via . All use subject to https://www.ebsco.com/terms-of-use

APPENDIX 13.1 *(continued)*

Measurement			*References*			
	Measurement Type	*Notes*	*Weidenreich (1943)*	*Wood (1991)*	*Martin (1928)*	*Other Authors*
Cranial breadth-basi-bregmatic index	I				no.8 ÷ no.17	
Cranial index I (max. temporal breadth/g-op)	I			no.10 ÷ no.1		
Cranial index II (eu-eu/g-op)	I				no.8 ÷ no.1	
Cranial index III, Length-breadth index	I	19	t.21, no.1		no.8* ÷ no.1(or 2)	
Foramen magnum shape index	I			no.77 ÷ no.76	no.16 ÷ no.7	
Frontal breadth index	I		t.21, no.22		no.9 ÷ no.8*	
Frontal curvature index	I		t.21, no.34		no.29 ÷ no.26	
Frontal torus breadth chord/arc index	I			no.66 ÷ no.67		
Frontal-supramastoid index	I			no.8 ÷ no.12		
Fronto-occipital arc index	I		t.21, no.29		no.28 ÷ no.26	
Fronto-patietal arc index	I		t.21, no.28		no.27 ÷ no.26	
Fronto-sagittal arc index	I		t.21, no.31		no.26 ÷ no.25	
Frontotemporal index	I			no.8 ÷ no.10		
Glabella-bregma chord/arc index	I			no.17 ÷ no.18		
Glabellar curvature index	I		t.21, no.36		no.29(1) ÷ no.26(1)	
Glabello-cerebral index	I		t.21, no.38		no.29(1) ÷ no.29(2)	
Inion height above (n-o) index	I		t.21, no.15			
Inion-opisthion chord/arc index	I			no.37 ÷ no.38		
Lambda height above (n-o) index	I		t.21, no.13			
Lambda position above (n-o) index	I		t.21, no.17			
Lambda-inion chord/arc index	I			no.35 ÷ no.36		
Lambdoid chord/arc index	I			no.31÷ no.32	no.30(3)	
Length-breadth chord (l-o/ast-ast) index	I			no.39 ÷ no.41		
Lower parietal breadth	I		t.21, no.26		no.8c ÷ no.11	

EBSCOhost - printed on 10/28/2022 4:53 AM via . All use subject to https://www.ebsco.com/terms-of-use

Best Daka Measurement					*Right or Midline*			*Left*		
Midline	*Right*	*Left*	*Error*	*Source*	*Original*	*Microscribe*	*CT*	*Original*	*Microscribe*	*CT*
109.9				**calc.**						
77.5				**calc.**						
73.9				**calc.**						
69.3				**calc.**						
81.4				**calc.**						
69.3				**calc.**						
87.1				**calc.**						
80.9				**calc.**						
63.8				**calc.**						
103.4				**calc.**						
85.3				**calc.**						
42.6				**calc.**						
63.1				**calc.**						
96.0				**calc.**						
73.6				**calc.**						
35.3				**calc.**						
24.7				**calc.**						
97.9				**calc.**						
70.4				**calc.**						
99.4				**calc.**						
86.7				**calc.**						
	87.6	**80.0**		**calc.**						
84.1				**calc.**						
96.2				**calc.**						

EBSCOhost - printed on 10/28/2022 4:53 AM via . All use subject to https://www.ebsco.com/terms-of-use

APPENDIX 13.1 *(continued)*

Measurement			*References*			
	Measurement Type	*Notes*	*Weidenreich (1943)*	*Wood (1991)*	*Martin (1928)*	*Other Authors*
Lower scale curvature index	I		t.21, no.42		no.31(2) ÷ no.28(2)	
Lower/upper occipital scale arc index	I			no.38 ÷ no.36		
Mandibular fossa breadth chord/arc index	I			no.82 ÷ no.83		
Mandibular fossa depth-breadth index	I			no.84 ÷ no.82		
Mandibular fossa depth-length index	I			no.84 ÷ no.82		
Mandibular fossa length chord/arc index	I			no.80 ÷ no.81		
Mandibular fossa length-breadth index	I			no.80 ÷ no.82		
Nasion-basion length index	I		t.21, no.43		no.5 ÷ no.5(1)	
Occipital length II index	I		t.21, no.19			
Occipital sagittal chord/arc index	I		t.21, no.40	no.39 ÷ no.40	no.31 ÷ no.28	
Occipital curvature index						
Occipital scale chord index	I			no.37 ÷ no.36		
Occipital upper-scale index	I				no.31(1) ÷ no.12	
Occipito-parietal arc index	I			no.40 ÷ no.26		
Occipito-parietal chord index	I			no.40 ÷ no.26		
Occipito-sagittal arc index	I		t.21, no.33		no.28 ÷ no.25	
Opisthcranion height above (n-o) index	I		t.21, no.14			
Parieto-occipital arc index	I		t.21, no.30		no.28 ÷ no.27	
Parieto-sagittal arc index	I		t.21, no.32		no.27 ÷ no.25	
Postglabellar sulcus-bregma chord/arc index	I			no.19 ÷ no.20		
Sagittal chord/arc index, Parietal curvature Index	I		t.21, no.39	no.25 ÷ no.26	no.30 ÷ no.27	
Sagittal cranial curvature index	I		t.21, no.20		no.5(1) ÷ no.25	
Sagittal-coronal arc index	I			no.26 ÷ no.30		
Temporal chord/arc index	I			no.27 ÷ no.28		

EBSCOhost - printed on 10/28/2022 4:53 AM via . All use subject to https://www.ebsco.com/terms-of-use

Best Daka Measurement					*Right or Midline*			*Left*		
Midline	*Right*	*Left*	*Error*	*Source*	*Original*	*Microscribe*	*CT*	*Original*	*Microscribe*	*CT*
96.5				**calc.**						
64.0				**calc.**						
	87.2	**81.8**		**calc.**						
	16.1	**19.9**		**calc.**						
	20.7	**26.7**		**calc.**						
	63.8	**64.8**		**calc.**						
	77.8	**74.4**		**calc.**						
72.3				**calc.**						
26.1				**calc.**						
79.2				**calc.**						
62.7				**calc.**						
47.6				**calc.**						
121.2				**calc.**						
101.1				**calc.**						
44.1				**calc.**						
39.3				**calc.**						
121.2				**calc.**						
36.4				**calc.**						
93.8				**calc.**						
94.9				**calc.**						
53.4				**calc.**						
86.8				**calc.**						
	89.1	**94.8**		**calc.**						

EBSCOhost - printed on 10/28/2022 4:53 AM via . All use subject to https://www.ebsco.com/terms-of-use

APPENDIX 13.1 *(continued)*

Measurement			*References*			
	Measurement Type	*Notes*	*Weidenreich (1943)*	*Wood (1991)*	*Martin (1928)*	*Other Authors*
Transverse cranial curvature index	I		t.21, no.21		no.11 ÷ no.24	
Transverse frontoparietal index	I		t.21, no.23		no.9 ÷ no.10	
Transverse parieto-occipital index	I	5	t.21, no.24		no.12 ÷ no.8*	
Transverse postorbital-biauricular index	I		t.21, no.25		no.9(1) ÷ no.11	
Tranverse frontoparietal index	I			no.8 ÷ no.9		
Upper scale curvature index	I		t.21, no.41		no.31(1) ÷ no.28(1)	
Vertical index	I			no.4 ÷ no.10		
Basion-bregma, Basi-bregmatic length	L		t.19, no.34	no.4	no.17	
Basion-nasion length	L		t.19, no.8	no.5	no.5	
Bregma position projected to g-op	L		t.19, no.11			
Bregma position projected to n-o	L		t.19, no.13			
Bregma-inion length	L					G, V
Foramen magnum length (ba-o)	L			no.76	no.7	
Glabella-inion length	L				no.2	
Glabella-lambda (g-l) length	L		t.19, no.5		no.3	
Glabella-nasion length	L					P
Glabella-opisthocranion length	L		t.19, no.1	no.1	no.1 & 2	
Glabella-porion length	L			no.118		
Inion position projected to n-o	L		t.19, no.15			
Lambda position projected to g-op	L		t.19, no.12			
Lambda position projected to n-o	L		t.19, no.14			
Maximum squamous length	L				no.4b	
Nasion-lambda (n-l) length	L		t.19, no.6		no.3a	
Nasion-opisthion (n-o) length	L		t.19, no.9		no.5(1)	
Nasion-opisthocranion [inion] (n-op [i]) length	L		t.19, no.4		no.1d & 2a	
Nasion-opisthocranion length	L				no.2a	
Nasion-porion length	L			no.119		
Ophryo-occipital (on-op [i])	L		t.19, no.3		no.1b & 2c	
Opisthocranion position projected to n-o	L		t.19, no.16			
Glabella projection	P					H
Supraorbital projection	P					H
Nasion radius	R					H
Vertex radius	R					H
Bregma-lambda (parietal) subtense	S					H
Lambda-opisthion (occipital) subtense	S					H

EBSCOhost - printed on 10/28/2022 4:53 AM via . All use subject to https://www.ebsco.com/terms-of-use

Best Daka Measurement					*Right or Midline*			*Left*		
Midline	*Right*	*Left*	*Error*	*Source*	*Original*	*Microscribe*	*CT*	*Original*	*Microscribe*	*CT*
50.4				**calc.**						
69.3				**calc.**						
90.3				**calc.**						
73.1				**calc.**						
71.8				**calc.**						
98.3				**calc.**						
115.3				**calc.**						
121.0			**±1**	**o**	121.0	121.1	121.2			
95.5			**±1**	**o**	95.5	96.0				
58.0			**±1**	**ct**			58.0			
28.0			**±1**	**ct**			28.0			
133.0			**±2**	**o**	133.0	136.8	135.4			
36.0			**±1**	**o**	36.0	38.2	36.5			
171.0			**±1**	**o**	171.0	170.2	169.7			
166.0			**±1**	**o**	166.0	164.7	164.6			
12.0			**±2**	**o**	12.0	14.4	13.0			
180.0			**±1**	**o**	180.0	180.4	179.9			
	116.8	**114.0**	**±1**	**o**	116.8			114.0		
156.0			**±1**	**ct**			156.0			
152.0			**±1**	**ct**			152.0			
130.0			**±1**	**ct**			130.0			
	55.0		**±1**	**o**	55.0					
165.0			**±2**	**o**	165.0	162.4	163.5			
132.0			**±1**	**o**	132.0	130.6	130.8			
175.0			**±1**	**o**	175.0	174.1	173.9			
175.0			**±1**	**o**	175.0					
	110.0	**108.4**	**±1**	**o**	110.0			108.4		
170.0			**±1**	**o**	170.0					
165.0			**±1**	**ct**			165.0			
9.0			**±1**	**o**			8.9			
16.0			**±1**	**o**	16.0					
90.5			**±2**	**o**	90.5		89.0			
95.5			**±2**	**o**	95.5		104.0			
16.0			**±1**	**o**	16.0		15.1			
34.0			**±1**	**o**	34.0		33.0			

EBSCOhost - printed on 10/28/2022 4:53 AM via . All use subject to https://www.ebsco.com/terms-of-use

APPENDIX 13.1 *(continued)*

Measurement			*References*			
	Measurement Type	*Notes*	*Weidenreich (1943)*	*Wood (1991)*	*Martin (1928)*	*Other Authors*
Nasion-frontal subtense	S					H
Nasion-bregma subtense	S		t.21, no.35			
Anteroposterior arc thickness of glabella	T			no.65		
Anteroposterior arc thickness of supraorbital torus	T			no.64		
Anteroposterior chord thickness of supraorbital torus	T			no.63		
Asterion thickness (occipital)	T			no.114		
Asterion thickness (parietal)	T			no.109		
Asterion thickness (temporal)	T			no.117		
Bregma thickness (frontal)	T		t.21, no.10	no.104		
Bregma thickness (parietal)	T		t.35	no.106		
Bregma/lambda thickness	T			no.112		
External occipital protuberance thickness	T			no.115		
Glabella-bregma thickness (frontal)	T			no.105		
Lambda thickness (occipital)	T			no.113		
Lambda thickness (parietal)	T			no.107		
Opisthocranion thickness	T					
Parietal eminence thickness	T		t.35	no.111		
Stephanion thickness	T			no.110		
Supraorbital torus lateral thickness	T					B
Supraorbital torus medial thickness	T		t.35			
Vertical thickness of supraorbital torus	T			no.62		

NOTE: Angles are reported in degrees, and capacities are reported in cubic centimeters. Without inferior orbits, the Frankfurt Horizontal plane was impossible to determine. Rather than producing inexact estimates, no metrics requiring the establishment of this plane were taken on the Daka calvaria. Bregma is estimated, and it is often associated with large error values.

Authors in "Other Authors" column are coded as follows: B: Baba et al. (2003); G: Gabunia et al. (2000); H: Howells (1973, 1980); P: Potts et al. (2004); V: Vekua et al. (2002); W/L= Walker and Leakey (1993).

Notes are as follows:

1. See Chapter 14 for a complete discussion of Daka cranial capacity.

2. Maximum horizontal circumference was measured with tape touching the cranium through the temporal fossa.

3. Mandibular fossa angle is taken from the posterior (larger) angle formed with sagittal. Wood (1991) is not always consistent here.

4. Petromedian and tympanomedian angles are the posterior (lesser) angles formed between the petrous axis and the tympanic axis, respectively, and the sagittal axis in a transverse plane. This differs from definitions presented in Wood (1991), but not the metrics published there.

5. Martin's number 8 is maximum cranial breadth (eu-eu). Weidenreich (1943) and others took the maximum breadth at various levels on the cranium, and Weidenreich (1943) opted to take an "average maximum breadth" of three dimensions. These are maximum temporoparietal, maximum intercrestal, and maximum torus angularis breadth. We follow Weidenreich in using average maximum breadth, and denote the difference by using 8* in the Martin number column.

Abbreviations; o = original; ct = tomography; calc. = calculation.

EBSCOhost - printed on 10/28/2022 4:53 AM via . All use subject to https://www.ebsco.com/terms-of-use

Best Daka Measurement					*Right or Midline*			*Left*		
Midline	*Right*	*Left*	*Error*	*Source*	*Original*	*Microscribe*	*CT*	*Original*	*Microscribe*	*CT*
10.0			**±1**	o	10.0					
16.0			**±0.5**	ct			16.0			
18.0			**±1**	o	18.0					
	25.0	**27.0**	**±1**	o	25.0			27.0		
	18.0	**18.0**	**±1**	o	18.0			18.0		
	10.6	**12.6**	**±1**	ct			10.6			12.6
	10.5	**10.9**	**±1**	o	10.5		10.2			10.9
	10.2	**11.0**	**±1**	ct			10.2			11.0
7.0			**±1**	o	7.0		6.8			
505.0			**±1**	ct			505.0			
6.6			**±1**	ct			6.6			
14.2			**±1**	ct			14.2			
6.8			**±1**	ct			6.8			
9.3			**±1**	ct			9.3			
8.5			**±1**	o	8.5		8.2			
12.0			**±1**	o	12.0		14.0			
		9.0	**±2**	o	7.8		8.8			9.0
	7.5	**7.3**	**±1**	ct			7.5			7.3
	12.0	**13.3**	**±1**	o	12.0			13.3		
	19.0	**18.0**	**±1**	o	19.0			18.0		
	19.0	**18.0**	**±1**	o	19.0			18.0		

EBSCOhost - printed on 10/28/2022 4:53 AM via . All use subject to https://www.ebsco.com/terms-of-use

This Page Left Intentionally Blank

EBSCOhost - printed on 10/28/2022 4:53 AM via . All use subject to https://www.ebsco.com/terms-of-use

14

Tomographic Analysis of the Daka Calvaria

W. HENRY GILBERT, RALPH L. HOLLOWAY, DAISUKE KUBO, REIKO T. KONO, AND GEN SUWA

This chapter presents observations made on distortion, subcortical structures, and endocranial features through the use of computed tomographic (CT) imagery of the Daka calvaria. It is organized into two sections: descriptions of the individual cranial vault bones (primarily by WHG) and a description of the endocast (primarily by RH). In addition, several cranial metrics and vault thicknesses were obtained from micro-CT data (presented in Tables 14.1 and 14.2 and in the text). These measurements were derived from coronal, sagittal, and transverse slices using the open-source navigation and display platform OsiriX version 2.1 (Rosset et al. 2004) on images with a resolution of 0.3528 mm per pixel, and cross-checked where necessary using the CT software Analyze 6.0 (Biomedical Imaging Resource, Mayo Clinic). The main Daka metrics table in Chapter 13 presents measurements of structures also measured with CT imagery. For consistency, measurements made on the original specimen are given priority. Where measurements reported in this chapter are derived from the original specimen or the stereolithographic model they are specifically identified. Other measurements reported in this chapter are derived from CT imagery.

High-resolution CT imagery was obtained by using the microfocal X-ray CT system TX225-ACTIS (Tesco Corporation), at the University Museum, The University of Tokyo. Original scans were taken at 170 kV and 0.2 mA with a 3-mm-thick copper plate prefilter to lessen beam-hardening effects. Slice thickness was set at 340 microns. A field of view of 174.08 mm was reconstructed for each slice in a 512 × 512 matrix, resulting in a pixel size of 340 microns. Pixel size was calibrated by scanning and measuring a cylindrical phantom of known diameter, and thereafter adjusting the source-to-object parameter, obtaining dimensional accuracy of ca. 0.1 percent to 0.2 percent. Serial slices (approximately coronal) were taken at 340-micron intervals, resulting in a total of approximately 550 slices. The original three-dimensional dataset thus consisted of isotropic voxels of 340-micron size. The entire volume dataset was then rotated and reformatted so that the horizontal plane exactly corresponded with the glabella-inion plane. The sagittal plane was adjusted with visually determined best fit. Serial slices were then produced in horizontal, sagittal, and coronal planes. Because of our high-resolution and isotropic dataset, reformatting the volume resulted in no noticeable degradation of gray scale data. Finally, for ease of metric

EBSCOhost - printed on 10/28/2022 4:53 AM via . All use subject to https://www.ebsco.com/terms-of-use

TABLE 14.1 CT Derived Metrics for the Daka Calvaria

Measurement	*Value*	*Unit*
Asterion thickness (occipital)	10.6	mm
Asterion thickness (temporal)	10.2	mm
Auricular-bregmatic height (po-b)	101.0	mm
Auriculo-lambda height	98.0	mm
Bregma height above g-op	73.0	mm
Bregma height above n-o	92.0	mm
Bregma position projected to g-op	58.0	mm
Bregma position projected to n-o	28.0	mm
Bregma thickness (parietal)	5.5	mm
Bregma/lambda thickness	6.6	mm
Calvarial height above g-l	51.0	mm
Calvarial height above g-op	73.0	mm
Calvarial height above n-op	80.0	mm
Cranial base angle (ba-n-o)	7.4	degrees
Endocranial capacity	986.0	ml
External occipital protuberance thickness	14.2	mm
Frontal angle	141.0	degrees
Frontal curvature (m-n-b)	17.0	degrees
Frontal inclination angle I (b-n-op)	55.0	degrees
Frontal inclination angle II (b-n-o)	70.0	degrees
Frontal profile angle (m-g-op)	65.0	degrees
Glabella-bregma thickness (frontal)	6.8	mm
Inclination of occipital foramen (n-ba-o)	154.0	degrees
Inclination of pars cerebralis (sg-b<n-op)	46.0	degrees
Inclination of pars glabellaris (sg-n-op)	80.0	degrees
Inclination of whole occipital (l-o-n)	92.0	degrees
Inclinaton of frontal squama (b-g-op)	52.0	degrees
Inion above n-o	33.0	mm
Inion position projected to n-o	156.0	mm
Inner skull breadth	112.3	mm
Lambda height above n-o	93.0	mm
Lambda position projected to g-op	152.0	mm
Lambda position projected to n-o	130.0	mm
Lambda thickness (occipital)	9.3	mm
Mandibular fossa angle	80.0	degrees
Mandibular fossa depth	4.9	mm
Maximum supramastoid, Maximum intercrestal breadth	139.5	mm
Median sagittal arc I (n-op)	282.0	mm
Median sagittal arc II (n-o)	336.0	mm
Nasion-bregma subtense	16.0	mm
Occipital curvature (Occipital angle) (l-op-o)	107.0	degrees
Occipital inclination I (l-op-n)	72.0	degrees
Occipital inclination II (l-op-g)	68.0	degrees
Opisthion-opisthocranion-nasion (o-op-n)	37.0	degrees
Opisthocranion position projected to n-o	165.0	mm
Parietal angle	147.0	degrees
Petromedian angle	41.0	degrees
Stephanion thickness	7.5	mm
Temporoparietal breadth	125.0	mm
Tympanomedian angle	80.0	degrees

NOTE: Right and left sides are averaged where applicable. See Table 13.1 for metric references. Additional vault thickness metrics and foramina diameters are reported in the text.

EBSCOhost - printed on 10/28/2022 4:53 AM via . All use subject to https://www.ebsco.com/terms-of-use

evaluations, gray scale sections were transformed to a 0.3528-pixel size so that images were depicted at natural size in 72 dpi representations.

Visualization of the external and internal cranial surfaces was done by using Analyze 6.0. For the external surface renderings, we first defined the osseous surface by using a global threshold value. The threshold was determined by averaging the CT values of bone and air, these sampled at representative locations of the external cranium. Because of the steep CT value profile of the air-bone interface, such a threshold widely approximates local half-maximum values. Next, areas such as the supraglabellar region that were affected by artifact noise were corrected by additional manual segmentation in order to obtain more accurate surface location in those regions.

The endocranial surface was visualized by first determining a global endocranial threshold, analogous to the external surface method. However, subsequent manual segmentation was done more extensively to contend with gaps between the bones and occasional patches of matrix. Two versions of endocranial segmentation were made. In the first version, we manually corrected for adhering matrix and connected wide bony gaps linearly, but retained the bone surfaces at the location of cracks. Thus, artificial projections were retained at the locations of cracks and gaps. Anatomical foramina were digitally "plugged" midway between endocranial and ectocranial levels. This version forms the basis of the endocranial description of the following sections. The volume (the sum of voxels) of this segmented region, including the projections, was 992 mL. A stereolithographic model was made by first transforming the CT volume data to surface polygon data using the marching cube algorithm available in Analyze 6.0, and then producing a stereolithographic model using a three-dimensional printer Z310 (Z corporation) at a layering resolution of 76 microns.

The second version of endocranial segmentation was made by manually modifying the first version. We electronically "shaved off" the projections at the seams and cracks between the individual pieces and adjusted the surface of the larger gaps and foramina openings to correspond to the projected local endocranial surface levels. The volume of this segmented region was thus smaller at 986 mL. This value of 986 mL thus forms the best estimate of the cranial capacity for the Daka calvaria as currently preserved.

Individual Cranial Vault Bones

Frontal

Tomographic images reveal little distortion in the frontal. Cracking through the right supraorbital torus is revealed by CT imagery to minimally affect its surface morphology. A perimortem puncture measuring 4.3 mm × 7.2 mm (measured on the original specimen) superior to left frontotemporale scars the outer cortex without penetrating it, whereas a puncture measuring 5.4 mm × 8.4 mm (measured on original specimen) just inferior to left frontotemporale extends through the outer cortex. These punctures, as discussed in Chapter 13, are consistent with animal gnawing and are adjacent to a set of shallow, parallel grooves on the frontal and left parietal that are not apparent on CT imagery.

The Daka frontal is approximately 7.0 mm (measured on original specimen) thick at bregma. This is not especially thick relative to other *Homo erectus* specimens such as

EBSCOhost - printed on 10/28/2022 4:53 AM via . All use subject to https://www.ebsco.com/terms-of-use

TABLE 14.2 Measurements of the Bony Labyrinth

	Standard Planes			*High Resolution*			*Homo erectus*			
	DAKA R	DAKA L	AVE.	DAKA R	DAKA L	AVE.	AVE.	OH9	SAN 2	SAN 4
n	1	1	1	1	1	1	3	1	1	1
ASCw	6.5	6.3	6.40	6.2	6.0	6.10	7.17	7.6	6.6	7.3
ASCh	5.7	5.9	5.80	6.5	6.3	6.40	5.50	5.3	5.8	5.4
LSCw	5.7	5.1	5.40	5.5	5.3	5.40	4.73	5.2	4.2	4.8
LSCh	5.7	5.0	5.35	4.9	5.1	5.00	3.70	4.4	3.7	3.0
PSCw	5.1	5.4	5.25	5.0	5.3	5.15	5.90	6.0	5.5	6.2
PSCh	5.2	5.6	5.40	5.8	6.0	5.90	6.43	6.5	5.8	7.0
COw	x	4.3	4.30	4.2	4.4	4.30	4.10	4.1	3.8	4.4
COh	x	5.3	5.30	5.3	5.4	5.35	5.77	5.7	5.6	6.0
SLI	x	x	x	45	48	46.5				
COt	x	105.0	105.00							
PSCm	131.5	132.5	132.00							
ASCm	31.3	30.0	30.65							

NOTE: Standard plane measurements were taken from sagittal and transverse sections. High-resolution dimensions of the semicircular canals were taken from CT data reformatted to capture planes aligned with each of the semicircular canals. See text for discussion. Non-Daka measurements are taken from Spoor (1993). Note that the *Homo erectus* average does not include Daka. Abbreviations are taken from the following: Spoor (1993); Spoor and Zonneveld (1994, 1995, 1998); Spoor et al. (2003). Angular measurements ASCm, PSCm, and COt refer to the angle made with the midline opening anterolaterally. Note that PSCh of the reformatted section does not follow its definition of Spoor and Zonneveld (1995), but was measured from the wall of the vestibule as with ASCh and LSCh. SLI of the high resolution sections uses the best fit plane of the LSC and superior-most and inferior-most lumen centers of the PSC. Cochlear dimensions of the high resolution dataset were measured in the sagittal and transverse sections.

Sangiran 17, Sangiran 12, Sangiran 3, KNM-ER 3883, Dmanisi D2282, and Dmanisi D2280, all of which have thicknesses of 7 mm or greater in this area. The Daka frontal is 6.7 mm thick along the midline halfway between bregma and glabella.

Frontal sinuses have long been appreciated for their utility in identifying individuals in forensic contexts (Asherson 1965; Yoshino et al. 1987; Christensen 2004). The septum dividing the left and right halves of the Daka frontal sinuses is relatively thin (approximately 0.5–1.0 mm) and is located to the left of the midline, especially superiorly (Plates 14.1 and 14.2). The Daka sinuses do not extend into the frontal squama toward bregma as they do in Petralona and Kabwe (Seidler et al. 1997) or Bodo, nor are they nearly as laterally extensive, expanding only to the approximate apices of the supraorbital torus arcs (the highest points on the supraorbital tori) on either side, ca. 30 mm lateral to the midline. They do not extend as far posteriorly as they do in the Maba specimen (Wu and Poirier 1995). The Ceprano specimen possesses frontal sinuses that are restricted laterally and toward bregma as in the Daka calvaria, but in Ceprano these do not meet at the midline as in the Daka calvaria (Bruner and Manzi 2005). In these ways the Daka frontal sinuses are similar to those reported for Sambungmacan 4 (Baba et al. 2003). There is some pneumatization in both right and left zygomatic processes and adjacent regions. It appears to be stronger on the right side than the left (Plates 14.1, 14.2, and 14.3). This pneumatization is not as extensive as in Sambungmacan 3 (Márquez et al. 2001).

EBSCOhost - printed on 10/28/2022 4:53 AM via . All use subject to https://www.ebsco.com/terms-of-use

Spoor (1993)						
Homo sapiens	*Pan troglodytes*	*Pan paniscus*	*Gorilla gorilla*	*Pongo pygmaeus*	*Hylobates* and *Symphalangus*	*Macaca fascicularis*
53	7	6	6	7	2	3
6.9	6.1	5.7	6.8	6.3	6.5	5.1
6.0	4.9	4.6	4.8	4.5	5.6	4.4
4.8	5.1	5.1	6.1	5.1	5.3	4.4
4.2	4.7	4.4	6.1	4.5	5.1	4.0
6.1	5.5	5.2	5.8	5.0	5.5	4.6
6.5	5.6	4.9	6.4	5.2	5.8	4.4
3.8	3.3	3.4	3.4	3.5	2.8	2.3
5.2	4.9	4.8	4.9	4.9	4.3	3.5

Parietals

Micro-CT imaging corroborates discussions of parietal distortion presented in Chapter 13. The compressed fragment of right parietal below the parietal boss protrudes endocranially approximately 2.0 mm. The fragment below the left parietal boss projects endocranially approximately 3.0 mm. In a coronal section through the parietal bosses, the calvaria is skewed to the right such that the subtense of an arc defined by the squamosal and sagittal boundaries of the parietals is 20.0 mm on the right and 26.0 mm on the left.

The parietals present significant endocranial thickening along the sagittal sulcus for the entire course of the sagittal suture. The thickness of parietals midway between bregma and lambda is 8.3 mm. Lateral to the endocranial keeling associated with the sulcus the thickness is less, about 5.5 mm in the areas between the sagittal suture and the transition to parietal wall verticality. The vertical walls measure approximately 8.3 mm thick in the superior part near the bosses and approximately 6.3 mm halfway between the bosses and the squamosal suture. Vault thickness is significantly greater near the squamosal suture. In some areas adjacent to the squamosal suture, for example, in the coronal plane through basion, the parietals are as thick as 10.0 mm. No signatures of the parietal foramina are present in the CT imagery or visible on the original.

Temporals

The zygomatic processes are broken, and the remaining zygomatic roots are cracked on both sides. These cracks, visible in CT imagery, produce only minimal distortion. The remaining temporal is relatively undistorted.

Mastoid air-cell function has received attention during the past decade. Witmer (1997) suggests eight possible functions: increased sensitivity to low-frequency sounds, enhanced

EBSCOhost - printed on 10/28/2022 4:53 AM via . All use subject to https://www.ebsco.com/terms-of-use

localization of sound, acoustic isolation of internally generated sounds, pressure equalization, shock absorption, thermal insulation, functional decoupling of inner and outer tables of bone, and strength per unit of bone mass maximization. Sherwood (1999) narrows this to four: hearing acuity, acoustic isolation, functional decoupling of the inner and outer cortices of the temporal, and maximization of strength per unit of bone mass. African apes have smaller mastoid processes that are much more extensively pneumatized than those of humans (Sherwood 1999). While the integration of temporal pneumatization into a functional unit is tenable for apes and other vertebrates, it appears that the pattern of pneumatization in *Homo* is more related to the development of surrounding structures (Balzeau and Grimaud-Hervé 2006). It is possible that selective pressures related to brain expansion and the biomechanics of bipedality have disrupted this unification in humans (see Penin et al. 2002 for a comparison of chimp and human basicrania).

As discussed in Chapter 13, the mastoid processes of the Daka calvaria are both damaged extensively. Neither side preserves the inferior portions, but pneumatization of the temporal bone superior to the mastoid tips extends superiorly nearly to asterion on both sides (see Plates 14.4 and 14.5). Pneumatization on the left is more readily visible and comprises numerous small air cells. On the more extensively damaged right side there is a relatively large vacuity in the posterior region of the mastoid area near asterion. The extensiveness of mastoid pneumatization is variable in humans, but rarely extends beyond the mastoid process and petrous region, while in apes, air cells are found throughout the temporal (Sherwood 1999). Air cells in the Daka calvaria extend beyond the mastoid process and petrous region toward asterion and extend into the inferior temporal squama above porion. They are least extensive adjacent to the occipitomastoid suture. The temporals, while highly pneumatized, are not as inflated as those of apes, and the individual cells are smaller.

A squamotympanic fissure is present in the Daka calvaria (see Plate 14.6) and the morphology of the posterior glenoid fossa in sagittal section is similar to the Sangiran 17 condition (Baba et al. 2003). The Daka temporal squamae are approximately 5.7 mm thick centrally, and the posterior temporal is approximately 10.6 mm thick adjacent to the occipitomastoid suture.

The semicircular canals (Plate 14.7) are visible in transverse and sagittal sections in the petrous portions of both temporals. The cochleae are also visible on both sides, but individual components of the right cochlea are difficult to discern, and only the left was measurable. Because the standard horizontal plane adopted in this study, the glabella-inion plane, approximates the nasion-porion plane considered to be close to the plane of the lateral semicircular canals, we were able to apply the metric methodology detailed in Spoor and Zonneveld (1995). Measurements of the Daka calvaria bony labyrinth are presented in Table 14.2. One set of metrics was derived from the cross-section images of the standard sagittal and transverse orientations and represents approximate measures that correspond to published comparative data (for example Spoor 1993). We checked further for accuracy of the above metric methodology by referring to a higher resolution micro-CT dataset. This consists of a close-up scan series of the ear region at 100-micron voxel resolution. The second set of metrics in Table 14.2 is based on this imagery, reformatted so that the plane of each of the newly derived sections corresponds to the best fit of the plane of the semicircular canals themselves. Cochleae were measured as in Spoor and Zonneveld (1995).

EBSCOhost - printed on 10/28/2022 4:53 AM via . All use subject to https://www.ebsco.com/terms-of-use

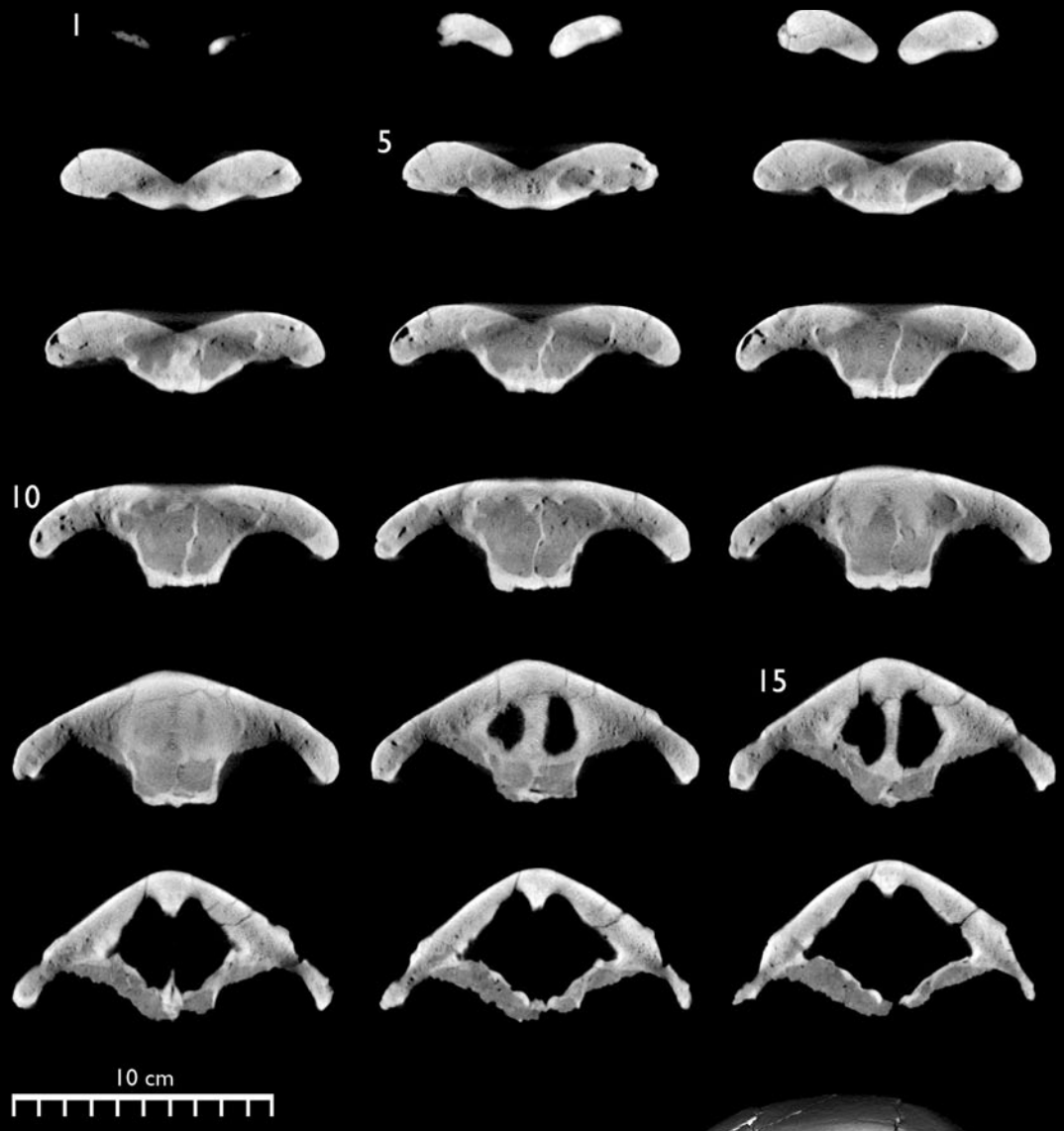

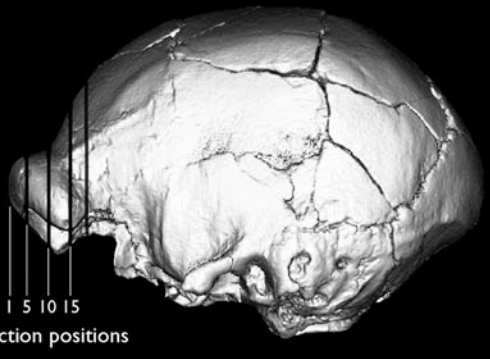

PLATE 14.1

Coronal sections through frontal sinuses of the Daka calvaria. Sections are 1.764 mm apart. Frame right is anatomical left for CT sections.

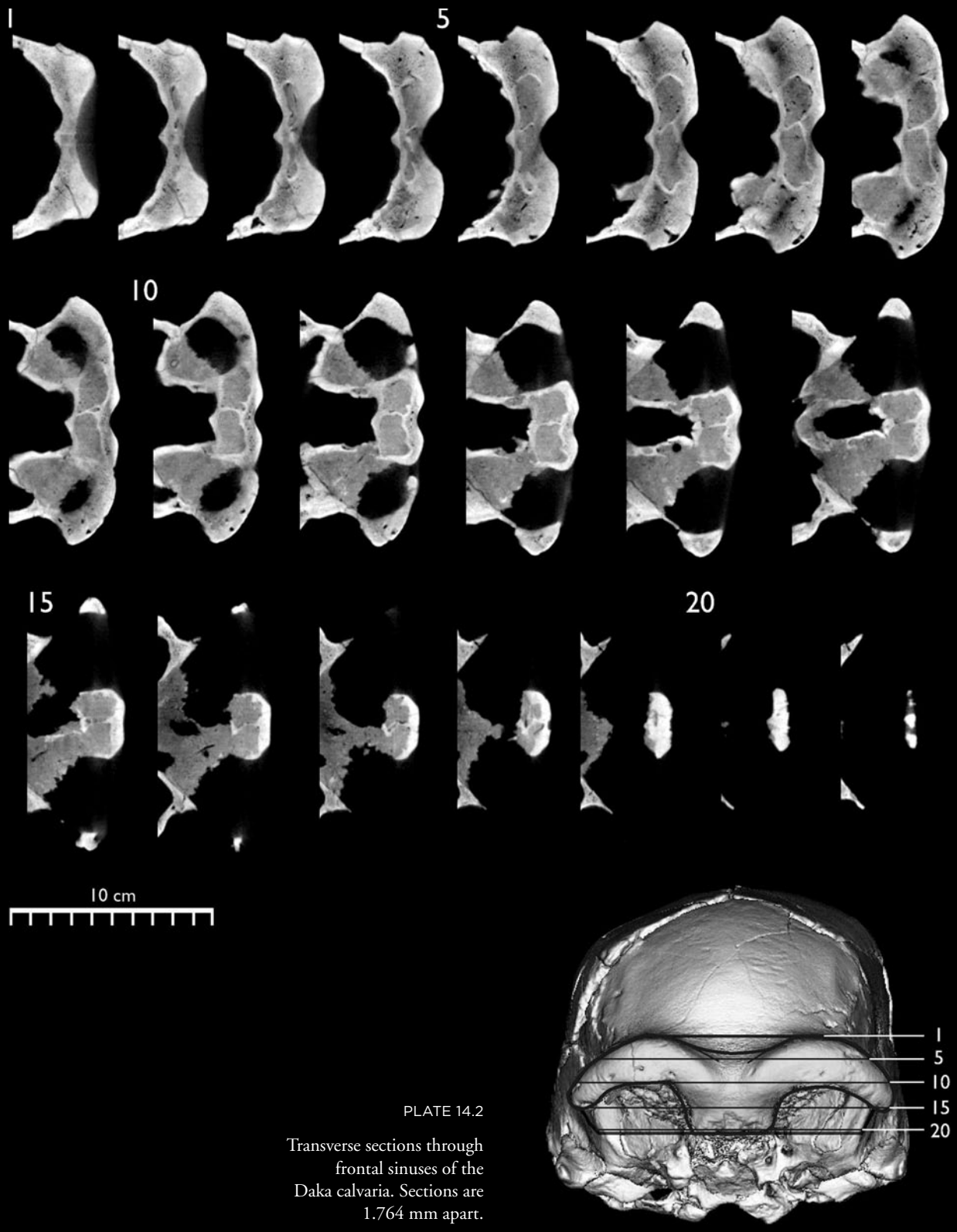

PLATE 14.2

Transverse sections through frontal sinuses of the Daka calvaria. Sections are 1.764 mm apart.

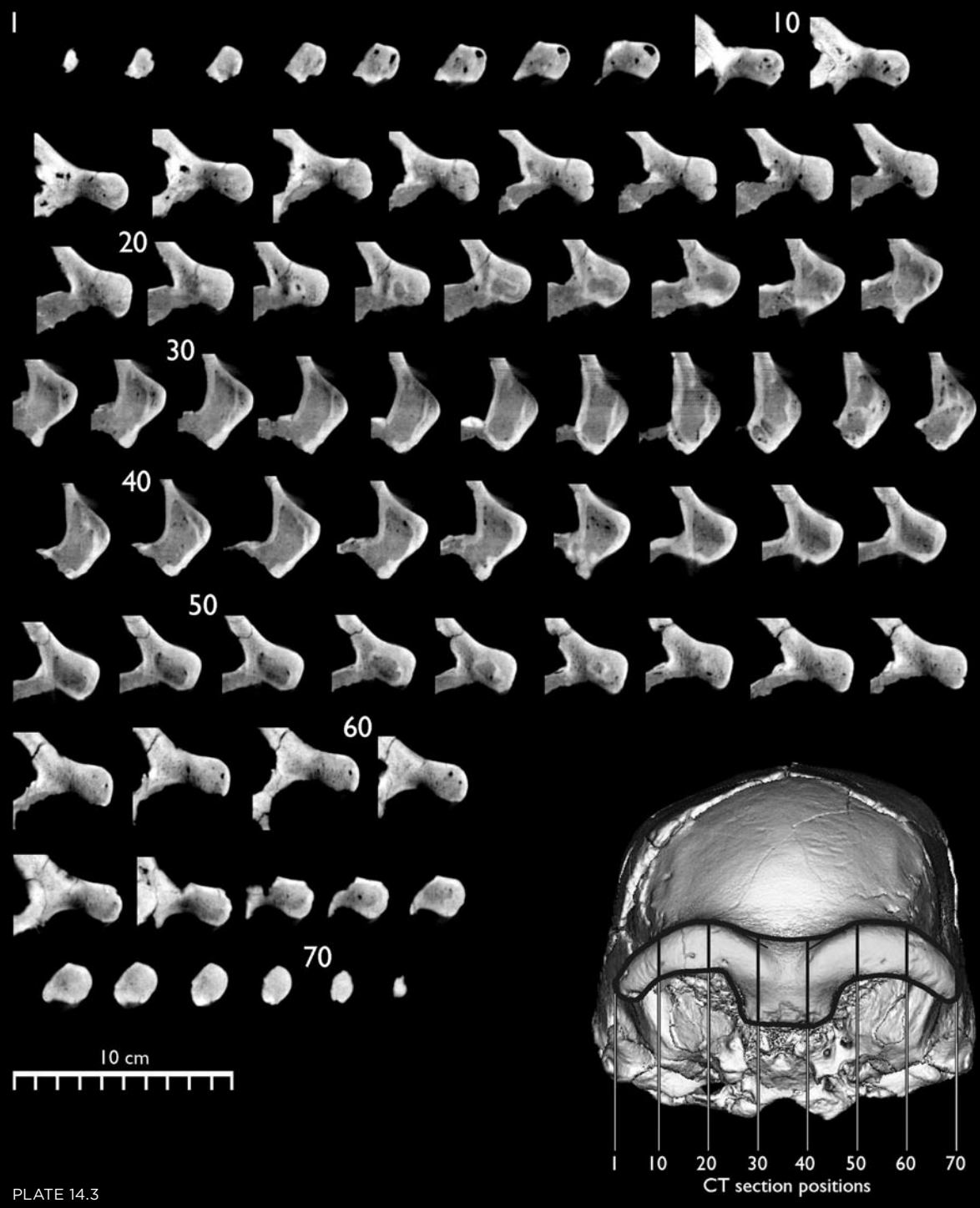

PLATE 14.3

Sagittal sections revealing frontal sinuses of the Daka calvaria. Sections are 1.764 mm apart.

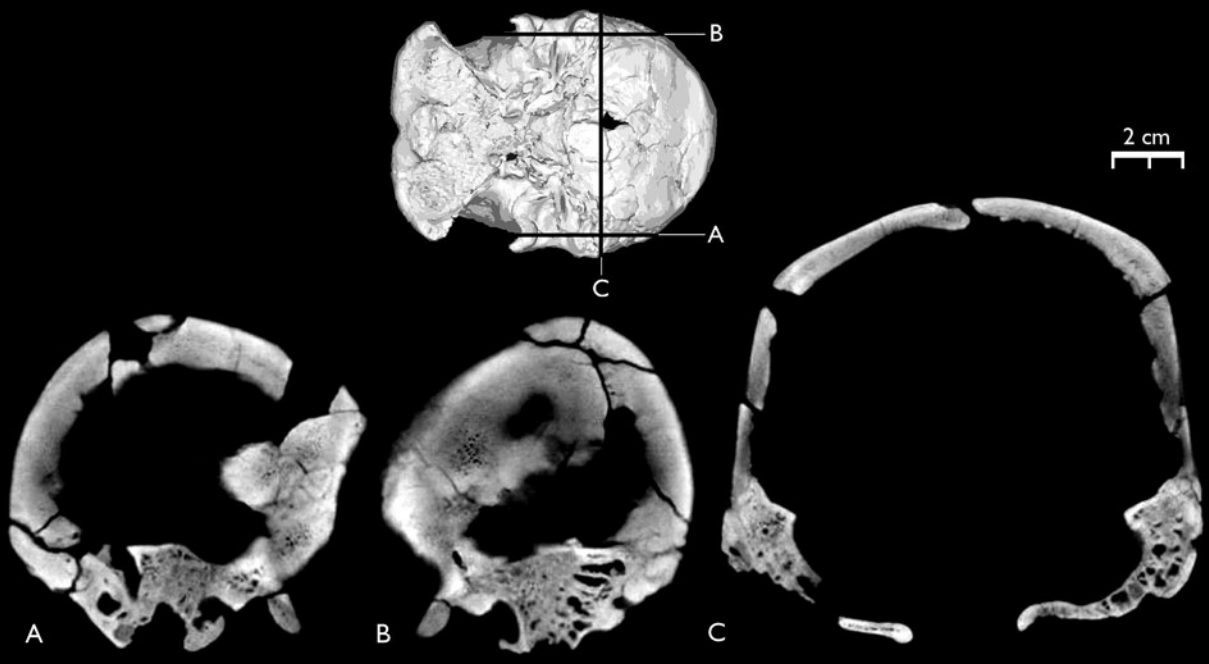

PLATE 14.4

Daka calvaria temporals and foramen magnum. A. Sagittal section through the right mastoid process. B. Sagittal section through the left mastoid process. C. Anatomically oriented (frame right is anatomical left) coronal section through the foramen magnum just posterior to the condylar bases.

PLATE 14.5

Daka calvaria temporals and foramen magnum. C. Taken in the transverse plane of the lateral semicircular canals. B. Approximately 8.8 mm below C. A. Approximately 14.1 mm below C.

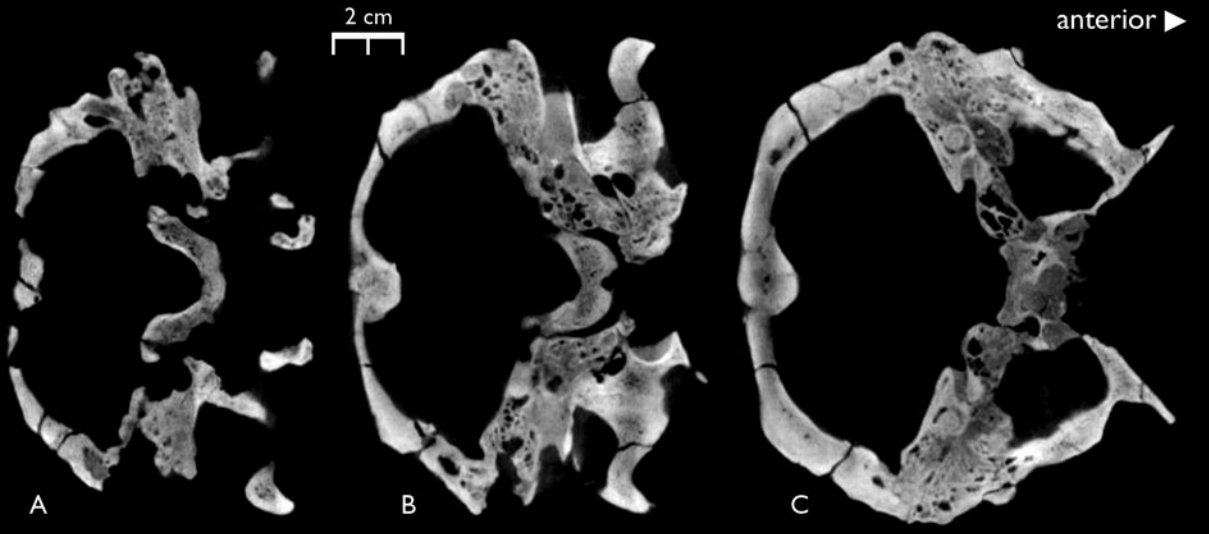

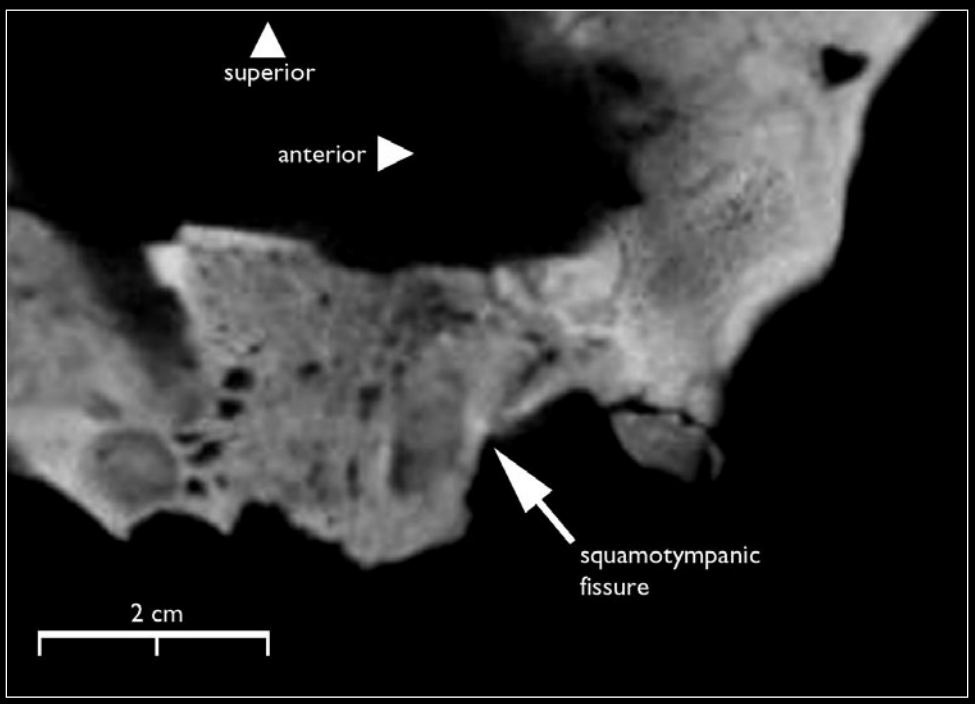

PLATE 14.6

Daka calvaria left squamotympanic fissure.

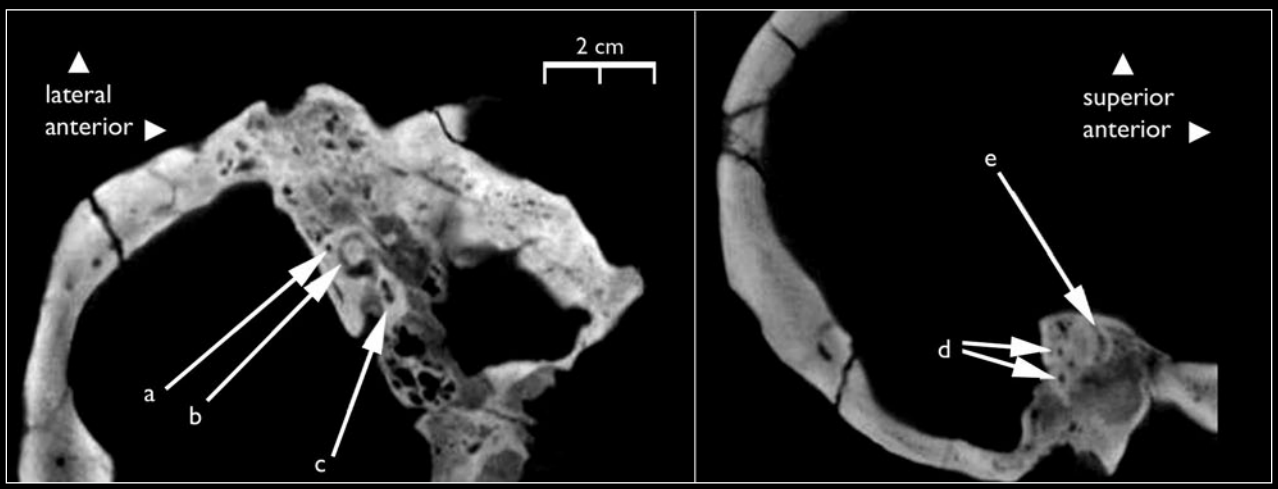

PLATE 14.7

Transverse section (left) and sagittal section (right) of Daka calvaria left bony labyrinth. A. Lateral tube of the posterior semicircular canal. B. Lateral semicircular canal. C. Cochlea. D. Superior and inferior tubes of the posterior semicircular canal. E. Anterior tube of anterior semicircular canal.

PLATE 14.8

Daka calvaria sagittal midline. Arrow A points to the pit in the inferior basilar region and the vacuity just superior to it. Arrow B shows rootcast penetration.

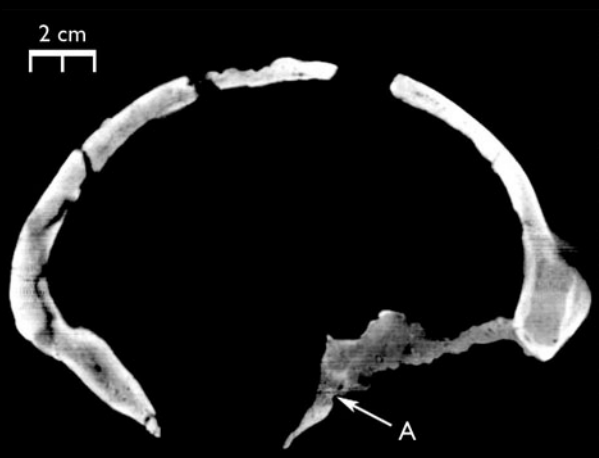

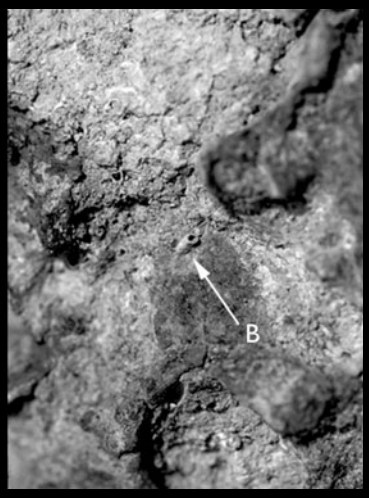

PLATE 14.9

Daka calvaria. A. Transverse section 35.7 mm superior to the base of the occipital condyles. B. Transverse section 46.3 mm superior to the base of the occipital condyles. C. Coronal section through the sphenoid taken 104.3 mm anterior to opisthocranion. D. Coronal section through the sphenoid taken 110.3 mm anterior to opisthocranion. E. Coronal section through the sphenoid taken 124.5 mm anterior to opisthocranion. Arrow f denotes the vacuity of the sphenoid referred to in the text. Views C, D, and E are oriented anatomically (frame right is anatomical left).

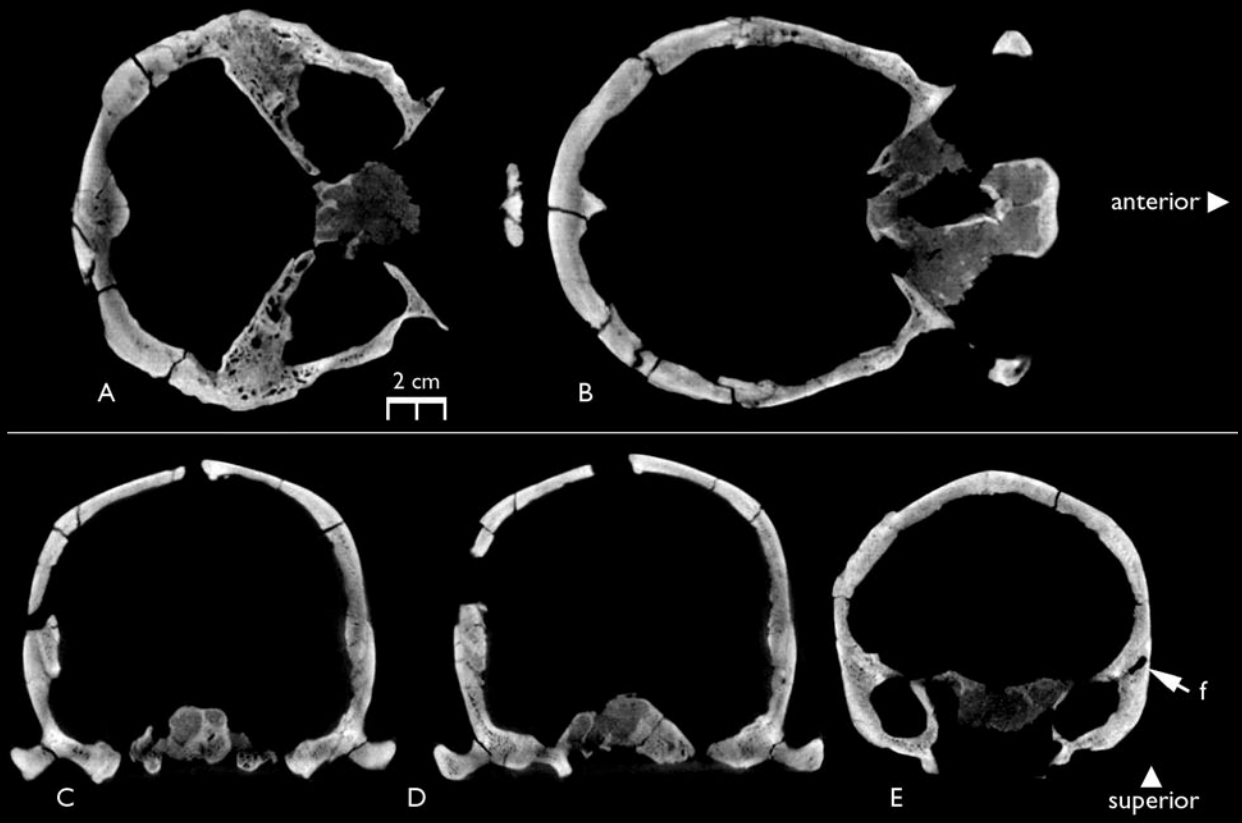

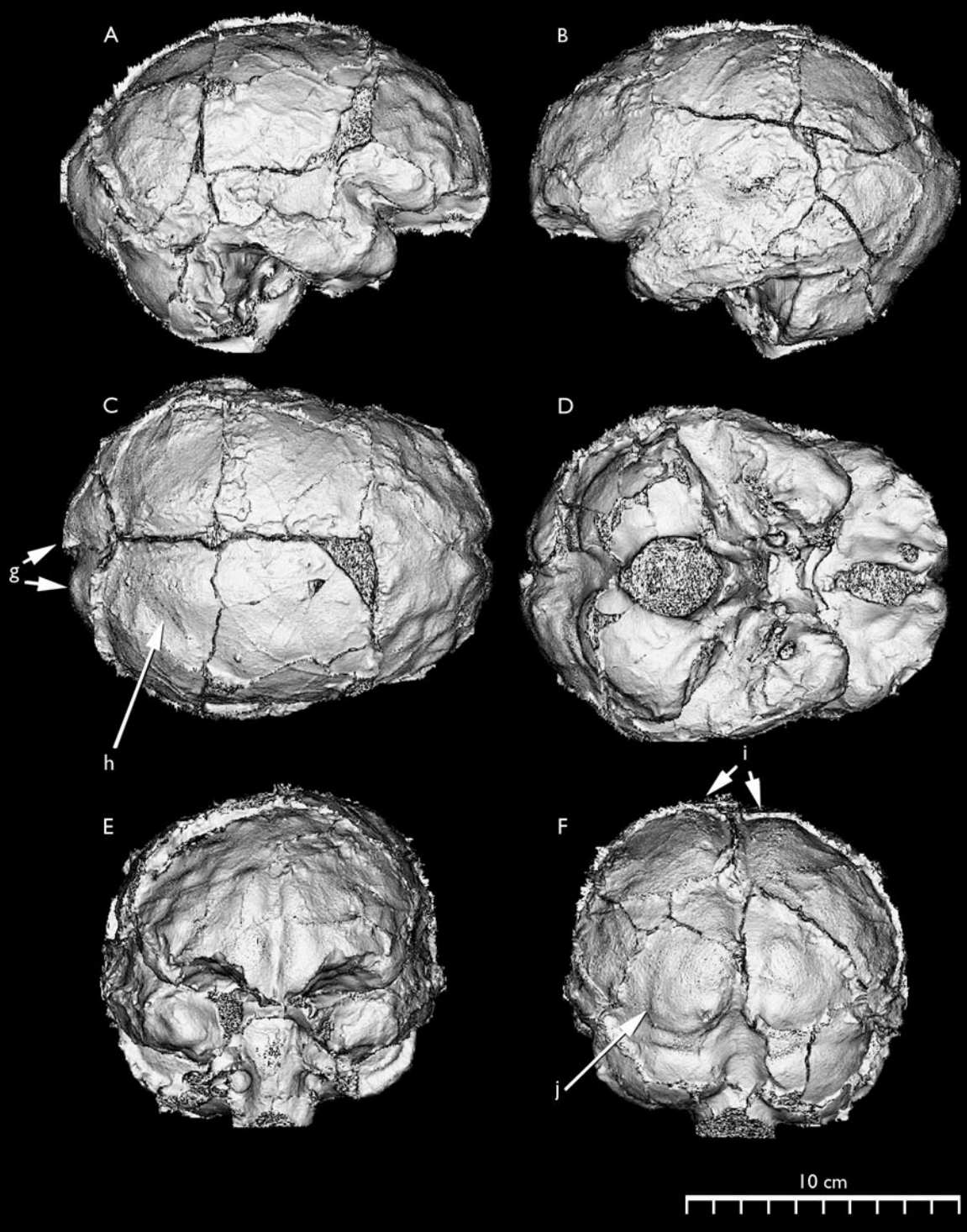

PLATE 14.10

Daka calvaria endocast: A. Right lateral view. B. Left lateral view. C. Superior view. D. Basal view. E. Frontal view. F. Occipital view. (g) Occipital petalia (visible on left). (h) Intraparietal sulcus. (i) Parasagittal keels. (j) Lunate sulcus.

The dimensions of the Daka semicircular canals are broadly comparable to other middle and late Pleistocene examples of *Homo,* and are at the upper end of the modern *H. sapiens* range of variation (Spoor 1993; Spoor and Zonneveld 1994, 1995, 1998; Spoor et al. 2003). Within Pleistocene *Homo,* Neanderthals have been characterized as having a distinct labyrinth, evinced most clearly in the relationship between the posterior and lateral canals. In this relationship (Spoor's index SLI), Daka clearly exhibits the generalized condition considered to be common in both modern *H. sapiens* and the few examples hitherto available for *H. erectus*.

Contrasting the condition reported by Spoor (2003) for three measured *Homo erectus,* Daka ASCh/ASCw is more similar to that of *H. sapiens* in having a relatively larger ratio. However, when we derived the same metrics using the higher resolution reformatted dataset, anterior canal height exceeded width in Daka, a condition not even reported in *H. sapiens*. We believe that this largely stems from inaccuracies in measuring anterior canal height, especially when this is based on low-resolution standard plane sections. Thus, any discussion of anterior canal shape must be received with caution. Spoor (1993) also suggested that *H. erectus* is characterized by large cochlear heights. Although cochlear dimensions of Daka were larger than the average of Spoor's (2003) *H. sapiens,* this difference is not significant.

The Daka cochlear helix is tightly spiraled and presents more twists than are found in apes. It is more similar to humans in this regard. The stylomastoid foramen is visible on both left and right sides, in both cases extending vertically as the facial canal from its inferior opening toward the central petrous. Daka bony labyrinth morphology examined above is consistent with the statement of Spoor and Zonneveld (1994) that the morphology found in *Homo erectus* is not significantly different from that of *H. sapiens*.

Occipital

Bone loss on the nuchal planum is detailed in Chapter 13. A network of cracks on the right side of the occipital combines to deflect the right margin of the foramen magnum approximately 3.0 mm inferiorly relative to the level of the left margin and to deflect the right cerebellar fossa approximately 7.0 mm inferior to the level of the left fossa (see Plate 14.4). This distortion appears on the CT imagery just posterior to the foramen magnum and continues anteriorly to immediately past the right condylar base. It is localized to the right nuchal plane of the occipital.

The thickness of the nuchal plane lateral to the lip of the foramen magnum is approximately 2.3 mm, and the thickness in the depths of the cerebral fossae is approximately 6.0 mm. The internal occipital crest is pronounced, protruding approximately 15 mm from the ectocranial surface at the transverse level of the nuchal crest. The right hypoglossal canal is damaged, but the left is intact. It has a diameter of approximately 5.5 mm. A pit occurs on the midline basilar portion of the occipital just posterior to hormion. CT imagery reveals that there is a 1.5 mm diameter vacuity in the basilar bone just superior to it. This area is the site of root penetration (see Plate 14.8 arrow A and discussion in Chapter 13).

EBSCOhost - printed on 10/28/2022 4:53 AM via . All use subject to https://www.ebsco.com/terms-of-use

Sphenoid

The posterior sphenoid body is present, as is most of the left lesser wing, some of the right lesser wing, the greater wings, the bases of the pterygoid processes, and the dorsum sellae. The anterior sphenoid, including the sphenoidal crest, is missing. The preserved portion of the sphenoid presents little damage. The sinuses of the sphenoid body are asymmetrical (Plate 14.9). The right sinus is larger superoinferiorly and anteroposteriorly. Sinuses are also present superior to the pterygoid plates on the left and the right. These lateral sphenoidal sinuses, which are exposed by breakage in the Daka calvaria, are not as extensive as those seen in the Bodo cranium. Both greater wings posses substantial diploe. A large vacuity is present in the left greater wing inferior to the sphenofrontal suture and anterior to sphenotemporal suture (see Plate 14.9 arrow F). This feature is not matched on the right side.

The undamaged pterygoid canal on the left is readily visible and is approximately 2.0 mm wide midway through the greater wing. Lateral to this is the left foramen rotundum, which is approximately 4.0 mm wide. The matrix-filled right foramen rotundum is approximately the same size. The optic canal is only preserved on the left and has a diameter of approximately 6.0 mm. The left and right greater wings present substantially different thicknesses. The left is approximately 5.2 mm thick at the most constricted point in the temporal fossa in the transverse plane of the pituitary fossa, and the right is approximately 3.0 mm thick.

Cranial Base Flexion

Sufficient portions of the basicranium are preserved, as described previously, to accurately estimate some measures of cranial base flexion. The endocranial metric landmarks sella (s) and foramen caecum (fc) can be located on closely spaced peri-midsagittal sections, although most of the planum sphenoideum is not preserved. We therefore measured the fc-s-basion angle (the CBA1 of previous studies), which value was determined to be 124 degrees. This is lower than 2 SD from the mean value for modern humans (136 to 138 degrees, summarized in Baba et al. 2003) and indicates a strong midsagittal cranial base flexion of the Daka cranium. The same measure was estimated at 141 degrees in Sambungmacan 4. The strong flexion seen in Daka strengthens the view that midsagittal cranial base flexion was strong in *Homo erectus* in general, while the difference in degree between Daka and Sambungmacan 4 may stem from any or all of the following factors: differences between *H. erectus* regional and/or temporal populations, individual variation, and bias in estimating the flexion values.

We previously suggested (Baba et al. 2003) that despite strong midsagittal cranial base flexion observed in *Homo erectus,* the structure of the more lateral endocranial base appeared to be distinct from that of modern humans. Specifically, we suggested that the anterior temporal pole was positioned relatively posteriorly (variable TP1 of Baba et al. 2003), and that the floor of the lateral anterior cranial fossa was oriented more anterosuperiorly (variable ORA1 of Baba et al. 2003) in Sambungmacan 4 relative to modern humans. We measured the same dimensions in Daka. The TP1 metric was 0.41 in Daka,

EBSCOhost - printed on 10/28/2022 4:53 AM via . All use subject to https://www.ebsco.com/terms-of-use

close to the modern human mean (0.40), and much higher than the Sambungmacan 4 value of 0.30. Together with visual assessments of temporal pole position relative to the sella turcica area in Daka, the previous metric evaluation does not suggest a posterior position of the anterior extent of the temporal pole. The difference between the two *H. erectus* crania in relative temporal pole position may be related to the difference in overall endocranial shape; Sambungmacan 4 is strongly platycephalic, in contrast to the more globular endocranial shape of Daka.

The ORA1 metric in Daka was estimated at 14.3 degrees, closer to the modern human mean (11.9) than to the Sambungmacan 4 value (20). This may also indicate that there are no significant differences in Daka from the modern human condition, although visual assessments, such as the virtually reconstructed endocranium, do suggest that the floor of the lateral anterior cranial fossa is actually inclined more anterosuperiorly than is the case in modern humans. More appropriate metric evaluations and/or a fuller assessment of basicranial structure and proportions are needed to unravel the significance of these observations.

Endocranium

The endocranial analysis provided here is based on the scanned dataset, scan images, and the physical stereolith model. In particular, the measurements provided were taken on the stereolith model, using spreading calipers and metric cloth tape. These measurements will vary somewhat from those taken from the scans, but the measurements are almost exactly the same, differing by 1 or 2 mm. Precise locations of landmarks such as the frontal and occipital poles can vary because they are seldom perfectly punctate. Measurement error of 1–2 mm is probable.

Distortion

The Daka endocast, as deduced from both the scan figures and the stereolith, shows minimal distortion. What does exist is mostly related to the occipital bone distortion described in Chapter 13 and again in the preceding section. Minor damage to the internal bony table has resulted in a dislocation of the right third inferior frontal portion, giving an attenuated Broca's cap, and scalloped inferior fronto-orbital margins. The right frontal lobe appears to be slightly depressed relative to the adjoining parietal lobe, due to a slight elevation of the anterior margin of the parietal bone. It is unlikely that these minor disruptions to the surface continuity would affect in any significant way the volume. Certainly, the minor distortions do not affect the overall asymmetry between left and right hemispheres.

Volume

As discussed in preceding sections, endocranial capacity of the Daka calvaria is estimated from CT scans at 986 mL. Cranial capacity was originally measured by Asfaw et al. (2002) using teff seeds and yielded a volume of 995 mL. The volume measured on the stereolith endocast, using water displacement technique, yielded a mean volume of 1,001 mL, based on six determinations ranging from 996 to 1,002 mL. This determination is expected to

EBSCOhost - printed on 10/28/2022 4:53 AM via . All use subject to https://www.ebsco.com/terms-of-use

be slightly high as a result of errors involved in the production of the endocast replica, but it is reported here as a third assessment of endocranial volume. This hominid thus had a volume squarely within the range of African and Asian *Homo erectus* specimens, which vary between 750 and 1220 mL, larger than the KNM-WT 15000 Nariokotome endocast (880 mL adolescent, 900 mL adult), but less than the 1,069 mL derived for OH 9. Crania KNM-ER 3373 and KNM-ER 3883 have volumes of 848 and 804 mL, respectively (see Holloway et al. 2004 for a newer compilation of hominid endocast volumes). In the view of RLH, the volume could be slightly larger or smaller depending on small adjustments made to the minor distortions discussed previously, and thus a volume of approximately 1,000 mL appears to be a reasonable and judicious estimate.

Morphological Description

The endocast does not appear to show the usual degree of platycephaly found in other *Homo erectus* endocasts, but instead appears to show a fairly high and arched dorsal profile. The degree of cerebral-over-cerebellar overhang is large, perhaps in part related to some anterior displacement of the cerebellar lobes and brain stem. The latter forms a rather acute angle with the rostral frontal portion, and in lateral view (with a horizontal plane passing through frontal and occipital poles), the anterior boundary of the brainstem appears to protrude forward compared to its usual position relative to the temporal lobe.

There is a marked asymmetry between left and right cerebral hemispheres as seen by the petalial pattern (Plate 14.10G), which on this endocast shows a strong left occipital petalia (both posteriorly projecting and in width) compared to the right side. If the right frontal Broca's cap were not slightly depressed from damage, the frontal width petalia would be wider on the right than the left sides, thus showing a configuration congruent with right-handedness (Holloway et al. 2004).

The frontal lobes show very marked superior frontal gyri, being roughly 18.0 mm in width at the level of the frontal poles. The minor depressions on the frontal lobe's surface indicate that the frontal lobe was well fissurated, even though it is impossible to delineate convolutional details. The left Broca's cap region shows strong lateral and inferior protrusion, perhaps more so than the damaged right side, but in any event similar to, if not identical with, that found in modern humans. As is most usual on hominid endocasts, the central sulcus separating frontal from parietal lobes is not visible. Its position can only be estimated and would be very close to the vertex of the dorsal surface with the endocast oriented with a horizontal plane passing through frontal and occipital poles. No convolutional details are present on either Broca's cap.

The parietal lobes show almost no sulcal details, except for the right side, suggesting a possible location for the intraparietal sulcus (Plate 14.10H), which separates the superior and inferior parietal lobules. This depression attenuates close to the remnant of the lambdoidal suture. If this identification is correct, it suggests that the angular gyrus was strongly developed, more on the right than left sides. More striking features of this endocast are the parasagittal keel (Plate 14.10I) on either side of the middle and posterior parts of the sagittal suture. The significance of this keeling is not known, but it might be related to Broca's area 5 of the superior parietal lobule. There is a strong depression just anterior

EBSCOhost - printed on 10/28/2022 4:53 AM via . All use subject to https://www.ebsco.com/terms-of-use

to the lambdoidal suture, which is not a cerebral sulcus but rather represents a thickening of the inferior posterior lip of the parietal bone.

The occipital lobes are large and protuberant, and are very similar in morphology to the Asian *Homo erectus* endocasts described in Holloway et al. (2004). The left occipital lobe shows a lateral and inferior concave crescent, strongly suggestive of the lunate sulcus (Plate 14.10J). If so, this placement is in a posterior location as in modern *Homo sapiens*. The left occipital lobe also shows more detailed fissuration than the right side, but the right side does indicate a dorsal portion of the lunate sulcus well posterior by 10.0 mm to the lambdoidal suture. The left occipital lobe shows a small part of the lateral calcarine fissure, extending from the occipital pole laterally for approximately 10–12 mm.

The temporal lobes show very little convolutional detail, and the superior temporal gyrus appears depressed from cranial damage, particularly on the right side. The temporal poles are strongly thrust forward, reminiscent of the OH 9 endocast, rather than the Asian form, best indicated by Sangiran 17. The basal aspects of the temporal lobes do show some convolutional details (middle and inferior temporal gyri) and a considerable amount of detail regarding foramina such as the foramina ovale and foramen rotundum (left side). The internal auditory foramina are present on both sides of the temporal/cerebellar cleft, and remnants of the arcuate depression and crest are also present.

The brainstem has a pronounced anterior curvature, and appears thrust anteriorly, possibly representing some distortion. The carotid canals are visible on the lateral and anterior limit of the brainstem. The cerebellar lobes appear somewhat reduced in size relative to the overlying cerebral hemispheres, suggesting some possible correlations with the observations of Weaver (2005). Both transverse and sigmoid sinuses are visible, being stronger on the left side, and the flow of blood from the superior sagittal sinus appears to have been predominantly to the left side.

Morphometric Data

The following measurements were taken directly on the stereolith model. Maximum chord length between frontal poles (FP) and occipital poles (OP) are 153 mm on the right side and 157 mm on the left side. The corresponding arcs (taken by flexible tape) between the same landmarks are: dorsal, right is 215 mm, left 225 mm. The lateral arcs are 200 mm right and 203 mm left. Maximum width, located on superior aspect of the temporal lobes is 124 mm, while the maximum arc width between these points, over the vertex, is 217 mm. The bregma-asterion chords are 118 mm right, 116 mm left. The corresponding arcs between these points are 150 mm right and 144 mm left. Bregma to deepest cerebellum is 125 mm, and the vertex to deepest temporal lobe (in the midline) is 105 mm. The bregma-lambda chord is 93 mm, while the arc is 100 mm. Biasterionic width is 101 mm. The maximum width of the cerebellum is 97 mm, while the widest width between the sigmoid sinuses is 108 mm. The chord distance between frontal poles is 18 mm, and the distance between occipital poles is 25 mm. The total lateral circumference through FPs and OPs is 445 mm, while the dorsal circumference, passing over the dorsal and basal surfaces in the midsagittal plane is 428 mm. The bregma-basion chord distance is 124 mm.

EBSCOhost - printed on 10/28/2022 4:53 AM via . All use subject to https://www.ebsco.com/terms-of-use

Discussion

Both the overall morphology and the volume of the endocast are perfectly congruent with the taxonomic designation of *Homo erectus*. As is so often the case with endocasts, there is little in the way of convolutional detail to merit comparisons with other *H. erectus* endocasts or to provide more than speculation regarding functional behavioral attributes. If the principle of uniformitarianism is adhered to, this endocast clearly indicates three important characteristics of the genus *Homo*: (1) the volume of ca. 1,000 mL is within the range of modern *H. sapiens*; (2) the cerebral asymmetries between left and right sides match those found in modern *H. sapiens,* as well as other *H. erectus* endocasts (see Holloway et al. 2004 for examples and discussion therein); (3) Broca's caps are asymmetrical and protuberant both inferiorly and laterally, another characteristic of modern *H. sapiens*. At the same time, the occipital lobes of the Daka endocast appear to show both derived and primitive characteristics, in that the posterior placement of the lunate sulcus is toward the modern condition, while the strong margins of the lunate sulcus are more primitive.

In sum, in terms of essential morphology, the Daka endocast shows clear continuities between *Homo erectus* and modern *H. sapiens* and suggests that complex social behavioral repertoires, including language, were available to this individual. This does not mean that neurological structures associated with social behavior and intelligence did not continue to evolve through to our own species. It only means that the essential behavioral repertoires were likely in place during the evolutionary time period of *H. erectus*.

Conclusions

Tomographic analysis reveals a great deal of information about the Daka calvaria. The individual had inner ear configurations similar to humans in their implications for balance and hearing. The Daka individual's brain was similar to that of humans in other important ways, and this individual was likely right-handed, perhaps with at least a rudimentary capacity for language. In addition to the functional determinations, the detail presented in this chapter should be useful in future work aimed at determining the systematic significance of endocranial features that supplement those more readily available from ectocranial observation. It is hoped that the future will bring an increased focus on less-accessible features, and that they will add significantly to the number of independent characters through which systematic hypotheses can be tested.

EBSCOhost - printed on 10/28/2022 4:53 AM via . All use subject to https://www.ebsco.com/terms-of-use

This Page Left Intentionally Blank

EBSCOhost - printed on 10/28/2022 4:53 AM via . All use subject to https://www.ebsco.com/terms-of-use

15

Hominid Systematics

W. HENRY GILBERT

The basic question of how fossils are allocated to species recurs throughout phylogenetic and taxonomic considerations of early and middle Pleistocene *Homo*. How are the available specimens best grouped and analyzed? Which specimens or groups of specimens represent direct human ancestors? Answers to these questions are presented to a broad audience, but the recipients may be unfamiliar with nuances and limitations of phylogenetic reconstruction.

Many workers have attempted to distinguish groups among Pleistocene *Homo* (von Koenigswald and Weidenreich 1939; Wood 1992; Rightmire 1996; Bermúdez de Castro et al. 1997; Foley and Lahr 1997; Gabunia et al. 2002; Mallegni et al. 2003; de Lumley et al. 2006). A pervasive hypothesis of the last few decades interprets early African and later, mostly Asian, *H. erectus* to represent distinct species lineages or clades, and suggests that the early African forms were more directly related to advanced *Homo* (Andrews 1984; Stringer 1984; Wood 1984, 1994). This notion has been controversial since its introduction in the 1980s (Rightmire 1984, 1994; Turner and Chamberlain 1989; Kennedy 1991; Kramer 1993; Bräuer 1994), but the distinction is widely held in scholarly literature (Wood and Richmond 2000; Manzi et al. 2001; Mallegni et al. 2003; Cameron 2003; Wang et al. 2004; Carbonell et al. 2005; Dennell and Roebroeks 2005). It is also popular for its heuristic appeal among the authors of textbooks and volumes intended for general audiences (Stanford and Bunn 2001; Alles and Stevenson 2003; Lewin and Foley 2003; Ridley 2004; Dawkins 2004; Arsuaga 2004). A second hypothesis involving Pleistocene *Homo* is that the earliest hominids from western Europe represent the direct ancestors of Neanderthals and *H. sapiens* to the exclusion of penecontemporary hominids from Africa (Bermúdez de Castro et al. 1997; Manzi et al. 2003; note that many of the authors of the former paper have altered their views based on recently discovered material [Carbonell et al. 2005]). Both hypotheses rely on the application of complex analytical methods for establishing phylogenetic relationships among taxa using morphological features. Unfortunately, these morphological features are often difficult to quantify, continuously variable, and functionally interdependent. They are therefore of dubious phylogenetic meaning. As more fossils have become available during the last 20 years, it has become increasingly clear that characters once thought to be geographically restricted among Pleistocene *Homo* specimens are not (see, for example, Asfaw et al. 2003; Spoor et al. 2007).

EBSCOhost - printed on 10/28/2022 4:53 AM via . All use subject to https://www.ebsco.com/terms-of-use

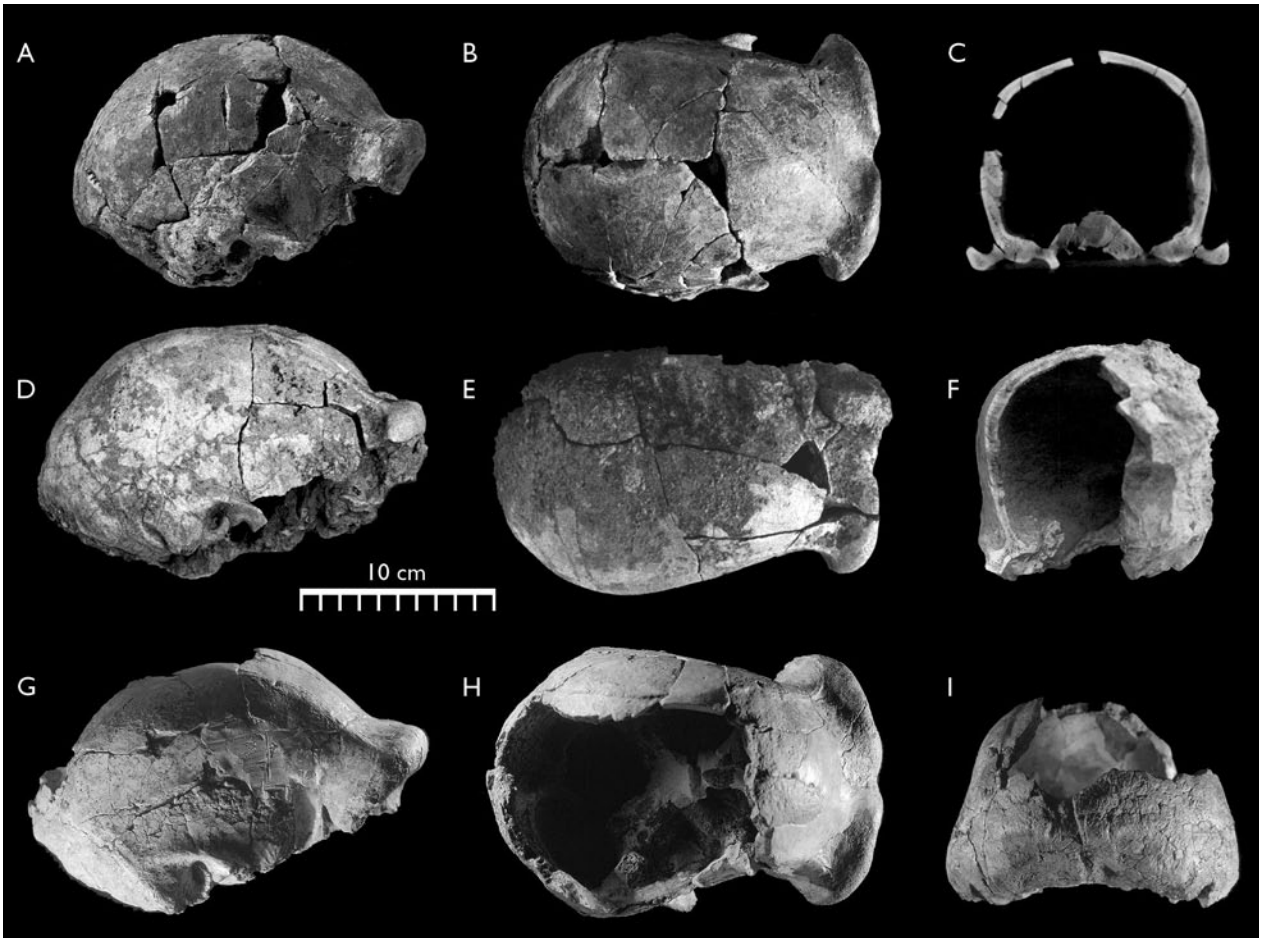

FIGURE 15.1

Comparison of the Daka calvaria (top row) with the Buia cranium (middle row) and Olduvai Hominid 9 (OH 9; bottom row). Images A, D, and G are lateral views. To make comparisons more effective in this column, Buia (D) has the facial skeleton masked and OH 9 (G) is mirrored. Images B, E, and H are vertical views, and C, F, and I are A-P views showing parietal wall verticality. In C the section is derived from CT imagery (see Chapter 14 for discussion). In F the section is witnessed via a natural break. In I the superiorly convergent parietal wall outline is readily apparent in a posterior view. Photographs by Tim White, except for Buia photographs by Danilo Torre and Lorenzo Rook (1997 record), courtesy of the Buia Project.

A simple example of this type of phenomenon can be seen in a comparison of the Daka calvaria with the Buia cranium (Figure 15.1). Both specimens are of roughly the same age and were found approximately 500 km from each other. Abbate et al. (1998) suggest that "morphology like that of *Homo sapiens* had begun to differentiate in Africa at ~1 Myr" based on the Buia specimen's possession of a high position of greatest cranial breadth (vertical parietal walls), implying that this was evidence of phylogenetic differentiation between African and Asian clades. Indeed, Buia's parietal walls are more vertical than those of the Daka calvaria, but the Buia cranium is long and low relative to Daka. This is a decidedly primitive feature classically associated with *H. erectus*. The roughly contemporary OH 9 specimen shows a long and low vault combined with parietals that show strong

EBSCOhost - printed on 10/28/2022 4:53 AM via . All use subject to https://www.ebsco.com/terms-of-use

superior convergence. What does it mean that three such geographically and temporally proximal specimens (the most complete available for the time period) could present such a mixed phenotypic message?

Inferring Evolutionary Relationships

Cladistics and Phenetics

There is no genetic material or soft tissue preserved or so far recovered from early and middle Pleistocene hominids. Therefore, inferring evolutionary relationships among these fossilized remains can only be done by sorting specimens based on arrays of bony morphological features. Using bony morphology, groupings between specimens are made either by overall similarity (phenetics) or by similarity of derived features (cladistics). Both methods make important assumptions, and both have serious limitations.

Phenetic methods cluster specimens based on overall similarity across a selected set of features. Phenetics-based methods yield hierarchical clusters of similar entities, but this hierarchical grouping does not directly relate to phylogenetic pattern because there is, by definition, no attempt made to distinguish primitive from derived features. Thus, phenetic analyses do not detect ancestry. Even if all features employed were phylogenetically meaningful, phenetic clusters are not necessarily consistent with a historically accurate evolutionary branching pattern. The shortcomings and dangers of relying solely on phenetics to construct phylogenetic hypotheses are well established (see, for example, Mayr 1981 and Sneath 1995). Phenetic methodology is inappropriate for addressing *Homo erectus* phylogeny (contra Manzi et al. 2003), and such methods seem better suited to developing taxonomies that do not address ancestry.

Cladistics, on the other hand, does distinguish between primitive and derived features and is thus theoretically capable of determining evolutionary branching patterns if certain assumptions are met. The central assumptions of cladistics are that divergent lineages exist and that these lineages are marked by change in characters over time (Mishler 1994). On the surface it would seem that any evolving group satisfies these assumptions. In practice, however, this can be problematic, especially when working on groups of individuals that are not certain to be discrete lineages (separate taxa are termed "operational taxonomic units" when used in a cladistic analysis and are referred to hereafter as OTUs). Such problems are pertinent to *Homo erectus* systematics, where the OTUs subject to analysis have never been established as discrete lineages (Trinkaus 1990; Sarmiento et al. 2002; Holliday 2003). Unfortunately, whether or not the OTUs analyzed actually represent divergent species lineages, a cladistic analysis will always generate a tree in which each OTU is a branch (see O'Brien et al. 2001). But this is only an illusion if the OTUs are invalid, for cladistic analysis cannot establish the authenticity of divergent groups. Rather, it will provide the most parsimonious branching pattern for the groups, *assuming* that they are divergent species lineages.

How, then, are divergent species lineages accurately delineated? In cladistic analyses of living taxa this poses a less significant problem than for fossil taxa. For example, lineage boundaries are more straightforward in living organisms, where species can be bound in

EBSCOhost - printed on 10/28/2022 4:53 AM via . All use subject to https://www.ebsco.com/terms-of-use

terms of reproduction and reticulation, than in fossils (Hennig 1966). Cladistic analyses performed separately on prehistoric taxa and living taxa regularly reveal discrepancies in tree topology (Gauthier et al. 1988; Lee 2005).

Establishment of divergent species lineages is an especially perplexing problem for hominid systematists, who deal with a short time frame, high degrees of morphological similarity among taxa analyzed, and substantial morphological intraspecific variation within the closest living analogs (humans and great apes). Perhaps the only reliable way of establishing multiple hominid lineages on morphological grounds is when two very different taxa coexist in contemporaneous units, as with the well-established examples of the coexistence of *Homo* species with *Australopithecus boisei* at several eastern African sites, including Konso-Gardula, Olduvai, and Koobi Fora (White 1988; Suwa et al. 1997). Similarly, middle Pleistocene African and European *Homo* specimens such as Bodo, Kabwe, Petralona, and the Sima de los Huesos specimens are demonstrably different from contemporaneous *H. erectus* from eastern Asia (Rightmire 2001; Asfaw et al. 2002). Does variation signal a similar dichotomy of species lineages within early Pleistocene *H. erectus*? The following sections address this question.

Caveats for Cladistics

Prior to engaging in any cladistic reconstruction of Pleistocene hominids, some important considerations must be made. Time, the meaning of "lineage," character definitions, variation, and homology must all be considered. The following paragraphs briefly explore each of these.

Cladograms portray only relative times of species divergence. However, absolute chronological depth represents phylogenetically informative data. For instance, many of the African *Homo erectus* specimens known before 1995 were from much earlier horizons than the Asian specimens they were compared to. Because change occurs in lineages over time, separately grouping earlier and later parts of an evolving lineage will create separate OTUs that do not represent a branching dichotomy (see Turner and Chamberlain 1989). Phyletic evolutionary change along a nonbranching lineage is a hypothesis not even considered in cladistic efforts that disregard chronology. Conversely, contemporaneity can represent very important evidence. *Homo erectus* specimens from the middle Pleistocene of eastern Asia are strikingly different from contemporary hominids in eastern Africa and Europe (Rightmire 2001), indicating that at least two divergent lineages of *Homo* coexisted at that time. *Homo sapiens* occurs in Africa contemporaneous with European Neanderthals (White et al. 2003), indicating that the hypothesis of a simple phyletic (chronospecies) relationship between these species is false. One must be aware that unless time information is specifically included (see, for example, Huelsenbeck 1994 and Wagner 1995), cladistic analysis ignores temporal information, a potentially vital piece of data for establishing evolutionary divergence and history.

Species lineages may be complex at the populational level, particularly for widespread species. This complexity is underappreciated when phylogenetic patterns are interpreted only via cladistic methodology. Do the OTUs that we recognize represent different lineages, or different populations, or different segments of these? In reality, lineages are the entities

EBSCOhost - printed on 10/28/2022 4:53 AM via . All use subject to https://www.ebsco.com/terms-of-use

that emerge from complex networks of interbreeding subspecies, demes, populations, and individuals (Holliday 2003). It is possible for incipient species to diverge from a larger lineage, become reproductively isolated for some time, and later become reunited with the main lineage (Graybeal 1995). Hybridization occurs between modern entities that appear to be biological species (Jolly 2001; Adams et al. 2003). Whereas *Homo erectus* crania from some single sites are similar in multivariate morphospace (Delson et al. 2001) and cluster together cladistically (Gilbert 2003a), other single-site samples show heterogeneity that has been interpreted at the level of the species lineage (Schwartz 2000). Some authors (Baba et al. 2003) suggest that region-bound groups of *H. erectus*, specifically those found on Java in Indonesia, might have evolved in isolation. The lineage structure of Pleistocene *Homo* was certainly complex, and the small sample of recovered cranial specimens is extremely unlikely to approximate pancontinental population structure. This renders the definition of OTUs from available specimens problematic. Cladistic methods depend on accurately defined OTUs representing separate species lineages. They cannot render accurate phylogenies unless this first, independent step has been accomplished.

Choosing good morphological features, termed "characters" in cladistics, is fundamentally important to solid cladistic analysis. Good characters should be heritable, they should not vary excessively within individual OTUs, they should be genetically and developmentally independent of each other, and they should be clearly defined (Thiele 1993; Pleijel 1995). It is unclear that any of the characters employed in this (or any other) analysis of Pleistocene hominid fossils fulfill these requirements. It is not the cladistic method, per se, that undermines this effort. Rather, it is our inability to define valid characters necessary in such analyses. When poorly chosen characters are employed, the analytical results are compromised because error can compound geometrically with the addition of each unsound character. Furthermore, cladistic methods assume that homologous characters (characters that are shared as a result of common descent) are more common than analogous characters (the "homoplastic" characters shared due to parallel or convergent evolution) (Hennig 1966). Many have pointed out the difficulties associated with the high incidence of homoplasy in hominid cranial characters (see Lieberman et al. 1996; Curnoe 2003).

Variation is a fundamental consideration in biology (see Hallgrímsson and Hall 2005 for a thorough review of this topic). Obviously, variation occurs not only between organisms from different lineages, but also among organisms within the same species, population, or brood. Variation even occurs between homologous features on different sides of a single organism (Willmore and Hallgrímsson 2005). Many of the features used in *Homo erectus* systematics vary in single modern human populations, as has been observed, for instance, in prehistoric Amerindian populations (Etler 1994). This poses problems for Pleistocene *Homo* systematists who deal with isolated specimens for which population-level variation cannot be established. The potential for variation makes it imperative that character state assessment be made on multiple individuals for any particular OTU, but this presents a problem when analyzing Pleistocene hominids, for there are very few single sites that have yielded more than one individual. Variation is addressed via the comparison of three analyses in the sections that follow. The first analysis makes no attempt to reconcile variation, analyzing individual specimens as OTUs. The second forms OTUs from groupings of crania that are based on geological age and geography, and the third groups

EBSCOhost - printed on 10/28/2022 4:53 AM via . All use subject to https://www.ebsco.com/terms-of-use

only specimens from the same site in two attempts to address the potentially confounding effect of individual variation.

Adjunct to variation is the concept of homology. Characters are homologous if they owe their shape similarity to evolutionarily equivalent morphogenetic pathways. Homology is thus directly related to genetics and development. Much recent work has focused on deciphering the complicated developmental underpinnings of bony and dental features (eg. Hlusko 2004). This work has made it clear that the proper units for phylogenetic and functional analysis, the true homologous features, are the morphogenetic fields behind traits rather that the traits themselves (Lovejoy et al. 2000). An array of several characters that are developmentally correlated may together indicate only a single homology, a single true character. Mathematically inclined cladists promote the inclusion of as many characters as possible (Landrum 1993), citing the statistical benefits that larger datasets imbue, but this is an analytical trap. Splitting a single morphogenetic homology into several cladistic characters might make a cladogram more statistically robust, but it will not make it any truer to phylogenetic history. Rather, it will have the opposite effect. It is thus incorrect to assume that naming a character for every feature discernible by sight or palpation can mitigate phylogenetic reconstruction error. Cladistic attempts at deciphering Pleistocene *Homo* phylogeny that have taken this approach (for example, Zeitoun 2000, with 122 characters recognized) are therefore at higher risk of error.

Morphological characters can be broken into two types: variable (continuous) characters and discrete (discontinuous) characters (Smith 1994; Curnoe 2003). Discrete characters are those that are based on the presence or absence of a feature. A feature state is scored as present if it is observed, or absent if it is not. Discrete characters do not present the problems of arbitrary subdivision that variable characters do (see below), but truly discrete characters are rare within groups of low taxonomic rank (Smith 1994). Pleistocene *Homo* exemplifies this problem, and there are relatively few well-established discrete characters. Often the morphology presented by specimens varies continuously between individuals such as to make accurate scoring very difficult, if not impossible.

Variable characters have more than two states, and are often based on metric values. For these character states are produced by subdividing the range of measurements into segments and then assigning scores to each metric subdivision, a procedure known as gap coding (see Chappill 1989). This is done either arbitrarily or based on a priori knowledge of the systematist (Smith 1994). Many of the characters used in the phylogenetic analyses that follow employ gap coding.

When considering all of the caveats presented here, one is left with a feeling of profound doubt over the utility of cladistics for resolving phylogenetic patterns among Pleistocene *Homo* fossil specimens and samples. Acknowledging this, the analyses that follow are not intended as hypotheses of evolutionary pattern. Rather, they represent tests of already established phylogenetic hypotheses. These hypotheses, that African and Asian *H. erectus* are cladistically distinct (Andrews 1984), that early African *H. erectus* is phylogenetically closer to advanced *Homo* than later African and Asian *H. erectus* (Stringer 1984; Wood 1984, 1994), and that early Pleistocene hominids from Europe are more directly ancestral to Neanderthals and *H. sapiens* than contemporary African specimens (Manzi et al. 2003), are borne of cladistic assessments of bony morphological features. They should, therefore, be consistent with any thorough cladistic analysis.

EBSCOhost - printed on 10/28/2022 4:53 AM via . All use subject to https://www.ebsco.com/terms-of-use

Homo erectus Cladistic Analysis

Without well-established taxonomies and lineages, cladistics can do little to determine evolutionary branching patterns within *Homo erectus* (see Sarmiento et al. 2002). However, it has some utility in testing preconceived phylogenetic hypotheses. First, the notion that Asian and early African *H. erectus* are discrete lineages, a phylogenetic prediction based on morphological characters, may be tested by performing a cladistic analysis. If a phylogenetic analysis of Pleistocene *Homo* does not reveal geographically bounded nested hierarchies, then this hypothesis is effectively falsified. If it does, then it is not falsified, but, regardless of the result, a cladistic analysis cannot demonstrate that the OTUs analyzed are nonreticulating. The first hypothesis addressed in the analyses below is: Asian *H. erectus* is a discrete phylogenetic entity from early *H. erectus* in Africa. The analyses presented here address this hypothesis, most clearly stated by Andrews (1984), who includes OH 9 within an African *H. erectus* group. A similar view is also promoted by Stringer (1984) and Wood (1984b, 1994), who differ in including OH 9 with Asian *H. erectus*, but exclude this group from *H. sapiens* ancestry. Thus, the second hypothesis tested by this analysis is that early African forms from Koobi Fora represent more direct ancestors to advanced *Homo* than do later African or Asian *H. erectus* specimens.

Manzi et al. (2003) have suggested that late early Pleistocene *Homo erectus* from Europe was a more direct ancestor of advanced *Homo* than its African contemporaries. This conclusion is based on a phenetic analysis, which is inappropriate for questions of ancestry. For the tests that follow, this third hypothesis can be distilled to the following: The Ceprano cranium is cladistically linked to advanced *Homo*, to the exclusion of Daka and Buia.

Three cladistic analyses are presented here to test these different hypotheses about Pleistocene hominid phylogenetics. The first employs individual specimens as OTUs. The second uses paleodemes (time- and geography-determined groupings, after Howell 1999) as OTUs. The third groups specimens from single sites into OTUs (it leaves isolated specimens as separate OTUs). These analyses are presented solely as tests of the phylogenetic hypotheses outlined previously. The cladograms derived from these analyses are explicitly not intended for interpretation as hypotheses of evolutionary pattern.

OTUs

All of the analyses presented here treat the same constellation of available fossil specimens. For the first, the OTUs are simple. They are the individual crania. For the second, OTUs are based on paleodemes defined by Howell (1999). Paleodemes are sets of fossils representing spatially and temporally bounded groupings below the species level. The demic analysis was undertaken to address the potential for error that would result from choosing a single representative from a highly variable population. See Appendix 15.2 for a list of the demes used. In the third analysis only specimens from single sites are grouped into OTUs, whereas the others are left as individual OTUs. In the latter analyses, character states for demes and sites were based on the dominant score of specimens in each grouping.

EBSCOhost - printed on 10/28/2022 4:53 AM via . All use subject to https://www.ebsco.com/terms-of-use

Characters

Characters used in the phylogenetic analyses that follow (presented in Appendix 15.1) were derived from a review of systematic literature related to early *Homo*. Similar characters and characters with a high likelihood of developmental correlation were synonymized. No implicit or explicit claim is made here for the phylogenetic or biological meaningfulness of the characters employed. On the contrary, it is certain that there is a high potential for homoplasy and population-level variation in each, and there is no published evidence for any of them being the unique products of discrete morphogenetic fields. The list is solely intended to represent the best compilation of characters that have been used to make phylogenetic inferences about Pleistocene *Homo* in the published literature. No defense of their phylogenetic meaning is intended, but since these are the characters most widely used in published analyses, their use here is appropriate to testing the phylogenetic inferences generated by those analyses.

There is a slight difference in the analyses presented here and those presented by Asfaw et al. (2002) and Gilbert (2003a). The method of gap coding for variable characters was changed, and intermediate characters were scored as intermediate rather than ambiguous. Because intermediate states truly are ambiguous, this does not improve the analysis per se, but does offer another dimension to the array of analyses already presented.

Specimen-Based Cladistic Analysis

The first analysis does not impose groupings. Rather, it uses individual specimens as OTUs. This means that individual variation may have a significant impact on tree topology. A heuristic analysis using PAUP 4.0 (Swofford 1998) resulted in 124,856 most parsimonious cladograms with scores of 127 steps. Figure 15.2 presents a strict consensus of these trees and a majority-rule consensus of branching patterns that occurred in 75 percent or more of the trees. There is no discernible separation between African and Asian groups. Early African forms from Koobi Fora do not fall out as closer sister taxa to advanced *Homo* than later African and Eurasian *Homo erectus*. Ceprano does not group more readily with more advanced specimens than do its African contemporaries.

In the specimen-based analysis, individuals from some single sites, such as Ngandong and Zhoukoudian, tended to cluster by site. While seemingly intuitive, the implications of this are nonetheless interesting. Populations of *Homo erectus* were likely morphologically distinctive. As more sites are discovered and more specimens become available, this phenomenon will likely come into clearer focus.

Deme-Based Cladistic Analysis

The second analysis groups specimens into demes in an attempt to mitigate the effect of individual variation. We employ previously defined paleodemes (Howell 1999) circumscribed primarily on the basis of time and space. This approach (Asfaw et al. 2002) has been criticized for overlooking the importance of morphological affinities (Manzi et al. 2003), but this was the explicit intent of the original analysis. Demes constructed

EBSCOhost - printed on 10/28/2022 4:53 AM via . All use subject to https://www.ebsco.com/terms-of-use

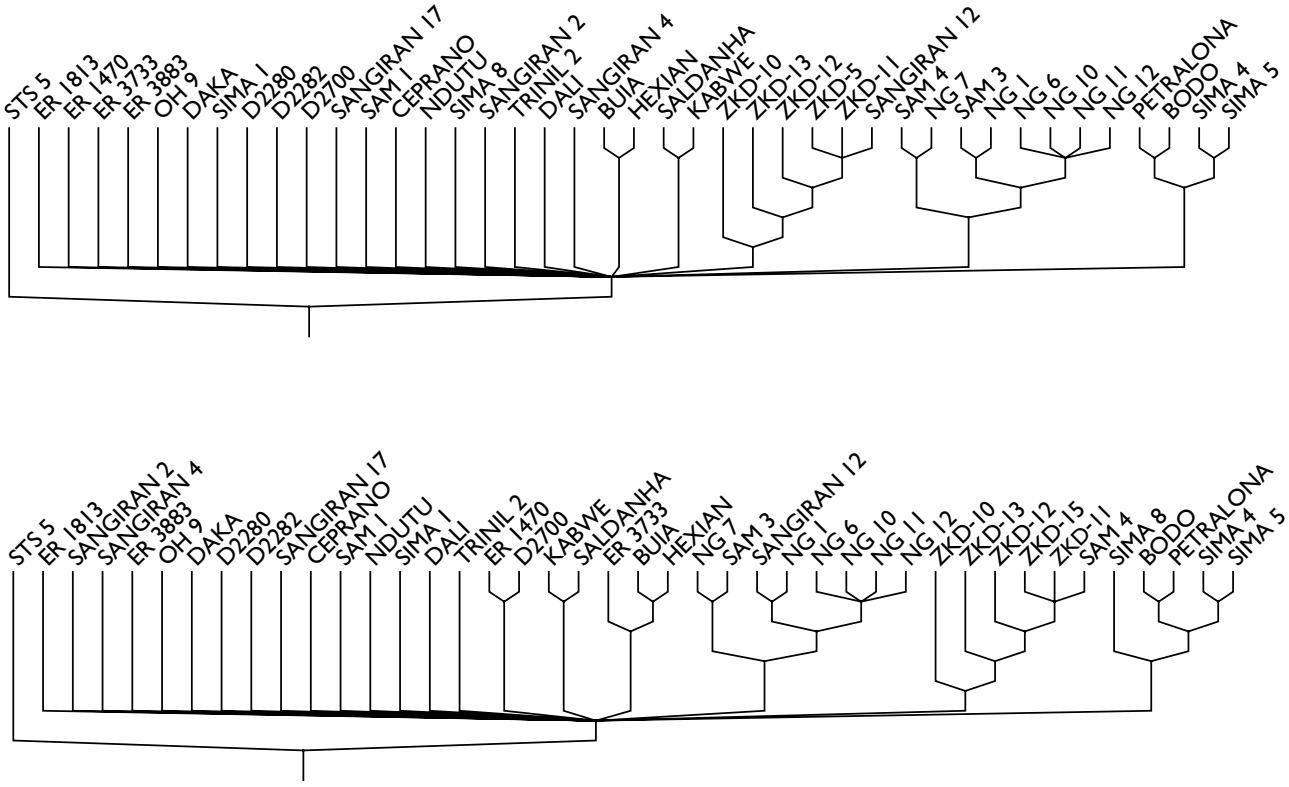

FIGURE 15.2

Strict consensus (above) and 75 percent majority rule consensus (below) of specimen-based cladistic analysis. See Appendix 15.1 for characters and definitions. See Appendix 15.2 for character scoring. This analysis was rendered with PAUP 4.0 (Swofford 1998). Of 22 total characters: 1 character, endocranial capacity, is of type "ord" (Wagner), 21 characters are of type "unord." All characters have equal weight. All characters are parsimony informative. Gaps are treated as "missing." Starting tree(s) obtained via stepwise addition. Addition sequence: simple (reference taxon = STS 5). Number of trees held at each step during stepwise addition = 1. Branch-swapping algorithm: tree-bisection-reconnection (TBR). Score of best trees found = 127. Number of trees retained = 124,856.

based on shared morphology would bias any cladistic analysis that was based on the same aspects of morphology. Obviously, Howell's paleodemes are not equivalent to true biological populations or metapopulations, but the creation of new OTUs based on shared anatomy would have introduced circularity. In any case, the point of Manzi et al. (2003) is muted by the specimen-based analysis presented in the previous section and the site-based analysis presented in the following section. Results of the deme-based analysis are presented in Figure 15.3. A heuristic analysis using PAUP 4.0 (Swofford 1998) resulted in 19 most parsimonious cladograms with scores of 67 steps. Neither a strict consensus nor a 75 percent majority rule consensus revealed cladistic separation of Asian and African Pleistocene *Homo*. The Nariokotome deme does not cluster more closely with advanced *Homo* than do later African and Eurasian demes. Cerpano does not group more readily with derived hominids than does the Olduvai LLK deme.

EBSCOhost - printed on 10/28/2022 4:53 AM via . All use subject to https://www.ebsco.com/terms-of-use

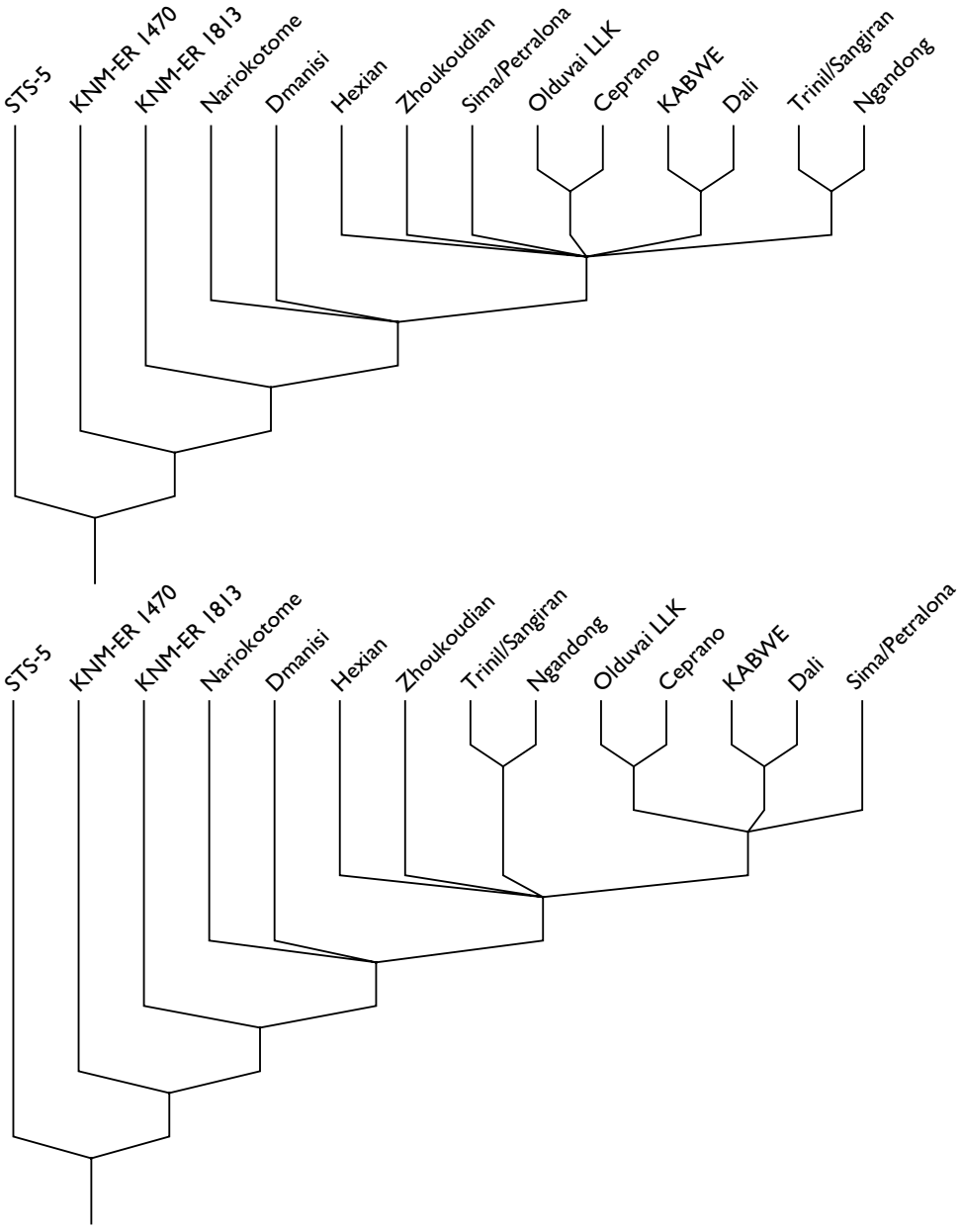

FIGURE 15.3

Strict consensus (above) and 75 percent majority rule consensus (below) of deme-based cladistic analysis. See Appendix 15.1 for characters and definitions. See Appendix 15.2 for deme composition and character scoring. This analysis was rendered with PAUP 4.0 (Swofford 1998). Of 22 total characters: one character, endocranial capacity, is of type "ord" (Wagner), 21 characters are of type "unord." All characters have equal weight. One character is parsimony uninformative. Number of parsimony-informative characters = 21. Gaps are treated as "missing." Starting tree(s) obtained via stepwise addition. Addition sequence: simple (reference taxon = STS 5). Number of trees held at each step during stepwise addition = 1. Branch-swapping algorithm: tree-bisection-reconnection (TBR). Score of best trees found = 67. Number of trees retained = 19.

Site-Based Cladistic Analysis

The third analysis imposes groupings only on specimens from the same sites and uses single specimens as OTUs for the others (see Appendix 15.3). Individual variation is also a potential bias in this analysis because most of the OTUs are of the latter variety. A heuristic analysis using PAUP 4.0 (Swofford 1998) resulted in 292 most parsimonious cladograms with scores of 88 steps. Figure 15.4 presents a strict consensus of the trees and

EBSCOhost - printed on 10/28/2022 4:53 AM via . All use subject to https://www.ebsco.com/terms-of-use

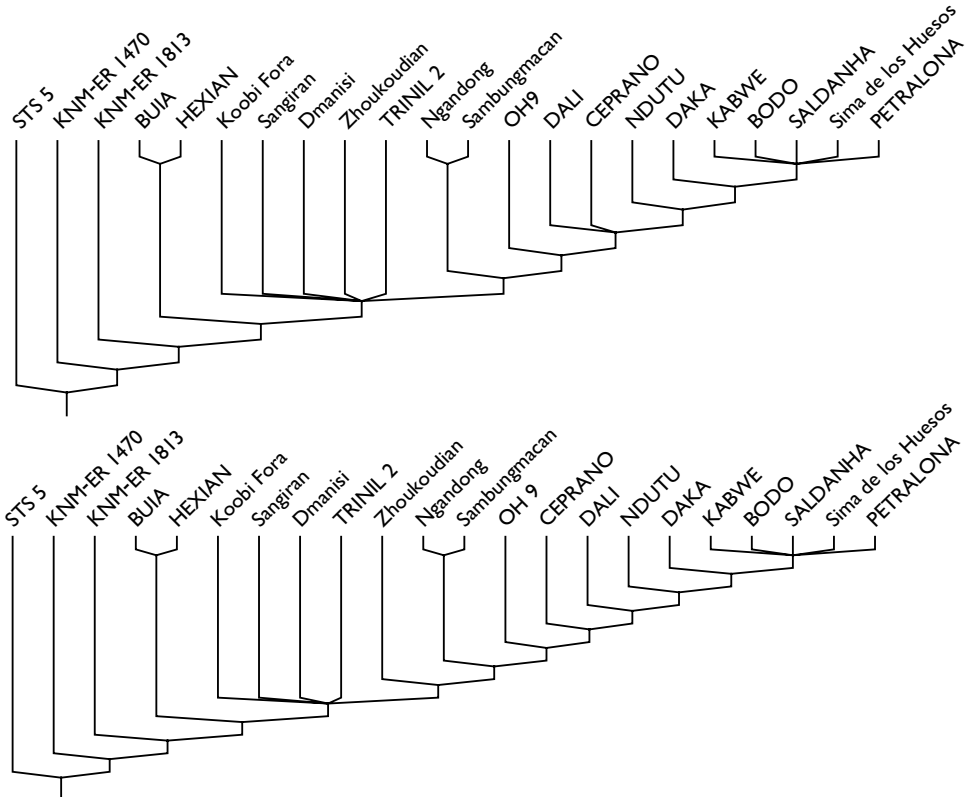

FIGURE 15.4

Strict consensus (above) and 75 percent majority rule consensus (below) of site-based cladistic analysis. See Appendix 15.1 for characters and definitions. Sites with only single specimens are denoted with all capital letters. See Appendix 15.2 for character scoring. This analysis was rendered with PAUP 4.0 (Swofford 1998). Of 22 total characters: one character, endocranial capacity, is of type "ord" (Wagner), 21 characters are of type "unord." All characters have equal weight. All characters are parsimony informative. Gaps are treated as "missing." Starting tree(s) obtained via stepwise addition. Addition sequence: simple (reference taxon = STS 5). Number of trees held at each step during stepwise addition = 1. Branch-swapping algorithm: tree-bisection-reconnection (TBR). Score of best trees found = 88. Number of trees retained = 292.

a majority rule consensus of branching patterns that occurred in 75 percent or more of the trees. As with both previous analyses, there is no discernible separation between African and Asian groups, early African forms from Koobi Fora do not fall out as closer sister taxa to advanced *Homo* than later African and Eurasian *Homo erectus*, and Ceprano does not group more readily with more advanced specimens than do its African contemporaries.

The trees derived from the site-based analysis cluster later early Pleistocene African and European specimens with middle Pleistocene African and Eurasian specimens that are more advanced than *Homo erectus*. This clustering is affected significantly by characters likely associated with larger brains: endocranial capacity, parietal wall verticality, and temporal squama shape. For reasons discussed, a cladistic analysis can never be taken as direct evidence for a speciation event. However, tree topology from this analysis does not refute the hypothesis that the middle Pleistocene divergence signaled by the apparent contemporaneity of very different hominids from Africa and eastern Eurasia (for example, Bodo and Broken Hill versus Zhoukoudian) began in the early Pleistocene of Africa.

Conclusions

Characters used in Pleistocene *Homo* phylogenetic reconstructions are subtle and often somewhat ambiguous (Bräuer 1994). Their phylogenetic meaning is therefore dubious (Lovejoy et al. 2000). The required circumscription of OTUs prior to analysis either forces the grouping of potentially unrelated specimens or dismisses the potential for individual

EBSCOhost - printed on 10/28/2022 4:53 AM via . All use subject to https://www.ebsco.com/terms-of-use

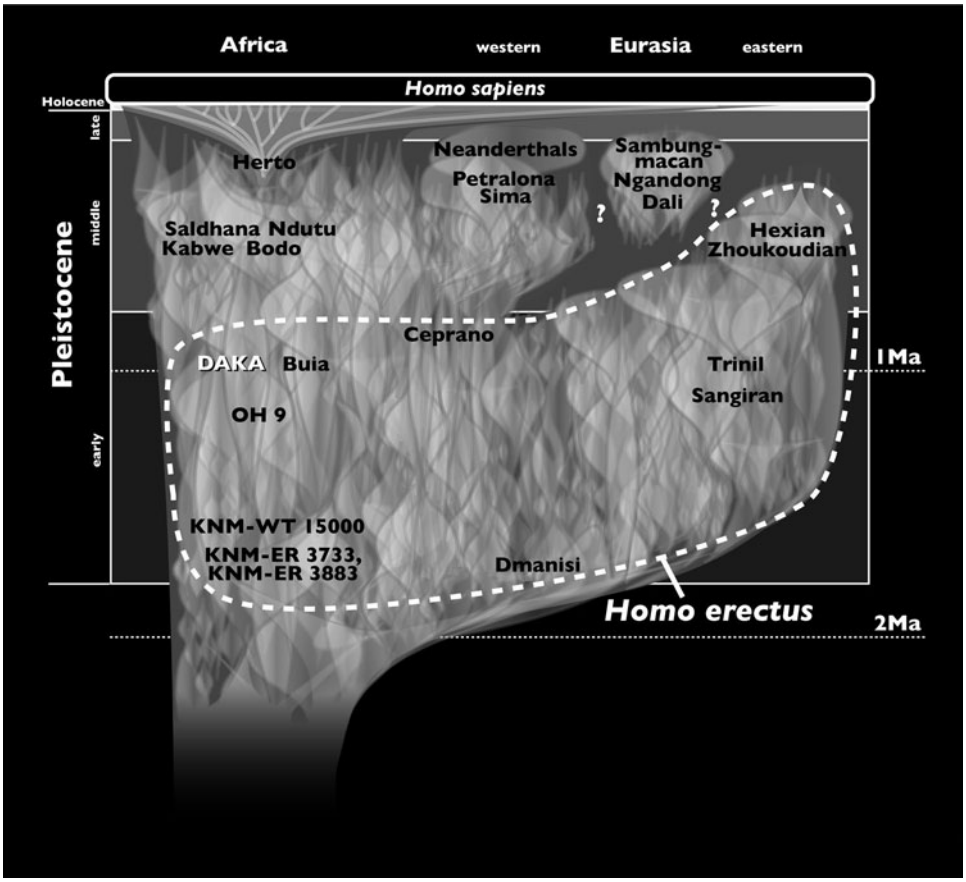

FIGURE 15.5
Diagram of a possible Pleistocene *Homo* phylogeny.

variation by analyzing individuals as OTUs. Even when these issues are ignored, resulting phylogenies for Pleistocene *Homo* are poorly resolved and show little consensus among high numbers of most parsimonious trees.

Little resolution on Pleistocene *Homo* phylogeny has been gained by the repeated use of cladistic analysis. However, the hypothesis that the African sample and the Asian sample represent distinct clades is readily falsified by these methods. Also, early African forms from Koobi Fora did not nest more closely with advanced *Homo* than later African and Eurasian *H. erectus* in any of the analyses. Thus, the taxonomic nomen *H. erectus* can be correctly applied to a large set of morphologically similar crania from the early and middle Pleistocene across the Old World. Additionally, no support was found for the osteomorphologically based claim that early Pleistocene *Homo* from Europe is closer than representatives from Africa to the clade of derived hominids that led to the emergence of Neanderthals and *H. sapiens* (Manzi et al. 2003). Figure 15.5 graphically portrays *H. erectus* phylogeny in a fashion consistent with the results of the analyses undertaken in this chapter. It is notably similar to the phylogeny presented by Rightmire (2001), and somewhat less complicated than those presented by Lahr and Foley (2001) and Stringer (2002).

EBSCOhost - printed on 10/28/2022 4:53 AM via . All use subject to https://www.ebsco.com/terms-of-use

EBSCOhost - printed on 10/28/2022 4:53 AM via . All use subject to https://www.ebsco.com/terms-of-use

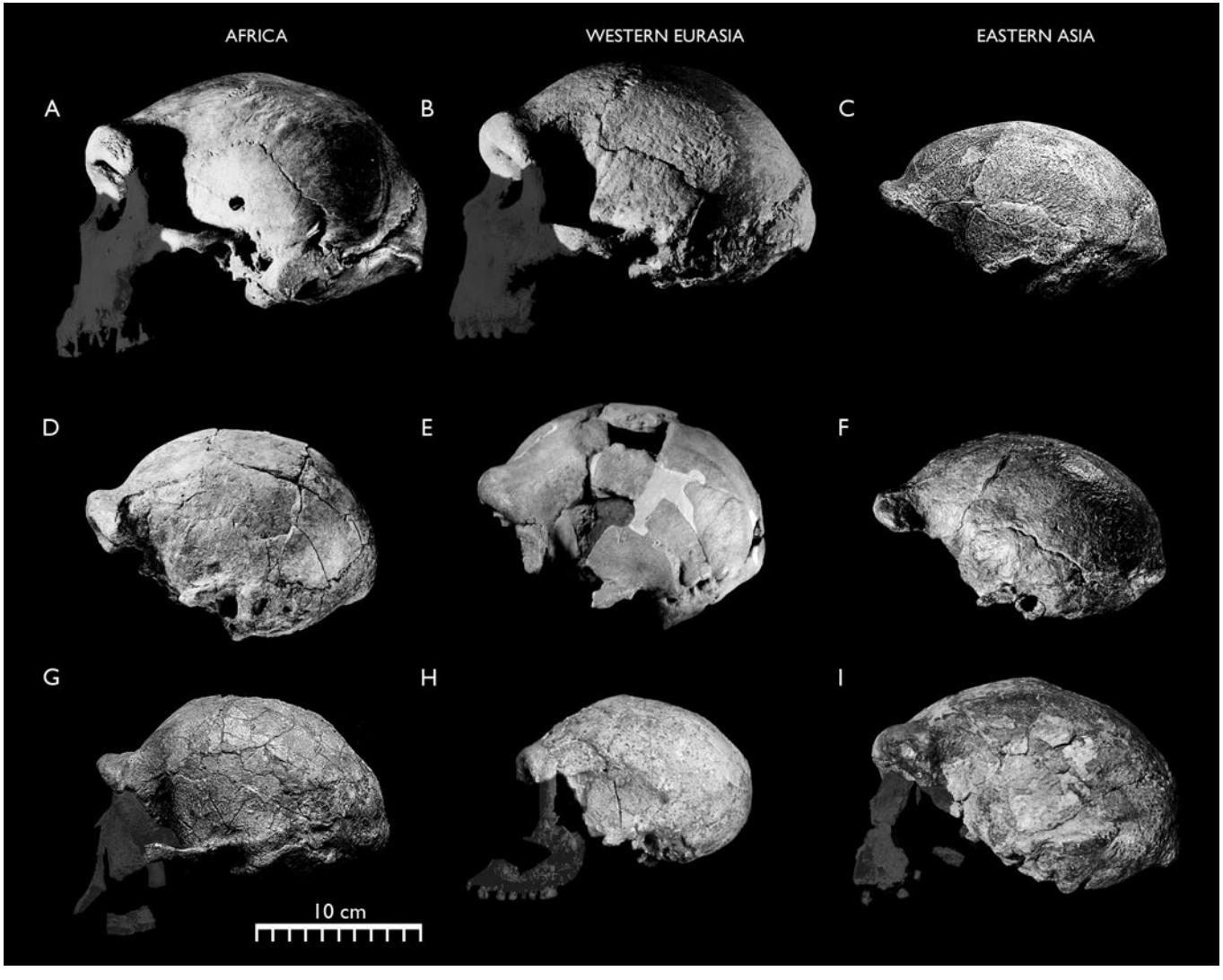

FIGURE 15.6

Comparison of Pleistocene *Homo* crania from different temporal intervals and geographic regions. Top row (middle Pleistocene): A. Kabwe. B. Petralona. C. ZKD 3. Middle row (later early Pleistocene): D. Daka calvaria. E. Ceprano. F. Sangiran 2. Bottom row (early Pleistocene): G. KNM-ER 3733. H. Dmanisi D2700. I. Sangiran 17. Photographs by Tim White, except for Dmanisi D2700 photograph courtesy of David Lordkipanidze.

While the analyses presented in this chapter discourage overzealous splitting within early Pleistocene *Homo* by dismantling cladistic arguments for dividing the group into clades, they are actually constructive in reaffirming the validity of contextual data and encouraging greater focus on what is actually knowable. Hominids emerged from Africa before the Pleistocene began at a time when *Australopithecus* coexisted with *Homo* in Africa (White 1988; Suwa et al. 1997; Dennel and Roebroeks 2005). There is evidence for a consistent increase in cranial capacity within *Homo* across the Pleistocene in noninsular Africa and Eurasia (Rightmire 2004). Contemporary African and Eurasian hominids are morphologically similar through the early Pleistocene (Asfaw et al. 2002; Vekua et al. 2002). While morphological differences exist among specimens assigned to *H. erectus*, the differences do not distinguish geography-based grouping beyond single sites (Asfaw et al. 2002; Gilbert 2003a; this chapter). *Homo erectus* crania from single sites tend to cluster cladistically (Gilbert 2003a; this chapter). *Homo erectus* appears to have persisted in eastern Asia through the middle Pleistocene, well after more derived forms of *Homo* appeared in Africa (Rightmire 2001; Asfaw et al. 2002; see Figure 15.6). *Homo sapiens* originated from advanced African *Homo* during the late middle Pleistocene (White et al. 2003) and subsequently became the sole hominid in the rest of the world.

EBSCOhost - printed on 10/28/2022 4:53 AM via . All use subject to https://www.ebsco.com/terms-of-use

EBSCOhost - printed on 10/28/2022 4:53 AM via . All use subject to https://www.ebsco.com/terms-of-use

APPENDIX 15.1 Descriptions and Scoring of Characters Used in Analysis

Character Number	*Character Name*	*Definition*	*Synonyms and Correlated Characters*	*Scoring*	*Remarks*
1	Endocranial capacity	Cranial capacity in cubic centimeters (cc)	Defined universally as the volume of the endocranium	Gap coded	Cranial capacity was gap coded using divisions at 650 cc, 950 cc, and 1200 cc. Cranial capacity is one of the most straightforward characters in the matrix. Its definition is precise and undebated. It is easily polarized and is unitary with respect to natural selection. While the small cranial capacity of *Homo floresiensis* (Morwood et al. 2004; Falk et al. 2005) would seem to suggest that a cladistic cranial capacity character cannot be treated as irreversible, there is a clear progression toward increasing cranial capacities across the Pliocene and Pleistocene (Rightmire 2001) in continental circumstances. This character was hence ordered for the cladistic analysis.
2	Cranial vault shape (length ÷ height)	Glabella-opisthocranion chord divided by basion-bregma chord	Lateral vault profile (Arsuaga et al. 1997); vault shape (Stringer et al. 1984); cranium long and low (Wood 1984; Tianyvan and Etler 1992; Schwartz and Tattersall 1996; Abbate et al. 1998; Gabunia et al. 2000; Manzi et al. 2001); platycephaly (Hublin 1998a, b)	Gap coded	Cranial vault shape was gap coded, with divisions at index values of 1.3, 1.5, and 1.8. While a long and low cranial vault shape has often been presented as a feature defining *Homo erectus,* it is rather vague with respect to homology. It does, however, appear to be more pronounced in *H. erectus* than in earlier or later hominids. Note that the Sima specimens, and STS 5 have low scores while others are high. A long and low vault is more likely, however, the result of the evolutionary path cranial shape took toward encephalization rather than a synapomorphy of *H. erectus,* as it is highly unlikely that all lower and middle Pleistocene hominids are a discrete clade with respect to *Australopithecus* and early *Homo* that excludes Neanderthals and modern humans.
3	Sutural keeling	Presence of keeling along the sagittal, coronal, and/or metopic sutures	Frontal keel (Wood 1984; Kennedy 1991; Etler 1992; Arsuaga et al. 1997; Rightmire 2001; Delson et al. 2001; Manzi et al. 2001); parietal keel (Arsuaga et al. 1997; Abbate et al. 1998); sagittal keel (Howells 1980; Etler 1994; Lahr 1996; Abbate et al. 1998; Arsuaga et al. 1999; Gabunia et al. 2000;); bregmatic eminence (Wu and Braüer 1993);	Present or absent	This character integrates keeling on the sagittal, coronal, and metopic sutures. Keeling is irregular in *Homo erectus.* In some specimens it is pronounced and continuous along the sagittal suture. In others it presents only subtly or in localized areas (as with a bregmatic eminence). Due to this variability, all sutural keeling is synonymized here and scored as present or absent.

(continued)

EBSCOhost - printed on 10/28/2022 4:53 AM via . All use subject to https://www.ebsco.com/terms-of-use

APPENDIX 15.1 *(continued)*

Character Number	*Character Name*	*Definition*	*Synonyms and Correlated Characters*	*Scoring*	*Remarks*
			prebregmatic eminence (Frayer et al. 1993); coronal ridge (Wood 1984); sagittal angulation or ridge (Wood 1984); ectocranial buttresses (Tianyvan and Etler 1992); coronal ridge (Manzi et al. 2001); anterior keel (Delson et al. 2001); frontal-sagittal keel (Kramer et al. 2001)		
4	Interorbital breadth (at nasion)	Interorbital chord measured between inner orbital rims at the level of nasion	Nasal bridge (Arsuaga et al. 1999); interorbital breadth (Tianyvan and Etler 1992)	Gap coded	Interorbital breadth was gap coded, with divisions at values of 30 and 35 mm.
5	Canial vault thickness (at bregma)	External to internal vault bone thickness taken at bregma	Vault thickness (Howells 1980; Arsuaga et al. 1997; Abbate et al. 1998; Delson et al. 2001; Manzi et al. 2001); robusticity (Stringer 1984); vault bones thickened (Wood 1984; Kennedy 1991; Frayer et al. 1993); bone thickness (Schwartz and Tattersall 1996)	Gap coded	Cranial vault thickness was gap coded, with divisions at values of 7.5 and 9.5 mm.
6	Forehead elevation	Pronounced convexity along the sagittal profile of the frontal bone between the supratoral sulcus and bregma	Frontal bone height (Stringer 1984); frontal squama (Frayer et al. 1993; Habgood 1989); frontal angle (Wood 1984); flatness (Tianyvan and Etler 1992; Rightmire 2001); elevation of the forehead (Abbate et al. 1998); frontal profile (Lahr 1996)	Present or absent	Forehead elevation was scored as present or absent by direct observation of the specimens. When the metopic area presented greater sagittal convexity at its middle than around bregma or the frontal trigon area, this character was scored as a 1. When the frontal presented more-or-less even convexity along the profile, it was scored as a 0. While intermediate cases did exist, the presence or absence of this feature was often easy to detect. Some specimens, like Sangiran 17, are clearly flat. Others, like the Zhoukoudian specimens, present a pronounced bulge on the frontal.
7	Glabellar inflexion	Transverse concavity separating supraorbital tori at glabella	Glabellar inflexion (Manzi et al. 2001); superior glabellar view (Wu and Braüer 1993)	Scored as minimal, moderate, or pronounced	Scoring was done by observation and palpation. No concavity was scored as a 0, slight concavity was scored as a 1, and pronounced concavity was scored as a 2.

EBSCOhost - printed on 10/28/2022 4:53 AM via . All use subject to https://www.ebsco.com/terms-of-use

8	Postorbital constriction	Chord between temporal lines at point of maximum constriction (Martin 9[1]) divided by maximum cranial breadth	Postorbital constriction (Howells 1980; Wood 1984; Turner and Chamberlain 1989; Rightmire 2001; Manzi et al. 2001)	Gap coded	Postorbital constriction was gap coded, with divisions at index values of .64, .7, and 1.0. The index used employed maximum cranial breadth rather than measurements on the orbits due to variation in supraorbital tori and the lack of zygomatics in many Pleistocene *Homo* specimens.
9	Supraorbital torus thickness	Vertical thickness of supraorbital torus above midorbit, in frontal view	Supraorbital torus thickness (Stringer 1984; Etler 1994; Abbate et al. 1998); supraorbital torus thickened and projecting (Rightmire 2001); supraorbital thickness (Manzi et al. 2001); supraorbital ridges (Lahr 1996); browridge size (Frayer et al. 1993); large, continuous supraorbital ridges with a supratoral sulcus (Wood 1984)	Gap coded	Supraorbital torus thickness was gap coded, with divisions at values of 10 and 15 mm. Midorbit is defined here as the apex of the supraorbital margin.
10	Supraorbital tori arching	Degree of arching found in the line defined by the anteriormost presentation of the supraorbital torus; assessed in frontal view	Double-arched supraorbital torus (Schwartz and Tattersall 1996; Bermúdez de Castro et al. 1997); supraorbital torus straight in anterior and superior view (Howells 1980; Tianyvan and Etler 1992); browridge straightness (Frayer et al. 1993)	Scored as minimal, moderate, or pronounced	Flattened supraorbital tori were scored as a 0, those with moderate arching, like KNM-ER 3733, were scored as a 1, and those with pronounced arching, like Kabwe, were scored as a 2. The line defined by the most anterior presentation of the supraorbital tori was used because often the infraorbital margin and the supraorbital margin differ in degree of arching.
11	Occipital angulation	Angle formed between the lambda-inion chord and the inion-opisthion chord	Occipital angulation (Wood 1984); occipital squama shape (Delson et al. 2001); occipital shape (Gabunia et al. 2000); lateral profile (Manzi et al. 2001)	Gap coded	Occipital angulation was gap coded, with divisions at index values of 100 and 110.
12	Occipital torus	Transverse bony thickening along the border of the nuchal and occipital planes; defined superiorly by a supratoral sulcus	Occipital torus (Wood 1984; Kennedy 1991; Tianyvan and Etler 1992, 1994; Lahr 1996; Schwartz and Tattersall 1996; Arsuaga et al. 1997; Hublin 1998a; Delson et al. 2001; Manzi et al. 2001); nuchal torus (Abbate et al. 1998); supratoral sulcus (Howells 1980; Manzi et al.	Scored as minimal, moderate, or pronounced	The occipital torus is a highly variable feature. For some specimens it is continuous from asterion to asterion as a raised bar. For others it is expressed medially, but not laterally. In many single sites with multiple specimens, like Ngandong, Sambungmacan, and Zhoukoudian, the morphology of this feature is similar between individuals, indicative of population-level homology. Unfortunately, across *Homo erectus* the feature is very irregular.

(continued)

EBSCOhost - printed on 10/28/2022 4:53 AM via . All use subject to https://www.ebsco.com/terms-of-use

APPENDIX 15.1 *(continued)*

Character Number	*Character Name*	*Definition*	*Synonyms and Correlated Characters*	*Scoring*	*Remarks*
			2001); occipital torus (Howells 1980); central occipital torus form (Kramer et al. 2001)		
13	Occipital/nuchal scale index	Lambda-inion chord divided by inion-opisthion chord	Occipital plane (Tianyvan and Etler 1992; Delson et al. 2001); upper scale length (Wood 1994); occipital vs. nuchal plane (Rightmire 2001)	Gap coded	Occipital/nuchal scale index was gap coded, with divisions at index values of 1.2 and 1.5.
14	Angular torus	A raised and thickened lower margin of the posterior temporalis muscle origin on the parietal	Angular torus (Wood 1994; Kennedy 1991; Wu and Braüer 1993; Abbate et al. 1998; Dean et al. 1998; Tianyvan and Etler 1992; Etler 1994); angular torus or swelling (Arsuaga et al. 1997)	Present or absent	Angular tori are defined for, and best observed in, the Zhoukoudian crania. In many specimens, including some modern humans, there is a raised area associated with the posteroinferior temporal line on the parietal above asterion. A readily discernable raised area at this position incurred a score of present.
15	Parietal wall verticality	Superior convergence of lateral parietal walls in posterior view	Parietal walls (Tianyvan and Etler 1992; Abbate et al. 1998)	Present or absent	This feature was scored in posterior view as present when external parietal walls below the parietal boss (or homologous region) were oriented sagittally.
16	Glenoid fossa depth (articular eminence height)	Index to express depth of fossa relative to height of eminence	Mandibular fossa (Gabunia et al. 2000); articular tubercle (Rightmire 2001); glenoid fossa (Delson et al. 2001); TMJ form (Picq 1983); anterior mastoid tubercle (Schwartz and Tattersall 1996; Arsuaga et al. 1997; Hublin 1998a); articular eminence shape (Martínez and Arsuaga 1997; Hublin 1998a)	Gap coded	Glenoid fossa depth was gap coded, with divisions at index values of 120 and 135.
17	Juxtamastoid eminence	Linear raised area of bone between the digastric groove and occipital artery groove	Juxtamastoid eminence (Martínez and Arsuaga 1997); juxtamastoid ridge (Wood 1984; Etler 1994; Manzi et al. 2001); occipitomastoid crest (Weidenreich 1943)	Present or absent	There is some confusion over this feature in the literature. We follow Walensky (1964); Aiello and Dean (1990) and Martínez and Arsuaga (1997) discuss the nomenclature of this variable feature extensively.

EBSCOhost - printed on 10/28/2022 4:53 AM via . All use subject to https://www.ebsco.com/terms-of-use

18	Tympanic plate inclination	General trend of lateral tympanic is relatively coronal in orientation or between sagittal and coronal	Tympanic plate orientation (Martínez and Arsuaga 1997; Tianyvan and Etler 1992; Etler 1994); tympanic and mastoid portions separate (Dean et al. 1998)	Binary scoring	Because the tympanic frequently changes orientation along its long axis, this character refers to the lateral portion adjacent to the glenoid fossa.
19	Postglenoid projection	Vertical height of the postglenoid process at its highest point relative to the glenoid fossa	Postglenoid process projection (Arsuaga et al. 1997); postglenoid process (Howells 1980; Hublin 1998a; Delson et al. 2001)	Gap coded	Postglenoid projection was gap coded, with divisions at values of 5 and 7.
20	Temporal squama shape	Squamosal suture path defined as long, low, and flat or short, high, and convex	Superior border of squama (Martínez and Arsuaga 1997; Arsuaga et al. 1999); temporal height (Turner and Chamberlain 1989); low squama (Wood 1984); superior squamosal margin (Tianyvan and Etler 1992); temporal squama height (Bermúdez de Castro et al. 1997; Hublin 1998a; Gabunia et al. 2000; Rightmire 2001; Delson et al. 2001; Manzi et al. 2001); temporal squama profile (Dean et al. 1998); flat squamal upper border (Manzi et al. 2001)	Binary scoring	Temporal squama shape was scored by observation. Specimens like the Zhoudoudian crania and OH 9 define the long, low, and flat condition, whereas specimens like Kabwe define the short, high, and convex condition.
21	Styloid process	Presence of a styloid process	Styloid process (Tianyvan and Etler 1992; Martínez and Arsuaga 1997; Bermúdez de Castro et al. 1997; Arsuaga et al. 1999; Delson et al. 2001)	Present or absent	Distinctive styloid bases where the process could be determined to have previously existed were scored as present.
22	Supramastoid/ suprameatal shelf	Presence of a protruding bony crest above the external auditory meatus and mastoid process	Supramastoid crest (Howells 1980; Turner and Chamberlain 1989; Etler 1994; Manzi et al. 2001); supramastoid/mastoid crests (Wood 1984); supramastoid-auriculare protrusion (Abbate et al. 1998)	Scored as minimal, moderate, or pronounced	A supramastoid/suprameatal shelf was scored as minimal when when the crest continuing from the zygomatic root lacked a clearly distinguishable concavity above auriculare. Moderate scores were applied when the concavity was detectable, but reduced; pronounced scores were applied when the suprameatal crest was ledge-like.

	Endocranial capacity	*Cranial vault shape (length÷ height)*	*Perisutural keeling*	*Interorbital breadth (at nasion)*	*Cranial vault thickness (at bregma)*	*Forehead elevation*	*Glabellar inflexion*	*Postorbital constriction*	*Supraorbital torus thickness*	*Supraorbital tori arching*
STS 5	0	1	0	?	0	?	0	0	0	1
KNM-ER 1813	0	2	0	0	0	1	1	0	1	1
KNM-ER 1470	1	?	0	2	0	1	1	0	0	1
KNM-ER 3733	1	2	1	0	?	1	1	1	0	2
KNM-ER 3883	1	3	1	0	1	0	1	0	1	1
Nariokotome deme	**1**	**?**	**1**	**0**	**1**	**?**	**1**	**?**	**?**	**?**
OH 9	2	2	?	3	1	?	2	1	2	1
DAKA	2	1	1	1	0	1	2	1	2	2
BUIA	1	?	?	?	0	1	?	?	2	2
Olduvai LLK deme	**2**	**?**	**1**	**?**	**0**	**1**	**2**	**1**	**2**	**2**
Dmanisi D 2280	1	2	1	1	1	0	0	0	1	1
Dmanisi D 2282	1	3	1	?	1	1	?	?	1	?
Dmanisi D 2700	0	?	1	2	1	1	0	0	0	1
Dmanisi deme	**1**	**?**	**1**	**?**	**1**	**1**	**0**	**0**	**1**	**1**
ZKD III	1	?	1	1	2	1	1	1	1	1
ZKD V	2	?	?	2	?	?	1	0	1	0
ZKD X	3	?	1	?	1	1	0	1	1	1
ZKD XI	2	2	1	?	0	1	0	1	1	0
ZKD XII	2	2	1	2	2	1	1	1	1	1
Zhoukoudian deme	**?**	**2**	**1**	**2**	**?**	**1**	**1**	**1**	**1**	**?**
CEPRANO	2	?	0	3	1	1	2	1	2	1
KABWE	3	2	1	1	?	0	1	2	2	2
NDUTU	2	?	?	?	0	?	?	?	1	?
BODO	3	?	1	2	2	0	1	2	2	1
SALDHANA	3	?	1	?	?	0	?	?	2	2
Kabwe deme	**3**	**2**	**1**	**?**	**?**	**0**	**1**	**2**	**2**	**2**
DALI	2	2	1	?	1	1	1	?	2	2
HEXIAN	2	?	1	?	?	1	1	0	2	2
TRINIL 2	1	2	1	?	1	0	?	0	?	?
SANGIRAN 2	1	2	1	?	1	0	?	0	1	?
SANGIRAN 4	1	?	1	?	?	?	?	?	?	?
SANGIRAN 12	2	?	?	?	0	?	?	?	?	?
SANGIRAN 17	2	3	1	1	1	0	1	0	1	1
Trinil Sangiran deme	**?**	**2**	**1**	**1**	**1**	**0**	**1**	**0**	**1**	**1**
NG 1	2	2	1	?	0	0	?	?	?	0
NG 6	3	?	1	?	2	0	2	2	1	0
NG 7	2	2	1	1	2	1	2	2	2	0
NG 10	?	?	?	?	1	0	?	?	?	0
NG 11	3	?	1	?	1	0	2	2	1	0
NG 12	2	?	1	2	1	0	2	2	1	0
SAM 1	?	?	1	?	?	1	?	1	2	?
SAM 3	2	?	1	?	2	1	2	2	?	0
SAM 4	2	?	1	?	2	1	1	?	1	0
Ngandong deme	**2**	**2**	**1**	**?**	**?**	**0**	**2**	**2**	**1**	**0**
SIMA 1	?	?	?	?	?	?	?	?	?	?
SIMA 4	3	0	1	?	?	1	?	?	1	?
SIMA 5	2	0	1	?	?	1	1	?	1	1
SIMA 8	?	?	1	?	2	?	?	?	?	?
PETRALONA	3	2	1	2	?	0	1	1	2	1
Sima Petralona deme	**3**	**0**	**1**	**2**	**2**	**1**	**1**	**1**	**1**	**1**

NOTE: Intermediate scores and missing data on individual specimens are recorded as (?). When over 66 percent of the specimens in a deme have the same score it is recorded as the deme score. Otherwise, when specimens in a deme present variable character states, the deme's overall score is recorded as unresolved (?).

EBSCOhost - printed on 10/28/2022 4:53 AM via . All use subject to https://www.ebsco.com/terms-of-use

Occipital angulation	*Occipital torus*	*Occipital/ Nuchal scale index*	*Angular torus*	*Parietal wall verticality*	*Glenoid fossa depth/ articular eminence height*	*Juxtamastoid eminence*	*Tympanic plate inclination*	*Postglenoid projection*	*Temporal squama shape*	*Styloid process*	*Supramastoid/-meatal shelf*
2	1	0	1	0	?	1	?	2	0	0	1
2	1	1	1	0	1	1	0	1	?	1	2
?	0	2	?	0	2	?	?	2	0	1	?
1	1	0	0	0	1	0	0	0	0	1	1
1	1	0	?	0	0	?	0	1	0	0	1
1	**1**	**0**	**0**	**0**	**?**	**0**	**0**	**?**	**0**	**?**	**1**
?	1	?	1	0	0	1	1	0	0	1	2
1	0	1	0	1	1	1	0	0	1	0	0
?	0	?	1	1	?	?	?	?	0	?	1
1	**0**	**1**	**1**	**1**	**?**	**1**	**?**	**0**	**0**	**?**	**?**
1	1	0	1	0	1	1	0	1	0	?	1
?	?	?	1	?	?	?	?	?	0	?	?
2	0	1	0	0	?	?	0	?	0	?	1
?	**?**	**?**	**1**	**0**	**1**	**1**	**0**	**1**	**0**	**?**	**1**
0	2	0	1	0	0	1	?	0	0	0	2
?	2	?	1	?	0	1	0	1	0	0	2
?	2	0	1	0	?	?	0	?	0	0	2
1	2	0	1	0	0	1	0	?	0	0	2
1	2	0	1	0	?	1	?	1	0	0	2
1	**2**	**0**	**1**	**0**	**0**	**1**	**0**	**1**	**0**	**0**	**2**
?	1	?	1	1	?	?	?	0	1	?	0
?	2	?	0	0	0	1	1	2	1	1	0
0	1	0	0	1	0	1	?	0	1	1	0
?	?	?	?	?	?	?	?	2	1	?	?
?	1	?	?	?	?	?	?	?	?	?	?
0	**1**	**0**	**0**	**1**	**0**	**1**	**1**	**2**	**1**	**1**	**0**
0	1	2	1	1	?	?	1	?	1	1	1
?	1	?	1	0	?	?	0	?	?	0	1
?	1	?	?	0	?	?	?	?	?	?	?
0	1	0	0	0	1	0	0	0	0	?	0
0	1	0	1	?	0	0	0	1	0	0	2
0	1	0	1	0	?	?	?	?	?	?	?
0	1	0	1	0	?	0	0	1	0	?	2
0	**1**	**0**	**1**	**0**	**?**	**0**	**0**	**1**	**0**	**0**	**2**
0	1	0	1	0	?	?	?	?	?	0	?
0	2	0	1	?	0	?	0	0	0	0	1
0	2	0	0	0	?	1	0	?	0	0	1
?	2	?	1	0	?	0	0	?	0	0	?
0	2	0	?	0	?	?	0	?	0	0	1
0	2	1	1	0	0	1	0	?	0	0	1
?	1	?	1	0	?	1	0	0	0	?	2
2	1	1	0	0	?	1	0	?	0	?	2
?	2	?	1	0	?	?	0	?	0	0	2
0	**2**	**0**	**1**	**0**	**0**	**1**	**0**	**0**	**0**	**0**	**?**
?	?	?	0	?	?	?	0	?	?	1	?
1	0	1	1	1	2	0	0	2	1	1	0
?	0	1	1	1	1	0	0	2	1	1	0
?	?	?	0	?	?	?	0	2	?	1	?
1	0	?	1	1	?	?	1	?	?	1	1
1	**0**	**1**	**?**	**1**	**?**	**0**	**0**	**2**	**1**	**1**	**0**

EBSCOhost - printed on 10/28/2022 4:53 AM via . All use subject to https://www.ebsco.com/terms-of-use

APPENDIX 15.3 Scoring of Site-Based Groups Using Characters Outlined in Appendix 15.1 and Data Outlined in Appendix 15.2

	Endocranial capacity	*Cranial vault shape (length ÷ height)*	*Perisutural keeling*	*Interorbital breadth (at nasion)*	*Cranial vault thickness (at bregma)*	*Forehead elevation*	*Glabellar inflexion*	*Postorbital constriction*	*Supraorbital torus thickness*	*Supraorbital tori arching*
KNM-ER 3733	1	2	1	0	?	1	1	1	0	2
KNM-ER 3883	1	3	1	0	1	0	1	0	1	1
Koobi Fora site	**1**	**?**	**1**	**0**	**1**	**?**	**1**	**?**	**?**	**?**
Dmanisi D 2280	1	2	1	1	1	0	0	0	1	1
Dmanisi D 2282	1	3	1	?	1	1	?	?	1	?
Dmanisi D 2700	0	?	1	2	1	1	0	0	0	1
Dmanisi site	**1**	**?**	**1**	**?**	**1**	**1**	**0**	**0**	**1**	**1**
ZKD III	1	?	1	1	2	1	1	1	1	1
ZKD V	2	?	?	2	?	?	1	0	1	0
ZKD X	3	?	1	?	1	1	0	1	1	1
ZKD XI	2	2	1	?	0	1	0	1	1	0
ZKD XII	2	2	1	2	2	1	1	1	1	1
Zhoukoudian site	**?**	**2**	**1**	**2**	**?**	**1**	**1**	**1**	**1**	**?**
SANGIRAN 2	1	2	1	?	1	0	?	0	1	?
SANGIRAN 4	1	?	1	?	?	?	?	?	?	?
SANGIRAN 12	2	?	?	?	0	?	?	?	?	?
SANGIRAN 17	2	3	1	1	1	0	1	0	1	1
Sangiran site	**?**	**?**	**1**	**1**	**1**	**0**	**1**	**0**	**1**	**1**
NG 1	2	2	1	?	0	0	?	?	?	0
NG 6	3	?	1	?	2	0	2	2	1	0
NG 7	2	2	1	1	2	1	2	2	2	0
NG 10	?	?	?	?	1	0	?	?	?	0
NG 11	3	?	1	?	1	0	2	2	1	0
NG 12	2	?	1	2	1	0	2	2	1	0
Ngandong site	**?**	**2**	**1**	**?**	**?**	**0**	**2**	**2**	**1**	**0**
SAM 1	?	?	1	?	?	1	?	1	2	?
SAM 3	2	?	1	?	2	1	2	2	?	0
SAM 4	2	?	1	?	2	1	1	?	1	0
Sambungmacan site	**2**	**?**	**1**	**?**	**2**	**1**	**?**	**?**	**?**	**0**
SIMA 1	?	?	?	?	?	?	?	?	?	?
SIMA 4	3	0	1	?	?	1	?	?	1	?
SIMA 5	2	0	1	?	?	1	1	?	1	1
SIMA 8	?	?	1	?	2	?	?	?	?	?
Sima de los Huesos site	**?**	**0**	**1**	**?**	**2**	**1**	**1**	**?**	**1**	**1**

NOTE: Intermediate scores and missing data on individual specimens are recorded as (?). When over 66 percent of the specimens in a site have the same score it is recorded as the site score. Otherwise, when specimens in a site present variable character states the site's overall score is recorded as unresolved (?).

EBSCOhost - printed on 10/28/2022 4:53 AM via . All use subject to https://www.ebsco.com/terms-of-use

Occipital angulation	*Occipital torus*	*Occipital/ nuchal scale index*	*Angular torus*	*Parietal wall verticality*	*Glenoid fossa depth/ articular eminence height*	*Juxtamastoid eminence*	*Tympanic plate inclination*	*Postglenoid projection*	*Temporal squama shape*	*Styloid process*	*Supramastoid/- meatal shelf*
1	1	0	0	0	1	0	0	0	0	1	1
1	1	0	?	0	0	?	0	1	0	0	1
1	**1**	**0**	**0**	**0**	**?**	**0**	**0**	**?**	**0**	**?**	**1**
1	1	0	1	0	1	1	0	1	0	?	1
?	?	?	1	?	?	?	?	?	0	?	?
2	0	1	0	0	?	?	0	?	0	?	1
?	**?**	**?**	**1**	**0**	**1**	**1**	**0**	**1**	**0**	**?**	**1**
0	2	0	1	0	0	1	?	0	0	0	2
?	2	?	1	?	0	1	0	1	0	0	2
?	2	0	1	0	?	?	0	?	0	0	2
1	2	0	1	0	0	1	0	?	0	0	2
1	2	0	1	0	?	1	?	1	0	0	2
1	**2**	**0**	**1**	**0**	**0**	**1**	**0**	**1**	**0**	**0**	**2**
0	1	0	0	0	1	0	0	0	0	?	0
0	1	0	1	?	0	0	0	1	0	0	2
0	1	0	1	0	?	?	?	?	?	?	?
0	1	0	1	0	?	0	0	1	0	?	2
0	**1**	**0**	**1**	**0**	**?**	**0**	**0**	**1**	**0**	**0**	**2**
0	1	0	1	0	?	?	?	?	?	0	?
0	2	0	1	?	0	?	0	0	0	0	1
0	2	0	0	0	?	1	0	?	0	0	1
?	2	?	1	0	?	0	0	?	0	0	?
0	2	0	?	0	?	?	0	?	0	0	1
0	2	1	1	0	0	1	0	?	0	0	1
0	**2**	**0**	**1**	**0**	**0**	**1**	**0**	**0**	**0**	**0**	**1**
?	1	?	1	0	?	1	0	0	0	?	2
2	1	1	0	0	?	1	0	?	0	?	2
?	2	?	1	0	?	?	0	?	0	0	2
2	**1**	**1**	**1**	**0**	**?**	**1**	**0**	**0**	**0**	**0**	**2**
?	?	?	0	?	?	?	0	?	?	1	?
1	0	1	1	1	2	0	0	2	1	1	0
?	0	1	1	1	1	0	0	2	1	1	0
?	?	?	0	?	?	?	0	2	?	1	?
1	**0**	**1**	**?**	**1**	**?**	**0**	**0**	**2**	**1**	**1**	**0**

EBSCOhost - printed on 10/28/2022 4:53 AM via . All use subject to https://www.ebsco.com/terms-of-use

This Page Left Intentionally Blank

EBSCOhost - printed on 10/28/2022 4:53 AM via . All use subject to https://www.ebsco.com/terms-of-use

16

Daka Member Hominid Postcranial Remains

W. HENRY GILBERT

This chapter outlines the postcranial remains of hominids from the Daka Member. The sample comprises three femora, one tibia, and one talus. The tibia and femora are presented here with descriptions of their preservation and anatomy relative to comparative specimens. The talus is only briefly presented, as it was discovered in late 2005 and has not yet been cleaned for detailed study.

Femora and tibiae of modern humans are variable in morphology (Lovejoy 1975; Grine et al. 1995; Lovejoy et al. 2002). Comparative samples of these elements among Pleistocene *Homo* are small. Several lower-limb bone features have been posited to differentiate early Pleistocene *Homo* and modern humans (Weidenreich 1941; Davis 1964; Day 1971; Kennedy 1983a, b, 1984; Grine et al. 1995, Stringer et al. 1998). Femora are given greater attention in this chapter because they are better represented in both the Daka Member and the Pleistocene fossil record in general. Comparisons are made with a robust modern human sample in which many features often cited as being associated with Pleistocene *Homo* are common.

Assignment of early Pleistocene hominid femora and tibiae to species without associated crania is not possible. This chapter compares Daka Member postcrania to a set of specimens from the early and middle Pleistocene that have been assigned to early *Homo* or *H. erectus*. Because of the difficulty inherent in identifying isolated postcranial elements to species, the most precise way to refer to the Pleistocene comparative material used in assessing the Daka postcranial specimens would be "early and middle Pleistocene hominids generally referred to *Homo*." However, in light of the awkwardness of repeating this string throughout the chapter, the sample of femora compared to the Daka material is here collectively referred to as "early Pleistocene *Homo*."

Femur Descriptions

Three hominid femora have been recovered from the Daka Member. Specimen BOU-VP-1/75 was found in 1992 by Tim White (Figure 16.1). Specimen BOU-VP-2/15 was found in 1992 by Gen Suwa, and BOU-VP-19/63 was found in 1998 by Tim White. See Figure 2.2 (Chapter 2) for stratigraphic positions of specimens. The three Daka Member femora are described here relative to other Pleistocene hominids. In the discussion

EBSCOhost - printed on 10/28/2022 4:53 AM via . All use subject to https://www.ebsco.com/terms-of-use

FIGURE 16.1
View northeast across the Daka Member at BOU-VP-1. Berhane Asfaw (left) and Gen Suwa (right) with the BOU-VP-1/75 femur shaft. The specimen was freshly exposed by recent rain, still in situ, cemented in the clay shown at the base of the excavation. Photograph by Tim White, December 28, 1992.

that follows, specific femoral features are discussed with respect to their occurrence in the Daka femora, in other early Pleistocene *Homo* specimens, and in a sample of femora from a robust modern human population.

Several femoral differences between modern humans and early Pleistocene *Homo* have been suggested in the literature (Weidenreich 1941; Day 1971; Kennedy 1983a, 1984). The most consistently cited are the following: early Pleistocene *Homo* femora have flat (platymeric) proximal shafts, early Pleistocene *Homo* specimens tend to lack a pilaster of obtuse triangular cross section deep to the linea aspera, early Pleistocene *Homo* minimum transverse breadths occur distal to the proximodistal midpoint of the femur shaft, and early Pleistocene *Homo* cortical bone is thick relative to that of modern humans and tends to be thicker medially than laterally. Absolute size does not distinguish early Pleistocene *Homo* femora, as wide femoral size variation has characterized hominids throughout the late Pliocene and Pleistocene (McHenry 1991). Workers have noted that robust modern human femora present many seemingly primitive features and that not all purported *H. erectus* features are present in all Pleistocene *Homo* specimens (Kennedy 1983a; Grine et al. 1995; Lovejoy et al. 2002).

Daka hominid femora and a sample of 80 early Pleistocene *Homo* and Holocene *H. sapiens* femora were assessed for nine features. In addition to those presented in the previous paragraph, several other features mentioned in the literature or emergent from comparing the

EBSCOhost - printed on 10/28/2022 4:53 AM via . All use subject to https://www.ebsco.com/terms-of-use

two samples were assessed: linea aspera position relative to the midline of the femur shaft, anteversion, the presence of a lateral supracondylar line, the presence of a lateral expansion of the proximal femur shaft at the level of the gluteal tuberosity, and the presence of a hypertrochanteric fossa (see Appendices 16.1 and 16.2 and Figure 16.2 for definitions and scoring).

The fossil sample, including the Daka femora, consists of 13 specimens generally placed in the genus *Homo* (McHenry and Corruccini 1978; Kennedy 1983a, b). Assessment of features was made on casts in the Human Evolution Research Center cast collection at the University of California, Berkeley, and measurements were taken from the literature (Weidenreich 1941; Day 1971; Kennedy 1983a; Grine et al. 1995). The oldest femora included in the comparative sample, KNM-ER 1472 and KNM-ER 1481, come from below the KBS tuff (Leakey et al. 1978), which dates to approximately 1.9 Ma (Feibel et al. 1989). These femora therefore predate known *H. erectus* fossils. The other Koobi Fora specimens examined, KNM-ER 737 and KNM-ER 803, are from the Okote Member and date to between 1.4 and 1.6 Ma (Feibel et al. 1989). It should be noted that *Australopithecus* coexisted with *Homo* in these units, and some workers conclude that the two genera are distinguishable based on femoral morphology (McHenry and Corruccini 1978; Kennedy 1983b). The Turkana Boy, KNM-WT 15000, is from the lowest part of the Natoo Member of the Nachukui Formation and dates to approximately 1.6 Ma (Feibel et al. 1989) but was excluded from the comparative sample because the individual is immature. Olduvai Hominid (OH) 28 is from Bed IV at Olduvai Gorge and dates to between 0.6 and 0.8 Ma (Hay 1994). Chinese specimens from Zhoukoudian, ZKD Femora 1 and 4, have been dated to between approximately 0.3 and 0.55 Ma (Grun et al. 1997). Arago specimens XLVIII and LVII date to the middle Pleistocene or latest early Pleistocene (de Lumley et al. 1984). Trinil Femur 2, which displays morphology characteristic of Pleistocene *Homo* (Kennedy 1983a), dates to between approximately 1.0 and 1.5 Ma (Larick et al. 2001).

The *Homo sapiens* comparative sample is composed of 70 femora from prehistoric Amerindian sites in North America. Individuals in this sample derive from the Phoebe Hearst Museum of Anthropology (PHMA), University of California, Berkeley. Individuals in the PHMA collections derive from archaeological contexts in California: eight localities in five counties, with the majority of them in northern California. Localities included in this subsample date to between approximately 4,500 BP to 100 BP. Individuals from these sites can be considered as representative of a hunter-gatherer mode of subsistence.

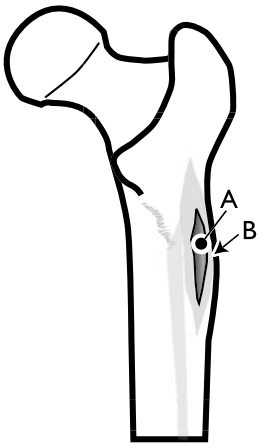

FIGURE 16.2

A. Illustration of the hypertrochanteric fossa. B. The lateral expansion of the gluteal tuberosity.

BOU-VP-1/75

PRESERVATION Femur BOU-VP-1/75 (Plate 16.1) is more complete and better preserved than BOU-VP-2/15. The entire specimen, however, is slightly hydraulically abraded, and primary surface relief is therefore slightly subdued. The specimen preserves the inferior portion of the neck and includes the entire shaft from just distal to the lesser trochanter (which is not present) to the proximal part of the popliteal surface. The anterolateral portion of the uneven proximal break shows signs of peeling, and it is possible that this break might have occurred around the time of death. Two circular impressions that appear to be puncture marks occur anteromedially on the distal shaft. The break occurring adjacent to the distal of these two marks also shows signs of peeling. Neither of the two impressions exhibits

EBSCOhost - printed on 10/28/2022 4:53 AM via . All use subject to https://www.ebsco.com/terms-of-use

adjacent striae, features often associated with carnivore activity. It is possible that carnivores are responsible for the depressions, but the morphology of the marks is inconclusive.

DISTORTION None.

DESCRIPTION Femur BOU-VP-1/75 is anteverted, with the supracondylar popliteal surface making an approximately 45° angle with the flattened posterior subtrochanteric surface. The subtrochanteric cross section is extremely platymeric (see Plate 16.1). This flattening produces a torus-like medial shaft margin, especially proximally. This torus-like margin extends onto the preserved portion of the neck and is similar to, but more pronounced than, what is seen in ZKD Femur 4. The pectineal line is faint but present below the base of the lesser trochanter, and it meets the gluteal line in an area of notable rugosity. There is a distinct hypertrochanteric fossa between the gluteal tuberosity and the lateral margin of the shaft, and the lateral margin bulges substantially in the adjacent area. A similar lateral expansion of the gluteal region occurs in ZKD Femur 1, OH 28, Arago LVII, and KNM-ER 737.

The linea aspera is well defined and occurs on a moderate pilaster. In contrast to BOU-VP-2/15, the linea aspera runs along the medial margin of the posterior femur, especially proximally. Distally, the linea trends medially, and it is positioned at the shaft midline where the divergence of the faint medial supracondylar line and the pronounced lateral supracondylar line occurs. This orientation of the linea aspera was not matched in any of the compared specimens. The lateral supracondylar line presents a pronounced ridge. The femur shaft is only slightly anteriorly convex when viewed laterally and is similar in this regard to ZKD Femur 4. It is much less convex than BOU-VP-2/15. The minimum shaft breadth on BOU-VP-1/75 occurs distally, at the approximate level of the divergence of the supracondylar lines.

BOU-VP-2/15

PRESERVATION Femur BOU-VP-2/15 (Plate 16.2) preserves the shaft starting proximally from the superior part of the spiral line and ending distally at the position of the diverging supracondylar lines. The proximal break occurs distal to the lesser trochanter and neck, but the specimen preserves most of the gluteal line. The distal break occurs at the point where the femur begins to widen toward the condyles. A clean transverse break separates the distal shaft from the proximal shaft, allowing observation of the cross section (Plate 16.3). Heavy abrasion and pitting occur on the anterior and lateral aspects of the proximal fragment. Most of the rest of the bone surface is well preserved, and the linea aspera and the gluteal line are readily observable.

DISTORTION None.

DESCRIPTION Because of the heavy weathering and pitting of the proximolateral shaft, platymery is not precisely measurable. However, the subtrochanteric cross section is certainly platymeric, similar to OH 28 in expression. Most of the gluteal line is observable, but the bone lateral to it is weathered heavily, and it is not clear whether the gluteal region would have projected laterally or possessed a hypertrochanteric fossa. The spiral line is present and runs from the posteromedial margin of the proximal break to join the gluteal tuberosity in

EBSCOhost - printed on 10/28/2022 4:53 AM via . All use subject to https://www.ebsco.com/terms-of-use

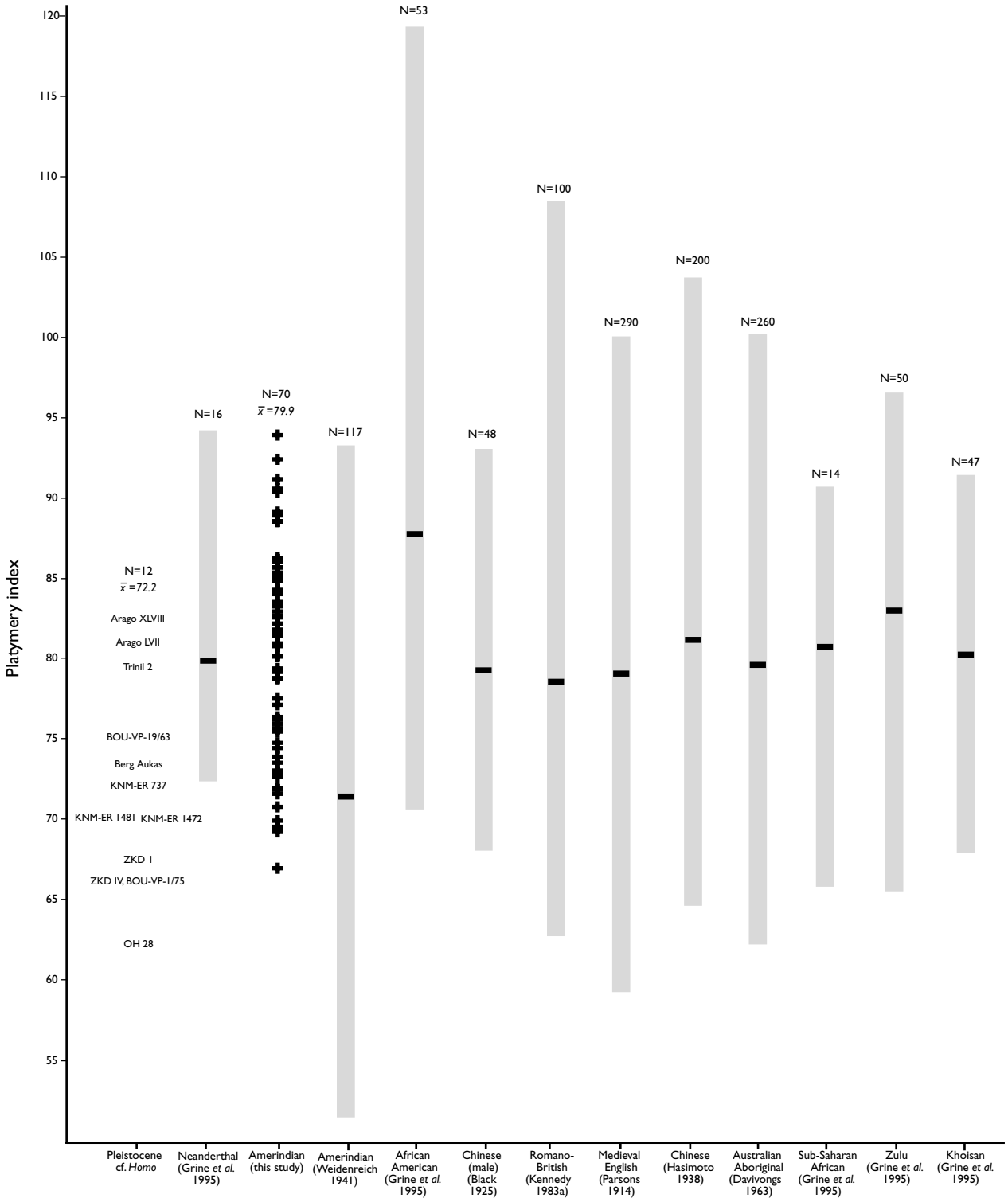

FIGURE 16.3

Platymery index scores for early Pleistocene *Homo* specimens and various populations of *Homo sapiens.* Specimen numbers of Pleistocene *Homo* specimens are placed at the level of their respective platymery index scores. Crosses (✚) represent individual Amerindian specimens measured in this analysis (see Section 16.2 for details on the PAHMA Amerindian sample). For other groups, vertical gray bars represent the range of scores and black horizontal lines represent the average for the group.

EBSCOhost - printed on 10/28/2022 4:53 AM via . All use subject to https://www.ebsco.com/terms-of-use

a highly rugose junction that extends approximately 40 mm from the proximal end of the linea aspera. The pectineal line is visible at the proximal end of this rugosity.

The femoral shaft is convex anteriorly. This curvature is similar in degree to OH 28, KNM-ER 737, and KNM-ER 1481. The linea aspera is positioned medial to the midline of the femur shaft, approximately one-third of the distance from the medial shaft margin to the lateral shaft margin, for its entire course down the shaft. Its position is more medial than in any of the specimens compared, including OH 28, which also has a medially positioned linea aspera. Femur BOU-VP-2/15 does not have a pronounced pilaster beneath the linea aspera. Again, this condition is similar to that observable in OH 28, but there is even less evidence of a pilaster in the Daka specimen. The portion of linea aspera distal to the transverse break is less distinct than that proximal to the break. The cross section of the BOU-VP-2/15 shaft is observable at the point of the break (Plate 16.2). Cortical thicknesses in this Daka femur are similar to other Pleistocene *Homo* specimens measured by Kennedy (1983a) and markedly larger than reported for *H. sapiens* (see Appendix 16.3). The medial cortex of BOU-VP-2/15 is thicker than the lateral cortex (Appendix 16.3), a relationship common in many *H. erectus* specimens and rare in modern humans (Kennedy 1983a). The minimum mediolateral breadth of BOU-VP-2/15 occurs distal to the midshaft.

BOU-VP-19/63

PRESERVATION Femur BOU-VP-19/63 (Plates 16.4, 16.5 and 16.6) preserves the shaft and lateral condyle. The specimen is broken just below the lesser trochanter, and the portion proximal to the break is absent. The bone surface is reasonably well preserved, but there is slight weathering on the shaft that likely occurred when the fossil was exposed by erosion. A large transverse break occurs slightly proximal to the midshaft. The cross section of the femur shaft is visible in this break (Plate 16.6). Some bone loss occurs along the lateral margin of the lateral condylar surface, exposing trabecular bone.

DISTORTION When viewed anteriorly, the shaft is somewhat convex medially. The apex of this convexity occurs at the level of the break, and a small part of the convexity is judged to be due to distortion caused by mineral matrix growth across the midshaft break.

DESCRIPTION Femur BOU-VP-19/63 is very anteverted, more so even than BOU-VP-1/75. The subtrochanteric cross section is platymeric, but not as platymeric as BOU-VP-1/75 (see Figure 16.3). As with BOU-VP-1/75, there is a torus-like medial shaft margin. The spiral line is present and well defined. The pectineal line is faint. The gluteal line is extremely rugose, and presents a crested ridge proximal and lateral to its intersection with the spiral line. There is a deeper hypertrochanteric fossa than is seen in BOU-VP-1/75, and there is a lateral expansion of the shaft margin adjacent to it, also more prominent than in BOU-VP-1/75. The prominence of the gluteal line and the adjacent concavity is similar to what is seen in Arago LVII, but even more pronounced.

The linea aspera is well defined, and it occurs on a relatively pronounced pilaster, especially proximally. As in BOU-VP-1/75, the linea aspera runs along the medial margin of the proximal femur and trends medially as it courses distally. Cortical thickness

EBSCOhost - printed on 10/28/2022 4:53 AM via . All use subject to https://www.ebsco.com/terms-of-use

PLATE 16.1

Femur BOU-VP-1/75.
A. Anterior view. B. Medial view. C. Posterior view.
D. Lateral view.

PLATE 16.2

Femur BOU-VP-2/15. A. Posterior view. B. Lateral view. C. Anterior view. D. Medial view.

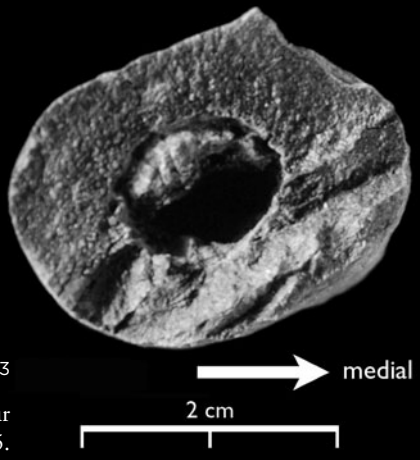

PLATE 16.3

Cross section of femur BOU-VP-2/15.

PLATE 16.4

Femur BOU-VP-19/63.
A. Anterior view. B. Medial view. C. Posterior view.
D. Lateral view.

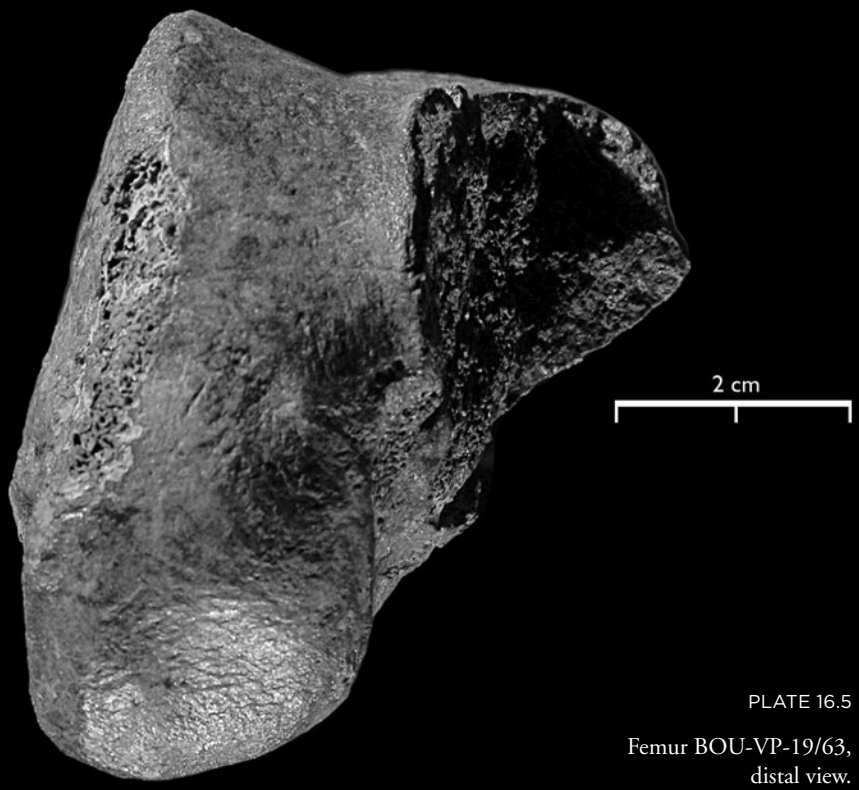

PLATE 16.5

Femur BOU-VP-19/63, distal view.

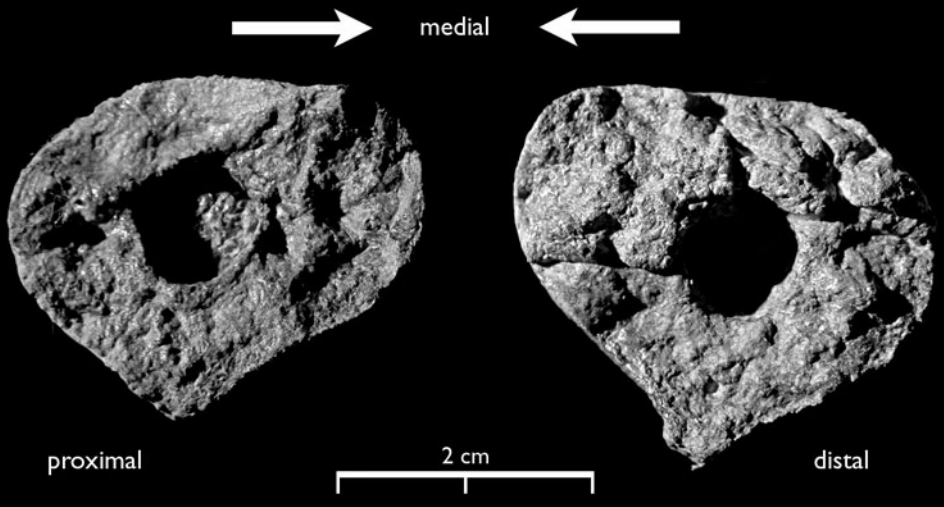

PLATE 16.6

Cross section of femur BOU-VP-19/63.

PLATE 16.7

Comparison of BOU-VP-1/75 (center) with other Pleistocene *Homo* femora, posterior view. A. Zhoukoudian femur 4. B. Trinil Femur 2. C. BOU-VP-1/75. D. KNM-ER 737. E. OH 28. All specimens except BOU-VP-1/75 are casts.

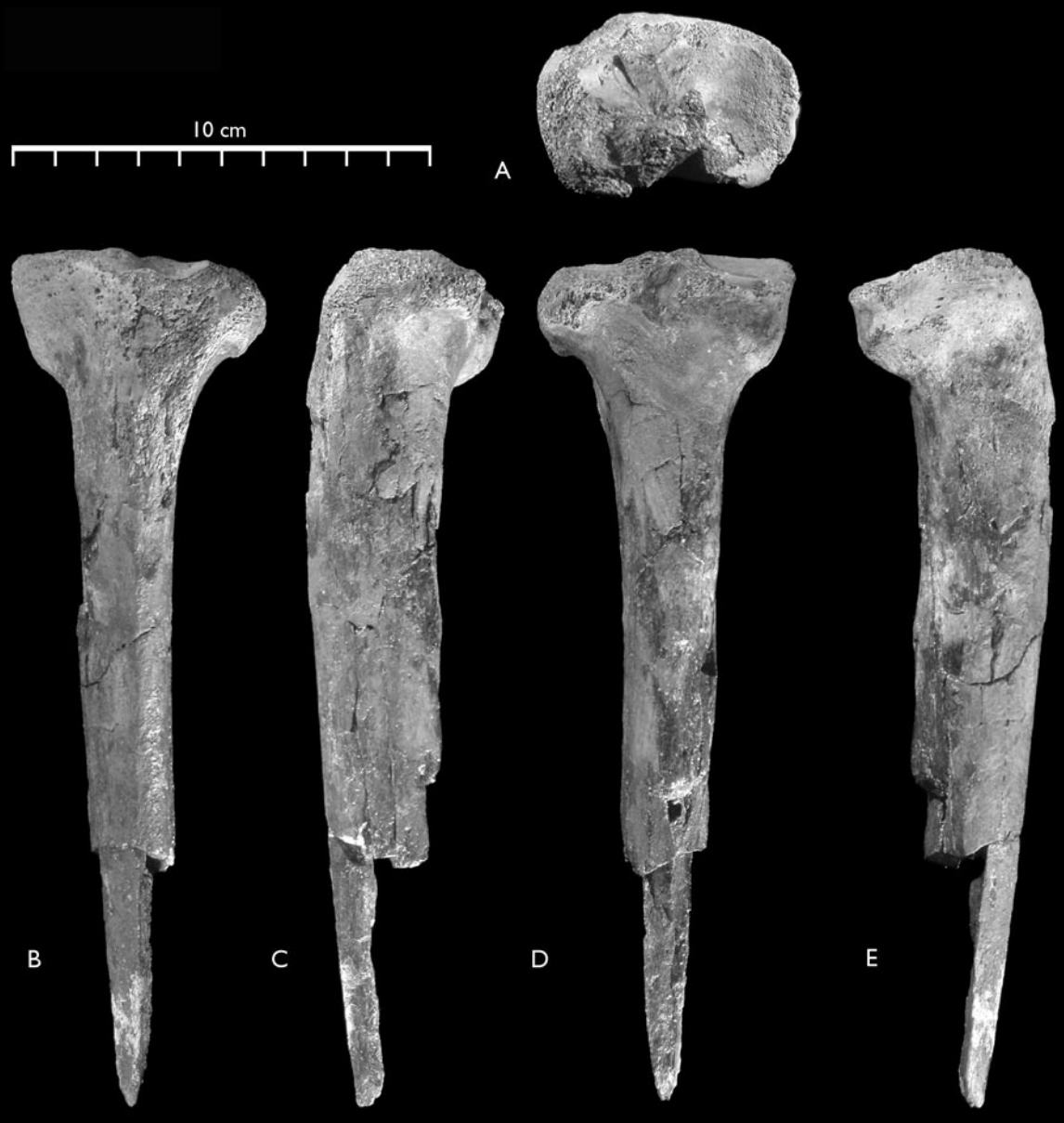

PLATE 16.8

Tibia BOU-VP-1/109. A. Proximal view. B. Anterior view. C. Lateral view. D. Posterior view. E. Medial view.

in BOU-VP-19/63 is pronounced. Medial and lateral cortices at the midshaft level are thicker than in any Pleistocene specimen reported by Kennedy (1983a). The cortex is thicker medially than laterally (Appendix 16.3). The lateral supracondylar line presents a pronounced ridge that takes a sigmoid course as it passes distally toward the condyle. The femur shaft is only slightly anteriorly convex when viewed from a lateral perspective. The minimum shaft breadth occurs distally, at the approximate level of the divergence of the supracondylar lines. The lateral condyle of BOU-VP-19/63, with a maximum anteroposterior dimension of 64.5 mm, does not differ markedly from modern humans in overall shape or popliteal groove morphology.

Femur Comparative Analysis

Appendix 16.2 presents the scores assigned to the Daka femora for the features presented in Appendix 16.1. Two of these features, the hypertrochanteric fossa and the lateral expansion of the gluteal tuberosity, are illustrated in Figure 16.2. Many of the features commonly associated with early Pleistocene *Homo* femora are ubiquitous in the Amerindian sample. Conversely, many early Pleistocene *Homo* specimens do not express these features. The following sections present each of these features and discuss their distribution in the sample observed. Where possible, data from the literature are incorporated into the discussions.

Platymery

Platymery (anteroposterior shaft flattening) has long been suggested to characterize *Homo erectus* (Weidenreich 1941). The early Pleistocene *Homo* specimens analyzed here have a lower average platymery index score (more exaggerated platymery) than the Amerindian sample analyzed and any of the *H. sapiens* sample averages presented in Figure 16.3, but the range of individual scores overlaps considerably. All three Daka Member femora have anteroposteriorly flattened (platymeric) shafts. For BOU-VP-2/15, which did not preserve enough of the proximal shaft to be measured accurately, this assessment was made by observation of the preserved proximal end. Metric assessment of platymery on the other femurs was made by obtaining the anteroposterior and mediolateral dimensions of femur shafts at the transverse level of the point at which the inferior margin of the lesser trochanter becomes flush with the femur shaft. Following other authors (Kennedy 1983a; Grine et al. 1995), an index was derived by dividing the anteroposterior dimension by the mediolateral dimension and multiplying the product by 100. Within the early Pleistocene *Homo* sample, only OH 28 (index of 62.3) is more platymeric than BOU-VP-1/75 (index of 66.2), although the ZKD Femur 4 (index of 66.2) presents an equivalent platymery index score. Femur BOU-VP-19/63 is less platymeric than most other early Pleistocene *Homo* femora in the sample. In general, early Pleistocene *Homo* femora present high platymery relative to *H. sapiens*. However, all of the platymery index scores reported for early Pleistocene *Homo* fall within the overall *H. sapiens* range (see Figure 16.3). Further, some *H. sapiens* populations present significantly increased incidences of femoral platymery and its associated morphology (Lovejoy and Heiple 1972; Lovejoy 1975; Kennedy 1983a; Gilbert and Gill 1990; Grine et al. 1995; Lovejoy et al. 2002), including both the Amerindian sample analyzed here and that reported by Gilbert and

EBSCOhost - printed on 10/28/2022 4:53 AM via . All use subject to https://www.ebsco.com/terms-of-use

Gill (1990). While Pleistocene hominid femora do express platymery index scores comparable to the more platymeric end of the Amerindian range, the overlap is substantial. Pronounced platymery cannot be considered a definitive feature of early Pleistocene *Homo*.

Linea Aspera Pilaster

Several authors discuss the lack of a linea aspera pilaster in early Pleistocene *Homo* (Kennedy 1983a, 1984; Grine et al. 1995). The term refers to the triangular column of bone underlying the linea aspera that gives the femur its characteristic teardrop shape in cross-section. This feature is present in all of the modern *H. sapiens* observed (13 percent have a moderate pilaster and 87 percent have a strong one), but it is much less common in early Pleistocene *Homo*. Of the early Pleistocene *Homo* sample, 31 percent of the specimens had no pilaster, 54 percent had a moderate pilaster, and 15 percent had a strong pilaster. The lack of a linea aspera pilaster is thus useful in differentiating many early Pleistocene *Homo* from *H. sapiens*. Of the Daka specimens, BOU-VP-2/15 lacks a pilaster, BOU-VP-1/75 has a moderate pilaster, and BOU-VP-19/63 has a strong pilaster.

Linea Aspera Position

The linea aspera is approximately centered on the posterior femur shaft in most (85 percent) *Homo sapiens* specimens observed, but in fewer than half of the early Pleistocene *Homo* specimens (44 percent). Whereas there is no clear trend of medial versus lateral displacement, mediolateral positioning of the linea aspera is more variable in early Pleistocene *Homo*. Of the Daka specimens, BOU-VP-2/15 has a linea aspera that is positioned medially relative to the femur shaft midline, whereas both the BOU-VP-1/75 and BOU-VP-19/63 lineae are set lateral to the midline.

Cortical Thickness

Femur shaft cortices in *Homo erectus* were recognized early as being relatively thick (Weidenreich 1941). Two observations were made regarding cortical thickness: the overall cortical thickness and the medial cortical thickness relative to the lateral cortical thickness. Daka femur cortical thicknesses are compared to metrics taken from Kennedy (1983a) in Appendix 16.3. Both measurable Daka femora had cortical thicknesses significantly higher than the *H. sapiens* average and similar to the early Pleistocene *Homo* femora. In fact, BOU-VP-19/63 has a cortex thicker than any early Pleistocene *Homo* in Kennedy's sample. Both measurable Daka femora, BOU-VP-2/15 and BOU-VP-19/63, have a thicker medial cortex than lateral cortex.

Position of Minimum Shaft Breadth

A distal position of minimum shaft breadth has been suggested to be a characteristic of *Homo erectus* femora (Weidenreich 1941; Day 1971; Kennedy 1983a). Over 50 percent of the early Pleistocene *Homo* femora studied have minimum shaft breadths that occur significantly distal to the midshaft. Nearly all of the Amerindian femora have minimum breadths

EBSCOhost - printed on 10/28/2022 4:53 AM via . All use subject to https://www.ebsco.com/terms-of-use

very close to the midshaft, and none of them have minimum breadths that occur distal to the midshaft. All three Daka femora have minimum shaft breadths that occur distal to the midshaft. This feature is one of the most consistently different between observed early Pleistocene *Homo* and *Homo sapiens*.

Anteversion

Anteversion is defined here as anterior torsion of the femoral neck axis with reference to the line defined by the most posterior surfaces of the femoral condyles. Anteverted femora present torsion along the entire shaft. In an anteverted femur, the medial portion of the distal femur is rotated posteriorly and laterally so that it forms an angle with the plane defined by the head and trochanters. Anteversion is easily assessed by placing the femur on a flat surface so that the head and trochanters are horizontal and then observing the orientation of the distal portion. Of the early Pleistocene *Homo* femora, 67 percent presented anteverted femora, as did 96 percent of the Amerindian femora. Both Daka specimens that could be assessed for the feature, BOU-VP-1/75 and BOU-VP-19/63, were anteverted.

Lateral Supracondylar Line

The lateral supracondylar line was not present in most (57 percent) of the early Pleistocene *Homo* specimens, but was present in almost all (99 percent) of the Amerindian sample. Both Daka specimens that could be assessed for the feature, BOU-VP-1/75 and BOU-VP-19/63, possessed a lateral supracondylar line.

Lateral Expansion of the Gluteal Tuberosity

This feature, illustrated in Figure 16.2, refers to the presence of a lateral bulge on the femur shaft adjacent to the hypertrochanteric fossa and associated with the gluteal tuberosity. Termed the "angulus lateralis superior" by Klaatsch (1901), it is mentioned by Weidenreich (1941), Day (1971), and Lovejoy et al. (2002). Most of the early Pleistocene *Homo* specimens (75 percent) and the Amerindian sample (83 percent) retain this feature. Both Daka specimens that could be assessed for this feature, BOU-VP-1/75 and BOU-VP-19/63, presented it.

Hypertrochanteric Fossa

This feature, also illustrated in Figure 16.2, refers to a depressed area located within the gluteal tuberosity (see Lovejoy et al. 2002 for discussion). Most of the early Pleistocene *Homo* specimens (64 percent) and the Amerindian sample (70 percent) retain this feature. Lovejoy et al. (2002) suggest that this feature is associated with platymery. Both Daka specimens that could be assessed for a hypertrochanteric fossa, BOU-VP-1/75 and BOU-VP-19/63, presented it.

Discussion

All of the Daka femora are platymeric and anteverted. Femoral platymery and anteversion are very likely associated with habitual postures that influence the developing femur. Growth plates have been shown to be responsive to transarticular forces during

EBSCOhost - printed on 10/28/2022 4:53 AM via . All use subject to https://www.ebsco.com/terms-of-use

development (i.e., those across the synchondrosis) and appear to underlie such phenomena as the bicondylar angle. Torsional forces, induced by habitual postures, seem likely to have similar effects (Lovejoy, personal communication). Anteversion is pronounced in femora of many Amerindian populations but minimal in contemporary European populations (Lovejoy et al. 2002). It is therefore possible that these morphological features are associated with habitual postures, possibly squatting, in both Amerindian populations and in early Pleistocene *Homo*. Platymery and anteversion are thus inappropriate for use in phylogenetic inquiry (see Lovejoy 2005).

In the sample analyzed, some features are common among early Pleistocene *Homo* specimens and very rare in *H. sapiens*. These features include a minimum shaft breadth that occurs distal to the femur midshaft and the lack of a pilaster underlying the linea aspera. An extremely thick cortex that is thicker medially than laterally is also associated with early Pleistocene *Homo* (Kennedy 1983a). The Daka femora express these features variably. With no pilaster, a distal position of minimum shaft breadth, and a thick cortex that is thicker medially, BOU-VP-2/15 presents all of the salient features of early Pleistocene *Homo*. Specimen BOU-VP-1/75 has a distal position of minimum shaft breadth but has not been assessed for cortical thickness and does retain a moderate linea aspera pilaster. Specimen BOU-VP-19/63, with a distally positioned minimum shaft breadth and extremely thick cortex that is thicker medially, presents most of the salient features but also presents a strong linea aspera pilaster. While two of the Daka femora present a linea aspera pilaster, this does not separate them from the overall early Pleistocene sample. Although all *H. sapiens* analyzed have a pilaster, only 31 percent of the early Pleistocene *Homo* specimens observed lacked it. Based on morphology, including size (Plate 16.7), the Daka femora fit well in the larger sample of early Pleistocene *Homo* femora. Additionally, they support the hypotheses that a minimum shaft breadth distal to the femoral midshaft, an overall thick femur shaft cortex, and a cortex that is thicker medially than laterally are characteristic of early Pleistocene *Homo*.

Other Postcranial Elements

Tibia

Tibia BOU-VP-1/109 (Plate 16.8) is incomplete and weathered and retains little morphological data. What morphology it has is compared here to several early Pleistocene tibiae. Specimens KNM-ER 803b, KNM-ER 741, and KNM-ER 1476 date to between approximately 1.4 and 1.6 Ma, and specimens KNM-ER 1471 and KNM-ER 1481c come from below the 1.9 Ma KBS tuff (Leakey et al. 1978; Feibel et al. 1989). These specimens cannot be certainly attributed to *Homo*. The other prehistoric comparative specimen observed, the Kabwe tibia, is not well dated, but it is generally agreed to be of later early Pleistocene or middle Pleistocene age (Avery 2003).

Many differences between human and chimpanzee tibiae are notable, but divergence in shape between the tibiae of various *Homo* species, all advanced bipeds, is subtler. Davis (1964) suggests that many features of early hominid tibiae differ from those in modern humans, but Lovejoy (1975) emphasizes that the features Davis cites are highly variable in humans and that early hominid tibiae and *H. sapiens* tibiae are very similar overall.

EBSCOhost - printed on 10/28/2022 4:53 AM via . All use subject to https://www.ebsco.com/terms-of-use

Stringer et al. (1998) reiterate several of the features cited by Davis in their description of the Boxgrove tibia, describing rounded shaft margins, a convex anterolateral shaft surface, and diminished concavities between various crests on the tibia as distinctive of Pleistocene *Homo* relative to *H. sapiens*. They additionally note that a distinct "tibial pilaster" (a vertically oriented crest on the posterior shaft) is characteristic of many specimens from Koobi Fora (KNM-ER 741, 803b, 1471, and 1476) and that of the Boxgrove tibia. Stringer et al. (1998), however, caution that it is unclear whether species-level taxonomic assignment of the Boxgrove tibia is possible.

PRESERVATION Tibia BOU-VP-1/109 preserves the proximal end of a left hominid tibia. The tibial plateau is relatively well preserved. The entire medial condylar surface is intact, while the lateral portion of the lateral condylar surface is eroded, exposing trabecular bone. Both the medial and lateral intercondylar tubercles are broken at their bases. The superior fibular articular facet is present. The tibial tuberosity is missing, and the associated cortical spalling runs from the tibial plateau approximately 55 mm along the anterior shaft. Approximately 145 mm of the proximal shaft is present. The shaft's anterior and lateral surfaces are relatively well preserved, but its medial and posterior surfaces exhibit considerable erosion and spalling of cortical bone. A 71 mm by 10 mm shaft fragment connects to the anterolateral aspect of the preserved shaft.

DISTORTION None.

DESCRIPTION The medial condyle of BOU-VP-1/109 is less concave than those of KNM-ER 1471 and 1481c and is more similar to that of KNM-ER 741. The fibular articular facet is present beneath the posterior portion of the eroded lateral condyle. Weathering prevents detailed observation of the posterior shaft surface. The Daka tibia presents a rounded anterior crest, and both anteromedial and anterolateral proximal shaft surfaces are slightly convex just distal to where the tibial tuberosity would have been. This condition is similar to that seen in the Kabwe tibia but differs markedly from KNM-ER 741 and KNM-ER 1476b, in which the shaft surfaces medially and laterally adjacent to the proximal portion of the anterior crest are concave. It also differs from KNM-ER 1481b and KNM-ER 1471, where shafts are concave medial to the proximal portion of the anterior crest, but convex lateral to it. Topography of the posterior shaft is not observable because of exfoliation of the surface, but what morphology is present does not exclude the possibility of a "tibial pilaster." A slightly raised line marks the interosseous crest. Specimen KNM-ER 1471 is very similar to the Daka fossil, bearing a subtle interosseous crest. Shaft specimen KNM-ER 803 also has a slight interosseous crest, as do KNM-ER 1476b, KNM-ER 1481c, and KNM-ER 741. The Kabwe tibia has a subtler interosseous crest with no pilaster.

Modern human tibiae vary considerably in all of the features discussed in this section (see Lovejoy 1975 for a discussion of Plio-Pleistocene hominid and *Homo sapiens* tibia morphology). Without a larger sample of complete Pleistocene *Homo* tibiae, little can be done to distinguish phyletically meaningful features. In summary, BOU-VP-1/109 is similar to other early Pleistocene *Homo* tibiae but does not present enough morphology to provide additional bases for differentiating early Pleistocene *Homo* tibiae from those of *H. sapiens*.

EBSCOhost - printed on 10/28/2022 4:53 AM via . All use subject to https://www.ebsco.com/terms-of-use

Talus

Specimen BOU-VP-2/95 preserves the body, neck, and head of a hominid talus. The trochlea and articular surface of the head are heavily eroded, exposing trabecular bone. This specimen was recovered recently (2005), and its fragility and the rigidity of the matrix encasing it have prohibited it from being cleaned and studied in time for the publication of this volume. It is, however, an important specimen because so few other specimens of early Pleistocene *Homo* tali are available.

Conclusions

The Daka Member hominid postcranial specimens add considerably to the relatively small sample of early Pleistocene hominid tibia and femora. The three Daka Member femora are similar to other contemporary specimens and corroborate the utility of three important features that distinguish early Pleistocene *Homo* from *H. sapiens*: the distal position of minimum femoral shaft breadth, the presence of very thick femoral shaft cortical bone, and the tendency for the medial shaft cortex to be thicker than the lateral shaft cortex. The Daka femora are platymeric and anteverted, which may indicate that the Daka hominids engaged in habitual squatting. The Daka tibia is similar to known early Pleistocene hominid and modern human tibiae. Whereas it does not provide any particular insight into phylogeny or biomechanics, it does add significantly to the very small sample of early Pleistocene hominid tibiae.

EBSCOhost - printed on 10/28/2022 4:53 AM via . All use subject to https://www.ebsco.com/terms-of-use

EBSCOhost - printed on 10/28/2022 4:53 AM via . All use subject to https://www.ebsco.com/terms-of-use

APPENDIX 16.1 Descriptions of Features and Scoring Procedure Applied to Compared Femora, and Distributions of Scores in Pleistocene *Homo* and Amerindian Samples

			Pleistocene cf. Homo Average Scores				*Amerindian Average Scores*			
Feature	*Description*	*Scoring*	N	0	1	2	N	0	1	2
Platymery index score	(Anteroposterior subtrochanteric cross section dimeter ÷ mediolateral subtrochanteric cross section diameter) × 100	0: <75 1: 75–85 2: 85	11	54.5%	36.4%	9.0%	70	25.7%	51.4%	22.9%
Linea aspera pilaster	Pedestal of cortical bone underlying linea aspera (note that this is not the robusticity of the linea aspera itself)	0: none 1: moderate 2: robust	13	30.8%	53.8%	15.4%	70	0.0%	12.9%	87.1%
Linea aspera position (medial or lateral)	General position of linea aspera along its entire course relative to the midline of the femur shaft	0: medial 1: midline 2: lateral	9	22.2%	44.4%	33.3%	69	1.4%	85.5%	13.0%
Cortical thickness (medial vs. lateral)	Thickness of femur shaft cortex (measured at approximate midshaft)	0: medial is thicker 1: equal 2: lateral is thicker	7	85.7%	0.0%	14.3%	5	20.0%	20.0%	60.0%
Position of minimum shaft breadth	Proximodistal position of minimum shaft breadth	0: distal to midshaft 1: at approximate midshaft 2: proximal to midshaft	10	60.0%	40.0%	0.0%	69	0.0%	97.1%	2.9%
Anteversion	Anterior torsion of the femoral neck axis with reference to the distal femur. Assessed by placing femoral neck axis on flat surface and observing orientation of condyles	0: anteverted 1: not anteverted	9	66.7%	33.3%	—	69	95.7%	4.3%	—
Lateral supracondylar line	Palpable lateral supracondylar line	0: absent 1: present	7	57.1%	42.9%	—	70	1.4%	98.6%	—
Lateral expansion of the gluteal tuberosity	Notable lateral torus-like expansion of the gluteal tuberosity (see Figure 16.5B)	0: absent 1: present	12	25.0%	75.0%	—	70	17.1%	82.9%	—
Hypertrochanteric fossa	Notable concavity on gluteal tuberosity (see Figure 16.2)	0: absent 1: present	11	36.4%	63.6%	—	70	30.0%	70.0%	—

APPENDIX 16.2 Measurements and Observations Made on Analyzed Femora

Specimen	*Sub-Trochanteric Shaft Cross Section (AP)*	*Sub-Trochanteric Shaft Cross Section (ML)*	*Platymery Index*	*Platymery Index Score*	*Linea Aspera Pilaster*	*Linea Aspera ML Position*
BOU-VP-1/75	26.4	39.9	66.2	0	1	2
BOU-VP-2/15				?	0	0
BOU-VP-19/63	27.4	36.5	75.1	2	2	2
KNM-ER 737	26	36	72.2	0	1	1
KNM-ER 803				?	2	0
KNM-ER 1472	21.8	31.4	69.4	0	0	2
KNM-ER 1481	22	31.3	70.3	0	1	1
OH 28	23.3	37.4	62.3	0	0	1
ZKD 1	23.2	34.3	67.6	0	1	?
ZKD 4	22.7	34.3	66.2	0	0	?
Arago XLVIII	28.5	34.5	82.6	1	1	?
Arago LVII	29.9	36.9	81.0	1	1	?
Trinil Femur 2	26.04	32.7	79.6	1	1	1
PAHMA Specimen Number						
1601	25.6	32.38	79.1	1	2	1
1623 A	25.81	31.44	82.1	1	2	1
1739	28.1	37.2	75.5	1	2	1
1740	27.7	36.52	75.8	1	2	1
3517	29.1	35.3	82.4	1	2	1
5528	22.15	33.15	66.8	0	2	1
5283	24.4	30	81.3	1	2	1
5527	25.9	34.3	75.5	1	2	2
5525	21.93	30.13	72.8	0	2	1
5531	24.5	35.3	69.4	0	1	1
5532	25.5	30.4	83.9	1	1	1
5530	25.3	35.8	70.7	0	2	2
5526	26.1	31.4	83.1	1	2	1
5519	22.1	29.6	74.7	0	2	1
5670	24.4	30	81.3	1	2	1
5669	24.4	32	76.3	1	2	1
5677	27.8	32.7	85.0	2	2	1
5679	26.5	31.5	84.1	1	2	2
5682	27.1	32.6	83.1	1	2	1
5845	28.7	31.1	92.3	2	2	1
5842	26.8	31.1	86.2	2	2	1
5808	30.3	36	84.2	1	1	1
5686	28.7	38.1	75.3	1	2	1
5811	28.4	35.2	80.7	1	1	1
5854	28.5	33.3	85.6	2	2	1
5861	25.3	31.3	80.8	1	2	1
5864	28.8	36	80.0	1	2	1
5847	25.5	35.5	71.8	0	2	1
5848	23.9	32.4	73.8	0	2	1
5856	27.4	33.2	82.5	1	1	?
5866	24.4	28.4	85.9	2	2	1

EBSCOhost - printed on 10/28/2022 4:53 AM via . All use subject to https://www.ebsco.com/terms-of-use

Cortical Thickness (Medial vs. Lateral)	*Position of Minimum Shaft Breadth*	*Ante-Version*	*Lateral Supra-Condylar Line*	*Lateral Expansion of the Gluteal Tuberosity*	*Hyper-Trochanteric Fossa*
?	0	0	1	1	1
0	0	?	?	?	?
0	0	0	1	1	1
0	1	0	0	1	1
2	0	0	0	1	?
?	1	1	1	0	0
0	1	0	0	1	1
0	0	0	0	1	1
?	?	?	?	1	0
?	0	1	?	0	0
?	?	?	?	1	1
0	?	?	?	1	1
?	1	1	?	0	0

?	2	0	1	0	0
?	2	0	1	1	1
2	1	0	1	1	1
2	1	0	1	1	1
?	1	0	1	1	0
?	1	0	1	1	1
?	1	0	1	1	1
?	1	0	1	0	0
?	1	0	1	1	1
?	1	0	1	1	0
?	1	0	1	1	0
?	1	0	1	0	0
?	1	0	1	0	0
?	1	0	1	0	0
?	1	0	0	1	1
?	1	0	1	1	0
?	1	0	1	1	1
?	1	0	1	1	1
?	1	0	1	1	1
2	1	0	1	1	1
?	1	0	1	1	0
?	1	0	1	1	0
?	1	0	1	1	1
?	1	0	1	0	0
?	1	0	1	1	1
?	1	0	1	1	1
?	1	0	1	1	1
1	1	0	1	1	1
?	1	0	1	1	1
0	?	?	1	1	1
?	1	1	1	0	0

EBSCOhost - printed on 10/28/2022 4:53 AM via . All use subject to https://www.ebsco.com/terms-of-use

APPENDIX 16.2 *(continued)*

PAHMA Specimen Number	*Sub-Trochanteric Shaft Cross Section (AP)*	*Sub-Trochanteric Shaft Cross Section (ML)*	*Platymery Index*	*Platymery Index Score*	*Linea Aspera Pilaster*	*Linea Aspera ML Position*
5867	26.9	33	81.5	1	2	1
5869	27.1	31.8	85.2	2	2	1
5870	25	30.6	81.7	1	2	1
5871	28.4	35.5	80.0	1	2	2
5874	25.1	29.6	84.8	1	1	1
5875	27.8	35.9	77.4	1	2	2
5879	28.7	30.6	93.8	2	2	1
5700	26.1	29.4	88.8	2	2	1
5884 A	28.4	33	86.1	2	2	2
5884 B	26.4	32.7	80.7	1	2	1
5884	26.5	29.3	90.4	2	2	1
5924 B	26.4	32.4	81.5	1	2	1
5924 E	24.6	33.9	72.6	0	2	2
5924 A	26.1	34.3	76.1	1	2	1
5926 A	25.1	30.3	82.8	1	2	1
5926 B	26.1	32	81.6	1	2	0
5921 A	19.7	28.4	69.4	0	1	1
5921 B	25.4	34.6	73.4	0	2	1
5921 C	19.6	28.25	69.4	0	2	1
5921 D	25.6	32.3	79.3	1	2	2
5916	25.9	32.1	80.7	1	2	1
5916 A	23.9	34.6	69.1	0	2	2
5916 B	25.9	35.6	72.8	0	2	1
5916 D	25.1	32.6	77.0	1	2	1
5916 G	23.8	33.3	71.5	0	2	1
5916 I	24.6	34.3	71.7	0	2	1
5919	27.6	35.1	78.6	1	2	1
5919 A	26.9	29.8	90.3	2	2	1
5919 B	22.4	32.1	69.8	0	2	1
5919 C	28.5	33.3	85.6	2	2	1
5919 D	24	30.5	78.7	1	2	1
5919 E	29.1	32.7	89.0	2	2	1
5608	31.3	35.4	88.4	2	1	1
5610	24.4	28.8	84.7	1	2	1
5613	25.7	30.8	83.4	1	2	1
5614	36.24	39.8	91.1	2	2	1
5604 A	26	29.4	88.4	2	2	1
5598	24.6	33.1	74.3	0	2	1
5593	23.4	32.1	72.9	0	1	1

NOTE: Four-digit identification numbers for Amerindian specimens refer to specimen numbers in the Phoebe Apperson Hearst Museum of Anthropology, University of California, Berkeley. Measurements for KNM-ER 737, KNM-ER 1481, and Trinil 2 taken from Kennedy (1983a). Measurements for ZKD 1 and ZKD 4 taken from Weidenreich (1941). Measurements for OH 28 taken from Day (1971). Measurements for KNM-ER 1472 taken from McHenry and Corruccini (2006). Measurements for Arago XLVIII and Arago LVII taken from casts.

EBSCOhost - printed on 10/28/2022 4:53 AM via . All use subject to https://www.ebsco.com/terms-of-use

Cortical Thickness (Medial vs. Lateral)	*Position of Minimum Shaft Breadth*	*Ante-Version*	*Lateral Supra-Condylar Line*	*Lateral Expansion of the Gluteal Tuberosity*	*Hyper-Trochanteric Fossa*
?	1	0	1	1	1
?	1	0	1	1	0
?	1	0	1	1	0
?	1	0	1	1	1
?	1	0	1	1	1
?	1	0	1	1	1
?	1	0	1	0	1
?	1	1	1	1	1
?	1	0	1	0	0
?	1	0	1	1	0
?	1	0	1	1	1
?	1	1	1	1	1
?	1	0	1	1	1
?	1	0	1	1	1
?	1	0	1	1	1
?	1	0	1	1	1
?	1	0	1	1	1
?	1	0	1	1	1
?	1	0	1	1	1
?	1	0	1	1	1
?	1	0	1	1	1
?	1	0	1	1	1
?	1	0	1	1	1
?	1	0	1	1	1
?	1	0	1	0	1
?	1	0	1	0	0
?	1	0	1	1	1
?	1	0	1	1	0
?	1	0	1	1	1
?	1	0	1	1	1
?	1	0	1	1	0
?	1	0	1	1	1
?	1	0	1	1	1
?	1	0	1	0	0
?	1	0	1	1	1
?	1	0	1	1	1

EBSCOhost - printed on 10/28/2022 4:53 AM via . All use subject to https://www.ebsco.com/terms-of-use

APPENDIX 16.3 Comparative *Homo erectus* Femur Cortex Thicknesses (in Millimeters) at the Midshaft Level

Specimen	*Medial Cortex*	*Lateral Cortex*
Homo sapiens (Romano-British) males	7.95	8.27
Homo sapiens (Romano-British) females	7.11	7.03
Homo sapiens (San)	5.68	6.51
ZKD 1	11.5	9.5
ZKD 4	10.3	9.5
OH 28	9.2	6
KNM-ER 737	10.5	8.9
KNM-ER 803	6.2	7.2
KNM-ER 1481	11.5	7.2
BOU-VP-19/63	**13.6**	**10.4**
BOU-VP-2/15	**10.8**	**9.1**

NOTE: Daka metrics taken from specimens with natural transverse breaks near the midshaft level. Non-Daka metrics taken from Kennedy (1983a).

EBSCOhost - printed on 10/28/2022 4:53 AM via . All use subject to https://www.ebsco.com/terms-of-use

17

Ecological and Biogeographic Context of the Daka Member

W. HENRY GILBERT

Deposition of Daka Member fossil remains took place in noncyclothemic lenticular channels (de Heinzelin et al. 2000a). Several episodes of sedimentation are observable, and some paleosols occur in what appears to have been a large river/lake system. The geography of the study area at the time of Daka deposition, with its lakes, rivers, and adjacent subaerial depositional environments, will have had a strong effect on the composition of the faunal assemblage. The components of living communities that accrue into paleontological assemblages are highly biased because the latter are defined by a combination of hydrology and habitat. These geospatial effects are easily observed in the modern Middle Awash, where, for example, *Kobus* (Figure 17.1) is abundant along the modern Awash River floodplain, whereas *Oryx* (Figure 17.2) is more abundant on the desiccated highlands of the immediately adjacent Central Awash Complex. These extant mammalian assemblages are synchronic, but the fossil record presently forming will incorporate abundant *Kobus* and virtually no *Oryx*.

Additionally, large rivers can carry bones for some distance prior to depositing them, and depositional systems potentially sample extended time periods. Large river systems mix remains of mammals preferring different habitats from different time periods, further blurring the paleontological "community," which, in fact, is a fossil assemblage partially sampling several different habitats over an extended time period. This effect becomes clear when one observes the area at the southeast tip of the Bouri Peninsula from an airplane (Figure 17.3). Both xeric scrub and swampy floodplain occur within one kilometer of each other, and the two will be taphonomically intermingled. Fossil assemblages therefore may not be directly equated with temporally uniform, habitat-circumscribed communities or ecosystems. Assemblages from the African Rift Valley, including the Daka Member (see faunal list, Table 1.2), are better equated with fluvial catchments sampled across long time periods in a nonrandom manner.

Biogeography

Geographic distributions of fossilized and recent taxa can be used to illuminate prehistoric connections between geographic regions. Several geographic levels of inquiry are

EBSCOhost - printed on 10/28/2022 4:53 AM via . All use subject to https://www.ebsco.com/terms-of-use

FIGURE 17.1
Herds of modern *Kobus* at the tip of the Bouri Peninsula, Middle Awash study area, Ethiopia. Predation by large felids in such habitats along the modern Awash River creates death assemblages mixing reduncine, alcelaphine bovids, and equids, much as is evidenced in the Pleistocene deposits of the Daka Member. Photograph by Tim White, December 21, 1997.

possible, ranging from continent-wide migrations to differences among localities in a single region. This section focuses the Daka data on three of these: continental provinciality within the eastern hemisphere, regional endemism within sub-Saharan Africa, and locality-level endemism within eastern Africa. This discussion is limited to genera because these form the most comparable units, given inconsistencies between published studies in species identifications.

Continental Provinciality

The continental zoogeographical realms outlined by Wallace (1880) are still used today (Spellerberg and Sawyer 1999). Wallace divided the Old World into the Palaearctic, Oriental, and Ethiopian realms. The Palaearctic realm includes all of Asia north of the Himalayas, Europe, North Africa, and northern Arabia. The Oriental realm extends from the Hindu Kush Mountains of Pakistan across India and southeast Asia south of the Himalayas. The Ethiopian realm includes southern Arabia and sub-Saharan Africa. The Sahara separates the Ethiopian realm from the Palaearctic, and the two regions have distinctive faunas. The Sahara has fluctuated in aridity and latitudinal expanse over the Neogene (Le Houérou 1997; Nichol 1999) and appears to have existed since the late

EBSCOhost - printed on 10/28/2022 4:53 AM via . All use subject to https://www.ebsco.com/terms-of-use

FIGURE 17.2
Modern *Oryx (Oryx beisa)* in the Messalu zone of the Middle Awash study area, east of the Awash River. Photograph by Tim White, October 29, 1981.

Miocene (Schuster et al. 2006). During periods of glacial maxima it appears that the hyperarid zones of the Sahara expanded almost to the equator. During interglacial periods much of what is now desert was more savanna-like. Interchange between the Ethiopian and Palaearctic realms is documented and is hypothesized to have occurred during these moister intervals (Tchernov 1992; Pickford and Morales 1994; Vrba 1995a).

Two taxa with potential Palaearctic affinities are present in the Daka Member: *Bouria anngettyae*, a caprine, and *Nitidarcus asfawi*, a possible ovibovine. *B. anngettyae* is known only from the Daka Member, where it is well represented. Its phylogenetic position within Caprini is unresolved (Vrba 1997), so specific discussion of its geographic origins is not possible. Caprini's distribution is predominantly Palaearctic, and there are numerous endemic genera and species in that realm. Caprini's current non-domestic distribution in Africa is north of the Sahara, along the Red Sea coast, and in the Ethiopian highlands. Agriculture and pastoralism have profoundly affected its habitats in these areas (Kingdon 1989b), and modern caprine distributions in Africa are likely quite restricted. Caprini is poorly represented in African Pleistocene faunas, including those from northern Africa. Its ubiquity in the Daka Member may indicate the existence of Palaearctic interchange around Daka times, but until the position of *B. anngettyae* can be resolved, any connection is speculative.

EBSCOhost - printed on 10/28/2022 4:53 AM via . All use subject to https://www.ebsco.com/terms-of-use

FIGURE 17.3
Low-altitude aerial photograph across the southern tip of the Bouri Peninsula (light-colored, barren patch to left center of frame). View is to the southeast from above Yardi Lake. Abida caldera and the eastern slope of Ayelu Volcano form the right skyline. The main channel of the Awash River is seen at frame center, edged by a thin band of riverine forest trees and surrounded on both sides by swamps. A. Xeric dunes and scrubland. B. Swamp and gallery forest near channel of Awash River draining Yardi Lake. C. Marshland of Awash River floodplain. This kind of mosaic physical and biological setting is also indicated for Daka times. Video frame capture by Rod Paul, January 11, 2003.

Nitidarcus asfawi, also known only from the Daka Member, is provisionally referred to Ovibovini by Vrba (1997). Ovibovini has a modern distribution in Asia, and fossil ovibovines are known from numerous Old World localities, including many in Africa. Unfortunately, evolutionary relationships within this group are not well resolved (Vrba 1997), and the Daka fossils differ substantially from living and fossil forms. It is therefore not possible to hypothesize Palaearctic-Ethiopian interchange with any certainty on the basis of Daka fossils.

African Regional Endemism

Within modern Africa there are several areas with high proportions of endemic species (Kingdon 1989b). Two of the commonly recognized areas of high endemism occur near the modern Awash drainage: the Ethiopian highlands and the Somali arid region (Grubb et al. 1999). Both of these regions have numerous endemic taxa. The Somali arid region is separated from the arid region of southwestern Africa by broad savannas but connected via a narrow drought corridor (Grubb et al. 1999). During glacial maxima, a broad xeric band would have existed from the Horn of Africa to the southwestern coast, and during interglacial periods the southern savannas would have extended farther north, possibly forming corridors to the Palaearctic realm (Tchernov 1992; Le Houérou 1997; Nichol 1999).

Some genera represented in the Daka Member have modern distributions that do not extend as far north as the Awash drainage, although humans have impacted modern distributions. Among these are *Aepyceros*, *Connochaetes*, *Giraffa*, *Ceratotherium*, and *Syncerus*. It is likely that these groups ranged into the Afar Depression prior to human pastoralism, and no comparison can be safely made between the Daka Member and modern distributions that does not invoke human influence.

EBSCOhost - printed on 10/28/2022 4:53 AM via . All use subject to https://www.ebsco.com/terms-of-use

Some Daka taxa are restricted to, but widespread within, sub-Saharan Africa during the Pliocene and Pleistocene: *Aepyceros*, *Megalotragus*, *Numidocapra*, *Antidorcas*, *Syncerus*, and Colobinae. The previously discussed genera *Bouria* and *Nitidarcus* are known only from the Daka Member and are, by default, endemic exclusively to the Daka Member and eastern Africa.

Other Daka genera are more cosmopolitan and have modern or historic ranges that include sub-Saharan Africa as well as northern Africa and Eurasia. These taxa include *Homo*, *Elephas*, *Gazella*, *Oryx*, *Hippopotamus*, *Tragelaphus*, *Panthera*, *Equus*, and *Crocuta*. *Connochaetes* is restricted to Africa, but it ranged to northern Africa during the early Pleistocene.

A number of Daka genera were more broadly distributed during the Pliocene and Pleistocene. *Pelorovis*, *Gazella*, *Parmularius*, *Giraffa*, *Sivatherium*, *Oryx*, *Kobus*, *Tragelaphus*, *Crocuta*, *Panthera*, *Theropithecus*, *Equus*, *Hipparion*, *Hippopotamus*, *Ceratotherium*, *Metridiochoerus*, *Kolpochoerus*, and *Elephas* are also known from sites across Africa and southwestern Eurasia.

Daka Member Endemism among Eastern African Early Pleistocene Sites

Daka Member endemism may be assessed relative to other contemporaneous sites in eastern Africa that are rich enough to provide a reasonable signal. Unfortunately, there are very few rich, well-dated Daka-age localities. Because climate is known to have fluctuated rapidly and intensely in the Pliocene and Pleistocene (deMenocal and Bloemendal 1995), age equivalence is mandatory for meaningful comparison. Other sites close to this time horizon include the following: Olduvai Bed IV, dating to between 0.78 and 1.2 Ma (Tamrat et al. 1995); Tighenif, biochronologically estimated to the middle Pleistocene (Geraads et al. 1986); Aïn Maarouf, biochronologically estimated to the early middle Pleistocene (Geraads et al. 1992); Buia, dated to approximately 1.0 Ma using biochronology and paleomagnetism (Abbate et al. 1998); Olorgesailie Member 1, dated to between 0.974 and 0.992 Ma (Potts et al. 1999); Olorgesailie Member 10, dated to between 0.662 and 0.746 Ma (Potts et al. 1999); Kanjera North, biochronologically and paleomagnetically approximated to the later early Pleistocene or the earlier middle Pleistocene (Ditchfield et al. 1999); Thomas Quarries, biochronologically approximated to the early to middle Pleistocene transition (Raynal et al. 2001); West Turkana Nariokotome Member, dated to between approximately 0.78 and 1.4 Ma (Harris et al. 1988a); East Turkana Chari Member, dated to between approximately 0.78 and 1.4 Ma (McDougall 1985; McDougall et al. 1985); and Omo Member L, radiometrically dated to between approximately 1.0 and 1.4 Ma (Feibel et al. 1989).

Few of these units are as precisely dated as the Daka Member, and few are as rich, imposing limitations on the interpretive value of signaled endemism. Genera limited to the Daka Member among these sites during the later early Pleistocene include *Bouria*, *Nitidarcus*, *Oryx*, and *Sivatherium*. As discussed, *B. anngettyae* and *N. asfawi* are unknown from anywhere but the Daka Member. The single occurrence of *Oryx* in the Daka Member is likely a factor of sampling more than environment, for, as discussed previously, *Oryx* behavior thwarts fossilization. The Daka Member is richer and therefore bound to

EBSCOhost - printed on 10/28/2022 4:53 AM via . All use subject to https://www.ebsco.com/terms-of-use

produce a greater diversity of rare mammals than penecontemporaneous comparative localities. *Oryx* and *Sivatherium* have ranges that extend outside eastern Africa in earlier and later times. This makes it impossible to characterize the Daka Member as a region of any particular endemism with respect to other eastern African sites at around 1.0 Ma.

Paleoecology

An initial caveat for any prehistoric reconstruction is that ecological webs are unstable over time and space. Further, except in cases of evolved obligate mutualism, species associations are also unstable. Even some very recent prehistoric "communities" are without modern analogs (Stafford et al. 1999). This instability hinders accurate extrapolation of deposystem paleoenvironments. As a consequence, macroscopic assemblage comparisons must be interpreted conservatively, with the range of ecological preferences of each taxon requiring independent consideration.

While structural constraints of organisms do allow for projection of function back in time, caveats apply at this level also. Incrementally small phyletic changes may be correlated with serious ecological shifts. Even lineages presenting relative morphological stasis can vary significantly in their ecological roles through time, as illustrated by the numerous modern taxa that have changed subsistence modes in the face of urbanization without pronounced phenotypic change: coyotes, raccoons, pigeons, starlings, deer, and many more. Put simply, paleoenvironment can potentially fluctuate faster than evolutionary change is able to track it, and clades have likely been sorted for their resilience to such perturbations (see discussion in the following chapter). This caveat applies particularly to animals with wide habitat tolerances—these are particularly poor indicators of paleoenvironment. The narrower a taxon's geographic distribution and ecological niche, the more useful its presence for identifying paleoenvironment becomes. Again, each taxon in an assemblage should be treated individually.

Catchment Paleoecology

In this section, Daka Member vertebrate taxa are presented individually, usually by family. Some groups, such as carnivores, are treated with minimal detail. Conversely, the most diverse and specialized group, the bovids, is given more detailed treatment and is presented at the end of the section out of the taxonomic order generally observed in this volume. Relative abundance data for the Daka bovid fossils are compared to tribal abundances in modern African game parks. This analysis is susceptible to many of the taphonomic and representational challenges previously outlined, but some meaningful generalizations about the paleoenvironment of the Daka Member emerge.

Carnivora

Both felids from the Daka Member are broadly distributed and lack specific ecological needs other than a healthy population of prey animals and an occasional drink. The occurrence of *P.* cf. *leo* and *P.* cf. *pardus* indicates little more than the site's richness.

Exceeding the modern ranges of the felids in the Daka Member, historic and prehistoric *Crocuta* is very broadly distributed across space and ecological circumstances. At

EBSCOhost - printed on 10/28/2022 4:53 AM via . All use subject to https://www.ebsco.com/terms-of-use

the level of ecological resolution provided by the Daka Member, the presence of *Crocuta* indicates only the presence of ample prey.

Cercopithecidae

Two monkey taxa are known from the Daka Member: *Theropithecus oswaldi* and *Cercopithecoides alemayehui*. Modern *T. gelada* is primarily a grazer, eating grass rhizomes, seeds, and blades (Simons and Delson 1978). It supplements these with other herbs and will sometimes eat invertebrates such as termites if the opportunity presents itself (Nowak 1991; Iwamoto 1993). Modern *Theropithecus* is restricted to cool, wet turf in the Ethiopian Highlands. Thus, the genus is today represented only in isolated outposts of its former pan-African geographic range. In spite of this potentially confounding factor, many of the features diagnosing *Theropithecus* within Papionini have been associated with feeding on grasses by reference to modern *T. gelada* (Jablonski 1993), and late *T. oswaldi* representatives are extremely derived in these features. Grassland habitats occur in a variety of African contexts, and even if grazing is accepted as *T. oswaldi*'s primary feeding mode, it is not possible to know how restricted to grassland habitats this taxon was.

Modern African colobine genera are generally restricted to wooded biomes, but within these they occupy a number of habitats, ranging from deep, moist lowlands in central Africa to the Ethiopian highland forests. They also inhabit narrow arboreal galleries along perennial rivers in many arid regions (Oates 1994). The new Daka species *Cercopithecoides alemayehui* is not associated with postcranial material, so its degree of arboreality is not possible to address.

In summary, *Cercopithecoides alemayehui* in the Daka Member suggests the presence of trees. *Theropithecus oswaldi* suggests the existence of grasses, although *T. gelada* is likely an imperfect ecological analog of the larger prehistoric species. Both of these ecological components are present in gallery forests and riverine sumplands.

Equidae

Without a modern analog, Daka Member hipparionines are of limited use in reconstructing paleoenvironment. Modern *Equus* is distributed globally. Non-domesticated modern *Equus* species inhabit a variety of habitats, usually ones that are more marginal and arid than those inhabited by other herbivores (Nowak 1991). All *Equus* species are grazers, but they may occasionally browse and will even resort to bark and roots in lean times (Estes 1991; Nowak 1991). While not as efficient at extracting protein from rich plant sources as are bovids, equids can process material with a higher fiber and lower protein content and compensate by eating more and digesting faster (Estes 1991). *Equus africanus* (Figure 17.4) is well adapted to xeric regions of Africa, and the Asian *E. hemionus* is also found in more arid regions. *Equus kiang* inhabits marginal habitats in the Himalayan steppe, where dietary richness is often seasonal. *Equus przewalskii* occupies semiarid steppe and grasslands. *Equus grevyi* occupies subdesert regions, sometimes migrating seasonally to follow water, and eats grasses inedible to other ungulates. *Equus zebra* lives in plateau grasslands and subdesert plains. *Eguus burchelli* is distributed across the most diverse environments of any living wild equid, from savanna to light woodland to scrub. With such a diverse array of modern habitat preferences, the presence of a large number of *Equus* fossils in the Daka Member must

EBSCOhost - printed on 10/28/2022 4:53 AM via . All use subject to https://www.ebsco.com/terms-of-use

FIGURE 17.4
Extant Ethiopian wild asses *(Equus africanus africanus)* in the Messalu zone of the Middle Awash study area, east of the Awash River. Photograph by Tim White, October 28, 1981.

be interpreted conservatively. Tropical rain forest and extreme desert may be ruled out, but a range of habitats between these two extremes is possible, and it is notable that Ethiopian wild asses were, at least as late as 1981 (Figure 17.4), present in the Middle Awash.

Giraffidae

There are no living sivatheres, and they are so different from species of living Giraffidae that specific ecological speculation is difficult. The living giraffid genera, *Okapia* and *Giraffa*, are very different in habitat preferences, but both rely heavily on browsing (Estes 1991). *Giraffa* is an obligate browser, focusing heavily on *Acacia* and *Combretum*. Giraffes are less water-dependent than many ungulates, obtaining much of their water through young vegetation and the dew that collects on it. When water is available, they will drink irregularly. Daka Member giraffids indicate the presence of browse, and *Giraffa* is likely associated with large acacia trees.

Hippopotamidae

Two species in two different African hippopotamid genera exist today: *Choeropsis liberiensis* and *Hippopotamus amphibius*. Daka hippopotamids are in the latter genus.

EBSCOhost - printed on 10/28/2022 4:53 AM via . All use subject to https://www.ebsco.com/terms-of-use

Living *Hippopotamus* has two ecological requirements: water deep enough to allow complete submersion, and adjacent grassland (Estes 1991). Its presence in the Daka Member indicates a large, perennial water body.

Elephantidae

Modern elephants, both *Loxodonta* and *Elephas*, are capable of inhabiting a wide variety of habitats. They graze and browse, eating small trees along with vines, shrubs, and grasses. Historic *Loxodonta* inhabited almost every part of Africa except for the most extreme arid regions. *Elephas* was similarly distributed across tropical Asian ecological space. Both species prefer cover during times of intense solar radiation (Estes 1991; Nowak 1991). Little specific ecological information is derived from the presence of *Elephas*.

Rhinocerotidae

There are two modern African rhinos: *Ceratotherium simum* and *Diceros bicornis*. Both have extremely circumscribed modern ranges but likely were distributed much more widely in the past. *Diceros bicornis* is a nearly exclusive browser, and *Ceratotherium* is an exclusive grazer. Both require water but can refrain from drinking for over three days (Estes 1991). Neither is found in highly arid environments. Daka Member *Ceratotherium* and *Diceros* indicate the presence of a standing water supply, grassland, and browse.

Suidae

Suid genera known from the Daka Member include *Phacochoerus*, *Metridiochoerus*, and *Kolpochoerus*. *Phacochoerus* and *Metridiochoerus* are included in the tribe Phacochoerini with the modern warthog. *Metridiochoerus modestus* is very similar in morphology to *Phacochoerus*. Modern *Phacochoerus* is a grazer and root feeder. It usually drinks daily and is generally found close to water, although it can tolerate semiarid conditions overall. Although it is possible that *Phacochoerus* and the large metridiochoeres had similar roles, it is also possible that the extinct species occupied a very different niche.

Kolpochoerus is in the tribe Potamochoerini with *Hylochoerus* and *Potamochoerus*. Modern *Potamochoerus* occupies a wide range of forest and woodland habitats. Modern *Hylochoerus* is rarely found outside dense rainforests. The modern potamochoerines are likely imperfect proxies for the habitat preferences of *Kolpochoerus* species.

Muridae

Muridae is represented in the Daka Member by a single cranium of *Arvicanthis*. *Arvicanthis*, the unstriped grass mouse or grass rat, is common in grasslands and savannas, where it feeds on leaves, grass, and seeds (Nowak 1991). In Ethiopia it is known from the highlands as high as 3,700 m. These broad-ranging rodents are not specific paleoenvironmental indicators.

Hominidae

Homo erectus, the hominid taxon from the Daka Member, is found throughout the tropical and warm temperate Old World. Modern humans, the taxon's closest living relative,

EBSCOhost - printed on 10/28/2022 4:53 AM via . All use subject to https://www.ebsco.com/terms-of-use

readily adapt to almost every climatic extreme known. While *H. erectus* was likely less adaptable, it is still not a good paleoenvironmental indicator.

Bovidae

A major synapomorphy of the bovids—a complex, four-chambered stomach—allows members of the family to extract a maximal amount of nutrition from consumed material. Digestive efficiency allows bovids to eat less and spend less time eating than other ungulates. Likely correlated with this—and, potentially, with bovid-specific mate recognition systems (Vrba 1987)—are the great number of bovid taxa and subsequent pronounced niche specialization with respect to other ungulates. Another trait of bovids that is very beneficial to paleontologists is horns and their osseous cores. These readily fossilized features are acted on directly by intense sexual selection and change rapidly through time. This allows for more specific identification than is possible in many other taxa. In the paragraphs that follow, each Daka bovid taxon is treated separately, and the group is then discussed as a unit. Many of the following accounts rely on Estes (1991) for bovid habitat and niche descriptions. Daka bovid genera are presented alphabetically except *Gazella* and *Antidorcas*, which are grouped into Antilopini and then listed alphabetically with the other bovid genera.

AEPYCEROS *Aepyceros* is currently distributed over much of sub-Saharan Africa in areas with available graze and browse, favoring woodland and shorter grasslands. Impalas are water-dependent during the dry season (Estes 1991). Their mixed reliance on browse and graze allows them to occupy a variety of different habitats and also to occupy those with a high degree of seasonal change (Estes 1991). This makes them less useful than other bovids as paleoenvironmental indicators, but Shipman and Harris (1988, 378) note that: "whatever the appropriate taxonomic status of impalas might be, ecologically they are clearly distinct from Alcelaphini in preferring more closed habitats."

ANTILOPINI Antilopine species, not water-dependent, are well adapted to arid conditions and can occupy areas uninhabitable by other bovids. *Gazella* species are currently found in savanna and arid zones of eastern Africa, and those of *Antidorcas* in southwestern Africa. Antilopine species are more nomadic than other bovids and are known to venture into very arid zones during the wet season, when highly nutritious growth occurs out of the range of other, more water-dependent competitors.

BOURIA *Bouria anngettyae* does not have any close modern analog. There are two modern African caprines, *Ammotragus lervia* (the Barbary sheep) and *Capra ibex* (ibex). Populations of ibex are still found in Ethiopia. *Ammotragus* lives in the arid highlands of the Sahara and northern Africa. The ibex is found in the scrub and sparse woodlands of the rocky hills of eastern Egypt and Sudan. It is also found in the somewhat wetter northeastern highlands of Ethiopia. Both African caprine taxa live in marginal habitats where other bovid taxa are rare. It is unclear whether *B. anngettyae* occupied a niche similar to these taxa.

CONNOCHAETES *Connochaetes* is currently distributed in open areas of southern and eastern Africa. Wildebeests occupy plains dominated by rhizome-spreading grasses that

EBSCOhost - printed on 10/28/2022 4:53 AM via . All use subject to https://www.ebsco.com/terms-of-use

grow and spread rapidly when being utilized, stimulated by cropping, trampling, and manure (Estes 1991). Although these animals do well in many environments that are somewhat arid, their distribution is limited to areas where fluctuating lake levels, seasonal thunderstorms, or somewhat higher general rainfall allow for this type of vegetation. The number of *Connochaetes* horn cores in the Daka member suggests that these types of environments ranged farther north during the early Pleistocene than they do presently.

DAMALISCUS AND *PARMULARIUS* Modern *Damaliscus* is found on the savanna of the southern margin of the Sahara from Mali to Sudan and has ranges in central and eastern Africa. Modern forms thrive in grasslands and are effectively exclusive grazers. When graze is green, *Damaliscus* individuals do not need to drink, but they become water-dependent when graze browns. They are found in greatest numbers near rivers that flood seasonally (Estes 1991). Daka *Damaliscus* and *Parmularius* (its close sister) suggest that grasses were prevalent in Daka Member times.

HIPPOTRAGUS Modern *Hippotragus* occupies wooded savanna or mosaics of woodland and grassland. They are capable of subsisting on perennial grasses in poor soils that are not capable of maintaining large numbers of other herbivores (Estes 1991). *Hippotragus* is not currently found in the Horn of Africa, and its presence may indicate richer ecological resources in Daka times, although Quaternary human predation and Holocene pastoralism may have influenced this pattern.

KOBUS Modern *Kobus ellipsiprymnus* is very closely associated with water and is one of the most water-reliant Daka Member bovids (Estes 1991). It is found in larger river galleries and lake margins across the middle latitudes of Africa. It is a grazer, must drink daily, and is not tolerant of dehydration in hot weather. Its presence in the Daka Member indicates the proximity of a large, perennial water body.

Modern *Kobus kob* is distributed along the Sahara-margin savanna of northern Africa and also in the savanna of the Democratic Republic of the Congo and Zambia. It is associated with floodplain grasses, does not require cover, and contracts to water-retaining floodplains during the dry season (Estes 1991). Like *K. ellipsiprymnus*, *K. kob* implies the proximity of a perennially running body of water during the Daka Member's deposition.

MEGALOTRAGUS *Megalotragus* is an alcelaphine that is closely related to living *Connochaetes*. *Connochaetes* specializes in eating turf grasses (see foregoing discussion of *Connochaetes*), although it is uncertain whether Daka *Megalotragus* would occupy a similar niche.

NITIDARCUS *Nitidarcus* is provisionally placed in Ovibovini. The relationship between African fossil ovibovines and living Asian representatives is essentially unstudied (Vrba 1997). Modern representatives of this taxon include the musk ox and the takin. The former has a tundra distribution, and the latter is native to the Himalayan foothills. It is not clear what the ecological implications of Daka *Nitidarcus* are.

EBSCOhost - printed on 10/28/2022 4:53 AM via . All use subject to https://www.ebsco.com/terms-of-use

NUMIDOCAPRA *Numidocapra* is an alcelaphine without any close living relatives. Other than the general alcelaphine trend of grazing, is not clear what the ecological implications of Daka *Numidocapra* are.

ORYX Modern *Oryx gazella* is suited to arid habitats uninhabitable by other bovids (Kingdon 1982; Estes 1991). It subsists on lower-quality graze than other bovids and does not rely on water. Modern *Oryx* is distributed in marginal and arid habitats in southwestern and eastern Africa and also Arabia. Its presence in the Daka Member, however, is not necessarily indicative of widespread arid conditions. Some marginal habitats inhabited by modern *Oryx* occur on the periphery of richer food sources and areas of high concentrations of other bovids (Kingdon 1982).

SYNCERUS AND *PELOROVIS* The modern African bovine *Syncerus* is found across the central latitudes of Africa. Its populations are densest in moist savanna and well-watered floodplains (Estes 1991), although the genus also penetrates into savannas (Klein 1994). It is able to process grasses too high and robust for most bovids. It is possible that *Pelorovis* and *Syncerus*, close sister taxa, filled similar niches. Daka *Syncerus* indicates the presence of grasses and available open water.

TRAGELAPHUS The greater kudu, *Tragelaphus strepsiceros*, is found in wooded patches across southern and eastern Africa. They are almost exclusively browsers. Although they will drink during the dry season, they can live in water-free areas (Estes 1991). They prefer thick cover and brush, but without being dependent on open water, they are not restricted to gallery forests. The lesser kudu, *T. imberbis*, is found in savannas retaining wooded patches in eastern Africa and relies on dense thickets for cover (Estes 1991). They are near-exclusive browsers and do not need to drink, even in the dry season.

Ecological Signal of Bovid Tribes

From the preceding discussions, it is apparent that modern bovid taxa are numerous and relatively habitat specific. Digestive synapomorphies and the tendency for bovids to specialize according to vegetation make them paleoecologically and evolutionarily interesting. Vrba (1980) documents percentages of bovid taxa from 16 ecologically diverse modern African game parks categorized as open or closed in terms of vegetative cover. Of the 16 parks she studied, she considered 10 closed and 6 open. Figures 17.5 and 17.6 plot Vrba's results. Figure 17.7 plots the ratios of bovid tribes in the Daka Member based on the minimum number of individuals (MNI) of each taxon derived from horn cores and crania, but not teeth, which are not such reliable identifiers.

Because different bovid tribes have established ecological roles, tribal abundance comparisons are potentially interesting, but not without caveats. The first problem is that there is no tight modern analog for a paleontological assemblage that includes many extinct large mammal taxa such as (in the case of the Daka Member) *Sivatherium*, *Metridiochoerus*, *Kolpochoerus*, *Megalotragus*, *Elephas recki*, *Parmularius*, *Bouria*, *Nitidarcus*, *Numidocapra*, *Theropithecus oswaldi*, *Eurygnathohippus*, *Homo erectus*, and *Pelorovis*. Presentation

EBSCOhost - printed on 10/28/2022 4:53 AM via . All use subject to https://www.ebsco.com/terms-of-use

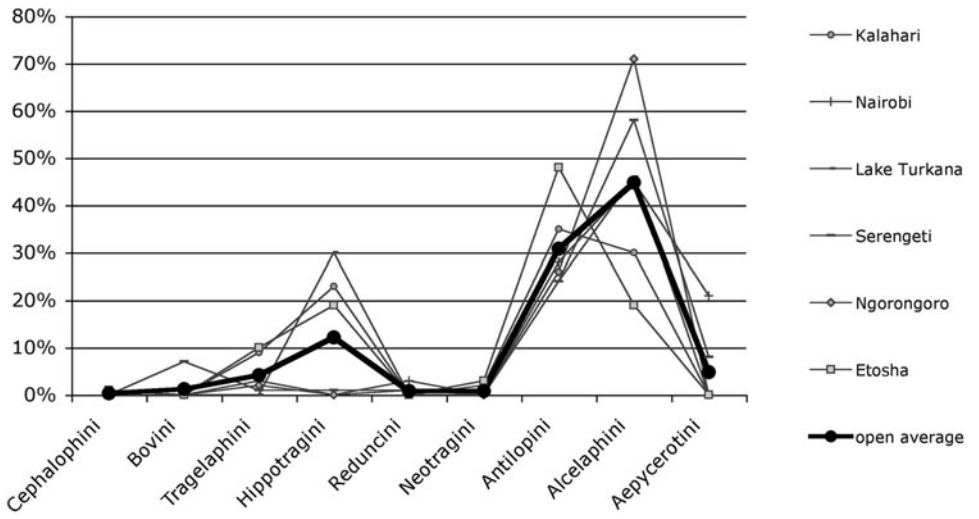

FIGURE 17.5
Relative proportions of bovid taxa collected in relatively open African game parks (Vrba 1980).

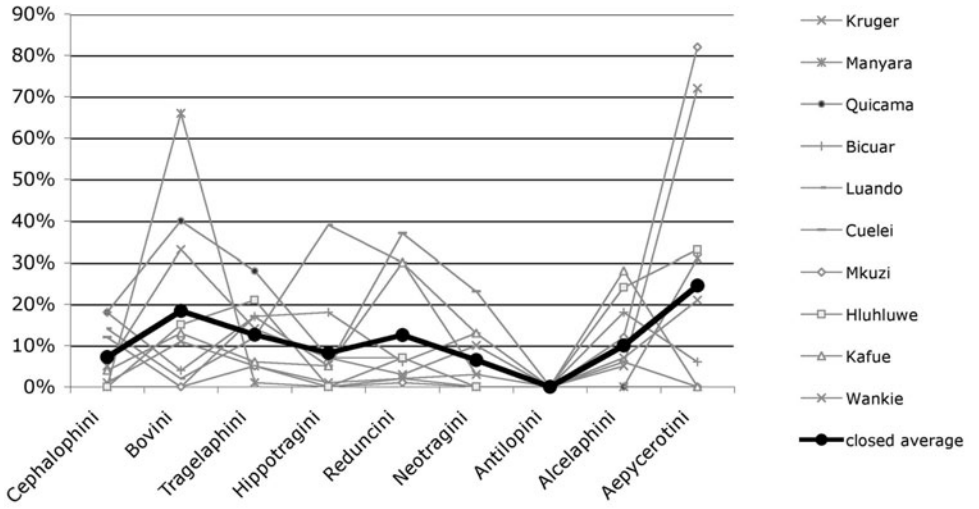

FIGURE 17.6
Relative proportions of bovid taxa collected in relatively closed African game parks (Vrba 1980).

of modern environments is provided here only as an example of what type of ecological patterning might be expected to correlate with bovid tribal ratios. A second problem involving the paleoecological use of bovid tribal representations based on census data from contemporary game parks is taphonomic. The Daka Member samples thousands of years from a very broad catchment.

Animals dependent on water are more likely to end up fossilized. Those that are less frequent at water holes are less likely candidates. For example, hippotragines have hooves that seem to be poorly suited to mud, and are especially aware of predators at water holes, around which they do not congregate (Kingdon 1982). Furthermore, even within small regions, hippotragines are found in the areas where other bovids are absent (Kingdon 1982). The presence or absence of hippotragines in an assemblage should therefore not

EBSCOhost - printed on 10/28/2022 4:53 AM via . All use subject to https://www.ebsco.com/terms-of-use

be expected to accurately indicate their abundance in the paleo-region. Gazelles get most of the water that they need from graze and do not frequent water holes regularly. Thus, they will also be under-represented in a fossil assemblage. Reduncines live along waterways and floodplains, exploit floodplain grasses, and will thus be over-represented. The most reliable indicators of paleoenvironment among fossil bovids should logically be those animals that forage in areas outside the large, ever-flowing river gallery forests, but still rely on open water. These are alcelaphines, neotragines, tragelaphines, cephalophines, and aepycerotines.

These problems notwithstanding, some general paleoecological conclusions can be drawn from Figures 17.5 through 17.7. First, in spite of biases against antilopine fossilization, a number are present in the Daka Member. There are no antilopines at all in *any* of the closed environment game parks studied by Vrba (1980). In Vrba's analysis, alcelaphines never dominated closed habitats. Alcelaphine frequency in the Daka Member is exceeded only by reduncines, riparian gallery dwellers that fossilize readily. Seeming to counter these conclusions, the Daka Member has a high percentage of tragelaphines. This does not imply more precipitation, because tragelaphines are not water-dependent, but it does suggest the presence of at least some woodlands or thickets. Additionally, there is a diversity of bovines: grazers that generally inhabit floodplains, glades, and woods around large waterways. These animals indicate a perennial water supply.

Conclusion

The Daka Member, like all fossil assemblages, must be conceptualized as a depositional system, not a living community. This bias imposes limits on characterizing the faunal assemblage as a group. In spite of this, some general statements can be made regarding its biogeographic and ecological dimensions.

The Daka Member has two taxa with potential Palaearctic affinities, *Bouria anngettyae* and *Nitidarcus asfawi*. Without a more detailed understanding of their systematic relationships, however, it is not prudent to propose geographic interchange between Ethiopian and Palaearctic realms based on their presence. A very interesting feature of the Daka Member is that many modern taxa recorded are no longer present in the Afar region, including *Aepyceros*, *Connochaetes*, *Giraffa*, *Ceratotherium*, and *Syncerus*. While there are many possible factors that could affect this, including human predation and competition with domestic animals, it is worth noting that during Daka times the region presented a much more diverse array of animals. Depositional biases ensure that this is a conservative appraisal. Apparent endemism in the Daka Member is more likely to be an effect of the site's richness with respect to contemporaneous sites.

The Daka Member samples some relatively open and grassy environments, as indicated by the large number of grazers, especially alcelaphine bovids, but likely also draws from areas with more closed habitats, as indicated by *Tragelaphus* and *Cercopithecoides*. There is a large representation of water-dependent taxa, including *Kobus*, Bovini, and *Hippopotamus*. Some animals in the Daka Member are tolerant of arid conditions, including antilopines and *Oryx*. When observing the overall abundances of different bovid tribes in the Daka

EBSCOhost - printed on 10/28/2022 4:53 AM via . All use subject to https://www.ebsco.com/terms-of-use

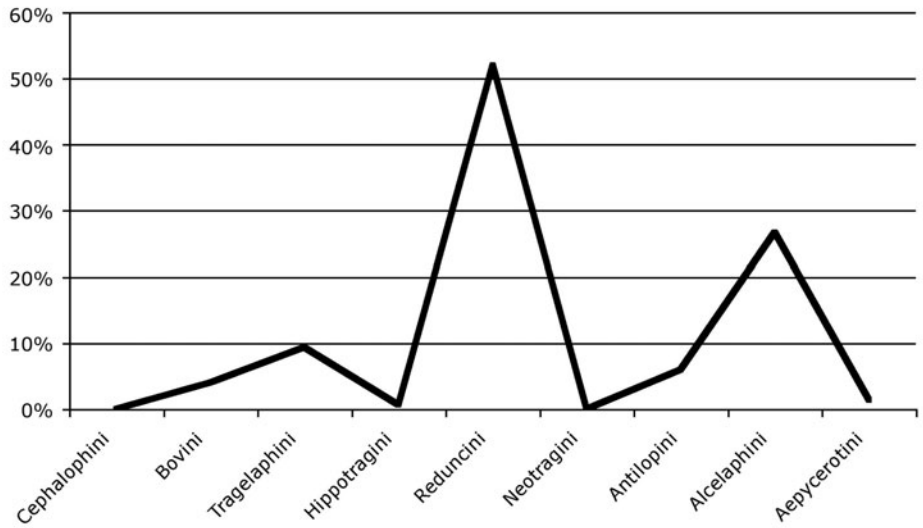

FIGURE 17.7

Relative proportions of bovid taxa in the Daka Member counted from horn cores.

Member and allowing for biases imposed by the depositional environment, the Daka Member, with a high frequency of alcelaphines and the presence of antilopines and hippotragines, more closely matches open, grassland- and savanna-dominated African game parks than closed, wooded parks. Aside from the numerous extinct taxa, the living community sampled by the Daka Member would have been easily recognizable as an ecologically rich African grassland/savanna with ample wooded areas, gallery forests, floodplains, and some xeric regions. Interestingly, this is very similar to the ecology of the region today, especially if the human impact is discounted.

EBSCOhost - printed on 10/28/2022 4:53 AM via . All use subject to https://www.ebsco.com/terms-of-use

EBSCOhost - printed on 10/28/2022 4:53 AM via . All use subject to https://www.ebsco.com/terms-of-use

18

Conclusions

W. HENRY GILBERT

Evolutionary Insights from the Daka Member

This volume has presented the Daka Member as understood in 2007. Work in the Daka Member will continue into the future. The fossil-bearing surfaces of the Bouri area have been systematically surveyed by organized groups of experienced collectors using tightly controlled geospatial techniques to ensure complete coverage. However, each year that the localities here are revisited, several additional fossils are found. We have learned that these subsequent visits always result in diminished rates of overall fossil acquisition (see White 2004); it is therefore certain that future collections will not again yield the abundant, well-preserved fossil mammal collections made at Bouri during the 1990s. Erosional activity, interseasonal variations in grass cover, survey time, and direction and collector competency all ensure that the collection of valuable fossils from the Daka Member will continue, rendering this volume a progress report rather than a definitive statement.

Daka Member archaeology and geology have previously received detailed treatment in the volume by de Heinzelin et al. (2000b). The Daka *Homo erectus* cranium was initially presented by Asfaw et al. (2002). Gilbert (2003b) provided the basic template for the current volume in his Ph.D. dissertation at the University of California at Berkeley. Here the contributions in earlier chapters of this volume are synthesized and the relevance of the Daka Member to broader questions of paleoclimate and evolution is discussed.

Volume Highlights

Geology

This volume significantly updates the stratigraphy presented in de Heinzelin (2000). This volume's geological map (Figure 2.1) details the Daka Member's boundaries based on numerous walked transects of the contact zones. Lithological units are also described, including detailed presentations of key sections and locality-by-locality descriptions of vertebrate paleontology collection areas. Stratigraphy is summarized in Figure 2.2. New radiometric dates for pumices centrally located in the Daka Member stratigraphic sequence are only slightly younger (average of 0.966 $\pm$ 0.006 Ma) than dates obtained for the basal unit, the HPU (average of 1.042 $\pm$ 0.009 Ma). This interval brackets the majority of Daka

EBSCOhost - printed on 10/28/2022 4:53 AM via . All use subject to https://www.ebsco.com/terms-of-use

fossils. It also suggests that Daka deposition was rapid and that the entire unit is closer in age to 1.0 Ma than to the minimum possible age of 0.78 Ma previously established by the universally reversed paleomagnetic polarity of the sediments. Soil stable isotope data corroborate geomorphological structures indicating a fluvial-lacustrine depositional system in open, seasonally dry, wooded grassland to open grassland environments with rainfall of less than 1,000 mm per year.

Paleontology

The Daka Member affords a wealth of new paleontological information. The Daka Member has yielded well-preserved cranial specimens from the following taxa: *Bouria anngettyae*, *Connochaetes taurinus olduvaiensis*, *Kobus kob*, *Megalotragus kattwinkeli*, *Nitidarcus asfawi*, *Parmularius angusticornis*, *Pelorovis oldowayensis*, *Pelorovis antiquus*, *Syncerus*, *Cercopithecoides alemayehui*, *Theropithecus oswaldi leakeyi*, *Elephas recki recki*, *Hippopotamus* cf. *gorgops*, *Homo erectus*, *Crocuta crocuta yangula*, *Kolpochoerus majus*, and *Kolpochoerus olduvaiensis*. There are two new species of bovids, a new species of colobine monkey, and a new subspecies of the spotted hyaena. Several first appearance dates (FADs) and last appearance dates (LADs) have been revised as a consequence. The following paragraphs, arranged according to the order of preceding chapters, outline the impacts that Daka fossils have had on each taxonomic group considered.

Bovidae

Vrba (1997) named two new genera and species, *Bouria anngettyae* and *Nitidarcus asfawi*, from Daka material. Additional material recovered since her publication has been presented. Daka Member bovid fossils document the last appearances of several taxa, including *Numidocapra crassicornis*. Daka Member *Syncerus* coexists with two *Pelorovis* species, including *P. antiquus*. This supports the hypothesis that *P. antiquus* is not a *Syncerus caffer* subspecies (contra Gautier and Muzzolini 1991). The Daka Member also presents a well-preserved cranium of a juvenile *Pelorovis*. Daka *Kobus ellipsiprymnus* is transitional between *K. sigmoidalis* and later *K. ellipsiprymnus*. This supports Gentry's (1985) hypothesis that the two are part of a single evolving lineage.

Carnivora

Daka carnivores include *Crocuta crocuta yangula*, *Panthera* cf. *pardus* and *P.* cf. *leo*. Perimortem modifications on *Homo erectus* cranium BOU-VP-2/66 are probably the result of carnivore activity. The Daka Member produced one of the best preserved Pleistocene *Crocuta* crania known. This cranium is larger than that of any recent or prehistoric eastern African *Crocuta* and has been placed in a new subspecies, *C. c. yangula*.

Cercopithecidae

While fossils of cercopithecid taxa are relatively rare in the Daka Member, there are three well-preserved cranial specimens. One cranium is a new species of colobine, *Cercopithecoides alemayehui*. The others are assigned to *Theropithecus oswaldi leakeyi*, also represented by several dental and postcranial specimens.

EBSCOhost - printed on 10/28/2022 4:53 AM via . All use subject to https://www.ebsco.com/terms-of-use

Equidae

The Daka Member presents a large sample of equids. There is both a form of *Equus* similar to modern zebra species and an extinct hipparionine, *Eurygnathohippus* cf. *cornelianus*. *Equus* outnumbers *Eurygnathohippus* in the Daka Member by approximately 2:1. The two taxa are very abundant, together representing approximately 20 percent of the Daka Member large mammal assemblage in terms of number of specimens.

Giraffidae

The Daka Member preserves both *Sivatherium* and *Giraffa* fossils. Daka *Giraffa* fossils are large and belong to the group of African *Giraffa* species that includes *G. jumae* and *G. camelopardalis*.

Hippopotamidae

Daka hippo fossils belong to the genus *Hippopotamus*. Compared to modern *H. amphibius*, the relatively advanced features of the skull and the more primitive aspects of the dentition are similar to *H. gorgops*. However, the anterior parts of the skull are narrower than in *H. gorgops*. Hippo material from Daka is thus provisionally assigned to *H.* cf. *gorgops*.

Elephantidae

Proboscidean remains from the Daka Member are tentatively identified as early representatives of *Elephas recki recki*. Cranial remains, including the only known complete skull of the species, show several derived features previously known only from Eurasian palaeoloxodonts. Presence of these features in Daka Member elephants suggest that the emigration of palaeoloxodonts from Africa to Eurasia took place at around 1.0 Ma.

Rhinocerotidae

Ceratotherium simum and *Diceros* are both present in the Daka Member. Daka *C. simum* comprises a mandible, maxilla, and several dental specimens, while *Diceros* is represented by a single premolar.

Suidae

Daka suid taxa include *Kolpochoerus majus*, *K. olduvaiensis*, *Metridiochoerus compactus*, *M. modestus*, and *Phacochoerus*. Until recently, *K. majus* was poorly known. Recent discoveries at several African localities have added substantially to its record. Now, particularly because of the new Daka material, this taxon has a rich eastern African record. *Kolpochoerus olduvaiensis* is abundant in the Daka Member and demonstrates that the elongation of M3 talons and talonids in this lineage during the early Pleistocene also took place in the Horn of Africa. Daka specimens substantially improve the quality of *K. olduvaiensis* as a biochronological indicator. Daka *M. modestus* co-occurs with distinctive *Phacochoerus*. This co-occurrence provides further evidence to support the metridiochoere status of the former and represents the earliest well-established African record of the latter.

EBSCOhost - printed on 10/28/2022 4:53 AM via . All use subject to https://www.ebsco.com/terms-of-use

Muridae

Micromammals are rare in the Daka Member. The assemblage includes a single specimen: a cranium of the murid *Arvicanthis*, the unstriped grass mouse or grass rat.

Other Vertebrates

In keeping with work on other sites in eastern Africa, little work has been done on the nonmammalian paleontology of the Daka Member. Crocodile scutes and teeth as well as fish vertebrae were not collected. One partial carpometacarpus of Aves and one fish cranium were recovered. The avian fossil has affinities with Ciconiiformes, the egret and stork order. The fish fossil is from the catfish order, Siluriformes. Further cleaning of the highly cemented matrix encasing the fragile cranial bones of this specimen will allow a more precise taxonomic assessment.

Hominidae

The Daka Member has yielded an assemblage of hominid fossils that includes a calvaria, three femora, a tibia, a talus, a partial mandible, and cranial fragments from two individuals. This volume presents a detailed comparative description, tomographic analysis, and systematic interpretation of the cranium. It also presents the postcranial elements in depth, discussing the functional and systematic information they provide.

Perhaps the most important conclusion to be drawn from comparison of the Daka *Homo erectus* calvaria to other cranial specimens referred to *H. erectus* is that ectocranial features were distributed in a complex mosaic across the Pleistocene within Africa and Eurasia. Features with any correlation to geography are rare or nonexistent outside of single-site assemblages. It is not possible to show regional morphological homogeneity in any group of *H. erectus* specimens from more than one site when more than a few features are considered simultaneously. The phylogenetic analysis presented in Chapter 15 investigates this phenomenon. It was unable to detect any consistently supported cladogenic events separating regional *H. erectus* subgroups.

The three Daka Member femora are similar to those of contemporary *Homo* specimens. These support the use of three often-cited features that appear to differentiate (older) Pleistocene *Homo* from *H. sapiens*: a distal position of minimum femoral shaft breadth, the presence of very thick femoral shaft cortical bone, and a tendency for the medial shaft cortex to be thicker than the lateral shaft cortex. The Daka femora are platymeric and anteverted, which suggests that the Daka hominids might have engaged in habitual squatting.

The Daka Member is also rich in archaeological remains. Several localities are known, and large samples of stone artefacts have been excavated and collected. The assemblage, characterized as early Acheulean, is thoroughly documented in de Heinzelin et al. (2000b).

Ecology

The mammal assemblage of the Daka Member contains a large number of grazers, particularly alcelaphine bovids, indicating that open and grassy regions must have been proximal

EBSCOhost - printed on 10/28/2022 4:53 AM via . All use subject to https://www.ebsco.com/terms-of-use

to the Daka depositional environment. However, the assemblage also draws from areas with woodland, brush, or forested habitats, as indicated by *Tragelaphus* and *Cercopithecoides*. There are numerous water-dependent taxa, including *Kobus*, Bovini, and *Hippopotamus*. Some elements of the Daka Member are tolerant of xeric environments, including antilopines and *Oryx*. The presence of antilopines and hippotragines more closely matches modern open, grassland- and savanna-dominated areas than closed, wooded ones. The living community sampled by the Daka Member is therefore interpreted as an ecologically rich African grassland/savanna with ample wooded areas, gallery forests, floodplains, and some xeric circumstances. Although the fauna was more diverse, the Daka Member presents an ecology very similar to that which would have characterized the extant region prior to the appearance of domestic livestock, which have degraded the modern landscape by overgrazing.

The Daka Member and Global Climate Change

Plio-Pleistocene paleoclimate has received substantial attention over the past few decades. Several recent studies have detected relatively punctuated shifts toward cooler, more arid conditions over these epochs (see deMenocal 2004 for a review). The Daka Member is temporally placed just prior to the onset of the intense glacial/interglacial cycles that characterized the second half of the Pleistocene, a period of increased climatic variability (deMenocal and Bloemendal 1995; Schefuss et al. 2003; deMenocal 2004; McClymont and Rosell-Melé 2005; Gasse 2006). For this reason, the Daka Member is especially relevant to studies seeking to examine potential relationships between climate change and mammalian evolution. The following sections consider some recent attempts to relate biotic evolution to paleoclimate. After a brief overview, the Daka fossil assemblage will be considered with reference to its contribution to such ongoing debates. Although very diverse and appropriately positioned temporally, the Daka mammal assemblage presents little additional evidence to support hypotheses of a causal link between paleoclimate and mammalian evolution.

While paleobiologists have long suspected that relationships must exist between large-scale climate changes and evolution (reviewed by Vrba 1995a), the chronological precision afforded by recent paleoclimate studies has given researchers a much more precise framework upon which to articulate hypotheses (deMenocal 2004). Several approaches directed to decipher complex relationships between climate and evolution have been attempted, with varying degrees of success. Some hypotheses are easily criticized for intrinsic logical problems or superficial appreciation of evolutionary processes. All are subject to the classic logical dilemma inherent in arguing causation from correlation. Problems are exacerbated by the imperfect fossil record (White 1995) and the still poor (but rapidly improving) resolution of the paleoclimate record.

Macroevolutionary Selection for "Generalists"

In 1994 Rick Potts published a paper titled "Variables versus Models of early Pleistocene Hominid Land Use." Potts observed that "fluctuations in habitats or resources may have

EBSCOhost - printed on 10/28/2022 4:53 AM via . All use subject to https://www.ebsco.com/terms-of-use

driven natural selection" (Potts 1994). From this beginning he posited a notion that he named "variability selection" (Potts 1996a). In subsequent publications (Potts 1998a, b, 2001, 2002, 2004), including a book-length treatment (Potts 1996b), Potts elaborated on his arguments. These have been widely and uncritically repeated in fields ranging from paleontology (Bobe et al. 2002) to geosciences (deMenocal 2004; Feakins et al. 2005; Deino et al. 2006) and archaeology (Gamble et al. 2004). The prominence of "variability selection" in the paleoanthropological landscape stands in stark contrast to its apparent limited impact within evolutionary biology; for example, Gould (2002) does not cite any of Potts's work in his over-1,400-page magnum opus on evolutionary theory. This is perhaps because "variability selection" as defined by Potts is perceived by most evolutionary biologists as derivative and unoriginal. Lloyd and Gould (1993) thoroughly and effectively delineated the macroevolutionary potential for selection on variability. Stevens (1989) suggested that the generalist tendencies of high-latitude species are the result of evolutionary processes related to climatic variability. Both contributions go uncited by Potts in any of his numerous publications on "variability selection" (Potts 1994, 1996a, b, 1998a, b, 2001, 2002, 2004).

Potts's version of "variability selection" posits that adaptations evolve "as a population confronts highly variable environments over many generations" (Potts 1998b, 85). Potts (2002) acknowledges that environmental variability occurs at several temporal scales (seasons, decades, centuries, millennia, multimillennia, and mega-anna), but, unlike preceding authors (Lloyd and Gould 1993), Potts puts forth little effort to disentangle the various biotic levels (gene, organism, species, clade) on which "variability selection" would have focused. His model frequently conflates species-level and organism-level selection:

> As a result, a lineage of organisms may face multiple, substantial disparities in selective environment over time . . . This process of adaptive evolution therefore enhances an organism's capacity to thrive in novel conditions. (Potts 1998a: 112)

In spite of this notable lack of specificity, Potts clearly focuses on long-term climate oscillations (those occurring at scales higher than 10^3 or 10^4 years) when framing his hypothesis (Potts 1998a, b, 2002). Because the duration of these oscillations is orders of magnitude greater than any single organism's life span, the "variability selection" hypothesized by Potts must have occurred across generations and therefore would constitute a form of selection operating above the level of the individual organism.

Species selection, well articulated by evolutionary biologists (Stanley 1975; and many others), goes unmentioned and unreferenced by Potts (1996a, b, 1998a, b, 2001, 2002, 2004). In contrast to natural selection operating as differential fitness among individual organisms, species selection (species sorting) occurs on features that emerge or aggregate (*sensu* Lloyd and Gould 1993) to characterize the individual competing species being sorted, and would manifest as differential survival of species lineages (Stanley 1975).

Differential survival of species adds a level of dimensionality to evolutionary patterns that makes it difficult to directly correlate survival or extinction with organism-level adaptations and dynamics. In a classic example, Vrba (1984) presents two closely related (but long distinct) clades of African bovids that arose at about the same time and have both survived all of the environmental vicissitudes of the Pliocene and Pleistocene. However, these clades have

EBSCOhost - printed on 10/28/2022 4:53 AM via . All use subject to https://www.ebsco.com/terms-of-use

very different clade-level emergent features. Alcelaphini is a diverse group of largely "specialist" grazers, with numerous morphologically variable genera and species, and a fossil record documenting high turnover rates (extinctions/speciations). Aepycerotini is monogeneric, with a single living representative species, *Aepyceros melampus*, the impala. The modern impala is a "generalist" and is very similar to, perhaps conspecific with, forms existing before the Pliocene and Pleistocene climate changes. This genus has never presented more than a single species for any particular temporal horizon (Vrba 1984). In census data from several African game parks (Vrba 1980), impalas outnumber all alcelaphine species combined except one: *Connochaetes taurinus*. Impalas (individual organisms) also outnumber *C. taurinus* alone and have higher population densities than any alcelaphine species. However, alcelaphine species (and individual organisms) outnumber aepycerotines.

How is it possible that a clade of specialists survived the Pliocene and Pleistocene with more species than a clade of generalists? Vrba's (1984) suggestion is that one of the features that emerges at a macroevolutionary level for Alcelaphini is its propensity to speciate and specialize. This implies that it is impossible to predict, without supplementary information, whether a clade of generalists or one of specialists will cope more successfully with environmental perturbations, regardless of the predilection of individual species within these clades. Both generalist and specialist strategies can be successful macroevolutionary tactics. Accordingly, several specialist species survived the Pleistocene, and several generalists did not.

These clade-level evolutionary processes are readily decoupled from organism-level selection. It is, however, possible for features to impact multiple biotic levels of selection (Vrba and Gould 1986). It is relatively easy to conceive of features selected at lower biotic levels (i.e., the organism) that might aggregate as features relevant at higher levels (i.e., the species). However, the relationship is not straightforward. It is, of course, less intuitive to imagine a phenotypic feature that is sorted at the species (or higher) level that has not been shaped by selection occurring at the individual level (Vrba and Gould 1986). This is precisely what Potts is arguing when he proposes that "variability selection" is responsible for bipedality, encephalization, stone tool transport, and cognitive sophistication (Potts 1998a). However, adaptations that confer advantages to individual organisms over individual lifetimes are certainly somewhat, if not mostly, shaped by organism-level selection. As such, they cannot simply be explained exclusively with appeals to selective forces that operated at higher biotic levels (Vrba and Eldredge 1984; Damuth and Heisler 1988; Lloyd and Gould 1993; Gould and Lloyd 1999). This completely undermines the explanatory value of "variability selection" for derived hominid features (e.g., Potts 1998a), or, for that matter, any feature impacted by selection operating at the organismal level. But it does not rule out the potential for mammalian species to have been sorted for resilience to ecological flux over the major climate changes of the Pliocene and Pleistocene via processes such as those outlined by Lloyd and Gould (1993).

Several authors have discussed the tendency for "generalist" species to withstand ecological instability better than "specialist" species (Stevens 1989; see Hernández-Fernández and Vrba 2005b, c for a recent review). Lister (2004) suggests that the ecological variation witnessed through the Pleistocene was severe enough (especially at high latitudes) and recent enough (too little time for speciation) to favor "generalists" over "specialists" through

EBSCOhost - printed on 10/28/2022 4:53 AM via . All use subject to https://www.ebsco.com/terms-of-use

differential extinction. Of course, the broad concepts of "generalist" and "specialist" make sense only with respect to a particular habitat or resource (Vrba 1987). The terms are frequently muddled in the literature.

> Variability selection results in organisms that are specialized in dealing with dynamic information about their surroundings and in buffering environmental disruptions. These same specializations may encourage the spread into diverse habitats, which usually is deemed to be a characteristic of a "generalist." (Potts 1998b)

"Generalist" and "specialist" are ecological terms referring to niche-breadth and are very difficult to define objectively. A real-world example provided by Vrba, *Syncerus caffer* (Cape buffalo), serves to illustrate this problem. The Cape buffalo is a "generalist" in its ability to both graze and browse on a variety of plants and to thrive under various conditions of temperature and vegetation cover, but it is a "specialist" in its dependence on permanent open water. Vrba also presents the antilopine *Antidorcas marsupialis* (springbok) a "generalist" in its propensity to engage in both grazing and browsing, but a "specialist" in terms of the overall number of plants that can be processed (it is restricted to xeric-adapted graze and browse). Vrba points out that every species is likely to have a mosaic of specialized and generalized features. Simplistic assessment of a taxon as a "specialist" or "generalist" based on a few features (e.g., Potts 1998b) is therefore wholly unwarranted.

Hernández-Fernández (2001) proposes the "biomic specialization index" (BSI) to address this problem of definition as applied to paleospecies. The BSI characterizes species by the number of different biomes they inhabit and is thus a proxy of their "specialist" or "generalist" tendencies. Unfortunately, while Hernández-Fernández and Vrba (2005b) apply this index to numerous African mammals, they do not publish index scores for individual taxa. It is beyond the scope of this chapter to develop a similar proxy, but the work of Hernández-Fernández (2001) and Hernández-Fernández and Vrba (2005b) serves to illustrate the problems with arbitrary classification of paleotaxa as "generalists" and "specialists." It also provides a conceptual basis for discussing the inclusion of taxa into either of the two categories.

The Daka faunal assemblage is germane to questions of whether the extreme glacial and interglacial cycles of the last half of the Pleistocene favored mammalian "generalists" or "specialists." Daka sediments are temporally situated near the beginning of the onset of the most intense period of glacial/interglacial cycles known. Lineages or clades that survived from the Pliocene or early Pleistocene, through the Daka Member, to the present, are certain to have been affected by climatic variation. By comparing Daka taxa that survived to the present from the beginning of the Pleistocene with those that went extinct after Daka times, trends in differential survivorship of "generalists" and "specialists" can be examined. To what extent have "generalists" represented in the Daka Member survived at the expense of "specialists"?

Addressing this question is not at all straightforward; identifying those Daka taxa that survived the climatic variation(s) of the Pleistocene, and comparing them with taxa that went extinct based on their "generalist" or "specialist" proclivities, is one approach. Daka taxa that survived through the Pleistocene to the Holocene include *Phacochoerus*, *Connochaetes taurinus*, *Kobus ellipsiprymnus*, *Tragelaphus strepsiceros*, *Oryx gazella*, *Homo erectus*, *Ceratotherium simum*, *Diceros*, *K. kob*, *Panthera* cf. *leo*, *P.* cf. *pardus*, *Crocuta crocuta*, *Aepyceros*,

EBSCOhost - printed on 10/28/2022 4:53 AM via . All use subject to https://www.ebsco.com/terms-of-use

Pelorovis antiquus, and *T. imberbis*. *Homo erectus* is included in this group because it is clear that at least one paleodeme of *H. erectus* is ancestral to *H. sapiens*. Those that did not survive the Pleistocene include *Theropithecus oswaldi*, *Elephas recki*, *Kolpochoerus majus*, *Parmularius angusticornis*, *Metridiochoerus compactus*, *M. modestus*, *Megalotragus kattwinkeli*, *Kolpochoerus olduvaiensis*, *Bouria anngettyae*, *Nitidarcus asfawi*, *Cercopithecoides alemayehui*, *Numidocapra crassicornis*, and *Pelorovis oldowayensis*. Whereas dichotomizing these lineages into "specialist" or "generalist" categories is somewhat specious (for reasons just discussed), it is not at all apparent that the most "generalized" taxa in this total set survived the climatic oscillations of the Pleistocene.

If "generalists" can be directly equated with a broad geographic distribution and "specialists" with a narrow one, then there appears to be some tendency for Daka "generalists" to have better survived the last half of the Pleistocene than did "specialists." But "generalist" and "specialist" most commonly refer to niche breadth, not geographic range. Using a geographic proxy for delimiting these ambiguous terms overlooks the potential for a niche "specialist" to be an evolutionary success with a broad geographic range. For example, the aardvark occurs in a wide variety of habitats in sub-Saharan Africa outside the tropical rain forests of western central Africa. Fossils of the genus are known from all of Africa and into Asia. It has survived all of the environmental perturbations of the Pliocene and Pleistocene. But can this creature, highly specialized for consuming fossorial insects, be considered a "generalist"? Is it possible that a successful "specialist" might attain a broad geographic distribution? It is clear that the meanings of the terms "specialist" and "generalist" are vague as they are commonly used in paleontology. Thus, definitions for these terms must be made explicit wherever they are used, especially in paleobiology.

Turnover Pulses

Authors have suggested that faunal turnover events, concentrations of species originations and extinctions, are correlated with periods of climate change (reviewed by Vrba 1995a). Vrba has elaborated and refined this concept into the "turnover pulse hypothesis" (Vrba 1985, 1992, 1993, 1995a, 1999, 2000, 2005). Essentially, this hypothesis postulates that speciations and extinctions, varying in scale, occur in response to changes in the physical environment (Vrba 1995a). Not all biologists agree that physical environment is the primary initiator of evolutionary change (e.g., the Red Queen Hypothesis, van Valen 1973; also Barnosky 2005), and some suspect that the incomplete fossil record might not afford adequate resolution to fully test Vrba's model (McKee 2001). The theoretical basis of the turnover pulse hypothesis is well-treated elsewhere (Vrba 1995a, 2000; Raia et al. 2005) and is not addressed in detail here.

With regard to the shift toward intense glacial/interglacial cycles that occurred around 1.0 Ma, Vrba (2005) suggests an extinction pulse without an origination pulse to have occurred between 1.0 and 0.5 Ma and significantly low origination and extinction to have occurred between 1.5 and 1.0 Ma. The Daka Member provides data relevant to these inferences. There are some first, as well as last, appearances in the Daka Member. By definition, the three new species named from the assemblage, *Bouria anngettyae*, *Cercopithecoides alemayehui*, and *Nitidarcus asfawi*, all have first and last appearances in the

EBSCOhost - printed on 10/28/2022 4:53 AM via . All use subject to https://www.ebsco.com/terms-of-use

Daka Member, but these data are obviously meaningless with regard to faunal turnover. *Pelorovis antiquus* and the *Phacochoerus* lineage have first appearances in the Daka Member. Both of these data points are consistent with Vrba's (1995a) suggestion of low origination between 1.0 and 0.5 Ma, as they push the dates of origination for these taxa back in time to the previous period (see Vrba 1995a). Both *Numidocapra crassicornis* and *Pelorovis oldowayensis* have last appearance dates in the Daka Member, implying that their true last appearances occurred after Daka Member times. These are also consistent with Vrba's (2005) suggestions. The sparse array of first and last appearance data provided by the Daka Member is consistent with Vrba's (2005) projections regarding the periods just before and just after 1 Ma, but the signal does not provide an adequate test of her overall hypothesis.

Phyletic Evolution

Another approach to understanding the interface between climate change and evolution is to analyze each lineage individually for evolutionary change. Do the changes witnessed within individual lineages indicate a climate-influenced pattern of morphological change? To address this question, the Daka fauna is presented here on a lineage-by-lineage basis. In this section, each Daka lineage is discussed relative to general morphological changes that occurred between approximately 1.5 Ma and 0.5 Ma.

Bovidae

Aepyceros has a reasonable fossil record dating back to the late Miocene. There is subtle indication of a gradual increase in size in the lineage from its first appearance to the Recent, but the modern form shows considerable size variation across its range (Vrba 1984). No potentially environmentally influenced morphological changes are noted in *Aepyceros* between 1.5 and 0.5 Ma.

Bouri anngettyae and *Nitidarcus asfawi* are only known from the Daka Member. With no other data points, no evolutionary change is observable.

Connochaetes first appears in the late Pliocene and persists to the present. There has been some evolutionary change from the first appearance of the *C. taurinus olduvaiensis* through modern *C. taurinus*, mostly manifested in horn cores. Horns, being intimately involved with sexual selection, are subject to intense selective pressures beyond climate and are poor indicators of any overall shift in ecological conditions.

Megalotragus kattwinkeli has several different forms in the period between 1.5 and 0.5 Ma, forms whose relationships are not well agreed upon. Some authors (Gentry 1985; Vrba 1997) argue for the existence of a single, variable species, whereas others (Harris 1991a) promote several species. No directional morphological change associated with time can be detected for this taxon in the period between 1.5 and 0.5 Ma.

Numidocapra crassicornis is the single species known from the genus. It is possibly present in the 2.5 Ma Hata Member of the Bouri Formation, but positively identified at the lower, early Pleistocene sites of Aïn-Hanech, Algeria, and Anabo Koma, Djbouti (Vrba 1997). The Daka Member represents its last appearance. There seems to be a trend of decreasing size from the earlier sites to the Daka Member (Vrba 1997). This morphological signal is impossible to interpret with respect to paleoclimate.

EBSCOhost - printed on 10/28/2022 4:53 AM via . All use subject to https://www.ebsco.com/terms-of-use

Parmularius angusticornis in the Daka Member is different in cranial proportions from earlier specimens from Olduvai Bed II and from Konso-Eardula. Its superior neurocranium is more transversely convex. It is not possible to interpret this morphology as an adaptation related to paleoclimate.

Kobus ellipsiprymnus and *K. kob* from the Daka Member fall within the size range of modern forms. *Kobus sigmoidalis* is smaller than Daka *K. ellipsiprymnus*, which, in turn, is smaller than the modern form. This morphological difference is not interpretable with respect to climate change. *Kobus kob* does not change substantially over the time interval between 1.5 and 0.5 Ma.

Oryx gazella in the Daka Member is indistinguishable from the modern form. Early representatives from the Pliocene differ little from the modern form, differing mainly in length and straightness of horn. This morphological transformation has little obvious connection to global climate change.

Pelorovis oldowayensis and *P. antiquus* in the Daka Member are the last and first appearances of these taxa, respectively. They do not present any evidence for climate-influenced evolutionary change when compared to earlier or later forms.

Tragelaphus strepsiceros and *T.* cf. *imberbis* from the Daka Member are not substantially different from modern forms. Daka forms fall within the metric ranges of both modern basal horn core dimensions and those from earlier localities for both taxa and do not indicate any evolutionary change.

Carnivora

Crocuta crocuta yangula is represented by a complete cranium in the Daka Member. Although larger than modern *Crocuta*, no climate-influenced evolutionary change can be detected across the 1.0 Ma mark.

Cercopithecidae

Cercopithecoides alemayehui is known only from the Daka Member. Thus, no evolutionary change is observable.

Theropithecus oswaldi evolutionary change is documented through the Plio-Pleistocene. During this period the lineage shortens its muzzle and increases the size of its molars, especially distally. Dental wear comparisons between modern *T. gelada*, which is a well-documented grazer, and fossil *Theropithecus* suggest a similarity in dental function (Jablonski 1993). Modern *T. gelada* feeds in large part on grasses and roots. This is one of the most robust associations of evolving form with function for any taxon in the Daka sample and suggests selective pressures associated with feeding on grasses were present throughout the Pleistocene. The trend toward increasing cheek tooth size begins in the Pliocene and does not culminate until the late Pleistocene (Jablonski 1993), indicating that the selective pressures producing it were not diminished across the ca. 1.0 Ma transition to increased glacial intensity.

Elephantidae

Elephas recki is subdivided into numerous temporal subspecies. Frequency of molar lamellae increases in successive members of the lineage in the period between 1.5 and 0.5 Ma

EBSCOhost - printed on 10/28/2022 4:53 AM via . All use subject to https://www.ebsco.com/terms-of-use

(Coppens et al. 1978). The generalized diet of modern elephants makes assigning specific function to tooth lamellar frequency difficult. No climate-induced evolutionary change is apparent in this lineage for the time period between 1.5 and 0.5 Ma.

Rhinocerotidae

Ceratotherium simum from Bed I at Olduvai Gorge is slightly larger than the modern form, the Daka Member form, and that from Olduvai Bed II. No evolutionary pattern is detectable across the 1.0 Ma horizon.

Suidae

Kolpochoerus olduvaiensis from the Daka Member possesses more elongate M3s than earlier specimens from eastern Africa. Because modern *Phacochoerus* uses its elongate and tall M3s in grazing and root feeding, it may well be that their function in *K. olduvaiensis* was congruent with such behaviors. It is likely that M3 lengthening in the *Kolpochoerus* group was similarly associated with selection stemming from grass eating, but this tendency stretches deep into the Pliocene, and so shows no correlation with global climatic change related to the ca. 1.0 Ma transition.

Kolpochoerus majus is well represented in the Daka Member. It demonstrates increasing crown height in third molars from early Pleistocene specimens to those found at Bodo (T. White, personal communication). It does not, however, exhibit the pronounced elongation seen in other suid lineages. Unlike the case of *K. olduvaiensis*, it is not possible to associate functionally *K. majus* third-molar morphology with that of modern *Phacochoerus*, and hence it is impossible to infer climate-influenced selection.

Metridiochoerus compactus from the Daka Member, while possessing elongate M3s, does not change considerably in this feature from earlier Pleistocene forms at Koobi Fora. It is substantially more derived in M3 morphology than its Pliocene parent, *M. andrewsi*. No evolution has been thus far documented for this taxon across the period spanning 1.5–0.78 Ma, after which the taxon apparently became extinct (White 1995).

Metridiochoerus modestus from the Daka Member does not differ significantly from counterparts recovered from Olduvai Bed I or Swartkrans, suggesting no third-molar evolution in this species over the 1.5–0.5 Ma period.

Phacochoerus in the Daka Member presents less elongate M3s than does the modern form. While it should be noted that modern phacochoere third-molar morphology is highly variable, it is clear that evolution toward increased third-molar length occurred over the Pleistocene. However, because Daka presents this taxon's first appearance, it is unclear what happened in the lineage prior to 1.0 Ma. As with *Kolpochoerus olduvaiensis*, it is likely that phacochoere M3 lengthening is associated with selection stemming from grass and root eating.

Hominidae

Homo erectus presents detectable evolutionary change through the Pleistocene. Postcranially, early *H. erectus* is very similar to modern humans. The most notable change is in cranial capacity, which increases in Africa from earlier forms from Koobi Fora and West Turkana through Daka times toward more derived hominids as from Bodo. Increased

EBSCOhost - printed on 10/28/2022 4:53 AM via . All use subject to https://www.ebsco.com/terms-of-use

cranial capacity is associated with larger brains involved with complex neurological information processing in modern humans. It is clear that much human brain function is devoted to negotiating complex social situations (see, for example, Barkow et al. 1992), and it is impossible to extricate runaway social selection pressures from those influenced by paleoclimate.

The overall signal of potentially climate-influenced evolutionary change in Daka taxa between 1.5 and 0.5 Ma is, at best, ambiguous. *Theropithecus oswaldi*, *Phacochoerus*, and *Kolpochoerus olduvaiensis* all show adaptations of their masticatory systems that appear to be associated with grass eating via modern analogs. While there is no obvious change in the rate of evolution during the million-year interval across the 1 Ma horizon in any of the Daka Member lineages, a general trend toward increasing adaptations for grazing can be discerned during the Plio-Pleistocene. It is not possible to detect any evolutionary change that may be specifically correlated with the 1.0 Ma initiation of intensified glaciation in a taxon-by-taxon analysis of Daka constituents across the 1.5–0.5 Ma interval.

The Way Forward

The time period sampled by the Daka Member is extremely important. Hominids had spread across the eastern hemisphere into temperate locations with post-Oldowan bifacial tool technologies. Cranial capacities of hominids had reached around 1,000 cm^3, and morphologically distinct populations of these creatures inhabited different geographic areas. Large mammal faunas were beginning to resemble those that presently exist. Global climate was on the verge of a major shift toward more intense glacial-interglacial cycles. The lineage of our ancestors had initiated the relatively rapid change toward intellectual and cultural primacy. The Daka Member now presents the most complete and best dated picture of this period of nascence.

The publication of this volume, representing more than a decade of work by a large team of specialists, is but one step in the compilation of knowledge about the human past in the Middle Awash Valley of Ethiopia. Work on the Daka Member will continue within the Middle Awash project as this set of localities is monitored for the appearance of new data. Fossils from the Daka Member presented here will continue to be analyzed in efforts to understand mammalian evolution in the Horn of Africa and beyond.

More sites like Daka are needed to fill in the emerging picture of human origins and evolution. Data derived from million-year-old paleontological sites such as Daka are still sparse, and their future assembly will require expertise from the disparate fields of geology, archaeology, and paleontology.

The task of extracting, synthesizing, and presenting paleoanthropologically relevant data from such operations will ultimately constitute a unified, accurate, and detailed prehistory of all humans. Thus, international, multidisciplinary projects, such as the Middle Awash project and those operating at Konso and Gona in Ethiopia, Dmanisi in Georgia, and Buia in Eritrea, will continue to be crucial to enriching our understanding of the critical period between the beginning of the Pleistocene and the initiation of cyclical Pleistocene glaciation at ca. 1.0 Ma.

EBSCOhost - printed on 10/28/2022 4:53 AM via . All use subject to https://www.ebsco.com/terms-of-use

This Page Left Intentionally Blank

EBSCOhost - printed on 10/28/2022 4:53 AM via . All use subject to https://www.ebsco.com/terms-of-use

Bibliography

Abbate, E., A. Albianelli, A. Azzaroli, M. Benvenuti, B. Tesfamariam, P. Bruni, N. Cipriani, R. J. Clarke, G. Ficcarelli, R. Macchiarelli, G. Napoleone, M. Papini, L. Rook, M. Sagri, T. M. Tecle, D. Torre, and I. Villa. 1998. A one-million-year-old *Homo* cranium from the Danakil (Afar) Depression of Eritrea. *Nature* 393:458–460.

Adam, K. D. 1985. The chronological and systematic position of the Steinheim skull. In E. Delson (ed.), Ancestors: The Hard Evidence, pp. 272–276. Alan R. Liss, New York.

———. 1986. Fossilfunde aus den Canstatter Sauerwasserkalken. *Fundberichte aus Baden-Wurttemberg* 11:25–61.

Adams, J. R., A. Leonard, and L. P. Waits. 2003. Widespread occurrence of a domestic dog mitochondrial DNA haplotype in southern US coyotes. *Molecular Evolution* 12:541–546.

Aguirre, E. 1969a. Evolutionary history of the elephant. *Science* 164:1366–1376.

———. 1969b. Revisión sistemática de los Elephantidae por su morfología y morfometría dentaria (segunda parte). *Estudios Geológicos* 25:123–177.

———. 1969c. Revisión sistemática de los Elephantidae por su morfología y morfometría dentaria (tercera parte). *Estudios Geológicos* 25:317–367.

Aiello, L., and C. Dean. 1990. An Introduction to Human Evolutionary Anatomy. Academic Press, London.

Alberdi, M. 1989. A review of Old World hipparionine horses. In D. Prothero and R. Schoch (eds.), The Evolution of Perissodactyls, pp. 234–261. Clarendon Press and Oxford University Press, New York and Oxford.

Alemseged, Z., and D. Geraads. 2001. A new middle Pleistocene fauna from the Busidima-Telalak region of the Afar, Ethiopia. *Comptes Rendus de l'Académie des Sciences, Sciences de la Terre et des Planètes* 331:549–556.

Allard, M., M. Miyamoto, L. Jarecki, F. Kraus, and M. Tennant. 1992. Systematics and evolution of the artiodactyl family Bovidae. *Proceedings of the National Academy of Sciences of the United States of America* 89:3972–3976.

Alles, D. L., and J. C. Stevenson. 2003. Teaching human evolution. *American Biology Teacher* 65:333–339.

Amrine-Madsen, H., K. P. Koep, R. K. Wayne, and M. S. Springer. 2003. A new phylogenetic marker, apolipoprotein B, provides compelling evidence for eutherian relationships. *Molecular Phylogenetics and Evolution* 28:225–240.

Andrews, P. J. 1984. An alternative interpretation of the characters used to define *Homo erectus. Courier Forschunginstitut Senckenberg* 69:167–175.

Andrews, R. C. 1945. Meet Your Ancestors: A Biography of Primitive Man. Viking, New York.

Aouadi, N. 2001. New data on the diversity of elephants (Mammalia, Proboscidea) in the early and early middle Pleistocene of France. In G. Cavarretta, P. Gioia, M. Mussi, and M. R. Palombo (eds.), The World of Elephants: Proceedings of the First International Congress (Oct. 16–21, 2001, Rome), pp. 81–84. Consiglio Nazionale delle Ricerche, Roma.

Arambourg, C. 1942. L'*Elephas recki* Dietrich. Sa position systématique et ses affinités. *Bulletin de la Société de la Géologique de France* 5:73–87.

———. 1947. Contribution à l'étude géologique et paléontologique du bassin du lac Rudolfe et de la basse vallée de l'Omo. Deuxième partie: Paléontologie. Mission scientifique de l'Omo 1932–1933. *Géologie-Anthropologie* 3: 231–562.

———. 1958. Les gros mammifères des couches tayaciennes. In H. Alimen, C. Arambourg, and A. Schreuder (eds.), La grotte de Fontéchevade, pp. 185–229. Memoire 29. Institut de Paleontologie Humaine, Paris.

———. 1979. Vertébrés villafranchiens de l'Afrique du Nord (artiodactyles, carnivores, primates, reptiles, oiseaux). Fondation Singer-Polignac, Paris.

EBSCOhost - printed on 10/28/2022 4:53 AM via . All use subject to https://www.ebsco.com/terms-of-use

Armour-Chelu, M., R. L. Bernor, and H.-W. Mittmann. 2006. Hooijer's Hypodigm for *"Hipparion" cf. ethiopicum* (Equidae, Hipparioninae) from Olduvai, Tanzania and comparative material from the East African Plio-Pleistocene. *Abhandlungen der Bayerischen Akademie der Wissenschaften* 30:15–24.

Arsuaga, J. L. 2004. The Neanderthal's Necklace: In Search of the First Thinkers. Four Walls Eight Windows, New York.

Arsuaga, J. L., I. Martínez, A. Garcia, and C. Lorenzo. 1997. The Sima de los Huesos crania (Sierra de Atapuerca, Spain): A comparative study. *Journal of Human Evolution* 33:219–281.

Arsuaga, J. L., I. Martínez, C. Lorenzo, A. Garcia, A. Muñoz, O. Alonso, and J. Gallego. 1999. The human cranial remains from Gran Dolina lower Pleistocene site (Sierra de Atapuerca, Spain). *Journal of Human Evolution* 37:431–457.

Asfaw, B. 1983. A new hominid parietal from Bodo, Middle Awash Valley, Ethiopia. *American Journal of Physical Anthropology* 61:367–372.

Asfaw, B., T. D. White, O. Lovejoy, B. Latimer, S. Simpson, and G. Suwa. 1999. *Australopithecus garhi:* A new species of early hominid from Ethiopia. *Science* 284:629–634.

Asfaw, B., W. H. Gilbert, Y. Beyene, W. K. Hart, P. R. Renee, G. WoldeGabriel, E. S. Vrba, and T. D. White. 2002. Remains of *Homo erectus* from Bouri, Middle Awash, Ethiopia. *Nature* 416:317–320.

Asherson, N. 1965. Identification by Frontal Sinus Prints: A Forensic Medical Pilot Survey. H. K. Lewis and Co., London.

Avery, D. 2003. Early and middle Pleistocene environments and hominid biogeography: micromammalian evidence from Kabwe, Twin Rivers and Mumbwa Caves in central Zambia. *Palaeogeography, Palaeoclimatology, Palaeoecology* 189:55–69.

Azzaroli, A. 1966. La valeur des caractères crâniens dans la classification des éléphants. *Eclogae Geologicae Helvetiae* 59:541–564.

———. 2003. Phylogeny of the genus *Equus*. *Palaeontographia Italica* 89:XI–XV.

Baba, H., F. Aziz, Y. Kaifu, G. Suwa, R. T. Kono, and T. Jacob. 2003. New *Homo erectus* calvarium from the Pleistocene of Java. *Science* 299:1384–1388.

Balzeau, A., and D. Grimaud-Hervé. 2006. Cranial base morphology and temporal bone pneumatization in Asian *Homo erectus*. *Journal of Human Evolution* 51:350–359.

Barkow, J., L. Cosmides, and J. Tooby. 1992. The Adapted Mind: Evolutionary Psychology and the Generation of Culture. Oxford University Press, New York.

Barnosky, A. D. 2005. Effects of Quaternary climatic change on speciation in mammals. *Journal of Mammalian Evolution* 12:247–264.

Barry, J. C. 1987. Large carnivores (Canidae, Hyaenidae, Felidae) from Laetoli. In M. D. Leakey and J. M. Harris (eds.), Laetoli: A Pliocene Site in Northern Tanzania, pp. 235–258. Clarendon Press, Oxford.

Beden, M. 1979. Les éléphants (*Loxodonta* et *Elephas*) d'Afrique Orientale: Systématique, Phylogénie, Intérêt Biochronologique. Ph.D. thesis, Université de Poitiers, Poiters.

———. 1980. *Elephas recki* Dietrich, 1915 (Proboscidea, Eleaphantidae): Evolution au cours de Plio-Pléistocène en Afrique Orientale. *Géobios* 13:891–901.

———. 1983. Family Elephantidae. In J. M. Harris (ed.), Koobi Fora Research Project. Volume 2: The Fossil Ungulates: Proboscidea, Perissodactyla, and Suidae, pp. 40–129. Clarendon Press, Oxford.

———. 1985. Les proboscidiens des grands gisements à hominidés Plio-Pléistocène d'Afrique Orientale. In Fondation Singer-Polignac (ed.), L'environnement des Hominidés au Plio-Pléistocène, pp. 21–44. Masson, Paris.

———. 1987. Les faunes Plio-Pléistocènes de la basse vallée de l'Omo (Éthiopie). Tome 2: Les éléphantides (Mammalia, Proboscidea). Cahiers de Paléontologie. Centre National de la Recherche Scientifique, Paris.

Behrensmeyer, A. K. 2006. Climate change and human evolution. *Science* 311:476–478.

Belmaker, M., E. Tchernov, S. Condemi, and O. Bar-Yosef. 2002. New evidence for hominid presence in the lower Pleistocene of the southern Levant. *Journal of Human Evolution* 43:43–56.

Beltrán, J. F., and M. Delibes. 1993. Physical characteristics of Iberian lynxes *(Lynx pardinus)* from Doñana, southwestern Spain. *Journal of Mammalogy* 74:852–862.

Benefit, B. 1999. *Victoriapithecus:* The key to Old World monkey and catarrhine origins. *Evolutionary Anthropology* 7:155–174.

Benefit, B., and M. L. McCrossin. 2002. The Victoripithecidae, Cercopithecoidea. In W. C. Hartwig (ed.), The Primate Fossil Record, pp. 241–254. Cambridge University Press, Cambridge, UK.

Berger, L. 1993. A preliminary estimate of the age of the Gladysvale australopithecine site. *Palaeontologia Africana* 30:51–55.

Bermúdez de Castro, J. M., J. L. Arsuaga, E. Carbonell, A. Rosas, I. Martinez, and M. Mosquera. 1997. A hominid from the Lower Pleistocene of Atapuerca, Spain: Possible ancestor to Neanderthals and modern humans. *Science* 276: 1392–1395.

Bernor, R. L., and M. J. Armour-Chelu. 1999a. Family Equidae. In Volker Fahlbusch Memorial Volume, pp. 193–202. Münchner Geowissenschaftliche Abhandlungen, Munich.

———. 1999b. Toward an evolutionary history of African hipparionine horses. In F. Schrenk and T. Bromage (eds.), African Biogeography, Climate Change and Human Evolution, pp. 189–215. The Human Evolution Series. Oxford University Press, New York and Oxford.

Bernor, R. L., and J. Franzen. 1997. The hipparionine horses from the Turolian Age (late Miocene) locality of Dorn Dürkheim, Germany. Courier Forschungsinstitut Senckenberg 197:117–185.

EBSCOhost - printed on 10/28/2022 4:53 AM via . All use subject to https://www.ebsco.com/terms-of-use

Bernor, R. L., K. Heissig, and H. Tobien. 1987. Early Pliocene Perissodactyla from Sahabi, Libya. In N. Boaz, A. El Arnauti, A. Gaziry, J. de Heinzelin, and D. D. Boaz (eds.), Neogene Paleontology and Geology of Sahabi. Alan Liss, New York.

Bernor, R. L., and J. M. Harris. 2003. Systematics and evolutionary biology of the late Miocene and early Pliocene hipparionine horses from Lothagam, Kenya. In J. M. Harris and M. Leakey (eds.), Lothagam: The Dawn of Humanity in Eastern Africa, pp. 387–438. Columbia University Press, New York.

Bernor, R. L., and R. S. Scott. 2003. New interpretations of the systematics, biogeography and paleoecology of the Sahabi hipparions (latest Miocene, Libya). *Geodiversitas* 25:297–319.

Bernor, R. L., G. D. Koufos, M. O. Woodbune, and M. Fortelius. 1996. The evolutionary history and biochronology of European and southwest Asian late Miocene and Pliocene hipparionine horses. In R. L. Bernor, V. Fahlbusch, and H.-W. Mittmann (eds.), The Evolution of Western Eurasian Neogene Mammal Faunas, pp. 307–338. Columbia University Press, New York.

Bernor, R. L., H. Tobien, L. A. Hayek, and H.-W. Mittmann. 1997. *Hippotherium primigenium* (Equidae, Mammalia) from the late Miocene of Höwenegg (Hegau, Germany). *Andrias* 10:1–230.

Bernor, R. L., R. S. Scott, M. Fortelius, J. Kappelman, and S. Sen. 2003. Systematics and evolution of the late Miocene hipparions from Sinap, Turkey. In M. Fortelius, J. Kappelman, R. L. Bernor, and S. Sen (eds.), The Geology and Paleontology of the Miocene Sinap Formation, Turkey, pp. 220–282. Columbia University Press, New York.

Bernor, R. L., T. M. Kaiser, and S. V. Nelson. 2004. The oldest Ethiopian hipparion (Equinae, Perissodactyla) from Chorora: Systematics, paleodiet and paleoclimate. *Courier Forschungsinstitut Senckenberg* 246:213–216.

Bernor, R. L., R. S. Scott, and Y. Haile-Selassie. 2005. A contribution to the evolutionary history of Ethiopian hipparionine horses (Mammalia, Equidae): Morphometric evidence from the postcranial skeleton. *Geodiversitas* 27:133–158.

Berthelet, A. 2001. L'outillage lithique du site de dépeçage à *Elephas recki ilretensis* de Barogali (république de Djibouti). *Comptes Rendus de l'Academie des Sciences, Sciences de la Terre et des Planètes* 332:411–416.

Bininda-Edmonds, O. R. P., J. L. Gittleman, and A. Purvis. 1999. Building large carnivore trees by combining phylogenetic information: A complete phylogeny of extant Carnivora (Mammalia). Biological Reviews of the Cambridge Philosophical Society 74:143–175.

Black, D. 1925. The human skeletal remains from Sha Kuo T'un cave deposit in comparison with those from Yang Shao Tsun and with recent North China skeletal material. *Palaeontologia Sinica,* series D 1(fasc. 3):1–120.

Blanco, J. C. 1998. Mamíferos de España I. Insectívoros, quirópteros, Primates y Carnívoros de la Península Ibérica, Baleares y Canarias. Planeta, Barcelona.

Bobe, R., A. K. Behrensmeyer, and R. E. Chapman. 2002. Faunal change, environmental variability and late Pliocene hominin evolution. *Journal of Human Evolution* 42:475–497.

Boeuf, O. 1990. Originalité et importance de la faune Plio-Pléistocène de Chilhac (Haute-Loire, France). *Quartärpaläontologie* 8:13–28.

Boisserie, J. 2004. A new species of Hippopotamidae (Mammalia, Artiodactyla) from the Sagantole Formation, Middle Awash, Ethiopia. *Bulletin de la Société Géologique de France* 175: 525–533.

———. 2005. The phylogeny and taxonomy of Hippopotamidae (Mammalia: Artiodactyla): A review based on morphology and cladistic analysis. *Zoological Journal of the Linnean Society* 143:1–26.

Boisserie, J., and T. D. White. 2004. A new species of Pliocene Hippopotamidae from the Middle Awash, Ethiopia. *Journal of Vertebrate Paleontology* 24:464–473.

Boisserie, J., M. Brunet, L. Andossa, and P. Vignaud. 2003. Hippopotamids from the Djurab Pliocene faunas, Chad, Central Africa. *Journal of African Earth Sciences* 36:15–27.

Boisserie, J., F. Lihoreau, and M. Brunet. 2005a. Origins of Hippopotamidae (Mammalia, Cetartiodactyla): Towards resolution. *Zoologica Scripta* 34:119–143.

———. 2005b. The position of Hippopotamidae within Cetartiodactyla. *Proceedings of the National Academy of Sciences of the United States of America* 102:1537–1541.

Boisserie, J., A. Likius, P. Vignaud, and M. Brunet. In press. A new late Miocene hippopotamid from Toros-Ménalla, Chad. *Journal of Vertebrate Paleontology.*

Bonifay, M. F. 1996. The importance of mammalian faunas from the early middle Pleistocene of France. In A. Turner (ed.), The Early Middle Pleistocene in Europe. Proceedings of the SEQS Cromer Symposium, pp. 255–262. Balkema, Rotterdam.

Bose, P. N. 1880. Undescribed fossil carnivora from the Sivalik Hills in the collection of the British Museum. *Quarterly Journal of the Geological Society of London* 36:119–136.

Bowler, P. J. 2005. Variation from Darwin to the modern synthesis. In B. Hallgrímsson and B. K. Hall (eds.), Variation: A Central Concept in Biology, pp. 9–28. Academic Press, London.

Brandon-Jones, D., A. A. Eudey, T. Geismann, C. P. Groves, D. J. Melnick, J. C. Morales, M. Shekelle, and C. B. Stewart. 2004. Asian primate classification. *International Journal of Primatology* 25:97–164.

Bräuer, G. 1994. How different are Asian and African *Homo erectus? Courier Forschungsinstitut Senckenberg* 171:301–318.

Bräuer, G., and H. Broeg. 1998. On the degree of Neanderthal: Modern continuity in the earliest Upper Paleolithic crania from Czech Republic—evidence from non-metrical features. In K. Omoto and P. V. Tobias (eds.), The Origins and Past of Modern Humans: Towards Reconciliation, pp. 106–125. World Scientific, Singapore.

EBSCOhost - printed on 10/28/2022 4:53 AM via . All use subject to https://www.ebsco.com/terms-of-use

Bräuer, G., and E. Mbua. 1992. *Homo erectus* features used in cladistics and their variability in Asian and African hominids. *Journal of Human Evolution* 22:79–108.

Brodkorb, B. 1980. A new fossil heron (Aves: Ardeidae) from the Omo Basin of Ethiopia, with remarks on the position of some other species assigned to the Ardeida. *Natural History Museum of Los Angeles County Contributions in Science* 330:87–92.

Brodkorb, B., and C. Mourer-Chauviré. 1982. Fossil anhingas (Aves: Anhingidae) from early man sites of Hadar and Omo (Ethiopia) and Olduvai Gorge (Tanzania). *Geobios* 15:505–515.

Bromage, T. G., and F. Schrenk. 1999. African Biogeography, Climate Change, and Human Evolution. Oxford University Press, New York and Oxford.

Brühl, E., and D. Mania. 2003. Neumark-Nord: A late middle Pleistocene lake shore with synchronous sites of different functional character. Données récentes sur les modalités de peuplement en Europe au Paléolithique inférieur et moyen, Rennes, Université de Rennes 1, September 22–25, 2003.

Bruner, E., and G. Manzi. 2005. CT-based description and phyletic evaluation of the archaic human Calvarium from Ceprano, Italy. *The Anatomical Record. Part A, Discoveries in Molecular, Cellular, and Evolutionary Biology* 285(1):643–657.

Brunet, M., and T. D. White. 2001. Two new suin species (Mammalia, Suidae) from Africa (Chad, Ethiopia). *Comptes Rendus de l'Academie des Sciences, Sciences de la Terre et des Planètes* 332:51–57.

Buntjer, J., M. Otsen, I. Nijman, M. Kuiper, and J. Lenstra. 2002. Phylogeny of bovine species based on AFLP fingerprinting. *Heredity* 88:46–51.

Cameron, D. W. 2003. Early hominin speciation at the Plio/Pleistocene transition. *Homo* 54:1–28.

Capasso Barbato, L., and C. Petronio. 1983a. Considerazioni sistematiche e filogenetiche su *"Hippopotamus pentlandi"* Von Meyer, 1832. *Atti della Società Italiana di Scienze Naturali e del Museo Civico di Storia Naturale di Milano* 124:229–248.

———. 1983b. Considerazioni sistematiche e filogenetiche su *Hippopotamus melitensis* Major, 1902. *Atti della Società Italiana di Scienze Naturali e del Museo Civico di Storia Naturale di Milano* 124:281–290.

Carbonell, E., J. M. Bermúdez De Castro, J. L. Arsuaga, E. Allue, M. Bastir, A. Benito, I. Cáceres, T. Canals, J. C. Díez, J. van der Made, M. Mosquera, A. Ollé, A. Pérez-Gonzáles, J. Rodríguez, X. P. Rodríguez, A. Rosas, J. Rosell, R. Sala, J. Vallverdú, and J. M. Vergés. 2005. An early Pleistocene hominin mandible from Atapuerca-TD6, Spain. *Proceedings of the National Academy of Sciences of the United States of America* 102:5674–5678.

Cerdeño, E. 1998. Diversity and evolutionary trends of the family Rhinocerotidae (Perissodactyla). *Palaeogeography, Palaeoclimatology, Palaeoecology* 141:13–34.

Cerling, T. E. 1984. The stable isotopic composition of modern soil carbonate and its relationship to climate. *Earth and Planetary Science Letters* 71:229–240.

Cerling, T. E., and R. L. Hay. 1986. An isotopic study of paleosol carbonates from Olduvai Gorge. *Quaternary Research* 25:63–78.

Cerling, T. E., J. R. Bowman, and J. R. O'Neil. 1988. An isotopic study of a fluvial-lacustrine sequence: The Plio-Pleistocene Koobi Fora sequence, East Africa. *Palaeogeography, Palaeoclimatology, Palaeoecology* 63:335–356.

Cerling, T. E., J. M. Harris, and M. G. Leakey. 2003. Isotope paleoecology of the Nawata and Nachukui Formations at Lothagam, Turkana Basin, Kenya. In M. G. Leakey and J. M. Harris (eds.), Lothagam: The Dawn of Humanity in Eastern Africa, pp. 605–624. Columbia University Press, New York.

Chappill, J. A. 1989. Quantitative characters in phylogenetic analysis. *Cladistics* 5:217–234.

Chavaillon, J., N. Chavaillon, F. Hours, and M. Piperno. 1979. From Oldowan to middle Stone Age at Melka Kunture: Understanding cultural changes. *Quaternaria* 21:87–114.

Chavaillon, J., A. Berthelet, J. L. Boisaubert, M. Faure, C. I. Guérin, and S. A. Warsama. 1990. Un *Elephas recki* en conexion anatomique dans le site de Haïdalo, prés de As Eyla (République de Djibouti). *Comptes Rendus de l'Academie des Sciences, Sciences de la Terre et des Planètes* 310:441–446.

Christensen, A. M. 2004. Assessing the variation in individual frontal sinus outlines. *American Journal of Physical Anthropology* 127(3):291–295.

Churcher, C. 1978. Giraffidae. In V. Maglio and H. Cooke (eds.), Evolution of African Mammals, pp. 509–535. Harvard University Press, Cambridge, MA.

———. 1982. Oldest ass recovered from Olduvai Gorge, Tanzania, and the origin of asses. *Journal of Paleontology* 56:1124–1132.

Churcher, C. S., and M. L. Richardson. 1978. Equidae. In V. J. Maglio and H. B. S. Cooke (eds.), Evolution of African Mammals, pp. 379–422. Harvard University Press, Cambridge, MA.

Clark, J. D., and K. D. Schick. 2000. Acheulean archaeology of the western Middle Awash. In J. de Heinzelin, J. D. Clark, K. D. Schick, and W. H. Gilbert (eds.), The Acheulean and the Plio-Pleistocene Deposits of the Middle Awash Valley, Ethiopia, pp. 123–137. Geological Sciences, Annals 104. Royal Museum for Central Africa, Tervuren, Belgium.

Clark, J. D., B. Asfaw, G. Assefa, J. W. K. Harris, H. Kurashina, R. C. Walter, T. D. White, and M. A. J. Williams. 1984. Paleoanthropological discoveries in the Middle Awash Valley, Ethiopia. *Nature* 307:423–428.

Clark, J. D., Y. Beyene, G. WoldeGabriel, W. K. Hart, P. R. Renee, W. H. Gilbert, A. Defleur, G. Suwa, S. Katoh,

EBSCOhost - printed on 10/28/2022 4:53 AM via . All use subject to https://www.ebsco.com/terms-of-use

K. R. Ludwig, J. Boisserie, B. Asfaw, and T. D. White. 2003. Stratigraphic, chronological, and behavioural context of Pleistocene *Homo sapiens* from Middle Awash, Ethiopia. *Nature* 423:747–752.

Clarke, R. J., and F. C. Howell. 1972. Affinities of the Swartkrans 847 hominid cranium. *American Journal of Physical Anthropology* 37:319–325.

Clark, W. E. Le Gros. 1971. The Antecedents of Man. Quadrangle Books, Chicago.

Colbert, E. H. 1935a. The phylogeny of the Indian Suidae and the origin of the Hippopotamidae. *American Museum Novitates* 799:1–24.

———. 1935b. Siwalik mammals in the American Museum of Natural History. *Transactions of the American Philosophical Society* 26:278–294.

Cooke, H. B. S. 1950. A critical revision of the Quaternary Perissodactyla of southern Africa. *Annals of the South African Museum* 31:393–479.

———. 1982. *Phacochoerus modestus* from Bed I, Olduvai Gorge. *Zeitschrift für Geologische Wissenschaften* 10: 899–908.

———. 1997. The status of the African fossil suids *Kolpochoerus limnetes* (Hopwood, 1926), *K. phacochoeroides* (Thomas, 1884) and *"K." afarensis* (Cooke, 1978). *Geobios* 30:121–126.

Cooke, H. B. S., and S. C. Coryndon. 1970. Pleistocene mammals from the Kaiso Formation and other related deposits in Uganda. In L. S. B. Leakey and R. J. G. Savage (eds.), Fossil Vertebrates of Africa. Volume 2, pp. 147–198. Academic Press, London.

Cooke, H. B. S., and A. F. Wilkenson. 1978. Suidae and Tayassuidae. In V. Maglio and H. Cooke (eds.), Evolution of African Mammals, pp. 435–482. Harvard University Press, Cambridge, MA.

Coppens, Y., V. J. Maglio, C. T. Madden, and M. Beden. 1978. Proboscidea. In V. J. Maglio and H. B. S. Cooke (eds.), Evolution of African Mammals, pp. 336–367. Harvard University Press, Cambridge, MA.

Coryndon, S. C. 1971. Evolutionary trends in East African Hippopotamidae. *Bulletin de l'Association Française des Études sur le Quaternaire* 1:473–478.

Craig, H. 1961. Isotopic variations in meteoric waters. *Science* 133: 1833–1834.

Curnoe, D. 2003. Problems with the use of cladistic analysis in palaeoanthropolgy. *Homo* 53:225–234.

Damuth, J., and I. L. Heisler. 1988. Alternative formulations of multilevel selection. *Biology and Philosophy* 3:407–430.

Davis, P. 1964. Hominid fossils from Bed I, Olduvai Gorge, Tanganyika: Fossil foot bones. *Nature* 221:230–233.

Davivongs, V. 1963. The femur of the Australian. *American Journal of Physical Anthropology* 21:457–467.

Dawkins, R. 2004. The Ancestor's Tale: A Pilgrimage to the Dawn of Evolution. Houghton Mifflin Company, New York.

Day, M. H. 1971. Postcranial remains of *Homo erectus* from Bed IV, Olduvai Gorge, Tanzania. *Nature* 232:383–387.

Dean, D., J. Hublin, R. Holloway, and R. Ziegler. 1998. On the phylogenetic position of the pre-Neandertal specimen from Reilingen, Germany. *Journal of Human Evolution* 34: 485–508.

de Beaulieu, J., V. Andrieu-Ponel, M. Reille, E. Grüger, C. Tzedakis, and H. Svobodova. 2001. An attempt at correlation between the Velay pollen sequence and the middle Pleistocene stratigraphy from central Europe. *Quaternary Science Review* 20:1593–1602.

Debruyne, R. 2005. A case study of apparent conflict between molecular phylogenies: The interrelationships of African elephants. *Cladistics* 21:31–50.

Dechow, P. C., and R. Singer. 1984. Additional fossil *Theropithecus* from Hopefield, South Africa: A comparison with other African sites and a reevaluation of this taxonomic status. *American Journal of Physical Anthropology* 63:405–435.

de Heinzelin, J. 2000. Stratigraphy. In J. de Heinzelin, J. D. Clark, K. D. Schick, and W. H. Gilbert (eds.), The Acheulean and the Plio-Pleistocene Deposits of the Middle Awash Valley, Ethiopia, pp. 11–25. Geological Sciences, Annals, 104. Royal Museum for Central Africa, Tervuren, Belgium.

de Heinzelin, J., J. D. Clark, T. D. White, W. K. Hart, P. R. Renne, G. WoldeGabriel, Y. Beyene, and E. S. Vrba. 1999. Environment and behavior of 2.5 million year old Bouri hominids. *Science* 284:625–629.

de Heinzelin, J., J. D. Clark, K. D. Schick, and W. H. Gilbert. 2000a. The Acheulean and the Plio-Pleistocene Deposits of the Middle Awash Valley, Ethiopia. Geological Sciences, Annals, 104. Royal Museum for Central Africa, Tervuren, Belgium.

de Heinzelin, J., G. WoldeGabriel, T. D. White, and W. H. Gilbert. 2000b. Geography, mapping and nomenclature. In J. de Heinzelin, J. D. Clark, K. D. Schick, and W. H. Gilbert (eds.), The Acheulean and the Plio-Pleistocene Deposits of the Middle Awash Valley, Ethiopia, pp. 5–10. Geological Sciences, Annals, 104. Royal Museum for Central Africa, Tervuren, Belgium.

Deino, A. L., J. D. Kingston, J. M. Glen, R. K. Edgar, and A. Hill. 2006. Precessional forcing of lacustrine sedimentation in the late Cenozoic Chemeron Basin, Central Kenya Rift, and calibration of the Gauss/Matuyama boundary. *Earth and Planetary Science Letters* 247:41–60.

Delson, E. 1975. Evolutionary history of the Cercopithecidae. In F. S. Szalay (ed.), Approaches to Primate Paleobiology. Volume 5: Contributions to Primatology, pp. 167–271. S. Karger, Basel.

———. 1993. *Theropithecus* fossils from Africa and India and the taxonomy of the genus. In N. G. Jablonski (ed.), *Theropithecus:* The Rise and Fall of a Primate Genus, pp. 157–189. Cambridge University Press, Cambridge, UK.

EBSCOhost - printed on 10/28/2022 4:53 AM via . All use subject to https://www.ebsco.com/terms-of-use

———. 1994. Evolutionary history of the colobine monkeys in paleoenvironmental perspective. In A. Davies and J. Oates (eds.), Colobine Monkeys: Their Ecology, Behavior and Evolution, pp. 11–43. Cambridge University Press, Cambridge, UK.

Delson, E., C. J. Terranova, W. L. Jungers, E. J. Sargis, N. G. Jablonski, and P. C. Dechow. 2000. Body mass in Cercopithecidae (Primates, Mammalia): Estimation and scaling in extinct and extant taxa. *American Museum of Natural History Anthropology Papers* 83:1–159.

Delson, E., K. Harvati, D. Reddy, L. F. Marcus, K. Mowbray, G. J. Sawyer, T. Jacob, and S. Marquez. 2001. The Sambungmacan 3 *Homo erectus* calvaria: A comparative morphometric and morphological analysis. *Anatomical Record* 262:380–397.

de Lumley, H., A. Fournier, Y. Park, Y. Yokahama, and A. Demouy. 1984. Stratigraphie du remplissage Pleistocene moyen de la Caune de l'Arago a Tautavel. *L'Anthropologie* 88:5–18.

de Lumley, M., L. Gabunia, A. Vekua, and D. Lordkipanidze. 2006. Les restes humains du Pliocene final du début du Pléistocene inférieur de Dmanissi, Géorgie (1991–2000). I. Les crânes, D2280, D2282, D2700. *L'Anthropologie* 110: 1–110.

deMenocal, P. B. 2004. African climate change and faunal evolution during the Pliocene-Pleistocene. *Earth and Planetary Science Letters* 220:3–24.

deMenocal, P. B., and J. Bloemendal. 1995. Plio-Pleistocene climatic variability in subtropical Africa and the paleoenvironment of hominid evolution. In E. S. Vrba, G. H. Denton, T. C. Partridge, and L. H. Burckle (eds.), Paleoclimate and Evolution, pp. 262–288. Yale University Press, New Haven, CT.

Dennell, R., and W. Roebroeks. 2005. An Asian perspective on early human dispersal from Africa. *Nature* 438:1099–1104.

Deocampo, D. M. 2002. Sedimentary structures generated by *Hippopotamus amphibius* in a lake-margin wetland, Ngorongoro Crater, Tanzania. *Palaïos* 17:212–217.

Diamond, J. M. 1992. Twilight of the pygmy hippos. *Nature* 359:15.

Dietrich, W. O. 1916. *Elephas antiquus recki* n. f. aus dem Diluvium Deutsch-Ostafrikas, nebst Bemerkungen über die stammesgeschichtlichen Veränderungen des Extremitäten Skeletts der Proboscidier. *Archiv für Biontologie/Gesellschaft naturforschender Freund zu Berlin* 4:1–80.

———. 1926. Fortschritte der Säugettierpaläontologie Afrikas. *Forschungen und Fortschritte* 15:121–122.

———. 1951. Daten zu den fossilen Elefanten Afrikas und Ursprung der Gattung *Loxodonta*. *Neues Jahrbuch für Geologie und Palaeontologie, Abhandlungen* 93:325–378.

Disotell, T. R. 1994. Generic level of relationships of the Papionini (Cercopithecoidea). *American Journal of Physical Anthropology* 94:47–57.

———. 2000. Molecular systematics of the Cercopithecidae. In P. F. Whitehead and C. J. Jolly (eds.), Old World Monkeys, pp. 29–56. Cambridge University Press, Cambridge, UK.

Ditchfield, P., J. Hicks, T. Plummer, L. C. Bishop, and R. Potts. 1999. Current research on the late Pliocene and Pleistocene deposits north of Homa Mountain, southwestern Kenya. *Journal of Human Evolution* 36:123–150.

Driese, S. G., C. I. Mora, C. A. Stiles, R. M. Joeckel, L. C. Nordt. 2000. Mass-balance reconstruction of a modern Vertisol: Implications for interpreting the geochemistry and burial alteration of paleo-Vertisols. *Geoderma* 95: 179–204.

Dubrovo, I. A. 1960. [The ancient elephant in USSR]. [Works of the Paleontological Institute of the Academy of Sciences of the USSR] 85:35–78.

———. 1977. Origin and migration of palaeoloxodont elephants. *International Geological Review* 19:1085–1088.

———. 1981. Die fossilen Elefanten Japans. *Quartärpaläontologie* 4:49–84.

Ducrocq, S. 1994. An Eocene peccary from Thailand and the biogeographical origins of the artiodactyl family Tayassuidae. *Palaeontology* 37:765–779.

Ducroz, J. F., V. Volobouev, and L. Granjon. 1998. A molecular perspective on the systematics and evolution of the genus *Arvicanthis* (Rodentia, Muridae): Inferences from complete cytochrome *b* gene sequences. *Molecular Phylogenetics and Evolution* 14:104–117.

Eck, G. G. 1987. *Theropithecus oswaldi* from the Shungura Formation, Lower Omo Basin, southwestern Ethiopia. In G. G. Eck, N. G. Jablonski, and M. L. Leakey (eds.), Les Faunes Plio-Pléistocènes de la Basse Vallée de l'Omo (Éthiopie). Tome 3, Cercopithecidae de la Formation de Shungura, pp. 123–139. Cahiers de Paléontologie. Centre National de la Recherche Scientifique, Paris.

Eggert, L. S., C. A. Rasner, and D. S. Woodruff. 2002. The evolution and phylogeography of the African elephant inferred from mitochondrial DNA sequence and nuclear microsatellite markers. *Proceedings of the Royal Society: Biological Sciences* 269:1993–2006.

Eisenberg, J. F. 1989. Mammals of the Neotropics. Volume 1: The Northern Neotropics: Panama, Colombia, Venezuela, Guyana, Suriname, French Guiana. University of Chicago Press, Chicago.

Eisenberg, J. F., and K. H. Redford. 1999. Mammals of the Neotropics. Volume 3: The Central Neotropics: Ecuador, Peru, Bolivia, Brazil. University of Chicago Press, Chicago.

Eisenmann, V. 1979. Les métapodes d'*Equus* sensu lato (Mammalia, Perissodactyla). *Geobios* 12:863–886.

———. 1983. Equidae. In J. Harris (ed.), Koobi Fora Research Project. Volume 2: The Fossil Ungulates, Proboscidea, Perissodactyla, and Suidae, pp. 156–214. Clarendon Press, Oxford.

———. 1985. Les equides des gisements de la Vallée de l'Omo en Éthiopie. In Y. Coppens and F. Howell (eds.), Les Faunes Plio-Pléistocènes de la Basse Vallée de l'Omo (Éthiopie). Tome

EBSCOhost - printed on 10/28/2022 4:53 AM via . All use subject to https://www.ebsco.com/terms-of-use

1. Périssodactyles, Artiodactyles (Bovidae), pp. 13–65. Centre National de la Recherche Scientifique, Paris.

———. 1995. What metapodial morphometry has to say about some Miocene hipparions. In E. S. Vrba, G. H. Denton, T. C. Partridge, and L. H. Burckle (eds.), Paleoclimate and Evolution, with Emphasis on Human Origins, pp. 148–163. Yale University Press, New Haven, CT.

Eisenmann, V., and M. Baylac. 2000. Extant and fossil *Equus* (Mammalia, Perissodactyla) skulls: A morphometric definition of the subgenus *Equus*. *Zoologica Scripta* 29:89–100.

Eisenmann, V., M. T. Alberdi, C. Giuli, and U. Staesche. 1988. Studying fossil horses, Volume I: Methodology. In M. O. Woodburne and P. Y. Sondaar (eds.), Collected Papers after the "New York International Hipparion Conference, 1981," pp. 1–71. Brill, Leiden.

Eltringham, S. K. 1993. The pygmy hippopotamus *(Hexaprotodon liberiensis)*. In W. L. R. Oliver (ed.), Pigs, Peccaries, and Hippos: Status Survey and Conservation Action Plan, pp. 55–60. The International Union for the Conservation of Nature and Natural Resources (IUCN), Gland, Switzerland.

———. 1999. The Hippos. Academic Press, London.

Essop, M., E. Harley, and I. Baumgarten. 1997. A molecular phylogeny of some Bovidae based on restriction-site mapping of mitochondrial DNA. *Journal of Mammalogy* 78: 377–386.

Estes, R. 1991. The Behavior Guide to African Mammals, Including Hoofed Mammals, Carnivores, Primates. University of California Press, Berkeley.

Etler, D. A. 1994. The Chinese Hominidae: New Finds, New Interpretations. Ph.D. thesis, University of California, Berkeley.

Ewer, R. F. 1954. Some adaptive features in the dentition of hyaenas. *Annals and Magazine of Natural History* 12:188–194.

———. 1958. Adaptive features of the skulls of African Suidae. *Proceedings of the Zoological Society of London* 131:135–155.

———. 1967. The fossil hyaenids of Africa—a reappraisal. In W. W. Bishop and J. D. Clark (eds.), Background to Evolution in Africa. University of Chicago Press, Chicago.

Falconer, H., and P. T. Cautley. 1846. Fauna Antiqua Sivalensis, Being the Fossil Zoology of the Siwalik Hills, in the North of India. Smith, Elder and Company, London.

Falk, D., C. Hildebolt, K. Smith, M. J. Morwood, T. Sutikna, P. Brown, Jatmiko, E. W. Saptomo, B. Brunsden, and F. Prior. 2005. The brain of LB1, *Homo floresiensis*. *Science* 308: 242–245.

Faure, M. 1983. Les Hippopotamidae (Mammalia, Artiodactyla) d'Europe occidentale. Thèse de 3° cycle, Université Claude Bernard—Lyon I, Lyons, France.

———. 1986. Les hippopotamidés du Pléistocène ancien d'Oubeidiyeh (Israël). *Mémoires et Travaux du Centre de Recherche Français de Jérusalem* 5:107–142.

———. 1994. Les Hippopotamidae (Mammalia, Artiodactyla) du rift occidental (bassin du lac Albert, Ouganda). Étude préliminaire. In B. Senut and M. Pickford (eds.), Geology and Paleobiology of the Albertine Rift Valley, Uganda-Zaïre. Volume II: Paleobiology, pp. 321–337. CIFEG, Orléans.

Feakins, S. J., P. B. deMenocal, and T. I. Eglinton. 2005. Biomarker records of late Neogene changes in northeast African vegetation. *Geology* 33:977–980.

Feibel, C. S., F. H. Brown, and I. McDougall. 1989. Stratigraphic context of fossil hominids from the Omo Group deposits—northern Turkana Basin, Kenya and Ethiopia. *American Journal of Physical Anthropology* 78:595–622.

Fernandez, M. H. 2001. Bioclimatic discriminant capacity of terrestrial mammal faunas. *Global Ecology and Biogeography* 10(2):189–204.

Ferretti, M. P., G. Ficcarelli, Y. Libsekal, T. M. Tecle, and L. Rook. 2003. Fossil elephants from Buia (northern Afar Depression, Eritrea) with remarks on the systematics of *Elephas recki* (Proboscidea, Elephantidae). *Journal of Vertebrate Paleontology* 23:244–257.

Ficarelli, G., and D. Torre. 1970. Remarks on the taxonomy of hyaenids. *Palaeontographia Italica* 66:13–33.

Fischer, K. 2004. Die Waldelefanten von Neumark Nord und Gröbern. *Praehistoria Thuringica* 10:47–62.

Fleagle, J. G. 1999. Primate Adaptation and Evolution. Academic Press, San Diego.

Fleagle, J. G., and W. S. McGraw. 1999. Skeletal and dental morphology supports diphyletic origin of baboons and mandrills. *Proceedings of the National Academy of Sciences of the United States of America* 96:1157–1161.

———. 2002. Skeletal and dental morphology of African papionins: Unmasking a cryptic clade. *Journal of Human Evolution* 42:267–292.

Foley, R. A., and M. M. Lahr. 1997. Mode 3 technologies and the evolution of modern humans. *Cambridge Archaeological Journal* 7:3–36.

Forsten, A. 1999. A review of *Equus stenonis* Cocchi (Perissodactyla, Equidae) and related forms. *Quaternary Science Reviews* 18:1373–1408.

Fortelius, M., and N. Solounias. 2000. Functional characterization of ungulate molars using abrasion attrition wear gradient. *American Museum Novitates* 3301:1–36.

Frayer, D. W., M. H. Wolpoff, A. G. Thorne, F. Smith, and G. Pope. 1993. Theories of modern human origins: The paleontological test. *American Anthropologist* 95:14–50.

Frost, S. R. 2001a. Fossil Cercopithecidae from the Afar Depression, Ethiopia: Species Systematics and Comparison to the Turkana Basin. Ph.D. thesis, City University of New York.

———. 2001b. New early Pliocene Cercopithecidae (Mammalia: Primates) from Aramis, Middle Awash Valley, Ethiopia. *American Museum Novitates* 3350:1–36.

Frost, S. R., and E. Delson. 2002. Fossil Cercopithecidae of the Hadar Formation and surrounding areas of the Afar Depression, Ethiopia. *Journal of Human Evolution* 43:687–748.

EBSCOhost - printed on 10/28/2022 4:53 AM via . All use subject to https://www.ebsco.com/terms-of-use

Gabunia, L., A. Vekua, D. Lordkipanidze, C. C. Swisher, R. Ferring, A. Justus, M. Nioradze, M. Tvalchrelidze, S. C. Anton, G. Bosinski, O. Joris, M. A. De Lumley, G. Majsuradze, and A. Mouskhelishvili. 2000. Earliest Pleistocene hominid cranial remains from Dmanisi, Republic of Georgia: Taxonomy, geological setting, and age. *Science* 288:1019–1025.

Gabunia, L., M. A. De Lumley, A. Vekua, D. Lordkipanidze, and H. De Lumley. 2002. Découverte d'un nouvel hominidé à Dmanissi (Transcaucasie, Georgie). *Comptes Rendus de l'Académie des Sciences, Palevol* 1:243–253.

Gamble, C., W. Davies, P. Pettitt, and M. Richards. 2004. Climate change and evolving human diversity in Europe during the last glacial. *Philosophical Transactions of the Royal Society of London Series B: Biological Sciences* 359: 243–253.

García, N. 2003. Osos y otros carnívoros de la Sierra de Atapuerca. Fundación Oso de Asturias, Gijón and Oviedo, Spain.

García, N., and J. L. Arsuaga. 1999. Carnivores from the early Pleistocene hominid-bearing Trinchera Dolina 6 (Sierra de Atapuerca, Spain). *Journal of Human Evolution* 37:415–430.

Gasse, F. 2006. Climate and hydrological changes in tropical Africa during the past million years. *Comptes Rendus de l'Académie des Sciences, Palevol* 5:35–43.

Gat, J. R. 1980. The isotopes of hydrogen and oxygen in precipitation. In P. Fritz and J. Ch. Fontes (eds.), Handbook of Environmental Isotope Geochemistry, Volume 1, pp. 21–47. Elsevier, Amsterdam.

Gatesy, J. 1992. Phylogeny of Bovidae (Artiodactyl, Mammalia), based on mitochondrial ribosomal DNA sequences. *Molecular Biology and Evolution* 9:433–446.

———. 1998. Molecular evidence for the phylogenetic affinities of Cetacea. In J. Thewissen (ed.), The Emergence of Whales, pp. 63–111. Plenum Press, New York.

Gatesy, J., G. Amato, E. S. Vrba, G. Schaller, and R. Desalle. 1997. A cladistic analysis of mitochondrial ribosomal DNA from the Bovidae. *Molecular Phylogenetics and Evolution* 7: 303–319.

Gauthier, J., A. G. Kluge, and T. Rowe. 1988. Amniote phylogeny and the importance of fossils. *Cladistics* 4:105–210.

Gautier, A., and A. Muzzolini. 1991. The life and times of the giant buffalo alias *Bubalis/Homioceras/Pelorovis antiquus* in North Africa. *Archaeozoologia* 4:39–92.

Geisler, J. H. 2001. New morphological evidence for the phylogeny of Artiodactyla, Cetacea, and Mesonychidae. *American Museum Novitates* 40:1–53.

Geisler, J. H., and Z. Luo. 1998. Relationships of Cetacea to terrestrial ungulates and the evolution of cranial vasculature in Cete. In J. Thewissen (ed.), The Emergence of Whales, pp. 163–212. Plenum Press, New York.

Geisler, J. H., and M. D. Uhen. 2003. Morphological support for a close relationship between hippos and whales. *Journal of Vertebrate Paleontology* 23:991–996.

Gentry, A. W. 1967. *Pelorovis oldowayensis* Reck, an extinct bovid from East Africa. *Bulletin of the British Museum (Natural History)* 14:243–299.

———. 1978. Bovidae. In V. J. Maglio and H. B. S. Cooke (eds.), Evolution of African Mammals, pp. 540–572. Harvard University Press, Cambridge, MA.

———. 1985. The Bovidae of the Omo group deposits, Ethiopia (French and American Collections). In Y. Coppens and F. C. Howell (eds.), Les Faunes Plio-Pléistocénes de la Basse Vallée de l'Omo (Éthiopie): Tome 1. Périssodactyles, Artiodactyles (Bovidae), 119–191. Éditions du Centre National de la Recherche Scientifique, Paris.

———. 1990. Evolution and dispersal of African Bovidae. In G. Bubenik and A. Bubenik (eds.), Horns, Pronghorns, and Antlers: Evolution, Morphology, Physiology, and Social Significance, pp. 195–227. Springer-Verlag, New York, Berlin.

———. 1992. The subfamilies and tribes of the family Bovidae. *Mammal Review* 22:1–32.

———. 1996. A fossil *Budorcas* (Mammalia, Bovidae) from Africa. In K. M. Stewart and K. L. Seymour (eds.), Palaeoecology and Palaeoenvironments of Late Cenozoic Mammals, pp. 571–578. University of Toronto Press, Toronto.

———. 1999. A fossil hippopotamus from the Emirate of Abu Dhabi, United Arab Emirates. In P. J. Whybrow and A. Hill (eds.), Fossil Vertebrates of Arabia, pp. 271–289. Yale University Press, New Haven, CT.

———. 2000a. Caprini and Hippotragini (Bovidae, Mammalia) in the upper Miocene. In E. S. Vrba and G. Schaller (eds.), Antelopes, Deer, and Relatives: Fossil Record, Behavioral Ecology, Systematics, and Conservation, pp. 65–83. Yale University Press, New Haven, CT.

———. 2000b. The ruminant radiation. In E. Vrba and G. Schaller (eds.), Antelopes, Deer, and Relatives: Fossil Record, Behavioral Ecology, Systematics, and Conservation, pp. 11–25. Yale University Press, New Haven, CT.

Gentry, A., and A. Gentry. 1978. Fossil Bovidae of Olduvai Gorge. Bulletin of British Museum of Natural History 29:289–446.

Geraads, D. 1986. Remarques sur la systématique et la phylogénie des Giraffidae. *Geobios* 19:465–477.

———. 1988. Revision des Rhinocerotinae (Mammalia) du Turolien de Pikermi: Comparison avec les formes voisines. *Annales de Paleontologie* 74:13–41.

———. 1992. Phylogenetic analysis of the tribe Bovini. *Zoological Journal of the Linnean Society* 104:193–207.

———. 1993. *Kolpochoerus phacochoeroides* (Thomas, 1884) (Suidae, Mammalia), from the upper Pliocene of Ahl-Al-Oughlam (Casablanca, Morocco). *Geobios* 26:731–743.

———. 1995. *Simatherium shungarense* n. sp., un nouveau Bovini (Artiodactyla, Mammalia) du Pleistocene terminal de l'Omo. *Annales de Paléontologie* 81:87–96.

EBSCOhost - printed on 10/28/2022 4:53 AM via . All use subject to https://www.ebsco.com/terms-of-use

———. 2005. Pliocene Rhinocerotidae (Mammalia) from Hadar and Dikka (Lower Awash, Ethiopia), and a revision of the origin of modern African rhinos. *Journal of Vertebrate Paleontology* 25:451-461.

Geraads, D., J. J. Hublin, J. J. Jaeger, H. Tong, S. Sen, and P. Toubeau. 1986. The Pleistocene hominid site of Ternifine, Algeria: New results on the environment, age and human industries. *Quaternary Research* 25:380-386.

Geraads, D., F. Amani, and J. J. Hublin. 1992. The middle Pleistocene site of Ain Maarouf near El-Hajeb, Morocco: Discovery of a fossil hominid. *Comptes Rendus de l'Académie des Sciences, Série II* 314:319–323.

Geraads, D., Z. Alemseged, and H. Bellon. 2002. The late Miocene mammalian fauna of Chorora, Awash basin, Ethiopia: Systematics, biochronology and ^{40}K-^{40}Ar age of associated volcanics. *Tertiary Research* 21:113–122.

Geraads, D., Z. Alemseged, D. Reed, J. Wynn, and D. C. Roman. 2004. The Pleistocene fauna (other than Primates) from Asbole, lower Awash Valley, Ethiopia, and its environmental and biochronological implications. *Geobios* 37:697–718.

Getty, R. 1982. Anatomía de los Animales Domésticos. Masson, Barcelona.

Gèze, R. 1980. Les Hippopotamidae (Mammalia, Artiodactyla) du plio-pléistocène de l'Ethiopie. Thèse de 3° cycle, Université Pierre et Marie Curie—Paris VI, New York.

Gilbert, R., and G. W. Gill. 1990. A metric technique for identifying American Indian femora. In G. W. Gill and S. Rhine (eds.), Skeletal Attribution of Race: Methods for Forensic Anthropology, pp. 97–99. Maxwell Museum of Anthropology Occasional Papers, Albuquerque, NM.

Gilbert, W. H. 2003a. Testing hypotheses of demes within *Homo erectus* using parsimony analysis. *American Journal of Physical Anthropology, Supplement* 36:100.

———. 2003b. The Daka Member of the Bouri Formation, Middle Awash Valley, Ethiopia: Fauna, Stratigraphy, and Environment. Ph.D. thesis, University of California, Berkeley.

Gilbert, W. H., B. Asfaw, and T. D. White. 2000. Paleontology. In J. de Heinzelin, J. D. Clark, K. D. Schick, and W. H. Gilbert (eds.), The Acheulean and the Plio-Pleistocene Deposits of the Middle Awash Valley, Ethiopia, pp. 183–192. Geological Sciences, Annals, 104. Royal Museum for Central Africa, Tervuren, Belgium.

Gingerich, P. D., M. Haq, I. S. Zalmout and M. Malkani. 2001. Origin of whales from early artiodactyls: Hand and feet of Eocene Protocetidae from Pakistan. *Science* 293:2239–2242.

Goren-Inbar, N., A. Lister, E. Werker, and M. Chech. 1994. A butchered elephant skull and associated artifacts from the Acheulian site of Gesher Benot Ya'aqov. Paléorient 20:99–112.

Goren-Inbar, N., C. S. Feibel, K. L. Verosub, Y. Melamed, M. E. Kislev, E. Tchernov, and I. Saragusti. 2000. Pleistocene milestones on the out-of-Africa corridor at Gesher Benot Ya'aqov, Israel. Science 289:944–947.

Gortani, M., and A. Bianchi. 1973. Missione geologica dell' Azienda Generale Italiana Petroli (AGIP) nella Dancalia meridionale e sugli altipiani Haraini (1936–1938). Accademia Nazionale dei Lincei, Rome.

Gould, S. J. 2002. The Structure of Evolutionary Theory. Harvard University Press (Belknap Press), Cambridge, MA.

Gould, S. J., and E. A. Lloyd. 1999. Individuality and adaptation across levels of selection: How shall we name and generalize the unit of Darwinism? *Proceedings of the National Academy of Sciences of the United States of America* 96:11904–11909.

Graybeal, A. 1995. Naming species. *Systematic Biology* 44:237–250.

Grey, J., and D. M. Harper. 2002. Using stable isotope analyses to identify allochthonous inputs to Lake Naivasha mediated via the hippopotamus gut. *Isotopes in Environmental and Health Studies* 38:245–250.

Grine, F., W. Jungers, P. Tobias, and O. Pearson. 1995. Fossil *Homo* femur from Berg-Aukas, northern Namibia. *American Journal of Physical Anthropology* 97:151–185.

Grubb, P. 2001. Review of family-group names of living bovids. *Journal of Mammalogy* 82:374–388.

Grubb, P., O. Sandrock, O. Kullmer, T. Kaiser, and F. Schrenk. 1999. Relationships between eastern and southern African faunas. In T. Bromage and F. Schrenk (eds.), African Biogeography, Climate Change, and Human Evolution, pp. 253–281. Oxford University Press, New York, Oxford.

Grubb, P., T. M. Butynski, J. F. Oates, S. K. Bearder, T. R. Disotell, C. P. Groves, and T. T. Struhsaker. 2003. Assessment of the diversity of African primates. *International Journal of Primatology* 24:1301–1357.

Grun, R., P. Huang, X. Wu, C. Stringer, A. Thorne, and M. McCulloch. 1997. ESR analysis of teeth from the paleoanthropological site of Zhoukoudian, China. *Journal of Human Evolution* 32:83–91.

Grzimek, B. 1988. Grzimek's Encyclopedia of Mammals. McGraw-Hill, New York.

Habgood, P. J. 1989. The origin of anatomically modern humans in Australasia. In P. Mellars and C. Stringer (eds.), The Human Revolution, pp. 245–273. Edinburgh University Press, Edinburgh.

Haile-Selassie, Y. 2001. Late Miocene Fauna from the Middle Awash Valley, Ethiopia. Ph.D. thesis, University of California, Berkeley.

Haile-Selassie, Y., and G. WoldeGabriel. 2008. *Ardipithecus kadabba*. Berkeley, CA: University of California Press.

Haile-Selassie, Y., G. WoldeGabriel, T. D. White, R. L. Bernor, D. DeGusta, P. R. Renne, W. K. Hart, E. S. Vrba, S. H. Ambrose, and F. C. Howell. 2004. Mio-Pliocene mammals from the Middle Awash, Ethiopia. *Geobios* 37:536–552.

Hallgrímsson, B., and B. K. Hall. 2005. Variation and variability: Central concepts in biology. In B. Hallgrímsson, and B. Hall (eds.), Variation: A Central Concept in Biology, pp. 1–7. Elsevier Academic Press, Burlington, MA.

EBSCOhost - printed on 10/28/2022 4:53 AM via . All use subject to https://www.ebsco.com/terms-of-use

Hamacho Naumannzou Kennkyu Gurupu (Hamacho Naumann's Elephant Study Group). 1978. Toukyou nihonnbashi hamacho ni okeru naumanzoukaseki no hakkutsu ni tsuite (On the excavation of the fossil of Naumann's elephant at Hamacho, Nihonnbashi, Tokyo). *Chikyu Kagaku* (Earth Science) 32: 83–85.

Hamilton, W. 1978. Fossil giraffes from the Miocene of Africa and a revision of the phylogeny of the Giraffoidea. *Philosophical Transactions of the Royal Society of London* 283:165–229.

Hamilton, W. J., R. L. Tilson, and L. G. Frank. 1986. Sexual monomorphism in spotted hyaenas *Crocuta crocuta. Ethology* 71:63–73.

Harris, E. E., and T. R. Disotell. 1998. Nuclear gene trees and the phylogenetic relationships of the mangabeys (Primates: Papionini). *Molecular Phylogenetics Evolution* 15:892–900.

Harris, J. 1983. Family Rhinocerotidae. In J. Harris (ed.), Koobi Fora Research Project Volume 2. The Fossil Ungulates: Proboscidea, Perissodactyla and Suidae. Clarendon Press, Oxford.

———. 1991a. Koobi Fora Research Project Volume 3. The Fossil Ungulates: Geology, Fossil Artiodactyls, and Paleoenvironments. Clarendon Press, Oxford.

———. 1991b. Family Giraffidae. In J. Harris (ed.), Koobi Fora Research Project. Volume 3: The Fossil Ungulates: Geology, Fossil Artiodactyls, and Paleoenvironments, pp. 93–138. Clarendon Press, Oxford.

———. 1991c. Family Hippopotamidae. In J. Harris (ed.), Koobi Fora Research Project.Volume 3: The Fossil Ungulates: Geology, Fossil Artiodactyls, and Paleoenvironments, pp. 31–85. Clarendon Press, Oxford.

———. 1991d. Family Rhinocerotidae. In J. Harris (ed.), Koobi Fora Research Project Volume 3. The Fossil Ungulates: Geology, Fossil Artiodactyls, and Paleoenvironments. Clarendon Press, Oxford.

Harris, J. M., and M. G. Leakey. 1993. The faunal context. In A. C. Walker and R. Leakey (eds.), The Nariokotome *Homo erectus* Skeleton, pp. 54–60. Harvard University Press, Cambridge, Massachusetts.

Harris, J. M., and T. D. White. 1979. Evolution of the Plio-Pleistocene African Suidae. *Transactions of the American Philosophical Society* 69:1–128.

Harris, J. M., F. Brown, and M. G. Leakey. 1988a. Stratigraphy and paleontology of Pliocene and Pleistocene localities west of Lake Turkana, Kenya. *Contributions in Science* 399:1–128.

Harris, J. M., F. H. Brown, M. G. Leakey, A. C. Walker, and R. E. Leakey. 1988b. Pliocene and Pleistocene hominid-bearing sites from west of Lake Turkana, Kenya. *Science* 239:27–33.

Harrison, T. 1997. The anatomy, paleobiology, and phylogenetic relationships of the Hippopotamidae (Mammalia, Artiodactyla) from the Manonga Valley, Tanzania. In T. Harrison (ed.), Neogene Paleontology of the Manonga Valley, Tanzania, pp. 137–190. Plenum Press, New York.

Hasegawa, Y. 1972. The Naumann's elephant, *Palaeoloxodon naumanni* (Makiyama) from the late Pleistocene. *Bulletin of the National Science Museum* 15:513–591.

Hasimoto, M. 1938. Ethnologische Untersuchungen über die Unterextremitäts-Knochen der Chinesen. *Journal of Oriental Medicine* 29:117–130.

Hassanin, A., and E. Douzery. 1999a. The tribal radiation of the family Bovidae (Artiodactyla) and the evolution of the mitochondrial cytochrome *b* gene. *Molecular Phylogenetics and Evolution* 13:227–243.

———. 1999b. Evolutionary affinities of the enigmatic saola *(Pseudoryx nghetinhensis)* in the context of the molecular phylogeny of Bovidae. *Proceedings of the Royal Society of London Series B Biological Sciences* 266:893–900.

Hay, R. 1994. Geology and dating of Beds III, IV and the Masek Beds. In M. Leakey and D. Roe (eds.), Olduvai Gorge: Excavations in Beds III, IV, and the Masek Beds. Volume 5, pp. 8–14. Cambridge University Press, Cambridge.

Hayward, N. J., and C. J. Ebinger. 1996. Variations in the along-axis segmentation of the Afar Rift system. *Tectonics* 15:244–257.

Hendey, Q. B. 1974. The late Cenozoic Carnivora of the southwestern Cape Province. *Annals of the South African Museum* 63:1–369.

Hennig, W. 1966. Phylogenetic Systematics. University of Illinois Press, Urbana.

Hernández-Fernández, M., and E. S. Vrba. 2005a. A complete estimate of the phylogenetic relationships in Ruminantia: A dated species-level supertree of the extant ruminants. *Biological Reviews* 80:269–302.

———. 2005b. Macroevolutionary processes and biomic specialization: Testing the resource-use hypothesis. *Evolutionary Ecology* 19:199–219.

———. 2005c. Rapoport effect and biomic specialization in African mammals: Revisiting the climatic variability hypothesis. *Journal of Biogeography* 32:903–918.

Hlusko, L. J. 2004. Integrating the genotype and phenotype in hominid paleontology. *Proceedings of the National Academy of Sciences of the United States of America* 101:2653–2657.

Holliday, T. W. 2003. Species concepts, reticulation, and human evolution. *Current Anthropology* 44:653–673.

Holloway, R. L., D. C. Broadfield, M. S. Yuan, J. H. Schwartz, and I. Tattersall. 2004. Brain Endocasts: The Paleoneurological Evidence. The Human Fossil Record 3. Wiley-Liss, Hoboken, NJ.

Hooft, W., F. Groen, and H. Prins. 2002. Phylogeography of the African Buffalo based on mitochondrial and Y-chromosomal loci: Pleistocene origin and population expansion of the Cape buffalo subspecies. *Molecular Ecology* 11:267–279.

Hooijer, D. A. 1955. Fossil Proboscidea from the Malay Archipelago and the Punjab. *Zoologische Verhandelingen* 28:1–146.

EBSCOhost - printed on 10/28/2022 4:53 AM via . All use subject to https://www.ebsco.com/terms-of-use

———. 1969. Pleistocene East African rhinoceroses. In L. S. B. Leakey (ed.), Fossil Vertebrates of Africa. Volume 1, pp. 71–98. Academic Press, London.

———. 1975. Miocene to Pleistocene hipparions of Kenya, Tanzania and Ethiopia. Zoologische Verhandelingen 142:1–80.

Hooijer, D., and B. Patterson, 1972. Rhinoceroses from the Pliocene of northwestern Kenya. *Bulletin of the Museum of Comparative Zoology, Harvard* 144:1–26.

Horwitz, L. K., and E. Tchernov. 1990. Cultural and environmental implications of hippopotamus bone remains in archaeological contexts in the Levant. *Bulletin of American Schools of Oriental Research* 280:67–76.

Howell, F. C. 1998. Evolutionary Implications of Altered Perspectives on Hominine Demes and Populations in the Later Pleistocene of Western Eurasia. Plenum, New York.

———. 1999. Paleo-demes, species clades, and extinctions in the Pleistocene hominin record. *Journal of Anthropological Research* 55:191–243.

Howell, F. C., and G. Petter. 1980. The *Pachycrocuta* and *Hyaena* lineages (Plio-Pleistocene and extant species of the Hyaenidae). Their relationships with Miocene ictitheres: *Palhyaena* and *Hyaenictitherium. Geobios* 13:579–623.

———. 1985. Comparative observations on some middle and upper Miocene hyaenids: Genera *Percrocuta* Kretzoi, *Allohyaena* Kretzoi, *Adcrocuta* Kretzoi (Mammalia, Carnivora, Hyaenidae). *Geobios* 18:419–476.

Howells, W. W. 1973. Cranial Variation in Man: A Study by Multivariate Analysis of Patterns of Difference among Recent Human Populations. Papers of the Peabody Museum of Archaeology and Ethnology, 67.

———. 1980. *Homo erectus*—who, when, and where: A survey. *Yearbook of Physical Anthropology* 23:1–23.

———. 1989. Skull shapes and the map. Papers of the Peabody Museum of Archaeology and Ethnology, 79.

———. 1998. Climatic changes, paleogeography, and the evolution of Neandertals. In T. Akazawa, K. Aoki, and O. Bar-Yosef (eds.), Neandertals and Modern Humans in Western Asia, pp. 293–310. Plenum, New York.

Hublin, J.-J. 1998a. Comments on Neanderthal acculturation of Western Europe? F. d'Errico, J. Zilhao, M. Julien, D. Baffier, and J. Pellegrin. *Current Anthology* 39 (Suppl.):24–25.

———. 1998b. Climatic changes, paleogeography, and the evolution of the Neandertals. In T. Akazawa, K. Aoki, and O. Bar-Yosef (eds.), Neandertals and Modern Humans in Western Asia, pp. 295–310. Plenum Press, New York.

Huelsenbeck, J. P. 1994. Comparing the stratigraphic record to estimates of phylogeny. *Paleobiology* 20:470–483.

Hulbert, R. C., and B. J. MacFadden. 1991. Morphological transformation and cladogenesis at the base of the adaptive radiation of Miocene hypsodont horses. *American Museum Novitates* 3000:1–61.

Inuzuka, N. 1977a. On a fossil skull of *(Palaeoloxodon naumanni)* from Saruyama, Shimosa-machi, Chiba Prefecture, central Japan. *The Journal of the Geological Society of Japan* 83:523–536.

———. 1977b. On the origin of *Palaeoloxodon naumanni:* A comparative osteology of the cranium. *The Journal of the Geological Society of Japan* 83:639–655.

———. 1991a. Naumannzou no koseibutsugaku. 2. Naumanzou no keitai, 3. Togai (Paleobiology of Naumann's elephant 2, Morphology of Naumann's elephant, 3. Cranium). In T. Kamei (ed.), Japanese Proboscidean Fossils. Tsukiji Shokan, Tokyo.

———. 1991b. Naumannzou no koseibutsugaku. 4. Naumanzou no henni, 4. Seisa (Paleobiology of Naumann's elephant 2, Morphological variation of Naumann's elephant, 3. Sexual dimorphism). In T. Kamei (ed.), Japanese Proboscidean Fossils, pp. 153–155. Tsukiji Shokan, Tokyo.

Inuzuka, N., and K. Takahashi. 2004. Discrimination between the genera *Palaeoloxodon* and *Elephas* and the independent taxonomic position of *Palaeoloxodon* (Mammalia: Proboscidea). In E. Baquedano and S. Rubio Jara (eds.), Miscelánea en homenaje a Emiliano Aguirre. Volume II, pp. 235–244. Alcalá de Henares Museo Arqueológico Regional, Madrid.

Inuzuka, N., Y. Hasegawa, H. Nogariya, and T. Kamei. 1975. On stylohyoid bone of Naumann's elephant (*Elephas naumanni* Makiyama) from Lake Nojiri. *Memoirs of the Faculty of Science, Kyoto University, Series of Geology & Mineralogy,* 41:49–65.

Irwin, D. M., and U. Arnason. 1994. Cytochrome *b* gene of marine mammals: Phylogeny and evolution. *Journal of Mammalian Evolution* 2:37–55.

Iwamoto, T. 1993. The ecology of *Theropithecus gelada*. In N. G. Jablonski (ed.), *Theropithecus:* The Rise and Fall of a Primate Genus, pp. 441–452. Cambridge University Press, Cambridge.

Jablonski, N. 1993. Evolution of the masticatory apparatus in *Theropithecus*. In N. Jablonski (ed.), *Theropithecus:* The Rise and Fall of a Primate Genus, pp. 299–329. Cambridge University Press, Cambridge, New York.

———. 2002. Fossil Old World monkeys: The late Neogene radiation. In W. C. Hartwig (ed.), The Primate Fossil Record, pp. 255–299. Cambridge University Press, Cambridge, UK.

Janis, C. M., and K. M. Scott. 1987. The interrelationships of higher ruminant families with special emphasis on the members of Cervoidea. *American Museum Novitates* 2893:1–85.

Johnson, W. E., and S. J. O'Brien. 1997. Phylogenetic reconstruction of the Felidae using 16S rRNA and NADH-5 mitochondrial genes. *Journal of Molecular Evolution* 44:S98–S116.

Jolly, C. J. 1972. The classification and natural history of *Theropithecus (Simopithecus)* (Andrews, 1916), baboons of the African Plio-Pleistocene. *Bulletins of the British Museum (Natural History), Geology* 22:1–122.

EBSCOhost - printed on 10/28/2022 4:53 AM via . All use subject to https://www.ebsco.com/terms-of-use

———. 2001. A proper study for mankind: Analogies from the papionin monkeys and their implications for human evolution. *Yearbook of Physical Anthropology* 116:177–204.

Kaiser, T. M., N. Solounias, M. Fortelius, R. L. Bernor, and F. Schrenk. 2000. Tooth mesowear analysis on *Hippotherium primigenium* from the Vallesian Dinotheriensande (Germany): A blind test study. *Carolinea* 58:103–114.

Kalb, J. E. 1993. Refined stratigraphy of the hominid-bearing Awash Group, Middle Awash Valley, Afar Depression, Ethiopia. *Newsletters on Stratigraphy* 29:21–62.

Kalb, J. E., C. B. Wood, C. S. Smart, E. B. Oswald, A. Mebrate, S. Tebedge, and P. Whitehead. 1980. Preliminary geology and palaeontology of the Bodo D'ar hominid site, Afar, Ethiopia. *Palaeogeography, Palaeoclimatology, Palaeoecology* 30:107–120.

Kalb, J. E., M. Jaegar, C. J. Jolly, and B. Kana. 1982a. Preliminary geology, palaeontology and paleoecology of a Sangoan site at Andalee, Middle Awash Valley, Ethiopia. *Journal of Archaeological Science* 9:349–363.

Kalb, J. E., C. J. Jolly, S. Tebedge, A. Mebrate, C. Smart, E. B. Oswald, P. F. Whitehead, C. B. Wood, T. Adefris, and V. Rawn-Schatzinger. 1982b. Vertebrate faunas from the Awash Group, Middle Awash Valley, Ethiopia. *Journal of Vertebrate Paleontology* 2:237–258.

Kalb, J. E., E. B. Oswald, A. Mebrate, S. Tebedge, and C. J. Jolly. 1982c. Stratigraphy of the Awash Group, Middle Awash Valley, Afar, Ethiopia. *Newsletters on Stratigraphy* 11:95–127.

Kamei, T., and H. Taruno. 1973. Note on the occurrence of the latest Pleistocene mammals from the Lake Nojiri (Part 1). *Memoirs of the Faculty of Science, Kyoto University, Series of Geology and Mineralogy* 39:99–122.

Kawamura, Y. 1998. Immigration of mammals into the Japanese islands during the Quaternary. The Quaternary Research (Daiyonki Kenkyu) 37:251–257.

Kennedy, G. E. 1983a. Some aspects of femoral morphology in *Homo erectus*. *Journal of Human Evolution* 12:587–616.

———. 1983b. A morphometric and taxonomic assessment of a hominine femur from the Lower Member, Koobi Fora, Lake Turkana. *American Journal of Physical Anthropology* 61:429–436.

———. 1984. The emergence of *Homo sapiens:* The postcranial evidence. *Man* 19:94–110.

———. 1991. On the autapomorphic traits of *Homo erectus. Journal of Human Evolution* 20:375–412.

Kingdon, J. 1979. East African Mammals: An Atlas of Evolution in Africa. Volume III Part B: Large Mammals. University of Chicago Press, Chicago.

———. 1982. East African Mammals: An Atlas of Evolution in Africa. Volume III Part C: Bovids. University of Chicago Press, Chicago.

———. 1989a. East African Mammals: An Atlas of Evolution in Africa, Volume III Part D: Bovids. Academic Press, London.

———. 1989b. Island Africa. Princeton University Press, Princeton.

———. 1997. The Kingdon Field Guide to African Mammals. Princeton University Press, Princeton.

Kingston, J. D. 1999. Environmental determinants in early hominid evolution: Issues and evidence from the Tugen Hills, Kenya. In P. Andrews and P. Banham (eds.), Late Cenozoic Environments and Hominid Evolution: A Tribute to Bill Bishop. pp. 69–84. Geological Society, London.

Klaatsch, H. 1901. Die wichtigsten Variationen am Skelett der freien unteren Extremität des Menschen. *Ergebnisse der Anatomie und Entwicklungsgeschichte* 10:599–719.

Klein, R. 1994. The long-horned African buffalo *(Pelorovis antiquus)* is an extinct species. *Journal of Archaeological Science* 21:725–733.

Klein, R., and K. Cruz-Uribe. 1999. Craniometry of the genus *Equus* and the taxonomic affinities of the extinct South African quagga. *South African Journal of Science* 95:81–86.

Koch, C. 1986. The vertebrate taphonomy and palaeoecology of the Olorgesaile Formation (middle Pleistocene, Kenya). Ph.D. thesis, University of Toronto, Toronto.

Konishi, S., and S. Yoshikawa. 1999. Immigration times of the two proboscidean species, *Stegodon orientalis* and *Palaeoloxodon naumanni*, into the Japanese Islands and the formation of land bridge. *Chikyu Kagaku* (Earth Science) 53:125–134.

Kostia, S., M. Ruohonen-Lehto, R. Vainola, and S. Varvio. 2000. Phylogenetic information in inter-SINE and inter-SSR fingerprints of the Artiodactyla and evolution of the Bov-tA SINE. *Heredity* 84:37–45.

Kramer, A. 1993. Human taxonomic diversity in the Pleistocene: Does *Homo erectus* represent multiple hominid species? *American Journal of Physical Anthropology* 91:161–171.

Kramer, A., T. L. Crummett, and M. H. Wolpoff. 2001. Out of Africa and into the Levant: Replacement or admixture in western Asia? *Quaternary International* 75:51–63.

Krentz, H. B. 1993. Postcranial anatomy of extant and extinct species of *Theropithecus*. In N. G. Jablonski (ed.), *Theropithecus:* The Rise and Fall of a Primate Genus, pp. 383–422. Cambridge University Press, Cambridge, UK.

Krull, E. S., and J. O. Skjemstad. 2003. ^{13}C and ^{15}N profiles in ^{14}C-dated oxisol and vertisols as a function of soil chemistry and mineralogy. *Geoderma* 112:1–29.

Kurtén, B. 1956. The status and affinities of *Hyaena sinensis* Owen and *Hyaena ultima* Matsumoto. *American Museum Novitates* 1764:1–48.

———. 1957. The bears and hyaenas of the interglacials. *Quaternaria* 4:1–13.

———. 1968. Pleistocene Mammals of Europe. Aldine Publishing Company, Chicago.

———. 1972. Fossil hyaenidae from the excavations at Stránská Skála. *Anthropos* 20:113–120.

Kuznetsova, M. V., and M. V. Kholodova. 2003. Revision of phylogenetic relationships in the Antilopinae subfamily on the

EBSCOhost - printed on 10/28/2022 4:53 AM via . All use subject to https://www.ebsco.com/terms-of-use

basis of the mitochondrial rRNA and beta-spectrin nuclear gene sequences. *Doklady Biological Sciences* 391:333–336.

Lahr, M. M. 1996. The Evolution of Modern Human Diversity: A Study of Cranial Variation. Cambridge University Press, Cambridge, UK.

Lahr, M. M., and R. A. Foley. 2001. Mode 3, *Homo helmei,* and the pattern of human evolution in the middle Pleistocene. In L. Barham and K. Robson-Brown (eds.), Human Roots: Africa and Asia in the Middle Pleistocene. Western Academic and Specialist Press, Bristol, UK.

Lahr, M. M., and R. V. S. Wright. 1996. The question of robusticity and the relationship between cranial size and shape in *Homo sapiens*. *Journal of Human Evolution* 31:157–191.

Landrum, L. R. 1993. Factors influencing the accuracy of the parsimony criterion and a method for estimating true tree length. *Systematic Biology* 18:516–524.

Larick, R., R. L. Ciochon, Y. Zaim, Sudijono, Suminto, Y. Rizal, F. Aziz, M. Reagan, and M. Heizler. 2001. Early Pleistocene $^{40}Ar/^{39}Ar$ ages for Bapang Formation hominins, central Jawa, Indonesia. *Proceedings of the National Academy of Sciences of the United States of America* 98:4866–4871.

Laws, R. M. 1968. Interactions between elephant and hippopotamus populations and their environments. *East African Agricultural and Forestry Journal* 33:140–147.

Leakey, L. S. B. 1934. Adam's Ancestors; an Up-to-Date Outline of What Is Known about the Origin of Man. Methuen, London.

———. 1942. Fossil Suidae from Oldoway. *Journal of the East Africa Natural History Society* 16:178–196.

———. 1963. Very Early East African Hominidae and Their Ecological Setting. In F. C. Howell and F. Bourlière (eds.), African Ecology and Human Evolution, pp. 418–446. Aldine, Chicago.

———. 1965. Olduvai Gorge Volume 1: A Preliminary Report on the Geology and Fauna. Cambridge University Press, Cambridge, UK.

Leakey, L. S. B., and T. Whitworth. 1958. Notes on the genus *Simopithecus* with description of a new species from Olduvai. Occasional Papers of the Coryndon Memorial Museum.

Leakey, M. D. 2000. The fauna. In D. Roe and M. D. Leakey (eds.), Olduvai Gorge: Excavations in Beds III, IV and the Masek Beds, 1968–1971, pp. 130–145. Cambridge University Press, Cambridge, UK.

Leakey, M. G. 1993. Evolution of *Theropithecus* in the Turkana Basin. In N. G. Jablonski (ed.), *Theropithecus:* The Rise and Fall of a Primate Genus, pp. 85–123. Cambridge University Press, Cambridge, UK.

Leakey, M. G., and J. M. Harris. 2003. Lothagam: The Dawn of Humanity in Eastern Africa. Columbia University Press, New York.

Leakey, M. G., M. T. Teaford, and C. V. Ward. 2003. Cercopithecidae from Lothagam. In M. G. Leakey and J. M. Harris (eds.), Lothagam: The Dawn of Humanity in Eastern Africa. Columbia University Press, New York.

Leakey, R. E., M. G. Leakey, and A. K. Behrensmeyer. 1978. The hominid catalogue. In M. G. Leakey and R. E. Leakey (eds.), Koobi Fora Research Project. Volume 1: The Fossil Hominids and an Introduction to Their Context, pp. 86–182. Clarendon Press, Oxford.

Lee, M. S. Y. 2005. Squamate phylogeny, taxon sampling, and data congruence. *Organisms Diversity and Evolution* 5:25–45.

Le Houérou, H. 1997. Climate, flora and fauna changes in the Sahara over the past 500 million years. *Journal of Arid Environments* 37:619–647.

Levin, N., J. Quade, S. Simpson, S. Semaw, and M. Rogers. 2004. Isotopic evidence for Plio-Pleistocene environmental change at Gona, Ethiopia. *Earth and Planetary Science Letters* 219:93–100.

Lewin, R., and R. A. Foley. 2003. Principles of Human Evolution, 2nd edition. Blackwell Publishing, Malden, MA.

Lieberman, D. E. 1995. Testing hypotheses about recent human evolution from skulls: Integrating morphology, function, development, and phylogeny. *Current Anthropology* 36:159–197.

Lieberman, D. E., D. R. Pilbeam, and B. A. Wood. 1996. Homoplasy and early *Homo:* An analysis of the evolutionary relationships of *H. habilis* sensu stricto and *H. rudolfensis*. *Journal of Human Evolution* 30:97–120.

Lindsay, E. H., N. D. Opdyke, and N. M. Johnson. 1980. Pliocene dispersal of the horse *Equus* and late Cenozoic mammalian dispersal events. *Nature* 287:135–138.

———. 1981. The arrival of *Equus* (reply). *Nature* 292:865.

Lister, A. M. 2004. The impact of Quaternary ice ages on mammalian evolution. *Philosophical Transactions of the Royal Society of London Series B: Biological Sciences* 359:221–241.

Lister, A. M., A. V. Sher, H. Van Essen, and G. Wei. 2005. The pattern and process of mammoth evolution in Eurasia. *Quaternary International* 126–128:49–64.

Liutkus, C. M., J. D. Wright, G. M. Ashley, and N. E. Sikes. 2005. Paleoenvironmental interpretation of lake-margin deposits using ^{13}C and ^{18}O results from early Pleistocene carbonate rhizoliths, Olduvai Gorge, Tanzania. *Geology* 33:377–380.

Lloyd, E. A., and S. J. Gould. 1993. Species selection on variability. *Proceedings of the National Academy of Sciences of the United States of America* 90:595–599.

Lock, J. M. 1972. The effects of hippopotamus grazing on grasslands. *Journal of Ecology* 60:445–467.

Lordkipanidze, D., A. Vekua, R. Ferring, G. P. Rightmire, J. Agusti, G. Kiladze, A. Mouskhelishvili, M. Nioradze, M. S. Ponce de León, M. Tappen, and C. P. Zollikofer. 2005. Anthropology: the earliest toothless hominin skull. *Nature* 434:717–718.

Lordkipanidze, D., A. Vekua, R. Ferring, G. P. Rightmire, C. P. Zollikofer, M. S. Ponce de León, J. Agusti, G. Kiladze, A. Mouskhelishvili, M. Nioradze, and M. Tappen. 2006. A fourth hominin skull from Dmanisi, Georgia. *The Anatomical Record. Part A: Discoveries in Molecular, Cellular, and Evolutionary Biology* 288(11):1146–1157.

EBSCOhost - printed on 10/28/2022 4:53 AM via . All use subject to https://www.ebsco.com/terms-of-use

Lovejoy, C. O. 1975. Biomechanical perspectives on the lower limb of early hominids. In R. H. Tuttle (ed.), Primate Morphology and Evolution, pp. 291–326. Mouton, Paris.

———. 2005. The natural history of human gait and posture Part 2. Hip and thigh. *Gait and Posture* 21:113–124.

Lovejoy, C. O., and K. G. Heiple. 1972. Proximal femoral anatomy of *Australopithecus*. *Nature* 235:175–176.

Lovejoy, C. O., M. J. Cohn, and T. D. White. 1999. Morphological analysis of the mammalian postcranium: A developmental perspective. *Proceedings of the National Academy of Sciences of the United States of America* 96:13247–13252.

———. 2000. The evolution of mammalian morphology: A developmental perspective. In P. O'Higgins and M. J. Cohn (eds.), Development, Growth, and Evolution: Implications for the Study of the Human Skeleton, pp. 41–55. Linnean Society Symposium Series, Volume 20. Academic Press, San Diego.

Lovejoy, C. O., R. S. Meindl, J. C. Ohman, K. G. Heiple, and T. D. White. 2002. The Maka femur and its bearing on the antiquity of human walking: Applying contemporary concepts of morphogenesis to the human fossil record. *American Journal of Physical Anthropology* 119:97–133.

Lydekker, R. 1884. Siwalik and Narbada Carnivora. *Paleontologia Indica* 10:178–363.

Maccagno, A. M. 1962. Gli elefanti fossili di Riano (Roma). *Geologica Romana* 1:33–131.

MacFadden, B. J. 1984. Systematics and phylogeny of *Hipparion, Neohipparion, Nannippus,* and *Cormohipparion* (Mammalia, Equidae) from the Miocene and Pliocene of the New World. *Bulletin of the American Museum of Natural History* 179:1–195.

———. 1992. Fossil Horses: Systematics, Paleobiology, and Evolution of the Family Equidae. Cambridge University Press, Cambridge, UK.

Mackie, C. 1976. Feeding habits of the hippopotamus on the Lundi River, Rhodesia. *Arnoldia* 7:1–16.

Maglio, V. J. 1970. Four new species of Elephantidae from the Plio-Pleistocene of nothwestern Kenya. *Breviora* 341:1–43.

———. 1973. Origin and evolution of the Elephantidae. *Transactions of the American Philosophical Society, New Series* 63:1–149.

Maglio, V. J., and A. B. Ricca. 1978. Dental and skeletal morphology of the earliest elephants. *Verhandelingen der Koninklijke Nederlandse Akademie van Wetenschappen, Afdeling Natuurkunde, 1st Series* 29:1–51.

Makiyama, J. 1924. Notes on a fossil elephant from Sahamma, Tôtômi. *Memoirs of the Faculty of Science, Kyoto University* B1:225–226.

Mallegni, F., E. Carnieri, M. Bisconti, G. Tartarelli, S. Ricci, I. Biddittu, and A. Segre. 2003. *Homo cepranensis* sp. nov. and the evolution of African-European middle Pleistocene hominids. *Comptes Rendus de l'Académie des Sciences, Palevol* 2:119–196.

Manlius, N. 2000. Biogéographie et écologie historique de l'hippopotame en Egypte. *Belgian Journal of Zoology* 130:59–66.

Manzi, G., F. Mallegni, and A. Ascenzi. 2001. A cranium for the earliest Europeans: phylogenetic position of the hominid from Ceprano, Italy. *Proceedings of the National Academy of Sciences of the United States of America* 98(17):10011–10016.

Manzi, G., E. Bruner, and P. Passarello. 2003. The one-million-year-old *Homo* cranium from Bouri (Ethiopia): A reconsideration of its *H. erectus* affinities. *Journal of Human Evolution* 44:731–736.

Martin, R. 1928. Lehrbuch der Anthropologie. Gustav Fischer, Jena.

Martínez, I., and J. L. Arsuaga. 1997. The temporal bones from Sima de los Huesos middle Pleistocene site (Sierra de Atapuerca, Spain): A phylogenetic approach. *Journal of Human Evolution* 33:283–318.

Martínez-Navarro, B. 1992. Revisión sistemática de la fauna de macromamíferos del yacimiento de Venta Micena (Orce, Granada, España). In J. Gibert (ed.), Proyecto Orce-Cueva Victoria (1988–1992), Presencia Humana en el Pleistoceno Inferior de Granada y Murcia, pp. 21–85. Museo de Prehistoria, Orce.

Martínez-Navarro, B., L. Rook, A. Segid, D. Yosief, M. Ferretti, J. Shoshani, T. Tecle, and Y. Libsekal. 2004. The large fossil mammals from Buia (Eritrea): Systematics, biochronology and paleoenvironments. *Rivista Italiana di Paleontologia e Stratigrafia* 110:61–88.

Márquez, S., K. Mowbray, G. J. Sawyer, T. Jacob, and A. Silvers. 2001. New fossil Hominid Calvaria from Indonesia—Sambungmacan 3. *The Anatomical Record* 262(4):344–368.

Matsumoto, H. 1924. Preliminary note on fossil elephants in Japan. *Journal of the Geological Society of Tokyo* 31:255–272.

Mattern, M. Y., and D. A. McLennan. 2000. Phylogeny and speciation in felids. *Cladistics* 16:232–253.

Matthee, C., and S. Davis. 2001. Molecular insights into the evolution of the family Bovidae: A nuclear DNA perspective. *Molecular Biology and Evolution* 18:1220–1230.

Matthee, C., and T. Robinson. 1999. Cytochrome *b* phylogeny of the family Bovidae: Resolution within the Alcelaphini, Antilopini, Neotragini, and Tragelaphini. *Molecular Phylogenetics and Evolution* 12:31–46.

Matthew, W. D. 1929. Critical observations upon Siwalik mammals. *Bulletin of the American Museum of Natural History* 56:437–560.

Mayr, E. 1981. Biological classification: Toward a synthesis of opposing methodologies. *Science* 214:510–516.

Mazo, A. Z. 1989. Nuevos restos de Proboscidea (Mammalia) en la cuenca de Guadix-Baza. *Trabajos Sobre el Neogeno-Cuatenario* 11:225–237.

Mazza, P. 1991. Interrelations between Pleistocene hippopotami of Europe and Africa. *Bolletino della Società Paleontologica Italiana* 30:153–186.

———. 1995. New evidence on the Pleistocene hippopotamuses of western Europe. *Geologica Romana* 31:61–241.

EBSCOhost - printed on 10/28/2022 4:53 AM via . All use subject to https://www.ebsco.com/terms-of-use

McClymont, E. L., and A. Rosell-Melé. 2005. Links between the onset of modern Walker circulation and the mid-Pleistocene climate transition. *Geology* 33:389–392.

McDougall, I. 1985. K-Ar and Ar-40/Ar-39 dating of the hominid-bearing Pliocene-Pleistocene sequence at Koobi Fora, Lake Turkana, Northern Kenya. *Geological Society of America Bulletin* 96:159–175.

McDougall, I., and C. S. Feibel. 2003. Numerical age control for the Miocene-Pliocene succession at Lothagam, a hominoid-bearing sequence in the northern Kenya Rift. In M. G. Leakey and J. M. Harris (eds.), Lothagam: The Dawn of Humanity in Eastern Africa, pp. 43–64. *Columbia University Press, New York.*

McDougall, I., T. Davies, R. Maier, and R. Rudowski. 1985. Age of the Okote Tuff Complex at Koobi-Fora, Kenya. *Nature* 316:792–794.

McHenry, H. M. 1991. Femoral lengths and stature in Plio-Pleistocene hominids. *American Journal of Physical Anthropology* 85:149–158.

McHenry, H. M., and R. S. Corruccini. 1978. The femur in early human evolution. *American Journal of Physical Anthropology* 49:473–488.

McKee, J. K. 2001. Faunal turnover rates and mammalian biodiversity of late Pliocene and Pleistocene eastern Africa. *Paleobiology* 27:500–511.

Mishler, B. D. 1994. Cladistic-analysis of molecular and morphological data. *American Journal of Physical Anthropology* 94:143–156.

Misonne, X. 1969. African and Indo-Australian Muridae: Evolutionary Trends. Muse Royal de l'Afrique Centrale, Tervuren, Belgium.

Miththapala, S., J. Seidensticker, and S. J. O'Brien. 1996. Phylogeographic subspecies recognition in leopards *(Panthera pardus):* Molecular genetic variation. *Conservation Biology* 10:1115–1132.

Montgelard, C., F. M. Catzeflis, and E. Douzery. 1997. Phylogenetic relationships of artiodactyls and cetaceans as deduced from the comparison of cytochrome *b* and 12S rRNA mitochondrial sequences. *Molecular Biology and Evolution* 14:550–559.

Montgelard, C., S. Ducrocq, and E. Douzery. 1998. What is a Suiforme (Artiodactyla)? Contribution of cranioskeletal and mitochondrial DNA data. *Molecular Phylogenetics and Evolution* 9:528–532.

Morwood, M. J., R. P. Soejono, R. G. Roberts, T. Sutikna, C. S. Turney, K. E. Westaway, W. J. Rink, J. X. Zhao, G. D. van den Bergh, R. A. Due, D. R. Hobbs, M. W. Moore, M. I. Bird, and L. K. Fifield. 2004. Archaeology and age of a new hominin from Flores in eastern Indonesia. *Nature* 431:1087–1091.

Murrill, R. I. 1981. Petralona Man: A Descriptive and Comparative Study with New Important Information on Rhodesian Man. Charles C. Thomas, Springfield, IL.

Mutter, R. J., L. R. Berger, and P. Schmid. 2001. New evidence of the giant hyaena, *Pachycrocuta brevirostris* (Carnivora, Hyaenidae), from Gladysvale cave deposit (Plio-Pleistocene, John Nash Nature Reserve, Gauteng, South Africa), *Palaeontologica Africana* 37:103–113.

Nadelhoffer, K., and B. Fry. 1988. Controls of natural nitrogen-15 and carbon-13 abundances in forest soil organic matter. *Soil Science Society of America Journal* 52:1633–1640.

Nakazato, H. 1993. Stratigraphic relationship between the Kiyokawa and Kamiiwahashi Formations of the middle-upper Pleistocene Shimosa Group, Chiba Prefecture, Central Japan. *The Journal of the Natural History Museum and Institute, China* 2:115–124.

———. 2001. Chronology of the Shimosa Group and movement of the "Kashima" uplift zone, Central Japan. *Daiyonki-Kenkyu* (Quaternary Research) 40:251–257.

Nakazawa, T., H. Nakazato, T. Komatsubara, and H. Tsukamoto. 2003. Reexamination of correlation between middle Pleistocene marker tephras TB-8 and Ky3, Kanto, central Japan. *Bulletin of the Geological Survey of Japan* 54:341–350.

Naylor, G. J. P., and D. C. Adams. 2001. Are the fossil data really at odds with the molecular data? Morphological evidence for Cetartiodactyla phylogeny reexamined. *Systematic Biology* 50:444–453.

Nelson, J. S. 2006. Fishes of the World. John Wiley, Hoboken, NJ.

Nichol, J. 1999. Geomorphological evidence for Pleistocene refugia in Africa. *Geographical Journal* 165:79–89.

Nickel, R., A. Schummer, and E. Seiferle. 1986. The Anatomy of the Domestic Animals. 1. The Locomotor System of the Domestic Mammals. Verlag Paul Parey, Berlin.

Nikaido, M., A. P. Rooney, and N. Okada. 1999. Phylogenetic relationships among cetartiodactyls based on insertions of short and long interpersed elements: Hippopotamuses are the closest extant relatives of whales. *Proceedings of the National Academy of Sciences of the United States of America* 96:10261–10266.

Nomura, O., and H. Yasue. 1999. Genetic relationships among hippopotamus, whales, and bovine based on SINE insertion analysis. *Mammalian Genome* 10:526–527.

Nowak, R. M. 1991. Walker's Mammals of the World, 5th edition. Johns Hopkins University Press, Baltimore and London.

———. 1999. Walker's Mammals of the World, 6th edition. Johns Hopkins University Press, Baltimore.

Oakenfull, E., and J. Clegg. 1998. Phylogenetic relationships within the genus *Equus* and the evolution of alpha and theta globin genes. *Journal of Molecular Evolution* 47:772–783.

Oates, J. F. 1994. Africa's Primates in 1992: Conservation issues and options. *American Journal of Primatology* 34(1):61–71.

O'Brien, M. J., J. Darwent, and R. L. Lyman. 2001. Cladistics is useful for reconstructing archaeological phylogenies: Palaeoindian points from the southeastern United States. *Journal of Archaeological Science* 28:1115–1136.

EBSCOhost - printed on 10/28/2022 4:53 AM via . All use subject to https://www.ebsco.com/terms-of-use

Ogen-Odoi, A., and T. Dilworth. 1987. Effects of burning and hippopotamus grazing on savanna hare habitat utilisation. *African Journal of Ecology* 27:47–50.

O'Leary, M. A. 1998. Phylogenetic and morphometric reassessment of the dental evidence for a mesonychian and cetacean clade. In J. Thewissen (ed.), The Emergence of Whales, pp. 133–161. Plenum Press, New York.

O'Leary, M. A., and J. H. Geisler. 1999. The position of Cetacea within Mammalia: Phylogenetic analysis of morphological data from extinct and extant taxa. *Systematic Biology* 48:455–490.

Omori, M., H. Isobe, K. Mano, and N. Inuzuka. 1971. Preliminary report on the discovery of the skull of *Elephas namadicus naumanni* Makiyama from the Yabu Formation at Saruyama, Chiba Prefecture. *Daiyonki-Kenkyu* (Quaternary Research) 10:92–97.

O'Regan, H. J. 2002. Defining cheetahs, a multivariate analysis of skull shape in big cats. *Mammal Review* 32:58–62.

Osborn, H. F. 1942. Proboscidea: A Monograph of the Discovery, Evolution, Migration and Extinction of the Mastodonts and Elephants of the World. Volume II: Stegodontoidea, Elephantoidea. The American Museum Press, New York.

Palombo, M. R. 2004. Dwarfing in insular mammals: The endemic elephants of Mediterranean islands. In E. Baquedano and S. Rubio (eds.), Miscelánea en homenaje a Emiliana Aguirre, pp. 354–371. Zona Arqueológica 4.2. Museuo Arqueológico Regional, Madrid.

Palombo, M. R., and M. P. Ferretti. 2005. Elephant fossil record from Italy: Knowledge, problems, and perspectives. *Quaternary International* 126–128:107–136.

Palombo, M. R., A. P. Anzidei, and A. Arnoldus-Huyzendveld. 2003. La Polledrara di Cecanibbio: One of the richest *Elephas (Palaeoloxodon) antiquus* sites of the late middle Pleistocene in Italy. In J. W. F. Reumer, J. de Vos, and D. Mol (eds.), Advances in Mammoth Research (Proceedings of the Second International Mammoth Conference, Rotterdam, May 16–20 1999), pp. 317–330. Natuurhistorisch Museum, Rotterdam.

Parsons, F. G. 1914. The characters of the English thighbone. *Journal of Anatomy and Physiology* 48:238–267.

Pavlakis, P. P. 1990. Plio-Pleistocene Hippopotamidae from the Upper Semliki. In N. T. Boaz (ed.), Results from the Semliki Research Expedition.Volume 1, pp. 203–223. Virginia Museum of Natural History Memoir, Martinsville.

Pei, W. C. 1934. On the Carnivora from Locality 1 of Choukoutien. *Paleontologica Sinica* 8:45–71.

Peters, J., A. Gautier, J. Brink, and W. Haenen. 1994. Late Quaternary extinction of ungulates in sub-Saharan Africa: A reductionist's approach. *Journal of Archaeological Science* 21:17–28.

Petter, G., and F. C. Howell. 1989. A new species of the genus *Crocuta* Kaup (Mammalia, Carnivora, Hyaenidae) in the Pliocene fauna of Laetoli (Tanzania): *Crocuta dietrichi* n. sp.: Origin of the genus. *Comptes Rendus de l'Académie des Sciences Serie II* 308:1031–1038.

Penin, X., C. Berge, and M. Baylac. 2002. Ontogenetic study of the skull in modern humans and the common chimpanzees: neotenic hypothesis reconsidered with a tridimensional procrustes analysis. *American Journal of Physical Anthropology* 118(1):50–62.

Pickford, M., and J. C. Morales. 1994. Biostratigraphy and paleobiogeography of East Africa and the Iberian Peninsula. *Palaeogeography, Palaeoclimatology, Palaeoecology* 112:297–322.

Picq, P. 1983. L'articulation Temporo-mandibulaire des Hominidés Fossiles: Anatomie Comparée, Biomécanique, Évolution, Biométrie. Ph.D. thesis, L'Université Pierre et Marie Curie, Paris.

Pilgrim, G. E. 1905. On the occurrence of *Elephas antiquus (namadicus)* in the Godavari alluvium with remarks on the species, its distribution and the age of the associated Indian deposits. *Records of the Geological Survey of India* 32:199–218.

———. 1932. The fossil Carnivora of India. *Paleontologia Indica* 18:1–232.

Pleijel, F. 1995. On character coding for phylogeny reconstruction. *Cladistics* 11(3):309–315.

Plummer, T., L. C. Bishop, P. Ditchfield, and J. Hicks. 1999. Research on late Pliocene Oldowan sites at Kanjera south, Kenya. *Journal of Human Evolution* 36:151–170.

Pons-Moyá, J. 1987. Los carnívoros (Mammalia) de Venta Micena (Granada, España). *Paleontologia i Evolucio, Mem. Esp.* 1:109–128.

Pope, G. 1991. Evolution of the zygomaticomaxillary region in the genus *Homo* and its relevance to the origin of modern humans. *Journal of Human Evolution* 21:189–213.

Port of Tokyo Geological Research Group. 2000a. Stratigraphy of the Port of Tokyo, Japan. In Port of Tokyo Geological Research Group (ed.), Geology of the Port of Tokyo, Monograph 47. pp. 10–22. The Association for the Geological Collaboration in Japan, Tokyo.

———. 2000b. Correlation of middle-upper Pleistocene tephra beds in cores from the Port of Tokyo, Japan. In Port of Tokyo Geological Research Group (ed.), Geology of the Port of Tokyo, Monograph 47, pp. 22–30. The Association for the Geological Collaboration in Japan, Tokyo.

Potts, R. 1994. Variables versus models of early Pleistocene hominid land use. *Journal of Human Evolution* 27:7–24.

———. 1996a. Evolution and climate variability. *Science* 273:922–923.

———. 1996b. Humanity's Descent: The Consequences of Ecological Instability. Morrow, New York.

———. 1998a. Environmental hypotheses of hominin evolution. *Yearbook of Physical Anthropology* 107:93–136.

———. 1998b. Variability selection in hominid evolution. *Evolutionary Anthropology* 7:81–96.

EBSCOhost - printed on 10/28/2022 4:53 AM via . All use subject to https://www.ebsco.com/terms-of-use

———. 2001. Mid-Pleistocene environmental change and human evolution. In L. Barham and K. Robson-Brown (eds.), Human Roots: Africa and Asia in the Middle Pleistocene, pp. 5–20. Western Academic and Specialist Press, Bristol.

———. 2002. Complexity and adaptability in human evolution. In M. Goodman and A. S. Moffat (eds.), Probing Human Origins, pp. 33–57. American Academy of Arts and Sciences.

———. 2004. Paleoenvironmental basis of cognitive evolution in great apes. *American Journal of Primatology* 62: 209–228.

Potts, R., A. K. Behrensmeyer, and P. Ditchfield. 1999. Paleolandscape variation and early Pleistocene hominid activities: Members 1 and 7, Olorgesailie Formation, Kenya. *Journal of Human Evolution* 37:747–788.

Potts, R., A. K. Behrensmeyer, A. Deino, P. Ditchfield, and J. Clark. 2004. Small mid-Pleistocene hominin associated with East African Acheulean technology. *Science* 305:75–78.

Prothero, D., C. Guerin, and E. Manning. 1989. The history of the Rhinocerotidae. In D. Prothero and R. Schoch (eds.), The Evolution of the Perissodactyls, pp. 321–340. Oxford University Press, New York.

Qi, G. 1999. On some problems of *Palaeoloxodon* of China. Proceedings of the Seventh Annual Meeting of the Chinese Society of Vertebrate Paleontology (Bejing), pp. 201–210.

Quade, J., N. Levin, S. Semaw, S. Simpson, M. Rogers, and D. Stout. 2004. Paleoenvironments of the earliest toolmakers. *Geological Society of America Bulletin* 116:1529–1544.

Raia, P., P. Piras, and T. Kotsakis. 2005. Turnover pulse or Red Queen? Evidence from the large mammal communities during the Plio-Pleistocene of Italy. *Palaeogeography, Palaeoclimatology, Palaeoecology* 221:293–312.

Rak, Y. 1983. The Australopithecine Face. Academic Press, New York.

Raynal, J. P., F. Z. Sbihi Alaoui, D. Geraads, L. Magoga, and A. Mohi. 2001. The earliest occupation of North-Africa: The Moroccan perspective. *Quaternary International* 75:65–75.

Reiff, W. 1986. Die Sauerwasserkalke von Stuttgart. *Fundberichte aus Baden-Wurttemberg* 11:2–24.

Renne, P. R. 2000. Geochronology. In J. de Heinzelin, J. D. Clark, K. D. Schick, and W. H. Gilbert (eds.), The Acheulean and the Plio-Pleistocene Deposits of the Middle Awash Valley, Ethiopia, pp. 47–50. Geological Sciences, Annals, 104. Royal Museum for Central Africa, Tervuren, Belgium.

Renne, P. R., C. C. Swisher, A. L. Deino, D. B. Karner, T. L. Owens, and D. J. DePaolo. 1998. Intercalibration of standards, absolute ages and uncertainties in $^{40}Ar/^{39}Ar$ dating. *Chemical Geology* 145:117–152.

Renne, P. R., G. WoldeGabriel, W. K. Hart, G. Heiken, and T. D. White. 1999. Chronostratigraphy of the Miocene-Pliocene Sagantole Formation, Middle Awash Valley, Afar Rift, Ethiopia. *Geological Society of America Bulletin* 111:869–885.

Retallack, G. J. 1994. The environmental factor approach to the interpretation of paleosols. *Soil Science Society of America Special Publication* 33:31–64.

———. 2001. Soils of the Past, 2nd edition. Blackwell Science, Oxford.

Ridley, M. 2004. Evolution, 3rd edition. Blackwell Publishing, Oxford.

Rightmire, G. P. 1984. Comparisons of *Homo erectus* from Africa and Southeast Asia. *Courier Forschungsinstitut Senckenberg* 69:83–98.

———. 1994. The relationship of *Homo erectus* to later middle Pleistocene hominids. *Courier Forschungsinstitut Senckenberg* 171:319–326.

———. 1996. The human cranium from Bodo, Ethiopia: Evidence for speciation in the middle Pleistocene? *Journal of Human Evolution* 31:21–39.

———. 2001. Patterns of hominid evolution and dispersal in the middle Pleistocene. *Quaternary International* 75:77–84.

———. 2004. Brain size and encephalization in early to mid-Pleistocene *Homo. American Journal of Physical Anthropology* 124:109–123.

Rightmire, G. P., D. Lordkipanidze, and A. Vekua. 2006. Anatomical descriptions, comparative studies and evolutionary significance of the hominin skulls from Dmanisi, Republic of Georgia. *Journal of Human Evolution* 50:115–141.

Roberts, A. 1954. The Mammals of South Africa. The Mammals of South Africa Book Fund, Johannesburg.

Roca, A. L., N. Georgiadis, J. Pecon-Slattery, and S. J. O'Brien. 2001. Genetic evidence for two species of elephant in Africa. *Science* 293:1473–1477.

Rosset, A., L. Spadola, and O. Ratib. 2004. OsiriX: An open-source software for navigating in multidimensional DICOM Images. *Journal of Digital Imaging* 17(3):205–216.

Saegusa, H. 1987. Cranial morphology and phylogeny of the stegodonts. *The Compass* 64:221–224.

———. 1993. A note on cranial materials of *Stegodon orientalis* Owen, 1870 (Stegodontidae, Proboscidea) from Yanjingou, Sichuan, China. *Human and Nature* 2:95–103.

Sahni, M., and E. Khan. 1988. Pleistocene Vertebrate Fossils and Prehistory of India. Books & Books, New Delhi.

Salles, L. 1992. Felid phylogenetics: Extant taxa and skull morphology (Felidae, Aeluroidea). *American Museum Novitates* 3047:1–67.

Sarich, V. M. 1985. Rodent macromolecular systematics. In W. Luckett and J. Hartenberger (eds.), Evolutionary Relationships among Rodents: A Multidisciplinary Approach, pp. 423–452. Plenum Press, New York.

Sarmiento, E. E., E. Stiner, and K. Mowbray. 2002. Morphology-based systematics (MBS) and problems with fossil hominoid and hominid systematics. *Anatomical Record* 269:50–66.

EBSCOhost - printed on 10/28/2022 4:53 AM via . All use subject to https://www.ebsco.com/terms-of-use

Schefuss, E., S. Schouten, J. H. F. Jansen, and J. S. S. Damste. 2003. African vegetation controlled by tropical sea surface temperatures in the mid-Pleistocene period. *Nature* 422:418–421.

Schick, K. D., and J. D. Clark. 2000. Acheulean archaeology of the western Middle Awash. In J. de Heinzelin, J. D. Clark, K. D. Schick, and W. H. Gilbert (eds.), The Acheulean and the Plio-Pleistocene Deposits of the Middle Awash Valley, Ethiopia, pp. 123–137. Geological Sciences, Annals 104. Royal Museum for Central Africa, Tervuren, Belgium.

Schreve, D. C., and D. R. Bridgland. 2002. Correlation of English and German middle Pleistocene fluvial sequences based on mammalian biostratigraphy. *Netherlands Journal of Geosciences* 81:357–373.

Schuster, M., P. Duringer, J. F. Ghienne, P. Vignaud, H. T. Mackaye, A. Likius, and M. Brunet. 2006. Revisiting the age of the Sahara desert—response. *Science* 312:1139.

Schutt, G. 1972. Fossil mammals of Java. IV. Zur Kenntnis des pleistozänen Hyänen Javas. *Proceedings Koninklijke Nederlandese Akademie van Wetenschappen* B74:261–288.

Schwalbe, G. 1899. Studien ueber *Pithecanthropus erectus* Dubois. *Zeitschrift für Morphologie und Anthropologie* 1:16–240.

———. 1902. Über die Beziehungen zwischen Innenform und Aussenform des Schaedels. *Deutsches Archiv für Klinische Medizin* 73:359–408.

———. 1907. Über das Gehirnrelief der Schlaefengegend des menschlichen Schaedels. *Zeitschrift für Morphologie und Anthropologie* 10:1–93.

Schwartz, J. H. 2000. Taxonomy of the Dmanisi crania. *Science* 289:55–56.

Schwartz, J. H., and I. Tattersall. 1996. Significance of some previously unrecognized apomorphies in the nasal region of *Homo neanderthalensis. Proceedings of the National Academy of Sciences of the United States of America* 93:10852–10854.

Seidler, H., D. Falk, C. Stringer, H. Wilfing, G. B. Mueller, and G. W. Weber. 1997. A comparative study of stereolithographically modeled middle Pleistocene skulls. *Radiology* 205:1605.

Sherwood, R. J. 1999. Pneumatic processes in the temporal bone of chimpanzee (*Pan troglodytes*) and gorilla (*Gorilla gorilla*). *Journal of Morphology* 241(2):127–137.

Shimamura, M., H. Yasue, K. Ohshima, H. Abe, H. Kato, T. Kishiro, M. Goto, I. Munechikak, and N. Okada. 1997. Molecular evidence from retroposons that whales form a clade within even-toed ungulates. *Nature* 388:666–670.

Shoshani, J., N. Goren-Inbar, and R. Rabinovich. 2001. A stylohyoideum of *Palaeoloxodon antiquus* from Gesher Benot Ya'aqov, Israel: Morphology and functional inference. In G. Cavarretta, P. Gioia, M. Mussi, and M. R. Palombo (eds.), The World of Elephants: Proceedings of the First International Congress (Oct. 16–21, 2001, Rome), pp. 665–667. Consiglio Nazionale delle Ricerche, Roma.

Shipman, P., and J. M. Harris. 1988. Habitat Preference and Paleoecology of *Australopithecus boisei* in Eastern Africa. In F. Grine (ed.), Evolutionary History of the "Robust" Australopithecines, pp. 383–404. Aldine de Gruyter, New York.

Sikes, N. E., R. Potts, and A. K. Behrensmeyer. 1999. Early Pleistocene habitat in Member 1 Olorgesailie based on paleosol stable isotopes. *Journal of Human Evolution* 37:721–746.

Simpson, G. 1945. The Principles of Classification and a Classification of Mammals. American Museum of Natural History, New York.

Simons, E. L., and E. Delson. 1978. Cercopithecidae and Parapithecidae. In V. J. Maglio and H. B. S. Cook (eds.), Evolution of African Mammals, pp. 100–119. Harvard University Press, Cambridge, MA.

Singer, R. 1962. *Simopithecus* from Hopefield, South Africa. *Bibliotheca Primatologica* 1:43–70.

Singer, R., and E. L. Bone. 1960. Modern giraffes and the fossil giraffids of Africa. *Annals of the South African Museum* 45:375–548.

Singh, A., K. Shailaja, A. Guar, and L. Singh. 2002. Development and characterization of novel microsatellite markers in the Asiatic lion *(Panthera leo persica). Molecular Ecology Notes* 2:542–543.

Smith, A. B. 1994. Systematics and the Fossil Record. Blackwell Scientific, Oxford.

Smith, R. J. 1993. Logarithmic transformation bias in allometry. *American Journal of Physical Anthropology* 90:215–228.

Sneath, P. H. A. 1995. 30 years of numerical taxonomy. *Systematic Biology* 44:281–298.

Spellerberg, I., and J. Sawyer. 1999. Applied Biogeography. Cambridge University Press, Cambridge, UK.

Spoor, F. 1993. The Comparative Morphology of the Human Bony Labyrinth. CIP-Gegevens Koninklijke Bibliotheek, Den Haag, The Netherlands.

———. 2003. The semicircular canal system and locomotor behaviour, with special reference to hominin evolution. *Courier Forschungsinstitut Senckenberg* 243:93–104.

Spoor, F., J. J. Hublin, M. Braun, and F. Zonneveld. 2003. The bony labyrinth of Neanderthals. *Journal of Human Evolution* 44:141–165.

Spoor, F., M. G. Leakey, P. N. Gathogo, F. H. Brown, S. C. Anton, I. McDougall, C. Kiarie, F. K. Manthi, and L. N. Leakey. 2007. Implications of new early *Homo* fossils from Ileret, East of Lake Turkana, Kenya. *Nature* 448:688–691.

Spoor, F., and F. Zonneveld. 1994. The bony labyrinth in *Homo erectus*: a preliminary report. *Courier Forschungsinstitut Senckenberg* 171:251–256.

———. 1995. Morphometry of the primate bony labyrinth: a new method based on high-resolution computed tomography. *Journal of Anatomy* 186(Pt 2):271–286.

———. 1998. Comparative review of the human bony labyrinth. *Yearbook of Physical Anthropology* 41:211–251.

EBSCOhost - printed on 10/28/2022 4:53 AM via . All use subject to https://www.ebsco.com/terms-of-use

Stafford, T., H. Semken, R. Graham, W. Klippel, A. Markova, N. Smirnov, and J. Southon. 1999. First accelerator mass spectrometry C-14 dates documenting contemporaneity of nonanalog species in late Pleistocene mammal communities. *Geology* 27:903–906.

Stanford, C. B., and H. T. Bunn. 2001. Meat Eating and Human Evolution. Oxford University Press, Oxford.

Stanley, S. M. 1975. Theory of evolution above species level. *Proceedings of the National Academy of Sciences of the United States of America* 72:646–650.

Steppan, S. J., R. M. Adkins, and J. Anderson. 2004. Phylogeny and divergence-date estimates of rapid radiations in muroid rodents based on multiple nuclear genes. *Systematic Biology* 53:533–553.

Steppan, S. J., R. M. Adkins, P. Q. Spinks, and C. Hale. 2005. Multigene phylogeny of the Old World mice, Murinae, reveals distinct geographic lineages and the declining utility of mitochondrial genes compared to nuclear genes. *Molecular Phylogenetics and Evolution* 37:370–388.

Stevens, G. C. 1989. The latitudinal gradient in geographical range—how so many species coexist in the tropics. *American Naturalist* 133:240–256.

Strasser, E., and E. Delson. 1987. Cladistic analysis of cercopithecid relationships. Journal of Human Evolution 16:81–99.

Stringer, C. 1984. The definition of *Homo erectus* and the existence of the species in Africa and Europe. *Courier Forschungsinstitut Senckenberg* 69:131–143.

———. 2002. Modern human origins: Progress and prospects. *Philosophical Transactions of the Royal Society of London, Series B, Biological Sciences* 357:563–579.

Stringer, C., and G. Bräuer. 1994. Methods, misreading, and bias. *American Anthropologist* 96:416–424.

Stringer, C. B., J. J. Hublin, and B. Vandermeersch. 1984. The origin of anatomically modern humans in Western Europe. In F. H. Smith and F. Spencer (eds.), The Origins of Modern Humans: A World Survey of the Fossil Evidence, pp. 51–135. Alan R. Liss, New York.

Stringer, C. B. 1984. The Definition of *Homo erectus* and the Existence of the Species in Africa and Europe. Courier Forschungsinstitut Senckenberg 69:131–143.

Stringer, C., E. Trinkaus, M. Roberts, S. Parfitt, and R. Macphail. 1998. The middle Pleistocene human tibia from Boxgrove. *Journal of Human Evolution* 34:509–547.

Stuart, A. J. 2005. The extinction of woolly mammoth *(Mammuthus primigenius)* and straight-tusked elephant *(Palaeoloxodon antiquus)* in Europe. *Quaternary International* 126–128:171–177.

Stuenes, S. 1989. Taxonomy, habits, and relationships of the subfossil Madagascan hippopotami *Hippopotamus lemerlei* and *H. madagascariensis. Journal of Vertebrate Paleontology* 9:241–268.

Sugiyama, Y. 1991. The middle Pleistocene deposits in the Atsumi Peninsula and along the east coast of Lake Hamana, Tokai district—sedimentary cycles formed by the glacio-eustatic sea-level change and their correlations to the comtemporaneous deposits in the Kanto and Kinki district. *Bulletin of the Geological Society of Japan* 42:75–109.

Suwa, G., B. Asfaw, Y. Beyene, T. D. White, S. Katoh, S. Nagaoka, H. Nakaya, K. Uzawa, P. R. Renne, and G. WoldeGabriel. 1997. The first skull of *Australopithecus boisei. Nature* 389: 489–492.

Suwa, G., H. Nakaya, B. Asfaw, H. Saegusa, A. Amazaye, R. T. Kono, Y. Beyene, and S. Katoh. 2003. Plio-Pleistocene terrestrial mammal assemblage from Konso, Southern Ethiopia. *Journal of Vertebrate Paleontology* 23:901–916.

Swofford, D. L. 1998. PAUP: Phylogenetic Analysis Using Parsimony (*and Other Methods). Version 4.0. Sinauer Associates, Sunderland, MA.

Szalay, F. S., and E. Delson. 1979. Evolutionary History of the Primates. Academic Press, San Diego, CA.

Takahashi, K., and N. Mazima. 1991. Morphological description and its variation in the molars of the Nauman's elephant (*Palaeoloxodon naumanni* [Makiyama]) from the Lake Nojiri, Nagano Prefecture, Central Japan. *Journal of Fossil Research* 24:7–32.

Takahashi, K., and K. Namatsu. 2000. Origin of the Japanese Proboscidea in the Plio-Pleistocene. *Chikyu Kagaku* (Earth Science) 54:257–267.

Tamrat, E., N. Thouveny, M. Taieb, and N. D. Opdyke. 1995. Revised magnetostratigraphy of the Plio-Pleistocene sedimentary sequence of the Olduvai Formation (Tanzania). *Palaeogeography, Palaeoclimatology, Palaeoecology* 114:273–283.

Tassy, P. 1988. The classification of Proboscidea: How many cladistic classifications? *Cladistics* 4:43–57.

Tchernov, E. 1992. The Afro-Arabian component in the Levantine mammalian fauna—a short biogeographical review. *Israel Journal of Zoology* 38:155–192.

Teilhard de Chardin, P., and M. Trassaert. 1937. The proboscidians of south-eastern Shansi. *Palaeontologica Sinica* 12:1–58.

Thewissen, J. G. M., E. M. Williams, L. J. Roe, and S. T. Hussain. 2001. Skeletons of terrestrial cetaceans and the relationship of whales to artiodactyls. *Nature* 413:277–281.

Thiele, K. 1993. The holy grail of the perfect character: the cladistic treatment of morphometric data. *Cladistics* 9(3):275–304.

Tianyuan, L., and D. A. Etler. 1992. New middle pleistocene hominid crania from Yunxian in China. *Nature* 357(6377):404–407.

Tobias, P. V. 1991. Olduvai Gorge: The Skulls, Endocasts, and Teeth of *Homo habilis*. Cambridge University Press, Cambridge, UK.

Todd, N. E. 2005. Reanalysis of African *Elephas recki:* Implications for time, space and taxonomy. *Quaternary International* 126–128:65–72.

Todd, N. E., and V. L. Roth. 1996. Origin and radiation of the Elephantidae. In J. Shoshani and P. Tassy (eds.), The Proboscidea:

EBSCOhost - printed on 10/28/2022 4:53 AM via . All use subject to https://www.ebsco.com/terms-of-use

Evolution and Palaeoecology of Elephants and their Relatives, pp. 193–202. Oxford University Press, Oxford.

Tosi, A. J., J. C. Morales, and D. J. Melnick. 2000. Comparison of Y-chromosome and mtDNA phylogenies leads to unique inferences of macaque evolutionary history. *Molecular Phylogenetics and Evolution* 17:133–144.

———. 2002. Y-chromosome and mitochondrial markers in *Macaca fascicularis* indicate introgression with *M. mulatta* and a biogeographic barrier in the Isthmus of Kra. *International Journal of Primatology* 23: 161–178.

Tosi, A. J., D. J. Melnick, and T. R. Disotell. 2004. Sex chromosome phylogenetics indicate a single transition to terrestriality in the guenons (tribe Cercopithecini). *Journal of Human Evolution* 46:223–237.

Tougard, C., T. Delefosse, C. Hanni, and C. Montgelard. 2001. Phylogenetic relationships of the five extant rhinoceros species (Rhinocerotidae, Perissodactyla) based on mitochondrial cytochrome *b* and 12S rRNA genes. *Molecular Phylogenetics and Evolution* 19:34–44.

Trevisan, L. 1947. Lo scheletro di *Elephas antiquu italicus* di Fonte Campanile (Viterbo). *Palaeontolographia Italica* 44:2–78.

Trinkaus, E. 1990. Cladistics and the hominid fossil record. *American Journal of Physical Anthropology* 83:1–11.

Turner, A. 1990a. The evolution of the guild of large carnivores during the Plio-Pleistocene in Africa. *Geobios* 23:349–368.

———. 1990b. Late Neogene/lower Pleistocene Felidae of Africa: Evolution and dispersal. *Quartärpaläontologie* 8:247–256.

Turner, A., and M. Antón. 1997. Big Cats and Their Fossil Relatives. Columbia University Press, New York.

Turner, A., and A. Chamberlain. 1989. Speciation, morphological change and the status of African *Homo erectus. Journal of Human Evolution* 18:115–130.

Turner, C. 1998. Volcanic maars, long Quaternary sequences and the work of the INQUA Subcomission on European Quaternary stratigraphy. *Quaternary International* 47/48:41–49.

Uphyrkina, O., W. E. Johnson, H. Quigly, D. Miquelle, L. Marker, M. Bush, and S. J. O'Brien. 2001. Phylogenetics, genome diversity and origin of modern leopard, *Panthera pardus. Molecular Ecology* 10:2617–2633.

Ursing, B. M., and U. Arnason. 1998. Analyses of mitochondrial genomes strongly support a hippopotamus-whale clade. *Proceedings of the Royal Society of London* 265:2251–2255.

van der Made, J. 1990. A range chart of European Suidae and Tayassuidae. *Paleontologia i Evolució* 23:99–104.

van der Made, J., and A. V. Mazo. 2001. Spanish Pleistocene Proboscidean diversity as a function of climate. In G. Cavarretta, P. Gioia, M. Mussi, and M. R. Palombo (eds.), The World of Elephants: Proceedings of the First International Congress (Oct. 16–21, 2001, Rome), pp. 214–218. Consiglio Nazionale delle Ricerche, Roma.

———. 2003. Proboscidean dispersal from Africa towards western Europe. *Deinsea* 9:437–452.

van Valen, L. 1973. A new evolutionary law. *Evolutionary Theory* 1:1–30.

Vaufrey, R. 1958. Proboscidea, étude systematique. In J. Piveteau (ed.), Traité de Paléontologie, Tome VI, pp. 203–295. Masson & Cie., Paris.

Vekua, A., D. Lordkipanidze, G. P. Rightmire, J. Agusti, R. Ferring, G. Maisuradze, A. Mouskhelishvili, M. Nioradze, M. Ponce De Leon, M. Tappen, M. Tvalchrelidze, and C. Zollikofer. 2002. A new skull of early *Homo* from Dmanisi, Georgia. *Science* 297:85–89.

Verheyen, R. 1954. Monographie éthologique de l'Hippopotame (*Hippopotamus amphibius* Linné). Institut des Parcs nationaux du Congo Belge, Morges, Belgium.

Vignaud, P., P. Duringer, H. T. Mackaye, A. Likius, C. Blondel, J. Boisserie, L. Bonis, V. Elsenmann, M.-E. Etienne, D. Geraads, F. Guy, T. Lehmann, F. Lihoreau, N. L.-L. Martinez, C. Mourer-Chauvier, O. Otero, J.-C. Rage, M. Schuster, L. Viriot, A. Zazzo, and M. Brunet. 2002. Geology and paleontology of the upper Miocene Toros-Menalla hominid locality, Chad. *Nature* 418:152–155.

Vijayan, S., and B. P. Pati. 2002. Impact of changing cropping patterns on man-animal conflicts around Gir protected area with specific reference to Talala sub-district, Gujarat, India. *Population and Environment* 23:541–559.

Vilá, C., J. Leonard, A. Götherström, S. Marklund, K. Sandberg, K. Lidén, R. Wayne, and H. Ellegren. 2001. Widespread origins of domestic horse lineages. *Science* 291:474–477.

von Koenigswald, G. H. R., and F. Weidenreich. 1939. The relationship between *Pithecanthropus* and *Sinanthropus*. *Nature* 144:926–929.

Vrba, E. S. 1980. The significance of bovid remains as indicators of environment and predation patterns. In A. Behrensmeyer and A. Hill (eds.), Fossils in the Making: Vertebrate Taphonomy and Paleoecology, pp. 247–271. University of Chicago Press, Chicago.

———. 1984. Evolutionary pattern and process in the sister-group Alcelaphini-Aepycerotini (Mammalia: Bovidae). In H. Eldredge and S. Stanley (eds.), Living Fossils, pp. 62–79. Springer-Verlag, New York.

———. 1985. Environment and evolution: Alternative causes of the temporal distribution of evolutionary events. *South African Journal of Science* 81:226–236.

———. 1987. Ecology in relation to speciation rates: Some case histories of Miocene-Recent mammal clades. *Evolutionary Ecology* 1:283–300.

———. 1992. Mammals as a key to evolutionary theory. *Journal of Mammalogy* 73(1):1–28.

———. 1993. Turnover-pulses, the Red Queen, and related topics. *American Journal of Science* 293A:418–452.

EBSCOhost - printed on 10/28/2022 4:53 AM via . All use subject to https://www.ebsco.com/terms-of-use

———. 1995a. On the connections between paleoclimate and evolution. In E. S. Vrba, G. H. Denton, T. C. Partridge, and L. H. Burckle (eds.), Paleoclimate and Evolution with Emphasis on Human Origins, pp. 24–45. Yale University Press, New Haven, CT.

———. 1995b. The fossil record of African antelopes (Mammalia, Bovidae) in relation to human evolution and paleoclimate. In E. S. Vrba, G. Denton, T. Partridge, and L. Burckle (eds.), Paleoclimate and Evolution with Emphasis on Human Origins, pp. 385–424. Yale University Press, New Haven, CT.

———. 1997. New fossils of Alcelaphini and Caprini (Bovidae, Mammalia) from Awash, Ethiopia, and phylogenetic analysis of Alcelaphini. *Palaeontologia Africana* 34:127–195.

———. 1999. Habitat theory in relation to the evolution in African Neogene biota and hominids. In T. G. Bromage and F. Schrenk (eds.), African Biogeography, Climate Change, and Human Evolution, pp. 19–34. Oxford University Press, Oxford.

———. 2000. Major features of Neogene mammalian evolution in Africa. In T. C. Partridge and R. R. Maud (eds.), The Cenozoic of Southern Africa, pp. 277–303. Oxford University Press, Oxford.

———. 2005. Mass turnover and heterochrony events in response to physical change. *Paleobiology* 31:157–174.

Vrba, E. S., and N. Eldredge. 1984. Individuals, hierarchies and processes: Towards a more complete evolutionary theory. *Paleobiology* 10:146–171.

Vrba, E. S., and J. Gatesy. 1994. New antelope fossils from Awash, Ethiopia, and phylogenetic analysis of Hippotragini (Bovidae, Mammalia). *Palaeontologica Africana* 31:55–72.

Vrba, E. S., and S. J. Gould. 1986. The hierarchical expansion of sorting and selection: Sorting and selection cannot be equated. *Paleobiology* 12:217–228.

Vrba, E. S., and G. Schaller. 2000. Phylogeny of Bovidae based on behavior, glands, skulls, and postcrania. In E. S. Vrba and G. Schaller (eds.), Antelopes, Deer, and Relatives: Fossil Record, Behavioral Ecology, Systematics, and Conservation, pp. 203–222. Yale University Press, New Haven, CT.

Vrba, E. S., J. Vaisnys, J. Gatesy, R. Desalle, and K. Wei. 1994. Analysis of pedomorphosis using allometric characters: The example of Reduncini antelopes (Bovidae, Mammalia). *Systematic Biology* 43:92–116.

Vrba, E. S., G. H. Denton, T. C. Partridge, and L. H. Burckle. 1995. Paleoclimate and Evolution with Emphasis on Human Origins. Yale University Press, New Haven, London.

Wagner, P. J. 1995. Stratigraphic tests of cladistic hypotheses. *Paleobiology* 21:153–178.

Walensky, N. 1964. A re-evaluation of the mastoid region of contemporary and fossil man. *The Anatomical Record* 149:67–72.

Walker, A., and R. E. Leakey. 1993. The skull. In A. Walker and R. E. Leakey (eds.), The Nariokotome *Homo erectus* Skeleton, pp. 63–96. Harvard University, Cambridge, MA.

Wallace, A. 1880. Island Life: Or, the Phenomena and Causes of Insular Faunas and Floras, Including a Revision and Attempted Solution of the Problem of Geological Climates. Macmillan & Co., London.

Wang, W., R. H. Crompton, T. S. Carey, M. M. Günther, Y. Li, R. Savage, and W. I. Sellers. 2004. Comparison of inverse-dynamics musculo-skeletal models of AL 288-1 *Australopithecus afarensis* and KNM-WT 15000 *Homo ergaster* to modern humans, with implications for the evolution of bipedalism. *Journal of Human Evolution* 47:453–478.

Wayne, R. K., R. E. Benveniste, D. N. Janczewski, and S. J. O'Brien. 1989. Molecular and Biochemical Evolution of the Carnivora. In J. Gittleman (ed.), Carnivore Behavior, Ecology, and Evolution. Cornell University Press, Ithaca, NY.

Wayne, R. K., B. Vanvalkenburgh, and S. J. O'Brien. 1991. Molecular distance and divergence time in carnivores and primates. *Molecular Biology and Evolution* 8:297–319.

Weaver, A. H. 2005. Reciprocal evolution of cerebellum and neocortex in fossil humans. *Proceedings of the National Academy of Sciences* 102:3576–3580.

Wei, G., H. Taruno, C. Jin, and F. Xie. 2003. The earliest specimens of the steppe mammoth, *Mammuthus trogontherii* from the early Pleistocene Nihewan Formation, North China. *Chikyu Kagaku* (Earth Science) 57:289–298.

Wei, Q. 1976. Recent find of fossil *Palaeoloxodon namadicus* from Nihewan Beds, NW Hebei. *Vertebrata PalAsiatica* 14: 51–58.

Weidenreich, F. 1941. The extremity bones of *Sinanthropus pekinensis*. *Palaeontologica Sinica, New Series D* 5:1–150.

———. 1943. The skull of *Sinanthropus pekinensis:* A comparative study of a primitive skull. *Palaeontologia Sinica, New Series D* 10:1–484.

Werdelin, L. 1989. Constraint and adaptation in the bone-cracking canid *Osteoborus* (Mammalia; Canidae). *Paleobiology* 15:387–401.

———. 1999. *Pachycrocuta* (hyaenids) from the Pliocene of East Africa. *Paläontologische Zeischrift* 73:157–165.

Werdelin, L., and B. Kurtén. 1999. Allohyaena (Mammalia, Carnivora): Giant hyaenid from the late Miocene of Hungary. *Zoological Journal of the Linnaean Society* 126:319–334.

Werdelin, L., and N. Solounias. 1990. Studies of fossil hyaenids: The genus *Adcrocuta* Kretzoi and the interrelationships of some hyaenid taxa. *Zoological Journal of the Linnaean Society* 98:363–386.

———. 1991. The Hyaenidae: Taxonomy, systematics and evolution. *Fossils and Strata* 30:1–104.

Werdelin, L., and A. Turner. 1996. The fossil and living Hyaenidae of Africa: Present status. In K. M. Stewart and K. Seymour (eds.), Palaeoenvironments of Late Cenozoic Mammals, pp. 637–659. University of Toronto Press, Toronto.

EBSCOhost - printed on 10/28/2022 4:53 AM via . All use subject to https://www.ebsco.com/terms-of-use

Wesselman, H. B. 1984. The Omo Micromammals: Systematics and Paleoecology of Early Man sites from Ethiopia. Karger, Basel.

Weston, E. M. 2000. Ontogeny and the evolution of body size in hippos. *Journal of Vertebrate Paleontology* 20:78A.

———. 2003. Fossil Hippopotamidae from Lothagam. In J. M. Harris and M. G. Leakey (eds.), Lothagam: The Dawn of Humanity in Eastern Africa, pp. 380–410. Columbia University Press, New York.

White, T. D. 1988. Context of robust *"Australopithecus."* In F. E. Grine (ed.), The Evolutionary History of the "Robust" Australopithecines, pp. 449–483. Aldine DeGruyter, New York.

———. 1995. African omnivores: Global climatic change and Plio-Pleistocene hominids and suids. In E. S. Vrba, G. H. Denton, T. C. Partridge, and L. H. Burckle (eds.), Paleoclimate and Evolution, pp. 369–384. Yale University Press, New Haven, CT.

———. 2000. A view on the science: Physical anthropology at the millennium. *American Journal of Physical Anthropology* 113:287–292.

———. 2004. Managing paleoanthropology's nonrenewable resources: A view from Afar. C*omptes Rendus de l'Académie des Sciences, Palevol* 3:341–351.

White, T. D., and P. A. Folkens. 2005. The Human Bone Manual. Elsevier Academic Press, Burlington, MA.

White, T. D., F. C. Howell, and W. H. Gilbert. 2006. The Earliest *Metridiochoerus* (Artiodactyla: Suidae) from the Usno Formation, Ethiopia. Transactions of the Royal Society of South Africa 61(2):75–80.

White, T. D., G. Suwa, W. K. Hart, R. C. Walter, G. WoldeGabriel, J. de Heinzelin, J. D. Clark, B. Asfaw, and E. S. Vrba. 1993. New discoveries of *Australopithecus* at Maka in Ethiopia. *Nature* 366:261–265.

White, T. D., G. Suwa, S. Simpson, and B. Asfaw. 2001. Jaws and teeth of *Australopithecus afarensis* from Maka, Middle Awash, Ethiopia. *American Journal of Physical Anthropology* 111:4568.

White, T. D., B. Asfaw, D. DeGusta, W. H. Gilbert, G. D. Richards, G. Suwa, and F. C. Howell. 2003. Pleistocene *Homo sapiens* from Middle Awash, Ethiopia. *Nature* 423:742–747.

White, T. D., F. C. Howell, and W. H. Gilbert. 2006. The earliest *Metridiochoerus* (Artiodactyla: Suidae) from the Usno Formation, Ethiopia. *Transactions of the Royal Society of South Africa* 61(2):75–80.

White, T. D., G. WoldeGabriel, B. Asfaw, S. Ambrose, Y. Beyene, R. L. Bernor, J. Boisserie, B. Currie, W. H. Gilbert, Y. Haile-Selassie, W. K. Hart, L. J. Hlusko, F. C. Howell, R. T. Kono, T. Lehmann, A. Louchart, C. O. Lovejoy, P. R. Renne, H. Saegusa, E. S. Vrba, H. Wesselman, and G. Suwa. 2006. Asa Issie, Aramis and the origin of *Australopithecus*. *Nature* 440:883–889.

Willmore, K. E., and B. Hallgrímsson. 2005. Within individual variation: Developmental noise versus developmental stability. In B. Hallgrímsson and B. K. Hall (eds.), Variation: A Central Concept in Biology, pp. 191–218. Elsevier Academic Press, Burlington, MA.

Witmer, L. M. 1997. The evolution of the antorbital cavity of Archosaurs: a study in soft-tissue reconstruction in the fossil record with an analysis of the function of pneumaticity. *Society of Vertebrate Paleontology Memoir* 3:1–73.

Wolanski, E., and E. Gereta. 1999. Oxygen cycle in a hippo pool, Serengeti National Park, Tanzania. *African Journal of Ecology* 37:419–423.

WoldeGabriel, G., Y. Haile-Selassie, P. R. Renne, W. K. Hart, S. H. Ambrose, B. Asfaw, G. Heiken, and T. D. White. 2001. Geology and palaeontology of the late Miocene Middle Awash Valley, Afar Rift, Ethiopia. *Nature* 412:175–178.

Wood, B. A. 1984. The origin of *Homo erectus*. *Courier Forschungsinstitut Senckenberg* 69:99–111.

———. 1991. Koobi Fora Research Project. Volume 4: Hominid Cranial Remains. Clarendon Press, Oxford.

———. 1992. Origin and evolution of the genus *Homo*. *Nature* 355:783–790.

———. 1994. Taxonomy and evolutionary relationships of *Homo erectus*. *Courier Forschungsinstitut Senckenberg* 171:159–165.

Wood, B., and B. Richmond. 2000. Human evolution: Taxonomy and paleobiology. *Journal of Anatomy* 196:19–60.

Woodburne, M. O., and R. L. Bernor. 1980. On superspecific groups of some Old World hipparionine horses. *Journal of Paleontology* 54:1319–1348.

Woodburne, M. O. 1996. Reappraisal of the Cormohipparion from the Valentine Formation, Nebraska. *American Museum of Natural History Novitates* 3163:1–56.

Wu, X., and G. Braüer. 1993. Morphological comparison of archaic *Homo sapiens* crania from China and Africa. *Zeitschrift für Morphologie und Anthropologie* 79:241–259.

Wu, X., and F. E. Poirier. 1995. Human Evolution in China: A Metric Description of the Fossils and a Review of the Sites. Oxford University Press, New York.

Wynn, J. G. 2000. Paleosols, stable carbon isotopes, and paleoenvironmental interpretation of Kanapoi, northern Kenya. *Journal of Human Evolution* 39:411–432.

Yellen, J., A. S. Brooks, D. Helgren, M. Tappen, S. H. Ambrose, R. Bonnefille, J. Feathers, G. Goodfriend, K. Ludwig, P. R. Renne, and K. Stewart. 2005. The archaeology of Aduma middle Stone Age sites in the Awash Valley, Ethiopia. *Paleoanthropology* 10:25–100.

Yoshino, M., S. Miyasaka, H. Sato, and S. Seta. 1987. Classification system of frontal sinus patterns by radiography. Its application to identification of unknown skeletal remains. *Forensic Science International* 34(4):289–299.

Zeitoun, V. 2000. Révision de l'espéce *Homo erectus* (Dubois, 1893). Utilisation des données morphologiques et métriques en cladistique, reconsidération du cas *Homo erectus*. *Bulletin et Mémoires de la Société d'Anthropologie de Paris* 12:1–200.

Zhang, Y., G. Zong, and Y. Liu. 1983. A new species of *Palaeoloxodon* from Pingliang, Kansu. *Vertebrata PalAsiatica* 21:64–68.

EBSCOhost - printed on 10/28/2022 4:53 AM via . All use subject to https://www.ebsco.com/terms-of-use

Index

The Acheulean and the Plio-Pleistocene Deposits of the Middle Awash Valley, Ethiopia, xvii
Acheulean artifacts, 6–8, 12, 20
Acinonyx jubatus (cheetah), 95, 96
Adcrocuta, 98
  A. exima, 98
Addax, 75
  A. nasomaculatus (Saharan addax), 75
Aepyceros (impala), 58–59, 400, 401, 406, 410, 420, 422
  Aepyceros cf. *melampus*, 59
Aepycerotini, 58–59
  Aepyceros (impala), 58–59, 406, 410
aerial photography, use of, xii, 8, 400
Aethomys, 262, 263
Afar Bouri Village, 3
Afar Rift, xi, 1, 3, 13
African game parks, proportions of bovid taxa collected in, 409
Alcelaphina, 48–54
  Alcelaphus (hartebeest), 48, 54
  Beatragus (hirola), 48
  Connochaetes (wildebeest), 48–50, 400, 401, 406–407, 410, 422
  Damalacra, 48
  Damalops, 48
  Megalotragus, 48, 50–52, 401, 407, 408
  Numidocapra, 48, 52–54, 401, 408
  Oreonager, 48
  Rabaticeras, 48, 53, 54
Alcelaphinae, 47–58
  Alcelaphina, 48–54
  Damaliscina, 47, 55–58
  horn morphologies, 48
  overview, 47–48
Alcelaphus (hartebeest), 48, 54
  A. buselaphus, 55, 56
Ammotragus lervia (Barbary sheep), 406
Andrews, Roy Chapman, xv
Antidorcas (springbok), 60, 61, 401, 406
  A. marsupialis (springbok), 420
  cf. *Antidorcas*, 60, 61
Antilopinae, 59–62
  Antilopini, 59, 60–62, 406
  Neotragini, 59, 62
Antilopini, 59, 60–62, 406
  Ammodorcas (dibitags), 60
  Antidorcas (springbok), 60, 61, 406
  Gazella (gazelles), 60–62
  Litocranius (gerenuks), 60
  Panthalops, 60
  Saiga, 60
Arari sandstone, 16, 17, 20
Archaeopotamus, 179–180
Ardipithecus, ix
  A. kadabba, xiii
  A. ramidus, xiii
argon ($^{40}Ar/^{39}Ar$) dates, 30–31, 32–37
Arvicanthis, 262–263, 405, 416
Asa Gita section, Daka Member, 22
Asfaw, Alemayehu, 3, 29, 46
Asfaw, Berhane, xviii, 5, 27, 29, 116, 374
A6 area, Daka Member, 24
Assebework, Tadewos, 8, 29, 46
A2 area, Daka Member. *See* Urugadehu section (A2 area), Daka Member
Australopithecus, 362
  A. afarensis, xi
  A. garhi, 19
Aves, 261–262
  aff. Piciniformes, 261–262
Awashia, 48, 55
Awash River, 40
  basin, paleoanthropological potential, 3
  floodplain, 13, 15, 17
  modern course of, 14–15, 19
Ayelu-Abidu volcanic complex, 13, 14, 19

Babyrousa, 231
  B. babyrousa, 231
badlands, 16
Beatragus (hirola), 48
biogeography, Daka Member, 397–402
biomic specialization index (BSI), 420
birds, 261–262, 264
Bison (buffaloes), 63
Bodo cranium, discovery of, 4
Bos (cows and allies), 63
Boselaphini, 62
  Boselaphus, 62
  Tetracerus, 62, 227
Boselaphus, 62
Bouria, 12, 72–74, 401, 406, 408
  B. anngettyae, 45, 56, 57, 72–74, 84, 399, 401, 406, 410, 414, 421, 422
Bouri Fault Block, 13, 14, 17, 40
Bouri Formation, xviii, 13, 17, 42. *See also* Daka Member
  history of fieldwork at, 3–5
  proximity to Quaternary axial rift zone, 13, 40

EBSCOhost - printed on 10/28/2022 4:53 AM via . All use subject to https://www.ebsco.com/terms-of-use

Bouri Horst, 15, 21
Bouri Peninsula
  aerial photograph of, 400
  chronostratigraphy of, 17–18
  erosion, influences of, 17, 18
  fault zone, 14
  landscape evolution of, 14–17
  sedimentary deposits, 17, 19
  topography, 16
  vitric tuff, 17
Bouri Village, 16, 23, 40
Bovidae, 12, 45–94, 406–408, 414–416, 422–423
  Aepycerotini, 58–59
  Alcelaphinae, 47–58
  Antilopinae, 59–62
  Bovinae, 62–71
  Caprinae, 71–75
  cranial metrics, 94
  dental metrics, 85–90
  early appearances, based on dental specimens, 46–47
  fossils
    identified by horn cores, 46
    recovery of, 46–47
  Hippotraginae, 75, 77–78
  horn core metrics, 91–93
  overview, 45–47
  phylogeny of, 48
  Reducinae, 78, 80–84
  tribal groupings, 45, 408, 410
Bovinae, 62–71
  Boselaphini, 62
  Bovini, 62–68
  Eotragus, 62
  Tragelaphini, 62, 68–71
Bovini, 62–68
  Bison, 63
  Bos, 63
  Bubalus, 63
  Pelorovis, 63–68, 84, 401, 408, 414
  Simatherium, 63
  Syncerus, 63
  Ugandax, 63
Bubalus (Asian water buffalo), 63
Bucorvus, 262

Canthumeryx, 167
capacity building, xii
Capra ibex (ibex), 72, 406
Caprinae, 71–75
  Caprini, 71, 72–74
  Naemorhedini, 71
  Ovibovini, 71, 74–75
  Rupicaprini, 71
Caprini, 71, 72–74
  Bouria, 12, 72–74, 401, 406, 408
  Sivacapra, 74
  Tossunnoria, 74
Carnivora, 95–113, 402–403, 414, 423
  Felidae, 95–97, 402
  Hyaenidae, 98–112, 402–403
castellated sandstone facies, 16, 25, 27, 28
catchment paleoecology, 402–408
catfish, 263–264
Ceratotherium, 227–229, 400, 401, 410
  C. neumayri, 227–228
  C. praecox, 228
  C. simum, 227, 228–229, 230, 405, 415, 420, 424
    C. s. cottoni, 229
    C. s. germanoafricanum, 229
    C. s. mauritanicum, 229
  first appearance of, 227
Cercocebus, 123
Cercopithecidae (nonhuman primates), 115–132, 403, 414, 423
  Cercopithecinae, 115, 122–132
  Colobinae, 115, 116–122
  Colobinae gen. et sp. indet. cf. *Colobus*, 122
  fossil evidence, 115
  overview, 115–116
  subfamily indet., 130–132
Cercopithecinae, 115, 122–132
  Cercopithecini, 123
  Papionini, 123
  Prohylobates, 115
  Theropithecus, 123–130, 401, 423
  Victoriapithecus, 115
Cercopithecini, 123
Cercopithecoides, 115, 116, 117–122, 411
  C. alemayehui, 117–122, 126, 132, 403, 414, 421, 423
  C. kerioensis, 117
  C. kimeui, 117, 119
  C. meaveae, 117, 119
  C. williamsi, 117, 119, 121
characters, 268, 353, 356
  description and sorting of, 363–367
  in scoring of site-based groups, 370–371
  scoring of specimens and demes based on, 368–369
Chasmaporthetes, 98
Choeropsis, 179, 181
  C. liberiensis (Liberian hippo), 179, 404
Ciconiiformes, aff., 261–262
cladistic analysis
  caveats for, 352–354
  characters, 268, 353, 356
  defined, 351
  deme-based, 356–358, 368–369
  Homo erectus, 355–359
  operational taxonomic units (OTUs), 351, 355
  and phenetic analysis compared, 351–352
  site-based, 358–359, 370–371
  specimen-based, 356
Clark, J. Desmond, ix–x, xi, xvii, xix, 5, 6, 24
Clark, W. E. Le Gros, xv
Climacoceras, 167
Colobinae, 116–122
  Cercopithecoides, 115, 116, 117–122, 411
  Colobinae gen. et sp. indet. cf. *Colobus*, 122
  Colobus, 115, 116, 119, 122
  cranial dimensions, 120
  dental dimensions, 121
  mandibular dimensions, 120
  overview, 116–117
Colobus, 115, 116, 119, 122
computed tomography (CT)
  microfocal x-ray system, 329
  use of to study Daka calvaria, 329–347
Connochaetes (wildebeest), 48–50, 400, 401, 406–407, 410, 422
  C. africanus, 49
  C. gentryi, 49
  C. gnou, 48, 50
  C. taurinus, 48–50, 420
    C. t. olduvaiensis, 49, 414
continental provinciality, 398–400
Coppens, Yves, 3
Cormohipparion, 133, 159
cranial anatomy, 265–328. *See also* Daka calvaria (BOU-VP-2/66)
cranial vault, 195, 214, 327
Cremohipparion, 133, 159
Crocuta (hyaena), 12, 95, 98–112, 401, 402, 423
  C. crocuta (spotted hyaena), 28, 95, 98, 100, 102–109, 111–112, 420
    C. crocuta angella, 99
    C. crocuta yangula, 96, 100, 102–109, 111–112, 113, 414, 423

EBSCOhost - printed on 10/28/2022 4:53 AM via . All use subject to https://www.ebsco.com/terms-of-use

C. dietrichi, 99, 100, 109
C. felina, 111, 112
C. sivalensis, 99, 100, 108, 109, 112
C. spelaea capensis, 99
C. ultra, 99
C. ul. latidens, 99
C. ul. ultra, 99
description, general, 102
measurements from fossil and modern, 101
rotated component loadings, 112
Curtis, Garniss, x
cyclical glaciation, 1, 421

Daba Boura section, Daka Member, 26
Daka calvaria (BOU-VP-2/66), xvii, 12, 28, 113, 274, 414
auditory meatus, 299–300
and Buia cranium compared, 350
carnivore activity, evidence of, 113, 292
coronal suture, 296
cranial anatomy, 265–328
descriptions, 268, 270–271, 273–275
protective jacket, removal of, 269
recovery, cleaning, and restoration, 265–268
robusticity, 274
specimen discovery, 265
tomographic analysis of, 329–347
uncleaned cavity, 271, 272
cranial base flexion, 343–344
cranial metrics, 312–327
cranial vault specimens, 310–311
endocranium, 341, 344–347
excavation of, 267
frontal bones, 291–293, 331–332, 335–337
frontal squama, 293–294
glabellar inflexion, 291–292
glenoid fossa/articular eminence, 301–302
jugular notch, 304
mandibular specimens, 311
mastoid region, 302–304
nuchal muscle attachments, 307–308
nuchal planum/foramen magnum, 306–307
occipital bones, 304–308
occipital torus, 308, 340, 342
and Olduvai Hominid 9 compared, 350
orbital plates, 292
overall size, shape, and proportions, 275–291
parietal bones, 294–297, 333
parietal foramina, 297
petrous portion, 299
recovery of, 25
scales, upper and lower, 305–306
sphenoidal angle, 295–296
sphenoid body, 308–310, 340, 343
supraorbital tori, 292–293
temporal bones, 297–304, 333–334, 338–340, 342
temporal lines and angular torus, 296–297
temporal squama, 298
tomographic analysis, 329–347
bony labyrinth, measurement of, 332–333, 339
cranial base flexion, 343–344
CT derived metrics, 330
endocranium, 341, 344–347
importance of, 347
tympanic plate, 299–301
views of, 273
basal, 282, 290–291
frontal, 275–276, 277
lateral, 272, 279–280, 287–289, 294
oblique, 274, 283
occipital, 281, 289–290
superior, 276, 278, 285–287
zygomatic process, 298–299
Daka Member, 17, 18, 20–30
Acheulean artifacts, 6, 8, 12, 20
African regional endemism, 400–401
archaeological evidence in, overview, 6–10
biogeography, 397–402
boundaries, 14, 413
Bovidae, 12, 45–94, 406–408, 414–416, 422–423
bovid taxa counted from horn cores, 411
Carnivora, 95–113, 402–403, 414, 423
Cercopithecidae, 115–132, 403, 414, 423
composition, 20–21
continental provinciality, 398–400
cranial remains. *See* Daka calvaria (BOU-VP-2/66)
dating of, xvii
ecological signal of bovid tribes, 408, 410
ecology, 416–417
Elephantidae, 193–225, 405, 415, 423–424
endemism among eastern African early Pleistocene sites, 401–402
Equidae, 133–165, 403–404, 415
evolutionary insights from, 413–425
fauna associated with, 5, 11
fieldwork
curation, and analytical methods, 6–11
history of, 3–5
fossil recovery protocols, 6–8
future developments, 425
geology of, 1, 413–414
Giraffidae, 167–177, 404, 415
global climate change, 417–425
Hippopotamidae, 179–191, 231, 404–405, 415
Hominidae, 405–406, 416, 424–425
hominid fossils recovered, general description of, xvii–xviii, 265
importance of to African Pleistocene studies, 1–3
location of, 13, 20
macroevolutionary selection for "generalists," 417–421
map of, 15, 413
miscellaneous vertebrates, 416
Muridae, 405, 416
paleoecology, 402–410
paleolandscape and paleoenvironmental features of, 39–42
paleontological localities, 26–30
BOU-A6, 24
BOU-VP-1, 26, 27
BOU-VP-2, 19, 26, 27–28
BOU-VP-3, 24–25, 26, 27, 28–29
BOU-VP-4, 20, 24, 29, 30
BOU-VP-19, 22, 23, 29, 30, 31, 39
BOU-VP-21, 28
BOU-VP-24, 26, 30
BOU-VP-25, 23, 24, 30
BOU-VP-26, 30
first, establishment of, 7–8
plotting of, 8
paleontology, 414–416
paleosol profile, 41–42
phyletic evolution, 422–425
postcranial remains, 373–396
femora, 373–388, 391–396
talus, 390
tibia, 384, 388–389
Rhinocerotidae, 227–230, 405, 415, 424

EBSCOhost - printed on 10/28/2022 4:53 AM via . All use subject to https://www.ebsco.com/terms-of-use

Daka Member *(continued)*
sections
A6 area, 24
Asa Gita, 22
Daba Boura, 26
Ley Gita/Dakanihylo, 23, 41
Lubaka Pass, 26
North Herto Gully, 25
overview of, 18, 21–22
Revenani section, 23–24
Urugadehu (A2 area), 22–23, 41
Wadi "M", 24, 41
Yanguli Mu'ul, 24–25
sedimentation and erosion, patterns of, 4, 16, 39–40, 397
Suidae, 233–234, 405, 415, 424
technology, classification of, 6
time period sampled by, 425
topography, 16
turnover pulses, 421–422
vertebrates, other, 425
Dakanihylo Member. *See* Daka Member
Damalacra, 48
Damaliscina, 47, 55–58
Awashia, 48, 55
Damaliscus (topi), 47–48, 55, 407
Parmularius, 47, 48, 55–58, 401, 407, 408
Damaliscus (topi), 47–48, 55, 407
D. ademassuai, 55
D. agelaius, 55
D. dorcas, 55
D. hadari, 55
D. lunatus, 55
D. lunatus lunatus, 55
D. niro, 55
Damalops, 48
de Heinzelin, Jean, ix, xvii, xix, 5, 6, 16, 24, 26, 30
deme-based cladistic analysis, 356–358
Dicerorhinus sumatrensis, 227
Diceros, 227, 228, 230, 415, 420
D. bicornis, 227, 230, 405
digital photography, use of, 10
Dinofelis, 97
divergent species lineages
delineating, 351–352
establishment of, 352
Dolichopithecus, 122
Dorcotragus, 62
Dulu Ali Basaltic Ridge, 13

Eastern Rift, ix
Elema, Hamed, 47
Elephantidae, 193–225, 405, 415, 423–424
biogeography, 213
cranial metrics, 201
cranial vault, 214
dental metrics, 210
Elephas, 12, 198–213, 401, 405
fossils, abundance of, 193
Loxodonta, 405
mandibular metrics, 202–203
"*namadicus* morph," 219–223
Paleoloxodon, 193, 198, 207, 213–223, 225
study methods, 197
"Stuttgart morph," 219–223
terminology, 195–197
cranial vault, 195, 214
frontoparietal crest, 196
frontoparietal surface/region/plane, 195–196
isthmus frontalis, 197
nuchal fossa, 197
nuchal plane, 197
occipitotemporal crest, 196
parietofrontal crest, 196
parietooccipital boss, 196
premaxillary fossa, 196–197
sinciput, 195
vertex, 195
Elephas, 12, 198–213, 401, 405. See also *Elephas (Palaeoloxodon), Palaeoloxodon*
cranial characters, 218
E. antiquus, 202–203, 205, 208, 211, 220–221
E. antiquus recki, 211
E. atlanticus, 211
E. ekorensis, 193, 204, 211, 214
E. hysudricus, 204, 207, 211, 214, 215, 218
E. iolensis, 225
E. maximus, 205, 206, 207, 225
E. meridionalis, 211
E. mnaidrensis, 211, 220
E. namadicus, 193, 202–203, 205, 206–207, 211, 219, 220–221
E. naumanni, 224
E. planifrons, 193, 204, 213, 214
E. recki, 27, 193, 204, 209–210, 211, 225, 408, 421, 423
E. r. atavus, 193, 194, 202–203, 204, 205, 206, 207, 208, 210, 211, 214, 215, 216–217, 218
E. r. brumpti, 193, 194, 204, 214, 215
E. r. ileretensis, 193, 194, 204, 205, 208, 210, 212
E r. recki, 193, 194, 204, 206, 207, 208, 209, 210, 212, 215, 225, 414, 415
E. r. shungurensis, 193, 194, 208, 210
E. zulu, 225
Palaeoloxodon and, suggested relationships, 217
systematics and paleobiogeography, revision of, 211–213
Elephas (Palaeoloxodon)
ancestry, 193
E. (P.) antiquus, 216, 220, 223
E. (P.) atavus, 211
E. (P.) mnaidrensis, 219, 220
E. (P.) namadicus, 196, 198, 213, 220, 221, 222, 223, 224
E. (P.) naumanni, 194, 198, 213, 214, 216, 221, 222, 223–225
E. (P.) recki, 198–211, 213, 214, 216
basicranial view, 207
cranium, 198–201, 204–207
E. (P.) r. atavus, 209, 211, 214, 216
E. (P.) r. ileretensis, 209
E. (P.) r. recki, 194, 214, 216
frontal view, 204–206
incisors, 208
lateral view, 207
mandible, 202–203, 208, 209
molars, 208, 209
occipital view, 206–207
E. (P.) turkmenicus, 221
evolutionary stages, 193
endemism
African regional, 400–401
Daka Member, among eastern African early Pleistocene sites, 401–402
endocranium, Daka calvaria (BOU-VP-2/66), 341, 344–347
distortion, 344
morphological description, 341
morphopometric data, 346
volume, 344–345
Eotragus, 62
Equidae, 133–165, 403–404, 415
astragali, 139–141, 147
Equus, 133, 136, 139, 153–159, 401, 403, 415
Eurygnathohippus, 133, 136, 139, 150, 154, 159–166, 408
Hyracotherium, 133
maxillary P^2, 139

EBSCOhost - printed on 10/28/2022 4:53 AM via . All use subject to https://www.ebsco.com/terms-of-use

metacarpal III, 141, 145–150
metatarsal III, 150–153
metric procedures, 134, 136
Sivalhippus, 133, 159
statistical analysis, 136, 139–166
terminology, 133–134
Equus, 133, 136, 153–159, 401, 403, 415
astragali, 139–141
cranium (BOU-VP-25/94), 155
E. africanus, 153, 403
E. a. africanus, 404
E. asinus, 150, 153, 166
E. burchelli (African wild zebra), 145, 149, 150, 152, 153, 157, 166, 403
E. b. boehemi, 145, 150–151
E. caballus (domestic horse), 153
E. grevyi (Grevy's zebra), 145, 148, 152, 153, 166
E. hemionus, 153
E. kiang, 153, 403
E. linnaeus, 154–158
E. przewalskii, 153, 403
E. quagga, 145, 151, 153, 157
E. simplicidens, 153
E. stenonis, 153
E. zebra (mountain zebra), 145, 149, 151, 152, 153, 157, 403
fossils, 403
mandible (BOU-VP-1/213), 158
mandible (BOU-VP-3/11), 155, 157
mandibular check teeth, 137–139
maxilla (BOU-VP-3/58), 156
maxillary check teeth, 135–136
maxillary P^2, 139
metacarpal III, 141, 145–150
nondental specimens, 140–141
proportions of, in Daka Member, 166
erosion, ix, 16–17, 18
patterns of, in Daka Member, 4, 16, 39–40
Ethiopian government, antiquities legislation, 5
Eurygnathohippus, 133, 136, 150, 154, 159–166, 408
astragali, 139–141
Eu. cf. *corelianus*, 150, 160–165, 415
Eu. cornelianus, 150, 160, 165
Eu. feibeli, 160
Eu. hasumense, 146, 151, 160
Eu. turkanense, 160
mandible, 163–165
maxilla, 161, 162–163
maxillary P^2, 139
metacarpal III, 141, 145–150
proportions of in Daka Member, 166
specimens, 142–144

faults, 14, 20, 40
Felidae, 95–97, 402
Panthera leo, 96, 97, 402
Panthera pardus, 95–97
femora
Daka member, 373–388, 391–396
cortex thickness compared, 396
features and scoring procedure, 391
measurements and observations, 392–395
differences between modern humans and early Pleistocene *Homo*, 374
fieldwork, curation, and analytical methods, 6–11
documentation and analysis, 10–11
field catalog entries, 9
fossil recovery protocols, 6–8
restoration and curation, 9–10, 265–268
survey, collection, and transportation, 6–9
water-washing and drying, 9, 10
first appearance dates (FADs), modification of, 414
fossils
accurate placement of, 8
allocating to species, system for, 349, 351
fields, identification of, 7
foot survey vs. excavation, 9
matrix removal, 9
pin-flagging of, 8
recovery protocols, 6–8
restoration methodology, 9–10
significant African sites dating to near 1.0 Ma, 2

Gazella, 60–62, 400, 401, 406
G. bennetti, 61
G. cuvieri, 61
G. dama, 61
G. dorcas, 61
G. granti, 62
G. leptoceros, 61
G. nanger, 62
G. rufifrons, 61
G. soemmerringi, 62
G. spekei, 61
G. subgutturosa, 61
G. thomsoni, 61
generalist species, 417, 419–420, 421
geology and geochronology, 13–43
argon ($^{40}Ar/^{39}Ar$) and paleomagnetic results, 30–31, 32–37
chronostatigraphy of the Bouri Peninsula, 17–18
Daka Member, 20–30, 413–414
Hata Member, 18–19
Herto Member, 20
landscape evolution of the Bouri Peninsula, 14–17
paleolandscape and paleoenvironmental features of the Daka Member, 39–42
paleosol stable isotope analysis, 31, 36–39, 43
Getty, Ann, 10
Gilbert, W. Henry, xvii, 5, 10, 24, 28, 29, 47, 266, 268
Giraffa, 167–169, 170, 177, 401, 404, 410, 415
G. camelopardalis, 167, 168, 177, 415
G. gracilis, 167
G. jumae, 167, 168, 177, 415
G. pygmaeus, 167
G. stillei, 167
Giraffidae, 167–177, 404, 415
Canthumeryx, 167
Clemaoceras, 167
first appearance of, 167
Giraffa, 167–169, 170, 177, 401, 404, 410, 415
Giraffokeryx, 167
Helladotherium, 167
Okapia, 167, 404
Palaeotragus, 167
Prolibytherium, 167
Propalacoryx, 167
remains, 167, 169
Samotherium, 167, 180
Sivatherium, 167, 168, 169, 171–177, 401, 402, 408
Giraffokeryx, 167
glaciation, cyclical, 1, 421
global climate change, 417–425
macroevolutionary selection for "generalists," 417–421
phyletic evolution, 422–425
turnover pulses, 421–422
global cooling, Plio/Pleistocene, effects of, 1

Hadar fossil field, xi
Haile-Selassie, Yohannes, 102
hard-hammer technique, 6

EBSCOhost - printed on 10/28/2022 4:53 AM via . All use subject to https://www.ebsco.com/terms-of-use

Hart, William, 5
Hata Member, 16, 17, 18–19, 24, 26, 28, 40, 42
Hatayae River, 13, 15, 22
Heis, Ounda, 30
Helladotherium, 167
Hereya Pumice Unit (HPU), 19, 21, 22, 24, 26, 29, 40
Herto Member, 17, 20, 25, 26, 40, 42, 191
Herto Village, 16, 19, 28
Hexaprotodon, 179, 180
Hex. karumensis, 181
Hex. protamphibius, 181
hipparion, 133
earliest known African, 159
Hipparion, 133, 159, 401
Hip. libycum, 160
hipparionine, 133
Hippopotamidae, 179–191, 231, 404–405, 415
Archaeopotamus, 179–180
Choeropsis, 179, 181
Hexaprotodon, 179, 180
Hippopotamus, 179, 180–190, 401, 405, 411
"hippo turnover" event, 190
phylogeny, 181
Saotherium, 180
Hippotamus, 179, 180–190, 401, 405, 411
fossils, 190
generic diagnosis, 181–182
Hip. amphibius (common hippo), 179, 181–182, 189, 190, 404, 415
Hip. antiquus, 181
Hip. behemoth, 181, 189
Hip. cf. *gorgops*, 182–190, 414, 415
cheek tooth measurement, 188
cranium, 182–184
cranium and mandible measurement ranges, 189
generic description, 182
lower dentition, 186–187
mandible, 184–186
postcrania, 187
upper dentition, 184
Hip. cf. *kaisensis*, 181
Hip. incognitus, 181
Hip. gorgops, 181, 188, 189, 190, 415
Hip. kaisensis, 181, 188, 189
Hip. karumensis, 187
remains found in association with stone tools, 191
Hippotherium, 133, 159
Hip. primigenium, 145, 150
Hippotraginae, 75, 77–78
Addax, 75
Hippotragus, 75, 77–78, 407
Oryx, 75, 78, 401–402, 408, 411
Hippotragus, 75, 77–78, 407
Hip. cf. *gigas*, 77–78
Hip. equines, 75, 78
Hip. niger, 75, 78
hominid(s), 425
activity, evidence of in Herto Member, 20
emergence of, 362
femora, 265, 373–388, 391–396
anteversion, 387
BOU-VP-1/75, 375–376, 378, 380
BOU-VP-2/15, 28, 376–378, 379, 380
BOU-VP-19/63, 29, 378, 381–382, 385, 396
cortex thicknesses compared, 396
cortical thickness, 386
features and scoring procedures, 391
femur comparative analysis, 385–389, 392–395
femur descriptions, 374–378, 385
gluteal tuberosity, lateral expansion of, 387
hypertrochanteric fossa, 375, 387
lateral supracondylar line, 387–388
linea aspera pilaster, 386
linea aspera position, 386–387
measurements and observations, 392–395
minimum shaft breadth, position of, 386–387
platymery, 378, 385–386
remains
cranial. See *Homo erectus,* Daka calvaria (BOU-VP-2/66)
postcranial, 373–396
recovery of in Middle Awash valley, xii, 265
systematics, 349–371
African forms, ancestry and, 349
allocating fossils to species, 349, 351
caveats for cladistics, 352–354
cladistics vs. phenetics, 351–352
European forms, ancestry and, 349
evolutionary relationships, inferring, 351–359
operational taxonomic units (OTUs), 351, 355
talus, 390
tibia, 384, 388–389
Hominidae, 405–406, 416, 424–425
Homo erectus, 405–406, 408, 414, 416, 420, 421, 424
ancestral relation to *Homo sapiens*, 273
cladistic analysis, 355–359
Daka calvaria (BOU-VP-2/66), xvii, 12, 28, 113, 272, 274, 414
auditory meatus, 299–300
basal view, 282, 290–291
bony labyrinth, measurement of, 332–333, 339
and Buia cranium compared, 350
carnivore activity, evidence of, 113, 292
coronal suture, 296
cranial anatomy, 265–328
cranial base flexion, 343–344
cranial metrics, 312–327
cranial vault specimens, 310–311
endocranium, 341, 344–347
excavation of, 267
frontal bones, 291–293, 331–332, 335–337
frontal squama, 293–294
frontal view, 275–276, 277
glabellar inflexion, 291–292
glenoid fossa/articular eminence, 301–302
jugular notch, 304
lateral view, 272, 279–280, 287–289, 294
mandibular specimens, 311
mastoid region, 302–304
nuchal muscle attachments, 307–308
nuchal planum/foramen magnum, 306–307
oblique view of, 274, 283
occipital bones, 304–308
occipital torus, 308, 340, 342
occipital view, 281, 289–290
orbital plates, 292
overall size, shape, and proportions, 275–291
parietal bones, 294–297, 333
parietal foramina, 297
petrous portion, 299
recovery of, 25
scales, upper and lower, 305–306
sphenoidal angle, 295–296

EBSCOhost - printed on 10/28/2022 4:53 AM via . All use subject to https://www.ebsco.com/terms-of-use

sphenoid body, 308–310, 340, 343
superior view, 276, 278, 285–287
supraorbital tori, 292–293
temporal bones, 297–304, 333–334, 338–340, 342
temporal lines and angular torus, 296–297
temporal squama, 298
tomographic analysis of, 329–347
tympanic plate, 299–301
zygomatic process, 298–299
descriptions, variations in, 270–271
environment of, 42
femoral specimens, 265
Daka Member, 373–388, 391–396
BOU-VP-1/75, 375–376, 378
BOU-VP-2/15, 28, 376–378, 379, 380
BOU-VP-19/63, 29, 378, 381–382, 385, 396
differences between modern humans and early Pleistocene *Homo*, 374
fossils, recovery, cleaning, and restoration of, xvii, 265–268
phylogeny, 360
Pleistocene crania, 361
protective jacket, removal of, 269
toolmaking capabilities, x
homology, 354
Homo sapiens, 287, 360, 416, 421
ancestral relationship to *Homo erectus*, 274, 349–350
evidence of in Middle Awash, ix
H. sapiens idaltu, xiii
platymery, 385–386
remains associated with origin of, 20
Howell, F. Clark, xv
human evolution, evidence of, ix, xv
Human Evolution Research Center, xiii
Hyaena, 98, 99, 100, 103
H. hyaena (striped hyena), 98, 102–108
"hyaena condominium," 16, 25, 28
Hyaenictitherium, 98
Hyaenidae, 98–112, 402–403
BOU-VP-1/204
cranium, 103–108
dentition, 108–112
phylogeny, 111
scores assigned to, 110
Crocuta (hyaena), 12, 95, 98–112, 401, 402, 423
Hyaena, 98, 99, 100, 102–108
Parahyaena, 98, 99, 100
Proteles cristacus (aardwolf), 98
hybridization, 353
Hylochoerus, 231, 234, 405
H. meinertzhageni, 231
Hyracotherium, 133

ice ages, 1, 12
Ictitherium, 98
Institute of Geophysics and Planetary Physics, Los Alamos National Laboratory, xiii, xx
International Afar Research Expedition (IARE), 3

Johanson, Donald, 3

Kadir, Hola, 30
Kalb, Jon, xi, 3–5
Kobus, 80–84, 398, 401, 407, 411
K. aff. *ancystrocera*, 83–84
K. ellipsiprymnus, 82–83, 84, 407, 414, 420, 423
K. kob, 12, 26, 30, 80–82, 407, 414, 420, 423
K. sigmoidalis, 82, 83, 84, 414, 423
Kolpochoerus, 29, 231, 233, 234–252, 401, 405, 408
K. afarensis, 234
K. cookei, 234
K. deheinzelini, 234
K. limnetes, 232, 234, 238, 239
K. majus, 12, 231, 234, 235, 237, 239–252, 260, 414, 415, 421, 424
BOU-VP-1/7, 239, 240, 247–252
BOU-VP-3/10, 239, 242, 249, 252
BOU-VP-3/33, 252
BOU-VP-3/50, 252
BOU-VP-25/71, 252
BOU-VP-25/98, 243
BOU-VP-25/107, 241, 243–247, 248, 252
cranium, 240, 241, 242, 247–251
dentition, 251–252
dental metrics, 253–254
mandibular measurements, 257
RM_3, 29
K. olduvaiensis, 231, 232, 233, 234–239, 260, 414, 415, 421, 424, 425
dental metrics, 255
description, 234–238
K. phacochoeroides, 234
molars, 30, 234, 239
Kuseracolobus, 122

last appearance dates (LADs), modification of, 414
Latimer, Bruce, 8
Leakey, Louis S. B., xv
Lemniscomys, 262
Ley Gita/Dakanihylo section, Daka Member, 23, 41
Libypithecus, 122
Lophocebus, 123
Loxodonta, 405
L. africana, 225
Lubaka Pass, Daka Member, 26

Macaca, 123
Machairodontinae, 95, 97
macroevolutionary selection, 417–421
Madoqua, 62
Mammuthus, 204, 208, 212, 214, 215
M. meridionalis, 212, 213
M. protomammonteus, 213, 224
M. rumanus, 212
M. trogontherii, 212
Mandrillus, 123
M. sphinx, 125, 132
Maoleem Vitric Tuff (MOVT), 18, 28
matrix removal, 9, 269, 270
Meadura Member, 5
Megalotragus, 48, 50–52, 401, 407, 408
M. kattwinkeli, 50–52, 414, 421, 422
Melka Kunture, discovery of, 3
Metarchidiskodon, 211
Metridiochoerus, 231, 233–234, 252, 255–259, 401, 405, 408
dental metrics, 256
M. andrewsi, 252, 259
M. cf. *hopwoodi*, 252
M. compactus, 252, 255, 257, 258, 415, 421, 424
M. hopwoodi, 252, 255
M. modestus, 231, 252, 255, 256, 258–259, 260, 405, 415, 421, 424
micromammals, 9, 264. *See also* Murinae
Middle Awash valley
hindrances to research in, 5
hominid remains, recovery of, xii
modern landscape of, xi
paleoanthropological work, overall goal of, 12, 425
paleoanthropological importance of, xi
record of human evolution in, ix

EBSCOhost - printed on 10/28/2022 4:53 AM via . All use subject to https://www.ebsco.com/terms-of-use

Middle Awash valley *(continued)*
study project
scope and purpose of, xii–xiv
study area, defined, xi
timing of, 5
Web site (middleawash.berkeley.edu), xiii, 10
Middle Awash Digital Map Archive (MADMA), 8
Muridae, 405, 416
Murinae, 262–263
Arvicanthis, 262–263, 405

Naemorhedini, 71
"namadicus morph," 219–223
Nannippus, 133
Nasalis, 122
National Museum of Ethiopia, xii, xix, 4, 6, 10, 47, 102
National Science Foundation, xiii, xx
natural selection, 418
Neohipparion, 133
Neotragini, 59, 62
Neotragus, 62
N. batesi, 58
N. moschatus, 58
Nitidarcus, 74–75, 407, 408
N. asfawi, 45, 74–75, 76, 84, 399, 400, 401, 410, 414, 421, 422
North Herto Gully, Daka Member, 25
Notochoerus, 231, 233
Notohipparion, 160
Numidocapra, 48, 52–54, 401, 408
N. crassicornis, 53–54, 84, 414, 421, 422
Nyanzachoerus, 231, 233

Okapia, 167, 404
Olduvai Bed IV, 3, 132, 150, 152
Olduvai Gorge, xi
Olduvai Hominid 9, 350
Omo Shungura Formation, xi
operational taxonomic units (OTUs), 351, 355
Oreonager, 48
Oreotragus, 62
Oryx, 75, 78, 401–402, 408, 411
O. beisa (modern oryx), 399
O. dammah (scimitar-horned oryx), 75
O. gazella (oryx), 75, 78, 79, 408, 420, 423
O. leucoryx (Arabian oryx), 75
Ourebia, 62
Ovibovini, 71, 74–75
Nitidarcus, 74–75

Pachycrocuta, 98
P. brevirostris, 100, 108
paleoanthropology, multidisciplinary nature of, xii, xiii
paleoecology, 402–410
catchment, 402–408
Palaeoloxodon, 193, 198, 207, 213–223, 225
ancestry, 211–213, 215
biogeography, 213
cranial view, 216
cranium, 197
Elephas and, suggested relationships, 217
Eurasian and African subgenus, 213–219
later African, 225
"*namadicus* morph," 219–223
occipitotemporal crest, 196
origin, 211
parietofrontal crest, 206
P. naumanni, 225
P. tokunagai, 212
spatiotemporal distribution and evolutionary history of in Eurasia, 219–223
"Stuttgart morph," 219–223
paleosol
profile, Daka Member, 41–42
stable isotope analysis, 31, 36–39, 43
Palaeotragus, 167
Panthera (big cats), 95, 96–97, 401
P. cf. *leo*, 95, 97, 113, 414, 420
P. cf. *pardus*, 95, 96–97, 113, 402, 414, 420
P. leo, 96, 97, 402
P. pardus, 95–97
Papio, 123
P. hamadryas, 125, 131, 132
P. h. kindae, 132
Papionini, 123
Lophocebus, 123
Macaca, 123
Papio, 123
Theropithecus, 123–130, 401, 423
Paracolobus, 119, 122
Paradiceros, 227
Parahyaena, 98, 99, 100
P. brunnea (brown hyena), 98
Parmularius, 47, 48, 55–58, 401, 407, 408
P. altidens, 55, 56
P. angusticornis, 56–58, 74, 414, 421, 423
P. braini, 55
P. eppsi, 55
P. pandates, 55
P. rugosis, 56
Pelomys, 262
Pelorovis, 63–68, 84, 401, 408, 414
cranium (BOU-VP-3/8), excavation of, 46, 47
juvenile, 66
P. antiquus, 63, 64, 67–68, 84, 414, 421, 422, 423
P. oldowayensis, 63, 64–67, 68, 414, 421, 422, 423
P. turkanensis, 63
Pennington, Doug, 10
Phacochoerus, 231, 234, 237, 238, 252, 259–260, 405, 415, 420, 424, 425
mandible, 258, 259
P. aethiopicus, 231
P. africanus, 258
Phanourios minor, 181
phenetics
and cladistics compared, 351–352
defined, 351
phyletic evolution, 422–425
Bovidae, 422–423
Carnivora, 423
Elephantidae, 423–424
Hominidae, 424–425
Rhinocerotidae, 424
Suidae, 424
Piliocolobus, 122
platymery, 378, 385–386
Plesiohipparion, 133, 159, 160
Pliocene Central Awash Complex, 13
Plioviverrops, 98
Potamochoerus, 231, 405
P. porcus, 231
Potts, Rick, 417
Proailurus, 95
Proboscidipparion, 133, 159, 160
Procapra, 60
Procolobus, 119, 120, 121, 122
Prohylobates, 115
Prolibytherium, 167
Propalaeoryx, 167
Propotamochoerus, 234
Proteles cristatus (aardwolf), 98
Pseudhipparion, 133
Puma concolor (puma), 95
Pygathrix, 122

Quaternary axial rift zone, 13, 14, 40, 42

EBSCOhost - printed on 10/28/2022 4:53 AM via . All use subject to https://www.ebsco.com/terms-of-use

Rabaticeras, 48, 53, 54
R. arambourgi, 53
Raphiceras, 62
rare taxa, 261–264
Aves, 261–262
Murinae, 262–263
Siluriformes, 263–264
Red Queen Hypothesis, 421
Redunca, 80
Reduncinae, 78, 80–84
Kobus, 80–84, 398, 401, 407, 411
Redunca, 80
Renne, Paul, 5
Revenani section, Daka Member, 23–24
Rhinoceros, 227
R. sondaicus, 227
R. unicornis, 227
Rhinocerotidae, 227–230, 405, 415, 424
Ceratotherium, 227–229, 400, 401, 410
dental metrics, 229
Diceros, 227, 228, 230, 415, 420
divergence of, 227
extinction, threat of, 227
Paradiceros, 227
Rhinoceros, 227
Teletaceras, 227
Rhinocolobus, 119, 122
Rift Valley Research Mission in Ethiopia (RVRME), xi, 3, 5
Rupicaprini, 71

Samotherium, 167, 180
Schick, Kathy, xvii
sedimentation
Eastern Rift, ix
Middle Awash valley, xi
patterns of in Daka Member, 4, 39–40, 397
selection
clade-based, 419
natural, 418
organism-level, 419
variability, 417–418
Semnopithecus entellus, 119
sexual dimorphism, 222, 239, 252, 260
Siluriformes, 263–264
Simatherium, 63
Simpson, Scott, 10
sinciput, 195
site-based cladistic analysis, 358–359, 370–371
Sivacapra, 74
Sivalhippus, 133, 159
Sivatherium, 167, 168, 169, 171–177, 401, 402, 408
dental metrics, 173
dental specimens, 176
description, 171–176
mandible, 171–172
maxilla, 174
S. giganteum, 169
S. hendeyi, 169
S. maurusium, 169
Smart, Charles, 4
soil, 38
paleosol profile, Daka Member, 41–42
paleosol stable isotope analysis, 31, 36–39, 43
vertisol, 36, 41
specialist species, 419–420, 421
species, 419–420
allocating fossils to, 349, 351
differential survival, 418
divergent lineages, establishing, 351–352
generalist, 417, 419–420, 421
selection, 417–418
specialist, 499–420, 421
specimen-based cladistic analysis, 356
Stegodon orientalis, 197
Stone Age artifacts, 20
study area, xi
exploration, xii
focused research, xii
long-term management, xii
three stages, xii
"Stuttgart morph," 219–223
Stylohipparion, 133, 160
Suidae, 231–260, 405, 415, 424
average third molar metrics, 239
Babyrousa, 231
cranial metrics, 260
Hylochoerus, 231, 234, 405
overview, 231, 233–234
Phacochoerus, 231, 234, 237, 238, 252, 259–260, 405, 415, 420, 424, 425
Potamochoerus, 231, 405
Suinae, 233–234
Sus, 231
Tetraconodontinae, 231, 233
Suinae, 233–234
Kolpochoerus, 29, 231, 233, 234–252, 401, 405, 408
Metridiochoerus, 231, 233–234, 252, 255–259, 401, 405, 408
Sus, 231
S. barbatus, 231
S. celebensis, 231
S. scrofa, 231
S. verrucosus, 231
Suwa, Gen, 8, 374
Syncerus (cape buffalo), 28, 63, 68, 69, 84, 400, 401, 408, 410, 414
S. acoelotus, 68
S. caffer, 63, 68, 84, 414, 420

Taieb, Maurice, xi, 3
talus, 390
Tayassuidae, 231
Tebedge, Seleshi, 3
Taurotragus (eland), 69
Teletacerus, 227
Tetracerus, 62
Tetraconodontinae, 231, 233
Notochoerus, 231, 233
Nyanzachoerus, 231, 233
Thallassictis, 98
Theropithecus, 123–130, 401, 423
T. brumpti, 123
T. gelada, 123, 129, 403, 423
T. imberbis, 421
T. oswaldi, 27, 123–124, 126, 129, 130, 403, 408, 421, 423, 425
T. o. darti, 123, 124
T. o. leakeyi, 115, 119, 122, 123, 124–130, 131, 132, 414
dental dimensions, 127
dentition, 128–129
description, general, 125–127
femur, 129
mandible, 127, 128
postcranial dimensions, 129
tibia, 129–130
tibia, 384, 388–389
tomographic analysis, Daka calvaria, 329–347
advantages and importance of, 347
endocranium, 341, 344–347
frontal bones, 331–332, 335–337
occipital bones, 340, 342
parietal bones, 333
sphenoid body, 340, 343
temporal bones, 333–334, 338–340, 342
Tossunnoria, 74
Tragelaphini, 62, 68–71
Taurotragus, 69
Tragelaphus, 69, 70–71

EBSCOhost - printed on 10/28/2022 4:53 AM via . All use subject to https://www.ebsco.com/terms-of-use

Tragelaphus (Kohi), 69, 70–71, 401, 408, 411
T. cf. *imberbis*, 69, 70, 408, 423
T. cf. *scriptus*, 69–70
T. imberbis (lesser kudu), 408
T. strepsiceros (greater kudu), 69, 70–71, 408, 420, 423
turnover pulse hypothesis, 421–422

Ugandax, 63
uplift, 40
Urugadehu section (A2 area), Daka Member, 22–23, 41

variability selection, 417–418
variation, 353
vertex, 195
vertisol, 36, 41
Victoriapithecus, 115
volcanic activity, 1, 13, 14, 19

Wadi "M" section, Daka Member, 24, 41
Waidedo Vitric Tuff (WAVT), 17, 20, 25
water, animal dependence on, 410
Wehaietu Formation, 4, 5
White, Tim, xiv, xix, 5, 27, 28, 29, 269, 373
Wokari Tuff, 16, 21, 23–24, 25, 26, 28, 29, 30, 40, 43
WoldeGabriel, Giday, 5

Yanguli Mu'ul section, Daka Member, 24–25
Yardi Lake, 13, 16, 18, 40

EBSCOhost - printed on 10/28/2022 4:53 AM via . All use subject to https://www.ebsco.com/terms-of-use